UNIVERSITÀ DEGLI STUDI DI TRIESTE

XXXVIII CICLO DEL DOTTORATO DI RICERCA IN

Earth Science, Fluid-Dynamics and Mathematics. Interactions and Methods

Finanziato dall'Unione europea – NextGenerationEU

Missione 4 – Componente 2 – Investimento 1.5 CUP J43C22000320006

Assessing Coastal Flood Hazard under Climate Change in the northern Adriatic Sea: Extreme Sea Level Analysis and Implications for Urban Adaptation

Settori scientifico-disciplinari: GEO/02 - GEO/04

DOTTORANDO

Sebastian Spadotto

COORDINATORE

PROF. Stefano Maset

SUPERVISORE DI TESI

PROF. Giorgio Fontolan

ANNO ACCADEMICO 2024/2025

Finanziato dall'Unione europea NextGenerationEU | Ministero dell'Università e della Ricerca | Italiadomani PIANO NAZIONALE DI RIPRESA E RESILIENZA | UNIVERSITÀ DEGLI STUDI DI TRIESTE

Finanziato dall'Unione europea NextGenerationEU
Ministero dell'Università e della Ricerca
Italiadomani PIANO NAZIONALE DI RIPRESA E RESILIENZA
UNIVERSITÀ DEGLI STUDI DI TRIESTE

Contents

Abstract 7

1. Introduction 8

1.1 Global climate change effect 8

1.2 Mediterranean as hot spot of Climate Change 8

1.3 Northern Adriatic 9

1.4 Coastal urban area 10

1.5 Statistical of extremes 10

1.6 Modellistic approach and downscaling analysis 12

2. Objective 13

3. Study area and drivers 14

3.1 Geographical settings: the Adriatic basin 14

3.2 Drivers of sea level 14

3.2.1 Tidal forcing 14

3.2.2 Storm Surge 15

3.2.2.1 Wind regime 15

3.2.2.2 Low pressure system 17

3.2.3 Seiches 17

3.3 Extreme sea level (ESL) composition 17

3.3.1 Tidal forcing 18

3.3.2 Metereological forcing 18

3.3.3 Meteotsunami 18

3.3.4 PAW surge 18

3.3.5 Seasonal sea level variability, inter-annual and inter-decadal (IDAS) 19

3.3.6 Long-term components 19

3.4 Wave regime 19

3.4.1 Wave run-up (R) 20

3.4.2 Wave set-up (η) 20

3.4.3 Swash (S) 20

3.4.4 Wave overtopping 21

3.5 Nearshore Total Water Level (TWL) 22

3.6 Factors of coastal risk exposure 23

3.6.1 Subsidence 23

3.6.2 Sea level rise (SLR) and Relative-Sea level rise (R-SLR) 25

3.6.3 Coastal morphology 28

3.6.3.1 Low-lying sandy coast 29

3.6.3.2 High and urbanized rocky coast 29

3.6.4 Coastal and urban flooding 30

3.6.4.1 Historical and recent storm surge event 32

3.6.5 Salt water intrusion 33

3.7 The coast of Friuli Venezia Giulia 34

Finanziato dall'Unione europea NextGenerationEU | Ministero dell'Università e della Ricerca | Italiadomani PIANO NAZIONALE DI RIPRESA E RESILIENZA | UNIVERSITÀ DEGLI STUDI DI TRIESTE

3.7.1 Coastal risk location and context ... 35
3.7.1.1 Lignano ... 36
3.7.1.2 Grado ... 37
3.7.1.3 Trieste ... 38
3.7.1.4 Muggia ... 40

4 Materials and methods ... 41

4.1 Flood Directive 2007/60/CE ... 43
4.1.1 Flooding scenarios ... 44
4.1.2 Flood Risk Management Plan of the Eastern Alps Hydrographic Basin (PGRA) ... 44

4.2 Assessment of Extreme Events in Grado: methodological setup ... 46
4.2.1 Tide gauge data processing and quality control ... 47
4.2.2 SLR rate detrending approach ... 48
4.2.3 Grado extreme analysis ... 48
4.2.3.1 Gumbel - Block Maxima (BM) ... 49
4.2.3.2 Annual exceedance of flooding threshold ... 50

4.3 Assessment of extreme events in Trieste: methodological setup ... 50
4.3.1 Tide gauge data processing and quality control ... 50
4.3.2 Sea level rise detrending approach ... 52
4.3.2.1 Annual mean sea level detrending ... 54
4.3.2.2 19-years mean move detrending ... 54
4.3.2.3 Detrending and drivers of sea level ... 55
4.3.3 Sea level dynamics statistical analysis ... 57
4.3.3.1 Non stationary analysis ... 57
4.3.3.2 Non linear interactions Tide-NTR ... 57
4.3.4 Trieste extreme values analysis ... 59
4.3.4.1 GEV-BM ... 59
4.3.4.2 GPD-POT ... 60
4.3.4.3 Multivariate Statistical Approach ... 61
4.3.4.4 Fit validation test ... 62

4.4 Grado vs. Trieste: Sea Level trend comparison ... 64

4.5 Downscaling flooding modelling ... 64
4.5.1 Bathtub modelling ... 64
4.5.2 Dynamic Modelling ... 66
4.5.2.1 MIKE21 Spectral Waves module (SW) ... 67
4.5.2.2 MIKE21 Hydrodynamic module (HD) ... 67
4.5.2.3 Domain setup ... 68

5. Results and discussion ... 70

5.1 Grado extreme statistical values ... 70
5.1.1 Gumbel-BM ... 70
5.1.2 Analysis of Mean vs. Max levels and Threshold exceedance ... 71

5.2 Trieste extreme analysis ... 73
5.2.1 GEV-BM ... 73
5.2.1.1 Extreme water levels ... 73
5.2.1.2 GEV-BM Validation test ... 75
5.2.2 GPD-POT ... 77

Finanziato dall'Unione europea NextGenerationEU
Ministero dell'Università e della Ricerca
Italiadomani PIANO NAZIONALE DI RIPRESA E RESILIENZA
UNIVERSITÀ DEGLI STUDI DI TRIESTE

5.2.2.1 Extreme water levels 77
5.2.2.2 GPD-POT Validation test 80
5.2.3 Multivariate Statistical Approach 84
5.2.3.1 Decomposition drivers of sea level 84
5.2.3.2 Non stationary analysis 86
5.2.3.3 Non linear interaction Tide-NTR 89
5.2.4 Analysis of Mean vs. Max levels and Threshold exceedance 93

5.3 Grado vs. Trieste: Sea Level trend comparison 94
5.3.1 Grado Long-term projections 95
5.3.2 Trieste Long-term projections 97

5.4 Muggia extreme values 98

5.5 Lignano extreme values 98

5.6 Downscaling bathtub approach analysis of Grado 99
5.6.1 Downscaling analysis of short-term flooding 99
5.6.1.1 The 2-Year Return Period Episodic Event 100
5.6.1.2 The 10-Year Return Period Episodic Event 101
5.6.1.3 The 30-Year Return Period Episodic Event 102
5.6.2 Lagoon promenade downscaling analysis 103
5.6.2.1 Riva Brioni - Mandracchio C. 103
5.6.2.2 Mandracchio C. 104
5.6.3 Bathtub vs. Dynamic modelling 105
5.6.4 Dynamic modelling: Event calibration of 4-5 November 2023 106
5.6.5 Future projections of the 4-5 November 2023 event 108

5.7 Downscaling analysis and flood modelling of Muggia 110
5.7.1 Water-front promenade analysis 111
5.7.1.1 Mandracchio Canal promenade waterfront 112
5.7.2 Bathtub vs. Dynamic modelling 117
5.7.3 Downscaling dynamic flood modelling 118
5.7.3.1 MIKE21 HD with R_P = 2 years 120
5.7.3.2 MIKE21 HD with R_P = 30 years 121
5.7.3.3 MIKE21 HD with R_P = 100 years 121
5.7.4 Muggia long-term projection 122

5.8 Downscaling analysis and flood modelling of Lignano 126
5.8.1 Downscaling analysis of lagoon promenade 126
5.8.1.1 Promenade C. Canottieri 127
5.8.1.2 Promenade Riva Zanelli 128
5.8.1.3 Dockyard Molo -A promenade 129
5.8.2 12 Novembre 2019 event calibration 131
5.8.3 Lignano long-term projections 132

5.9 Downscaling analysis and flood modelling of Trieste 133
5.9.1 Downscaling of marine waterfront and promenade 133
5.9.1.1 Ponterosso promenade: Via Rossini 134
5.9.1.2 Ponterosso promenade: Via Bellini 136
5.9.1.3 Marine waterfront: Le Rive 137
5.9.2 Bathtub vs. Dynamic modelling 139
5.9.3 12 Novembre 2019 event calibration 140
5.9.4 SLR projections (SSP5-8.5) applied on nuisance extreme events 143

6 Adaptation Plans and Conclusions 145
6.1 Grado adaptation plans 146
6.2 Muggia adaptation plans 148
6.3 Lignano adaptation plans 152
6.4 Trieste adaptation plans 153
7 Final remarks 154
8 References 156
9 Acknowledgements 183
10 Appendix I – Papers and scientific contributions related to PhD project 185

a Valentina

Finanziato dall'Unione europea NextGenerationEU
Ministero dell'Università e della Ricerca
Italiadomani PIANO NAZIONALE DI RIPRESA E RESILIENZA
UNIVERSITÀ DEGLI STUDI DI TRIESTE

Abstract

Coastal flooding represents one of the most critical and rapidly evolving hazards affecting low-lying and urbanized coastal areas under climate change, particularly in semi-enclosed basins such as the Mediterranean Sea. The ongoing rise in mean sea level, combined with the intensification of meteomarine extreme events, is increasing both the frequency and severity of coastal inundation events, with significant socio-economic and infrastructural impacts. Within this context, the northern Adriatic Sea represent a hotspot of vulnerability, owing to its shallow bathymetry, elongated basin geometry, and strong sensitivity to wind-driven storm surges and basin-scale oscillations. This doctoral research investigates extreme sea level dynamics and coastal flood hazard along the Friuli Venezia Giulia coastline (NE Italy), focusing on the urban areas of Grado Lignano Sabbiadoro, Muggia and Trieste. The study integrates long-term tide-gauge observations, advanced extreme value statistics, physical process decomposition, and hydrodynamic modelling to characterize present-day and future coastal flood hazard at the urban scale. For Trieste, one of the longest and most reliable tide-gauge records in the Mediterranean (1939-2024) is analysed. Extreme sea levels are estimated using both the block maxima approach (GEV distribution) and the Peaks Over Threshold method (GPD), following detrending procedures based on annual mean sea level and a 19-year running mean to isolate meteomarine extremes from long-term sea-level rise oscillations. Statistical robustness is ensured through diagnostic tests and non-parametric trend analysis. A multivariate decomposition of total water levels allows the relative contribution of astronomical tide, storm surge, seiches, and low-frequency components to be quantified. Results show that extreme sea levels in Trieste are predominantly governed by barotropic processes, with the non-tidal residual becoming the dominant contributor during the most severe events. Seiches play a key amplifying role under persistent Scirocco conditions, leading to resonance effects that substantially enhance coastal water levels. Despite the observed increase in mean sea level, no statistically significant trends in storm intensity or frequency are detected over the analysed period, indicating that rising baseline sea level remains the primary driver of increasing flood hazard. For Grado and Lignano Sabbiadoro, characterized by low-lying sandy and lagoonal morphologies, extreme levels are assessed using annual maxima calibrated against the Trieste reference record. High-resolution digital terrain models are employed within a GIS-based framework to map inundation scenarios through a static “bathtub” approach, highlighting the critical role of lagoon connectivity and urban elevation in controlling flood propagation. In Muggia, a semi-enclosed bay setting promotes surge accumulation and prolonged inundation despite limited wave exposure. Hydrodynamic simulations performed with the MIKE 21 modelling suite further elucidate the interaction between sea level, waves, and coastal morphology, confirming that flooding mechanisms differ substantially among the analysed sites. Overall, the research provides an integrated and operational framework for coastal flood hazard assessment, supporting urban adaptation strategies and the implementation of the European Floods Directive. The findings underscore the urgency of targeted adaptation measures, particularly in lagoon-connected urban systems, where even modest sea-level rise may transform currently infrequent events into chronic flooding conditions.

Finanziato dall'Unione europea NextGenerationEU | Ministero dell'Università e della Ricerca | Italiadomani PIANO NAZIONALE DI RIPRESA E RESILIENZA | UNIVERSITÀ DEGLI STUDI DI TRIESTE

1. Introduction

1.1 Global climate change effect

In the most recent climate change assessment reports –the Sixth Assessment Report prepared by the IPCC (Masson-Delmotte et al., 2021; Pörtner et al., 2022)– as well as during the latest United Nations Climate Change Conference (COP29, Baku, 2024. https://cop29.az/en/home), the main global challenges to be addressed in the coming years in relation to the effects of climate change were highlighted, as its consequences are becoming increasingly evident worldwide. At the global scale, the impacts of sea-level rise expected in the near future will lead to a marked increase in coastal risks, including erosion and salinisation, and above all flooding (Vitousek et al., 2017; Taherkhani et al., 2020). The most significant consequences will involve the loss of low-lying and sandy coastal areas, shoreline retreat, saltwater intrusion (Ku, 2021), and the degradation or loss of coastal ecosystems (Neumann et al., 2015; Ranasinghe, 2016; Vousdoukas et al., 2018; Nicholls et al., 2020). Moreover, it is well established that since ancient times coastal zones have represented major centres of societal development, owing to the presence of key subsistence resources, their role as gateways for trade and maritime transport, and their importance for cultural and recreational activities. As a result, even relatively small increases in mean sea level can generate severe impacts on these territories (Xie et al., 2022). Such impacts may be morphological in nature –such as coastal erosion or the inundation of wetlands– geochemical, through the contamination of groundwater and agricultural soils due to increased salinity (Masson-Delmotte et al., 2021; Pörtner et al., 2022), as well as economic, ecological, cultural, and infrastructural losses.

1.2 Mediterranean as hot spot of Climate Change

Sea-level rise, the most significant slow-onset consequence of climate change, is already affecting the coasts of the Mediterranean (Lionello et al., 2017; Pörtner et al., 2022) and the Adriatic Sea (Ferrarin et al., 2022). Identified as a climate change hot spot (Tuel & Eltahir, 2020), particularly with respect to extreme events (Paxian et al., 2015), this region is experiencing a warming rate approximately 20% higher than the global average (Cramer et al., 2018; Lionello & Scarascia, 2020; MedECC, 2020; Pörtner et al., 2022; Chiggiato et al., 2023; Lionello et al., 2023). Consequently, climate-related impacts in this area are expected to be more severe than in many other regions of the world (Giorgi et al., 2006; Giorgi & Lionello, 2008). Over recent decades, both the intensity and frequency of coastal flooding events in the Mediterranean have increased, driven by highly impactful storms as well as by particularly intense storm surge phenomena (Bakkensen et al., 2017; Portmann et al., 2020; Scicchitano et al., 2021). Furthermore, as highlighted in Mediterranean studies, the vulnerability of these areas (Rizzi et al., 2017; Bonaldo et al., 2019) is strongly linked to the effects of sea-level rise (Melet et al., 2018) acting on a high population density that is predominantly concentrated along coastal zones (Lagarias et al., 2023). According to McEvoy et al. (2021), approximately one third of the European population currently lives within 50 km of the coastline, with an average density of around 100 inhabitants per km², while nearly 75% of the Mediterranean population is distributed along coastal strips. Current trends indicate that migration towards these areas is ongoing and is expected to intensify further in the future. As a result, the development and utilisation of coastal zones have

Finanziato dall'Unione europea NextGenerationEU
Ministero dell'Università e della Ricerca
Italiadomani PIANO NAZIONALE DI RIPRESA E RESILIENZA
UNIVERSITÀ DEGLI STUDI DI TRIESTE

increased substantially, leading to profound environmental changes due to the strong pressure exerted on these vulnerable systems, as well as to significant human-induced transformations (Crossland et al., 2005; Patterson & Hardy, 2008; Antonioli et al., 2017; Pasquali & Marucci, 2021). These factors, combined with the aforementioned climatic drivers, are expected to significantly constrain the adaptive capacity of European coastal systems, as demonstrated by van de Wal et al. (2024). Consequently, the risk associated with coastal flooding phenomena is progressively increasing.

1.3 Northern Adriatic

Flooding represents a particularly critical issue in the Adriatic Sea, where the dominant contribution of storm surge is more pronounced than in other sectors of the Mediterranean basin (Marcos et al., 2009; Conte & Lionello, 2013). More specifically, the Northern Adriatic is of particular interest from the perspective of both meteorological and marine forcings (Raicich, 2010; Lionello et al., 2012; Ferrarin et al., 2022). The most extreme sea levels generated by storm surge events are observed in its northern sector, where water levels can, in some cases, exceed one metre above the mean sea level (Međugorac et al., 2018). These extreme levels typically occur during the autumn season, particularly in November, when storm surge intensity is maximised as a result of the concurrence of multiple factors. These include the combined action of strong south-easterly Scirocco winds (Lionello et al., 2012) and the inverse barometric effect associated with low atmospheric pressure systems. Winds blowing from the south-east are channelled along the Adriatic basin, pushing large volumes of water northwards over timescales ranging from several hours to days. This mechanism significantly contributes to the occurrence of so-called *acqua alta* events, which are favoured by the shallow bathymetry of the basin and are responsible for frequent coastal flooding (Lionello et al., 2012; Mel et al., 2014; Međugorac et al., 2018; Ferrarin et al., 2020; Pervan et al., 2023). Within this framework, sea-level rise combined with storm surge can produce an amplified response, particularly when acting in conjunction with land subsidence, especially along low-lying and sandy coastlines. In this context, Venice and its lagoon represent the most emblematic and globally recognised example of climate change impacts related to *acqua alta* (i.e., storm surge) events. Over the years, numerous studies have been conducted to investigate the forcings governing the increase in extreme sea levels in this unique environment (Tomasin & Pirazzoli, 2007, 2009; Zanchettin et al., 2021). Owing to its specific exposure and orientation with respect to meteorological and oceanographic drivers, the Venice Lagoon constitutes an exceptionally important natural laboratory for both numerical and statistical analyses (Ferrarin et al., 2022; Umgiesser et al., 2022; Ragno et al., 2023).Nevertheless, within the broader Northern Adriatic context, other lagoonal systems –such as the Grado–Marano Lagoon– and the Po River Delta also rank among the Mediterranean areas most exposed to the effects of sea-level rise and extreme events (Perini et al., 2017; Gallina et al., 2019; Noon et al., 2021), as well as to marine flooding, particularly during extreme conditions (Ferrarin et al., 2021). Further exacerbating the intrinsic vulnerability of these territories is the presence of some of the most economically and touristically significant coastal settlements of the Northern Adriatic, including Venice and other major centres such as Jesolo, Bibione, Lignano, Grado, and Trieste.

Finanziato dall'Unione europea NextGenerationEU
Ministero dell'Università e della Ricerca
Italiadomani PIANO NAZIONALE DI RIPRESA E RESILIENZA
UNIVERSITÀ DEGLI STUDI DI TRIESTE

1.4 Coastal urban area

For these reasons, densely populated coastal areas of high economic and tourist value are at risk of severe degradation, and in some cases potential disappearance, due to the concurrence of multiple interacting drivers (Masson-Delmotte et al., 2021; Lionello et al., 2022). In addition to the impacts of sea-level rise at both global and regional scales, the effects of rapid urban development (Merkens et al., 2016; Andreadis et al., 2022) must also be considered, as they have substantially amplified flood risk in coastal settings. This combination of pressures has resulted in significant socio-economic damages (Nicholls et al., 2007; Wong et al., 2014; Hlodversdottir et al., 2015; Harley et al., 2017; Wu et al., 2017; Locatelli et al., 2020), driven both by the increasing concentration of populations exposed to flooding hazards (Rufat et al., 2015) and by the recurrent vulnerabilities inherent to densely urbanised environments (Neumann et al., 2015). The resulting impacts range from the disruption of transport systems and road networks (Hammond et al., 2015), traffic accidents, and structural failures or collapses (Agonafir et al., 2023), to broader effects on land-use patterns (Nicholls et al., 2020) and human activities (Cooley et al., 2023). These processes also pose a growing threat to valuable cultural heritage assets (Reimann et al., 2018; Vousdoukas et al., 2022) located in many coastal regions. For this reason, it is essential to undertake detailed and robust studies aimed at characterising the increasingly severe and persistent issues associated with marine flooding, which is becoming more frequent in urbanised coastal areas (Tong et al., 2022). The growing need to develop adaptation and mitigation plans (Rafiq et al., 2016; Shah et al., 2018; Chen et al., 2019) in response to climate change impacts –often requiring substantial modifications to territories exposed to extreme events (Pörtner et al., 2022; UNFCCC, 2024)– has heightened public awareness and concern regarding political responsibility in translating these challenges into effective urban planning policies (Mariano et al., 2021). Since 2008, following the launch of the Covenant of Mayors, European local governments have committed to the implementation of Sustainable Energy and Climate Action Plans (SECAPs), aiming to increase energy efficiency and the use of renewable energy sources, while also integrating climate adaptation measures and mitigation strategies (Melica et al., 2022). Within this framework, it has been possible to develop, for instance in the urban area of Trieste (Manzan et al., 2022), coastal flood hazard maps to assess the local-scale impacts of marine flooding. A wide range of studies (Bisht et al., 2016; Mignot et al., 2019; Habel et al., 2020; Mariano et al., 2021; Gao et al., 2022; Shi et al., 2022; Balaian et al., 2024) emphasise that the implementation of tailored simulation approaches is crucial, not only for the design of flood risk management plans –essential for mitigating the impacts described above– but also as part of routine urban maintenance programmes. Such approaches support regional and municipal authorities in the development of more effective planning strategies and mitigation actions, while substantially reducing short-term management costs (Xie et al., 2022).

1.5 Statistical of extremes

A fundamental step in assessing the current frequency of events and, equally, in defining effective urban planning strategies lies in the adoption of a statistical approach capable of describing the behaviour of extreme sea levels as realistically as possible. This requires consideration of the statistical framework provided by Extreme Value Theory (EVT). The assessment of extreme meteo-marine events is in fact grounded in EVT, originally

Finanziato dall'Unione europea NextGenerationEU | Ministero dell'Università e della Ricerca | Italiadomani PIANO NAZIONALE DI RIPRESA E RESILIENZA | UNIVERSITÀ DEGLI STUDI DI TRIESTE

developed through the seminal works of Fisher and Tippett (1928) and later formalised by Gnedenko (1943). Within this framework, the family of Generalised Extreme Value (GEV) distributions (von Mises, 1936) is identified as the appropriate model for describing the distribution of maxima extracted over equal-length time intervals, such as annual maxima, according to the Block Maxima (BM) method (Gumbel, 1958). Although widely applied in oceanographic and hydrological studies, this approach presents several limitations: (i) it considers only a single maximum per year; (ii) it relies on the assumption of independence and stationarity of the maxima; and (iii) it may prove inefficient when applied to short time series –requiring, according to Pugh and Vassie (1980), at least 25 years of data– or to discontinuous records (Castillo & Sarabia, 1994; Coles & Tawn, 2005; Haigh et al., 2010; Muis et al., 2016; Katalinić & Puranov, 2020; Anghel, 2024). To overcome some of these limitations, EVT also provides the Peaks Over Threshold (POT) approach, based on the Generalised Pareto Distribution (GPD) (Balkema & de Haan, 1974; Pickands, 1975), whereby all events exceeding a sufficiently high threshold are modelled as GPD exceedances (Davison & Smith, 1990). In the context of marine extremes –where the observed signal results from the combination of a deterministic component (astronomical tide) and a stochastic component (storm surge), typically sampled at an hourly resolution– the POT method allows a larger number of extreme observations to be exploited compared to the sole use of annual maxima. For this reason, it is often preferred to the BM–GEV approach (Coles & Tawn, 2005; Haigh et al., 2010; Caruso & Marani, 2022), despite requiring careful threshold selection, which can significantly influence the uncertainty of the estimated parameters (Scarrott, 2012; Benito et al., 2024). Nevertheless, the choice of a simpler approach (Wahl et al., 2017), such as the BM method, may still prove highly effective when the primary objective concerns the design calculations of coastal or urban defence structures (Vanem, 2015; Muis et al., 2016; Wahl et al., 2017; Buchanan et al., 2017). An example of such a methodological choice is provided by the application presented by Spadotto et al. (2025) in the context of urban planning for the city of Grado, in the Friuli Venezia Giulia region.

Extreme Value Theory (EVT) is currently applied across a wide range of disciplines –from hydrogeology and climatology to wave modelling and urban flood studies– with applications encompassing both pluvial and fluvial events as well as marine-driven phenomena (Coles, 2001; Beirlant, 2004; Castillo et al., 2005; de Haan & Ferreira, 2006; Reiss & Thomas, 2007; Masina & Ciavola, 2011; Barbariol et al., 2019; De Leo et al., 2020; Nimac et al., 2022; Iliadis et al., 2023; Ferrarin et al., 2022; Green et al., 2025). Within the Italian context, and particularly in the Northern Adriatic region, EVT has been extensively employed to characterise coastal flood risk in a number of scientific studies and technical reports. These include the *Methodological Report on Coastal Flooding in Sardinia* (SAR, update 2018), the analyses carried out within the MICORE project for the Emilia-Romagna region (Masina & Ciavola, 2011; Perini et al., 2015), more recent investigations focused on Venice (Zanchettin et al., 2021; Caruso & Marani, 2022; Ferrarin et al., 2022; Ragno et al., 2023), as well as local-scale applications for Trieste and Grado (Tomasin & Pirazzoli, 2009; Spadotto et al., 2025). In the current climate change driven context, robust estimates of the probability of occurrence of extreme meteomarine events have become indispensable for hazard assessment and for adaptation planning and mitigation measures in coastal and lagoonal

Finanziato dall'Unione europea NextGenerationEU
Ministero dell'Università e della Ricerca
Italiadomani PIANO NAZIONALE DI RIPRESA E RESILIENZA
UNIVERSITÀ DEGLI STUDI DI TRIESTE

environments (Hamdi et al., 2018; Ferrarin et al., 2022; Mariano et al., 2021; van de Wal, 2024; Ramirez et al., 2024; Spadotto et al., 2025).

1.6 Modellistic approach and downscaling analysis

To complement the statistical analyses applied within a given coastal sector –essential for both the historical assessment and future projection of extreme events and sea-level trends– it is necessary to integrate a supporting tool that is fundamental for the prevention and mitigation of flood-related impacts. This tool is the modelling approach, which has become increasingly prevalent in this field of research. Compared to the use of coastal flood hazard maps –which are highly valuable for the correct interpretation of vulnerable areas as a function of event type and are therefore useful for impact mitigation and urban planning, as well as for the definition of future adaptation strategies (Perini et al., 2015; Habel et al., 2020; Mariano et al., 2021)– numerical modelling accounts for a much wider range of additional components. As a result, the analysed event can be represented in a more comprehensive and realistic manner. Over recent decades, a broad variety of modelling approaches have been developed, reflecting the diversity of boundary conditions and processes that need to be considered. Examples include the explicit investigation and incorporation of tide-surge-wave interactions within modelling frameworks (Lyddon et al., 2020), the assessment of potential failure or overtopping of natural and/or artificial coastal defences (Brown et al., 2007; de Moel et al., 2012), and the use of hydrodynamic models to support coastal planning and decision-making processes (Louisor et al., 2022). Other numerical approaches focus on wave overtopping processes affecting urban coastal defences (Santiago-Collazo et al., 2019). Additional modelling studies concentrate on the dynamics of individual drivers contributing to total water level increases, such as storm surge (Umgiesser et al., 2022; Vogt et al., 2024), in order to assess potential urban flood risk (Zheng & Sun, 2020). Conversely, more holistic approaches aim to evaluate the effectiveness of coastal protection systems through hydrodynamic modelling that simultaneously considers multiple drivers within the selected study area (Sah et al., 2025). In this context, the combined use of modelling and downscaling techniques enables the derivation of more reliable information on flood dynamics within the urban fabric. In particular, these approaches allow for a more accurate identification of flood ingress points and propagation pathways, as well as the characterisation of key parameters such as flow velocities, dominant flow routes, water depths, and subsequent drainage or recession areas. Therefore, to complement the statistical analysis, this study adopts dynamic modelling approaches to evaluate the response of the urban fabric in the coastal settlements of Lignano, Grado, Trieste, and Muggia under the storm surge scenarios considered. Hydrodynamic and wave models are employed in order to characterise both the pure water-level elevation driven by tidal and meteorological forcings, analysed individually, and the combined contribution of wave processes, thereby allowing an assessment of the total water level associated with storm events. Accordingly, two main events are considered, selected on the basis of the orientation and exposure of each coastal sector to wave dynamics. This approach enables a more comprehensive evaluation of potential hazard and flooding risk across all the coastal settings examined in the study.

2. Objective

The present study aims to produce flood hazard maps related to meteomarine events, which constitute the basis for flood risk assessment and management in accordance with the Floods Directive 2007/60/EC of the European Parliament and of the Council of 23 October 2007, subsequently transposed into Italian legislation through Legislative Decree No. 49 of 23 February 2010. Within this framework, a detailed investigation has been carried out focusing on the most relevant urban areas along the coastlines of the Friuli Venezia Giulia region, located in the eastern sector of the Northern Adriatic. In this specific environmental context, the combined effects of sea-level rise and rapid urbanisation have substantially amplified flood risk in coastal settlements, both due to the increased concentration of population and to the recurrent criticalities observed within the urban fabric. In recent years, the regional Civil Protection authorities of Friuli Venezia Giulia have been extensively engaged in flood emergency management. The coastal resorts of Grado and Lignano Sabbiadoro, characterised by a strong beach-tourism vocation and located along the western coastal sector, have experienced significant impacts due to water mass ingress, primarily from the lagoonal side, resulting in widespread disruption and critical conditions within the urban areas. Similarly, the more eastern sector, characterised by a high and densely urbanised coastline hosting the regional capital Trieste and the town of Muggia, has also suffered considerable consequences as a result of increasingly frequent marine flooding events. The main objective of this work therefore arises from the need to investigate coastal flooding processes at the urban scale, where sufficiently accurate topographic data are available to support different types of flood simulations. However, the analysis does not focus exclusively on present-day events assessed through statistical methods, but also addresses their evolution under future sea-level rise projections over both short- and long-term horizons. In this regard, an improved understanding of coastal flooding dynamics is of fundamental importance for local-scale municipal management of impacts, enabling risk reduction for exposed populations as well as the preservation of cultural heritage located within historic urban centres. A progressively more detailed characterisation of extreme sea levels observed over recent decades would allow for a more robust assessment of the impacts associated with extreme events expected to occur in the near future.

Consequently, rigid defence systems along the coastline, including backshore protection structures and perimeter embankments bordering lagoonal environments, must be subject to structural verification and careful elevation control, ensuring that their design levels are consistent with projected sea-level rise and the extreme events developing upon it. Such a strategy is essential for the effective mitigation of future flood risk.

Finanziato dall'Unione europea NextGenerationEU
Ministero dell'Università e della Ricerca
Italiadomani PIANO NAZIONALE DI RIPRESA E RESILIENZA
UNIVERSITÀ DEGLI STUDI DI TRIESTE

3. Study area and drivers

3.1 Geographical settings: the Adriatic basin

The Adriatic Sea is a semi-enclosed basin located in the eastern sector of the Mediterranean Sea. It extends approximately from 46° N, 12° E to 40° N, 19° E, covering a length of about 800 km and reaching a maximum width of roughly 200 km (Umgiesser et al., 2021). From a geographical perspective, the basin can be subdivided into three main sectors– northern, central, and southern– and is characterised by depths that are, on average, significantly lower than those of the rest of the Mediterranean Sea, with a mean depth of approximately 260 m (Medvedev et al., 2020). More than 50% of the Adriatic Sea area is shallower than 100 m (Vrdoljak et al., 2021). The northern Adriatic represents the shallowest sector of the entire basin, with depths generally not exceeding 50 m (Foglini et al., 2020; Vrdoljak et al., 2021). Within this northern portion, two major sub-regions can be distinguished: the Gulf of Venice to the west and the more easterly Gulf of Trieste. These areas host two important lagoonal systems, namely the Venice Lagoon and the Grado–Marano Lagoon, respectively. Despite being a narrow, semi-enclosed, and relatively shallow sea, the Adriatic basin exhibits a highly complex circulation system (Bisci et al., 2021). In particular, especially in the northern sector (Marcos et al., 2009; Lionello et al., 2012, 2019; Zanchettin et al., 2021), meteomarine forcings play a key role in driving the processes responsible for coastal flooding phenomena, which are described in the following sections.

3.2 Drivers of sea level

The following sections describe the three main drivers contributing to the increase in extreme sea levels under storm conditions within the northern Adriatic region.

3.2.1 Tidal forcing

The tidal regime in the Adriatic Sea can be described as a co-oscillation with the Mediterranean Sea, enhanced by resonance phenomena along the basin's longitudinal axis from south to north after crossing the deeper Strait of Otranto (Polli, 1961; Defant, 1961; Vilibić et al., 2017). In the northern Adriatic, tidal forcing plays a crucial role among the processes governing sea-level variability. In particular, within the Gulf of Trieste, the tidal regime is characterised as mixed semidiurnal (Ferrarin et al., 2015; Lionello et al., 2021), with a mean tidal range of approximately 76 cm (Petti et al., 2019), a mean spring-tide range of about 105 cm (Medvedev et al., 2020), and maximum observed values reaching up to 120 cm (Janeković et al., 2005), while the mean neap tide is around 22 cm (Dorigo et al., 1965). In this area, the seven main tidal constituents –four semidiurnal (M2, S2, N2, and K2) and three diurnals (K1, O1, and P1)– provide a substantial contribution to the attainment of very high sea levels within the Gulf of Trieste (Polli, 1961; Orlić, 2001). These characteristics make the Northern Adriatic one of the Mediterranean environments exhibiting the largest tidal ranges (i.e., the difference in height between high and low tide), together with the Gulf of Gabès in Tunisia. By contrast, mean tidal ranges in the rest of the Mediterranean generally do not exceed 30 cm (Tsimplis et al., 1995). Tides also represent the primary component in the overall balance of sea-level oscillations in the Adriatic Sea, particularly in its northern sector (Vilibić et al., 2017). Both diurnal and semidiurnal tidal components reach their maximum amplitudes in the northern Adriatic basin (Lionello et al., 2021). In the Adriatic Sea, the tidal wave propagates in an anticlockwise direction, initially affecting the Croatian

Finanziato dall'Unione europea NextGenerationEU
Ministero dell'Università e della Ricerca
Italiadomani PIANO NAZIONALE DI RIPRESA E RESILIENZA
UNIVERSITÀ DEGLI STUDI DI TRIESTE

coast before reaching the western coasts of the northern Adriatic, with a propagation speed of approximately 2 km per minute. The most important semidiurnal constituent (M2) completes an anticlockwise rotation in about 12.42 h (Cushman-Roisin et al., 2001). Starting from Trieste, the tidal wave amplitude progressively decreases as it propagates westwards across the northern Adriatic. Within the lagoonal systems mentioned above, tidal propagation from the open sea towards the inner lagoon is slower due to shallow bathymetry. The time lag from Trieste to Grado is approximately 25 minutes, while the delay towards Lignano Sabbiadoro is around 12 minutes (Stravisi et al., 1985). The importance of tidal forcing in the Adriatic Sea, and particularly in its northern part, is closely linked to resonance effects associated with the two main seiche nodes at periods of 10.7 h and 21.8 h (Raicich, 1999; Lionello et al., 2005), which are close to the periods of the dominant semidiurnal (M2) and diurnal (K1) tidal constituents, respectively.

3.2.2 Storm Surge

Storm surge can be described as an abnormal rise in sea level generated by synoptic-scale meteorological events, which develops above the astronomical tide component. Within the Adriatic Sea, storm surge represents the dominant driver of coastal flooding, with water-level elevations that are significantly higher than those typically observed in other parts of the Mediterranean basin (Marcos et al., 2009; Conte & Lionello, 2013). Historically, the coastal area most severely affected by this phenomenon has been Venice (Lionello et al., 2012; Zampato et al., 2016; Ferrarin et al., 2019, 2021; Umgiesser et al., 2021), owing to its location along the main axis of Scirocco winds. However, in recent decades, increasingly intense storm surge events have also been recorded in Grado (Spadotto et al., 2025), located along the western coastal sector of the Friuli Venezia Giulia region, at the eastern boundary of the Grado and Marano Lagoon. More specifically, within semi-enclosed and shallow basins, the magnitude of storm surge levels is primarily controlled by the combined action of two main forcings: wind stress induced by strong winds and the inverse barometric effect associated with intense local low-pressure systems, as discussed below. Depending on the structure and spatial configuration of the wind field, flooding impacts may be more severe along either the western or the eastern Adriatic coastlines (Međugorac et al., 2018).

3.2.2.1 Wind regime

There are two main winds that blow in the northern Adriatic, each with distinct physical and seasonal characteristics: the Scirocco and the Bora. The first is the Scirocco, which blows from the south-east towards the northern Adriatic. It is a marine wind, typically warm and humid in nature. Owing to the elongated and semi-enclosed geometry of the Adriatic basin, together with the influence of regional orography (Pašarić et al., 2009), strong Scirocco winds are channelled along the longitudinal axis of the Adriatic Sea, pushing large volumes of water towards the northern Adriatic coastlines. As a result, Scirocco winds are characterised by a very long fetch, of the order of 800 km. Wind speeds associated with Scirocco events within the basin typically range between 10 and 15 m/s (Lionello et al., 2012). Under persistent conditions, Scirocco can generate significant precipitation and offshore wave heights along the northern Adriatic coasts (Ferla et al., 2012). Nevertheless, its intensity is generally lower than that of Bora winds. The second dominant wind regime affecting the Northern Adriatic is the Bora. Bora is a continental, katabatic wind (Grisogono & Belušić, 2009) with characteristics that are essentially opposite to those of the Scirocco.

Finanziato dall'Unione europea NextGenerationEU
Ministero dell'Università e della Ricerca
Italiadomani PIANO NAZIONALE DI RIPRESA E RESILIENZA
UNIVERSITÀ DEGLI STUDI DI TRIESTE

In this case as well, the orography of the Dinaric Alps, which run along the eastern Adriatic coastline, plays a fundamental role. The strong thermal gradient between relatively warm air over the sea surface and cold continental air masses inland leads to the generation of intense wind energy (Umgiesser et al., 2021). The resulting wind is highly gusty and violent in nature, with peak gusts reaching up to 200 km/h and hourly mean speeds exceeding 20 m/s at Trieste (Raicich, 2003), blowing predominantly from the E-NE direction across the Northern Adriatic. This characteristic strongly influences circulation patterns in the northern Adriatic basin (Belušić et al., 2004). Consequently, in terms of frequency, Bora winds from the E-NE represent the dominant wind regime in this sector (Bezzi et al., 2018; RAFVG, 2019).

An additional characteristic shared by Scirocco and Bora winds is their strong seasonal signature, which is particularly pronounced in the northern Adriatic and plays a key role in controlling the timing and severity of coastal flooding and related criticalities. This seasonality leads to either increases in storm surge levels (*positive surge*) or sea-level depressions (known as *negative surge*). In particular, during the autumn season (Battistin & Canestrelli, 2006) –notably from October to December, with a peak in November (Lionello et al., 2012)– the action of the Scirocco reaches its maximum intensity, especially when combined with deep low-pressure systems. This configuration favours the development of positive storm surge anomalies. The most severe storm surge events of the last century, which produced record extreme sea levels recorded by the Venice Punta della Salute and Trieste Molo Sartorio tide gauges, occurred on 4 November 1966 in Venice, with an extreme sea level (ESL) of 194 cm ZMPS (including 107 cm of storm surge; Ferrarin et al., 2022), and on 26 November 1969 in Trieste, with an ESL of 193 cm (datum IGM42). During the autumn period, Scirocco winds are generally stronger (Raicich, 2010) and are responsible for very large water-level elevations, commonly referred to as *acqua alta* in the Northern Adriatic. Consequently, Scirocco winds are primarily responsible for the extreme sea levels observed throughout the northern Adriatic region. By contrast, the Bora exerts its strongest influence during the winter season (Raicich, 2003), from December to March/April, affecting the entire transect of the northern Adriatic, but producing markedly different effects along the eastern and western coastal sectors. In the Gulf of Trieste, Bora winds play a particularly important role, as they generate a local high-pressure system linked to the strong wind forcing acting on the sea surface. This results in a pronounced depression of sea level, giving rise to negative storm surge anomalies. However, this effect is largely confined to the eastern Adriatic coast. As Bora winds intensify, water levels progressively increase towards the Gulf of Venice, leading to positive storm surge conditions along the western coasts of the northern Adriatic, although generally less intense than those associated with Scirocco events. Other wind-driven currents affecting the Northern Adriatic include Libeccio winds, originating from the SSW direction. These winds act over a fetch of approximately 200 km and generate wave conditions that impact both the low-lying sandy coast between Grado and the Isonzo River mouth, as well as the high and rocky coastal sectors of the Gulf of Trieste (Busetti et al., 2024).

3.2.2.2 Low pressure system

The main synoptic conditions leading to coastal flooding and storm surge events along the coastlines of the Northern Adriatic –and more generally throughout the Adriatic basin– are associated with the presence of low-pressure centres over Central Europe, and in particular with cyclogenesis occurring in the Gulf of Genoa (Robinson et al., 1973; Trigo & Davies, 2002; Lionello et al., 2012, 2019).

3.2.3 Seiches

Seiches are oscillatory components, or normal modes, characteristic of enclosed or semi-enclosed water bodies such as lakes, channels, bays, harbours, and lagoons. They are standing waves with a single characteristic frequency, determined by the geometry and depth of the basin in which they occur. During a seiche oscillation, sea level oscillates around a nodal point located within the basin, where sea level remains unchanged. In the Adriatic Sea, the seiche component is described as a free oscillation of the sea surface, with periods determined by the normal modes of the basin and is typically triggered by preceding storm surge events following the decay of the external meteorological forcing (Međugorac et al., 2018; Ferrarin et al., 2022). The primary mode exhibits the longest period, approximately 21.8 h (Raicich et al., 1999; Lionello et al., 2005). The associated decay time in the Adriatic is on the order of about 78 h ± 24 h (Raicich, 1999), which is consistent with estimates reported for the Croatian coast by Cerovečki et al. (1997), approximately 3.2 ± 0.5 days, and by Vilibić et al. (2000), who reported values of 81 ± 19 h. The second mode is characterised by a shorter period of approximately 11 h (≈10.7 h) and contributes much less to overall sea-level variability compared to the primary mode (Leder & Orlić, 2004).

3.3 Extreme sea level (ESL) composition

Once the main contributing components have been described, it is possible to define the observed sea level. Pugh and Vassie (1978) describe the observed sea level Z_T as the sum of the two previously discussed components acting above mean sea level, together with a third component defined with respect to a specific vertical datum.

$$Z_T = \mathrm{msl}_{(t)} + X_{(t)} + \Upsilon_{(t)}$$

$\mathrm{msl}_{(t)}$ = mean sea level-waves and tidal components area averaged out.
$X_{(t)}$ = tidal forcing driven by astronomical forcing.
$\Upsilon_{(t)}$ = meteorological contribute (storm surges) influenced by topography and orography.

The analysis of these three main components characterising observed sea levels is therefore essential for the study of what are defined as Extreme Sea Levels (ESLs). An extreme sea level event refers to an anomalous rise in sea level driven by meteomarine forcings –primarily storm surge and tidal components– and, where present to a significant extent, also by wave processes. In most applications, extreme sea levels are observed and analysed by focusing predominantly on the storm surge component (Haigh et al., 2011). However, depending on the environmental context and the dominant forcings, the investigation of interactions between tidal forcing and storm surge is fundamental for a proper understanding of the characteristics of a given event. For instance, quadratic bottom

friction in shallow waters tends to dampen the storm surge component during high tide conditions (Tawn & Vassie, 1989). Moreover, shallow-water effects and seasonality can lead to a temporal mismatch between storm surge maxima and high tides in non-tropical regions (Pirazzoli & Tomasin, 2007; 2009), such as the northern Adriatic. For this reason, over recent decades, in response to the increasingly frequent occurrence of extreme events, there has been a growing need to further investigate meteomarine components and their interactions, which are essential for the development of appropriate coastal defence measures and adaptation strategies (Arns et al., 2020; van de Wal et al., 2024), particularly in urban settings. Recent studies focusing on the interaction between meteo-marine forcings –including investigations at the global scale (Arns et al., 2020), at the national scale (Ragno et al., 2023), and at the local scale for Venice (Ferrarin et al., 2022)– have demonstrated the importance of quantifying the non-linear contributions of the different drivers involved in order to accurately describe extreme sea levels, especially from a statistical perspective and in terms of their probability of occurrence. For this reason, a detailed analysis has been carried out for Trieste, in the eastern sector of the Northern Adriatic, where extreme sea-level components are decomposed into multiple contributions associated with distinct meteo-marine processes. According to Lionello et al. (2021) and Šepić et al. (2022), the contributions governing sea-level variability in the Northern Adriatic can be broadly discretised as follows:

3.3.1 Tidal forcing

Describe as a high frequency component (see section “3.2.1” for more details)

3.3.2 Metereological forcing

Low frequency component <10 days (see section “0” for more details) sub-divided in:
- storm surges
- seiches

3.3.3 Meteotsunami

Meteotsunamis are described as long waves generated by mesoscale atmospheric pressure disturbances associated with thunderstorms or fast-moving squall lines propagating over water, whose development depends on the interaction between intensity, direction, and propagation speed (Monserrat et al., 2006; Rabinovich et al., 2009; Denamiel et al., 2021). They are generated through resonance in open sea conditions when the propagation speed of the atmospheric disturbance matches that of shallow water barotropic waves (Ferrarin et al., 2022). Meteotsunamis are typically high-frequency oscillations (periods < 10 h) of non-seismic origin and are particularly relevant in microtidal basins (Vilibić & Šepić, 2017). Semi-enclosed structures, such as harbours, may induce resonant effects capable of significantly amplifying the impact of these waves (Vilibić et al., 2009).

3.3.4 PAW surge

Planetary atmospheric waves (PAWs) are low-frequency oscillations that induce variations in sea level. They are generated by pressure disturbances (Pašarić & Orlić, 1992) and wind forcing (Pašarić & Orlić, 1998) and are characterised by wavelengths ranging between approximately 6,000 and 8,000 km. PAWs provide a significant contribution to sea-level variability in the northern Adriatic (Pašarić & Orlić, 2001).

Finanziato dall'Unione europea NextGenerationEU
Ministero dell'Università e della Ricerca
Italiadomani PIANO NAZIONALE DI RIPRESA E RESILIENZA
UNIVERSITÀ DEGLI STUDI DI TRIESTE

3.3.5 Seasonal sea level variability, inter-annual and inter-decadal (IDAS)

In the northern Adriatic, the occurrence of ESLs is closely linked to seasonal, inter-annual, and inter-decadal variability (Vilibić et al., 2017), associated with large-scale atmospheric and oceanic circulation patterns (Zanchettin et al., 2021). Inter-annual variability of mean sea level in this region has been described as the result of interactions and/or interference between solar activity and lunar precession (Valle-Levinson et al., 2021).

3.3.6 Long-term components

The long-term component is driven by climate change at the global scale and by local vertical land movements (VLM). In Trieste, a mean sea-level rise rate of 1.4 mm/yr has been recorded over the last century. The main components governing sea-level variability (and hence the occurrence of ESLs) can therefore be discretised as follows:

- Short-term contribution (high frequency): meteotsunamis, seiches, and storm surges associated with meteorological phenomena.
- Long-term contribution (low frequency): PAW surge, seasonal to inter-annual and inter-decadal variability (IDAS), and relative sea-level rise (R-SLR; secular trend).

Once the components controlling extreme sea-level events and processes have been defined, it is possible to describe the component that propagates above the sea surface, namely the wave component.

3.4 Wave regime

In the northern part of Adriatic, Bora and Sirocco generate a bimodal wave regime, with the mean significant wave height (Hs) less than 0.5 m, according to data collected at the wave buoy DWRG1 placed at the coordinates 13.24°E, 45.56°N (-15.2 m depth) managed by the National Institute of Oceanographic and Applied Geophysics (OGS). Events with Hs greater than 0.5 m represent the 25.2% of the overall record (Figure 1), with prevailing waves from the SSE (10.7%) and ENE (10.5%): even if Sirocco is weaker than Bora, its fetch above 800km, one order of magnitude longer than the Bora's fetch, causes its waves to record the highest Hs values of 4.4 m (RAFVG, 2019).

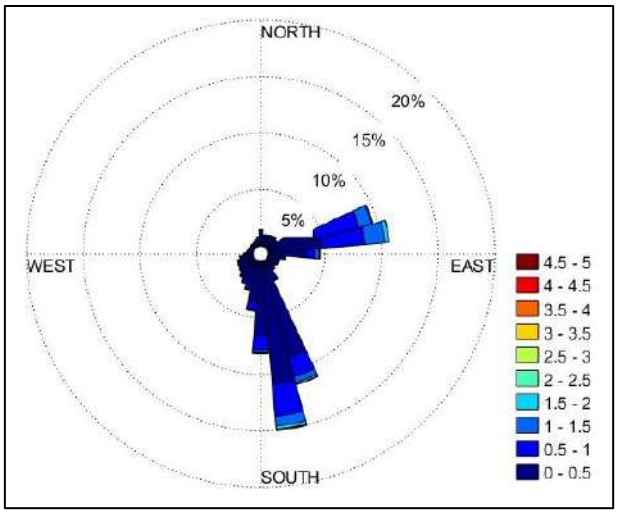

Figure 1**.** Wave rose of the DWRG1 relating to the time interval from 2004 to 2023.

Finanziato dall'Unione europea NextGenerationEU
Ministero dell'Università e della Ricerca
Italiadomani
UNIVERSITÀ DEGLI STUDI DI TRIESTE

The yearly wave energy flux for the northern Adriatic area is 1.95 kW/m; The longshore drift is directed from the Isonzo River mouth toward west (Casagrande et al., 2023). The wave regime in the Northern Adriatic is characterised by a bimodal structure, primarily driven by Bora and Scirocco winds (Bezzi et al., 2018). Over the last decade, winds blowing from the south-west, commonly referred to as Libeccio, have also played an increasingly important role, particularly in driving meteo-marine events affecting Trieste. These winds are now recognised as a key contributor to coastal flooding processes along the stretch extending from Grado to the high and rocky coastline of the eastern Friuli Venezia Giulia region.

3.4.1 Wave run-up (R)

In the vicinity of the shoreline along coastal sectors, under both calm and storm conditions, waves generate a resultant component associated with the accumulation and transformation of wave energy in the nearshore zone. This variable is defined as wave run-up (hereafter referred to simply as *run-up*), a process of major importance as it contributes to both coastal deposition and erosion (Alsina et al., 2018). The study of run-up is of particular relevance for the present and future design of coastal defence structures (EurOTop, 2018; Bujak et al., 2023). Run-up is defined as the ensemble of maximum water-level elevations measured at the shoreline (Stockdon et al., 2006) relative to the offshore still water level, which corresponds to the mean sea level outside the surf zone and includes both tidal and storm surge components (Dodet et al., 2019). The magnitude and intensity of run-up are intrinsically linked to wave characteristics such as wave height (H_0 or H_s), wave period (T), and wave direction (FIRM, 2023). Run-up typically occurs over time scales ranging from seconds to minutes (Dodet et al., 2019). The two main components constituting wave run-up are wave setup (or *set-up*) and swash, which are described below.

3.4.2 Wave set-up (η)

Wave set-up is defined as the increase in the mean water level that develops as a result of the partial transfer of wave energy during wave breaking within the surf zone (Longuet-Higgins & Stewart, 1963, 1964). It exhibits an oscillatory behaviour that can persist over time scales ranging from several minutes to several hours (Dodet et al., 2019).

3.4.3 Swash (S)

The remaining portion of wave energy is transferred shoreward, where it generates an irregular oscillatory motion at the shoreline, consisting of uprush and backwash (Miche, 1951), leading to a further elevation of the water level at the coast. The swash component is often decomposed into two distinct frequency bands: swell waves (SS, 4-20s) and infragravity waves (IG, 20-250s) (Dodet et al., 2019; Fiedler et al., 2020). Once these components have been described, it is possible to define the most commonly used empirical formulation for run-up, namely R_2%**,** which represents the run-up level exceeded by 2% of the incident waves (Stockdon et al., 2006). Accordingly, R_2% can be expressed as the sum of the setup and swash contributions:

$$R_{(2\%)} = \eta + \frac{S}{2} \quad \textit{where } S = \frac{1}{2}(S_{SS}^2 + S_{IG}^2)^{\frac{1}{2}}$$

The formulation proposed by Stockdon et al. (2006) is representative of run-up behaviour in highly dissipative and high-energy coastal environments (such as the Australian Pacific

Finanziato dall'Unione europea NextGenerationEU | Ministero dell'Università e della Ricerca | Italiadomani PIANO NAZIONALE DI RIPRESA E RESILIENZA | UNIVERSITÀ DEGLI STUDI DI TRIESTE

coast, where it was originally calibrated). Nevertheless, it provides a reasonable approximation also for strongly dissipative beaches along the coastlines of Friuli Venezia Giulia (as described in Section 3.6.3). In these coastal sectors, the Total Water Level (TWL) reached during an extreme storm event can be expressed as the sum of the following components.

$$TWL = R_{(2\%)} + ESL$$

The TWL is therefore obtained by combining the run-up contribution with the Extreme Sea Level (given by the sum of the tidal component and the residual contribution NTR). The second type of coastline has characteristics that differ completely from the first, both in terms of structure and type of wave contribution.

3.4.4 Wave overtopping

The impulsive nature of wave run-up does not manifest exclusively along low-lying, sandy and dissipative coastlines (Stockdon et al., 2006), or along reflective gravel beaches (Poate et al., 2016), but may also occur in a different form when waves interact with coastal structures such as vertical walls, seawalls, bulkheads, and other impermeable defences. In this case, the run-up process takes the form of wave overtopping. Wave overtopping occurs when the maximum crest elevation of the incoming waves exceeds the crest height of the coastal structure (EurOTop, 2007; 2018). This exceedance is quantified in terms of the volumetric discharge rate of water passing over the structure per unit length. The phenomenon is referred to as **"**green water**"** overtopping (FIRM, 2023) when wave breaking occurs continuously on or just in front of the coastal defence or vertical wall, and the overtopping discharge is quasi-continuous (EurOTop, 2018). A commonly adopted formulation to estimate the overtopping contribution is given by:

$$\frac{q}{\sqrt{gH^3}} = aexp\left(-\frac{bZ_c}{H}\right)$$

where *q* is the mean overtopping discharge, *g* is the acceleration due to gravity, *H* (typically evaluated at a water depth of 10 m) is the significant wave height, and *Zc* is the crest freeboard of the structure above the still water level. The coefficients *a* and *b* depend on the type of coastal structure considered (e.g. berms, vertical walls, etc.) (EurOTop, 2007; 2018).

3.5 Nearshore Total Water Level (TWL)

Once the different components contributing to sea-level variability have been described in detail –ranging from low-frequency forcings (astronomical tide, meteorological storm surge, PAWs, and seasonal to inter-annual variability) to high-frequency contributions associated with wave propagation processes (infragravity waves, sea–swell, wave setup, swash, and run-up)– it becomes possible to integrate these elements into a single conceptual framework representing the formation of the TWL along the coast.

The central idea is that extreme sea-level conditions do not arise from a single dominant process, but rather from the non-linear combination of multiple components acting across different temporal and spatial scales. This overlap determines the level actually observed near the shoreline and, in particularly severe conditions, the overflowing of coastal areas and the onset of flooding phenomena. The conceptual scheme shown in Figure 2 illustrates this cumulative effect, highlighting how the transition from offshore waters to the shoreline is characterised by a progressive increase in water level. This increase is initially governed by background components (tide and surge) and subsequently modulated by wave-driven processes responsible for local amplification (set-up and run-up). This integrated approach is essential for correctly interpreting extreme events and supporting hazard analysis and coastal defence design.

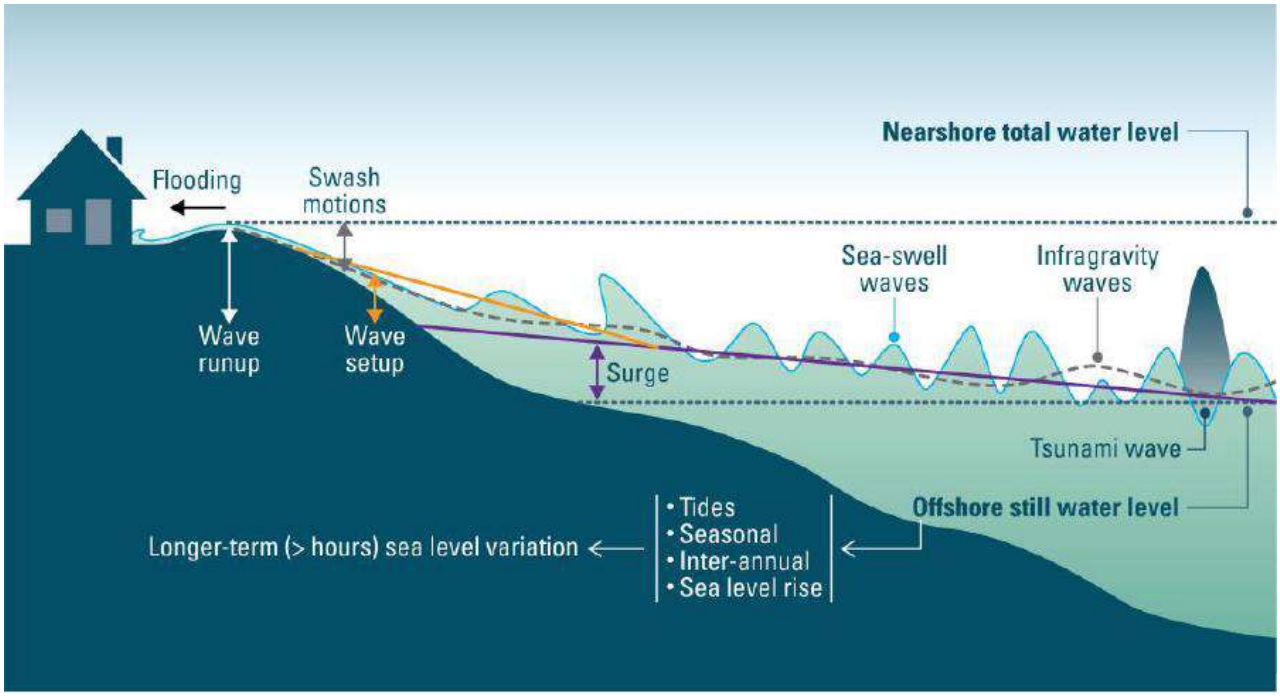

Figure 2. Contribution of total nearshore water level by coastal flooding phenomenon (from Morris et al., 2021).

Finanziato dall'Unione europea NextGenerationEU
Ministero dell'Università e della Ricerca
Italiadomani
UNIVERSITÀ DEGLI STUDI DI TRIESTE

3.6 Factors of coastal risk exposure

Given the heterogeneous environmental setting of the northern Adriatic and the meteomarine forcings previously described that characterise the coastal region of Friuli Venezia Giulia, it is essential to account for the main controlling factors in baseline assessments. These factors may lead to varying levels of hazard and risk across the territory, depending on the specific area considered. Among the most relevant factors are:

- Subsidence
- Sea Level Rise (SLR) and Relative-sea level rise (R-SLR)
- Coastal morphology
- Coastal and urban flooding
- Salt water intrusion

Sea-level rise and vertical land movements (VLM) are generally regarded as medium- to long-term drivers. By contrast, coastal flooding –and, to some extent, saltwater intrusion– are primarily associated with short-term or episodic processes, triggered by specific meteorological and marine conditions such as storm surges and severe sea storm events.

3.6.1 Subsidence

Subsidence is a geological process consisting of a gradual lowering of the ground surface (Gregory et al., 2019), and is particularly relevant in lagoonal and peri-lagoonal environments (Fontolan et al., 2012), estuaries, and more generally in low-lying coastal areas (Nicholls et al., 2007; Tosi et al., 2010; Fox-Kemper et al., 2021; Jevrejeva et al., 2023). The main causes of subsidence are related both to natural geological processes (as tectonic, thermal, and isostatic subsidence) and to the increasing intensity of anthropogenic pressure on coastal territories. Human activities may induce or exacerbate subsidence processes, often amplifying the natural background signal (Tosi et al., 2010; Anzidei et al., 2014; Zerbini et al., 2017; Da Lio et al., 2018). In general, naturally driven subsidence may affect areas of varying spatial extent and typically occurs at rates of a few millimetres per year, although it can locally reach values of several tens of millimetres per year (e.g. the Po Delta plain; Tosi et al., 2016). These rates depend on multiple factors, including tectonic movements, Holocene sediment compaction (Antonioli et al., 2017b), and lithospheric cooling processes associated with magmatic bodies (thermal subsidence). A different and often more critical situation arises when subsidence is induced or significantly intensified by anthropogenic activities, such as the extraction of gas or groundwater from the subsurface (Herrera-García et al., 2021). In particular, the pumping of artesian groundwater for industrial cooling purpose such as historically documented in the Venice Lagoon (Zanchettin et al., 2021), can increase ground settlement rates, in extreme cases leading to cumulative subsidence on the order of several metres. In the present study, subsidence primarily affects the eastern coastal sectors of the northern Adriatic, which are characterised by a fragile environmental setting (Zerbini et al., 2017), particularly along the western stretch extending from the Tagliamento River mouth to the Isonzo River mouth. This process is especially relevant across the entire lagoonal domain (Fontolan et al., 2012; Zerbini et al., 2017) of the lower Friulian plain, with specific reference to the coastal arc between Lignano and Grado (Tosi et al., 2010; Antonioli et al., 2017; Da Lio et al., 2018), which is characterised by spatially heterogeneous subsidence rates. According to the recent study by Da Lio and Tosi

(2018), along the regional coastal sector and moving in a south-westerly direction, the mean subsidence rate ranges from approximately 2.5 mm/yr in the central portion near the lagoonal boundary, up to about 4 mm/yr in the vicinity of the Tagliamento delta system. Further eastwards, within the lagoonal environment, average subsidence rates increase to around 5 mm/yr (Antonioli et al., 2017). More specifically, the westernmost portion of the lagoonal ecosystem, represented by the Marano Lagoon, exhibits internal subsidence rates on the order of 5-7 mm/yr (Da Lio & Tosi, 2018). Continuing along the coastline, the sector extending eastwards from the Grado Lagoon to the town of Monfalcone is characterised by highly heterogeneous subsidence rates, with mean annual values of approximately 2.5 mm/yr**.** More specifically, certain areas within the urban fabric of Grado are affected by peak subsidence rates reaching up to 10 mm/yr**,** followed by the industrial area of Monfalcone, where rates of about 8 mm/yr have been observed, and finally by the estuarine environment associated with the Isonzo River mouth, where ground settlement reaches values of approximately 4 mm/yr (Da Lio & Tosi, 2018). In addition, the effects of induced subsidence related to anthropogenic forcing must be taken into account (Fontolan et al., 2012). Most human-induced modifications in this region have occurred over a relatively short time span, largely within the last century, with a marked acceleration during recent decades. Major interventions have included extensive land reclamation (*bonifica integrale*), the reinforcement of lagoonal embankments, the construction of fish-farming enclosures (*valli da pesca*), the excavation of navigable channels, maritime works aimed at stabilising lagoon inlets, and the hardening of barrier island sectors through the construction of embankments and breakwaters (https://www.atlantedeiluoghirivierafriulana.it/; Cosolo M. et al., 2015). These intensive modifications have led to an apparent advantage from a conservation and protection perspective; however, at the same time, they have produced a progressive imbalance between the artificial stability imposed on the ecosystem by human interventions and the inherent dynamism driven by eustatic and meteo-marine conditions. Furthermore, a reduction in lagoonal areas available for the free circulation of water has occurred as a result of several factors, including extensive reclamation works in circum-lagoonal zones, urban development, and the expansion of lagoon-based aquaculture activities (Cosolo et al., 2015). In particular, land reclamation operations –especially hydraulic reclamation– represent one of the most significant anthropogenic transformations of the environment and are responsible for severe subsidence-related issues (Management Plan of the SCI/SPA IT3320037 *Laguna di Marano e Grado*: Agriconsulting, 2008). In general, the subsidence rate of reclaimed soils is directly proportional to the lowering of the groundwater table and occurs through two main mechanisms: a geomechanical process, causing volumetric reduction due to compaction, and a biogeochemical process, driven by the oxidation of soils with high organic content, such as peat deposits (Carbognin et al., 2011). The situation is different for the eastern coastal area, which stretches from Villaggio del Pescatore, through Trieste, to Muggia. This area is predominantly defined by a high, rocky coastline, with the exception of the urbanised coastal stretches within the municipalities of Trieste and Muggia. This coastal sector, analysed through both GNSS station data deployed across the territory and SAR interferometry, is considered to be tectonically stable (Sanchez et al., 2018; Zerbini et al., 2021; Areggi et al., 2023; Anzidei et al., 2025), as also indicated by the Sea Level Projection Tool provided by NASA (https://sealevel.nasa.gov/ipcc-ar6-sea-level-projection-tool).

3.6.2 Sea level rise (SLR) and Relative-Sea level rise (R-SLR)

Eustatism refers to the global rise or fall of sea level relative to the Earth's surface. These phenomena, associated with oscillations in sea level, occur as a result of natural processes and generally lead to either a transgression or regression of the coastline with respect to the sea. The primary natural drivers responsible for global and regional sea-level variations are glaciation and deglaciation processes, which induce substantial changes in ocean water volume and consequently cause sea-level lowering or rise. It should also be noted that the present-day rise in sea level includes an additional component generated by rapid, anthropogenically driven global warming (Busetti, 2011; IPCC, 2022). The second major component responsible for sea-level rise, directly linked to glacial-interglacial cycles and to the rapid increase in temperatures of anthropogenic origin, is the steric contribution (Meier & Wahr, 2002; Carton et al., 2005; Galassi & Spada, 2014). This component is defined as the contraction or expansion of ocean water masses driven by changes in temperature and salinity (Lambeck et al., 2011). An additional contribution at both global and local scales that controls sea-level rise or fall is isostatic adjustment (Lambeck et al., 2011), associated with crustal movements related to the presence or melting of continental ice sheets and to tectonic processes. Moreover, at the local scale, coastal areas may be affected by Vertical Land Motion (VLM)**,** expressed as either uplift or subsidence, of natural or anthropogenic origin. Such movements can amplify or attenuate the effects of sea-level rise (Vecchio et al., 2024). Once the main components contributing to sea-level rise have been described, the concept of Relative Sea-Level Rise (R-SLR) can be introduced, resulting from the interaction between global sea-level rise (SLR) and local vertical land motion (VLM). In the Northern Adriatic, three tide-gauge stations have been operating for more than 140 years: Trieste Molo Sartorio since 1859 (Raicich et al., 2006; Raicich, 2007), Venice Punta della Salute since 1871 (Magrini et al., 1908; Battistin & Canestrelli, 2006), and Marina di Ravenna (Porto Corsini) since 1873 (Italian Geodetic Commission, 1900). The latter, however, has not been included in the comparative analysis between stations. Since 1992, satellite altimetry has provided sea-level measurements referenced to a global datum (Fournier et al., 2022; Srinivasan & Tsontos, 2023). As a result, much of the historical knowledge of sea-level changes in this region relies on relative sea-level measurements derived from long-term tide-gauge records. The following section presents data on mean sea-level rise at Trieste (Figure 4) over the period 1890–2024, as recorded at the Molo Sartorio tide-gauge station, located at 13.76° E and 45.38° N (Figure 3a), The measurements are referenced locally to benchmarks fixed to the ground and therefore incorporate both marine contributions and vertical land movements (source: courtesy of Dr. Raicich, CNR–ISMAR Trieste).

Figure 3. Locations of tidal gauges considered in this study: Trieste (a), Grado (b), Venice (c).

Figure 4 shows the recorded mean sea-level values, the corresponding linear trend, and the 18.61-year lunar nodal cycle (≈19 years). The lunar nodal cycle represents the period required for the plane of the Moon's orbit to oscillate around the plane of the ecliptic. This cycle –also referred to as the Metonic cycle– produces the primary decadal-scale modulation of tidal amplitude (Pugh, 1987). Consequently, accounting for this factor is particularly important when analysing inter-annual variability of extreme events in terms of relative sea-level rise (R-SLR) and coastal flooding (Bult et al., 2024). Inspection of the time series indicates a secular trend with a rate on the order of 1.4 mm/yr, superimposed on marked positive and negative anomalies. In particular, the positive anomalies recorded in 2010 (10.6 cm), 2024 (9.13 cm), and 2014 (8.28 cm) represent the highest mean sea-level values ever observed in the record. All mean sea-level values are referenced to the Italian national vertical datum IGM42 (Istituto Geografico Militare, Genova, 1942).

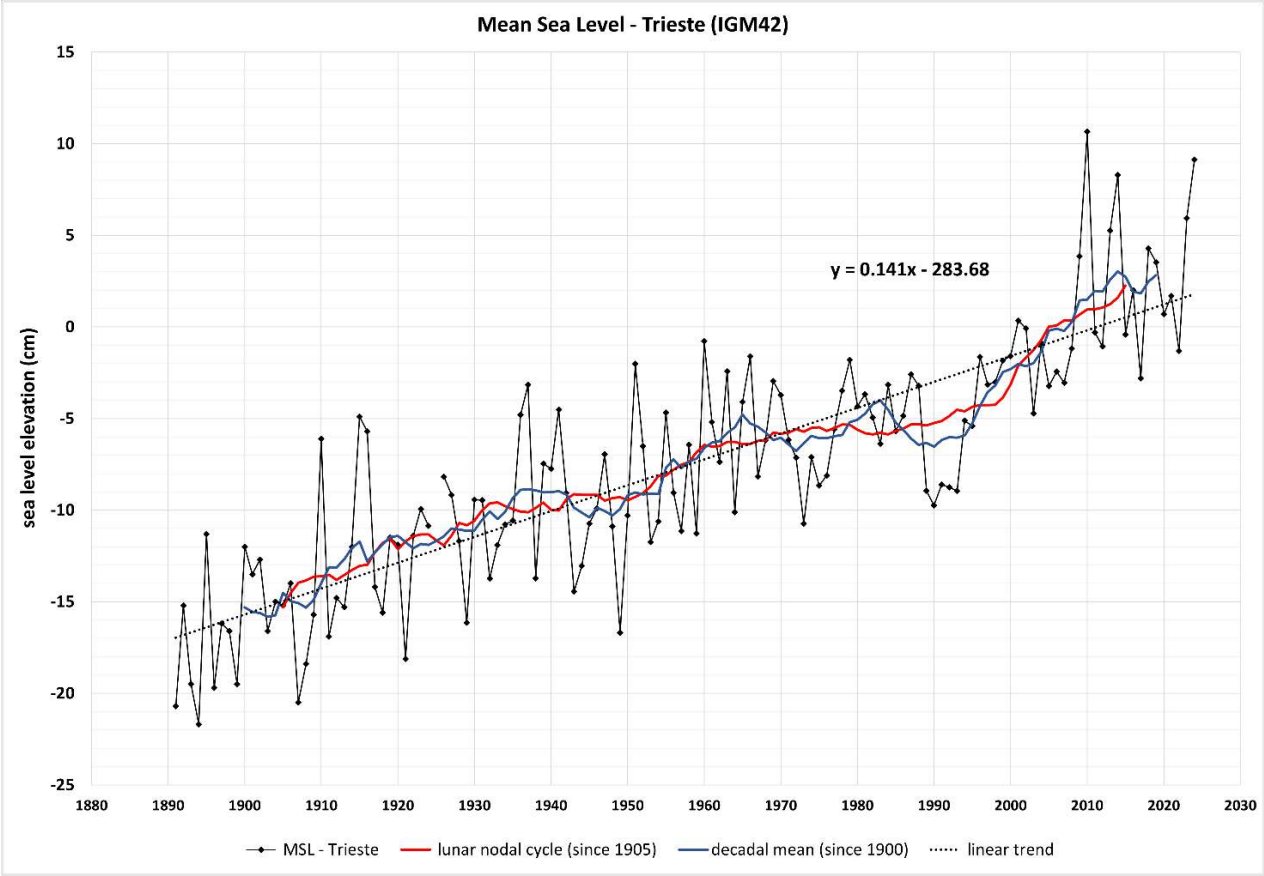

Figure 4. Mean annual water level (black line) registered in Molo Sartorio tidal gauge from 1890 to 2024. Blue line represents decadal mean of 10 years. Red line represents nodal lunar cycle of 19 years.

Mean sea level at Trieste exhibits a rise rate of approximately 1.4 mm/yr, whereas at Venice, over the same time interval, the rate is around 2.5 mm/yr, broadly consistent with the estimates reported by Baldin and Crosato (2017). Compared to Trieste, Venice has experienced a significant lowering of the ground surface due to the well-documented phenomenon of anthropogenically induced subsidence that occurred mainly between the 1930s and the 1970s (Zanchettin et al., 2021). For this reason, the Trieste time series is commonly used as a reference for comparison with other tide-gauge stations, as the site is considered tectonically stable (Zerbini et al., 2017; Anzidei et al., 2024). Within the western

Finanziato dall'Unione europea NextGenerationEU
Ministero dell'Università e della Ricerca
Italiadomani
UNIVERSITÀ DEGLI STUDI DI TRIESTE

coastal sector of the Friuli Venezia Giulia region, the Grado tide gauge (Figure 3b), operated by the Italian national tide-gauge network managed by ISPRA (https://www.venezia.isprambiente.it/rete-meteo-mareografica), is also present. Unlike the Trieste tide gauge (Figure 3a), the Grado station, located at 13.38° E and 45.68° N, is situated within the lagoonal environment**.** Although data are available only for the period 1991-2023 (the most recent year currently available), this time series was used to provide a direct local comparison of the multi-decadal evolution of mean sea level at Grado. In addition, it was employed to assess the behaviour of maximum sea levels recorded over the same temporal window. The 32-year historical series of mean sea level (Figure 5), measured with respect to the tide gauge zero of Punta della Salute (ZMPS) in Venice (+23.56 cm above the Italian datum IGM42 and subsequently converted to IGM42), indicates a progressive increase in mean sea level, with an estimated rate of +4.85 mm/yr**.** All sea-level values shown in Figure 5 are referenced to the IGM42 national vertical datum.

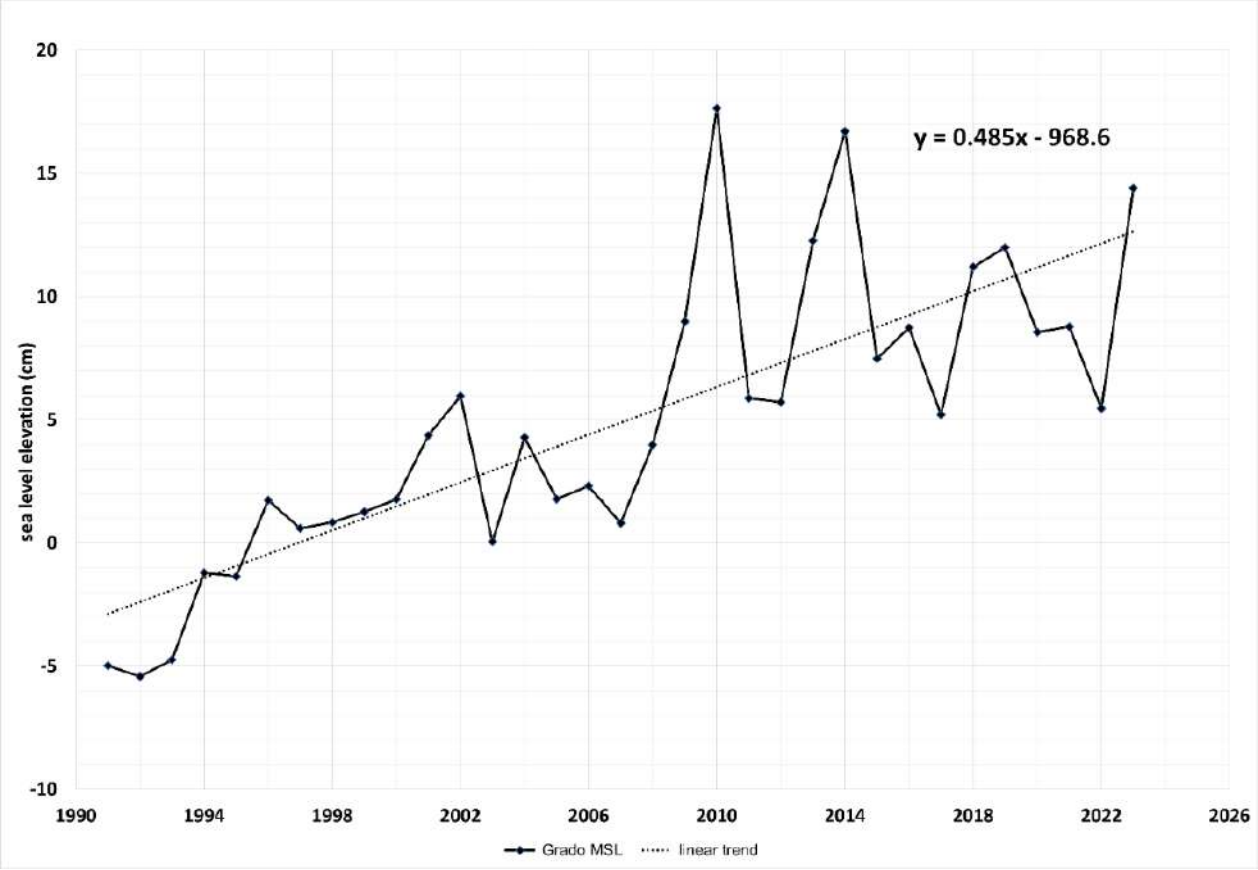

Figure 5. Mean annual water level trend (blue line) registered in Grado tidal gauge from 1991 to 2023.

Unlike the Trieste tide gauge, the Grado station is located within a lagoonal geological setting, characterised by lagoonal sediments reaching thicknesses of several hundreds of metres. Such substrates are particularly prone to surface settlement and to generalised subsidence affecting the entire stratigraphic column. As reported by Areggi et al. (2023), who analysed VLM using satellite differential interferometry (InSAR), the Friulian-Venetian plain –composed of Quaternary deposits with thicknesses of hundreds of metres (Tosi et al., 2010)– tends to undergo compaction-driven subsidence of approximately 2 mm/yr in the Grado area. In contrast, Trieste is essentially stable or exhibits slight uplift, due to the

influence of active Dinaric tectonics. The sea-level data recorded over the 1991-2023 period for Grado and Trieste were subsequently compared with those from Venice (Figure 6), referenced to the Zero Mare Punta della Salute (ZMPS) datum and converted to IGM42. This approach allowed for a direct comparison across tide-gauge networks spanning the entire northernmost sector of the Adriatic Sea.

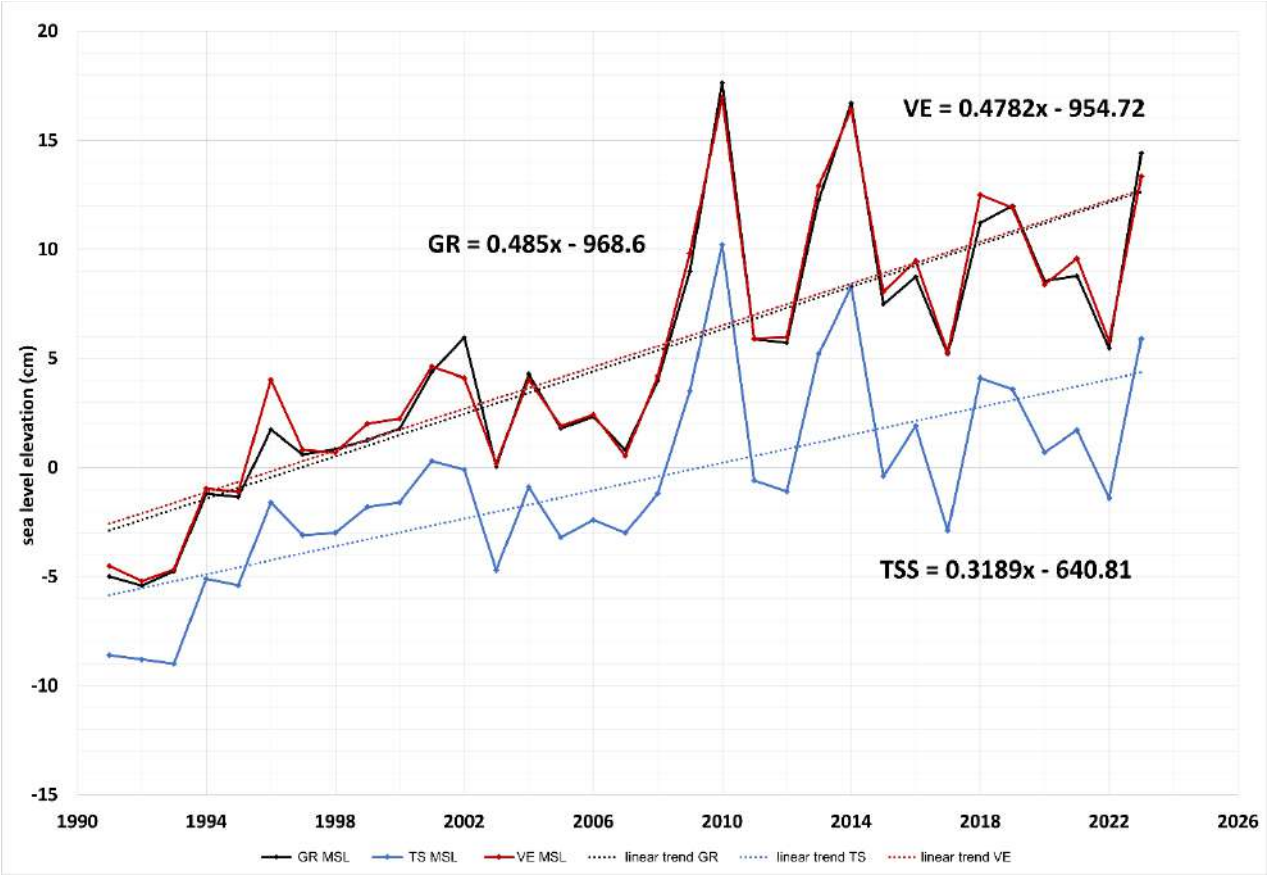

Figure 6. Mean annual water level trend (black line) registered in Grado, Venice (red line) and Trieste (light blue line) tidal gauge from 1991 to 2023.

The graph shows a pronounced discrepancy between the rates recorded at Trieste (TSS=3.2 mm/yr), which is tectonically stable, and Grado (GR=4.85 mm/yr). The latter exhibits a rate of sea-level rise that is almost identical to that observed at Venice (VE=4.78 mm/yr).

3.6.3 Coastal morphology

Along the eastern Northern Adriatic coastal sectors, belonging to the Gulf of Trieste and extending from Lignano, at the Tagliamento River mouth, to Muggia, two main types of coastal systems can be distinguished. These systems influence both the characteristics and the behaviour of the water level response –commonly referred to as surge or storm surge– and the wave related run-up component, as described in the previous sections (sections 3.3; 0). In addition to the R_2% contribution, the properties of the surf zone and the shore barrier also play a significant role in determining the run-up regime (EurOTop, 2018; FIRM, 2023). The coastline of Friuli Venezia Giulia is therefore characterised by a mixed setting, which is described in detail in the following sections.

Finanziato dall'Unione europea NextGenerationEU
Ministero dell'Università e della Ricerca
Italiadomani
UNIVERSITÀ DEGLI STUDI DI TRIESTE

3.6.3.1 Low-lying sandy coast

The coastal sector predominantly characterised by low-lying sandy shores extends between the Tagliamento River mouth and the Primero tidal inlet (Figure 7, red line). Within this stretch, the two main sandy coastal domains of the Friuli Venezia Giulia region can be identified. The first corresponds to Lignano Sabbiadoro, which represents the left wing of the Tagliamento River delta and includes approximately 7.3 km of sandy beach. This coastal strip is almost entirely urbanised, and the beach is intensively exploited for tourism and recreational activities. The second coastal stretch extends between the Grado and Primero tidal inlets and is characterised by a total length of approximately 9.4 km. It represents the easternmost portion of the barrier island system bordering the lagoon, which has been historically modified for agricultural and tourism-related purposes through land reclamation, urban development, and the construction of coastal defence structures. The beaches are largely used for tourism, while certain coastal segments are devoid of beaches and are protected by embankments located directly along the shoreline. In the nearshore area in front of the beaches, the distinctive morphology of the Banco della Mula di Muggia is present, consisting of a system of sandbanks that partially emerge at low tide and sandy bars extending down to depths of approximately 5 m. These features are arranged in an arcuate configuration and are located at distances of up to 2 km from the shoreline (Fontolan et al., 2023). These sandbanks represent the outer boundary of an extensive tidal flat dominated by muddy sands and covered by dense submerged seagrass meadows. The coastal systems from Lignano to Grado are located at the seaward margin of the Grado-Marano Lagoon. Both systems are characterised by beaches that are largely devoid of dune systems, with the exception of a short central sector along the Lignano coastline. These coastal environments can therefore be classified as strongly dissipative beaches, with an almost complete absence of dune barriers.

3.6.3.2 High and urbanized rocky coast

This coastal sector includes the remaining portion of the Friuli Venezia Giulia coastline and extends from the Timavo River mouth to the coast of Muggia. The first stretch, from the Timavo mouth to Trieste, covers approximately 18 km of coastline and is almost entirely composed of rocky or urbanised shores (Figure 7). In its western part (up to the Sistiana Bay), the coastline consists mainly of steep limestone cliffs or gently sloping rocky coasts, with only a single, limited pocket beach (the small beach below Duino Castle). In the eastern sector, rocky coastal platforms and urbanised shorelines are predominant. The coastal strip extending between the town of Muggia and the state border at San Bartolomeo, over a length of about 4 km, is mainly characterised by rocky coastal platforms composed of flysch, almost entirely affected by anthropogenic structures and constructions related to port, tourism, and recreational uses (Fontolan et al., 2023). The slope of the surrounding hilly relief varies between 20% and 30% (VAS, 2015), with elevations reaching up to approximately 200 m above mean sea level. The coastal sector including Sistiana, Trieste, and Muggia is commonly referred to as a high and urbanised coast. Throughout this sector, nearshore bathymetry is typically characterised by relatively deep waters even close to the shoreline. As discussed previously, the nature of the seabed, the structural characteristics of the coastline, and the presence of coastal structures require the adoption of alternative formulations for run-up estimation. Indeed, Poate et al. (2016) and Almeida et al. (2017)

have shown that, in the presence of gravel beaches with intermediate-to-reflective behaviour, run-up heights are significantly higher than those observed along sandy coastal systems. However, in the context of the present thesis, the focus is placed on the high and urbanised coastline commonly referred to as the “Trieste coastline”. In this sector, owing to the impulsive interaction between wave motion and vertical coastal structures, the relevant process considered is wave overtopping.

3.6.4 Coastal and urban flooding

A coastal storm can be defined as a meteorological disturbance of local marine conditions within a given area –affecting either water levels and/or wave forcing– that has the potential to modify low-lying coastal morphologies and, as a consequence, expose the backshore to wave action, strong currents, or flooding processes (Harley, 2017). Focusing more specifically on the Adriatic context at the local scale, Perini et al. (2015) define a coastal flooding event (sea storm or storm surge event) as a complex meteo-marine phenomenon, characterised by intense wave activity and strong wind regimes, responsible for the onshore displacement of water masses along the coastline and for substantial sediment mobilisation.

In particular, the following definition can be adopted to describe the extreme coastal flooding events that characterise the Northern Adriatic. In the vicinity of the shoreline, breaking waves induce a rise in the mean sea surface (set-up) and run up along the beach profile or coastal defence structures (run-up). Storm conditions are often accompanied by an additional elevation of the sea surface (surge), commonly referred to as “acqua alta”, resulting from the combined effects of the astronomical tide, atmospheric pressure gradients associated with low-pressure systems, and the tangential action of wind in the nearshore zone, which drives water accumulation along the coastlines of the Northern Adriatic. These parameters can exhibit strong spatial variability along the coastal strip and evolve significantly over the duration of a flooding event (Perini et al., 2015; Perini et al., 2019; 2020). The coastal environment of the Northern Adriatic is geomorphologically highly fragile, as it is composed of several vulnerable elements such as beaches (Bonaldo et al., 2019), which are predominantly low-lying and sandy, as well as transitional wetland areas including lagoons and peri-lagoonal zones. These sectors are therefore exposed to a high level of risk (Fontolan et al., 2012). The main associated impacts include coastal erosion (Rizzi et al., 2017; Gallina et al., 2019), groundwater contamination, the inundation of low-lying areas, and saltwater intrusion, leading to the loss of cultivable land. In addition, as discussed in the previous sections, subsidence combined with sea-level rise plays a crucial role, as it may prevent the natural system from rapidly achieving a new equilibrium through shoreline retreat or regression of coastal barriers and barrier islands. Such a scenario could result not only in the drowning of these morphologies, but potentially in the disappearance of the entire lagoonal system. Consequently, low-lying, sandy, and narrow coastlines –of high ecological value and fundamental importance for tourism– are at risk of being lost (Lionello, 2022). Beyond the issues related to the natural setting, particular attention must be paid to anthropogenic environments developed near the coastline. In these areas, coastal settlements with a strong tourism and/or economic vocation, together with infrastructure and port facilities, are highly exposed to flood hazards. The most emblematic example in this respect is Venice, located in the western sector of the Northern Adriatic, which has long been affected by recurrent “acqua alta” events (Lionello et al., 2019; Lionello et al., 2020;

Zanchettin et al., 2021; Umgiesser et al., 2021; Ferrarin et al., 2021, 2022; Mel et al., 2023). Fontolan et al. (2023a) developed a database of storm events impacting the coasts of Veneto, the Italian region located west of Friuli Venezia Giulia, and identified a total of 79 storm events between 1980 and 2022. The analysis revealed a marked increasing trend in the number of recorded events since the 2000s, partly attributable to the greater availability of online data sources. Most events occurred during the autumn months, particularly in November (Lionello et al., 2012), while only a limited number of events were recorded during the summer season. However, in recent years even coastal areas that are less well known at national and international levels have been affected by recurrent flooding issues, originating both from the open sea and from the adjacent lagoonal environments. Along the coastal sectors of Friuli Venezia Giulia, the impacts of these meteo-marine phenomena increasingly affect municipalities located close to the shoreline, which plays a crucial role in the regional economy. This stretch of coast hosts the two most important urban centres with a strong seaside tourism vocation in the region, namely Lignano and Grado. Both locations are characterised by low-lying, sandy coastlines. In addition, these settlements are situated at elevations close to mean sea level along the coast, while moving inland ground elevations locally reach values between -2 and -4 m a.m.s.l. Consequently, given the low topographic setting and the reduced dissipative capacity of the present-day beaches –compromised by intense urbanisation and strong anthropogenic pressure– future flooding events could result in substantial socio-economic damages. In particular, over the last decades the town of Grado has been affected by numerous flooding events, with water ingress occurring predominantly along lagoonal promenades and quays (Spadotto et al., 2025), generating significant challenges for local Civil Protection authorities. To a lesser extent, with the notable exception of the event of 12 November 2019, the resort of Lignano, located along the western margin of the Grado-Marano Lagoon, has also experienced several flooding-related issues. A different situation characterises the eastern coastal sector of the region, where storm events generally do not pose significant hazards, as most urban development is located above the Karst plateau, which provides natural protection through the high rocky cliffs forming the coastal escarpments. However, one of the settlements potentially affected by storm events is Sistiana, located to the west of the Karst structure. Between 27 October 2023 and 5 November 2023, an intense multi-event storm dominated by Libeccio winds occurred, generating several critical impacts along portions of the Sistiana coastline (Busetti et al., 2024). A different situation is observed along the so-called “Trieste coastline”, which includes the regional capital Trieste and the town of Muggia, corresponding to the easternmost and highly urbanised sector of the region. Along this stretch, particularly in Trieste and neighbouring areas such as Barcola, numerous storm events and episodes of acqua alta of varying intensity have occurred over the years, causing several disruptions along the waterfront (Le Rive) and within the port area.

Finanziato dall'Unione europea NextGenerationEU
Ministero dell'Università e della Ricerca
Italiadomani PIANO NAZIONALE DI RIPRESA E RESILIENZA
UNIVERSITÀ DEGLI STUDI DI TRIESTE

3.6.4.1 Historical and recent storm surge event

From a historical perspective, it is important to recall that the impulsive nature of the most severe and destructive flood events affecting the north-eastern sector of Italy has often been influenced by meteorological conditions responsible for dramatic river flooding. The most well-known and emblematic case is represented by the meteo-marine event of 4 November 1966. The combination of widespread river flooding and the simultaneous occurrence of violent storm surges resulted in civil and hydrogeological damages (from the flooding of the Arno River in Florence to the overflow of the Tagliamento River) unprecedented in recent history. In particular, the Venice Punta della Salute tide gauge recorded a sea level of 194 cm relative to the Zero Mare Punta della Salute datum (Canestrelli et al., 2001). During this extreme event, coastal defences were breached at several locations, causing extensive flooding of the adjacent hinterland and leading to the mixing of marine waters with those originating from fluvial overflow (PGRA, 2016). During the same decade, between the 1960s and 1970s, another disastrous event occurred within the Gulf of Trieste, particularly along the Trieste coastal sector. During the night between 25 and 26 November 1969, a severe storm surge caused significant impacts, affecting the entire eastern sector of the northern Adriatic (https://archiviodistatotrieste.it/documento-del-mese/novembre-2023-mareggiate-a-trieste/) In this case, the maximum sea level reached approximately 360 cm with respect to the ZIT reference (Zero Istituto Talassografico). Data for this event had to be reconstructed, as the measuring instruments were submerged and ceased recording before the peak was reached. Fortunately, the 1969 event was unique in its magnitude, and no sea levels equal to or exceeding this value have been recorded since the tide gauge became operational. Nevertheless, over the last century, several events classified as exceptional “acqua alta” have been recorded in Trieste. As reported by Ferraro and Crisciani in *La mareografia a Trieste: aspetti scientifici e storici* (2001), an exceptional sea-level event is defined as one in which overtopping occurs due to the exceedance of the maximum elevation along the urban waterfront (Le Rive), resulting in damage and disruption to the population. In this context, the reference threshold is approximately 278 cm relative to the ZIT datum, corresponding to about 111 cm with respect to the national IGM42 datum (in Venice, a comparable threshold is around 110 cm, referenced to ZMPS). Events exceeding the threshold of 278 cm ZIT between 1900 and 1997, considering the annual maximum sea level, amount to approximately 19 occurrences (Ferraro & Crisciani, 2001, Table 5, p. 73). In contrast, during the period from 1997 to 2024, around 11 such events were recorded. These figures indicate that, when considering only annual maximum sea levels exceeding the reference threshold, there has been an increase in the frequency of exceptional events. The following table (Table 1) reports the most significant events between 2004 and 2024, referenced to the ZIT datum and converted to the national IGM42 datum.

Data	Elevation (cm) *ZIT reference*	Elevation (cm) *IGM42 reference*
31/10/2004	281	114
01/12/2008	**303**	**136**
23/12/2009	285	118
24/12/2010	283	116
11/02/2013	288	121
05/03/2016	289	122
29/10/2018	284	117
12/11/2019	**308**	**141**
08/12/2020	281	114
22/11/2022	**302**	**135**
27/10/2023	**301**	**134**

Table 1. Episodes of “acqua alta” in Trieste. Hourly water levels are referenced to the ZIT datum (Zero Istituto Talassografico) and to the IGM42 datum (Istituto Geografico Militare, 1942).

The table shows that particularly in recent years four vents have exceeded the threshold of 300 cm ZIT.

3.6.5 Salt water intrusion

The final issue addressed concerns the hydrogeological phenomenon of saltwater intrusion into aquifers, which is now widely recognised as an environmental, economic, and social problem across Europe (Scheidleger et al., 2004), and particularly in Italy, where it has been documented in numerous studies, especially in the Po Delta and the Venice Lagoon sectors (e.g. Antonellini et al., 2008; Pezzetta et al., 2010; Tosi et al., 2021; Tarolli et al., 2023). The coastal territory of Friuli Venezia Giulia represents an area of considerable economic, social, and environmental relevance, as it hosts land uses of very different nature, including agricultural areas, residential settlements, seaside resorts, forested zones, and wetlands. Saltwater intrusion is a typical issue in coastal areas, where seawater –often in conjunction with mean sea-level rise and/or during storm events– penetrates into phreatic and artesian aquifers. This process is facilitated by the low elevation of reclaimed land, which in some cases lies 2-3 m below mean sea level. For this reason, saltwater intrusion represents one of the major concerns for coastal zones, particularly where low-lying plains are present and drainage systems are predominantly artificial (Poulter et al., 2008; Rasmussen et al., 2013). Extensive human interventions, such as the reclamation of lagoonal and coastal areas and the exploitation of groundwater resources, have promoted the inland expansion of saline intrusion within aquifer systems. In addition, climate change–related processes, including sea-level rise and increased drought frequency, have further exacerbated salinisation processes (IPCC, 2022), with severe consequences for agricultural land management. The presence of salt constitutes a major stress factor for vegetation, adversely affecting crop yields and reducing soil fertility and overall productivity (Tarolli et al., 2023).

3.7 The coast of Friuli Venezia Giulia

From a geographical perspective, the coastline of the Friuli Venezia Giulia region can be subdivided according to its geological and environmental setting and the presence of the most relevant coastal settlements, not only in economic, commercial, and tourism terms, but also in relation to their cultural value (Figure 7). The coastal realities considered in this study are located within the western coastal sector, at the margins of the lagoonal system (Lignano and Grado), and along the high and urbanised coastal stretch known as the “Trieste coastline”, corresponding to the easternmost coastal sector of the region, where the urban areas of Trieste and Muggia are located. The total length of the Friuli Venezia Giulia coastline is approximately 169 km, of which about 119 km remain when excluding port areas and heavily urbanised and anthropogenically modified sectors such as Monfalcone, Trieste, and Muggia (Fontolan et al., 2023). The resident population within coastal municipalities of the Northern Adriatic is estimated to be slightly over one million inhabitants. More specifically, the coastal municipalities of Friuli Venezia Giulia host approximately 274.000 residents distributed across eight municipalities, with an average population density of about 675 inhabitants/km^2. These values are approximately three times higher than those of the Veneto region and twice those of Emilia-Romagna (ISTAT-ASI, 2024). The intense urbanisation of these areas, combined with the environmental vulnerabilities of the coastal setting and the strong influence of meteomarine forcings, results in a particularly high exposure to flood risk compared to other coastal sectors at the national scale.

Figure 7. Coastal arc of the Northern Adriatic showing the coastal urban centres analysed in this study (Lignano, Grado, Trieste, and Muggia) and the different coastal sectors: the western low-lying coast sector (red line); the eastern high coast sector (yellow line); and the eastern high and urbanised coast sector (light blue line) (modified from ArcGIS Pro 3.10, 2025).

Finanziato dall'Unione europea NextGenerationEU
Ministero dell'Università e della Ricerca
Italiadomani PIANO NAZIONALE DI RIPRESA E RESILIENZA
UNIVERSITÀ DEGLI STUDI DI TRIESTE

As previously noted, it is important to recall the impulsive nature of the most severe and destructive flood events that have historically affected the north-eastern sector of Italy. These events were driven by meteorological conditions that caused dramatic fluvial flooding, such as the event of 4 November 1966 (Canestrelli et al., 2001; De Zolt et al., 2006), and simultaneously favoured the occurrence of violent storm surges. In several locations, coastal defences were breached, leading to extensive inundation of the adjacent hinterland and to the mixing of marine waters with those originating from fluvial overflow (PGRA, 2016). The event affected numerous Italian regions but had particularly severe consequences along the coasts of Veneto and Friuli Venezia Giulia. Along the entire coastal sector, marine water intrusion occurred as a result of intense storm activity in areas such as Riviera and Pineta in Lignano, accompanied by the partial dismantling of the coastal dune system. At that time, coastal defence structures along the seaward shoreline were either absent or very limited. Following the event, several protective works were constructed, including seawalls, breakwaters, and groynes, both to enhance the hydraulic safety of tourist settlements and to reinforce the coastline and the lagoon island system, with the aim of counteracting the natural erosive action of wave dynamics and the consequent shoreline retreat. A second major event dated 26 November 1969 (Canestrelli et al., 2001), reached the highest sea-level values ever recorded by the Trieste tide gauge. This storm surge caused extensive damage to infrastructure and to the waterfront in several areas, including the Barcola seafront promenade. (https://archiviodistatotrieste.it/documento-del-mese/novembre-2023-mareggiate-a-trieste/).

3.7.1 Coastal risk location and context

The entire coastal area investigated, between the mouth of the Tagliamento River and Muggia, is affected by dynamics and conditions directly linked to the Adriatic Sea. However, it shows several morphodynamic reactions based on the characteristics of the different segments of coastline and the water levels achieved during extreme events. The division of coastal areas into two macro-sectors, low and sandy coast and high and urbanised coast, is not solely attributable to morphological factors, such as the presence of the Grado and Marano lagoons or stretches of high and rocky coastline, but also reflects different levels of vulnerability in response to meteorological and marine forces and extreme events. In this case, the orientation of the coastline and its ensuing exposure to the primary forces under analysis –particularly those originating from the Sirocco and Libeccio winds– were taken into consideration in addition to the geomorphological features of the coastal sector to which they belong. The low-lying, sandy coastal areas where Lignano and Grado are located (Figure 7) are totally exposed to the Scirocco wind and, to a lesser extent, to the Libeccio wind. These areas are extremely susceptible to SLR and high water and storm surge events, with increasingly frequent consequences, due to the exposure factor, low altitude, and sandy terrain. In contrast, mountainous and rocky coastal regions are shielded from the Scirocco wind's force. The Istrian peninsula's shielding effect, which tends to lessen the effects of storm surges and waves created by the Scirocco wind, is very beneficial to Trieste and the town of Muggia, which is situated inside the Gulf of Trieste. However, these locations are more exposed to the Libeccio wind, which in some circumstances, especially in recent years, has generated high-intensity waves in this area (Busetti et al., 2024). The strongest storm surge events in the northern Adriatic are linked to the Scirocco wind, although being less

immediately exposed to it. Muggia is a particularly noteworthy example in this regard since the low elevation of the urbanized region on which it is located encourages the occurrence of more severe and widespread floods than in other high coast locations. It is consequently underlined how the response to extreme occurrences is highly impacted by the interaction between meteorological and sea forces, direction and the local peculiarities of the terrain.

3.7.1.1 Lignano

The Municipality of Lignano Sabbiadoro (45°39′18″ N; 13°05′35″ E) is located in the westernmost portion of the Friuli Venezia Giulia region (Figure 7), along the western boundary of the Grado–Marano Lagoon. The municipal territory extends over the south-western edge of the Province of Udine, bordering the Province of Venice near the mouth of the Tagliamento River, while to the north it is bounded by Marano Lagoon. The municipality covers an area of approximately 15.7 km². Lignano is a town with a resident population of about 7000 inhabitants and a strong tourism vocation, reaching up to approximately 3.7 million visitors during the summer season. Historically, the settlement was already inhabited in Roman times when a military outpost was established to control the lagoonal area. Initially, however, the territory where present-day Lignano is located was largely uninhabited. Historically, the settlement was already inhabited during Roman times, when a military outpost was established to control the lagoonal area. Initially, however, the territory where present-day Lignano is located was largely uninhabited. At the beginning of the nineteenth century, the population of the peninsula amounted to only about seventy inhabitants (https://www.lignanoonline.eu/it/storia.php). In the early twentieth century, Lignano was still a narrow strip of land covered by pine forests, interspersed with sand dunes shaped by winds towards the sea, and by marshes, salt meadows, and tidal flats on the lagoonal side, connected to the mainland through river channels flowing into the lagoon. The first bathers arrived from Marano in the early 1900s (Valussi, 1986; Nicoloso, 1992), marking Lignano as one of the oldest seaside resorts in Italy. During the same period, the first bathing establishment “Bagni di Porto Lignano” was founded. The construction of the first road connecting Lignano to the mainland enabled, between 1903 and 1910, the development of the first hotels and holiday residences. (https://www.lignanoonline.eu/it/storia.php). The development of the Lignano area occurred only after the land reclamation works carried out in the immediate post-war period, aimed at draining marshy and unhealthy areas affected by malaria, which had represented a major obstacle to tourism and leisure activities in the wetlands surrounding the peninsula. Major reclamation interventions were therefore undertaken in the Pantani and Lovato valley areas, on the inner side of the peninsula (Consorzio Bonifica Bassa Friulana, 2012). Around 1930, the first church and the seaside colony were built, and Lignano officially became a “Stazione di Soggiorno” (holiday resort). After the Second World War, holiday homes in Lignano became a symbol of the improved living standards achieved by the middle class. After 1950, a key role in shaping the urban development of the area was played by the new master plan for Lignano Pineta, designed by the well-known Udine-based architect Marcello D’Olivo. (https://www.domusweb.it/it/dall-archivio/2023/07/11/a-lignano-il-progetto-di-marcello-dolivo.html). From that period to the present day, Lignano has experienced a substantial increase in holiday homes, hotels, and accommodation capacity. Today, it represents one of the most important seaside tourism centres in the region, attracting millions of visitors during the summer season and becoming

the most populated town in Friuli Venezia Giulia during peak periods, as well as one of the most renowned and vibrant destinations along the Adriatic coast (https://www.lignanoonline.eu/it/storia.php). The town is characterised by a high level of tourist appeal, primarily due to the wide sandy beaches facing the Adriatic Sea. The most sought-after coastal sector is Lignano Sabbiadoro, owing to the presence of numerous bathing establishments, often associated with rigid backshore defence structures. As a result of intense tourism activity and rapid urban development, beach profiles have been significantly altered. At present, the only remaining soft coastal defence system, represented by dune ridges with discontinuous vegetation, is confined to a stretch of approximately 1 km between Pineta and Sabbiadoro, with elevations slightly exceeding 7 m.

3.7.1.2 Grado

The Municipality of Grado is located in the easternmost part of the Grado–Marano Lagoon, Italy (Figure 7). The municipal territory covers a total area of approximately 115.5 km², of which about 45 km² consist of mainland and 70.5 km² of lagoonal environment (https://comune.grado.go.it/it/vivere-il-comune-22477/luoghi-22478/la-laguna-di-grado-69770). The mainland represents the easternmost portion of the barrier island system bordering the Grado Lagoon and is almost entirely devoted to tourism and agriculture (Bezzi et al., 2018). Despite having just over 7550 permanent residents (https://demo.istat.it/app/?a=2024&i=D7B), a number that roughly triples during the summer season, Grado represents one of the most important tourist destinations in the region, attracting approximately 1.4 million visitors per year (ISTAT, 2023). Grado has a very long history, originating around the second century AD as a fishing village and as the harbour outpost of the Roman city of Aquileia (https://www.archeocartafvg.it/portfolio-articoli/grado-go-il-castrum/). Grado, after Aquileia, represents an important archaeological site. Over the decades, significant cultural heritage has been uncovered, spanning from the Roman period to the Palaeochristian and early medieval eras. Numerous archaeological remains have been identified along the coastline, particularly offshore of the Grado breakwater, including ancient church dykes and Roman structures (De Grassi, 1952; Gaddi, 2001; Tortorici, 1997). The most significant remains are located within what is known as the castrum, corresponding to the historic centre, which represents the original urban nucleus. The Palaeochristian architectural heritage includes the Cathedral of Santa Eufemia, the baptistery, the church of Santa Maria delle Grazie, and the remains of the Basilica delle Corte. The settlement is connected to the mainland by a long artificial causeway and includes a distinctive lagoonal core, around which more recent urban districts have developed. In the early twentieth century, the built-up area was concentrated around the Mandracchio Canal and the Roman castrum historic centre. However, the small fishing village remained isolated until 1905, when a road was constructed across the lagoon to connect Aquileia with Grado (Touring Club Italiano, 2009). The earliest traces of land reclamation in the peri-lagoonal area date back to Roman times, with the construction of the Anfora Canal and a drainage network serving the Aquileia area. In the modern era, the most significant reclamation works aimed at draining marshy areas for agricultural, industrial, and urban uses were initiated under the Austro-Hungarian Empire, notably with the reclamation of the Isola Morosini basin in 1912 and were subsequently interrupted by the outbreak of the First World War. The major land reclamation activities within the Grado lagoonal territory,

however, began in the 1920s, with the construction of numerous pumping stations, and continued for more than three decades, significantly influencing the evolution of the lagoon system. One of the most important reclamation projects, centred on the Fossalon area within the Municipality of Grado, was the Bonifica della Vittoria, initiated in 1928. This project aimed to create land suitable for agricultural use (Agriconsulting, 2008). In 1936, Grado was definitively connected to the mainland through the construction of a swing bridge, bringing an end to its long-standing isolation (Touring Club Italiano, 2009). In the post-war period, the town experienced rapid urban expansion, accompanied by land reclamation works and water management interventions, alongside the growth of coastal tourist and bathing facilities, including the well-known “Costa Azzurra” beach, the breakwater protecting the historic centre, and the main urban beach (Marocco, 2000). The numerous human interventions have led to profound changes within the Grado-Marano Lagoon system, particularly from a tourism-related perspective. Permanent and seasonal settlements within the lagoon consist mainly of small historic villages originally developed in connection with fishing activities (Consorzio di Bonifica Bassa Friulana, 2008; 2012). Only the more recent urban expansion around the historic centre of Grado and Grado Pineta has promoted the construction of second homes, apartment blocks, and tourist accommodation facilities. Other structures present in the area include isolated dwellings near fish farms and several traditional straw huts (known as *casoni*), found both in the Grado and Marano lagoons. From an environmental and landscape perspective, the Grado and Marano lagoons exhibit markedly different characteristics. In Marano, emerged land and built-up areas are quantitatively more limited than in the Grado Lagoon, resulting in a more natural system, whereas the Grado lagoonal area appears more anthropogenically modified and therefore more heterogeneous. Focusing on the Grado coastline, which is characterised by approximately 120 m of beach width, the western sector shows the highest tourist interest, hosting numerous bathing establishments with predominantly rigid backshore defence structures. As observed for Lignano, dune systems are very scarce also in Grado, both due to unfavourable exposure conditions and to the extensive reshaping of beaches for tourism and recreational purposes. Having described the localities of Lignano and Grado, the focus now shifts to the high and rocky coastal sector extending beyond the mouth of the Timavo River, starting from Villaggio del Pescatore, which marks the transition from a low-lying coast to a predominantly high and rocky shoreline. More specifically, the high coast extends between the Timavo River mouth and the San Bartolomeo border crossing, excluding the urban and port area of Trieste, which also includes Muggia and is commonly referred to as the “Trieste coastline”.

3.7.1.3 Trieste

The Municipality of Trieste (45°39′13″ N, 13°46′42″ E) is located in the eastern coastal sector (Figure 7), and specifically belongs to the high and urbanised coastal stretch extending from Barcola to Muggia. Trieste is the capital of the Friuli Venezia Giulia Region and is situated in the north-easternmost part of Italy, approximately 6 km from the border with Slovenia (RAFVG, 2015). The municipality covers an area of about 84 km², accounting for approximately 40% of the total provincial territory, with elevations ranging from sea level to 672 m a.m.s.l. Its administrative boundaries are defined to the north by the municipalities of Duino-Aurisina, Sgonico, and Monrupino, to the east by Slovenia, and to the south by the

municipalities of Muggia and San Dorligo della Valle. Trieste has very ancient origins, linked to protohistoric settlements dating back to the second millennium BC. Between around 50 BC and the first centuries AD, the small fishing village developed into a Roman colony known as Tergeste (https://www.regionestoriafvg.eu/tematiche/tema/404/Dedizione-di-Trieste-allAustria). During the Middle Ages, following numerous conflicts with its rival Venice for control of the Adriatic Sea, Trieste placed itself under Austrian protection in 1382, while retaining a degree of autonomy until the seventeenth century. In 1719 it was declared a free port and, as the only Adriatic outlet of the Austrian Empire, Trieste benefited from substantial investments and underwent rapid development, becoming in 1867 the capital of the Austrian Littoral region (https://trieste-di-ieri-e-di-oggi.it/2016/11/15/storia-di-trieste-in-sintesi/). The coastal belt of the municipal territory is characterised by two distinct geomorphological settings: a hilly sector and a sub-planar sector. The hilly belt connects the Trieste Karst plateau to the coastline and is characterised by flysch reliefs, which include both the coastal zone and the entire urban area of Trieste, incised by an erosive drainage network. Slopes range between 23° and 35° within the urbanised belt, increasing to values between 35° and 70° along the predominantly coastal sector. (RAFVG, 2019). The sub-planar belt has been almost entirely obliterated by the urban development of the city of Trieste. In particular, the coastline has been extensively modified by various anthropogenic interventions, including land reclamation, infilling, and port-related works (https://www.arpa.fvg.it/temi/temi/suoli-siti-contaminati-e-biodiversit/sezioni-principali/siti-contaminati/il-sin-di-trieste/). Within the Municipality of Trieste, the Porto Vecchio area has historically been affected by marine water ingress, favoured by specific meteo-climatic conditions, such as the combination of intense precipitation, southerly winds, and low atmospheric pressure, which have caused episodic flooding over time. In the “Relazione Tecnica di Fase A” and in the geomorphological and surface hydrology maps of the Geological Study of the Trieste Urban Master Plan (P.R.G.), this area is identified as being prone to flooding. Indeed, the area under consideration is characterised by a sub-planar topography, with elevations ranging between +1.00 m and +2.00 m a.m.s.l., and is entirely enclosed within the “upper limit of the zone subject to verification of safe elevation with respect to marine water ingress”, as defined by the geotechnical zoning map of the Geological Study of the Trieste P.R.G., which establishes a safety elevation of +2.5 m a.m.s.l. (RAFVG, 2020). Along the coastline, the main industrial area of the city has also developed, representing a key economic hub for Trieste. This area is characterised by productive activities such as the storage and handling of petroleum products, metal processing, and the manufacture of plastic materials, which are particularly critical in terms of potential environmental impacts in the event of major flooding or marine intrusion events. In addition, one of the most relevant factors for environmental risk assessment within the Municipality of Trieste is related to traffic and mobility. The primary transport axis is represented by the SS14 road, which runs from Grignano and crosses the coastal belt of the city of Trieste, namely the waterfront area known as Le Rive. Consequently, extreme events of acqua alta or severe storm surges would cause serious disruptions to traffic circulation, especially during high-intensity events, potentially damaging port infrastructure and leading to the interruption of road transport activities.

3.7.1.4 Muggia

The Municipality of Muggia (45°36′ N, 13°46′ E), located close to the Slovenian border, forms part of the final stretch of high and urbanised coastline extending from Barcola to the town of Muggia (Figure 7). Muggia also has origins dating back to the Roman period, shortly after the foundation of Aquileia in 181 BC (https://www.archeocartafvg.it/portfolio-articoli/muggia-ts-il-centro-storico/). The Romans established the first settlement in an elevated position, known as Castellum Mugla. Only around the fifteenth century did the urban centre begin to develop along the shoreline, mainly around the harbour area. In more recent history, following a brief period of Venetian rule, Muggia, together with Trieste, came under Habsburg control, during which time shipbuilding activities developed. Despite this, the town has retained an atmosphere reminiscent of the Venetian Republic, particularly in the architecture of its historic centre, characterised by narrow streets resembling Venice's streets (RAFVG, 2023). At present, the Municipality of Muggia covers an area of just under 14 km² and hosts approximately 13,000 residents, with the highest population density concentrated along the coastal zone. It also represents the southernmost municipality of Friuli Venezia Giulia. These figures tend to increase slightly during the tourist seasons, when up to an additional 3,000 people may be present, placing Muggia within the same range as the Municipality of Trieste (RAFVG, 2024). Similarly, to Grado, although located within a coastal setting characterised by different physical features, Muggia has experienced increasing impacts from coastal flooding over recent decades. The most vulnerable area involves the small Mandracchio channel and, consequently, the entire historic centre of the town. In recent years, one of the most significant events recorded was the acqua alta of 12 November 2019, which affected the entire Northern Adriatic coastal sector and caused disruptions to the local population in Muggia. A further episode of acqua alta combined with storm conditions, occurring between 27 October and 5 November 2023, resulted not only in flooding within the historic centre but also in substantial damage to the SP14 road network ("Strada del Lazzareto"), which connects Muggia to the Slovenian border.

4 Materials and methods

The analyses developed within this thesis include: (a) a set of preliminary assessments of extreme sea levels reached during episodic events such as *acqua alta* and/or storm surges, as reported in the Flood Risk Management Plan (PGRA) of the Eastern Alps River Basin District, together with the application of different statistical approaches to update extreme-value estimates based on the most recent trends; and (b) the production of coastal flood hazard maps.

Part (a) focuses on the statistical processing of data extracted from the Venice tide gauge for the updated extreme levels at Grado and Lignano, and from the Trieste tide gauge for Trieste itself and for the town of Muggia. This approach preserves the natural geological subdivision of the four sites, distinguishing between low, sandy coasts and high, urbanized coasts, while also accounting secondarily, for the orientation of each location with respect to the dominant forcings acting in the Northern Adriatic. This activity can be summarized as follows:

- Preliminary assessment of the local Floods Directive (PGRA) and of the definition of extreme water levels reached during meteomarine events, which form the basis for the development of flooding scenarios (Section 4.1);
- Statistical analyses to update extreme water levels for Grado (Section 4.3), using data recorded by the Venice tide gauge and applying a detrending procedure to the observed levels, followed by the application of the Gumbel statistical distribution over the period 1950–2023. The derived extreme levels were subsequently adopted also for Lignano, as it lies within the same lagoonal context;
- Definition of the urban flooding threshold for the city of Grado and estimation of the frequency of occurrence and potential exceedance above this threshold;
- Statistical analyses to update extreme water levels for Trieste over the period 1939–2024 (Section 4.4), applying different detrending approaches (with respect to annual mean sea level and/or to the lunar nodal cycle) and subsequently adopting several statistical frameworks, including GEV-BM (Pirazzoli & Tomasin, 2009), POT-GPD (Caruso & Marani, 2022), and multivariate statistical analysis (Ferrarin et al., 2022; Ragno et al., 2023). The resulting extreme levels were also applied to the nearby town of Muggia;
- Estimation of relative sea-level rise (RSLR) for Grado, by comparing IPCC AR6 projections (Masson-Delmotte et al., 2021), tide gauge records from Trieste and Grado, and existing literature, in order to infer the contribution of vertical land motion (VLM);
- Combination of RSLR projections for 2050 and 2100 with episodic event statistics and associated R_P, to evaluate the reduction of R_P values corresponding to given flooding thresholds.

The second part (b), building on the statistical analyses described above, focuses on the development of models aimed at producing flood hazard maps for the selected locations. Two distinct approaches are considered. The first approach consists of a statistical “bathtub” flooding model, which is particularly suitable for very low-lying and gently sloping urban environments such as Grado. The second approach is more advanced and involves the

Finanziato dall'Unione europea NextGenerationEU | Ministero dell'Università e della Ricerca | Italiadomani PIANO NAZIONALE DI RIPRESA E RESILIENZA | UNIVERSITÀ DEGLI STUDI DI TRIESTE

dynamic simulation of extreme events using the MIKE 21 hydrodynamic model developed by DHI. Both methodologies were implemented following the steps outlined below and were applied in a complementary manner, depending on the geomorphological and urban characteristics of each study area, as described below:

- Bathtub approach: using the LiDAR-derived digital terrain model (DTM), the Grado area was subdivided into sectors characterized by different levels of vulnerability, in order to produce a set of downscaling maps of episodic flood-inducing extreme events associated with different R_P. The analysis also includes a detailed assessment of the elevation of the promenade along the lagoon boundary.

Initially, a static bathtub technique was contemplated for the town of Grado. The local Civil Protection operating requirements, which call for rapid qualitative analytic tools for the quick evaluation of metropolitan areas that can be impacted by extreme events, served as the main driving force behind this decision. The bathtub model offers a useful representation for identifying flood-prone locations and extremely vulnerable sectors in territorial and city contexts with relatively low elevations, like the Grado lagoon front, and a fairly flat urban fabric. Second, the bathtub approach served as a reference and preliminary model while dynamic modeling was applied to a particular severe event that actually happened to get the answers. Thus, the MIKE21 hydrodynamic model was used to recreate the severe event under consideration in static form. This enables both additional calibration and a comparative evaluation of the static model's dependability within the Grado environment. The results of the testing indicate that the two methods are fairly consistent.

After the calibration process was finished, the dynamic model was used as Muggia and Trieste's primary analysis tool. The development of flooding in these urban settings, which are distinguished by more noticeable topographical gradients, is greatly impacted by local morphology and flow dynamics. For an accurate portrayal of flooding patterns in these situations, dynamic modeling is crucial. In order to compare the two approaches and enable site-specific assessments, the static approach was nevertheless used in a complimentary manner.

- Dynamic modelling: using the LiDAR-derived digital terrain model (DTM), the areas of Trieste, Muggia, and Lignano were subdivided into sectors with different levels of vulnerability, allowing the generation of downscaling maps of episodic flood-inducing extreme events associated with different R_P. In addition to the DTM, topo-bathymetric data were incorporated to construct the computational mesh required for dynamic flood simulations. Within the urban areas, land-use information was also included to account for surface roughness effects and to better represent the interaction between the urban fabric and the incoming water mass.

Finanziato dall'Unione europea NextGenerationEU
Ministero dell'Università e della Ricerca
Italiadomani PIANO NAZIONALE DI RIPRESA E RESILIENZA
UNIVERSITÀ DEGLI STUDI DI TRIESTE

4.1 Flood Directive 2007/60/CE

The present study aims to develop flood hazard maps related to meteomarine events, which constitute the basis for flood risk assessment and management, in accordance with the Floods Directive 2007/60/EC of the European Parliament and of the Council of 23 October 2007 (EUR-lex, 2007), subsequently implemented in Italy through Legislative Decree No. 49 of 23 February 2010. More specifically, rather than addressing a purely hydraulic phenomenon that is slowly varying and essentially unidirectional, such as river flow, this study focuses on a fundamentally periodic process, namely marine dynamics associated with storm surge and wave motion. The main objectives of Directive 2007/60/EC remain unchanged for both fluvial flooding and coastal inundation events. The overarching goal is the mitigation of potential adverse consequences for the environment, human health, economic and touristic activities, and cultural heritage. In this context, the Flood Risk Management Plan required by the Directive addresses all aspects of flood risk management, with particular emphasis on prevention, protection, and preparedness, including flood forecasting and early warning systems, as well as planning, mitigation measures, and emergency management activities typically undertaken by Civil Protection authorities. Article 7 of Directive 2007/60/EC (EUR-lex, 2007, see "*piani di gestione del rischio da alluvioni"*), explicitly highlights the need to account for spatial and land-use planning in areas exposed to flood risk. Similarly, Legislative Decree No. 49/2010, Article 7, paragraph 6, refers to urban planning and structural measures implemented by the directly involved local authorities, underlining the close interconnection between flood risk management strategies and territorial planning instruments (ISPRA, update 2014). It should also be emphasized that the time scales associated with Civil Protection actions, which are aimed at ensuring the prompt management and response to hazardous events, differ substantially from the time frames and processes characterizing urban transformation and territorial development, which are instead oriented toward land conservation and spatial planning over medium- to long-term horizons. Furthermore, Italian legislation incorporates the European requirement to consider flooding caused by marine inundation of coastal areas through Article 2 of Legislative Decree No. 49/2010. Article 6, paragraph 6 of Directive 2007/60/EC allows Member States to focus exclusively on extreme events, provided that this choice is supported by an assessment of the level of protection. However, several national methodological reports on coastal flooding (e.g. Sardinia), in light of the absence of a clear regulatory definition of what constitutes an "adequate level of protection" (RAS, update 2018), have recommended not making use of this option. Conversely, based on territorial urban planning practices and Civil Protection interventions, and considering, for instance, the Storm Surge Catalogue of Emilia-Romagna (Perini et al., 2015) –a region that shares, in several respects, similarities with Friuli Venezia Giulia both in terms of geological setting and dominant forcing mechanisms– it was decided to also assess the effects of meteomarine events characterized by short return periods, namely events with a high probability of occurrence. The guidelines adopted in the present study are inspired by the structure defined within the Flood Risk Management Plan (PGRA, 2021). It is therefore appropriate to outline some considerations regarding the objectives of the PGRA, in relation to the Hydrogeological Asset Management Plans (PAIR, 2016) and to urban planning instruments, which together support territorial planning and land-use management activities. The Flood Risk Management Plans (PGRA) have been prepared by the District Basin

Authorities of the five hydrographic districts into which the national territory is divided (Po River, Eastern Alps, Northern Apennines, Central Apennines, Southern Apennines), as well as by the Regions of Sardinia and Sicily. The periodic review and possible update of the Plans every six years allows flood risk management strategies to be adapted to changing territorial conditions, also taking into account the increasingly plausible impacts of climate change on the occurrence of flood events. With reference to the coastal environmental context of the Friuli Venezia Giulia Region, the Flood Risk Management Plan of the Eastern Alps Hydrographic District is considered. This district is characterized by approximately 280 km of coastline, extending from the Veneto Region (with the exception of a short stretch falling within the Po River District) to the easternmost boundary of Friuli Venezia Giulia, along the border with Slovenia. Within this area, the relevant river basins and the lagoon systems of Venice and Marano-Grado are included, with estimated surface extents of approximately 550 km² and 160 km², respectively, together with smaller wetland areas (PGRA, 2016).

4.1.1 Flooding scenarios

This section addresses the evaluation and analysis of data processing aimed at deriving the total water level (H_{TOT}) near the shoreline (Morris et al., 2021) for short-term episodic events, such as storm surges or exceptional “acqua alta” events, which occur over a limited time window in a given area as a direct function of the return period. In the case of coastal flooding, the return period defines the probability that an event of a given intensity will occur within a one-year time horizon. As a reference framework, sea-level data reported under the Floods Directive, as transposed into Italian legislation by Legislative Decree No. 49/2010, are adopted, based on the Flood Risk Management Plan (PGRA) of the Eastern Alps Hydrographic District. These values derive from the statistical analysis of extreme sea levels carried out by Tomasin and Pirazzoli (2009). This approach enables a region-scale assessment of extreme water levels along the eastern sector of the northern Adriatic Sea, extending from the Lignano coastline to the Trieste-Muggia coastal area, using the Trieste tide gauge as the primary reference.

4.1.2 Flood Risk Management Plan of the Eastern Alps Hydrographic Basin (PGRA)

The first step concerns the description of the threshold levels reported in the Flood Risk Management Plans (PGRA), prepared by the District Basin Authorities for the five hydrographic districts into which the national territory is divided. Under the Floods Directive, for the Eastern Alps Hydrographic District and specifically for the northern Adriatic sector, the statistical representation of total water level values (H_{TOT}), associated with medium and high probabilities of occurrence is based on the statistical characterization of extreme tidal levels, following the approach developed by Tomasin and Pirazzoli (2009). This methodology considers, for both Venice and Trieste, the historical sea-level time series recorded over the period 1939-2006. In the case of Trieste, the available observations are sampled at hourly resolution. The Eastern Alps Hydrographic District is subdivided into two zones:

- zone 1: extended from Adige River mouth to Tagliamento River mouth.
- zone 2: extended from Tagliamento River mouth to Trieste littoral.

The return periods considered by the Floods Directive for a flood event are the following:

- R_P *30 years* = representative of frequent events with high probability of occurrence.
- R_P *100 years* = representative of events with medium probability of occurrence.
- R_P *300 years* = representative of rare events with low probability of occurrence.

Below (Table 2a,b) the reference values used for the computation dell'H_{TOT} representing the total water level that the marine water mass can reach along the coastline, are reported:

Zone 1: from Adige mouth to Tagliamento mouth			
	R_P = 30	**R_P = 100**	**R_P = 300**
L_{MM} + H_{ASTR} + H_{SURGE}	145 cm	155 cm	170 cm
H_{SET-UP} + H_{RUN-UP}	+ 40 cm for each scenario		
Values in cm on zero I.G.M			

Table 2a: Reference H_{TOT} values for Zone 1 of the Eastern Alps Hydrographic Basin District (PGRA, 2021).

Zone 1: from Tagliamento mouth to Trieste littoral			
	R_P = 30	**R_P = 100**	**R_P = 300**
L_{MM} + H_{ASTR} + H_{SURGE}	140 cm	160 cm	200 cm
H_{SET-UP} + H_{RUN-UP}	+ 40 cm for each scenario		
Values in cm on zero I.G.M			

Table 2b. Reference H_{TOT} values for Zone 2 of the Eastern Alps Hydrographic Basin District (PGRA, 2021).

From the table it emerges that the maximum total water level (HTOT) is generally defined as the sum of several contributing components:

$$H_{TOT} = L_{MM} + H_{ASTR} + H_{SURGE} + H_S + (H_{SET-UP} + H_{RUN-UP})$$

where:
L_{MM} = mean sea level.
H_{ASTR} = astronomical tide.
H_S = maximum seiche high wave (included in H_{SURGE}).
H_{SURGE} = represents the meteorological contribution and does not include the astronomical tide.
H_{SET-UP} = set-up of the sea surface near the shore induced by wave breaking.
H_{RUN-UP} = maximum run-up level.

Based on the levels reported in Table 2 and on the definition of the total water level, the detrending methods adopted in this study are described below. These procedures are required to correctly apply the statistical approaches used to update extreme sea-level values, accounting for the most recent trends observed over the last decades.

Subsequently, studies carried out at the local scale for Venice were considered, focusing on the statistical analysis of extreme sea levels at the secular scale. In particular, the work by Caruso and Marani (2022) was analysed with respect to the statistical characterization of extreme sea levels, with special attention to the most recent trends. Subsequently, the

Finanziato dall'Unione europea NextGenerationEU
Ministero dell'Università e della Ricerca
Italiadomani
UNIVERSITÀ DEGLI STUDI DI TRIESTE

statistical framework proposed by Ferrarin et al. (2022) and Ragno et al. (2023) for Venice was examined and replicated, adapting it to the environmental context of Trieste. The aim is to investigate in detail the complexity of extreme sea-level behaviour, in order to assess the different factors contributing to extreme levels and, consequently, to coastal flooding, both under present conditions and future projections. The overarching objective is to achieve a robust understanding of the dynamics governing extreme sea-level hazards, supporting the assessment and management of flood risk in urban coastal areas, particularly in the context of climate change.

In addition, an ad hoc analysis was carried out for the town of Grado, given the severe flooding issues that have affected the area over recent decades. This allowed a more site-specific assessment of extreme events, analysing recent trends in both maximum and mean sea levels, as well as their long-term behaviour. The focus on Trieste, and partly on Grado, is driven by the availability of tide-gauge records, which are essential for a robust analysis of past and recent sea-level extremes. The Trieste tide gauge provides a secular time series, continuously recorded since 1890, and therefore represents a key dataset for statistical analyses of extreme sea levels. In contrast, the Grado tide gauge has been operating continuously only since 1991. For this reason and given the inherent limitations of a roughly 30-year statistical record, interpolation procedures were applied in order to derive the most reliable possible extreme-level statistics for the lagoonal setting of Grado. Once the datasets and results derived from the aforementioned studies were processed, a comparative analysis was performed to estimate the final rate of water-level increase, with a specific focus on Trieste, owing to the length and robustness of its time series, and to relate this increase to the return periods of episodic extreme events. The final step consisted in producing flood-inundation maps based on the updated extreme sea-level thresholds, incorporating the most recent trends and the corresponding return periods. The main targets of the simulations for the western coastal sector of Friuli Venezia Giulia are Grado and Lignano, using Grado as the reference for extreme sea levels. Conversely, for the eastern coastal sector, the selected targets are the regional capital Trieste and the town of Muggia, with extreme levels derived from the statistical analysis of the Trieste tide-gauge record. This subdivision is motivated by the different orientation of the coastal sectors where the urban centres are located, and by their differing exposure to the meteomarine forcings acting in the northern Adriatic basin.

4.2 Assessment of Extreme Events in Grado: methodological setup

To robustly characterise the frequency and intensity of extreme meteomarine events in the northern Adriatic, it is necessary to adopt a statistical framework based on Extreme Value Theory (EVT). This theoretical approach allows an appropriate modelling of extreme sea-level values through the use of Gumbel distributions within a Block Maxima (BM) framework, as well as the more general Generalized Extreme Value (GEV) distribution (BM method) and the Generalized Pareto Distribution (GPD) within the Peaks Over Threshold (POT) approach. These methods enable a more reliable estimation of return levels and their associated probabilities of occurrence. The combined use of these models is particularly relevant in vulnerable coastal settings such as Trieste and Grado, where storm surge, astronomical tide, and low- and high-frequency variability interact in a non-linear manner.

Finanziato dall'Unione europea NextGenerationEU
Ministero dell'Università e della Ricerca
Italiadomani PIANO NAZIONALE DI RIPRESA E RESILIENZA
UNIVERSITÀ DEGLI STUDI DI TRIESTE

The statistical approach therefore represents a fundamental first step for the assessment of present and future coastal hazard and for supporting adaptation strategies in response to the irreversible rise in mean sea level.

For the town of Grado, a different analytical approach was adopted compared to that applied to Trieste. This choice is primarily justified by the need of the Friuli Venezia Giulia Civil Protection Authority to address coastal flooding issues mainly on the lagoonal front. In recent years, extreme sea-level events have caused recurrent public safety problems within the urban fabric, highlighting the urgency of improving local flood protection measures. Given this context, an ad hoc study focused on extreme-value statistics was required, with particular emphasis on the increasing frequency observed over recent decades. For the purpose of updating the analysis of extreme sea levels in the north-eastern sector of the Adriatic, the extreme levels recorded at the Venice tide-gauge station were adopted for Grado (Table 3). In this case, a classical Block Maxima approach was applied using the Gumbel distribution. Unlike the methodology adopted for Trieste, the observed sea level was treated according to the formulation proposed by Pugh and Vassie (1978), without explicitly decomposing the signal into astronomical tide, meteorological contribution, and mean sea-level components. As discussed above, the application of extreme value models requires the sea-level time series to be made as stationary as possible. This condition is a fundamental prerequisite to ensure the statistical validity of the adopted distributions (GEV, GPD) and, consequently, also of the classical Gumbel formulation within the Block Maxima (BM) framework. Accordingly, for Grado, unlike Trieste, the reference levels above which extreme values are defined were obtained through a detrending procedure relative to a specific reference year, selected as a temporal centroid. A sea-level rise rate representative of the most recent mean sea-level trend was then applied to account for the ongoing increase in mean sea level. In parallel, trends in mean sea level and in recorded maximum sea levels from the Grado tide-gauge station were compared over the 1991-2023 period. This allowed the hazard associated with extreme peak levels to be evaluated in relation to event duration. Subsequently, a downscaling analysis of impacts on the urban fabric was carried out by subdividing the town into sectors characterized by different levels of vulnerability. Based on LiDAR surveys, a high–spatial-resolution digital terrain model (DTM) was derived and used to simulate flooded areas through a static bathtub approach implemented in ESRI ArcGIS Pro 3.1.0. This procedure enabled the assessment of both flood extent and exposure of the urban context to inundation risk. The developed scenarios therefore address, first, individual episodic (short-term) events using updated threshold levels, and subsequently episodic events combined with projected sea-level rise (long-term) for 2050 and 2100, based on the latest IPCC Sixth Assessment Report (AR6, 2021). Finally, considering the current defensive conditions of the site –which do not fully guarantee protection against water ingress during surge events– preliminary mitigation and adaptation measures were also outlined at a conceptual level.

4.2.1 Tide gauge data processing and quality control

For the statistical characterization of extreme sea levels at Grado, along the Friuli Venezia Giulia coastline, tide-gauge records from the Grado and Venice stations were selected (Table 3). Prior to the application of the statistical analysis methods described in the

following sections, the datasets were subjected to preliminary quality control and temporal consistency checks.

Site	Station Name	Latitude (°)	Longitude (°)
Venice	RMLV	45° 25′ 50.49”	12° 20′ 11.97”
Trieste	Molo Sartorio	45° 38′ 50.00”	13° 45′ 33.90”
Grado	RMLV	45° 40′ 59.26”	13° 23′ 00.38”

Table 3. List of tide gauges in the northern Adriatic considered in this study.

The first operation concerned the data recorded by the Venice tide gauge and made available by the Centro Previsioni e Segnalazioni Maree of the Municipality of Venice (https://www.comune.venezia.it/it/content/grafici-e-statistiche). The values provided by the institution were not subjected to additional in-depth quality control, as this step was aimed at extracting the annual maximum sea levels recorded in Venice over the 1950-2023 period and subsequently calibrating them for the Grado site. The adopted approach is described in detail in Section 4.2.3.1.

For both Venice and Grado, sea-level observations are referred to the Zero Mareografico di Punta della Salute, which corresponds to the national vertical reference of the Italian Altimetric Network established in 1897 and lies 23.56 cm below the present mean sea level (https://www.comune.venezia.it/it/content/riferimenti-altimetrici). These values were then converted to the national vertical datum of the Istituto Geografico Militare (Genova, 1942), commonly referred to as IGM42. In contrast, sea-level data recorded at Trieste are referenced to the ZIT (Zero Istituto Talassografico) and subsequently converted to the IGM42 datum.

4.2.2 SLR rate detrending approach

The detrending approach adopted in this study differs from that applied for Trieste. In this case, detrending was applied exclusively to the extreme sea levels estimated for the city of Grado, derived from the Venice tide-gauge record (ZMPS). This approach is based on a sufficiently long time series of annual maxima (1950-2023) and involves a calibration that accounts for sea-level rise. Specifically, the mean sea level is computed over a selected temporal window representative of the most recent trend (here 1996-2023), and the resulting rate is then applied to the annual maximum levels extracted year by year. Subsequently, a temporal barycentre reflecting recent conditions is identified. In this study, the detrending of the full series of annual maxima was performed by adjusting all values to the reference barycentre year 2006. Accordingly, the estimated sea-level rise rates are subtracted from values corresponding to years after the reference period and added to those before it, consistently with the observed trend of the historical series.

4.2.3 Grado extreme analysis

The definition of the reference mean sea level and the subsequent detrending procedure represent an essential step to ensure data stationarity. Once the time series has been cleared of slow-varying components and long-term secular trends, it is possible to proceed with the application of statistical methodologies for the analysis of extreme values for the town of Grado.

4.2.3.1 Gumbel - Block Maxima (BM)

The extreme sea-level data were derived from records of the Venice Lagoon Meteo-Mareographic Network (RMLV), referenced to the Zero Mare Punta della Salute 1897 datum (ZMPS). The historical series from 1950 to 2023 was analysed to assess the probability of severe sea-level events. Given the long temporal coverage, the analysis was simplified by adopting the Gumbel distribution, a specific case of the Generalized Extreme Value (GEV) family, using the Block Maxima (BM) approach (Coles, 2001) to extract annual maxima over uniform time intervals. The availability of more than 70 years of observations provides a sufficiently large sample of annual maxima to support a statistically robust application of the GEV-BM framework. As shown by Caruso and Marani (2022), the GEV-BM method applied to the long Venice time series yields low estimation uncertainty for return periods up to approximately 100 years, particularly when long calibration windows are used. Moreover, from a risk-management perspective, the moderate overestimation of return levels by the GEV-BM approach in the short- to medium-return-period range identified by Caruso and Marani (2022) can be regarded as conservative, providing an additional safety margin for applications such as coastal risk assessment and infrastructure planning, as in the case of Grado. Annual maximum sea-level values exceeding 110 cm, referenced to the ZMPS datum, were extracted from the time series. Data for the period 1950-2020 (prior to the activation of the Venice Lagoon closure system, Mo.S.E.) were obtained from the Centro Previsioni e Segnalazioni Maree of the Municipality of Venice, while data from 2021 to 2023 were provided by the same institution but recorded offshore of Venice by the ISMAR-CNR Acqua Alta Oceanographic Platform during Mo.S.E. operation. The subsequent step consisted of calibrating the analysed historical series to account for sea-level rise (SLR). An SLR rate of approximately 2.5 mm/yr was adopted. This reference rate was derived from the 1996–2023 period in order to capture the most recent trends, based on the local tide-gauge record of Trieste (Table 3), expressed with respect to the national vertical datum IGM42 (Genova 1942). The extreme-value analysis adopted 2006 as the reference year, within a baseline period spanning 1995-2014, consistently with the latest IPCC report (Masson-Delmotte et al., 2021), which is representative of recent conditions. A detrending procedure was therefore applied to the full historical series (1950-2023), adjusting all values relative to 2006 as the temporal barycentre of the reference period. Accordingly, the SLR contribution was subtracted from years following the reference period and added to years preceding it, in line with the long-term trend observed over 1950-2023. The resulting sample of extreme values was then subjected to statistical inference to estimate the parameters of the Gumbel distribution (Gumbel, 1958). The data were ranked in descending order and, for each m-th observation, the non-exceedance probability was computed using the Gringorten plotting-position formula (Goda, 1988). Parameter estimation was subsequently performed using the least-squares method. Once the non-exceedance probability function was defined, and given its direct relationship with the return period, it was possible to estimate the extreme sea-level value associated with a given R_P. Finally, the derived thresholds were converted to the national IGM datum by subtracting 23.56 cm from values originally referenced to ZMPS.

4.2.3.2 Annual exceedance of flooding threshold

he analysis first evaluated the mean SLR trend for Grado in relation to the duration of exceedances of the previously updated extreme thresholds. Sea-level records from the Grado tide gauge (Table 3), referenced to the ZMPS datum, were retrieved from the ISPRA database. The dataset is available from 1991 onward and was sampled at 10-minute intervals until 2019 and at 5-minute intervals from 2020 to 2023. All records were subsequently converted to the national IGM datum by subtracting 23.56 cm from values referenced to ZMPS. The mean sea-level trend was then compared with the evolution of the maximum levels recorded at Grado, in order to assess whether an increase in extreme events is also evident, as reported by Caruso and Marani (2022). After comparing the trends, the analysis focused on event duration, so as to retain only exceedances associated with a potentially significant impact. Specifically, the analysis was carried out by jointly evaluating the maximum levels reached and their persistence in time, accounting for the total number of observations available for each year. The flooding threshold was defined in terms of cumulative exceedance duration at the 99.96th percentile of the distribution, corresponding to approximately 0.04% of the total time, i.e., about 3 hours.

4.3 Assessment of extreme events in Trieste: methodological setup

The theoretical framework outlined in the previous section is here applied to the northern Adriatic sector, with specific reference to the Trieste tide-gauge station. This section describes the datasets used, the quality-control procedures adopted, the detrending techniques applied to ensure signal stationarity, and finally the use of the GEV-BM and GPD-POT distributions for estimating extreme sea levels and their associated return periods.

4.3.1 Tide gauge data processing and quality control

For the statistical characterization of extreme sea levels along the Friuli Venezia Giulia coastline, tide-gauge data recorded at the Trieste station (Table 3) were selected. As in the previous cases, the station data were subjected to preliminary quality-control and temporal-consistency checks prior to the application of the statistical analysis methods described in the following sections. After completing the analyses for Venice and Grado, additional preliminary and quality checks were carried out on the data recorded by the Trieste tide gauge. This step was necessary because most of the statistical analyses and the comparisons among the different methodologies adopted to derive updated extreme sea-level estimates were based on observations from this station. This choice is motivated by the fact that Trieste not only provides one of the longest available tide-gauge records, but also represents the only station within the study area capable of supplying the temporal coverage required for robust statistical analyses. In this context, the Trieste sea-level record is therefore assumed to provide the most reliable representation of extreme sea-level dynamics in the eastern sector of the northern Adriatic. The Trieste tide gauge is located at Molo Sartorio and is operated by the Institute of Marine Sciences (ISMAR) of the National Research Council (CNR). Sea-level records are available at hourly frequency (Raicich, 2003). The historical time series considered in this study spans from 1 January 1939 to 31 December 2024 and includes approximately 753398 hours of data. Of these, about 490

hours correspond to missing values, as reported in Table 4. The choice of the temporal interval adopted for the analysis is based on the previous work carried out by Tomasin and Pirazzoli (2009). This allows a direct comparison between the statistics derived from the historical series used in their study (1939-2006) and the updated dataset extended to 2024.

Quality control was performed to assess the consistency and validity of the data acquired at the Molo Sartorio tide-gauge station in Trieste. Preliminary quality checks were carried out following the guidelines of the European Sea Level Service (Garcia et al., 2007). According to this framework, the adopted procedure includes the following steps:

- ensure regularity and continuity of the time series.
- verification of gaps within the series (Table 4); assessment of seasonal gaps that may affect the statistics of the surge component; evaluation of data coverage through linear interpolation between consecutive observations over short intervals. In this case, gap filling for Trieste was applied only for gaps ≤ 2 hours.
- detection and verification of anomalous spikes.
- The application of the stationarity test aimed at identifying sequences of consecutively repeated values was carried out in accordance with the guidelines reported in the *Manual of Quality Control Procedures for Validation of Oceanographic Data* (IOC, 1993) and subsequently adopted in the *IOC Manuals and Guides No. 83* (IOC, 2020). A quality flag will be assigned to samples that show no variation for a number of time steps greater than that considered compatible with natural sea level variability, as such situations may indicate a sensor blockage or acquisition anomaly.

	1945	1954	1960	1961	1965	1966
Lak data	162 1.85%	78 0.89%	38 0.43%	41 0.47%	96 1.09%	75 0.85%

Table 4. Total number and percentage of missing data from 1939 to 2024 for the Trieste Molo Sartorio station.

In the present case, since the Trieste tide-gauge time series is sampled at hourly intervals, the original threshold of 12 consecutive samples (recommended for 10-minute data, equivalent to 2 hours of constant measurements) was converted into an equivalent temporal limit of 2 hours, corresponding therefore to 2 consecutive hourly samples. Spikes within the hourly time series for Trieste (1939-2024) were identified by applying two complementary algorithms, described below. The first is the delta check, used to detect levels affected by anomalous variations relative to the immediately preceding and subsequent records, considering the following relationship:

$$|\chi_{T-1} - \chi_T| > \tau_T \text{ e } |\chi_T - \chi_{T+1}| > \tau_T$$

τ_T = tolerance threshold calculated as:

$$\sigma_T = 0.58 \cdot 3 \cdot \sigma_T \cdot \sqrt{T}$$

as proposed in the *Handbook of Automated Data Quality Control Checks and Procedures* of the National Data Buoy Center (NDBC, 2003). In this formulation, σ represents the

Finanziato dall'Unione europea NextGenerationEU | Ministero dell'Università e della Ricerca | Italiadomani PIANO NAZIONALE DI RIPRESA E RESILIENZA | UNIVERSITÀ DEGLI STUDI DI TRIESTE

standard deviation of the sample and *T* the sampling interval, expressed in hours. In the specific case of Trieste, with hourly sampled data and a global standard deviation of 0.306 m, the resulting tolerance threshold is equal to 141.1 cm. No samples exceeded this value, indicating the absence of impulsive-type spikes in the dataset. For a more refined validation, a second control was therefore applied based on cubic smoothing splines (csaps, p = 0.999) and on the analysis of residuals with respect to the smoothed curve. Points with residuals exceeding 5σ (σ=11.34 cm, threshold=56.7 cm) were identified as outliers and subsequently corrected through local linear interpolation, limited to sequences of three consecutive samples or fewer. Overall, the algorithm identified 9 anomalous values out of a total of 753398 observations, without loss of valid data. The Jarque-Bera and Lilliefors tests, although indicating a statistical deviation from normality ($p<0.001$), confirm in practical terms the correctness of the despiking process, as the residuals are symmetric, exhibit constant variance, and show no significant autocorrelation.

4.3.2 Sea level rise detrending approach

For the purpose of updating the analyses of sea-level extremes in the north-eastern sector of the Adriatic Sea, the historical sea-level series recorded at the Trieste Molo Sartorio tide gauge from 1939 to 2024 was considered (Table 3).The selected and subsequently discussed approach is based on a comparison among the main statistical methodologies commonly used in the northern Adriatic. The first analysis refers to the method applied by Tomasin and Pirazzoli (2009) for the Trieste station, using the historical series from 1 January 1939 to 31 December 2006. In this case, a purely statistical treatment was carried out through the GEV–Block Maxima (GEV-BM) methodology applied to the recorded annual maximum levels. The resulting values are reported in Table 2b, with reference to the total water levels. Subsequently, this methodology was compared with the values obtained using the GPD-POT approach, following the criterion applied by Caruso and Marani (2022) for Venice and adapted to the Trieste context. The third and final purely statistical approach refers to the methodology proposed by Ferrarin et al. (2022) and Ragno et al. (2023). This criterion integrates a physical–statistical framework based on the decomposition of the different drivers of sea level, such as the tidal component and the non-tidal residual, and on the use of multivariate copulas to model their non-linear interactions. All three approaches were implemented in MATLAB, using state-of-the-art and advanced toolboxes specifically developed for generalized extreme-value distributions and harmonic analysis. In general, all the analysed approaches rely on the following definition of the observed sea level Z_T, expressed as the sum of three main components (as described by Pugh & Vassie, 1978):

$$Z_T = \mathrm{msl}_{(t)} + X_{(t)} + \Upsilon_{(t)}$$

where:

$\mathrm{msl}_{(t)}$ = mean sea level (including both the long-term component and the slow variations related to the local datum, such as subsidence or uplift).

$X_{(t)}$ = deterministic tidal components.

$\Upsilon_{(t)}$ = meteorological component, or stochastic surge residual.

Such a decomposition represents the fundamental basis for the development of the method proposed by Tomasin and Pirazzoli (2009), following the application of an annual harmonic

fit to the main tidal constituents and a detrending with respect to the annual mean sea level, as well as for the method of Caruso and Marani (2022), who adopt a direct approach based on the sum of the tide and surge components. The method proposed by Ferrarin et al. (2022) also relies on a similar criterion, albeit modified in some aspects, as will be described below. Before applying the statistical methods aimed at extracting extreme sea-level values, it is essential to introduce a key concept for the correct analysis of extreme-level variability: detrending. The first step requires the definition of a mean sea-level reference against which variations in extreme levels can be measured. As explained in the previous paragraph, the observed sea level Z_T can be decomposed into three main contributions $\mathrm{msl}_{(t)}$, $\mathrm{X}_{(t)}$ and $\Upsilon_{(t)}$ (Pugh & Vassie, 1978; Dixon & Tawn, 1999). As observed by Dixon and Tawn (1999) and more recently by Caruso and Marani (2022) for Venice, the application of extreme value models requires that the analysed sea-level series be made as stationary as possible over time. This condition represents a fundamental prerequisite to ensure the statistical validity of the GEV and GPD distributions, which assume that the data originate from a process with probabilistic characteristics that are invariant over the analysed period (Coles, 2001). In this context, it is necessary to remove from the observed signal the long-term component, namely the mean sea level $\mathrm{msl}_{(t)}$, which incorporates both the secular trend associated with eustatic rise, steric effects and local subsidence, as well as slow variations of the vertical datum. Pugh and Woodworth (2014) emphasize that this operation allows the stochastic part of the signal, composed of meteorological oscillations, to be isolated, thereby making the residual series more suitable for extreme value analysis and for the estimation of return levels. This implies that failing to remove the secular trend and/or interannual or seasonal fluctuations may render sea level a non-stationary process, for which the statistical extraction of extremes is not constant over time (Dixon & Tawn, 1999). Non-stationarity may therefore lead to (i) an overestimation of extremes and, consequently, to a distortion in the estimation of return periods (Méndez et al., 2007), and (ii) biased parameter estimates in GEV or GPD models, which by definition assume stationarity (Coles, 2001). This issue is particularly relevant in the Northern Adriatic, where the reference sea level may exhibit variability across multiple temporal scales. As observed by Tomasin and Pirazzoli (2009), Ferrarin et al. (2022), and more recent basin-scale analyses in the Mediterranean, such oscillations may be linked to eustatic rise driven by global warming and to local subsidence, resulting in a positive long-term trend. Moreover, as analysed by Valle-Levinson et al. (2021) and Ferrarin et al. (2015) in the context of the Venice Lagoon and the northern Adriatic, interannual and interdecadal oscillations associated with luni-solar activity are present, modulating the amplitude of the astronomical tide and, consequently, mean sea-level fluctuations. In addition, meteorological variability –such as Bora wind events at the northern Adriatic microscale– can generate higher or lower mean sea levels depending on seasonality and exposure to the forcing. Therefore, in order to remove the influence of these factors, isolate short-duration level variations (e.g., surge, seiches), and thus achieve the stationarity required by EVT, a detrending operation must be applied. This consists of removing an estimate of the time-varying mean sea level $\mathrm{msl}_{(t)}$ from the observed sea level Z_T recorded by the tide gauge. In this way, fluctuations are analysed relative to a consistent mean reference level. In the following analyses, mainly based on studies carried out at the

Finanziato dall'Unione europea NextGenerationEU
Ministero dell'Università e della Ricerca
Italiadomani PIANO NAZIONALE DI RIPRESA E RESILIENZA
UNIVERSITÀ DEGLI STUDI DI TRIESTE

scale of the northern Adriatic, two application approaches were considered for the detrending procedure described above:

- the annual mean sea level, following the approach adopted by Tomasin and Pirazzoli (2009) and, in part, by Caruso and Marani (2022).
- the 19-year moving average, associated with the lunar nodal cycle of 18.61 years (Valle-Levinson et al., 2021; Caruso and Marani, 2022; Ferrarin et al., 2022).

The two approaches lead to slightly different results in the detrended series, as will be discussed in the Results and Discussions section.

4.3.2.1 Annual mean sea level detrending

The first application considers the approach adopted by Tomasin and Pirazzoli (2009) and concerns detrending with respect to the mean sea level calculated on a yearly basis. For each year, the average of the observed hourly sea levels is first computed and then subtracted from all hourly values belonging to the same year. As will be discussed later, the two authors refine this approach by reconstructing the astronomical tide for each year through harmonic analysis using the seven main tidal constituents (M_2, S_2, N_2, K_2, K_1, O_1, P_1 from Stravisi e Purga, 1997). In this way, extremes are represented as purely meteorological anomalies relative to the mean sea level and the tide of that year. By contrast, Caruso and Marani (2022) choose not to separate surge and tide, but instead analyse the extreme sea level as a whole above the annual mean sea level, combining tidal and meteorological fluctuations. Compared to the approach of Tomasin and Pirazzoli, the choice adopted by Caruso and Marani offers several advantages: (i) it reduces secular effects governed by eustatism and subsidence; (ii) annual maxima retain interannual and decadal oscillations of mean sea level (e.g., the lunar nodal cycle); and (iii) from the perspective of coastal defence planning and management, all extremes are referenced to a mean sea level. This procedure was also adopted by Baldan et al. (2022) in the comparison between GEV and GPD models applied to the Venice tide-gauge series. The authors show that this detrending procedure, compared to the use of non-detrended sea-level data, significantly reduces residual non-stationarity and improves the coherence of the estimated parameters, yielding more conservative and robust estimates of extreme sea levels and the corresponding return periods. In conclusion, detrending with respect to the annual mean sea level emphasises deviations of sea level during storm surge events relative to the average conditions of the corresponding year. In this sense, it provides a physically intuitive and statistically stable representation of the meteorological component of the total sea-level signal.

4.3.2.2 19-years mean move detrending

This second approach is based on the use of a 19-year moving average, selected to define the reference mean sea level (Pugh & Woodworth, 2014), in relation to the lunar nodal cycle (18.61 years), which is responsible for modulating, over long timescales, the amplitude of the main tidal constituents. A 19-year average tends to remove all long-period tidal components from the mean sea-level signal (Woodworth, 2012). This approach makes it possible to obtain a more stable “climatic mean sea level”. As demonstrated by Valle-Levinson et al. (2021) in the Northern Adriatic, low-frequency variations in mean sea level

Finanziato dall'Unione europea NextGenerationEU
Ministero dell'Università e della Ricerca
Italiadomani PIANO NAZIONALE DI RIPRESA E RESILIENZA
UNIVERSITÀ DEGLI STUDI DI TRIESTE

can be expressed as a combination of harmonic constants associated with lunar cycles (from 8.85 to 18.61 years) and the solar cycle (generally 10-11 years), as well as the interferences they generate. Valle-Levinson et al. (2021) highlight that using a temporal window on the order of 20 to 30 years is particularly suitable for filtering out slow astronomical oscillations from mean sea level, while retaining in the residual signal the variability of mean sea level at interannual and/or interdecadal scales. A similar concept is also discussed by Orlić et al. (2018) and subsequently adopted in the study by Ferrarin et al. (2022) in the context of non-stationary extreme sea-level analysis. The applied procedure can be described as follows. Starting from the observed hourly sea-level values, the annual mean sea level was first computed. Subsequently, for each year, a 19-year centred moving average was calculated, appropriately adjusting the boundaries at the beginning and end of the reference time series. Finally, the corresponding 19-year moving-average value was subtracted from the hourly sea-level observations belonging to the selected year. In this way, a detrended series was obtained that represents sea-level deviations with respect to a climatic baseline, rather than with respect to the annual mean sea level alone. This approach was adopted by Ferrarin et al. (2022) to extract extreme sea-level values for Venice. Baldan et al. (2022) compared the 19-year moving-average approach with detrending relative to the annual mean sea level, showing that in both cases the stationarity of the series improves. However, the multi-decadal moving-average approach provides more consistent results when dealing with non-stationary models and long-term projections. The resulting value represents the deviation of sea level with respect to a long-term baseline, which incorporates both the secular trend of sea-level rise and decadal to multi-decadal oscillations (Haigh et al., 2011; Bult et al., 2024), associated with luni-solar cycles (Valle-Levinson et al., 2021), as well as potential variations related to morphological changes (Ferrarin et al., 2022). With regard to the subsequent statistical extraction of extreme sea-level values, the use of a multi-decadal moving average acts as a form of low-pass filter on the sea-level signal. This is because slow-varying trends are absorbed by the selected moving average, while the resulting detrended series preserves variability at the annual scale driven by the coupling between tide and surge. In this sense, extreme sea levels become “climatically homogeneous”, as demonstrated by Ferrarin et al. (2022). From the perspective of stationarity –a key statistical assumption for the application of Extreme Value Theory (EVT)– this approach is consistent with the recommendations of Coles (2001) and Dixon and Tawn (1999) for the application of extreme value models.

4.3.2.3 Detrending and drivers of sea level

Trieste's time series from 1939 to 2024 was treated to guarantee the signal's temporal regularity and climatic uniformity. A monotonic cubic interpolation technique was used to interpolate hourly data (Ferrarin et al., 2022). The next phase involved using a detrending process based on a 19-year centered moving average that was in line with the previously described lunar nodal cycle. This method eliminates the multidecadal variability, subsidence effects, and secular sea-level component related to luni-solar cycles. This process makes the extreme-event signal "climatically homogeneous," according to Pirazzoli et al. (2007).
Harmonic analysis was carried out once the detrended series was acquired. The detrended series was subjected to a least-squares harmonic analysis using the UTide toolbox created by Codiga (2011) in order to extract the harmonic component from the overall observed sea level. Diurnal, semidiurnal, and long-period oscillations were among the maximum of 68 tidal

elements that were taken into account. In accordance with Ferrarin et al. (2022), a 19-year moving window was used in the analysis to capture probable tidal oscillations associated with astronomical and nodal variability, anthropogenic changes (such as port infrastructure and coastal urbanization), and possibly local morphological changes.
After obtaining the astronomical tidal component, the Non-Tidal Residual (NTR) component has to be extracted. A preliminary study of the reconstructed harmonic tide was done to guarantee a precise separation between the astronomical tide and the non-tidal residual. Despite the reconstruction's great accuracy, it has a low-frequency residual (about >72 h) that can be attributed to noise, other interactions, and delayed changes in harmonic parameters. To prevent distortions in the total NTR, this low-frequency part must be eliminated before deducting the tidal component from the detrended signal.
In order to achieve this, the traditional Godin filter (24-24-25 h), which is frequently utilized in tide-gauge applications (Godin, 1972; Pugh, 1987), was first used. Frequency-domain analysis, however, revealed that this filter was insufficiently selective for the case study under consideration. Specifically, it introduced amplitude distortions in the main tidal harmonics (K1, O1, M2, S2) and partially attenuated diurnal and semidiurnal oscillations, making it unsuitable for a refined decomposition of the NTR signal, according to the methodology used by Ferrarin et al. (2022). A FIR sinc–Kaiser high-pass filter with a pass-band ≥ 72 h and a stop-band ≤ 36 h was developed and calibrated to get around these restrictions (see https://tomroelandts.com/articles/how-to-create-a-configurable-filter-using-a-kaiser-window; acknowledgements to Dr. Raicich, CNR-ISMAR Trieste). The complementary high-pass component served as the "pure" astronomical tide, and the filter was applied while maintaining the gaps in the data that already existed (see Table 4). The variance budget and the strong connection with the tidal signal recovered by UTide both support the result's physical correctness.

A targeted harmonic fit was carried out directly on the NTR for the O1, K1, N2, M2, and S2 constituents, eliminating any spurious contribution related to each frequency in order to remove any remaining traces of the primary tidal harmonics inside the NTR. The energetic contribution of various tidal parts was significantly decreased in this instance (for example, the false M2 component was reduced by almost 98%). Therefore, in order to produce a very clean tidal component and a physically consistent NTR that are completely compatible with the decomposition and multivariate analysis approach created by Ferrarin et al. (2022) and modified here for the Trieste case study, the Kaiser filter must be applied.
At this point, the detrended NTR, which had been cleared of astronomical residuals, was broken down into a number of physical components according to their distinctive frequency ranges, using the method suggested by Ferrarin et al. (2022) and modified for Trieste. Fourth order IIR Butterworth filters (high-pass, low-pass, and band-pass) were used to perform the decomposition in the time domain while taking into consideration the existence of gaps in the otherwise continuous hourly series. In particular, the following elements were separated: (i) a high-frequency component (<10 h), accounting for the combined effects of meteotsunamis and local set-up; (ii) a storm surge component with periods between 10 h and 10 days, obtained after removal of seiche oscillations; (iii) two Adriatic seiche contributions centred on the fundamental modes at approximately 21.8 h and 10.7 h; (iv) a low-frequency PAW surge component (10-120 d), associated with the barotropic response of the Adriatic Sea to atmospheric forcing on synoptic and sub-seasonal scales; (v) an IDAS

Finanziato dall'Unione europea NextGenerationEU
Ministero dell'Università e della Ricerca
Italiadomani
UNIVERSITÀ DEGLI STUDI DI TRIESTE

component with periods longer than 120 days, representing the residual inter-seasonal and multi-annual variability not explained by the 19-year moving mean.
The application of a declustering method was the final preliminary step. In this instance, events were identified using the independence criterion adopted by Ferrarin et al. (2022), in contrast to common approaches in the literature that sought to ensure temporal independence between extreme events by imposing a fixed separation (e.g., 78 hours between events; Masina and Ciavola, 2011, or 72 hours; Caruso and Marani, 2022). The hourly data were subsampled for the full historical period from 1939 to 2024 in order to produce uniformly distributed "high" and "low" water levels. In accordance with the semidiurnal tidal regime typical of the northern Adriatic, this was accomplished by applying a 6-hour filter each day, producing about two high-water and two low-water values each day (Ferrarin et al., 2022). For the years 1939-2024, a total of about 119820 values were found.

4.3.3 Sea level dynamics statistical analysis

Both the time evolution of extreme values and the dependent mechanisms governing the combination of the various components regulating marine dynamics must be taken into account in the statistical study of extremes. In order to do this, it is essential to analyse the existence of non-stationarity on multi-decadal scales in order to confirm if extremes show consistent fluctuations over time. Simultaneously, because astronomical and meteorological components do not occur independently in the northern Adriatic (Tomasin and Pirazzoli, 2009), it is crucial to measure the kind and intensity of their non-linear interactions, particularly during the most intense episodes. The purpose of these two analyses is to provide an additional essential component for both accurate probabilistic calculation of extreme sea levels and a thorough characterization of severe variability.

4.3.3.1 Non stationary analysis

The levels corresponding to the 99th percentile was subjected to a non-stationarity analysis in order to confirm the potential existence of trends in extreme sea levels between 1939 and 2024. The non-tidal residual (NTR) was further broken down into its primary meteorological and climatic components, storm surge and seiches (short-term variability) and longer-scale contributions like PAW surge and IDAS, after the astronomical contribution (tide) was separated from the NTR. In accordance with the method suggested by Orlić et al. (2018), which enables the isolation of slow and decadal fluctuations in extreme sea levels in the Adriatic, the diagnosis of non-stationarity was carried out by applying a centered 30-year moving average to the 99th percentiles. Ferrarin et al. (2022) used and modified the same methodological framework for the Venice site. As a result, the studies that follow are based on Ferrarin et al. (2022)'s methodology, which was tailored to the Trieste case study.

4.3.3.2 Non linear interactions Tide-NTR

An additional analysis concentrated on the non-linear interaction between these two factors, which are crucial to the North Adriatic, in order to thoroughly examine the behavior between the tidal component and the NTR contribution. Because of the basin's semi-enclosed shape and the existence of persistent free oscillations like seiches, which frequently coincide with extreme weather events, it can be difficult to distinguish between tide and surge in this situation (Tomasin & Pirazzoli, 1999; Canestrelli et al., 2001; Pirazzoli & Tomasin, 2007). Because of this feature, the North Adriatic is an environment where the assumption of independence among sea-level components is frequently invalid, especially in severe

circumstances. Previous research has demonstrated that, depending on the true dependence structure in the data, assuming independence between astronomical tide and surge (an assumption underlying Joint Probability Method formulations) may result in either an overestimation or an underestimation of extreme sea levels (Pugh & Vassie, 1979; Pirazzoli et al., 2006; Tomasin & Pirazzoli, 2007). When tide and NTR have a positive association, combined extremes tend to be amplified, raising the likelihood that high values in both components may co-occur. On the other hand, compared to the independent situation, a negative reliance may produce a compensatory impact that considerably lowers extreme levels (Ferrarin et al., 2022; Ragno et al., 2023). Numerous studies have demonstrated the existence of substantial tidal–residual interactions within the North Adriatic's shallow-water environment, even if these interactions are not always contiguous in space and time. In this sense, Tomasin & Pirazzoli (2007, 2009) demonstrate that these interactions significantly contribute to the non-linearity of recorded extreme sea levels when paired with the seasonality of meteorological occurrences. As a result, tide and surge may have reciprocal effects, producing more noticeable extreme levels that frequently happen during low tide or just before a high-tide phase (Williams et al., 2016). In a similar vein, Ferrarin et al. (2022) emphasize that a joint study of sea-level components, conditioned on extreme occurrences, reduces distortions associated with simplified independence assumptions by isolating the effective contribution of dynamic dependencies. Given these results, a copula-based method was used to analyse the non-linear dependence between the tidal component and the non-tidal residual (NTR), which enables the dependence structure to be modelled independently of the marginal distributions. The use of copulas is driven by the possibility that extreme sea levels may be overestimated or underestimated if tide and NTR are assumed to be independent (Tomasin & Pirazzoli, 2009; Ferrarin et al., 2022). The copula formalism (Sklar, 1959; Nelsen, 2006), which allows the marginal distributions to be modelled independently from the joint dependence structure between variables, serves as the foundation for the multivariate analyses carried out in this paper. Because it overcomes the simplifying assumption of independence that is frequently used in classical approaches, this framework is especially well suited to the analysis of extreme sea levels because it enables the effect of dependence and/or independence among the various contributions to total sea level to be explicitly quantified.

The methodology was expanded to evaluate the dependence between the variables involved, particularly between the astronomical tidal component and the non-tidal residual (NTR), in a manner similar to that of Ragno et al. (2023). Non-parametric measures were used to examine dependence, with special reference to Kendall's rank correlation coefficient τ (Kendall, 1938), which enables the identification of dependence structures even in the presence of asymmetries and non-linear correlations typical of extreme events. The use of copula-based models in the ensuing modelling stage is justified by the existence of statistically significant dependence. Following the method used by Ferrarin et al. (2022) for Venice, a bivariate copula was fitted to characterize the relationship between tide and NTR after the existence of dependence was confirmed. In particular, percentile criteria of the detrended sea-level series (99th, 99.5th, and 99.9th), specified throughout the whole period from 1939 to 2024, were used to identify extreme sea-level values. According to Ferrarin et al. (2022), the reference time series was sampled at high- and low-tide instants to reduce false dependence between the forcings and produce a representation consistent with tidal oscillations. Thus, astronomical tidal maxima and minima with a temporal gap of roughly 6 hours were identified using a declustering approach, which is compatible with the

Finanziato dall'Unione europea NextGenerationEU
Ministero dell'Università e della Ricerca
Italiadomani PIANO NAZIONALE DI RIPRESA E RESILIENZA
UNIVERSITÀ DEGLI STUDI DI TRIESTE

semidiurnal tidal regime typical of the northern Adriatic (Ferrarin et al., 2015). The time intervals at which sea level surpasses the thresholds of the chosen extreme-level dataset were thus designated as extreme events. A “t” copula was used to represent the dependence structure, and the marginal distributions of the examined forcings were obtained empirically. The t copula was selected in accordance with the methods described by Ferrarin et al. (2022) and Ragno et al. (2023), where this copula shown efficacy in depicting dependency in the distribution tails. After estimating the copula parameters, 50.000 samples were produced using Monte Carlo simulations to reconstruct extreme sea levels under both independent and dependent assumptions between the two drivers. Non-Linear Interactions (NLI), which are defined as the difference between the extreme level simulated under dependency and that obtained assuming total independence, are used to compare the two scenarios. Finally, the study was expanded to include the application of multivariate copulas to five variables (tide, seiches, storm surge, PAW surge, and IDAS) that are indicative of extreme sea-level pulsations. This method provides a more comprehensive and physically consistent depiction of the mechanisms controlling extreme sea levels in the eastern sector of the northern Adriatic by explicitly modelling the joint reliance among all relevant processes (Ferrarin et al., 2022).

4.3.4 Trieste extreme values analysis

The definition of the reference mean sea level and the subsequent application of detrending represent a crucial preliminary step to ensure the stationarity of the analysed signal. Only once a time series free from slowly varying components and secular trends has been obtained is it possible to proceed with the application of statistical methodologies for extreme value analysis –namely GEV (Generalized Extreme Value) and GPD (Generalized Pareto Distribution)– which require an underlying stationary process.

4.3.4.1 GEV-BM

The first reference methodology is that proposed by Tomasin and Pirazzoli (2009), based on the analysis of annual maxima of sea level and on the application of the GEV-BM distribution. In this study, the full Joint Probability Method (JPM) was not adopted; however, the underlying logical framework of the approach remains analogous. Starting from the hourly time series, the data were detrended with respect to the annual mean sea level, treating the astronomical tide and the surge component separately, in order to analyse extreme total sea-level events relative to their interannual variability. The approach is based on the construction of an hourly time series cleaned from the secular trend and referenced to the annual mean sea level, computed year by year to ensure long-term stationarity. The astronomical tide was reconstructed annually through least-squares harmonic analysis of the main tidal constituents. Seven constituents were considered –four semidiurnal (M2, S2, N2, K2) and three diurnals (K1, O1, P1)– which are deemed sufficient to describe the tidal regime of the northern Adriatic. This criterion allows the harmonic coefficients to be updated annually and accounts for interannual variations related to astronomical and local processes. The meteorological residual was then obtained by subtracting from the observed sea level both the astronomical component and the annual mean sea level, which represents the reference sea-level elevation for each year, thereby removing both tidal effects and long-term variations (e.g. mean sea-level oscillations). Annual detrending ensures that the resulting surge series is stationary and thus comparable over time, avoiding distortions

induced by secular changes in mean sea level. This approach enables a more robust and physically interpretable estimation of return levels of extreme events, as the residual peaks reflect solely the meteorological response of the basin, while the astronomical component is treated separately (Tomasin and Pirazzoli, 2009). The parameters of the GEV distribution were estimated using the Maximum Likelihood Estimation (MLE) method, which identifies the three parameters (ξ, σ, μ) that maximise the probability of observing the sample of annual maxima. This method represents the standard in extreme value modelling (Coles, 2001; Castillo et al., 2005) and provides consistent and asymptotically efficient parameter estimates, particularly given the length of the historical time series analysed.

4.3.4.2 GPD-POT

The second methodology adopted refers to the approach developed by Caruso and Marani (2022), based on the Peaks Over Threshold (POT) framework and on the application of the Generalized Pareto Distribution (GPD) to exceedances of extreme sea levels. Unlike the GEV-BM approach described above, the POT methodology exploits all extreme values exceeding a selected threshold, allowing a more efficient use of the information contained in the hourly time series. This results in a more accurate representation of the tail of the distribution. Compared to the application by Tomasin and Pirazzoli (2009), in this case the hourly series of observed sea levels was detrended according to two different criteria: (i) with respect to the annual mean sea level msl(t), and (ii) with respect to the 19-year moving average (consistent with the approach also adopted by Ferrarin et al. (2022), as discussed in the following section). Both detrending procedures aim to remove the secular component of mean sea level and to obtain a time series that is as stationary as possible, referenced to the local mean sea-level baseline. Starting from these detrended series, independent sea-level peaks were identified through a temporal declustering window of 78 hours, in order to ensure statistical independence between successive events. This choice allows the separation of individual events while accounting for the temporal decay of seiche oscillations following storm-surge events (Masina and Ciavola, 2011). For each cluster, the maximum peak associated with the storm-surge event was retained. Threshold selection, which is a critical step for the application of the GPD, was performed through a detailed analysis of peak percentiles ranging between the 90th and the 99th percentile. The optimal threshold was identified as the one satisfying the following criteria:

Number of exceedances

The choice of the threshold must ensure that the number of exceedances is sufficiently large to allow a reliable estimation of the GPD parameters (Coles, 2001). As reported by Lang et al. (1999) and Scarlett and MacDonald (2012), it is essential to find a trade-off between bias and variance: a small number of exceedances increases the variance of the estimates, whereas a low threshold introduces bias. In the present study, a minimum number of exceedances was selected such that $N \geq 86$, corresponding to the number of years covered by the historical record between 1939 and 2024.

Stability of the shape parameter (ξ)

The shape parameter is fundamental for assessing the behaviour of the tail of the extreme value distribution, determining which events can be classified as rare extremes. In addition, it directly influences coastal risk estimates as a function of the return period (Coles, 2001),

providing physical insight into the environmental context in which extremes occur. In the vicinity of the optimal threshold, ξ should remain approximately constant as the threshold varies, a condition that confirms the correct applicability of the GPD model (Coles, 2001). The analysis of the stability of ξ therefore represents one of the key operational criteria for threshold selection (Lang et al., 1999). Following the guidelines of Scarrott and MacDonald (2012), an empirical tolerance of ±0.05 between adjacent thresholds is adopted, which is considered indicative of numerical stability and is thus used as a quantitative constraint for automatic threshold selection.

Statistical consistency and interpretation

Beyond stability, the shape parameter ξ directly affects the statistical validity of the model and the correct physical interpretation of extremes. Values of ξ >0.5 compromise the regularity of maximum likelihood estimators (MLE), which lose their properties of normality and efficiency (Smith, 1985; Coles, 2001). For this reason, the range ξ ≤0.5 is commonly considered appropriate in extreme value applications. The consistency of the GPD model was further verified using the Kolmogorov-Smirnov (KS) and Anderson-Darling (AD) tests, as well as QQ-plots comparing theoretical and observed quantiles, in order to ensure statistical goodness of fit and robustness of parameter estimation. When these conditions were not satisfied, a conservative threshold corresponding to the 95th percentile was adopted. Both detrended series yielded an optimal threshold corresponding to approximately the 90th percentile, consistently with the results reported by Caruso and Marani (2022) for Venice. Exceedances above the selected threshold were modelled using the GPD, whose shape (ξ) and scale (σ) parameters were estimated via maximum likelihood estimation (MLE). Assuming that the exceedance process follows a Poisson distribution with a constant rate λ over time, return levels for different return periods were then estimated according to the following relationship:

$$RL_T = u + \frac{\sigma}{\xi}\left[(\lambda_u \mathrm{T})^{\xi} - 1\right]$$

where λ_u represents the mean number of events exceeding the threshold per year. The validation of the GPD model was carried out using the Kolmogorov–Smirnov (KS) and Anderson-Darling (AD) tests applied to the normalized residuals, complemented by a visual inspection of QQ-plots. Finally, to verify the stationarity of the underlying signal, the Mann–Kendall (MK) test was applied to the detrended annual maxima with respect to mean sea level; no statistically significant trend was detected (p-value > 0.05). This result confirms the stationarity assumption required for the application of the GPD-POT model and supports the validity of the detrending procedure adopted.

4.3.4.3 Multivariate Statistical Approach

In addition to the univariate approaches based on the GEV-BM distribution (Tomasin and Pirazzoli, 2009) and the GPD-POT framework (e.g., Caruso and Marani, 2022), the physico-statistical approach proposed by Ferrarin et al. (2022) for Venice, and subsequently extended by Ragno et al. (2023), was applied and adapted to the Trieste case study. This methodology aims to quantify the relative contribution of the different physical components of sea level to extreme events and to explicitly model the non-linear dependencies among

them. The underlying concept is that extreme sea-level events are not driven by a single dominant forcing, but rather result from the combination of multiple contributions, such as the tidal component, storm surge, low-frequency oscillations, seiches, and related processes, which may interact in a non-linear manner and generate compound extreme events.

4.3.4.4 Fit validation test

The validity of the statistical models adopted, such as Gumbel BM, GEV-BM and GPD-POT, was assessed through a set of validation procedures, including QQ-plot analyses comparing empirical and theoretical quantiles estimated from the fitted distributions. To complete the validation process, additional goodness-of-fit tests were applied to evaluate the agreement between empirical and theoretical distributions. The first test considered was the Kolmogorov-Smirnov (KS) test (Chakravarti, Laha and Roy, 1967), which is sensitive to overall differences between the empirical and theoretical distributions. The second test was the Anderson-Darling (AD) test (Anderson and Darling, 1952), which places greater emphasis on the tails of the distribution and is therefore more suitable for the assessment of extreme-value models. Finally, predictive performance was evaluated through cross-validation following the approach of Caruso and Marani (2022), and the Mann-Kendall test was applied to assess the presence of any residual trends in the analysed extremes.

Probability integral transform (PIT)

The validation of the GEV-BM model applied to annual maxima was performed following the approach described by Coles (2001) and Majumder et al. (2024), who adopt the Probability Integral Transform (PIT) to assess the consistency between the observed data and the theoretical distribution estimated by extreme-value models. For each annual maximum X_i the transformed value was computed as:

$$u_i = F_{GEV}(x_i|\hat{\theta})$$

where F_{GEV} denotes the cumulative distribution function of the GEV with the estimated parameters θ. If the model is adequate, the values u_i are expected to be distributed as a Uniform (0,1), regardless of the specific form of the GEV distribution. This property allows the application of non-parametric goodness-of-fit tests, such as the Kolmogorov-Smirnov (KS) and Anderson-Darling (AD) tests, which compare the empirical distribution of the PIT values with the theoretical uniform distribution. In the absence of statistically significant deviations (p-value ≥0.05), the GEV-BM distribution can be considered to satisfactorily represent the statistical behaviour of the annual maxima, with no significant departures from the theoretical model.

Cross validation analysis

In addition to evaluating the goodness of fit of the models through QQ-plots and KS and AD tests, it was also considered necessary to assess the *out-of-sample* predictive skill of the extreme value models. To this end, a cross-validation procedure developed by Caruso and Marani (2022) for Venice was applied. The aim is to quantify how reliable the estimation of extreme levels remains when the model is calibrated on sub-samples with different temporal lengths Starting from a total number of available years *M*, a calibration sub-sample of size

Finanziato dall'Unione europea NextGenerationEU
Ministero dell'Università e della Ricerca
Italiadomani
UNIVERSITÀ DEGLI STUDI DI TRIESTE

S is selected. The remaining years, equal to *M−S*, are excluded from calibration and constitute an independent validation period *V*. This procedure is repeated n times, randomly reshuffling the available years at each iteration. For each calibration sub-sample, the model (either GEV-BM or POT-GPD) is estimated and the corresponding theoretical return levels are derived. Similarly, for the validation period, empirical return levels are estimated from the ordered annual maxima using standard plotting position formulations (e.g., Gringorten). The comparison between estimated and observed values is summarized through the Non-Dimensional Error (NDE), a metric that allows the assessment of bias and stability in the estimated return levels. The procedure was applied for different sizes of the calibration sub-sample (S=10, S=20, S=30), enabling an analysis of how the amount of available information affects model performance. Unlike the application by Caruso and Marani (2022), the case S=5 years was not considered due to the insufficient number of extreme values in such short windows, which prevents a reliable estimation of model parameters using the GEV-BM approach. Consequently, larger values of *S*, such as S=30, simulate more favourable calibration conditions. For each value of *S*, the distribution of the NDE obtained from 1000 resampling iterations provides a quantitative indicator of model robustness and of its sensitivity to the choice of the calibration sub-sample. Consistently with Caruso and Marani (2022), in addition to standard return periods ranging from 10 to 50 years, the maximum return period observable within the validation window (*T≈V+1*), corresponding to approximately 57 years for the Trieste series, was also considered. This value allows the synthesis of model performance into a single indicator for each combination of *S*, facilitating a direct comparison between the GEV-BM and POT-GPD approaches and between short and long calibration windows.

Mann-Kendall test

Once the two series detrended with respect to mean sea level were reconstructed, a further aspect becomes important, namely the possible presence of “residual” trends in the analysed annual maxima. The objective is to verify that the extreme values under investigation can be regarded as fully stationary over time, thereby excluding systematic long-term variations that are not attributable to mean sea-level rise. To investigate this aspect, the Mann-Kendall (MK) test (Mann, 1945; Kendall, 1975) was applied. This test is widely used in climatological studies to detect monotonic trends in time series. The MK test evaluates the deviations of annual maxima relative to their reference mean value and allows assessment of whether the temporal evolution exhibits an increasing trend, a decreasing trend, or does not significantly depart from statistical randomness. The application of the Mann-Kendall test therefore makes it possible to verify the robustness of the no-trend assumption in the detrended series and to confirm the validity of the stationarity requirement necessary for the subsequent use of GEV-BM and GPD-POT models in the extreme value analyses.

4.4 Grado vs. Trieste: Sea Level trend comparison

To develop a medium- to long-term projection of relative sea-level rise (RSLR), mean sea level at Grado was analysed for the period 1991-2023. To compare the sea-level data from Grado and assess their significance, the dataset recorded at the Trieste tide-gauge station was used as a reference. The temporal evolution of sea level at Trieste is monitored by CNR-ISMAR and is available through the Permanent Service for Mean Sea Level (PSMSL) database (https://www.psmsl.org/data/obtaining/stations/154.php). The analysed data include both observed sea level and the subsidence component, which represents a critical factor for long-term projections. To enable a long-term assessment, published subsidence estimates by Da Lio and Tosi (2010) and Areggi et al. (2023) were adopted as reference. The subsidence rate for Grado, derived from SAR interferometry and GNSS measurements for the periods 2003-2010 (Da Lio and Tosi, 2010) and 2015-2019 (Areggi et al., 2023), was subsequently compared with the residual obtained from the correlation between sea-level variations at Grado and Trieste. The resulting mean value was then used to generate long-term RSLR projections for 2050 and 2100. Using satellite derived sea-level projections for Trieste provided by the NASA Sea Level Projection Tool (https://sealevel.nasa.gov/ipcc-ar6-sea-level-projection-tool), the RSLR estimates and the tectonic contribution were adjusted through a correction factor averaged over the Grado area. After computing the projected sea-level increases for 2050 and 2100 under ongoing climate-change scenarios, the corresponding reductions in return periods were evaluated for selected significant episodic events. This analysis assessed both the magnitude of flooding and the exposure of the urban environment to flood risk. The considered scenarios focus first on a single short-term episodic event associated with the updated flooding threshold, and subsequently on the same event combined with mean sea-level projections for 2050 and 2100, as described in detail in the Sixth Assessment Report of the IPCC (Masson-Delmotte et al., 2021).

4.5 Downscaling flooding modelling

This chapter presents the modelling methodologies applied to the coastal settings of Grado, Muggia, Trieste, and Lignano. The first section addresses the application of a static modelling approach, namely bathtub modelling, which was applied exclusively to Grado. For the localities of Muggia, Trieste, and Lignano, dynamic models were adopted, specifically MIKE21, considering selected events that have recently occurred along the coastlines of Friuli Venezia Giulia.

4.5.1 Bathtub modelling

Flood risk maps were developed for the urban and territorial context of the city of Grado. A static “bathtub approach” (NOAA, 2012) was applied using a high-resolution Digital Terrain Model (DTM) and the ESRI ArcGIS Pro 3.1.0 software. The objective was to assess the elevations of the city’s perimeter waterfront (Figure 8a) in order to identify critical points with respect to both current water levels and those projected for the future. To analyse the elevation of the lagoon promenade and the perimeter embankment, the following procedure was adopted. First, the Digital Terrain Model (DTM) of Grado, derived from a LiDAR survey conducted in 2018 (courtesy of the Friuli Venezia Giulia Region), was used. The resulting DTM has a spatial resolution of 0.5 × 0.5 m. The resolution of the DEM/DTM plays a key

Finanziato dall’Unione europea NextGenerationEU
Ministero dell’Università e della Ricerca
Italiadomani
UNIVERSITÀ DEGLI STUDI DI TRIESTE

role in determining the reliability of static flooding outputs (van de Sande et al., 2012; Leon et al., 2014; Wolff et al., 2016). A 6-m-wide buffer was generated from the DTM elevations, starting from the outermost section of the promenade –specifically from the portion closest to the water– and extending landward. Given the spatial variability in elevation statistics, the promenade was subdivided into four sectors, as shown in Figure 8b. This approach allowed a detailed analysis of promenade elevations and of the entire embankment system bordering the town on the lagoon side, enabling the identification of both localized critical points and broader area-scale vulnerabilities. The calculation of the elevation value of the extracted cells was necessary in order to obtain information on the mean elevation surrounding each cell, based on a fixed-width buffer. To perform this operation, a GIS analysis tool (*Cell Statistics*, part of the Spatial Analyst extension in ArcGIS Pro 3.1.0) was used, allowing the computation of an average elevation value within a 6 m radius along the entire length of the embankment section under investigation. Finally, to complete the analysis, elevation values at the centre of the previously selected cells were extracted and subsequently subjected to statistical analysis. The analysed elevation points were filtered to exclude negative elevation values exceeding a predefined threshold. To assess embankment heights in relation to extreme events, a range of elevations from 70 cm up to a maximum of 155 cm was considered, depending on the specific sector of the lagoon promenade and/or embankment analysed. The resulting elevations were represented through a graph illustrating cumulative statistics as a function of the considered height intervals, indicating the percentage of embankment remaining safe with respect to the threshold value associated with an extreme event and its corresponding return period. The same downscaling approach, aimed at assessing the condition of the perimeter embankments along the lagoon margin (lagoon promenade) and evaluating the state of the urban waterfront, was also applied to the municipalities of Lignano, Muggia, and Trieste. In these cases, the range of elevations analysed varies according to the local context: from 70 cm to 160 cm for Lignano; from 70 cm to 170 cm for Muggia; and up to 220 cm for Trieste. To represent the effects of storm-surge events through updated water-level thresholds based on trends observed over recent decades, scenarios with different probabilities of occurrence were analysed. The aim of this processing is to produce flood hazard maps derived from extreme events, which serve as a basis for flood risk assessment and management, in accordance with the Floods Directive 2007/60/EC, subsequently transposed into Italian law by Legislative Decree 49/2010. As explained previously (see Section 4.1), the Floods Directive allows reference to extreme events only, subject to an evaluation of the level of protection. Some Italian methodological reports on coastal flooding, such as those produced for the Sardinia region (RAS, update 2018), have pointed out that the lack of a precise regulatory definition of an “adequate level of protection” suggests refraining from making use of this option. Conversely, on the basis of territorial urban planning and civil protection measures –particularly in Emilia-Romagna (Perini et al., 2011; Perini et al., 2012; Perini et al., 2016), a region with coastal physiographic characteristics comparable to those of Friuli Venezia Giulia– an assessment was carried out to estimate the impact of marine events with short return periods, thus focusing on nuisance and therefore recurrent flooding events.

Figure 8. Downscaling area analysis: (a) elevation of the lagoon promenade considered in the study, represented by 10 classes subdivided every 0.10 m of elevation. (b) The subdivision of the promenade and lagoon embankment into 4 macro sectors; the extent of the inhabited area of Grado municipality is also reported, treating the streets as unobstructed surfaces for water flow while omitting buildings and uninhabited areas (from Spadotto et al, 2025).

Accordingly, flood risk maps were produced for return periods (R_P) of 2, 10, 30, and 100 years. The maps were developed by analysing inhabited areas within the administrative boundaries of the municipality of Grado, considering roads as surfaces free of obstacles to water flow and excluding buildings and uninhabited areas. The analysis focused primarily on the historic centre, which exhibits the highest vulnerability, and was extended eastwards. The analysed municipal area of Grado covers approximately 0.96 km².

4.5.2 Dynamic Modelling

Coastal areas, increasingly exposed to the effects of sea level rise and to the intensification of extreme events, require tools capable of complementing statistical analyses with a dynamic assessment of impacts. Numerical modelling (see Section 1.5) today represents an essential support for understanding the non-linear interaction between tide, surge, and waves, as well as for simulating realistic flooding scenarios, even in the presence of defence failures or morphodynamical changes. The use of hydrodynamic and wave models makes it possible to reconstruct, in greater detail, the propagation of the water mass within the urban fabric, identifying pathways of water ingress, flood depths, and flow velocities. For this reason, the present study integrates MIKE21 by ©DHI modelling, applied to different coastal typologies and to various meteomarine events, in order to evaluate the response of coastal urban areas in Friuli Venezia Giulia to the extreme scenarios considered. The MIKE21 by ©DHI package relies on three different modules, each with a specific field of application.

The Spectral Waves (SW) module is a two-dimensional spectral wave model used to simulate and propagate waves from their generation area towards the selected coastal sector. Subsequently, the Flow Model Hydrodynamic (HD) two-dimensional module was employed to simulate widespread flooding, where the main driver is the variation of the hydrodynamic water-level component, neglecting the purely wave-related contribution such as run-up and the subsequent overtopping effect.

4.5.2.1 MIKE21 Spectral Waves module (SW)

The SW module was used to reproduce wave generation, propagation, and transformation, including processes such as refraction, shoaling, breaking, bottom friction, and simple reflection (DHI, 2023a). The model resolution is based on the full spectral formulation of the wave action balance equation, in which the fundamental variable is the directional-frequency wave action spectrum. This formulation allows the representation of the main physical mechanisms governing wave dynamics: energy transfer from wind according to the theory of Janssen (1989, 1991), non-linear wave-wave interactions (approximated using the DIA model by Hasselmann et al., 1985), dissipation due to depth-induced breaking following Battjes and Janssen (1978), white capping dissipation according to the classical formulation of Hasselmann (1974), and bottom friction following Johnson and Kofoed-Hansen (2000). This physically based structure makes the SW module suitable for providing a comprehensive description of wave evolution up to the breaking zone, delivering as output key parameters such as significant wave height (Hs), peak period (Tp), mean wave direction, radiation stress components (Sxx, Syy, Sxy), and wave energy (P).

4.5.2.2 MIKE21 Hydrodynamic module (HD)

The HD module, which is devoted to simulating two-dimensional hydrodynamic circulation and coastal flooding processes, was used in the modelling phase that followed the SW module's propagation of the wave field toward the coastal zones. Under the hydrostatic pressure assumption, the HD model solves the Nonlinear Shallow Water Equations (NLSWE), which are the fully nonlinear formulation of the shallow-water momentum equations obtained from the depth-averaged Navier-Stokes equations. This assumption is true in situations when the velocity fields are primarily horizontal, and the water depth is minimal in relation to the wavelength. These conditions are common in coastal environments, particularly in storm-surge and wave-driven occurrences. The NLSWE are particularly useful in describing processes like run-up, wave-induced set-up, and breaking-driven currents that are characterized by rapid water-level variations and steep wave fronts. They describe a non-dispersive flow regime in which wave propagation speed depends on water depth rather than wave period. The NLSWE are commonly used to predict widespread coastal inundation and offer a strong foundation for hazard assessment under extreme events because of their numerical robustness and capacity to precisely replicate wave kinematics inside the surf zone. (RAS, update 2018; DHI, 2023b). These equations are discretized using a finite-volume technique on an unstructured triangular mesh in the MIKE21 HD model, which provides a thorough description of coastal geometry, channels, and the urban fabric and permits the domain resolution to be adjusted to local morphological features. First-order numerical techniques in both space and time are used to guarantee numerical stability and maximum computational efficiency. These approaches enable the steady simulation of steep water fronts and rapid water-level oscillations, despite the

moderate amount of numerical dissipation they introduce. The bottom in MIKE21 HD is taken to be fixed and impermeable, just like in many shallow-water, wave-resolving models. This simplification is suitable for analyses intended to represent coastal inundation and water-level propagation, even though it does not permit the simulation of erosion or sediment transport processes. Free-surface elevation, still and total water depth, current velocities and their constituent parts, current direction, and associated hydrodynamic variables are among the model's outputs. The decision was made to develop smaller but higher-resolution urban downscaling models after creating a wave model that covered the entire Gulf of Trieste, from the mouth of the Tagliamento River in the east to Muggia in the west, due to the different layout and orientation of the coastal areas under consideration. One or both models were employed, as explained below, depending on the exposure of the coastline area.

4.5.2.3 Domain setup

The boundaries of the calculation mesh were drawn based on specific criteria. The northern border was drawn following the shoreline, giving it directional continuity in the presence of lagoon mouths and river mouths, up to the border with the Gulf of Panzano. The eastern and south-eastern border, from Panzano, following the rocky coast and Trieste littoral to Punta Salvore, was drawn parallel to the coastline, simplifying its course. The border towards the north Adriatic was drawn by connecting the Tagliamento river mouth to the DWRG1 buoy and going further, in the same direction, for about 3 km. Finally, it was closed perpendicularly to the shoreline. For the triangular mesh creation, we set the smallest allowable angle to 28°. The mesh for the SW module was just one huge zone with the resolution offshore of 45 × 45 m. The maximum area for the mesh elements was set to satisfy the criterion $\frac{1.25 \cdot (\text{spacing})^2}{2}$. The mesh for the north-eastern Adriatic basin is characterised by 100079 nodes and 228084 elements. To construct the model, bathymetric datasets from different sources were combined, with high-resolution sources considered more reliable. Specifically, the bathymetric input data for the Gulf of Trieste, extended to cover the entire regional coastal area (Figure 9), consists of multiple sources: (i) the model of the European Marine Observation and Data Network (EMODnet) of 2022 (http://www.emodnet-bathymetry.eu) on a grid of 1/16 × 1/16 arc minute of longitude and latitude (approx. 115 × 115 m) integrated with (ii) the bathymetric model provided by Petti et al. (2019), and higher resolution bathymetric models of the northern coastal area on a grid of 2 × 2 m, and finally (iii) the bathymetric surveys carried out by Trobec et al. (2017). The different bathymetric models were then interpolated, removing any discontinuities, especially in the areas where the different data sources connected. This made it possible to obtain a bathymetric map of the Gulf of Trieste and the Friuli Venezia Giulia coastline that did not contain any obvious errors or discontinuities that could cause problems for the model simulations. As input data for the construction of the calculation domain, hydrodynamics and wave motion modelling also require a digital terrain model (DTM) with a resolution accurate enough to simulate both the distribution of physical quantities at sea and flooding within the urban fabric. The DTM was obtained by means of a LiDAR survey in 2018 (courtesy of the Friuli Venezia Giulia Region) covering the entire regional coastal area. The spatial resolution of the resulting digital model is 0.5 × 0.5 m. The use of high-resolution DTM tools is a fundamental element in assessing coastal flooding associated with extreme events. In Spadotto et al. (2025), for the town of Grado, and in Mannarini et al. (2025), for the case study of the city of Lecce, it is emphasised that the use of a high-resolution DTM allows the

identification of area vulnerabilities and specific critical points that control or contribute to the propagation of water masses, even considering thresholds that are not particularly high (Spadotto et al., 2025). Similarly, Baldoni et al. (2024) demonstrate that integrating high-resolution DTM tools with current and future extreme level scenarios allows the boundaries of water mass expansion in urban grids to be defined, highlighting the hydraulic connection between the sea and/or lagoon and the urban fabric. The DTM therefore plays a crucial role in hazard analysis and in supporting the planning of coastal adaptation strategies. Finally, the EMODnet bathymetry was cropped externally compared to the 2019 DTM, and the mesh was interpolated on the basis of the two rasters. To obtain a hydraulic flow that is accurately represented and consistent with reality, it was also necessary to integrate land-use values. Generally, the impact of soil on hydraulic flow is represented by the bottom friction parameter defined as roughness, which takes on different values depending on the type of soil considered. As a rule, roughness is parametrised using the Manning or Strickler coefficient. Land use values were obtained from the Manning values reported by Papaioannou et al. (2023). The reciprocal was applied to the Manning values to obtain the Strickler Corine values used to complete the calculation domain.

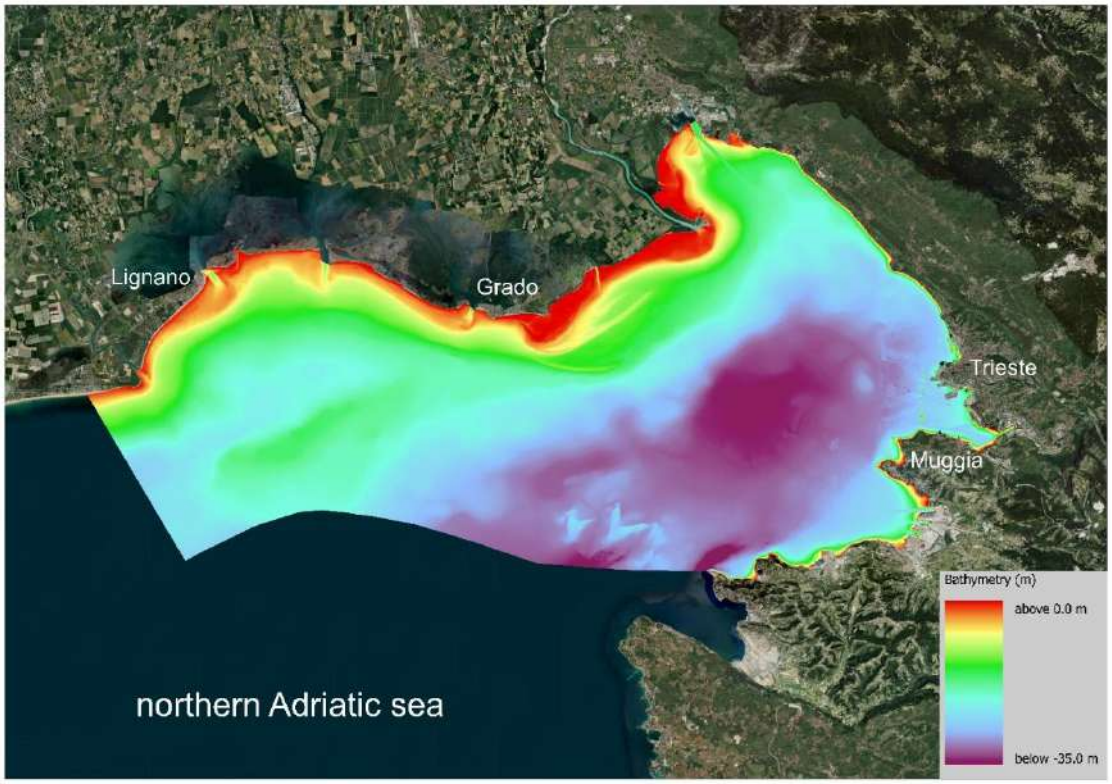

Figure 9. Bathymetry of the mesh used in MIKE21 modules.

Finanziato dall'Unione europea NextGenerationEU
Ministero dell'Università e della Ricerca
Italiadomani
UNIVERSITÀ DEGLI STUDI DI TRIESTE

5. Results and discussion

Within Section 5.1, the results obtained from the statistical analyses performed for Grado, as described in the methodological Section 4.2, are presented. For Trieste, the results related to the statistical extrapolation are reported in Section 5.2, based on the statistical methodology outlined in Section 4.3.

5.1 Grado extreme statistical values

5.1.1 Gumbel-BM

The results of the Gumbel distribution applied within the Block Maxima (BM) framework to extreme water levels are shown in Figure 10. The return periods (R_PS) reported in Table 5 (reference period: 1995-2014; central year: 2006) are associated with the corresponding updated extreme thresholds. According to the Flood Risk Management Plan of the Eastern Alps River Basin District for Zone 2 (PGRA), the derived values refer exclusively to the combined contribution of the meteorological component, the astronomical tide, and the mean sea-level component (section 4.1.1).

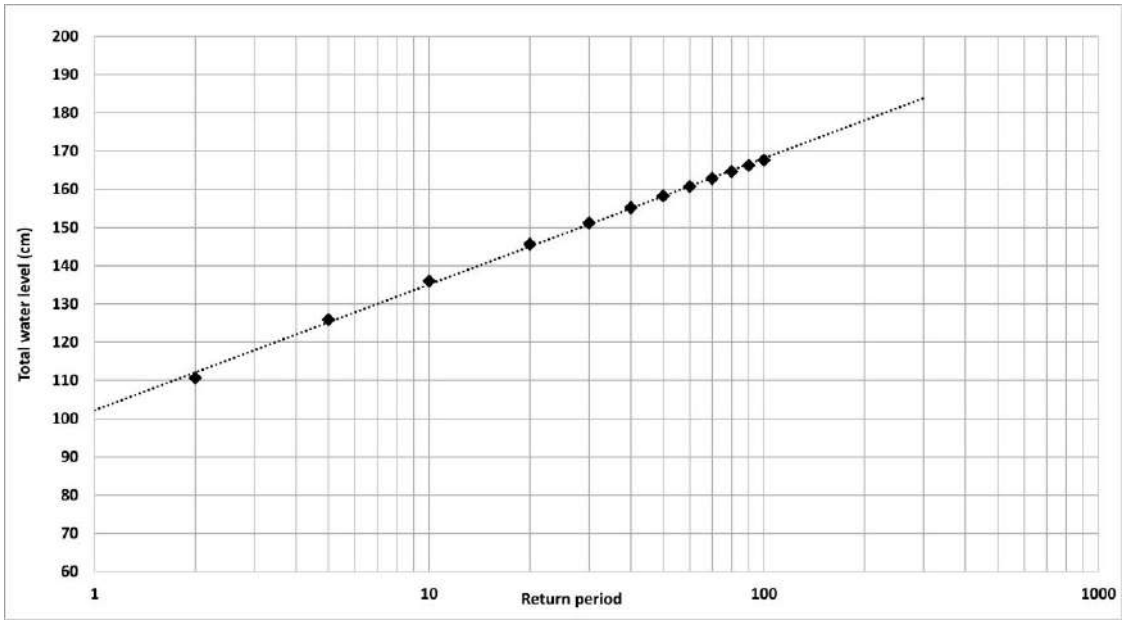

Figure 10. Extreme water level statistical analysis (Gumbel distribution) observed at the RMLV meteo-mareographic station in Venice, reference period 1950–2023 (from Spadotto et al, 2025).

The values reported in Table 5 represent an update of those provided in the PGRA, which is based on the reference period 1985-2005 and incorporates the extreme tide-level statistics compiled by Tomasin and Pirazzoli (2009). The extreme water levels reported in the PGRA for events with return periods (R_P) of 30 and 100 years are approximately 8-10 cm lower than those calculated in the present analysis, as also observed for Trieste (see Table 2b for Trieste).

R_P (years)	Extreme level (cm)	CI 95% (cm)
2	111	107-115
10	136	125-146
30	151	136-165
100	168	147-186

Table 5. Updated extreme level values as a function of return period (reference year 2006, Gumbel distribution) (from Spadotto et al, 2025).

5.1.2 Analysis of Mean vs. Max levels and Threshold exceedance

The evolution of mean sea level is widely used to derive long-term projections within a given environmental context. Such projections can be developed at the global scale, as in the assessments of the IPCC (Masson-Delmotte et al., 2021), at the Mediterranean basin scale (Cramer et al., 2020), or, as in the present study, at a more local scale, drawing on recent works developed particularly for Venice (Zanchettin et al., 2021; Lionello et al., 2021; among others). However, for a proper understanding of the increasingly pronounced temporal variability observed at short- to medium-term scales, maximum sea-level values can provide more relevant information with respect to flood risk. In this context, the aim of this analysis is to compare the temporal evolution of mean sea level with the trend of annual maximum levels, as shown in Figure 11. he time interval considered spans from 1991 to 2024, covering slightly more than 30 years and providing a sufficiently long time series to assess the interannual variability of the meteorological component (Arguez et al., 2011).

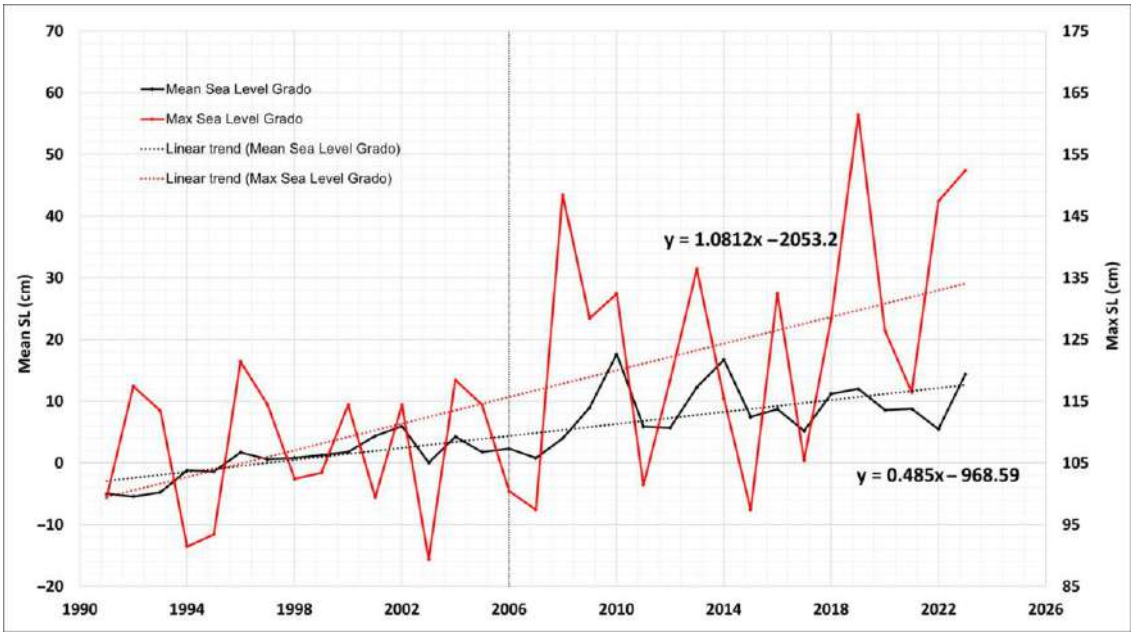

Figure 11. Comparison of the mean sea level (black line) and the maximum sea level (red line) observed in Grado from 1991 to 2023 (IGM42 reference). The left axis indicates the scale for mean sea level, whereas the right axis signifies the maximum levels (from Spadotto et al, 2025).

As shown in Figure 11, the observed annual maximum sea levels exhibit an increasing rate of approximately 10.8 mm/yr, more than twice the trend estimated for mean sea level, which

Finanziato dall'Unione europea NextGenerationEU
Ministero dell'Università e della Ricerca
Italiadomani
UNIVERSITÀ DEGLI STUDI DI TRIESTE

is about 4.9 mm/yr. Within the limitations of a roughly 30-year record, this result suggests that flood risk is increasing more substantially than would be inferred from mean sea-level projections alone. In general, when referring to risk, it is often implicitly associated with flooding events. However, risk is not determined solely by the peak water levels reached, but also by the duration of such events. For this reason, the analysis was extended to assess sea-level exceedances over a given time interval within each year, specifically considering events persisting for a minimum duration of 3 hours. Figure 12 illustrates the temporal evolution of maximum sea levels recorded at Grado that persisted for at least 3 hours. The year 2006, which represents the centroid of the 30-year reference period, is consistent with the temporal framework adopted in the IPCC AR6 report (Masson-Delmotte et al., 2021), thereby allowing projections that are approximately aligned with the most recent observed trends.

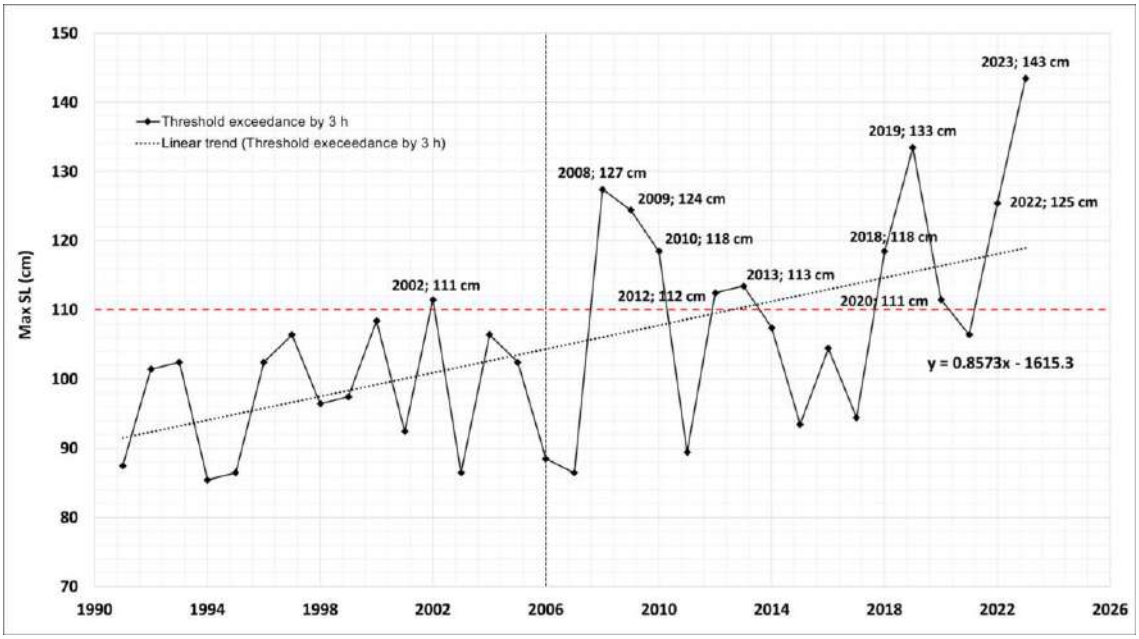

Figure 12. The 30-year trend of maximum sea levels recorded in Grado that persisted for a minimum of 3 h (threshold exceedance by 3 h). The threshold level of 110 cm (ref. IGM42 datum) is here reported as a reference value for flooding phenomena in the 'Old Town' area (from Spadotto et al, 2025).

By examining Figure 12, it is possible to analyse the average trend of the maximum sea levels that persist for at least 3 hours within a given year. The estimated slope of the linear trend is 8.6 mm/yr. The mean value represented by the trend line indicates a 3-hour event level of approximately 93 cm at the beginning of the series in 1991, increasing to about 118 cm by 2023. Over a period of just over 30 years, maximum sea levels associated with persistent events have therefore increased by approximately 25 cm. The figure also highlights a minimum threshold value of 110 cm, which is adopted as a precautionary reference level. This threshold corresponds to an event with an approximate return period of 2 years and a high probability of occurrence (Table 5). In the city of Grado, a water level of 110 cm implies substantial inundation of the historic centre, particularly along the quays of the Mandracchio Canal. From 2006 to the present, Grado has experienced 10 flooding events, corresponding to an average frequency of 1.8 events per year, with water levels exceeding 110 cm for durations close to 3 hours.

5.2 Trieste extreme analysis

As described in the Materials and Methods section, the analysis of extreme events based on sea-level data extracted from the Trieste tide gauge, considering the 1939-2024 time series, was carried out using three different methodologies, the results of which are presented below: the GEV-BM approach, the GPD-POT approach, and a multivariate statistical framework.

5.2.1 GEV-BM

The parameters μ (location), σ (scale), and ξ (shape) determine the GEV distribution. The latter governs how the distribution tail behaves: values of ξ>0 denote a heavy tail (Fréchet type), ξ=0 denotes the Gumbel case with an exponential tail, and ξ<0 denotes a bounded tail (Weibull type). This analysis's predicted shape parameter is ξ=0.0319, which is extremely near to zero and indicates a behavior that is similar to the Gumbel type with an exponential tail. This arrangement is in line with the dynamics of exceptional sea levels in the Northern Adriatic, where storm surges and tidal processes produce powerful but physically limited events (Tomasin & Pirazzoli, 2009; Ferrarin et al., 2022).

5.2.1.1 Extreme water levels

The results of the goodness-of-fit analysis of the sample to the GEV-BM distribution applied to extreme sea levels measured above the running mean sea level are shown in Figure 13. The derived values have been updated to the year 2024 with respect to the analysis performed by Tomasin and Pirazzoli (2009), which was based on the Trieste time series covering the period 1939-2006.

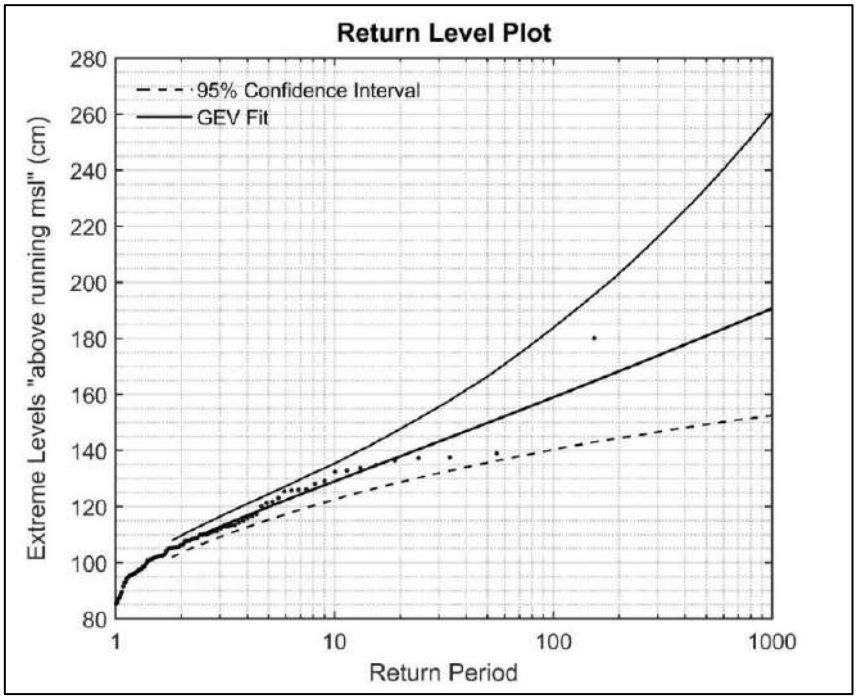

Figure 13. Extreme water level “above running msl” (GEV-BM distribution) observed at Molo Sartorio meteomareographic station in Trieste (reference period: 1939-2024). 95% Confidence interval in lower and upper limits.

When taking into account possible effects within the urban fabric, the return periods shown in Table 6 are especially pertinent because they begin at a value of two years, which corresponds to a fairly frequent recurrence interval. In this context, return periods of two to

ten years are typically categorized as nuisance flooding, which refers to those extremely frequent occurrences that cause considerable and ongoing disruption to the population despite not being catastrophic.

R_P (years)	Extreme levels "above running msl" (cm)	CI 95% (cm)
2	107	104-110
5	120	115-125
10	129	122-135
30	143	132-156
50	150	136-166
100	159	140-184

Table 6. Updated extreme sea level values above running msl, as a function of return period (GEV-BM distribution), reference period: 1939-2024.

However, in the paper by Tomasin and Pirazzoli ("Extreme sea levels on the Adriatic coasts: a comparison of estimation methods"), the 100-year return period (R_P = 160 cm) shown in Table 2b of the PGRA, is not directly acquired through a formal statistical extrapolation. The estimates in that study are presented as exploratory or tentative applications of the GEV and Gumbel approaches rather than as definitive return level values explicitly supporting the 100-year R_P adopted in the PGRA, as shown in *table 3* ("Tentative application of GEV simulations and of the Gumbel method to yearly maximum sea-level hourly heights -cm above the running MSL-"). In fact, applying the GEV distribution to 68 years of records provides an extreme sea level of 143 cm for a 100-year return period, according to testing the methodology across the 1939-2006 period and closely adhering to the two authors' criterion. The extreme meteomarine event of November 26, 1969, which reached an extreme level of 194 cm and constitutes the highest value ever recorded since the Trieste tide gauge has been in service, is excluded from the yearly maxima series for calculating this number. The extreme elevation "above running MSL" rises to about 158 cm when the identical scientific technique is repeated with the 1969 meteomarine event explicitly included. This figure is generally similar with the value stated in the PGRA for a 100-year return period event, despite some discrepancies pertaining to the reference used to assess the maximum level reached. Based on this, the extreme sea levels were updated until 2024 using the same selection criterion. Therefore, the predicted extreme level associated with a 100-year return period is roughly 159 cm by applying the GEV distribution to the entire set of 86 years of available observations and taking into account all recorded yearly maxima, including the event of November 26, 1969 (Table 6). It should be mentioned that the reference utilized in the Flood Risk Management Plan is the total extreme water level Z_T (Pugh & Vassie, 1978), which is reached during a meteomarine event, rather than the "above running MSL" method employed by Tomasin and Pirazzoli. Therefore, while still taking into consideration a 100-year return period, updated values that also take into account the contribution of the mean sea level reference –whose magnitude depends on the criterion adopted (e.g., annual mean sea level, decadal mean, moving average)– are anticipated to

surpass the 160 cm value reported in the PGRA. For example, the reference values for Trieste are approximately +3 cm above the IGM42 datum if the mean sea level of the most recent decade is chosen as the reference, roughly corresponding to the 2010-2024 interval, and using an approach consistent with that used in the PGRA (updated to 2021). At this point, the updated extreme sea levels are obtained as the sum of the values derived from the GEV application and the corresponding mean sea level, as reported in Table 7.

R_P (years)	**Extreme levels "above running msl" (cm)**	**Average MSL (cm) interval 2010-2024**	**Updated Total water level (cm)**
2	107	+3	110
10	129		132
30	143		146
100	159		162

Table 7. Updated total water level values for Trieste considering an average msl of +3 cm (interval from 2010-2024), as a function of return period (GEV-BM distribution), reference period: 1939-2024.

5.2.1.2 GEV-BM Validation test

This section presents the statistical analyses carried out for the validation tests. The aim is to verify whether the results obtained from the analysis are statistically robust and methodologically sound. The validation of the GEV-BM approach is assessed through QQ-plot analysis and goodness-of-fit validation tests.

QQ-plot analysis

A diagnostic tool for determining whether a theoretical distribution is adequate in relation to observed data is the QQ-plot (Quantile-Quantile plot). The empirical quantiles of the observed annual maxima (y-axis) and the theoretical quantiles of the fitted GEV distribution (x-axis) are contrasted in Figure 14. With no appreciable departures from the 1:1 bisector, the theoretical distribution accurately replicates the empirical one, as the picture illustrates. The block maxima approach's restricted sample size (n=86 years) and the greater variability linked to the rarest extreme events are responsible for the tiny deviations seen in the upper tail, which correlate to the highest quantiles. These variances show the statistical uncertainty influencing the calculation of high return levels rather than a systematic model distortion.

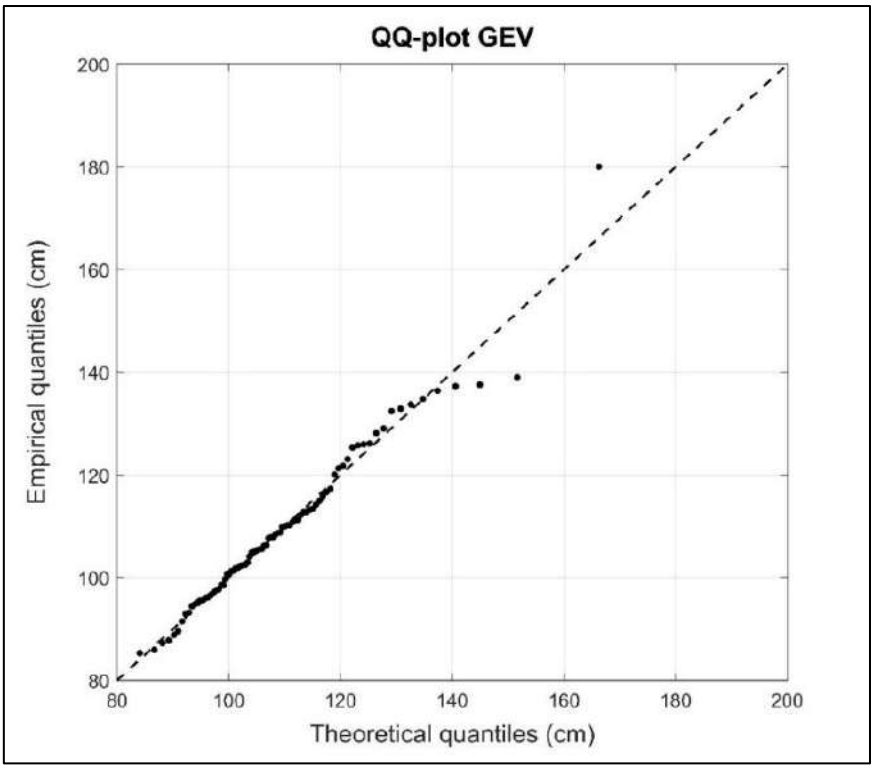

Figure 14. Diagnostic QQ-plot of the GEV distribution via MLE applied to annual maximum sea levels at Trieste (reference period: 1939-2024).

Fit validation test

The validation of the GEV model, carried out through Probability Integral Transform (PIT) tests following the criterion proposed by Coles (2001) and the application described by Majumder et al. (2024), confirms a good level of consistency between the observed annual maxima and the fitted theoretical distribution. The estimated shape, location and scale parameters are reported in Table 8.

ξ	σ	μ	KS	p-value (KS)	AD	p-value (AD)
0.0319	11.432	102.32	0.0424	0.955	0.2087	0.795

Table 8. Parameters estimated using the GEV distribution and results of the GEV model validation based on the Kolmogorov–Smirnov and Anderson–Darling tests.

From an interpretive standpoint, the value of ξ=0 places the fitted distribution in a near-Gumbel regime, which is consistent with the Northern Adriatic's physical environment, where severe occurrences can have large amplitudes but are still limited by clearly defined physical boundaries. When the converted data are subjected to the Kolmogorov-Smirnov (KS) test, the test statistic is 0.0424, and the bootstrap-based p-value (10000 resamples) is 0.955. The Anderson-Darling (AD) test yields a statistic of 0.2087 with a p-value of 0.795; this test is more sensitive to variations in the distribution tails. The null hypothesis of uniformity of the Probability Integral Transforms is supported by the p-values in both situations, which are significantly higher than the traditional significance level (α=0.05). Overall, these findings support the derivation of trustworthy return-level estimates up to a 100-year R_P and verify that the GEV distribution, calculated by MLE, offers a statistically sound and physically realistic representation of the annual maxima "above running msl" for the period 1939-2024.

Finanziato dall'Unione europea NextGenerationEU
Ministero dell'Università e della Ricerca
Italiadomani
UNIVERSITÀ DEGLI STUDI DI TRIESTE

5.2.2 GPD-POT

The Peaks Over Threshold (POT) method was used to apply the GPD to extreme sea-level exceedances. A threshold for extreme events was established after the recorded sea levels were detrended in relation to the mean sea level and the 19-year moving mean. The threshold was established at the independent peak distribution's 90th percentile, or roughly 74 cm above the chosen reference level. This decision guarantees an enough number of exceedances for a reliable GPD parameter estimation. Approximately 785 exceedances were found between 1939 and 2024, which translates to an average rate of 9.13 occurrences annually. Table 9 reports the estimated GPD parameters.

GPD-POT series	Interval (1939-2024)	Threshold u (90th)	exceedances (N>u)	λ	ξ	σ
Extreme "above msl"	86	74.21	785	9.13/yr	-0.0417	13.798
Extreme "above mm19"	86	74.53	785	9.13/yr	-0.0525	14.196

Table 9. Estimated parameters of the Generalized Pareto Distribution (GPD) applied using the Peaks Over Threshold (POT) method, considering extremes "above msl" and "above mm19" for Trieste (reference period: 1939-2024).

For both detrended series, the MLE approach was used to estimate the GPD shape (ξ) and scale (σ) parameters. The data shown in Table 9 indicate that the upper tail behaves roughly exponentially, with ξ values near zero (ξmsl= -0.0417; ξmm19= -0.0525). The GPD precisely reduces to an exponential distribution when ξ=0 (Serinaldi & Kilsby, 2015). According to Merz et al. (2022), meteomarine extreme statistics are characterized by an exponential tail in the GPD framework. These findings validate that the chosen threshold is suitable and that the severe sea-level behaviour at Trieste is coherently represented by the GPD-POT model. The adoption of the ~19-year lunar nodal cycle does not change the structure of threshold exceedances while improving fit stability, according to the almost identical parameter estimates obtained from the two detrending procedures.

5.2.2.1 Extreme water levels

Figure 15 and Figure 16 how the return level plots obtained for the extreme sea-level series at Trieste (1939-2024), detrended with respect to the annual mean sea level ("above msl") and the 19-year moving mean ("above mm19"), respectively. The curves represent the relationship between the expected extreme level and the corresponding return period (years), estimated using the Generalized Pareto Distribution (GPD), while the dashed lines indicate the 95% confidence intervals.

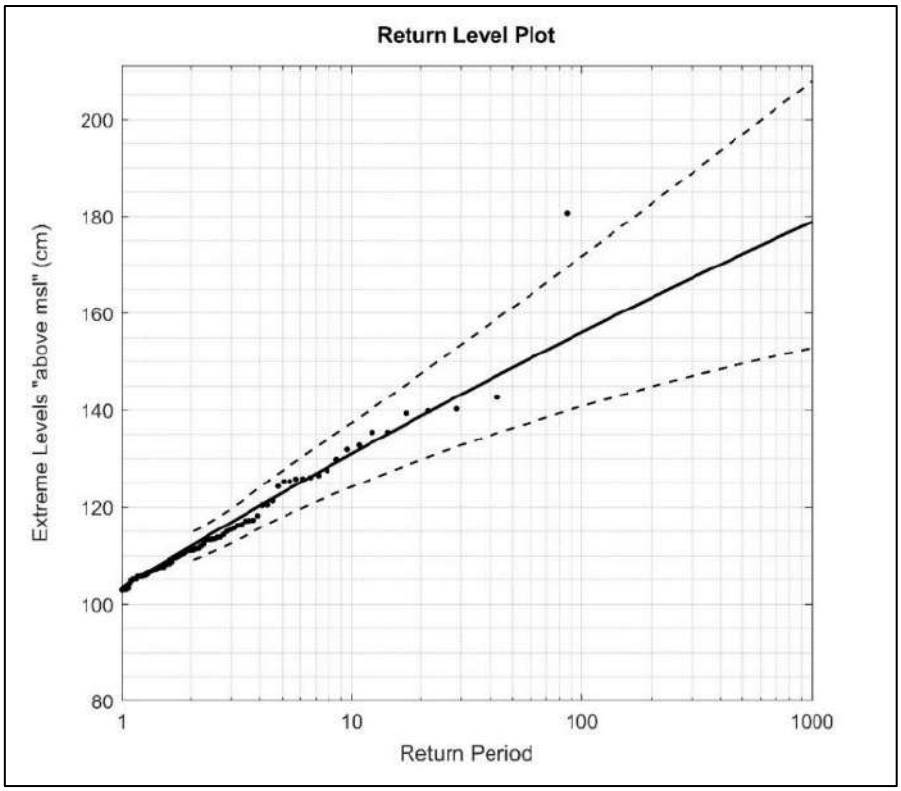

Figure 15. Extreme return level curves estimated using the GPD (solid line) with 95% confidence intervals (dashed lines) applied to the series of extremes relative to mean sea level. Dots represent the empirical maxima ordered by return period.

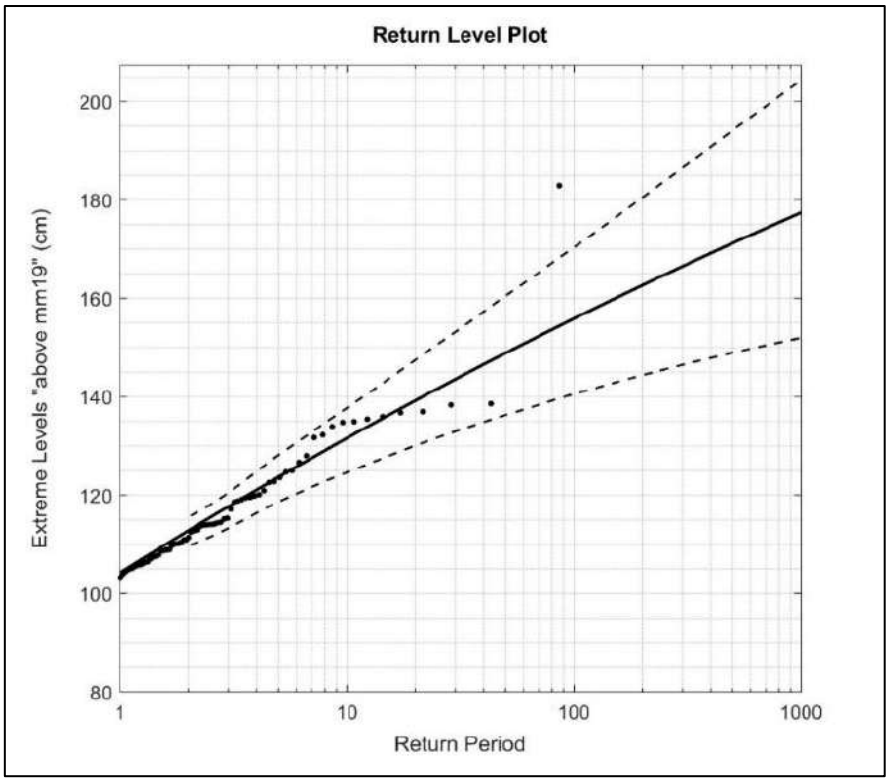

Figure 16. Extreme return level curves estimated using the GPD with 95% confidence intervals, applied to the series corrected for the lunar nodal cycle (mm19); the fit remains stable and consistent with the empirical distribution up to return periods of 100 years.

For both the "above msl" and "above mm19" series, the GPD curves displayed in the plots show good agreement with the empirical point estimates, demonstrating the GPD's usefulness in depicting the tail behaviour of extreme sea levels. In particular, the estimated confidence intervals for R_P up to around 50 years stay quite narrow, suggesting low uncertainty in the prediction of moderately common (30-50 years) and frequent (up to 10 years R_P) events. The confidence intervals gradually get wider for uncommon events, as those connected to a 100-year return time. The small sample size of extreme events in this range is reflected in this behaviour. The estimated extreme levels along with their confidence ranges and matching return durations are shown in Table 10a, 10b (for the "above msl" and "above mm19" scenarios, respectively).

R_P (years)	**Extreme levels "above msl" (cm)**	**CI 95% (cm)**
2	112	109-115
5	123	118-128
10	131	124-137
30	143	133-154
50	149	136-161
100	156	141-172

Table 10a. Updated extreme sea level values "above msl", as a function of return period (GPD-POT distribution) and 95% confidence interval, reference period: 1939-2024.

R_P (years)	**Extreme levels "above mm19" (cm)**	**CI 95% (cm)**
2	113	110-116
5	124	119-128
10	132	125-138
30	144	133-153
50	149	136-161
100	156	141-170

Table 10b. Updated extreme sea level values above running 19-years mean move (mm19), as a function of return period (GPD-POT distribution), and 95% confidence interval, reference period: 1939-2024.

The extreme levels obtained after the preliminary detrending procedure and analysed using the GPD are effectively equivalent. In fact, the estimated return levels for periods ranging from 2 to 100 years are very similar for the two detrending approaches, with differences smaller than ±1 cm.

5.2.2.2 GPD-POT Validation test

Similarly, to the approach adopted for the GEV-BM, the results obtained from the GPD-POT distribution were validated through the following diagnostic tests: QQ-plot analysis, goodness of fit validation tests, cross-validation tests, and the Mann-Kendall trend test.

QQ-plot analysis

Figure 17 and Figure 18 show the QQ-plots obtained for the detrended series “extreme above mm19” and “extreme above msl”, respectively. In both cases, the points are well aligned along the 1:1 line, indicating a close agreement between empirical and theoretical quantiles. This confirms that the adopted GPD model accurately reproduces the distribution of exceedances above the selected threshold. Minor positive deviations are observed for the most extreme events; however, these departures remain within the associated confidence intervals and do not indicate a systematic lack of fit.

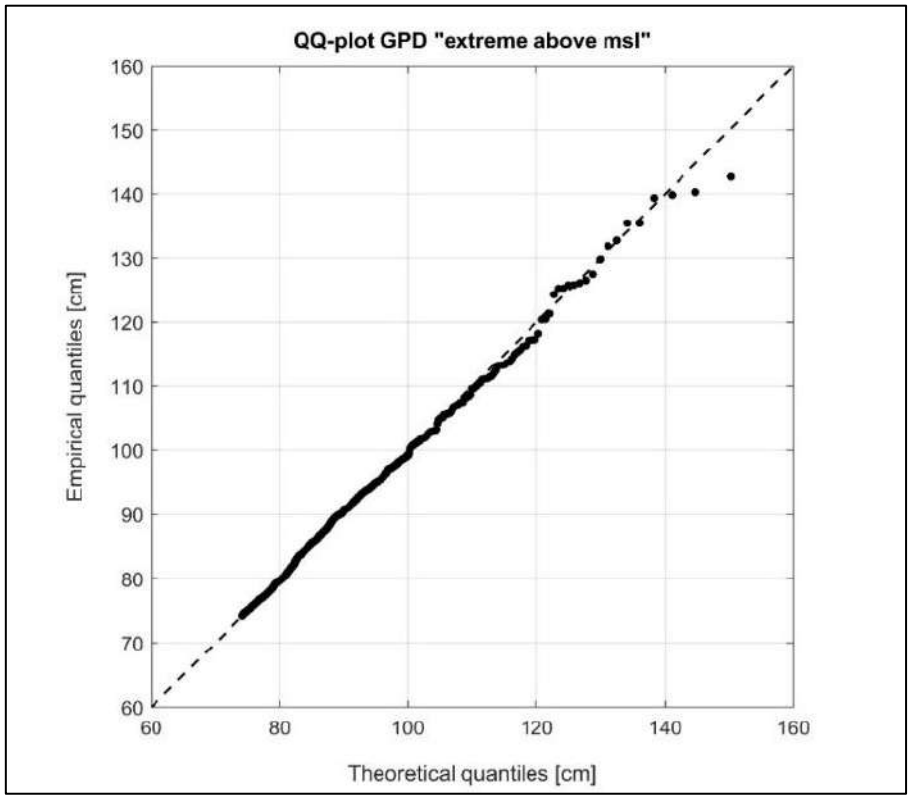

Figure 17. Diagnostic QQ-plot of the GPD distribution via MLE applied to exceedances of extreme sea levels at Trieste (reference period: 1939-2024). Series detrended with respect to the 19-year moving mean (“extreme above mm19”). The close agreement between empirical and theoretical quantiles confirms the adequacy of the GPD-POT model in representing the statistical distribution of extreme events.

Finanziato dall'Unione europea NextGenerationEU
Ministero dell'Università e della Ricerca
Italiadomani
UNIVERSITÀ DEGLI STUDI DI TRIESTE

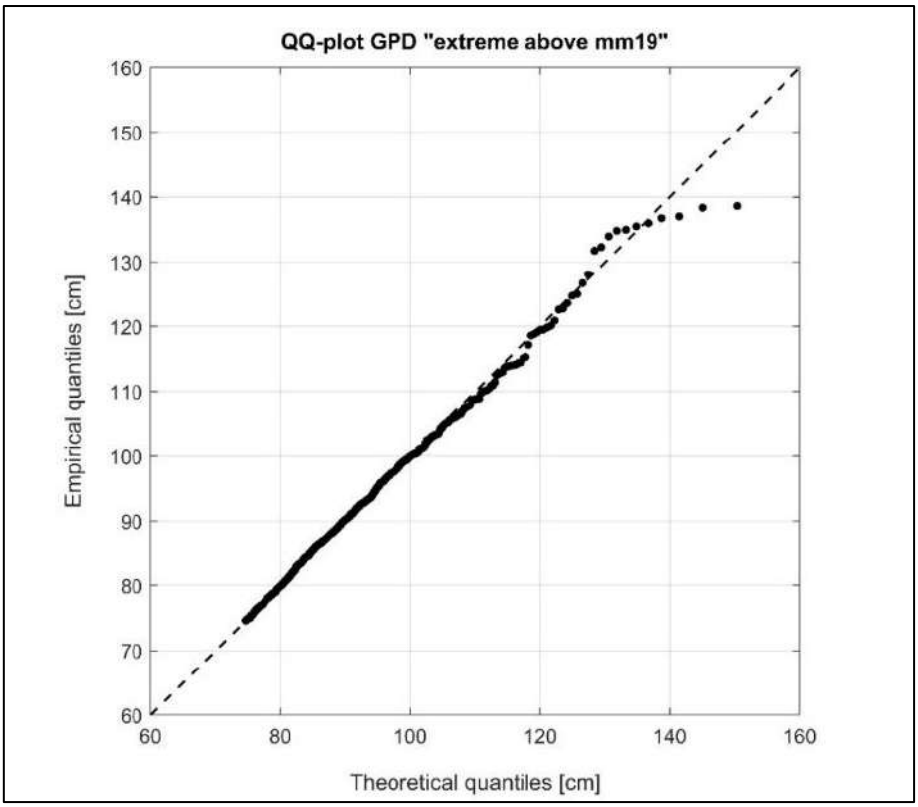

Figure 18. Diagnostic QQ-plot of the GPD distribution via MLE applied to exceedances of extreme sea levels at Trieste (reference period: 1939-2024). Series detrended with respect to mean sea level ("extreme above msl"). The close agreement between empirical and theoretical quantiles confirms the adequacy of the GPD-POT model in representing the statistical distribution of extreme events.

Fit validation test

The Kolmogorov-Smirnov (KS) and Anderson-Darling (AD) statistics were used in goodness-of-fit tests to further evaluate the correctness of the chosen distribution model. The findings shown in Table 11, demonstrate that the KS statistics are extremely low (0.0194 and 0.0283, respectively) for both detrended series ("above msl" and "above mm19"), with corresponding p-values of 0.546 and 0.921, considerably over the standard significance criterion of α=0.05. These results corroborate the robustness of the fit by showing no statistically significant variations between the theoretical GPD model and the empirical distribution of exceedances.

GPD-POT series	**Interval**	**Threshold u (90th)**	**KS**	***p-value* (KS)**	**AD**	***p-value* (AD)**
"above msl"	1939-2024	74.21	0.0283	0.546	0.644	0.093
"above mm19"		74.53	0.0194	0.921	0.338	0.504

Table 11. Parameters derived from the validation of the GPD-POT model as a function of the threshold u (90th percentile), assessed using the Kolmogorov–Smirnov and Anderson–Darling tests.

The results of the KS test are further supported by the AD test. The "above msl" series displays AD=0.644 with a p-value of 0.093, but the "above mm19" series provides an AD of 0.338 with a p-value of 0.504. Given that the AD statistic is explicitly intended to highlight

deviations in the top tail of the distribution, these values fall within the range associated with a successful GPD fit (Stephens, 1974). These findings are in line with Choulakian and Stephens's (2001) demonstration of the usefulness of the AD test in evaluating the GPD's goodness of fit. They also showed that AD<1 indicates a satisfactory fit, particularly when parameters are estimated using MLE, as in this study, using critical values and Monte Carlo simulations. Additionally, the classification that was achieved is consistent with the reference criteria outlined in Stephens (1974, 1976, 1979) and Pettitt and Stephens (1977), which show that the theoretical model is strongly supported by tiny KS and AD values along with high p-values. Overall, the GPD model's capacity to accurately depict the distribution of threshold exceedances is confirmed by the consistently high p-values ($p \geq 0.05$) and the well-aligned dots in the QQ-plots.

Cross validation test

The GEV-BM and POT-GPD models' stability and dependability as a function of the calibration window length are quantitatively evaluated using the cross-validation process. A calibration window of S=5 years could not be used because of inadequate data, as indicated in the Materials and Methods section. As a result, more reliable windows (S=10, S=20, and S=30 years) were chosen. These windows produce rather consistent parameter estimations by ensuring a sufficient number of annual maxima and threshold exceedances. The validation based on the Normalized Deviation Error (NDE) was only carried out on the series detrended using the 19-year moving mean, in accordance with the methodological framework suggested by Caruso and Marani (2022). This detrending approach is supported by the length of the examined period (1939-2024), which eliminates multi-decadal sea-level variability that may otherwise skew the model assessment. The NDE statistics for each calibration window, namely the median, mean, and standard deviation, are reported in Table 12 The models were validated on the remaining M−S years and calibrated on a subset of S years for a particular window length S, where M=86 is the entire length of the available record. [R_P=(M−S)+1] is the return level that is used to compare simulated and observed values. As a result, the validation is carried out over 56 years for S=30 years, and the comparison relates to the extreme level linked to R_P=57 years.

variables	S=10 years		S=20 years		S=30 years	
	BM	POT	BM	POT	BM	POT
NDE median	-0.186	-0.218	-0.186	-0.205	-0.183	-0.199
NDE mean	0.252	-0.120	-0.070	-0.099	-0.046	-0.064
NDE SD	4.24	0.305	0.254	0.224	0.217	0.207

Table 12. Parameters derived from the cross-validation procedure, considering calibration on subsamples S = 10, 20, and 30 years, applied to the BM and POT approaches.

The median NDE stays roughly constant (about -0.19) across all the calibration windows when the BM is applied to the GEV distribution. This suggests a persistent tendency to underestimate the observed return level throughout the validation phase. For both the BM and POT techniques, the mean NDE falls as S rises (from 0.25 to -0.046), indicating an overall improvement in model performance with larger calibration windows. As the number of calibration years grows, there is a gradual decrease in variability and an increase in estimate stability. When looking at the NDE standard deviation for the BM model, this behavior is especially clear: values are very high for S=10 (≈4.24), indicating strong

instability when short calibration windows are used, while they become significantly lower for S=20 and S=30 (≈0.25 and 0.22, respectively), reflecting much more stable and reliable estimates. In a similar vein, the median NDE for the POT model stays roughly constant at -0.20, suggesting a consistent propensity to underestimate the return values. However, the POT model shows significantly less fluctuation and more stable mean values when compared to the BM approach. As S grows, the standard deviation drops from 0.30 to 0.21 and the mean NDE falls from -0.12 to -0.064, indicating a smoother behaviour and less susceptibility to the number of the calibration subsamples than the GEV-based BM model. Overall, when calibrated on brief temporal frames, both approaches exhibit a minor underestimating of extreme return levels. However, expanding the calibration window enhances model reliability; the most stable and methodologically sound setup is S=30.

Mann Kendall test

The annual maximum sea-level values for detrended series were subjected to the Mann-Kendall (MK) test. To separate long-term behaviour from more recent changes, the entire database from 1939 to 2024 was then split into three temporal intervals (1939-1990, 1991-2024, and 2006-2024). Theil-Sen slope estimator (Sen, 1968), a reliable indicator of trend size, was used in conjunction with the MK test for each chosen period. Table 13 reports the outcomes for each interval.

series	N	p-value	*Theil-Sen slope*
1939-2024			
“above msl”	86	0.817	0.017 cm/yr
“above mm19”		0.788	0.014 cm/yr
1991-2024			
“above msl”	34	0.213	0.426 cm/yr
“above mm19”		0.091	0.477 cm/yr
2006-2024			
“above msl”	19	0.6243	0.676 cm/yr
“above mm19”		0.6243	0.385 cm/yr

Table 13. Parameters derived from the Mann-Kendall test and corresponding Theil-Sen slope estimates, as a function of the selected temporal interval.

The findings presented in Table 13 demonstrate that the MK test does not reveal a statistically significant trend (p-value≥0.05) for any of the temporal intervals taken into consideration. Once the mean sea-level component and the 19-year Metonic cycle are eliminated, Trieste shows no discernible trend in annual maximum sea levels for the whole 1939-2024 period. The "above msl" and "above mm19" series had p-values of 0.817 and 0.788, respectively. P-values for the more recent years 1991–2024 are 0.213 ("above msl") and 0.091 ("above mm19"), which are lower but still above the significance level. *P*-values, which are 0.624 for both detrended series, are non-significant even when the study is limited to the most recent period (2006-2024). In every instance, the Theil-Sen slope estimates are weakly positive: roughly +0.19–0.20 cm/yr for the entire period, +0.38–0.48 cm/yr for 1991–2024, and +0.38–0.68 cm/yr for 2006-2024. The MK test, however, indicates that these

Finanziato dall'Unione europea NextGenerationEU
Ministero dell'Università e della Ricerca
Italiadomani PIANO NAZIONALE DI RIPRESA E RESILIENZA
UNIVERSITÀ DEGLI STUDI DI TRIESTE

slopes cannot be statistically separated from zero. Overall, the findings suggest that there is no discernible trend in the yearly maximum sea levels at Trieste, either throughout the whole record or in the most recent decades, once the long-term mean sea-level component is eliminated. This behavior is in contrast to Caruso and Marani's findings for Venice, where a notable trend was found and linked to local characteristics such lagoon structural changes and subsidence (Zanchettin et al., 2021). The findings for Trieste are consistent with the theory that mean sea-level oscillations and meteorological forcing are the main factors influencing yearly maximum variability, with no discernible extra signal associated with local morphological changes like uplift or subsidence

5.2.3 Multivariate Statistical Approach

5.2.3.1 Decomposition drivers of sea level

By considering the various combinations between the tidal component and the residual component known as non-tidal residual (NTR), the first analysis inside the multivariate framework seeks to determine the primary factor governing extreme sea levels.

Choosing the proper threshold is a crucial first step. Threshold selection is not unique and relies on the analysis's goal, as Ferrarin et al. (2022) explain for Venice. The elevation of the urban waterfront (Le Rive), which is roughly 111 cm in relation to the IGM42 datum, could serve as a potential reference in the instance of Trieste. The criterion used in this analysis, however, is based on the distribution of observed sea levels detrended with respect to the 19-year centred moving mean, taking into account the entire historical record from 1939 to 2024, in accordance with the methodology suggested by Ferrarin et al. (2022).

With values of 66.2 cm, 73.8 cm, and 91.3 cm for Trieste, respectively, the chosen thresholds represent the 99th, 99.5th, and 99.9th percentiles of the detrended sea-level distribution, corresponding to 1956, 966, and 176 extracted events. These thresholds, which are discretized based on the semidiurnal tidal regime, reflect hourly exceedances of sea level, assuming temporal independence between "high-water" values that occur twice in a single day. Following the definition of the extreme-level percentiles, the primary causes of sea-level variability –the astronomical tidal component and the non-tidal residual– were broken down using frequency-band filtering. The latter include PAW surge, storm surge, seiches, meteotsunami, and the low-frequency variability linked to mean sea-level pulsations related to IDAS. The decomposition results (Table 14) show that, for Trieste, the tidal component largely controls extreme sea levels at the 99th percentile, while the NTR component predominates over the tidal contribution at the 99.5th and 99.9th percentiles. The NTR makes up around 58% of the overall sea-level signal in the most extreme scenario (99.9th percentile). Lionello et al. (2021) and Ferrarin et al. (2022) have also observed a similar domination of the NTR component for the highest percentiles for Venice. At the 99th percentile, there is a more evident difference between Trieste and Venice. In Trieste, the tidal contribution accounts for roughly 57% of the total sea level, while in Venice it is only about 49% (Ferrarin et al., 2022). The specific factors influencing the non-tidal residual were further examined after the relative contributions of tide and NTR were measured. Specifically, processes like meteotsunami-related events that have characteristic frequencies between 10 h and 10 d are included in the storm surge component. Seiches were handled and examined separately inside the storm surge component.

Forcings		99th	99.5th	99.9th
Astronomical tide		57.4	52.6	42.3
Non Tidal Residual (NTR)		42.6	47.4	57.7
NTR	Storm surge	25.7	27.6	34.4
	Seiches	17.1	17.4	16.6
	PAW surge	35.2	35.1	32.5
	IDAS	22.0	19.9	16.5

Table 14. Average contribution of the different components to extreme sea levels, as a function of the 99th, 99.5th, and 99.9th percentiles.

In particular, the storm surge contribution rises with the extreme event's severity and overtakes the other contributions, accounting for up to 34% of the overall NTR. The most intense incident on November 26, 1969, saw the largest storm surge event ever recorded in Trieste, measuring 97 cm (sea level measured at 194 cm IGM42 with a 10-minute sampling frequency; rescaled to 177 cm IGM42 when considering hourly data). Additional extremely strong storm surge incidents were noted on December 10, 1954 (91 cm), November 4, 1966 (87 cm), and during the more recent Vaia storm in 2018 (76 cm). The two Adriatic seiche modes' contributions are distinguished by their greatest magnitudes, which were measured in March 1958 and exceeded 56 cm. The numbers reported by Godin and Trotti (1975; *table 14, p. 23*) are consistent with this order of magnitude. December 2019 saw another high value of about 52 cm. A value of roughly 43 cm was noted, which is comparable to what Ferrarin et al. (2022) found for Venice over the same time period. In all situations, the storm surge component did not significantly contribute to the same events.
The largest magnitude of the high-frequency component (<10 h), which is solely described in this study as a meteotsunami contribution, was recorded in November 1965 and exceeded 48 cm. Lastly, the PAW surge and the IDAS component are the final two contributions taken from the NTR. According to Ferrarin et al. (2022) for Venice, these two contributions typically decline as event magnitude increases. In contrast to Venice, where they make up roughly 44% and 29% of the total NTR, respectively, the storm surge and PAW surge contributions in Trieste are very closer to one another. For the IDAS contribution, a significant variation is also noted. For a 99.9th percentile occurrence, IDAS makes up about 16–17% of the total NTR in Trieste, which is similar to the entire contribution of seiches; in Venice, this percentage is about 11%. In December 1954, the PAW surge reached a maximum value of 48 cm, which was greater than what was reported for Venice (Ferrarin et al., 2022). Although it is commensurate with levels seen in Venice, the maximum positive IDAS result is roughly 25 cm (November 2010).

Finanziato dall'Unione europea NextGenerationEU
Ministero dell'Università e della Ricerca
Italiadomani PIANO NAZIONALE DI RIPRESA E RESILIENZA
UNIVERSITÀ DEGLI STUDI DI TRIESTE

5.2.3.2 Non stationary analysis

Following the definition and breakdown of the detrended sea level into its constituent parts, a further analysis was carried out, concentrating on the 99th percentile, to find a potential rising trend in extreme sea levels as a function of the previously determined components. As previously mentioned, this process is a supplementary method to the Mann-Kendall test applied to the GPD-POT framework by Caruso and Marani (2022). In particular, the 99th percentiles were subjected to a centered 30-year moving average (Orlić et al., 2018), which eliminated decadal fluctuation in sea level over the northern Adriatic and allowed for the examination of gradual changes in extremes. The detrended levels (black line) and their breakdown into the tidal component (blue dashed line) and non-tidal residual component, NTR (red dashed line), expressed in terms of the rise and/or fall of the representative 99th percentile extreme, are compared in Figure 19 with reference to a centered 30-year moving average. The dynamics of extreme values seem to be steady within a range of about ±1 cm for the whole historical period from 1939 to 2024. The 99th percentile of total sea level shows a period of comparatively high values between 1950 and 1970, a marked minimum between the late 1970s and the mid-1980s, and a fairly monotonic increase beginning in the 1990s.After 2000, this growth becomes more noticeable and persists to this day. Between 2015 until 2020, there was a small decline; but, from then on, there has been a sharp increase, totalling almost +1.5 cm. The tidal component's variations have a small amplitude and exhibit a sluggish oscillation without a distinct trend. There is a rise of about +1 cm from 1990 and 2020. In line with Ferrarin et al. (2022), this conclusion generally validates the tidal component's essentially stationary contribution to extreme sea levels. The behaviour of the total NTR curve, which exhibits a greater excursion than the total sea level, is especially significant since it suggests that residual contributions are primarily responsible for the variability of the 99th percentile. The analysis specifically shows that, up to about 2010, the decade 1960-1970, historically linked to two of the most significant events ever documented in the northern Adriatic (1966 in Venice and 1969 in Trieste), exhibits the biggest increases in NTR. NTR decreased until 1970, then had a period of relative stasis at levels of about −1 cm until around 2000. Following this, a distinct and ongoing increase is seen, culminating in a total rise of roughly +3 cm in recent decades.

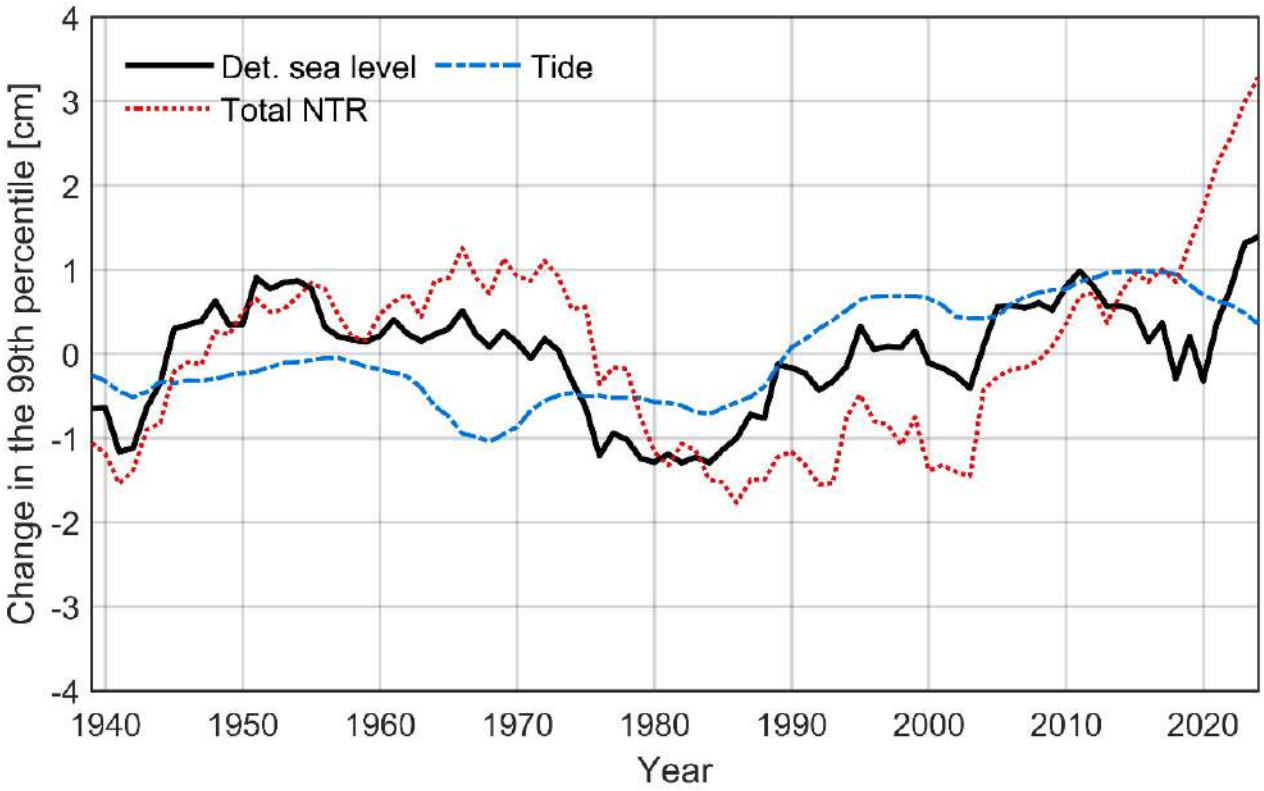

Figure 19. Fluctuation of the 99th percentile extreme from 1939 to 2024, comparing the detrended sea level (black line) with its two components: tide (blue dashed line) and non-tidal residual, NTR (red dots line).

Thus, it can be concluded, within the bounds of a non-stationary analysis, that the recent rise in the 99th percentile of sea level is mainly due to an intensification of NTR extremes rather than changes in the tidal component, especially between 2000 and 2024, when a total increase of about +4.8 cm has been observed.

The variability of the 99th percentile of the NTR is broken down into its primary components in Figure 20: PAW surge and IDAS (climatic components) and seiche and storm surge (meteorological contributions). In this instance as well, 99th percentile anomalies are presented in relation to the mean for the years 1939-2024.

With mostly positive values and a peak between the 1960s and the mid-1970s, the meteorological factors linked to storm surge and seiche account for a significant amount of the variations of the chosen extreme up until the 1970s. The dynamics shift starting in the 1980s. While the storm surge contribution decreases, the seiche component becomes comparatively more stationary. The PAW surge and IDAS components, on the other hand, show a longer-term, climatically driven pattern that is more noticeable. Between 1950 and 1960, their evolution reveals highly positive values for the IDAS component and moderately positive values for PAW surge. The IDAS component thereafter had a noticeable downward inflection until the 1980s and 1990s. With a considerably less noticeable decline soon after 1980, the PAW surge component is almost same. With a slightly more noticeable increase in recent decades, the PAW surge contribution appears to be generally steady, consistent with the behaviour of storm surge and seiche. In contrast, during the historical period 1939-2024, the IDAS component exhibits a considerably more noticeable growth. The IDAS component shows periods of relative stagnation in the 1990s and early 2000s, followed by a gradual and noticeable increase to the present.

Finanziato dall'Unione europea NextGenerationEU
Ministero dell'Università e della Ricerca
Italiadomani
UNIVERSITÀ DEGLI STUDI DI TRIESTE

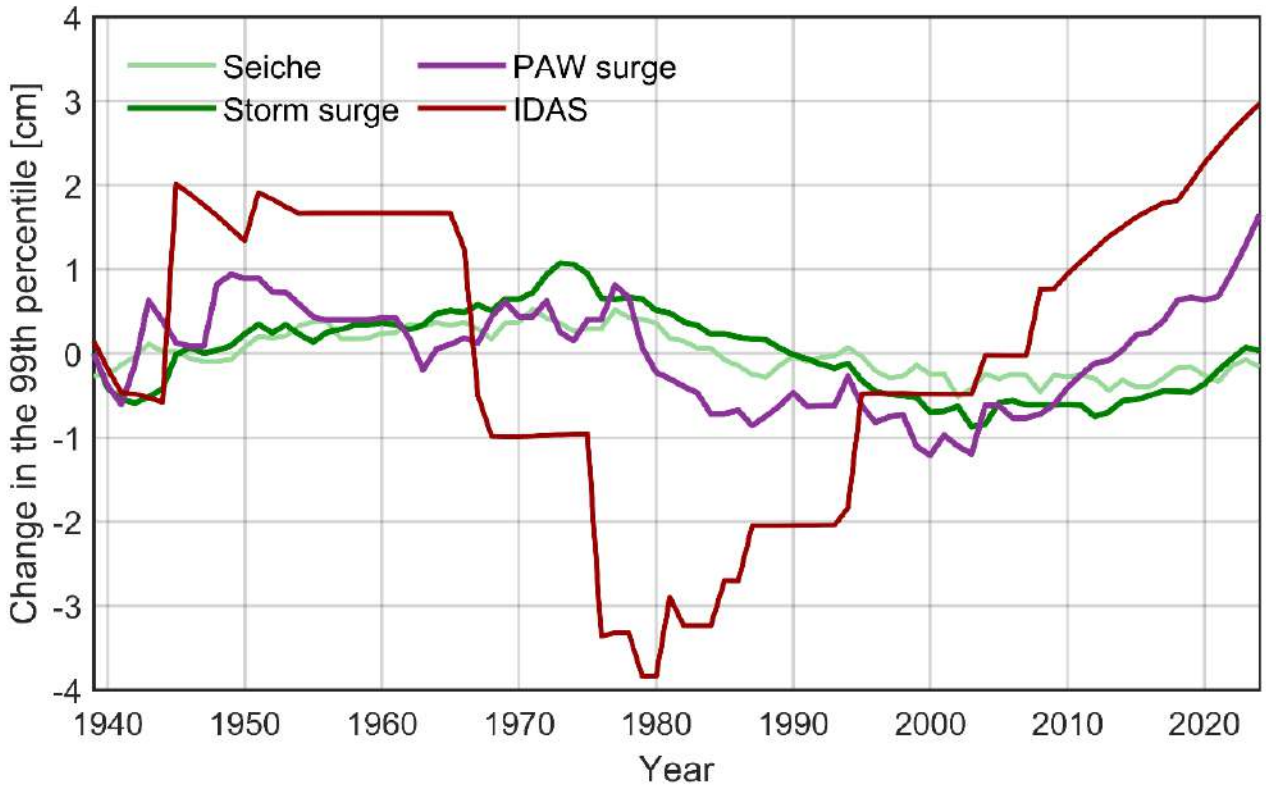

Figure 20. Comparison between the different components of the non-tidal residual (NTR), distinguishing between meteorological components (<10 days) and climatic components (>10 days).

An oscillation between roughly −3.8 cm and +3 cm has been seen since 1980, which corresponds to a trend of roughly 0.18 cm/yr. In conclusion, the study shows that during the time under investigation, the solely climatic IDAS component has experienced particularly notable variations. Therefore, rather than a straightforward amplification of individual storm events, this behaviour probably suggests that the rise in severe NTR levels is increasingly associated with low-frequency components, such as barometric persistence and seasonal/interannual circulation patterns. According to multiple studies (Crisciani et al., 1994; Supić et al., 1999; Raicich, 2010), this kind of sea-level behaviour is typical of the northern Adriatic and has a clear seasonal signature. In the final analysis of this kind, meteorological and climatic contributions were essentially contrasted by comparing short-term components (approximately shorter than 10 days) and long-term components (>10 d). The data presented in Figure 20 is summarized in Figure 21 which separates the long-term (PAW + IDAS, green dashed line) and short-term (seiches + storm surge, red line) contributions to the 99th percentile of total NTR. Similar to earlier figures, a 30-year moving frame is used to report anomalies of the 99th percentile. With positive anomalies of around 1-1.5 cm, the short-term component reaches its peak between the late 1960s and the late 1970s. Around 2000, it gradually declines into weakly negative values. Values have been essentially constant over the past 20 years, fluctuating between −1 cm and 0 cm. This research indicates that there hasn't been a systematic increase in storm strength or daily-scale oscillations over the long run. On the other hand, beginning in the 1980s, the long-term component clearly displays a growing signal. With an amplitude that is on par with or even higher than the overall 99th percentile of total NTR, long-term anomalies change from negative values in the 1970s to clearly positive values in recent decades.

Finanziato dall'Unione europea NextGenerationEU
Ministero dell'Università e della Ricerca
Italiadomani
UNIVERSITÀ DEGLI STUDI DI TRIESTE

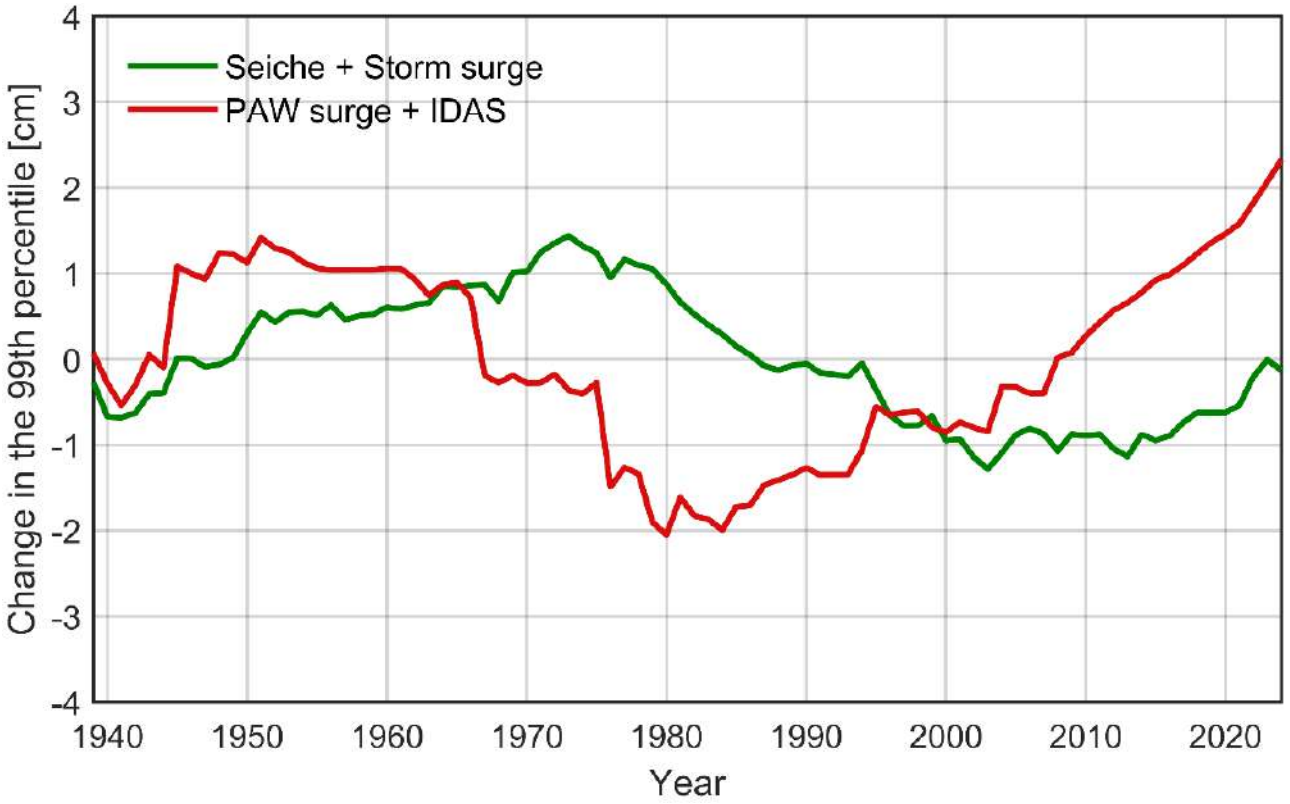

Figure 21. Summarize comparison between the different short-term components (green line) and the long-term components (red line).

The long-term component's greatest value to date is more than +2 cm (led by the combined contribution of IDAS and PAW surge). With the exception of a few periods of standstill, there has been a fairly constant increase of about +4.4 cm during the past 40 years.
These results are broadly consistent with those obtained for Venice by Ferrarin et al. (2022), although evaluated over a shorter temporal window. It follows that the increase in extreme sea levels at Trieste appears to be primarily explained by the growth of the low-frequency, and therefore climatic, component of the NTR (PAW surge + IDAS), namely by a rise in the "background level" upon which tides and storm-surge events are superimposed. In other words, even in the presence of storms with characteristics comparable to those observed historically, the elevation of the seasonal–interannual background level makes the exceedance of critical sea-level thresholds more likely.

5.2.3.3 Non linear interaction Tide-NTR

A substantial and negative non-linear relationship between the astronomical tidal component and the non-tidal residual (NTR) across the examined percentile thresholds is revealed by the study performed on the declustered severe events. Estimated on extreme events, Kendall's τ coefficient (which ranges from −1 to 1) takes values of −0.51, −0.53, and −0.56 for the 99th, 99.5th, and 99.9th percentiles, respectively, with 95% confidence intervals continually deviating from zero. These findings confirm what has previously been documented in the literature for the Northern Adriatic (Tomasin & Pirazzoli, 2007; Tomasin & Pirazzoli, 2009; Ferrarin et al., 2022; Ragno et al., 2023) and show a clear tendency for NTR maxima to occur in conjunction with decreasing tidal contributions or, more generally, during low-tide phases. Therefore, it may be said that systems that are very temporally conditioned by the tidal phase govern the most extreme sea-level events. This behaviour is

in line with the physical interpretation, which states that the strongest storm surges typically form outside of high-tide phases (Horsburgh & Wilson, 2007). This is partially due to dynamical constraints and increased dissipation over shallow waters in the Northern Adriatic basin (Tawn & Vassie, 1989). The same analysis was then applied solely to the storm-surge component in respect to the tidal component in order to gain a more thorough understanding and determine whether there was any reliance or independence between the two. This decision is in line with standard procedure in statistical evaluations of extreme sea levels, which usually concentrate on the interplay between surge and tidal components (e.g., Tomasin & Pirazzoli, 2009). According to the data, the reliance between tide and storm surge shows a different behaviour from what was seen for the tide-NTR interaction. The reliance between the two forcings reduces with increasing extreme event severity, falling from −0.28 (99th percentile) to −0.26 (99.5th) and finally to −0.21 (99.9th). This result suggests that the interaction strength attenuates little towards the distribution's tail.
This implies that the most severe sea levels are more in line with the results of Ragno et al. (2023) rather than being tightly controlled by the co-occurrence of the greatest storm surge with the minimum tidal phase, as noted by Ferrarin et al. (2022). Because the storm-surge component may occur during slightly different tidal phases and/or in conjunction with other processes like seiches, PAW surge, or low-frequency contributions like IDAS, the most extreme events seem to arise from more heterogeneous interactions. As a result, even if there is still a tide-storm surge compensation mechanism, its impact diminishes in the most extreme regime. The physical mechanisms governing the maximum elevations of extreme sea levels are more complex, as evidenced by this behaviour. Further and more thorough investigations were carried out to better understand the various dynamical behaviours of the forcings in order to further explore the potential dependence among them.
By specifically taking into account the relationship between storm surge and seiches, additional evaluations concentrated on the NTR contribution.
The level of the significant anti-correlation between the two factors increases with the severity of the extreme event under consideration, ranging from −0.11 (99th percentile) to −0.12 (99.5th) and up to −0.17 (99.9th). The results are in line with what Ferrarin et al. (2022) reported for Venice. The distinct temporal dynamics between the climatic forcing and the ensuing free oscillation of the northern Adriatic basin can account for this behaviour (Tomasin and Pirazzoli, 1999; Ragno et al., 2023). Following the description of potential meteorological interactions, additional analyses were performed for the slow-variability component with a characteristic climatic signature, represented by the IDAS forcing, and the low-frequency PAW surge component. Despite operating on separate temporal scales, the link between storm surge and PAW surge is very weak or non-existent, suggesting that the two processes are not synchronous. Similar to this, a mild negative reliance that tends to weaken toward the most extreme percentiles characterizes the relationship between storm surge and IDAS. The idea that IDAS represents seasonal to decadal-scale processes unrelated to extreme weather events is supported by this behaviour. Lastly, an analysis of the PAW surge–IDAS pair was conducted. Kendall's τ values are around zero in this instance as well, indicating that there is no significant dynamical interaction between the two contributions. In accordance with what was tested for Venice by Ferrarin et al. (2022) and Ragno et al. (2023), the Student's t copula was used for the examination of interdependence among the various sea-level components. This decision is driven by the t copula's capacity to depict dependency in the distribution's tails, which is crucial for accurately interpreting extreme occurrences. Extreme sea level was assessed as the sum of the tidal component (tide) and the residual part (NTR), taking into account the bivariate case. Simulated samples

were created assuming both dependence and independence between tide and NTR for each dataset of extremes defined by the 99th, 99.5th, and 99.9th percentiles of the detrended series. The 99th, 99.5th, and 99.9th percentiles of the corresponding distributions were then extracted in order to compare the simulated values. The findings demonstrate that there is a negative difference between the quantiles simulated under independence and dependency assumptions, which causes an overestimation of extremes when independence is assumed in contrast to scenarios that take into account the dependence seen in the recorded data. In particular, the bivariate tide-NTR copula yields values that vary from −21 cm to −56 cm, with the biggest reductions linked to the highest extremes. For the 99th, 99.5th, and 99.9th percentiles and the associated non-linear interactions, Table 15 presents the extreme levels calculated by the Student's “t” copula model, taking into account both the dependence (NLIdip) and independence (NLIind) assumptions.

Dataset	***Percentile***	***bivariate copula (tide,NTR)***		
		Extreme DEP (cm)	***Extreme IND (cm)***	***NLI***
99th	99th	115	136	-21
	99.5th	123	150	-26
	99.9th	146	201	-55
99.5th	99th	122	147	-25
	99.5th	131	161	-30
	99.9th	159	215	-56
99.9th	99th	147	201	-54
	99.5th	164	215	-51
	99.9th	196	224	-28

Table 15. Assumption of extreme dependence and independence through a bivariate copula model of tide and NTR, accounting for their non-linear interaction.

The values shown in Table 15 are in line with what Ferrarin et al. (2022) found for Venice. Tail dependence, which restricts the likelihood of co-occurrence of tidal maxima and residual maxima, is linked to the decrease in extreme values. Consequently, extreme occurrences are limited in their severity. These findings are consistent with the qualitative data for the North Adriatic provided by Tomasin and Pirazzoli (2009). There is no obvious monotonic relationship between dataset, percentile, and NLI for the 99.9th percentile dataset. Even while this behaviour might seem unusual, it is consistent with what is expected when estimates are based on simulated samples and a small number of extreme occurrences (176 events for the 99.9th percentile) are analysed. According to Ferrarin et al. (2022), this behaviour results from the non-linear dependence between the tide and NTR components as well as the inherent variability of extreme-event data.

The same method was used with a multivariate copula once the bivariate analysis was finished, taking into account the five primary variables that determine the NTR. Therefore,

Finanziato dall'Unione europea NextGenerationEU
Ministero dell'Università e della Ricerca
Italiadomani PIANO NAZIONALE DI RIPRESA E RESILIENZA
UNIVERSITÀ DEGLI STUDI DI TRIESTE

the explicit combination of the tidal contribution, seiches, storm surge, PAW surge, and IDAS is used to analyse the entire extreme sea level. The non-linear interactions between the many dynamic factors that define the overall extreme level can be more precisely quantified by simultaneously analysing these five variables. The resulting differences are still negative when using the multivariate copula, but their size is more constrained, ranging from −22 cm to −38 cm. In order to account for non-linear interactions through the multivariate copula, Table 16 presents the extreme levels calculated using the t-copula model for the 99th, 99.5th, and 99.9th percentiles under the assumptions of dependence (NLIdip) and independence (NLIind). The effect of breaking down the NTR into its physical components, which effectively minimizes the amplification of co-occurrence commonly observed between tide and NTR, is responsible for the narrower range. As a result, the multivariate copula offers an estimate that is both potentially more accurate in capturing the non-linear interactions underlying extreme events and unquestionably more conservative than the bivariate model. Overall, it can be said that the co-occurrence of the forcings controlling extreme sea levels in the North Adriatic can be better realistically explained by using both bivariate and multivariate models. The distortions brought about by the straightforward independent accumulation of individual contributions are lessened by this method.

Dataset	***Percentile***	***multivariate copula (tide,storm surge, seiches, PAW surge, IDAS)***		
		***Extreme DEP** (cm)*	***Extreme IND** (cm)*	***NLI***
99th	99th	108	130	-22
	99.5th	113	137	-24
	99.9th	123	150	-27
99.5th	99th	115	139	-24
	99.5th	120	147	-27
	99.9th	131	164	-33
99.9th	99th	133	164	-32
	99.5th	138	171	-33
	99.9th	148	186	-38

Table 16. Assumption of extreme dependence and independence through a multivariate copula model of *(tide,storm surge, seiches, PAW surge, IDAS)*, accounting for their non-linear interaction.

In this way, more reliable estimates of the non-linear effects among meteomarine forcings are made possible by the multivariate approach. Lastly, episodes with extremely high storm surge forcings were identified and analysed by assessing the matching astronomical tidal level at the time of the peaks in order to validate the statistical interpretation. Within the bounds of the statistical method, the results, which are presented in Table 17, offer empirical proof of the tidal component's influence on the intensity of extreme occurrences.

Data event	*Storm surge (peak)*	*Tide*
26/11/1969	+96.9	+2.1
10/12/1954	+90.6	-46.5
04/11/1966	+84.6	+19.1
29/10/2018	+75.8	-24.7
07/11/2000	+75.6	-28.2

Table 17. Major storm surge events recorded at their peak and correlated with the tidal level measured at the same time. The values were extracted during the decomposition of the NTR component using different frequency spectra.

As reported by Ferrarin et al. (2022) for Venice, also with regard to the most significant surge events recorded in Trieste, the observed peak is consistently associated with a falling tide or a low-tide phase. By way of example, the 4 November 1966 event in Venice produced a storm surge of about 107 cm (Ferrarin et al., 2022), while the sea level at the time of the surge peak was only about 10–15 cm (see figures on p. 26 in Canestrelli et al., 2001). Moreover, as documented by Tomasin and Pirazzoli (2007; 2009) for the 99.9th percentile, the typical surge peak occurring between October and December (linked to severe meteorological conditions) and the typical tidal peak associated with equinoctial tides occur in different periods of the year in the Northern Adriatic. This further highlights the presence of a non linear anticorrelation between surge and astronomical tide, as previously identified.

5.2.4 Analysis of Mean vs. Max levels and Threshold exceedance

To analyse the behaviour of extreme sea levels and to further substantiate the interpretation of the observed increase in maximum water levels, the same comparison previously applied to Grado, was also performed for Trieste. In particular, the analysis focuses on the different rates of increase of mean sea level and annual maximum sea levels over the last 30 years. The trends were directly derived from observations recorded by the Trieste tide gauge over the period 1991-2024. Both trends are shown in Figure 22.

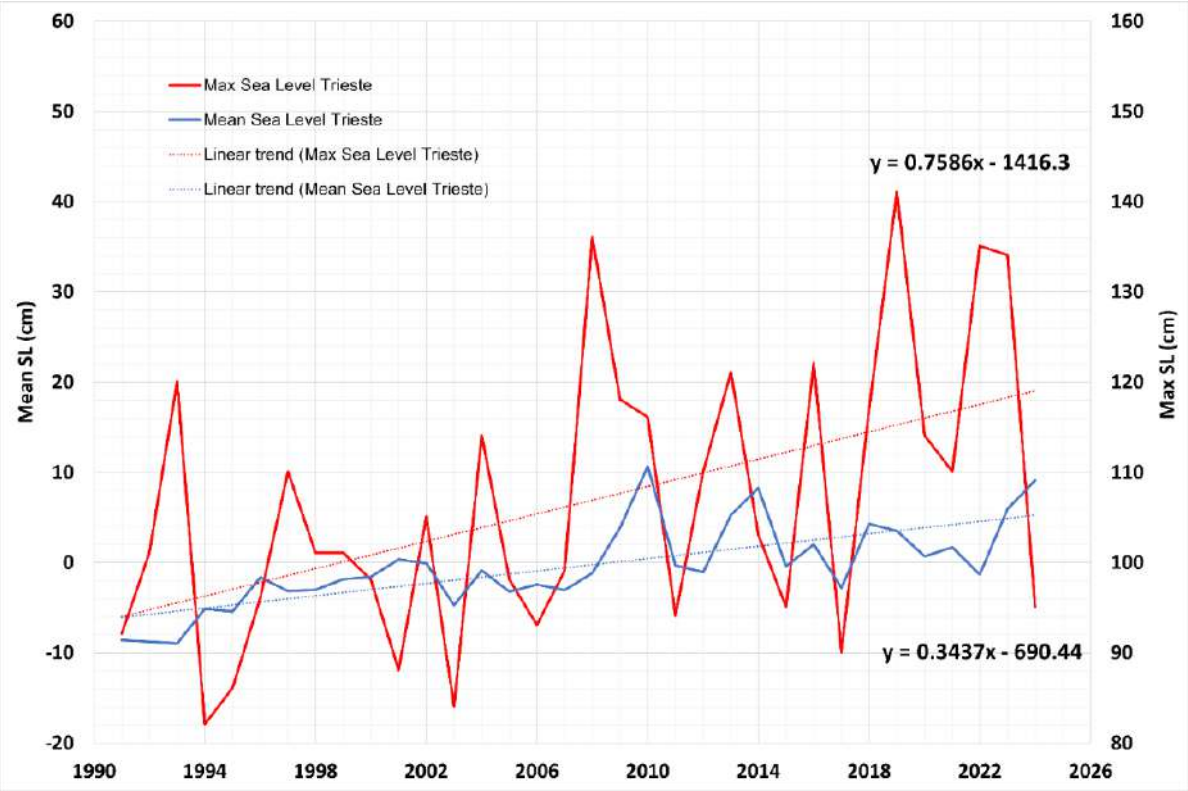

Figure 22. Comparison of the mean sea level (blue line) and the maximum sea level (red line) observed in Trieste from 1991 to 2024 (IGM42 reference). The left axis indicates the scale for mean sea level, whereas the right axis signifies the maximum levels.

As shown in Figure 22, the observed annual maximum sea levels are increasing at a rate of 7.6 mm/yr, more than twice the rate estimated for mean sea level, which is approximately 3.4 mm/yr. Within the limits imposed by a 30-year statistical window, this result indicates that flood-related risk is increasing more rapidly than suggested by projections based solely on mean sea level rise. Risk is commonly associated with the occurrence of flooding events; however, it is not determined exclusively by the maximum levels reached, but also by the duration of such events.

5.3 Grado vs. Trieste: Sea Level trend comparison

Once the extreme-value statistics for Grado and Trieste had been updated, and the comparison between mean and maximum sea levels had been assessed for both sites over a comparable time window, the need emerged to directly compare the two locations. The aim is to discuss the recorded values and to quantify the potential influence of factors not yet explicitly addressed, namely coastal exposure and orientation with respect to the dominant forcings The analysis is based on the trends of mean and maximum sea levels for Grado shown in Figure 11, and the corresponding trends for Trieste reported in Figure 22. The comparison indicates that Grado exhibits a higher vulnerability to extreme events in terms of maximum sea levels reached. This behaviour is most likely related to its exposure and orientation with respect to the Scirocco wind, combined with the strong inverse barometric pressure gradient that characterises the northern Adriatic (Lionello et al., 2012). In recent years, however, intense Libeccio-driven events have also been observed, such as the multi-day storm between 27 October and 5 November 2023.

Finanziato dall'Unione europea NextGenerationEU
Ministero dell'Università e della Ricerca
Italiadomani PIANO NAZIONALE DI RIPRESA E RESILIENZA
UNIVERSITÀ DEGLI STUDI DI TRIESTE

In contrast, Trieste is located in a more sheltered setting within the Gulf of Trieste. The Istrian Peninsula provides partial protection from the Scirocco fetch, which may explain the generally lower extreme levels observed. Compared to Grado, the Trieste coastline is more favourably oriented towards Libeccio winds, which tend to generate not only a significant sea level rise but also an enhancement of wave forcing. This effect is particularly relevant along the high and urbanised eastern coasts of the Gulf of Trieste, as documented by Busetti et al. (2024).

5.3.1 Grado Long-term projections

After analysing the maximum sea levels, the trends in mean sea level were also compared for the two locations. Considering the last 30 years (1991-2023), the sea level rise trend at Grado is characterised by a rate of about 4.8 mm/yr (Figure 11). When the reference time window is shortened, the estimated trend increases, and interannual sea-level fluctuations can reach up to +10 cm, as observed in 2010.The mean sea-level trends at Grado and Trieste show notable similarities. This is expected, as both tide gauges are located within the same regional context, namely the northern Adriatic, although they are embedded in markedly different environmental settings. As discussed in Section 3.6.2 (see Figure 3) the Trieste tide gauge is located directly along the open coast, whereas the Grado tide gauge is situated within the Grado Lagoon and is therefore more likely affected by ground subsidence related to the stratigraphic characteristics of the underlying sediments (Tosi et al., 2010). It is therefore plausible that the difference between the observed rates approximately 4.8 mm/yr at Grado and 2.8 mm/yr at Trieste (Figure 23 from Spadotto et al., 2025), can be at least partly attributed to subsidence, i.e. vertical land motion (VLM). Trieste represents the only coastal site in the northern Adriatic where subsidence is minimal compared to the surrounding areas (Sanchez et al., 2018; Zerbini et al., 2021). The vertical land motion (VLM) inferred from the comparison between observed sea-level trends and values reported in the literature (Da Lio et al., 2018; Areggi et al., 2023) falls within the range of 1-2 mm/yr. Accordingly, a mean subsidence rate of 1.5 ± 0.5 mm/yr was adopted for Grado, as a representative value for the formulation of relative sea-level rise (RSLR) projections for 2050 and 2100. Using sea-level projections closest to Trieste from the NASA Sea Level Projection Tool (https://sealevel.nasa.gov/ipcc-ar6-sea-level-projection-tool), the VLM contribution was computed by multiplying this rate by the number of years elapsed since the reference year 2006. This corresponds to 44 years for the 2050 horizon and 94 years for the 2100 horizon. The resulting VLM contributions to be incorporated into the SLR scenarios are therefore 6.6 ± 2.2 cm by 2050 and 14.1 ± 4.7 cm by 2100.

Finanziato dall'Unione europea NextGenerationEU
Ministero dell'Università e della Ricerca
Italiadomani PIANO NAZIONALE DI RIPRESA E RESILIENZA
UNIVERSITÀ DEGLI STUDI DI TRIESTE

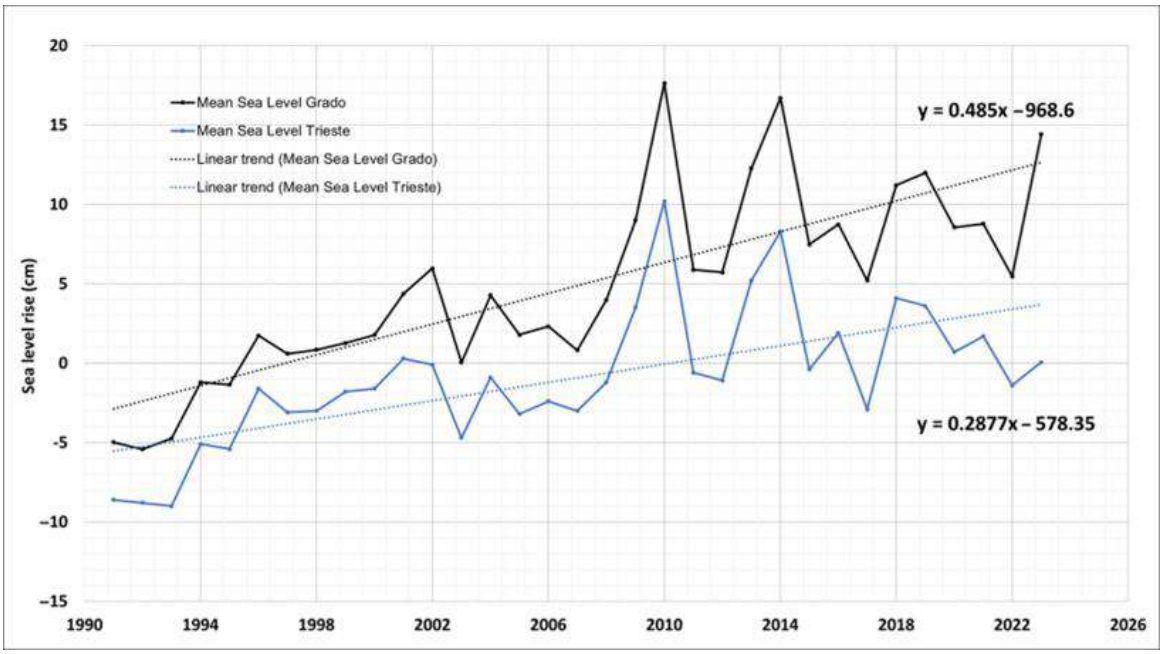

Figure 23. The 30-year trend of sea level change in Grado (black line) and Trieste (blue line) with IGM42 reference. Elevation in ordinate has been kept to scale for each series. Trends can be calculated based on linear regression (form Spadotto et al., 2025).

Table 18 summarizes the projected sea-level values for 2050 and 2100 based on the calculations described above.

Year	**SLR Scenario Reference 2006 Baseline (1995-2014)**	**Trieste Sea Level (cm)**	**Total VLM (cm) for Grado (Average Rate)**	**Total Sea Level for Grado (cm)**
2050	SSP1-2.6 (median)	17	6.6	23.6
	SSP5-8.5 (median)	21	6.6	27.6
2100	SSP1-2.6 (median)	39	14.1	53.1
	SSP5-8.5 (median)	67	14.1	81.1

Table 18. Projection of sea level in 2050 and 2100 according to IPCC AR-6 (Masson-Delmotte et al., 2021), as reported in the NASA Sea Level Projection Tool. Sea level projections refer to the city of Trieste. Vertical land motion (VLM) for Grado is assumed at a rate of 1.5 ± 0.5 mm/yr. The total sea level for Grado is calculated by adding the two components.

At this point, focusing on the most relevant rare events for urban planning namely the 10-, 30-, and 100-year return periods (R_Ps) –it is possible to assess how the effective R_Ps may shift by accounting for the projected sea-level rise by 2050 and 2100 under both best- and worst-case scenarios. In particular, for an episodic extreme event with low probability of occurrence (R_P=100 years), combining the projected sea-level rise for 2050 and 2100 under the high-emission scenario SSP5–8.5 allows anticipating the following potential situation:

$$\boldsymbol{Critical\ threshold_{2050}} = current\ R_P100y - RSLR_{2050} = 168\ cm - 28\ cm = \mathbf{140\ cm}$$

Finanziato dall'Unione europea NextGenerationEU
Ministero dell'Università e della Ricerca
Italiadomani
UNIVERSITÀ DEGLI STUDI DI TRIESTE

Considering a worst-case scenario, the 168 cm level in 2050 becomes, after subtracting 28 cm of sea-level rise, approximately 140 cm. This adjusted level corresponds to an episodic event with an estimated return period (R_P) of about 14-15 years. In probabilistic terms, exceedance of the 168 cm threshold by 2050 would therefore occur at a frequency almost seven times higher than under present-day conditions. This implies a marked increase in the occurrence of extreme sea-level events in the near future. The same reasoning can be applied to an episodic event currently associated with R_P=100 years when considering projections to 2100. In this case, subtracting 53 cm yields an adjusted level of about 115 cm. This value is consistent with an episodic event with an R_P of roughly 2-3 years. Probabilistically, exceedance of the 168 cm threshold by 2100 could therefore occur about 33 times more frequently. These shifts in effective return periods, derived for the eastern sector of the northern Adriatic, are broadly consistent with the results reported by Lionello et al. (2021), who quantify analogous R_P changes under projected sea-level rise for the western northern Adriatic by 2050 and 2100.

5.3.2 Trieste Long-term projections

The same approach adopted for Grado can be applied to Trieste by using the VLM estimates reported in Table 18, while updating the statistical thresholds with the GPD-POT results provided in Table 10b, derived for the "above mm19" series. The analysis is performed in terms of total extreme sea level, defined as the sum of: (i) a reference mean sea level and (ii) the storm-related contribution, i.e., the combined effect of astronomical tide and meteorological surge. Consistently with the mm19 detrending framework (section 4.3.2.2), the reference mean sea level is taken from the most recent period coherent with the centred 19-year moving mean, i.e., approximately 2006-2024. This choice also ensures consistency with the operational convention adopted in the PGRA (see Table 2b Under this reference, mean sea level at Trieste over 2006–2024 is approximately +2 cm relative to the IGM42 datum. Accordingly, the updated extreme levels used for the projections are obtained by adding the Trieste reference mean sea level (+2 cm, IGM42) to the return levels estimated through the GPD-POT model (above mm19). The resulting updated extreme thresholds –adopted here to support the long-term projections for the Trieste-Muggia sector– are reported in Table 19.

R_P (years)	**Extreme levels "above mm19" (cm)**	**Average MSL (cm) interval 2006-2024**	**Updated Total water level (cm)**
2	113	+2	115
10	132		134
30	144		146
100	156		158

Table 19. Updated total water level values for Trieste, considering an average msl of +2 cm (interval from 2006- 2024), as a function of return period (GPD-POT distribution), 1939-2024 reference period.

Still focusing on the most severe extremes and on urban planning relevant return periods (R_P = 10, 30, and 100 years), changes in recurrence can be assessed by accounting for the projected mean sea-level rise by 2050 and 2100 under both optimistic and pessimistic

Finanziato dall'Unione europea NextGenerationEU
Ministero dell'Università e della Ricerca
Italiadomani PIANO NAZIONALE DI RIPRESA E RESILIENZA
UNIVERSITÀ DEGLI STUDI DI TRIESTE

scenarios (see Table 18). For a rare episodic event associated with R_P=100 years, combining the baseline extreme threshold with the projected sea-level rise under the SSP5–8.5 pathway allows anticipating a potential shift in effective return periods, as outlined below:

$$\boldsymbol{Critical\ threshold_{2050}} = current\ R_P 100y - RSLR_{2050} = 158\ cm - 21\ cm = \mathbf{137\ cm}$$

Assuming a pessimistic scenario, the 158 cm threshold in 2050 becomes approximately 137 cm after subtracting 21 cm of projected mean sea-level rise. This adjusted level corresponds to an episodic event with an estimated return period of about 14-15 years. In probabilistic terms, exceedance of the 158 cm threshold by 2050 could therefore occur almost six to seven times more frequently. Consequently, the frequency of extreme events is expected to increase substantially in the near future. The same logic can be extended to a 100-year episodic event under an optimistic projection to 2100. In this case, subtracting 67 cm yields an adjusted level of roughly 92 cm in 2100. This value corresponds to an event with a return period well below annual recurrence. A level of 92 cm has a high likelihood of being reached even under the occurrence of a single very intense surge event (see Table 17) making it plausible that –under future conditions– it could shift to multi-annual recurrence. In probabilistic terms, exceedance of the 158 cm threshold by 2100 could occur more frequently than once per year, potentially at semi-annual frequency or even higher.

5.4 Muggia extreme values

This section presents and discusses the updated statistically derived extreme sea levels for the town of Muggia. Given its close proximity to Trieste, the same extreme-level estimates obtained from the statistical analysis of the Trieste tide-gauge record (1939-2024) are adopted. Specifically, the values used for Muggia are those derived from the GPD-POT analysis based on extremes referenced “above mm19” (see Table 10b). Since the statistical extraction was performed relative to the centred 19-year moving mean, the total extreme sea level is reconstructed as the sum of the reference mean sea level and the astronomical tide plus surge components. Accordingly, adopting as reference the mean sea level of the most recent decade (approximately 2006-2024), and following the application framework used in the PGRA (see Table 2b the reference mean sea level for Trieste is about +2 cm relative to the IGM42 datum. The updated extreme sea levels for Muggia are therefore obtained by summing the GPD-POT derived extreme values and the above reference mean sea level from Trieste, as reported in Table 19. Once defined, these extreme levels were used as boundary conditions for the subsequent dynamic modelling, carried out with the MIKE21 hydrodynamic model.

5.5 Lignano extreme values

This section presents and discusses the updated statistically derived extreme sea levels for the town of Lignano. The site is located along the western margin of the Grado–Marano Lagoon and is therefore in close proximity to Grado. For this reason, the same extreme sea-level values estimated for Grado using the Gumbel Block Maxima (Gumbel-BM) approach were adopted for Lignano. Accordingly, the values used for Lignano were derived following the methodology described in Section 4.3 and are reported in Table 5. As for the other study sites, once the extreme levels were defined for Lignano, they were subsequently employed

Finanziato dall'Unione europea NextGenerationEU
Ministero dell'Università e della Ricerca
Italiadomani PIANO NAZIONALE DI RIPRESA E RESILIENZA
UNIVERSITÀ DEGLI STUDI DI TRIESTE

as input conditions for the dynamic simulations performed with the MIKE21 modelling framework.

5.6 Downscaling bathtub approach analysis of Grado

This chapter presents and discusses the results obtained from the application of the static bathtub approach, implemented using ArcGIS Pro 3.10. For each generated inundation scenario, the updated flood thresholds reported in Table 5 are adopted as reference levels.

5.6.1 *Downscaling analysis of short-term flooding*

This section presents the set of marine flooding hazard maps derived from the developed inundation scenarios. Each scenario represents an episodic event associated with a specific return period (R_P) and is defined by a critical threshold corresponding to the total water-level rise reached during the event. The simulations were carried out using a static (bathtub) approach combined with a qualitative assessment of the results, deliberately neglecting dynamic variables such as inflow velocity and flood duration. The wave component was excluded from the analysis, as water enters through the Grado inlet and propagates within the lagoonal system, where wave set-up is progressively damped. Table 20 provides a summary of the analysed scenarios, reporting the R_P associated with each threshold value and the total extent of the urbanised area affected by flooding, expressed both in square kilometres and as a percentage of the entire municipality.

R_P (years)	Extreme levels (cm)	Inhabitated Area (km^2)	Flooded Area (%)
2	111	0.016	1.67
10	136	0.20	20.8
30	151	0.40	41.7
100	156	0.61	63.5

Table 20. Extreme water levels with return periods, which correspond to the relative flooded areas, expressed in terms of size (km^2) and percentage value with respect to the built-up area of the Municipality of Grado of 0.96 km^2 (from Spadotto et al., 2025).

The following section presents the hazard maps derived from the analysed episodic events. The hazard maps are constructed by representing the water depth, defined as the maximum hypothetical elevation of water above the ground surface reached during each flooding event. Water depth is computed as a function of the initial DTM elevations and the spatial extent of the inundated area.

Finanziato dall'Unione europea NextGenerationEU
Ministero dell'Università e della Ricerca
Italiadomani PIANO NAZIONALE DI RIPRESA E RESILIENZA
UNIVERSITÀ DEGLI STUDI DI TRIESTE

5.6.1.1 The 2-Year Return Period Episodic Event

In the case of a meteomarine event with a R_P=2 years, the water level has a total elevation of approximately 111 cm. The flood hazard map is shown in Figure 24.

Figure 24. Flood hazard map representing an event with a 2-year R_P (111 cm). The blue colours represent the water depths as a function of the city's DTMs elevations. As for the Old Town, the water enters from the Riva Brioni promenade and the docks of the Mandracchio Canal. The eastern part of the town (Grado East) is not affected by ingress because it is characterized by higher embankments (from Spadotto et al., 2025).

The downscaling analysis (scale 1:5000) enables detailed verification of the problems caused by flooding. On the map, it is possible to establish that the criticalities occur mostly around the Mandracchio Canal and the Brioni promenade. Both stretches correspond to the lowest urban areas that allow the water mass to advance inwards. The criticalities found mostly concern the propagation of the water mass into the interior of the old town by means

of the urban network. The nearby historic centre, located south of the Mandracchio Canal, does not exhibit any particular criticality.

5.6.1.2 The 10-Year Return Period Episodic Event

In the case of a meteomarine event with a R_P=10 years, the water level has a total elevation of 136 cm. The flood hazard map is shown in Figure 25.

Figure 25. Flood hazard map representing an event with a 10-year R_P (136 cm). The blue colours represent the water depths as a function of the city's DTM elevations: (a) The inundation map of the 'Old Town' sector shows that this area is almost entirely affected by the extent of the flooding. Flooding also affects parts of the historic centre. (b) It depicts the slight expansion of flooding to the east as well, with some ingressions of the water mass toward the built-up area by the Moreri Canal. (c) Flooding in the western part of the historic centre during 27 October 2023 (photo credits: Cester E.). (d) Expansion of the water mass along the western docks of the Mandracchio Canal during 27 October 2023 (photo credits: Cester E.). (e) expansion flooding along A. Manzoni Street during 29 October 2018 (photo credits: Folla M.) (from Spadotto et al., 2025).

The 1:5000 downscaling analysis made it possible to observe more clearly the extended criticality along the lagoon promenade of Riva Brioni, the town's primary western encroachment area. We could also observe a generalised extension of the water mass around the Mandracchio Canal through its perimetral docks. Compared to the previous simulation, the water mass extends both to the east and west of Mandracchio, almost completely affecting the old town and partially affecting the historic core to the south. There

is also an eastern expansion of the water mass through two areal criticalities of the lagoon promenade along the Moreri Canal.

5.6.1.3 The 30-Year Return Period Episodic Event

Compared to the previous scenario, in the simulation of a storm surge event with a return time of 30 years and a total elevation of 151 cm, the urban flooding also extends along the eastern part of the town (Figure 26).

Figure 26. Flood hazard map representing an event with a 30-year R_P (151 cm). The blue colours represent the water depths as a function of the city's DTMs elevations: (a) The inundation map of the 'Old Town' sector shows that this area is completely flooded. The extent of the flooding also affects much of the historic centre. (b) The widespread flooding in the city's 'Grado East' area. Water flows inland through the Moreri Canal's embankment at several places. (c) Flooding near the southwest dock of the Mandracchio Canal during 27 October 2023 (photo credits: Cester E.). (d) Flooding in front of the St. Eufemia Cathedral during 12 November 2019 (photo credits: Patruno V.). (e) Extensive flooding along the end of the Moreri Canal embankment, Monfalcone Street during 27 October 2023 (photo credits: Rai Tgr Fvg website) (from Spadotto et al., 2025).

The flooding affects the entire old town, particularly the historic core surrounding the St. Eufemia Cathedral and the Baptistery. It extends approximately 2000 metres along the lagoon promenade of the Moreri Canal, impacting many areas in the eastern part of the city. The additional 15 centimetres, compared to the 10-year R_P scenario, clearly illustrate how

Finanziato dall'Unione europea NextGenerationEU
Ministero dell'Università e della Ricerca
Italiadomani PIANO NAZIONALE DI RIPRESA E RESILIENZA
UNIVERSITÀ DEGLI STUDI DI TRIESTE

a meteomarine event of this magnitude can lead to an expansion of the water mass covering a significant portion of the urban fabric.

5.6.2 *Lagoon promenade downscaling analysis*

This section presents the results of the downscaling analysis applied along the entire promenade bordering the interface between the city and the lagoon. The assessment encompasses the full perimeter embankment stretching from Riva Brioni to the easternmost part of the Moreri Canal, divided into four macro-sectors (Figure 8). This approach enabled a more thorough examination of the embankments, assessing both specific and broader critical issues. Table 21 presents the analysed promenade/embankment sectors along with their respective lengths, the total length of the embankments, and the percentage of each section in relation to the total length.

Promenade/embankment sector	Length (m)	Percent (%) of total lenght
Riva Brioni - Mandracchio C.	573	9
Mandracchio C.	1392	22
Schiusa Island	1681	27
Mandracchio C - Moreri C.	2685	42
Total embankment	6334	100

Table 21. Lagon promenade/embankment sectors analysed for elevation analysis aimed at the flooding assessment (from Spadotto et al., 2025).

The two-lagoon promenade and docks sectors most vulnerable to marine ingression are described below. The first stretch considered concerns the Riva Brioni-Mandracchio sector. The second section concerns the Mandracchio Canal. The other two sectors, Moreri Canal and Schiusa Island, are shown and described in the Supplementary Materials in Spadotto et al., (2025).

5.6.2.1 Riva Brioni - Mandracchio C.

The section considered has a total length of 260 m. La Figure 27 displays the analysis of the promenade's heights along the entire Riva Brioni. The survey covered a total of 6188 measured points within an elevation range of 70 to 125 cm. Hence, approximately 85% of the height of the promenade section considered is below 111 cm (Figure 27b). This means that, already with a meteomarine event with a high probability of occurrence, having a R_P of 2 years, the perimeter promenade is not in a safe condition. On the other hand, considering an episodic event with a R_P of about 5 years and approximately 125 cm of water level, the entirety of the promenade is not in a safe condition, causing the expansion of the water mass in the western area of the urban centre.

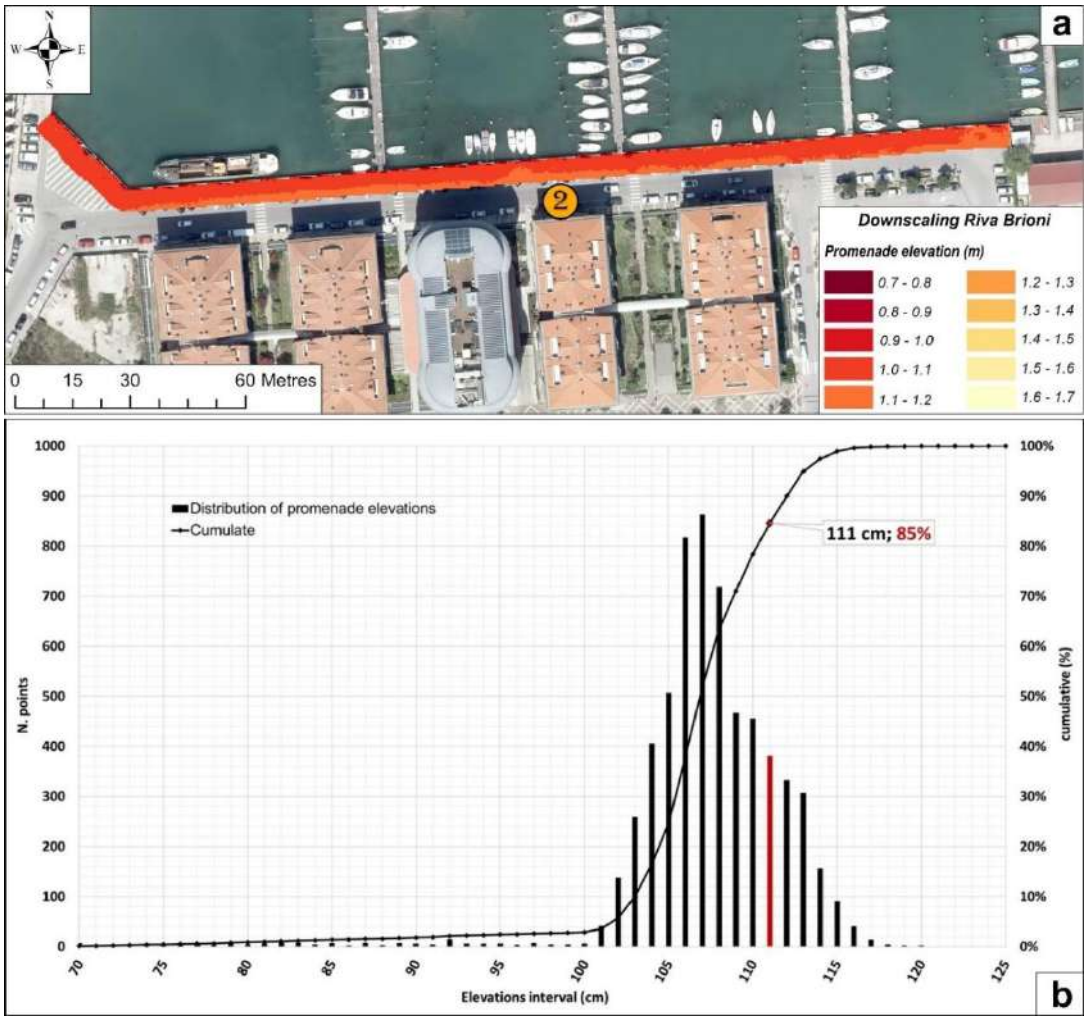

Figure 27. Critical sector promenade of Riva Brioni: (a) represents the elevations extracted from the 6-m buffer of the promenade. The elevation values of the promenade range from 70 to 125 cm. (b) represents the statistical distribution of the elevations extracted from the promenade of Riva Brioni. Shown in red is the 111-cm elevation column, which represents about 85% of the cumulative statistics. The promenade is then flooded with an event with a very high probability of occurrence (R_P=2 years) (from Spadotto et al., 2025).

5.6.2.2 Mandracchio C.

The Mandracchio Canal has a total length of 1392 m, corresponding to 22% of the total lagoon promenade. The analyses of the canal's banks covered a total of 31782 measured points within an elevation range of 70 to 155 cm. Historically, the main flooding within the built-up area of Grado occurs through the docks of the Mandracchio Canal, the preferential route of water ingression within the ancient centre. Infatti, come descritto nella sezione 5.1.2 (see Figure 12), la soglia di 110 cm è stata superata per 3 ore in un anno quasi 9 volte negli ultimi 15 anni (2008-2023). This statistic is corroborated by the graph in Figure 28b, which shows that 50% of the Mandracchio docks are not in a safe condition for an event with a R_P-2 year. It follows that even with a very low elevation threshold, the historic centre is experiencing significant flooding. On the other hand, considering a R_P of 10 years, with a medium-high frequency of occurrence and a level of 136 cm, the entire docks of the Canal do not guarantee any safety, entailing extensive flooding both to the west and east of the Mandracchio itself, also affecting the portion of the historic core post south of the Canal (Figure 25a,c).

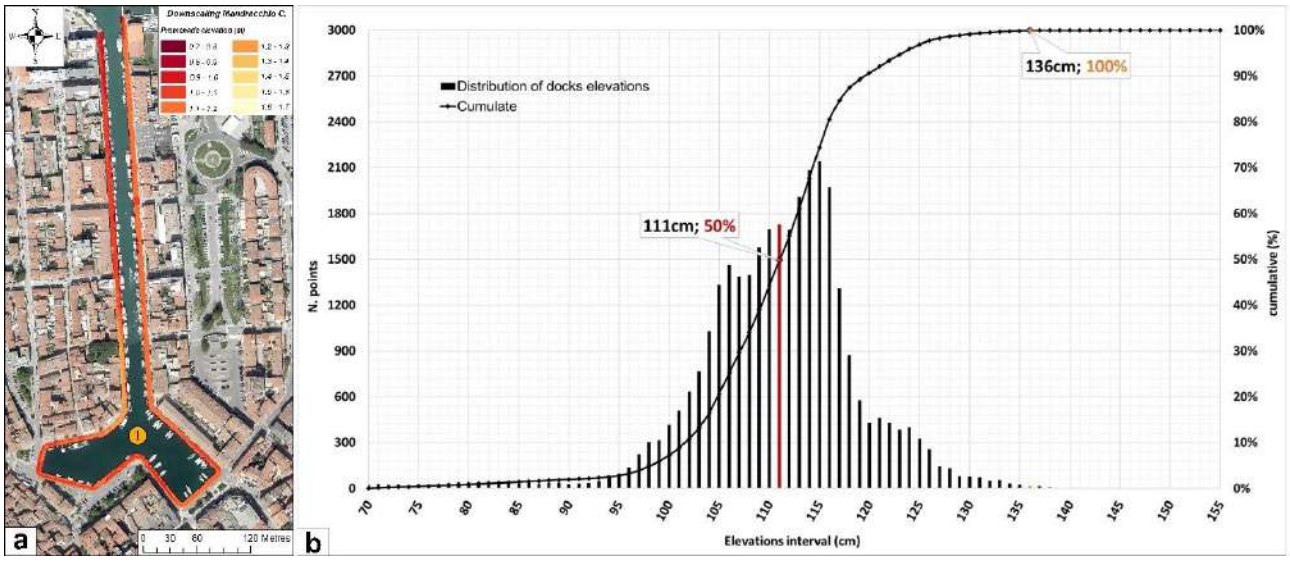

Figure 28. Critical sector of Mandracchio Canal docks: (a) represents the elevations extracted from a 6-m buffer of the docks. The elevation values of the canal docks range from 70 to 155 cm. (b) represents the statistical distribution of the elevations extracted from the Mandracchio Canal docks. Shown in red is the 111 cm elevation column, which represents about 50% of the cumulative statistics. Shown in orange is the elevation of 136 cm, the level of an event with a medium to high probability of occurrence (R_P=10 years), resulting in complete submergence of the canal docks (from Spadotto et al., 2025).

5.6.3 *Bathtub vs. Dynamic modelling*

In according to applications at the territorial and urban scales (e.g., Mariano et al., 2021, Mannarini et al., 2025), the static bathtub approach was employed as a first screening tool to confirm possibly flooded urban regions, as detailed in Section 4 of the materials and methods. Nevertheless, the static model ignores friction losses and local hydraulic restrictions, as well as the dynamic mechanisms that control the spread of the extreme event's peak. As emphasized by Vousdoukas et al. (2016) and Didier et al. (2019), if these factors are not taken into account, they can nearly always result in overestimations of flooded regions, with occasionally serious inaccuracies. In order to quantify any spatial differences and evaluate the static model's applicability limits, the results of the static approach were compared by simulating the event of November 4-5, 2023, in hydrodynamic form, using the town of Grado as the first case study under analysis. This was done in accordance with recent literature (Sanders et al., 2024).

The comparison between the static bathtub approach and the hydrodynamic simulation highlights clear spatial discrepancies in the predicted inundation event (Figure 29). A more consistent and laterally continuous flood pattern is produced by the static model, which is distinguished by a “horizontal filling” of low-lying areas once the threshold elevation is surpassed. This causes water to penetrate farther inland, especially in areas where small topographic depressions are connected by narrow passageways. On the other hand, the hydrodynamic model displays a flooding pattern that is more spatially selective. Local hydraulic controls, such as friction effects, urban impediments, and temporary water-level gradients, have a significant impact on the simulated inundation, which is restricted along preferential flow pathways. Because of this, certain regions that the bathtub approach indicated as flooded stay dry in the dynamic simulation, while, other regions, show more constrained spatial distributions and lower flood depths.

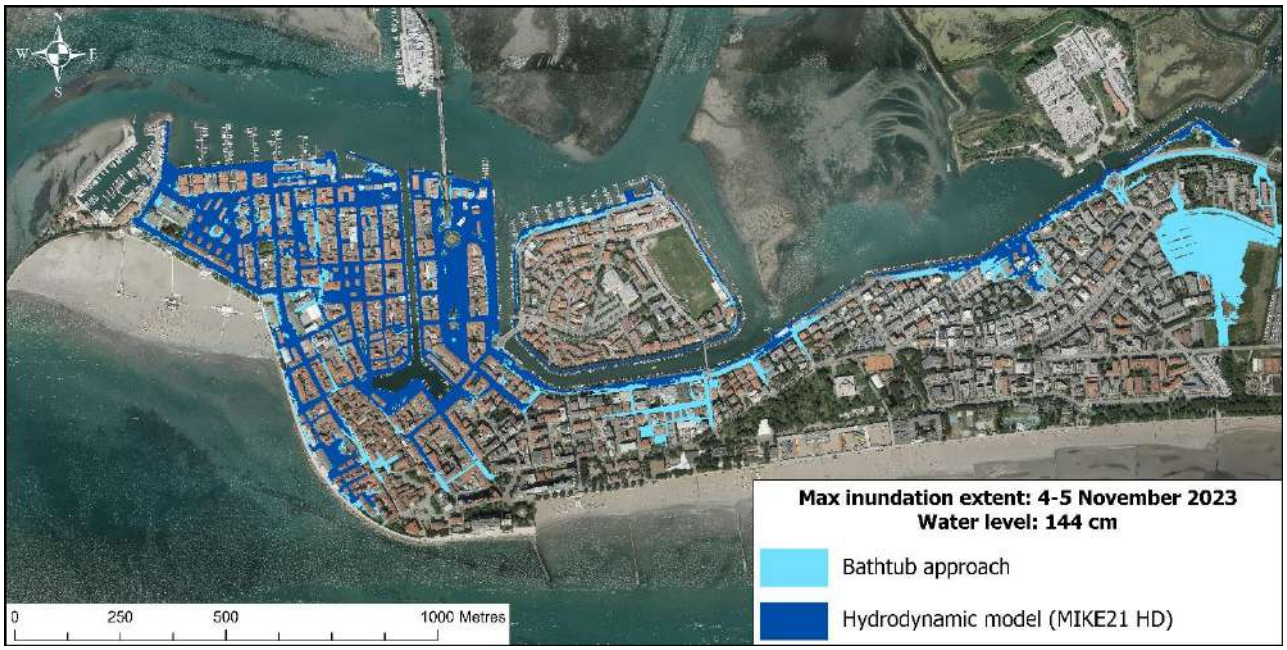

Figure 29. Maximum inundation extent for the 4–5 November 2023 event in Grado (peak water level: 144 cm, IGM42), comparing the static bathtub approach (light blue) and the dynamic hydrodynamic model MIKE21 HD (dark blue). The dynamic simulation accounts for hydraulic constraints and flow processes, resulting in a more physically consistent flood pattern compared to the static assumption of uniform water spreading.

The bathtub approach ignores energy dissipation and momentum redistribution process and assumes instantaneous hydraulic connection, which is the main cause of these discrepancies. By taking into account flow resistance, boundary conditions and the temporal evolution of the event peak, the dynamic model, explicitly resolves the propagation of the water mass through the urban fabric.

5.6.4 *Dynamic modelling: Event calibration of 4-5 November 2023*

To verify whether the inundated areas associated with R_P of 2, 10, 30, and 100 years are broadly reliable, a calibration was performed using a recent flood event that affected the coasts of the Friuli Venezia Giulia region. The selected case study corresponds to the event of 4-5 November 2023. The event reached a maximum sea level of 132 cm at Trieste at 04:20, while higher values were recorded at Grado, with a peak of 144 cm at 05:20, approximately one hour later than Trieste. Based on the previously estimated return periods (Table 5), the peak level observed at Grado is representative of an event with an approximate return period of 20 years.The onset of urban inundation occurred at around 02:25 in the areas adjacent to Riva Brioni (Figure 27), when the water level reached approximately 117 cm (Figure 30a). Up to levels of about 130 cm, recorded shortly after 03:00, flooding remained limited to a small number of streets near the Mandracchio Canal (Figure 28) and Riva Brioni (Figure 30b). The maximum spatial extent of inundation (Figure 30c) occurred between 05:00 and 06:00, corresponding to water levels close to 144 cm, with the involvement of a significant portion of the urban fabric north of the port area (excluding the Schiusa Island). Despite the wide spatial extent, flood depths were generally moderate, reaching approximately 40-45 cm in some inner sectors.

Finanziato dall'Unione europea NextGenerationEU
Ministero dell'Università e della Ricerca
Italiadomani
UNIVERSITÀ DEGLI STUDI DI TRIESTE

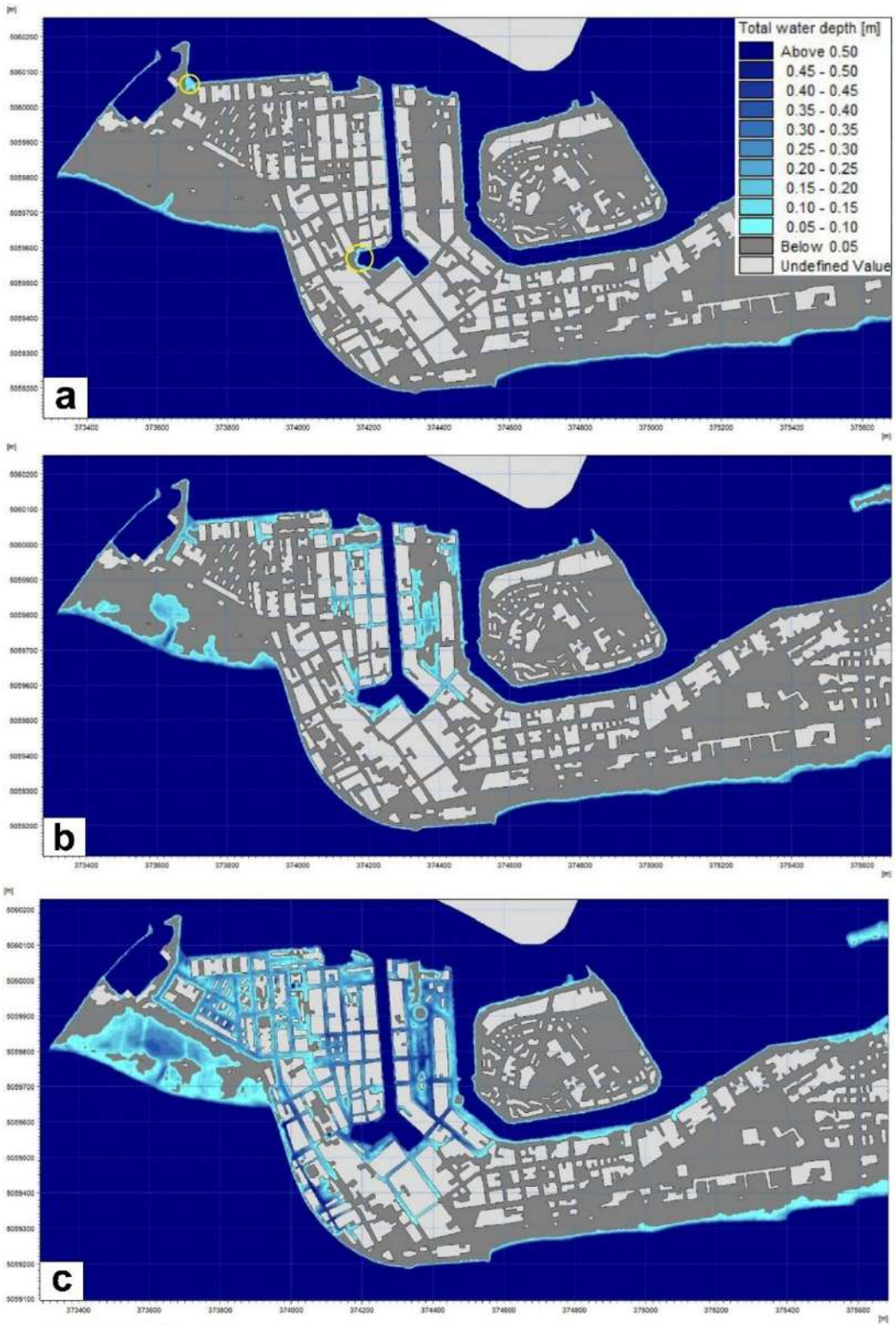

Figure 30. Onset of marine flooding along Riva Brioni and adjacent areas, with partial inflow also occurring from the south-western banks of the Mandracchio Canal. Ingress points are marked by yellow circles. (b) Flood extent at a water level of 130 cm. The affected areas remain confined to zones adjacent to the Mandracchio Canal and Riva Brioni. (c) Maximum flood extent at the peak water level of 144 cm. Flood depths is generally limited, reaching approximately 40-45 cm. Results derived from a 2D hydrodynamic simulation.

Finanziato dall'Unione europea NextGenerationEU
Ministero dell'Università e della Ricerca
Italiadomani PIANO NAZIONALE DI RIPRESA E RESILIENZA
UNIVERSITÀ DEGLI STUDI DI TRIESTE

5.6.5 *Future projections of the 4-5 November 2023 event*

By considering mean sea-level projections, it is possible to simulate the November 2023 storm surge as if it were to occur again in the future. The analysed episodic event is associated with an approximate return period of 20 years, and it is therefore statistically plausible that a similar or more severe event may occur within the next 25-75 years. The simulation was carried out using the MIKE21 HD model, allowing the identification of critical urban areas under medium- and long-term conditions. Accordingly, the sea-level projections for Grado reported in Table 18, were expressed both relative to the reference baseline (1995-2014) and relative to 2022. In the latter case, the observed mean sea-level rise rate at Grado over the period 1991-2022 (+4.7 mm/yr) was applied and multiplied by the 18 years elapsed since the baseline period (Table 22).

Year	**SLR Scenario Reference 2006 Baseline (1995–2014)**	**Total VLM (cm) for Grado (Average Rate)**	**Total Sea Level for Grado (cm)**	**Total Sea Level for Grado (cm) (2006-2022)**
2050	SSP1-2.6 (median)	6.6	23.6	15
	SSP5-8.5 (median)	6.6	27.6	19
2100	SSP1-2.6 (median)	14.1	53.1	44
	SSP5-8.5 (median)	14.1	81.1	72

Table 22. Global and local sea-level values at Grado under SSP1-2.6 and SSP5-8.5, projected for 2050 and 2100 and expressed in cm, considering the time interval between the 2006 baseline and 2022.

The projection of the November 2023 storm surge to 2050 and 2100 highlights markedly different scenarios. In the medium term, under the pessimistic scenario –characterized by a mean sea level approximately 4 cm higher than in the optimistic case– the flooded area (Figure 31) is clearly more extensive than that affected by the present-day event. In the western sector of the town, an increase in water depths is observed, while the spatial expansion of the inundated area remains relatively limited. If one considers the simple superposition of the 2023 episodic event peak (144 cm) onto the projected mean sea-level rise under the SSP5-8.5 scenario for 2050, the resulting water level would reach approximately 163 cm (144 cm + 19 cm by 2050). Under these conditions, the November 2023 storm, when projected to 2050, would produce impacts comparable to those of an event with a return period of about 70-80 years relative to the 2006 baseline (Figure 10), This clearly illustrates the strong reduction in return periods induced by sea-level rise, with significant implications for flood risk amplification in the coming decades.

Figure 31. Maximum extent of flooding scenario for 2050, corresponding to a peak water level of 163 cm. Results derived from a 2D hydrodynamic simulation.

Therefore, from a probabilistic perspective, consistently with the framework described in Section 5.3.1, the resulting situation can be summarized as follows:

$$\boldsymbol{Critical\ threshold_{2050}} = 2023\ event\ R_P20y - RSLR_{2050} = 144\ cm - 28\ cm = \mathbf{116\ cm}$$

Under a pessimistic scenario, the 144 cm level observed in 2023 would, in 2050, effectively correspond to about 116 cm once the projected sea-level rise of 28 cm is subtracted. This value is consistent with a threshold associated with an episodic event having a return period slightly greater than 3 years (Figure 10). From a probabilistic standpoint, exceedance of the 163 cm threshold in 2050 would therefore occur with a frequency almost seven times higher than under present-day conditions. As a consequence, the frequency of extreme flooding events is expected to increase substantially in the near future.

This effect becomes even more pronounced under long-term projections to 2100. In this case, a water level of approximately 190 cm, reachable under an optimistic scenario (SSP1-2.6), would place the urban fabric in a condition of severe and widespread criticality. Nearly the entire town would be inundated, with water depths frequently exceeding 50 cm (Figure 32). Also in this case, considering the simple superposition of the November 2023 episodic event (144 cm) onto the water table represented by the projected mean sea-level rise under the pessimistic SSP5-8.5 scenario for 2100, a total water level of about 188 cm would be reached (144 cm +44 cm by 2100). Consequently, the November 2023 storm, if projected to 2100 under a pessimistic scenario, would produce impacts comparable to those of an event with an associated return period of about 250 years, referred to the 2006 baseline.

Finanziato dall'Unione europea NextGenerationEU
Ministero dell'Università e della Ricerca
Italiadomani PIANO NAZIONALE DI RIPRESA E RESILIENZA
UNIVERSITÀ DEGLI STUDI DI TRIESTE

Figure 32. Maximum extent of flooding scenario for 2100, corresponding to a peak water level of 188 cm. Results obtained from a 2D hydrodynamic simulation.

The same reasoning can be applied to the same episodic event under an optimistic SSP1-2.6 projection for 2100. In this case, subtracting the projected sea-level rise of about 44 cm (Table 22) the reference level of 144 cm would effectively be reduced to approximately 100 cm. This value corresponds to an episodic event with a return period close to annual or even semi-annual recurrence. From a probabilistic perspective, the exceedance of the 144 cm threshold by 2100 could therefore occur with a frequency up to about 20 times higher than under present-day conditions.

5.7 Downscaling analysis and flood modelling of Muggia

This chapter presents and discusses the results obtained from the downscaling analysis for Muggia, carried out using statistical analyses within ArcGIS Pro 3.10. For each flood simulation, the inundation thresholds reported in Table 19 are adopted as reference values. The application of the downscaling analysis to the town of Muggia is essential to identify the main critical factors controlling seawater intrusion during extreme “acqua alta” events. Similar to Grado, Muggia represents one of the most vulnerable coastal settlements in Friuli Venezia Giulia with respect to extreme sea-level conditions. The primary issue is related to the local elevation of the urban waterfront, particularly within the inner harbour basin (darsena), as discussed below. The low-lying topography promotes increasingly frequent seawater intrusion events over recent decades. A key difference with respect to Grado, in addition to the different orientation and exposure of Muggia (see Figure 7), concerns the coastal setting. Unlike Grado, Muggia is located along a high and highly urbanised rocky coast, where the local topographic gradient plays a dominant role in controlling inland propagation of floodwaters.

5.7.1 *Water-front promenade analysis*

This section presents the results of the downscaling analysis applied to the waterfront promenade, which represents the main pathway for seawater intrusion into the historic centre of Muggia (Figure 33) along the entire boundary separating the city from the lagoon.

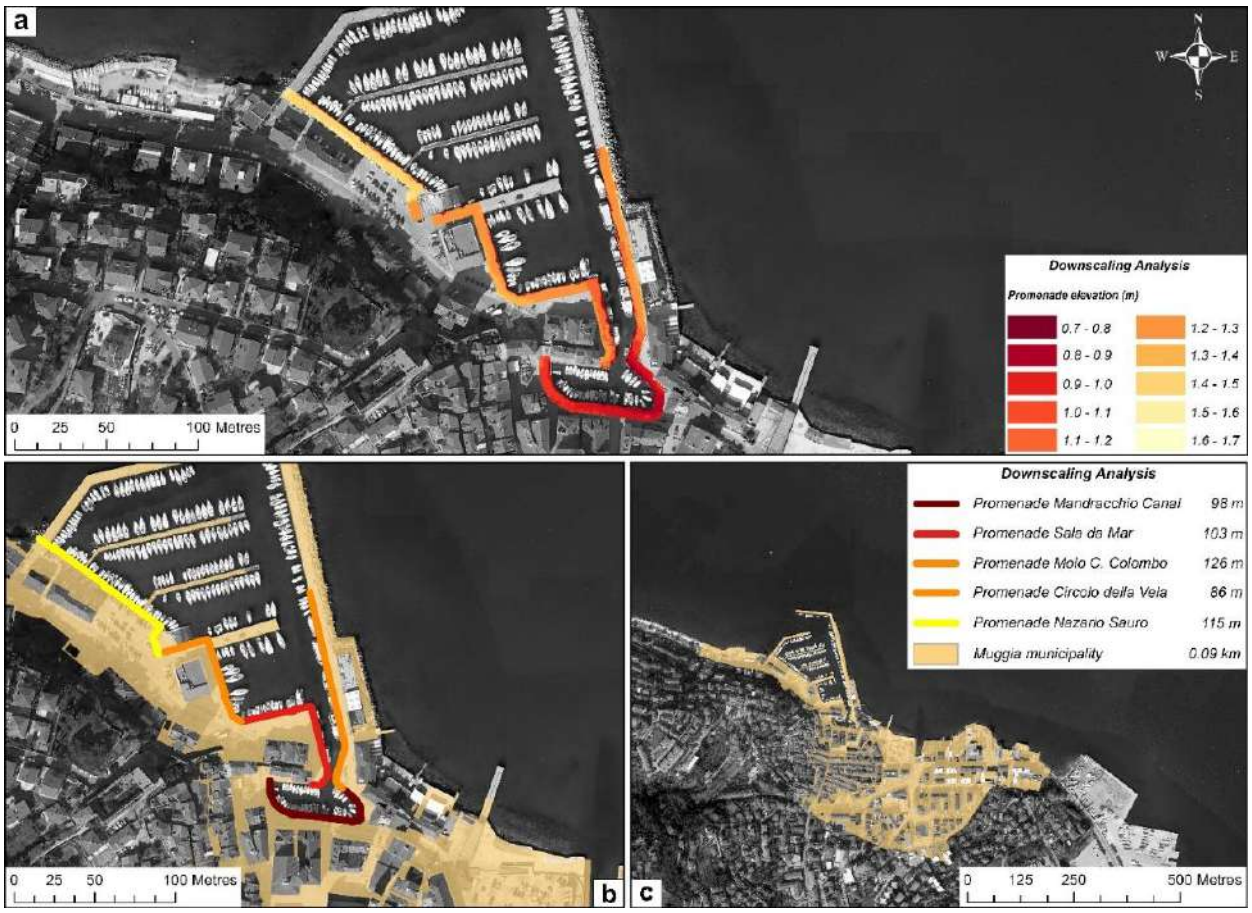

Figure 33. Downscaling area analysis: (a) elevation of the waterfront promenade considered in the study, represented by 10 classes subdivided every 0.10 m of elevation. (b) The subdivision of the promenades into 4 micro sectors; (c) the extent of the inhabited area of Muggia municipality is also reported, treating the streets as unobstructed surfaces for water flow while omitting buildings and uninhabited areas.

The assessment covers the full waterfront surrounding the Mandracchio Canal. Specifically, four waterfront sectors were analysed, extending from the area adjacent to the historic centre towards the outer harbour basin in the seaward direction, following both the right and left banks of the Mandracchio (see Figure 33b). This approach allows a detailed investigation of the primary ingress pathways, addressing both site-specific criticalities and more general vulnerability patterns. Table 23 summarises the analysed waterfront sectors, reporting their individual lengths, the total waterfront length, and the relative contribution of each sector expressed as a percentage of the overall waterfront extent.

Water-front promenade sector	Length (m)	Percent (%) of total lenght
Mandracchio C.	98	19
Sala da Mar restuarant	103	19
Molo C. Colombo	126	24
Circolo della Vela	86	16
Nazario Sauro park	115	22
Total promenade	528	100

Table 23. Muggia water-front promenade sectors analysed for elevation analysis aimed at the flooding assessment.

The following section describes the sectors of the waterfront promenade that are vulnerable to seawater intrusion. The analysed stretches encompass the entire waterfront along the Mandracchio Canal, subdivided into four micro-areas that characterise the portion closest to the historic centre of Muggia. A second sector corresponds to the Mandracchio Canal itself. The municipal area of Muggia considered in this analysis was selected because of the generally very low elevations on which the historic centre is developed, which represents the primary focus of the following assessments. Within this area, as discussed in the subsequent sections, the progressive inland propagation of seawater occurs as a function of the severity of the extreme event considered.

5.7.1.1 Mandracchio Canal promenade waterfront

The Mandracchio Canal waterfront considered in this analysis has a total length of 413 m. Based on the elevation of the promenade, the sector was subdivided into four micro-areas.

Mandracchio Canal waterfront

This sector accounts for 19% of the total waterfront promenade. The analysis of the canal banks was carried out on a total of 2572 measurement points, with elevations ranging between 70 and 120 cm. The main flooding pathways affecting the built-up area of Muggia occur through the Mandracchio Canal waterfront, which represents the primary preferential route for seawater ingress into the historic centre. This evidence is confirmed by the graph in Figure 34b, which shows that nearly the entire waterfront (≈99%) of the Mandracchio Canal is not in safe conditions for an event with R_P=2 years. Consequently, even for an elevation threshold of 115 cm, the historic centre remains highly vulnerable to very frequent flooding events.

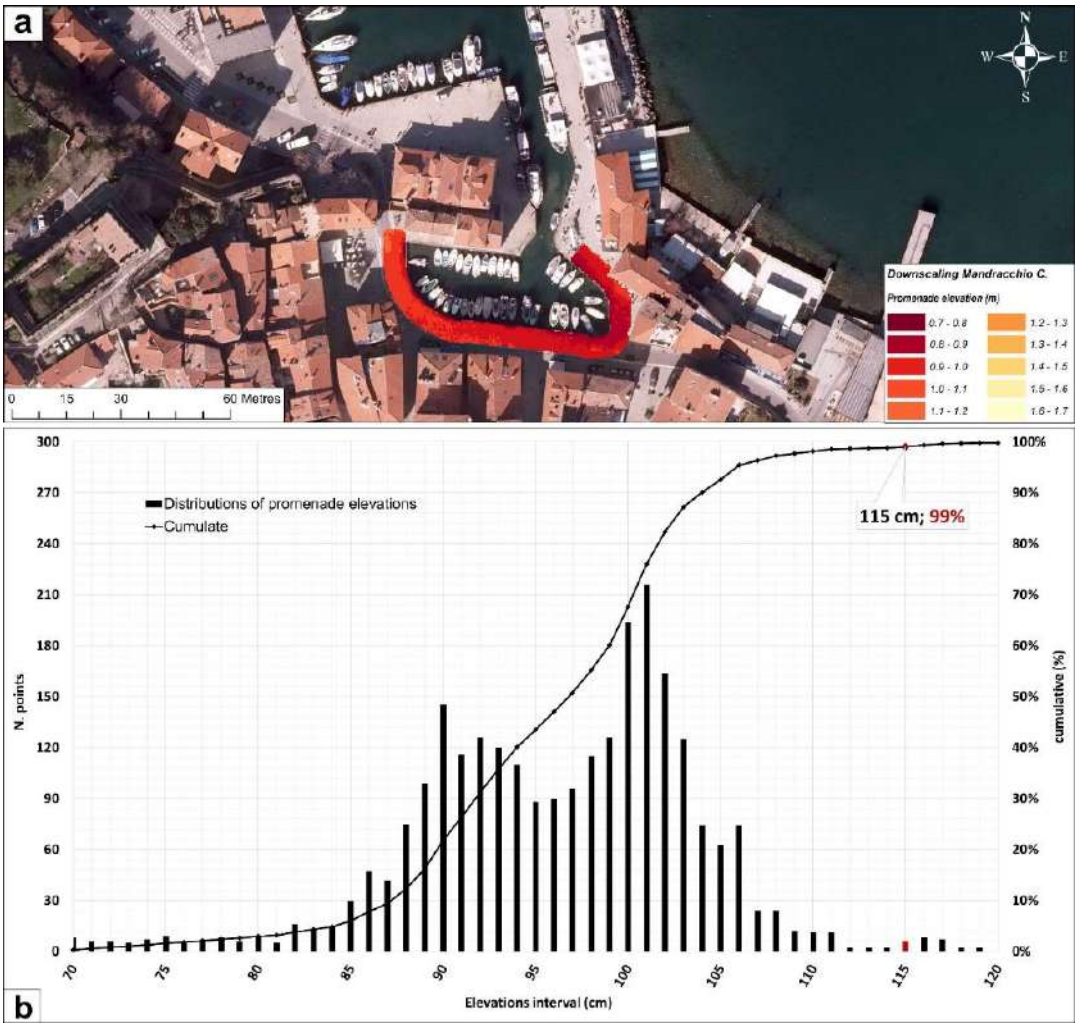

Figure 34. Critical sector promenade of Mandracchio canal promenade: (a) represents the elevations extracted from the 6-m buffer of the promenade. The elevation values of the promenade range from 70 to 120 cm. (b) represents the statistical distribution of the elevations extracted from the promenade of Mandracchio docks. Shown in red is the 115-cm elevation column, which represents 99% of the cumulative statistics. The promenade is then flooded with an event with a very high probability of occurrence (R_P=2 years).

Sala da Mar restaurant waterfront

The adjacent sector located to the left of the main Mandracchio Canal waterfront corresponds to the promenade of the restaurant Sala da Mar. This stretch has a length of approximately 103 m and represents the second critical micro-sector of the Mandracchio Canal. The analysis of the canal banks was conducted on a total of 2126 measurement points, with elevations ranging between 70 and 150 cm. This area does not constitute a primary flooding pathway toward the historic centre, as it is partially shielded by the built structure of the restaurant itself. Nevertheless, it still represents a potential ingress route due to the generally low elevation of the promenade. This is confirmed by the graph in Figure 35b, which shows that about 21% of the surveyed elevations lie below the 115 cm threshold. More critical conditions emerge when considering events with a 10-year return period. In fact Figure 35b indicates that the western waterfront of the Mandracchio Canal is largely not in safe conditions for an R_P=10 years event. Consequently, with an elevation threshold of 134 cm, the historic centre becomes vulnerable to relatively frequent flooding events.

Finanziato dall'Unione europea NextGenerationEU
Ministero dell'Università e della Ricerca
Italiadomani PIANO NAZIONALE DI RIPRESA E RESILIENZA
UNIVERSITÀ DEGLI STUDI DI TRIESTE

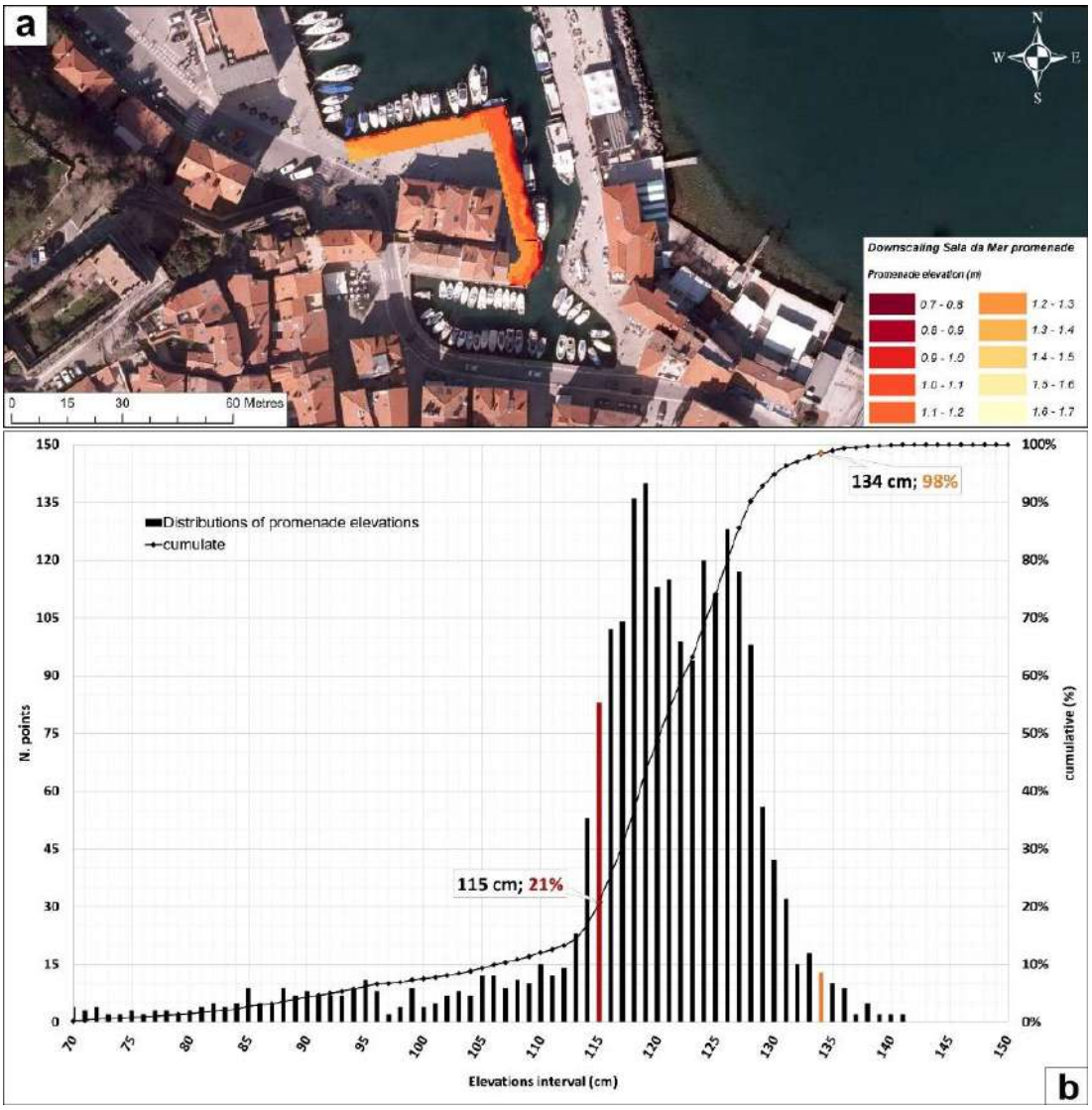

Figure 35. Critical sector promenade of Sala da Mar restaurant promenade: (a) represents the elevations extracted from the 6-m buffer of the promenade. The elevation values of the promenade range from 70 to 150 cm. (b) represents the statistical distribution of the elevations extracted from the promenade of Sala da Mar restaurant. Shown in red is the 134-cm elevation column, which represents 98% of the cumulative statistics. The promenade is then completly flooded with an event with a very high probability of occurrence (R_P = 10 years.

C. Colombo waterfront promenade

The sector adjacent to the right side of the main Mandracchio Canal waterfront corresponds to the C. Colombo pier waterfront. This stretch is approximately 126 m long and represents the third critical micro-sector of the Mandracchio Canal. The analysis of the canal banks was carried out on a total of 2904 measurement points, with elevations ranging between 70 and 170 cm. This sector represents a secondary flooding pathway, as it does not directly affect the historic centre. Nevertheless, it still constitutes a potential route for water ingress due to the generally low elevation of the waterfront. This is confirmed by the graph in Figure 36b, which shows that about 22% of the surveyed elevations lie below the 115 cm threshold. The most critical condition again emerges for events with a 10-year return period. As shown in Figure 36b the quays of this sector of the Mandracchio Canal waterfront are largely not in

Finanziato dall'Unione europea NextGenerationEU
Ministero dell'Università e della Ricerca
Italiadomani PIANO NAZIONALE DI RIPRESA E RESILIENZA
UNIVERSITÀ DEGLI STUDI DI TRIESTE

safe conditions for an R_P=10 years event, highlighting its vulnerability to relatively frequent extreme water levels.

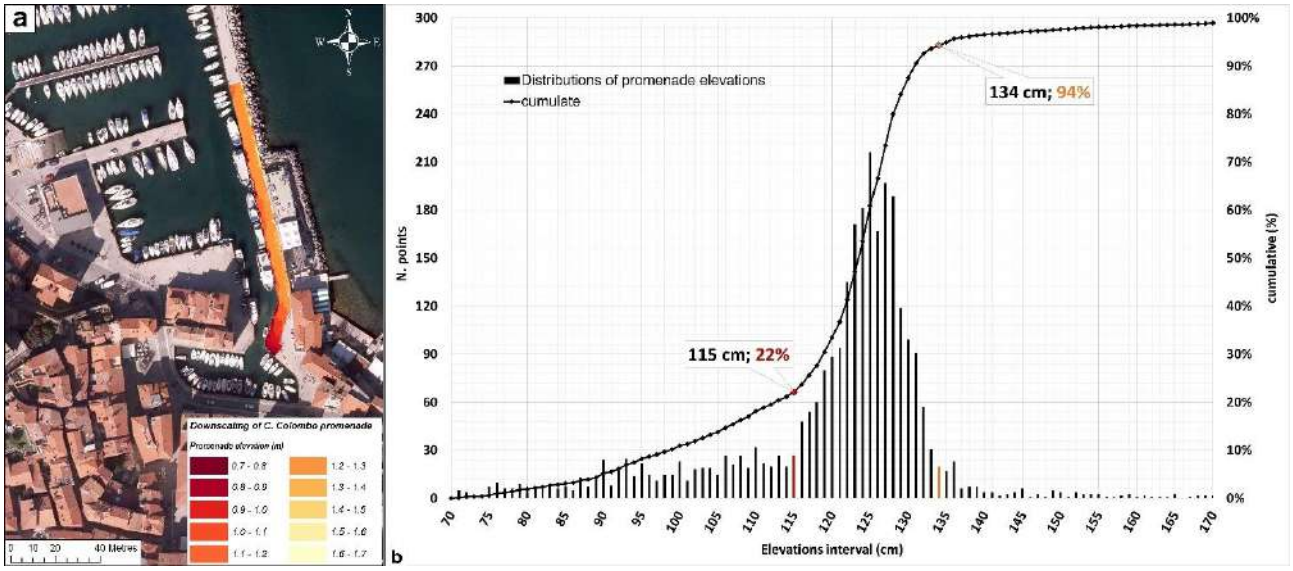

Figure 36. Critical sector promenade of Cristoforo Colombo promenade: (a) represents the elevations extracted from the 6-m buffer of the promenade. The elevation values of the promenade range from 70 to 170 cm. (b) represents the statistical distribution of the elevations extracted from the promenade of Cristoforo Colombo docks. Shown in orange is the 134-cm elevation column, which represents 94% of the cumulative statistics. The promenade is then completely flooded with an event with a very high probability of occurrence (R_P=10 years).

Circolo della Vela waterfront

This stretch represents the last sector analysed and includes the most critical portion of the Mandracchio Canal. It has a length of approximately 86 m and constitutes the second critical micro-sector of the Mandracchio Canal. The analysis of the canal banks was performed on a total of 1967 measurement points, with elevations ranging between 70 and 150 cm. Although it does not represent a primary flooding pathway towards the historic centre, potential water ingress may still cause significant issues along the waterfront area of Muggia. The elevation statistics for this sector are among the lowest within the Mandracchio system. As shown in Figure 37b the quays of this waterfront are largely unsafe for an event with a 10-year return period, with approximately 90% of the analysed elevations being overtopped. Consequently, for an elevation threshold of 134 cm, the western waterfront area of Muggia is highly vulnerable to relatively frequent flooding events.

Finanziato dall'Unione europea NextGenerationEU
Ministero dell'Università e della Ricerca
Italiadomani PIANO NAZIONALE DI RIPRESA E RESILIENZA
UNIVERSITÀ DEGLI STUDI DI TRIESTE

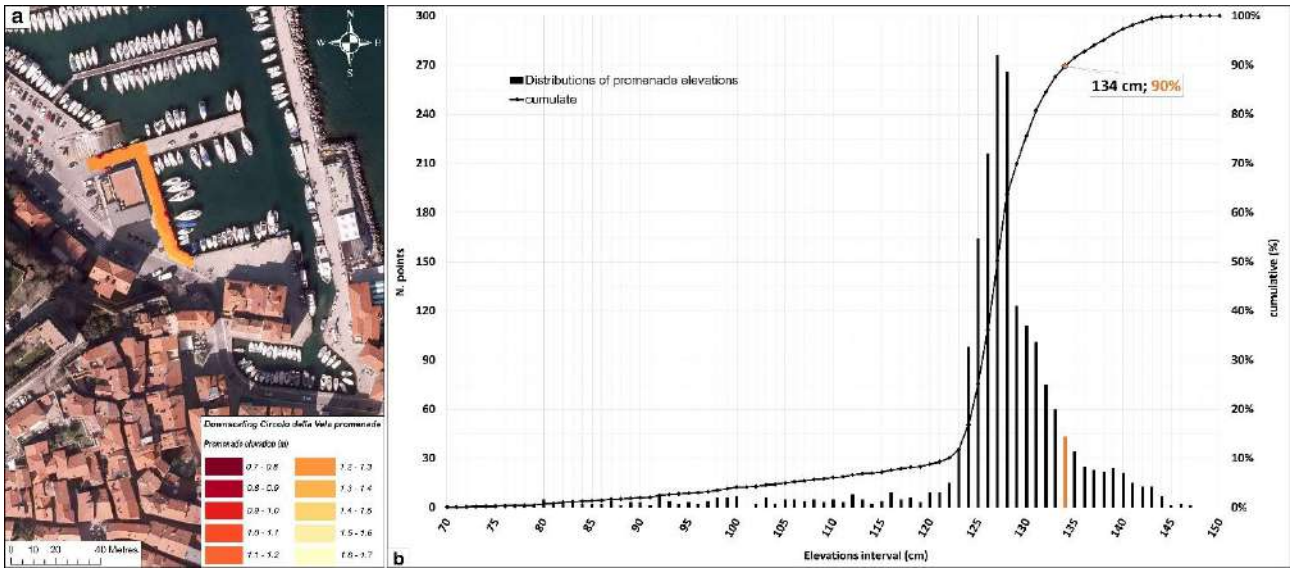

Figure 37**.** Critical sector promenade of Circolo della Vela promenade: (a) represents the elevations extracted from the 6-m buffer of the promenade. The elevation values of the promenade range from 70 to 150 cm. (b) represents the statistical distribution of the elevations extracted from the promenade of Circolo della Vela promenade. Shown in orange is the 134-cm elevation column, which represents 90% of the cumulative statistics. The promenade is then almost completly flooded with an event with a very high probability of occurrence (R_P=10 years).

Nazario Sauro park promenade

The last micro-sector considered corresponds to the Nazario Sauro parking promenade. This stretch is located in a more marginal area compared to the previously described sectors and has an approximate length of 115 m. The analysis of the waterfront elevations was carried out on a total of 2616 measurement points, with elevations ranging between 70 and 160 cm. This sector does not represent a primary flooding pathway towards the historic centre. However, potential water ingress may still generate critical conditions along the waterfront of Muggia, especially during less frequent events, such as extremes with a 30-year return period, or even rarer events with a 100-year return period. The elevation statistics extracted for this sector are the highest among those analysed along the Mandracchio Canal. As shown in Figure 38b approximately 46% of the waterfront elevations are not safe under a 30-year return period event. At a water level of 158 cm, the quays are completely overtopped. Consequently, for an elevation threshold of 146 cm, the western waterfront area of Muggia becomes highly vulnerable to high-magnitude flooding events.

Finanziato dall'Unione europea NextGenerationEU
Ministero dell'Università e della Ricerca
Italiadomani
UNIVERSITÀ DEGLI STUDI DI TRIESTE

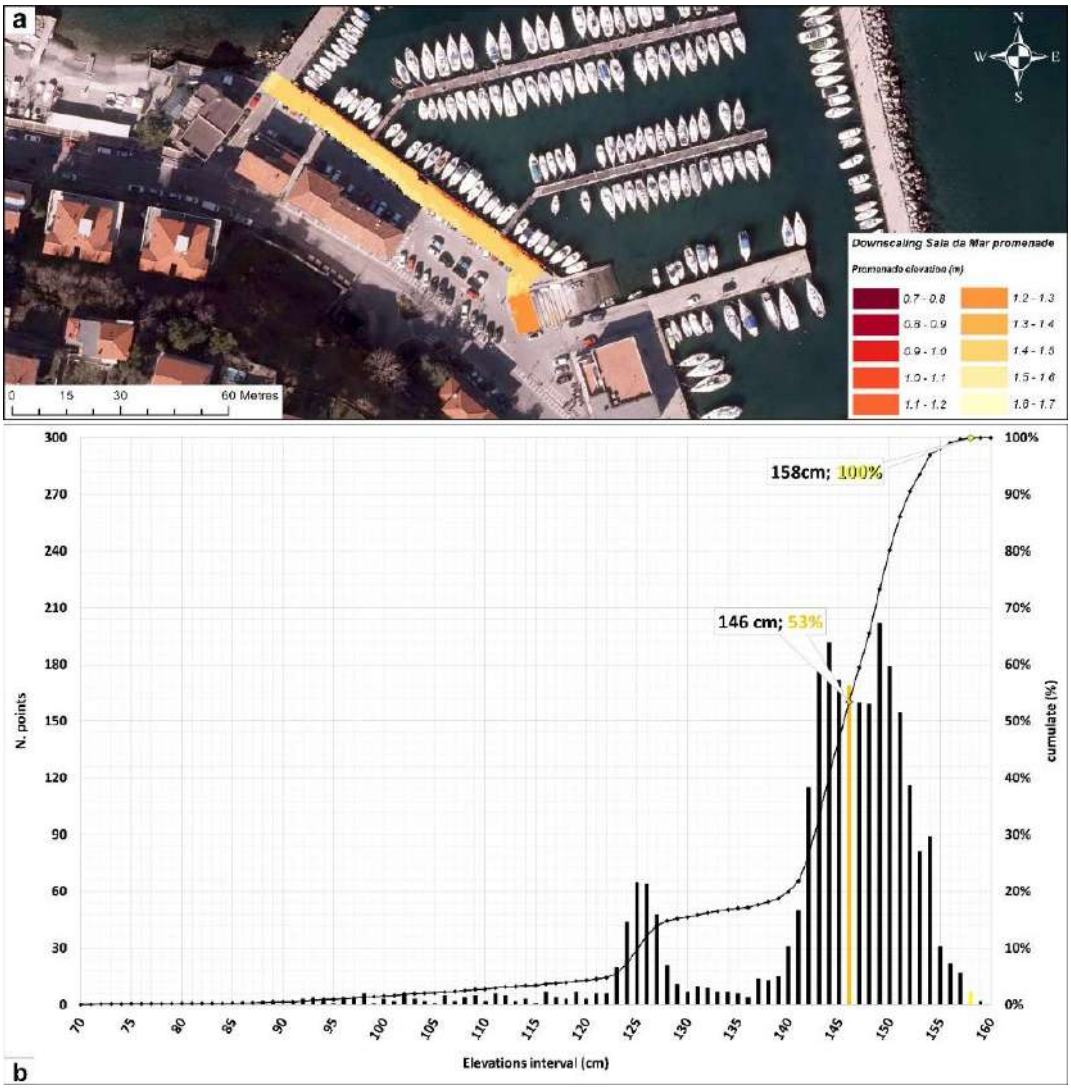

Figure 38**.** Critical sector promenade of Circolo della Vela promenade: (a) represents the elevations extracted from the 6-m buffer of the promenade. The elevation values of the promenade range from 70 to 160 cm. (b) represents the statistical distribution of the elevations extracted from the promenade of Nazario Sauro park promenade. Shown in red is the 146 cm elevation column, which represents 53% of the cumulative statistics, considering a R_P=30 years. The promenade is then almost completely flooded with 158 cm, extreme level with a very rare probability of occurrence (R_P = 100 years).

5.7.2 *Bathtub vs. Dynamic modelling*

Using the event of November 4-5, 2023, as a case study, a preliminary comparison between the bathtub approach and dynamic modelling was also conducted for Muggia, as was done for Grado (Figure 39). The event reached a maximum level of 132 cm (R_P=10 years). The static approach was initially applied as a rapid screening tool, aimed at identifying areas potentially subject to flooding based solely on altimetric criteria. However, unlike Grado, the morphological context of Muggia is characterised by a more pronounced topographical gradient, a complex port configuration and a greater presence of morphological and infrastructural constraints that significantly influence the propagation of water masses.

Finanziato dall'Unione europea NextGenerationEU
Ministero dell'Università e della Ricerca
Italiadomani PIANO NAZIONALE DI RIPRESA E RESILIENZA
UNIVERSITÀ DEGLI STUDI DI TRIESTE

Figure 39. Maximum inundation extent for the 4-5 November 2023 event in Muggia (peak water level: 132 cm, IGM42), comparing the static bathtub approach (dark blue) and the dynamic hydrodynamic model MIKE21 HD (light blue). The dynamic simulation accounts for hydraulic constraints and flow processes, resulting in a more physically consistent flood pattern compared to the static assumption of uniform water spreading.

Significant variations in the scope and trajectories of flooding are revealed by comparing the two scenarios. Specifically (i) the dynamic model exhibits a larger flooded area expansion than the bathtub model; (ii) preferential propagation paths are revealed, associated with the harbour's configuration and the quays' geometry; (iii) a local amplification contribution is identified, probably, due to seiche wave within the harbour basin (+3 cm), which cannot be captured by a static approach. The static approach, based exclusively on exceeding an altitude threshold, is unable to represent any losses due to friction, peak timing, possible local accumulation phenomena and any interactions between port oscillations and meteorological forcing. In this case study, the dynamic model not only modifies the extent of flooding, but also changes its spatial geometry and depth distribution, providing a more realistic picture of the physical processes governing the event.

5.7.3 *Downscaling dynamic flood modelling*

Once the downscaling analysis of the critical segments along the Mandracchio Canal waterfront –the primary pathway for water ingress– was completed, a high-resolution dynamic modelling approach at the urban scale of Muggia was adopted. Compared to the static bathtub simulations applied to Grado, this approach allows the dynamics of extreme events to be explicitly resolved, making it possible to capture their temporal evolution and propagation within the urban network. This provides a more accurate interpretation of how flooding develops and spreads in this specific urban context. In the case of Muggia, similarly to Grado, flooding is mainly driven by high water level events ("acqua alta"). Therefore, wave action was not included in the simulations, as it is expected to be significantly damped. This

Finanziato dall'Unione europea NextGenerationEU
Ministero dell'Università e della Ricerca
Italiadomani PIANO NAZIONALE DI RIPRESA E RESILIENZA
UNIVERSITÀ DEGLI STUDI DI TRIESTE

assumption is consistent with the coastal setting and the orientation of the town with respect to the dominant wave forcing, which is likely shielded by the Istrian Peninsula (Figure 7). Under these conditions, the adoption of a 2D hydrodynamic model for downscaling proved to be the most appropriate and comprehensive choice. The preliminary step consists of using the updated sea-level thresholds derived for Trieste and transferring them to the Muggia context, given the close proximity of the two sites and their exposure to the same extreme hydrometric forcing. As for Grado and Trieste, the same reasoning can be applied by directly considering the VLM values reported in Table 18, while updating the statistical thresholds using the results obtained from the GPD-POT approach Table 10b, extracted with reference to the “above mm19” series. The total extreme water level is defined as the sum of the reference mean sea level and the combined contribution of astronomical tide and storm surge. Accordingly, the mean sea level of the most recent decade is adopted as reference, approximately spanning the 2006-2024 period, which is consistent with the last 19 years of the recent trend and with the centred 19-year moving-average detrending applied in Section 4.3.2.2. This choice also follows the methodological framework adopted within the PGRA (see Table 2b). Under this assumption, the reference mean sea level for Trieste over 2006-2024 is approximately +2 cm relative to the IGM42 datum. The updated extreme levels for Muggia are therefore constructed by adding this reference mean sea level to the extreme values obtained from the GPD-POT analysis, as reported in Table 19. The hydrodynamic (HD) model developed for the town of Muggia was built starting from the implementation of a wave model at the scale of the Gulf of Trieste, as described in Section 4.5.2.3. The hydrodynamic model for Muggia was configured to generate an unstructured computational mesh with a spatial resolution of 1×1 m over the urban area of interest (see Figure 33). The resulting mesh, shown in Figure 40 consists of a total of 100079 nodes and 348694 elements.

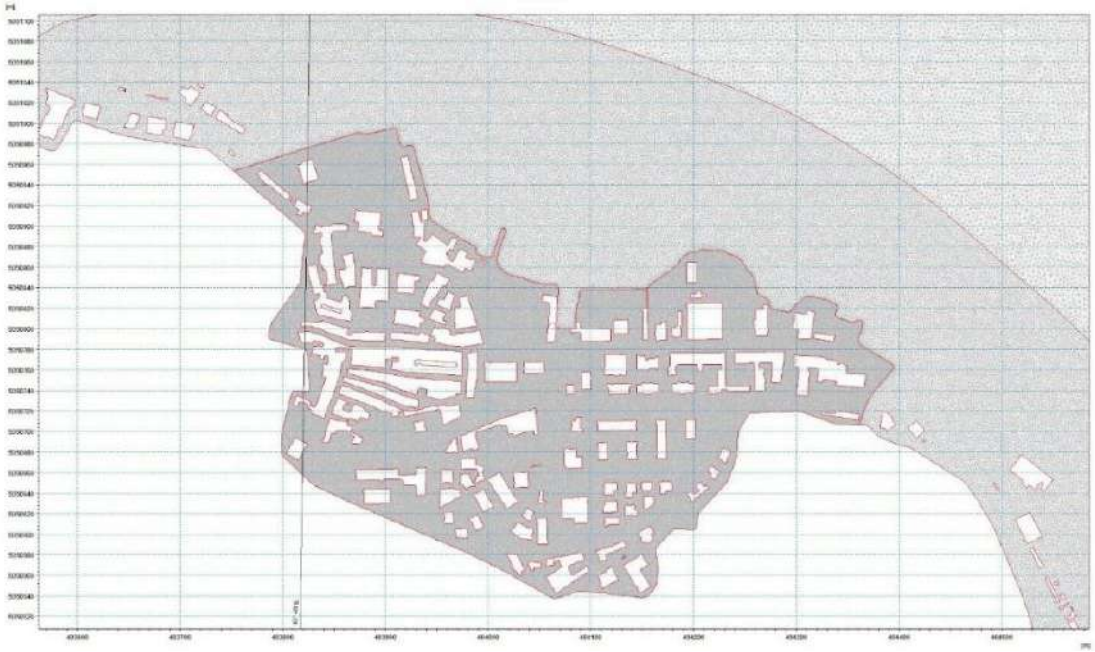

Figure 40. Mesh used for Muggia municipality.

The selected spatial resolution was dictated by the presence of narrow alleys and piers within the historic centre of the town. This choice allows the model to accurately capture and interpret the propagation dynamics of the water mass once it overtops the Mandracchio Canal waterfront (Figure 34). The final computational mesh also incorporates land-use information derived from CORINE data through Strickler coefficients. In this way, spatially varying surface roughness is accounted for, reflecting the different flow resistances encountered by the water mass after entering the urban fabric. Buildings were explicitly excluded from the computational domain (see Figure 40). Within the dynamic-model outputs, in addition to the flooded areas, the five previously defined micro-sectors are also displayed. This representation facilitates the identification of the critical zones responsible for water ingress (section 5.7.1, Figure 33a). For all the simulations presented and discussed below, the selected extreme water level (i.e., the hydrometric level) is imposed continuously at the external boundary of the computational domain constructed for Muggia.

5.7.3.1 MIKE21 HD with R_P = 2 years

Once the computational mesh was completed, the 2D hydrodynamic model was propagated starting from the external boundary of the Muggia downscaling domain. The selected total water-level threshold Z_T was set to 115 cm, corresponding to a return period of R_P = 2 years (Table 19). The results of the maximum water-mass propagation for an extreme level of 115 cm are shown in Figure 41.

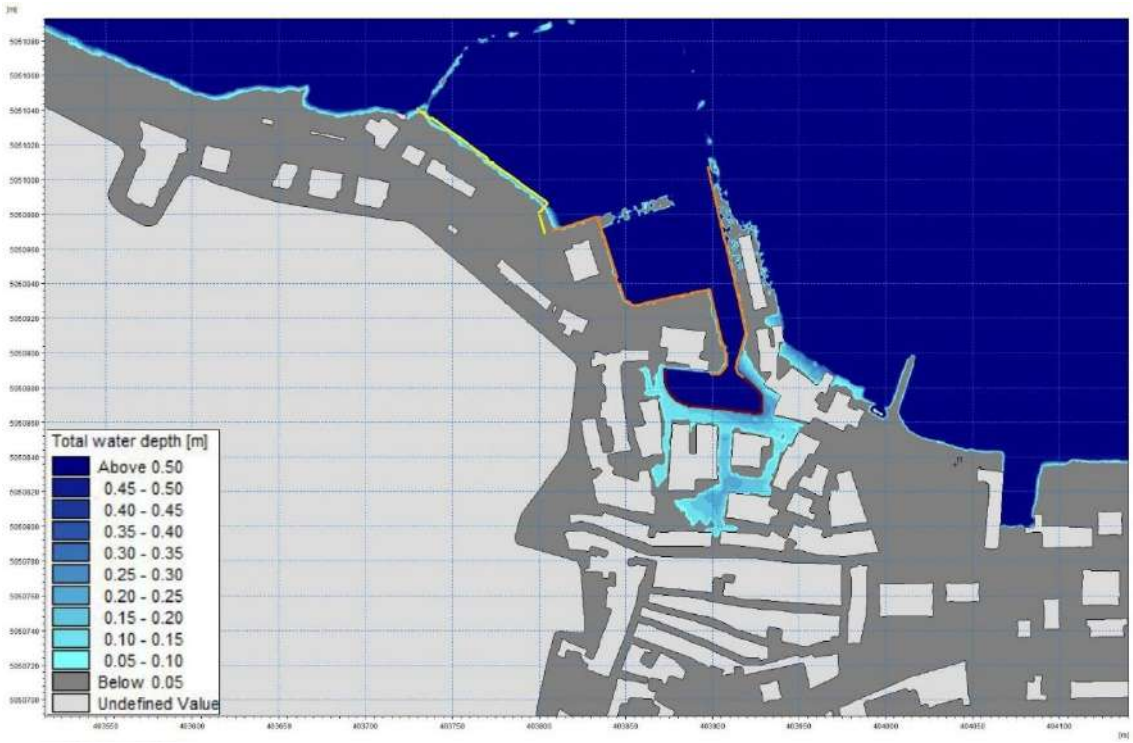

Figure 41. Maximum flood extent at a water level of 115 cm (R_P = 2 years), obtained using the 2D HD hydrodynamic model. Water depths are limited to a maximum of 50 cm.

Figure 41 shows that water ingress occurs exclusively through the Mandracchio Canal waterfront, which represents the primary entry pathway into the historic city centre (see Figure 34). From this point, the water mass progressively propagates inland, mainly affecting the areas adjacent to the harbour basin. The resulting water depths reach approximately 23

Finanziato dall'Unione europea NextGenerationEU
Ministero dell'Università e della Ricerca
Italiadomani PIANO NAZIONALE DI RIPRESA E RESILIENZA
UNIVERSITÀ DEGLI STUDI DI TRIESTE

cm within the core of the historic centre, exceeding the local ground elevations of the urban fabric.

5.7.3.2 MIKE21 HD with R_P = 30 years

Once the extreme threshold of 115 cm was dynamically analysed and calibrated, the same modelling framework was applied to an event with a return period of R_P=30 years, characterised by a total extreme water level Z_T of 146 cm (Table 19). The results of the maximum propagation of the water mass under this extreme level are shown in Figure 42. Compared to an event with R_P=2 years, in this case the propagation of the water mass also affects areas located farther from the historical centre. Flooding extends to the entire historical core adjacent to the Mandracchio Canal waterfront (dark red area in Figure 33b).

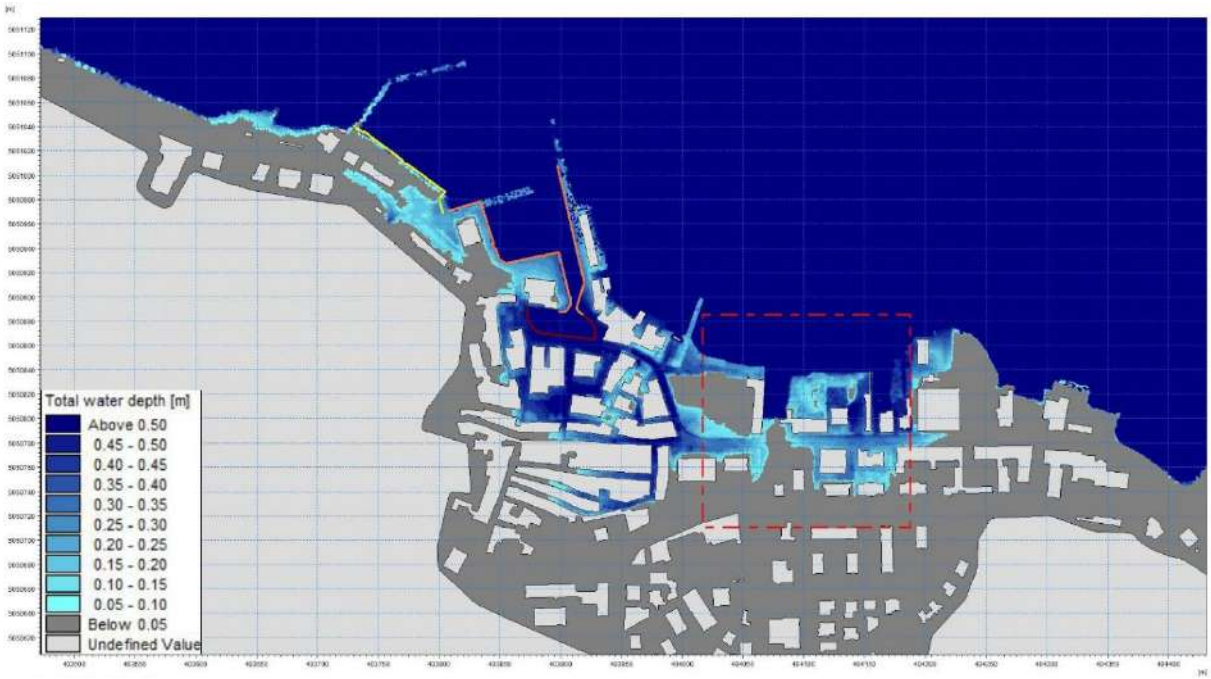

Figure 42. Maximum flood extent at a water level of 146 cm (R_P=30 years), obtained using the 2D HD hydrodynamic model. Water depths are limited to a maximum of 50 cm.

An additional flooded area is identified east of the historical centre. However, this sector is associated with a relatively high level of uncertainty, mainly due to the elevations extracted from the reference DTM (LiDAR survey, 2018) used in the present modelling framework. It is likely that the waterfront in this sector is characterised by vertical structures with thicknesses smaller than 50 cm, which corresponds to the effective resolution limit of the LiDAR-derived DTM. Consequently, the areas highlighted within the dashed red quadrant are interpreted as zones potentially affected by flooding rather than as definitively inundated areas.

5.7.3.3 MIKE21 HD with R_P = 100 years

The final simulation for Muggia concerns an extreme water level corresponding to a total threshold Z_T of 158 cm (Table 19) associated with an extreme event with a return period of R_P=100 years. The results obtained from the dynamic model for this scenario are shown in Figure 43. The propagation of the water mass extends across a large portion of the municipal

area considered in this analysis. Although Muggia is located within a high and urbanized coastal setting, with urban development occurring along sloping sectors, an extreme water level of 158 cm results in the complete inundation of the historic centre. In several areas close to the Mandracchio Canal waterfront, water depths exceed 50 cm.

As in the previous case (R_P=30 years), the western sector is highlighted by a dashed red rectangle, indicating a potential flood extent in areas not fully constrained by point-based topographic surveys. Nevertheless, the water mass propagates southward relative to the orientation of the municipality of Muggia, spreading along urban drainage pathways characterized by elevations exceeding 130 cm.

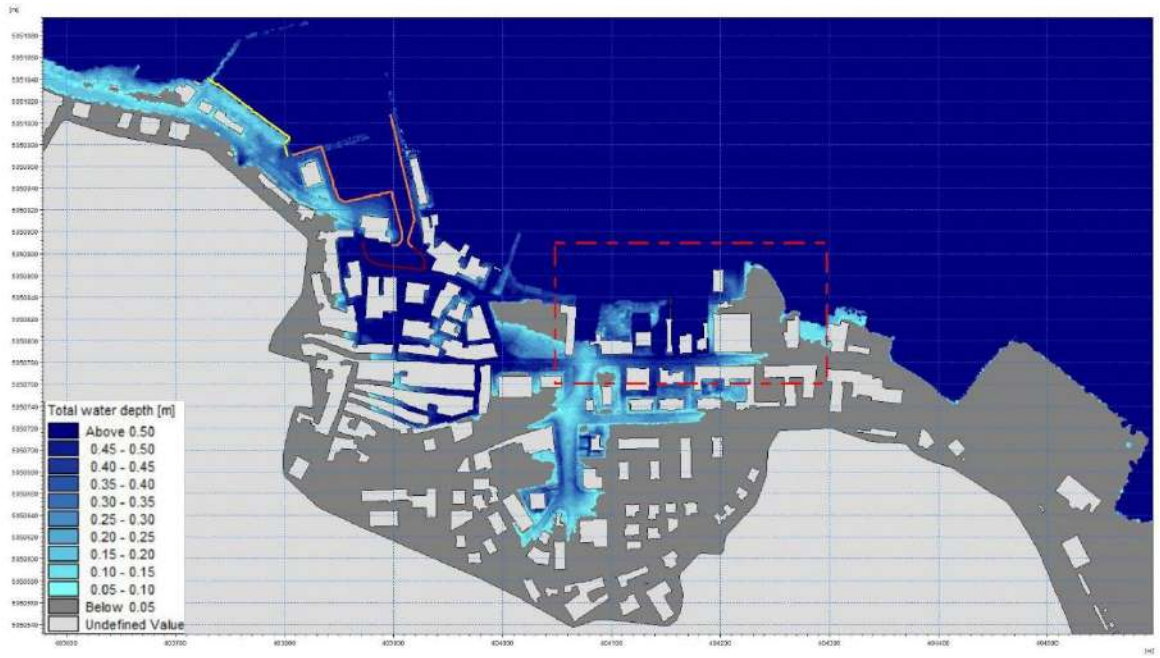

Figure 43. Maximum flood extent at a water level of 158 cm (R_P=100 years), obtained using the 2D hydrodynamic (HD) model. Water depths are limited to a maximum of 50 cm.

5.7.4 *Muggia long-term projection*

By focusing on the most relevant extreme events and considering urban planning horizons associated with return periods of 10 and 30 years, it is possible to assess how return periods are expected to change as a function of projected sea-level rise by 2050. By considering mean sea-level projections, it is possible to simulate the November 2023 storm surge as if it were to occur again in the future. The analysed episodic event is associated with an approximate return period of 10 years. Accordingly, the projections for Trieste reported in Table 18, were expressed both with respect to the reference baseline (1995-2014) and relative to the year 2022. In the latter case, the observed mean sea-level rise rate at Trieste over the period 1991-2022 (+2.8 mm/yr) was adopted and multiplied by the 18 years elapsed since the baseline, as reported in (Table 24). This consideration is motivated by the fact that Muggia is frequently affected by marine flooding associated with episodic events characterised by very high occurrence probabilities (return periods of 2-10 years) and moderately high probabilities (around 30 years). For this reason, from an urban planning and risk mitigation perspective, it is particularly important to prioritise the assessment of

Finanziato dall'Unione europea NextGenerationEU
Ministero dell'Università e della Ricerca
Italiadomani PIANO NAZIONALE DI RIPRESA E RESILIENZA
UNIVERSITÀ DEGLI STUDI DI TRIESTE

those events that are expected to recur most frequently, as they represent the dominant source of impact on the urban fabric and local infrastructure.

Year	SLR Scenario Reference 2006 Baseline (1995–2014)	Trieste Sea Level (cm)	Total Sea Level Trieste - Muggia (cm) (2006-2022)
2050	SSP1-2.6 (median)	17	12
	SSP5-8.5 (median)	21	16
2100	SSP1-2.6 (median)	39	34
	SSP5-8.5 (median)	67	62

Table 24. Local sea-level values for the Trieste-Muggia area under SSP1-2.6 and SSP5-8.5, projected for 2050 and 2100 (cm), considering the interval from the 2006 baseline to 2022.

The projection of the storm surge to 2050 and 2100 highlights markedly different scenarios. In the medium term, under the optimistic scenario, the area affected by flooding (Figure 44) is clearly larger than that impacted by the present-day event. In the western sector of the town, an increase in water depths is observed, accompanied by only a limited expansion of the flooded area. As described in Figure 42 and Figure 43, in Figure 44 the areas highlighted within the dotted red quadrant are also interpreted as areas potentially subject to flooding.

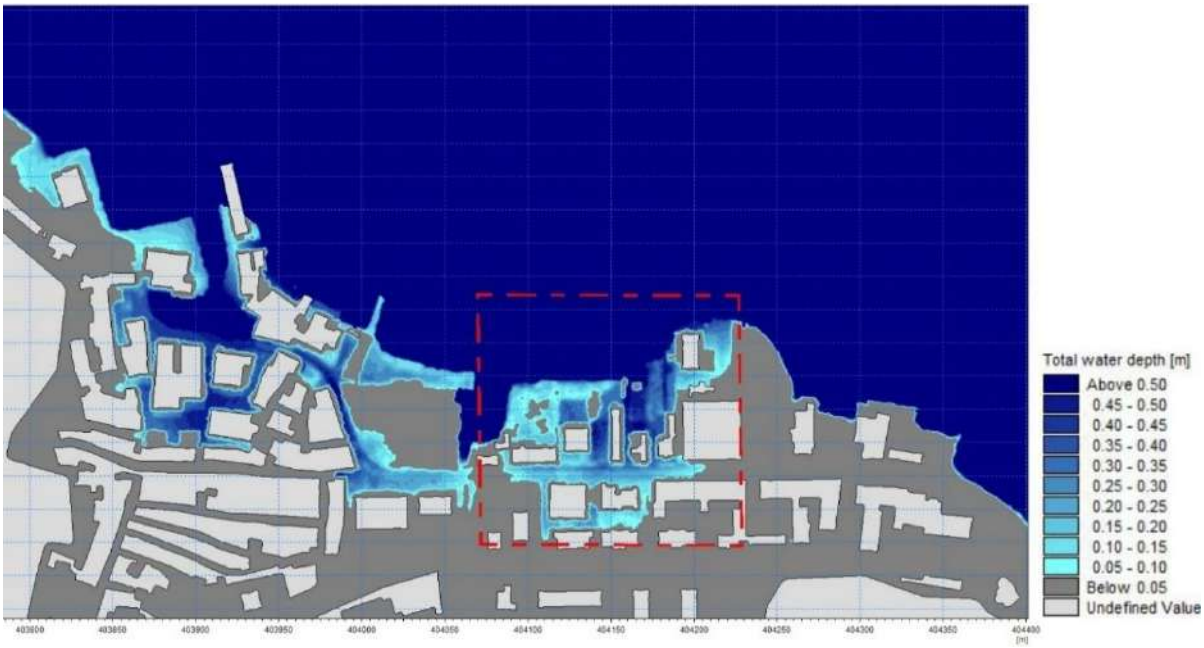

Figure 44. Maximum flood extent projected for 2050 at a peak water level of 144 cm, obtained through 2D hydrodynamic simulation.

By considering the simple superposition of the 2023 episodic event (132 cm) and the mean sea-level rise projected under the optimistic SSP1-2.6 scenario for 2050, a total water level of approximately 144 cm would be reached (132 cm + 12 cm). Consequently, if the November 2023 storm surge were to occur under 2050 mean sea-level conditions, it would exhibit the effects of an event with an approximate return period of 30 years relative to the 2006 baseline, clearly highlighting the significant reduction in return periods induced by sea-

Finanziato dall'Unione europea NextGenerationEU
Ministero dell'Università e della Ricerca
Italiadomani PIANO NAZIONALE DI RIPRESA E RESILIENZA
UNIVERSITÀ DEGLI STUDI DI TRIESTE

level rise (Table 19). Therefore, from a probabilistic perspective and following the framework described in Section 5.3.1, the resulting situation can be summarized as follows:

$$\boldsymbol{Critical\ threshold_{2050}} = 2023\ event\ R_P10y - RSLR_{2050} = 132\ cm - 12\ cm = \mathbf{120\ cm}$$

Under an optimistic scenario, the 132 cm level observed in 2023 would effectively correspond to approximately 120 cm in 2050 after subtracting the projected mean sea-level rise of 12 cm. This value is consistent with a threshold associated with an episodic event characterized by a return period of about 4 years (Figure 10). From a probabilistic standpoint, exceedance of the 120 cm threshold in 2050 could occur with a frequency nearly six times higher than at present, affecting essentially the same flooded areas shown in Figure 42. This indicates that even moderate-intensity extreme events are expected to become significantly more frequent in the near future. The same reasoning can be extended to rarer episodic events, such as those associated with a 100-year return period, under optimistic projections toward 2100. As previously observed for Grado, the effect becomes even more pronounced for the town of Muggia when projecting the current conditions to 2100. Under an optimistic scenario (SSP1-2.6), the hydrometric level could reach approximately 166 cm, placing the urban fabric in a state of critical vulnerability. Most of the town would be flooded, with impacts exceeding those associated with a present-day event characterized by a 100-year return period (Figure 32). In the long term, even under the optimistic SSP1-2.6 scenario, the flooded area (Figure 45) is therefore substantially larger than that affected by the current event.

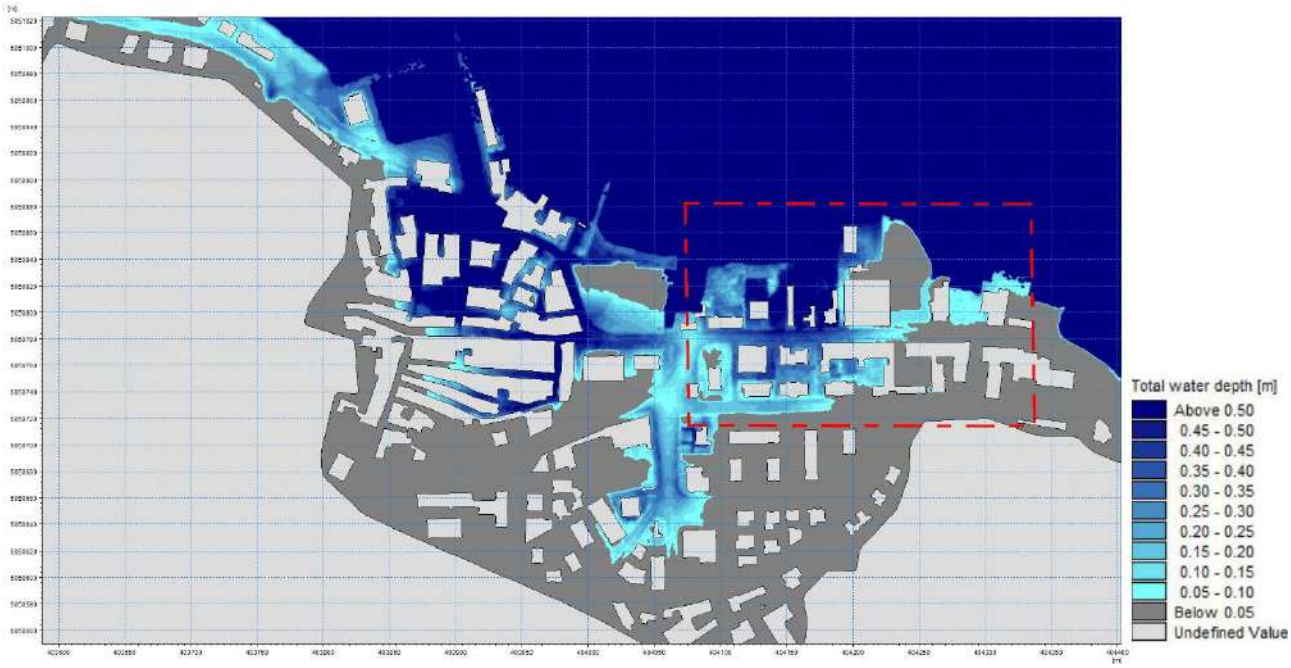

Figure 45. Maximum extent of flooding projected for 2100, at the attainment of a maximum water level of 166 cm. Results obtained using a 2D hydrodynamic simulation model.

Compared to the episodic event of 2023 projected to 2050 in an optimistic scenario (Figure 44), the area represented by the red dotted rectangle increases if we consider an optimistic projection to 2100 of the same event (Figure 45). Also in this case, considering the simple superposition of the 2023 episodic event (132 cm) onto the mean sea-level increase

Finanziato dall'Unione europea NextGenerationEU
Ministero dell'Università e della Ricerca
Italiadomani PIANO NAZIONALE DI RIPRESA E RESILIENZA
UNIVERSITÀ DEGLI STUDI DI TRIESTE

projected under the SSP1-2.6 scenario for 2100, a total water level of approximately 166 cm would be reached (132 cm at present + 34 cm by 2100). Consequently, the November 2023 storm surge, if projected to 2100, would produce effects comparable to an event with a return period exceeding 100 years, referred to the 2006 baseline. Conversely, in 2100 the present-day level of 132 cm would correspond to an effective level of approximately 98 cm. This value is consistent with an episodic event characterised by a multi-annual recurrence (Table 19). From a probabilistic perspective, exceedance of the 132 cm threshold by 2100 could therefore occur about 15 times more frequently than under present-day conditions. This hypothetical, yet not unrealistic, future scenario is further exacerbated by the elevation of the Mandracchio Canal waterfront promenade (Figure 34b) within the historic town centre, where most of the surveyed elevation points fall within the 90-100 cm range. Once this waterfront threshold is overtopped, the incoming water mass would directly impact the historic core located landward of the promenade, triggering a progressive, oil-spill–like expansion of flooding across the historic urban fabric. Figure 46 provides a detailed representation of the elevations extracted from the topographic survey within the historic centre, highlighting the particularly low-lying nature of this area.

Figure 46. Topographic detail survey on historic centre area point elevation.

As can be observed, most of the topographic elevations derived from point-based GPS surveys (using the STONEX S900+ model) fall within the 90-120 cm range. Within the historic centre, elevations generally do not exceed 100 cm. This implies that once the water mass overtops the Mandracchio Canal promenade under an event with R_P=2 years (see Figure 41) flooding rapidly propagates into the historic core, flowing along the narrow streets that characterize the local urban layout. Only by considering long-term projections, such as those for 2100, and by analysing rare episodic events (e.g., R_P=100 years) in combination

Finanziato dall'Unione europea NextGenerationEU
Ministero dell'Università e della Ricerca
Italiadomani PIANO NAZIONALE DI RIPRESA E RESILIENZA
UNIVERSITÀ DEGLI STUDI DI TRIESTE

with projected sea-level rise, do the implications become evident: this coastal setting is highly sensitive even to small sea-level fluctuations, such that modest increases in mean sea level can substantially amplify flooding impacts for events of comparable meteorological intensity.

5.8 Downscaling analysis and flood modelling of Lignano

This chapter presents and discusses the results of the downscaling analysis for Lignano, carried out using statistical analyses within ArcGIS Pro 3.10. For each simulated flooding scenario, the updated inundation thresholds reported in Table 5 are adopted. The application of the downscaling approach to Lignano is essential to identify the critical conditions leading to seawater intrusion during extreme high-water events. Compared with Grado and Muggia –both highly vulnerable to extreme events– Lignano exhibits a more conservative response, despite its greater exposure to meteorological forcings. Nevertheless, the downscaling analysis allowed a detailed assessment of the most critical sectors, particularly in relation to the 12 November 2019 event, which reached sea levels of approximately 150 cm (IGM42) and required the activation of the regional Civil Protection system. The primary criticality concerns the area near the private marina, located along the lagoon-side promenade, which represents the main pathway for water ingress during extreme events, as discussed in the following sections.

5.8.1 *Downscaling analysis of lagoon promenade*

This section presents the results of the downscaling analysis applied to specific sectors of the promenade separating the town from the lagoon. The assessment covers the entire perimeter of the urban marina, the promenade of the private marina (Circolo dei Canottieri), and Riva Zanelli. The analysed promenade is therefore subdivided into three micro-sectors (see Figure 47). his approach enables a more detailed examination of the waterfront embankments, allowing both sector-specific criticalities and more general issues to be identified. Table 25 reports the analysed promenade sectors together with their respective lengths, the total length of the investigated stretch, and the percentage contribution of each section relative to the overall length.

Lagoon promenade sector	Length (m)	Percent (%) of total lenght
C. Canottieri	86	7
Riva Zanelli	28	2
Molo A	1103	91
Total promenade	1217	100

Table 25. Lignano lagoon promenade sectors analysed for elevation analysis aimed at the flooding assessment.

Below, the three sectors of the lagoon-side promenade and the piers most vulnerable to water ingress are described. The first sector considered corresponds to the promenade of the Circolo dei Canottieri. The second sector includes Riva Zanelli and the dockyard Molo A.

Finanziato dall'Unione europea NextGenerationEU
Ministero dell'Università e della Ricerca
Italiadomani PIANO NAZIONALE DI RIPRESA E RESILIENZA
UNIVERSITÀ DEGLI STUDI DI TRIESTE

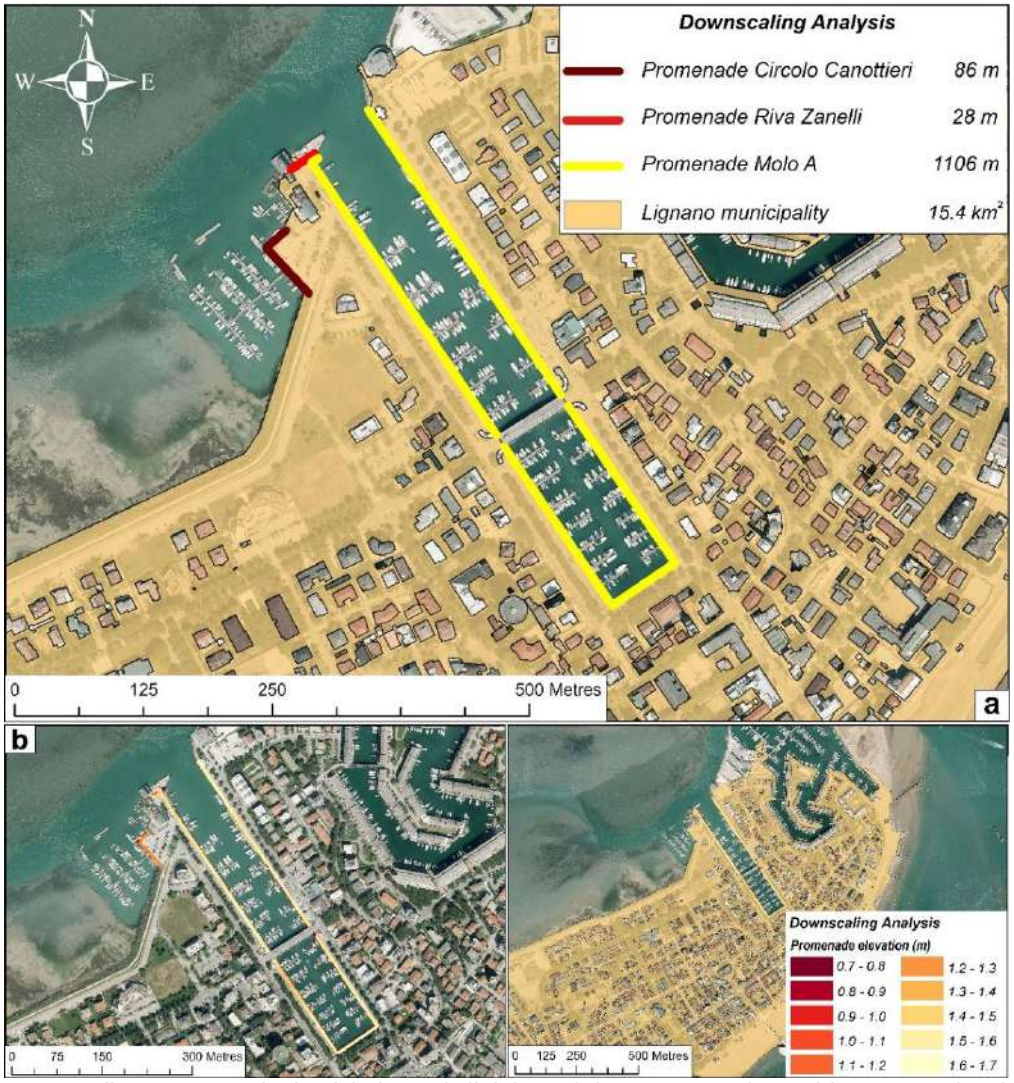

Figure 47. Downscaling area analysis: (a)The subdivision of the promenade and lagoon embankment into 3 micro sectors; (b) Elevation of the lagoon promenade considered in the study, represented by 10 classes subdivided every 0.10 m of elevation. (c) the extent part of the inhabited area of Lignano municipality is also reported, treating the streets as unobstructed surfaces for water flow while omitting buildings and uninhabited areas.

5.8.1.1 Promenade C. Canottieri

The total length of the lagoon-side promenade in this sector is 86 m, corresponding to 7% of the lagoon promenade analysed for Lignano. The elevation analysis was performed on a total of 1792 points, with elevations ranging between 70 and 140 cm. The main flooding processes affecting the built-up area of Lignano occur through the promenade in this sector, which represents the primary pathway for water ingress. This is confirmed by the histogram shown in Figure 48b, indicating that almost the entire promenade of the Circolo dei Canottieri (about 99%) is not in safe conditions for an event with a R_P=5 years. Consequently, even for a threshold elevation of 126 cm, the promenade experiences significant water ingress (Figure 48).

Finanziato dall'Unione europea NextGenerationEU
Ministero dell'Università e della Ricerca
Italiadomani PIANO NAZIONALE DI RIPRESA E RESILIENZA
UNIVERSITÀ DEGLI STUDI DI TRIESTE

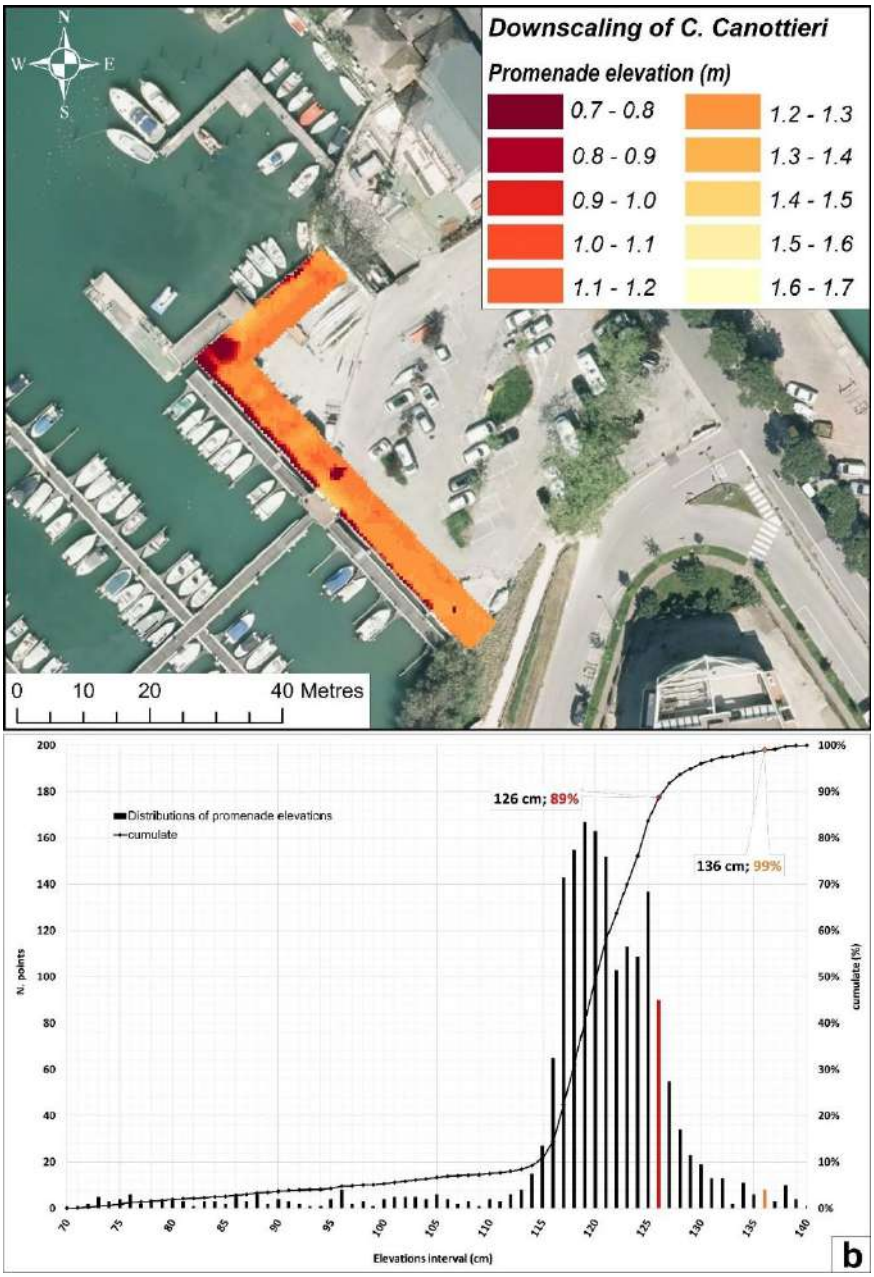

Figure 48. Critical sector promenade of C. Canottieri: (a) represents the elevations extracted from the 6-m buffer of the promenade. The elevation values of the promenade range from 70 to 140 cm. (b) represents the statistical distribution of the elevations extracted from the promenade of C. Canottieri. Shown in red is the 126-cm elevation (R_P=5 years, Table 5) column, which represents 89% of the cumulative statistics. The promenade is then completely flooded with an event with a very high probability of occurrence (R_P=10 years).

5.8.1.2 Promenade Riva Zanelli

This small promenade sector, adjacent to the main marina of the town, accounts for about 2% of the analysed lagoon-side promenade. The elevation analysis was carried out on a total of 550 points, with elevations ranging between 70 and 160 cm. This sector represents a secondary pathway for water ingress into the urban area. This behaviour is confirmed by the histogram shown in Figure 49b, which indicates that about 36% of the promenade is inundated for an event with a R_P of 10 years. For an R_P of 30 years (e.g. the 12 November 2019 event), characterised by a medium–low frequency of occurrence and a water level of

151 cm, approximately 84% of the embankments are submerged, thus activating a secondary ingress pathway compared to the Circolo dei Canottieri promenade (Figure 49b).

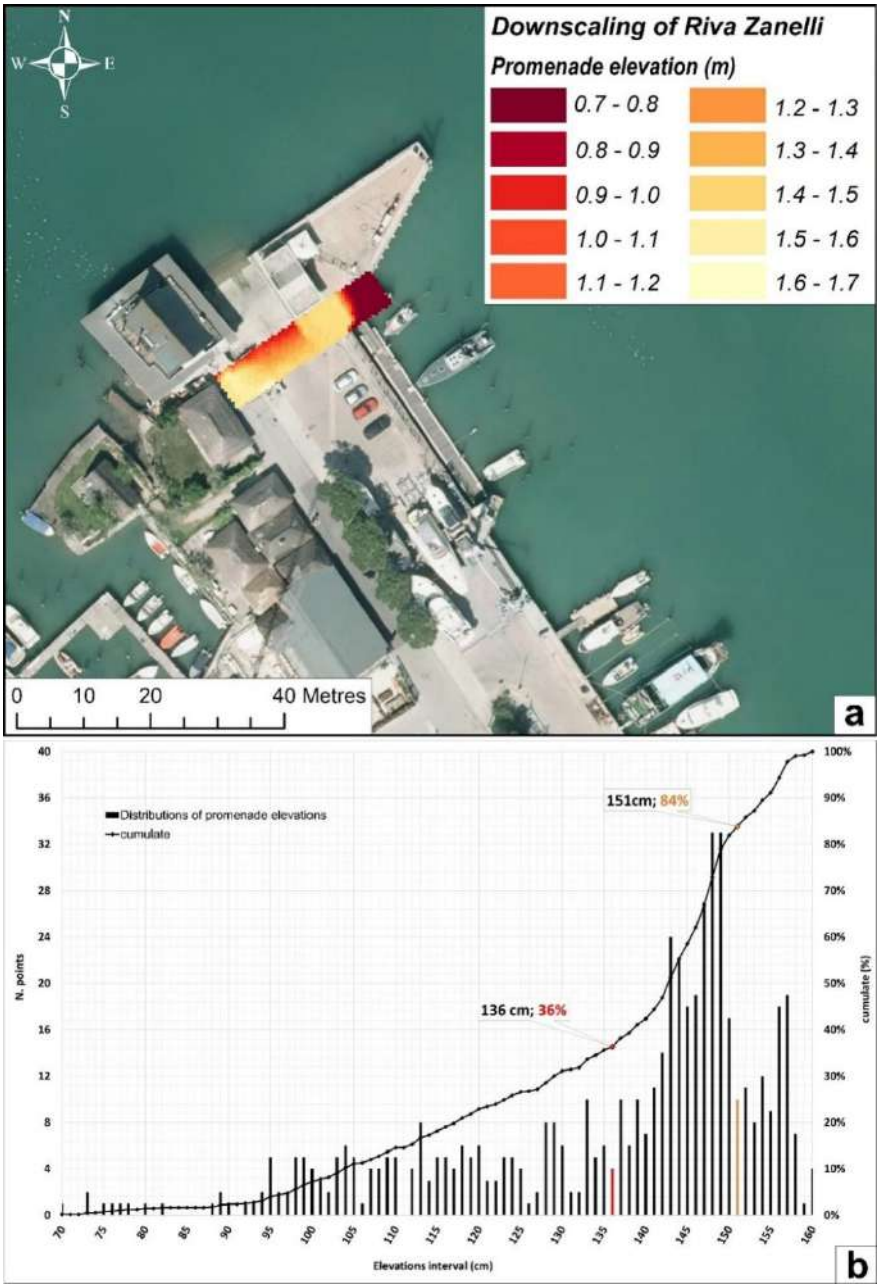

Figure 49**.** Critical sector promenade of Riva Zanelli: (a) represents the elevations extracted from the 6-m buffer of the promenade. The elevation values of the promenade range from 70 to 160 cm. (b) represents the statistical distribution of the elevations extracted from the promenade of C. Canottieri. Shown in red is the 136-cm elevation (R_P=10 years) column, which represents 36% of the cumulative statistics. The promenade is then almost completely flooded with an event with a very medium probability of occurrence (R_P=30 years).

5.8.1.3 Dockyard Molo -A promenade

This sector represents the most extensive stretch of promenade, with a total length of 1107 m. The analysis of the embankments was carried out on 26115 surveyed points, with elevations ranging between 70 and 180 cm. Based on the extracted elevation statistics, it is plausible that this sector may act as a potential pathway for water ingress when extreme

events reach threshold levels between 151 and 168 cm, corresponding to very extreme events with progressively lower probabilities of occurrence and R_P between 30 and 100 years. This interpretation is supported by Figure 50 which shows that about 31% of the promenade is inundated for an R_P=30 years, considering a 6 m buffer. Conversely, for an R_P of 100 years, characterised by a rare occurrence and a water level of 168 cm, approximately 99% of the embankments are submerged (Figure 50b) activating a potential ingress pathway that would likely lead to the inland propagation of floodwaters towards the urban centre.

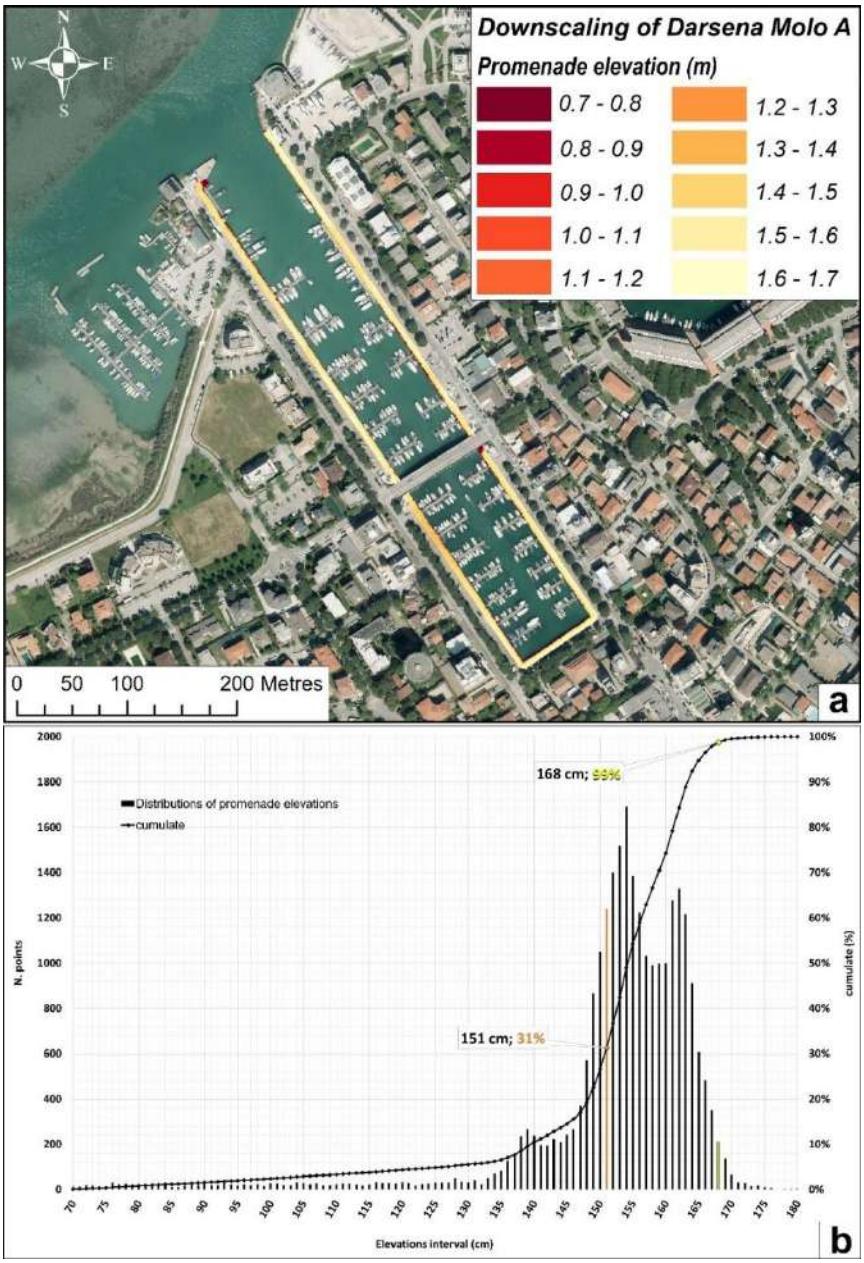

Figure 50. Critical sector Dockyard -A promenade: (a) represents the elevations extracted from the 6-m buffer of the promenade. The elevation values of the promenade range from 70 to 180 cm. (b) represents the statistical distribution of the elevations extracted from the dockyard -A promenade. Shown in orange is the 151-cm elevation (R_P=30 years) column, which represents 31% of the cumulative statistics. The promenade is then completly flooded with an event with a very medium probability of occurrence (R_P=100 years).

Finanziato dall'Unione europea NextGenerationEU
Ministero dell'Università e della Ricerca
Italiadomani
UNIVERSITÀ DEGLI STUDI DI TRIESTE

5.8.2 *12 Novembre 2019 event calibration*

Once the downscaling analysis of promenade performance and the associated potential ingress pathways was completed, data provided by the Regional Civil Protection allowed the effects of the event that affected the entire Northern Adriatic coastal sector on 12 November 2019 to be evaluated. This event was analysed and subsequently modelled by the Civil Protection using HEC-RAS 5.0, developed by the Hydrologic Engineering Center (HEC), which enables two-dimensional hydrodynamic flow modelling. For Lignano, the recorded peak water level reached 1.73 m relative to ZMPS, corresponding to approximately 23.56 cm above the national datum, i.e. about 150 cm IGM42. The following section presents screenshots of the simulations (Figure 51) produced using a dynamic modelling approach, explicitly accounting for water depth (hydraulic head), flow velocity at the points of ingress, and flooding duration within the urban area of Lignano.

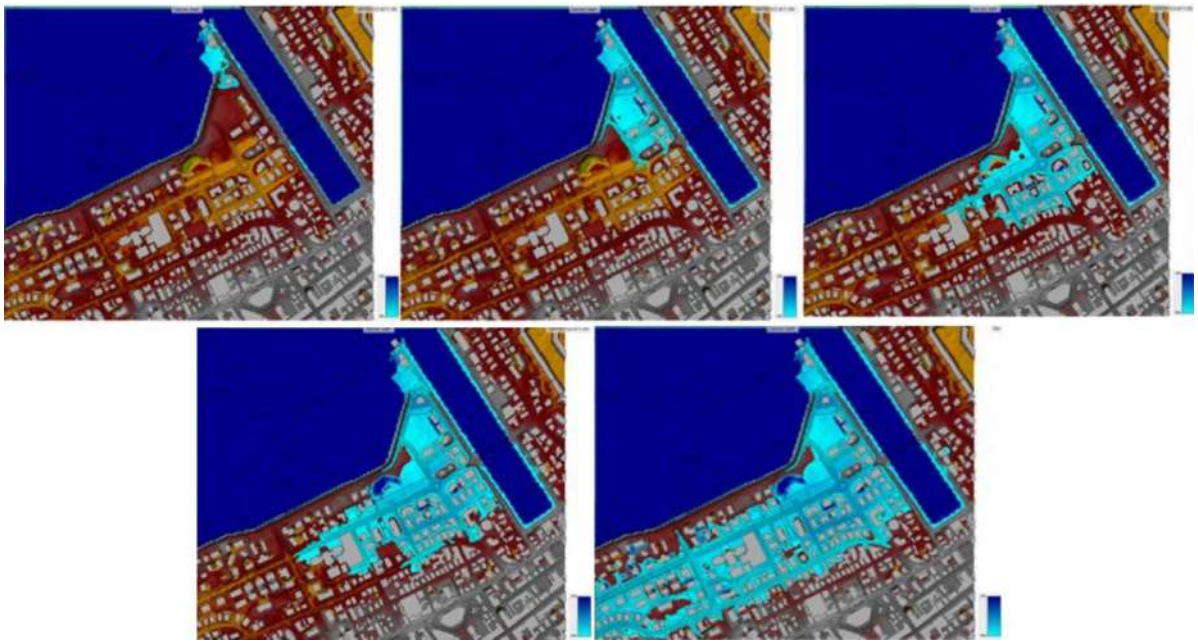

Figure 51. screenshots of the critical area analysed through the modelling of the 12 November 2019 event (HEC-RAS 5.0; courtesy of Dr. Peressi, Regional Civil Protection of Friuli Venezia Giulia).

The main access point for floodwater ingress into the urban area of Lignano occurs through the promenade adjacent to the Circolo Canottieri parking area. As previously shown (Figure 48), the elevations along the Circolo Canottieri promenade reach a maximum of about 136 cm, corresponding to an R_P=10 years when applying the Grado-based thresholds to Lignano (Table 5). Consequently, an event such as that of 12 November 2019, led to overtopping and subsequent ingress of water through this sector. To further support this interpretation, the downscaling analysis also verified the local DTM elevations around the breach point identified by Dr. Peressi. Based on the LiDAR survey conducted in 2018, ground elevations in this area generally range between 120 and 135 cm (Figure 52 a,b), confirming the intrinsic vulnerability of this sector to relatively frequent extreme events. These values are well below the water level recorded on 12 November 2019. Consequently, it became necessary to verify –through a targeted GPS topographic survey (STONEX S900$^+$)– whether the ingress breach responsible for the inland propagation of floodwaters within the urban area of Lignano (see Figure 51) had been raised following the 2019 event (Figure 52a,b).

Finanziato dall'Unione europea NextGenerationEU
Ministero dell'Università e della Ricerca
Italiadomani PIANO NAZIONALE DI RIPRESA E RESILIENZA
UNIVERSITÀ DEGLI STUDI DI TRIESTE

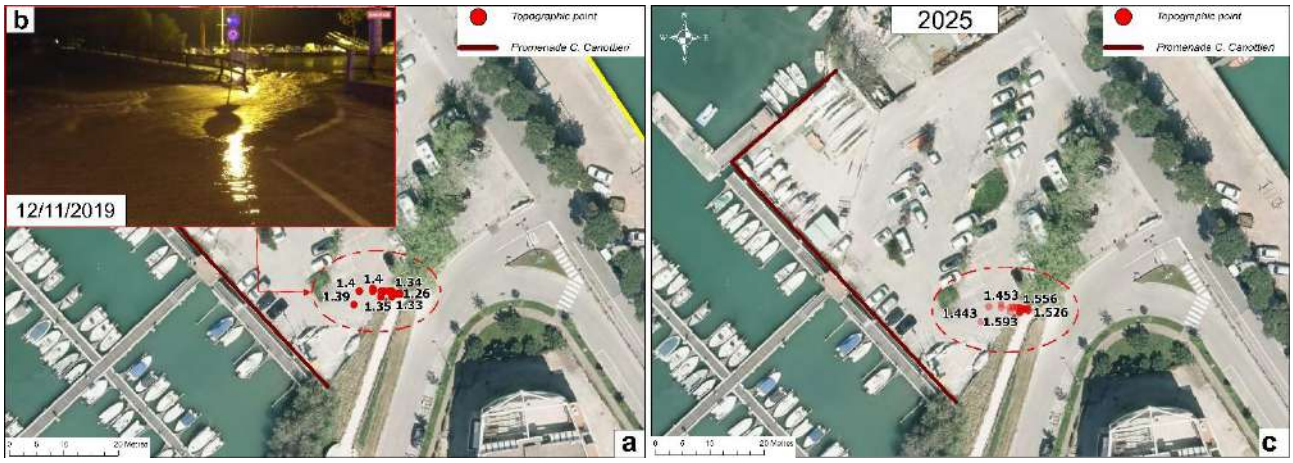

Figure 52. Temporal comparison of the topography at the flood ingress breach located near the Circolo Canottieri promenade. (a) Point-based DTM elevations derived from the 2019 dataset; (b) detailed extraction in the vicinity of the breach (dashed circle) overtopped during the 12 November 2019 extreme event (source: https://www.telefriuli.it/cronaca/piogge-e-alta-marea-lacqua-tracima-a-lignano-grado-e-trieste/);
(c) comparison with the topographic survey conducted in November 2025.

During the topographic survey carried out in November 2025, measurements were collected at the identified ingress location (Figure 52c). The elevations at this breach were found to have been raised by approximately 20-30 cm. As shown in Figure 52 the maximum elevation now reaches about 159 cm, i.e., roughly 9 cm higher than the peak level of the 12 November 2019 event (R_P=30 years). Based on this evidence, the primary ingress point responsible for the 2019 flooding has been effectively mitigated. As a result, Lignano can currently be considered in a condition of relative safety with respect to events exceeding R_P=30 years, and plausibly also for events up to R_P≈50 years (Figure 10). Accordingly, future assessments of the structural performance of the waterfront promenade should focus on rare events, such as R_P=100 years, which for Lignano corresponds to a level of 168 cm (Table 5).

5.8.3 *Lignano long-term projections*

The Lignano setting proves to be markedly different from the nearby town of Grado. Although both localities are located along lagoon margins in proximity to their respective tidal inlets, they experience different impacts, not so much due to the intensity of the extreme event itself –which, as discussed in the previous sections, is plausibly controlled by exposure and orientation, as well as by the peak expression of specific forcings such as deep low-pressure systems (Lionello et al., 2012)– but rather due to the elevation of the urban context in which the two tourist hubs have developed. In contrast to Grado, Lignano exhibits a much more conservative geomorphological and topographic setting. From an urban-planning perspective, it therefore appears reasonable to focus on rarer events, with R_P ranging between 50 and 100 years (Figure 10). This approach allows an assessment of how return periods are expected to change as a function of projected sea-level rise by 2050 and 2100 under both optimistic and pessimistic scenarios. For Lignano, Vertical Land Motion (VLM) values consistent with those reported in Table 18 for Grado were adopted. This choice is supported by unpublished analyses carried out by Dr. Piovesan, showing that VLM rates derived for the Lignano area from InSAR data, and cross-validated with nearby GNSS

stations, are broadly consistent with the values inferred from the tide-gauge comparison between Grado and Trieste over the 1991-2023 period (Figure 23).

Within the context of a rare episodic extreme event, characterized by a low probability of occurrence and associated with an R_P of 100 years, and accounting for the projected sea-level rise by 2050 and 2100 under the pessimistic SSP5-8.5 scenario, the following potential situation can be anticipated:

$$\boldsymbol{Critical\ threshold_{2050}} = current\ R_P100y - RSLR_{2050} = 168\ cm - 28\ cm = \mathbf{140\ cm}$$

Under a pessimistic scenario, the threshold of 168 cm projected for 2050 effectively decreases to approximately 140 cm once the expected sea-level rise of 28 cm is removed. This level corresponds to an episodic event with an R_P of about 14-15 years. In probabilistic terms, exceedance of the 168 cm threshold by 2050 would therefore occur with a frequency nearly seven times higher than at present. As a result, the occurrence of extreme events is expected to increase substantially in the near future. The same reasoning applies to a 100-year episodic event projected to 2100 under an optimistic scenario. In this case, subtracting 53 cm of sea-level rise yields an effective level of approximately 115 cm. This value corresponds to an event with an R_P of roughly 2-3 years. From a probabilistic perspective, exceedance of the 168 cm threshold by 2100 could occur up to 33 times more frequently.

5.9 Downscaling analysis and flood modelling of Trieste

This chapter presents and discusses the results obtained from the downscaling analysis applied to the city of Trieste, carried out using ArcGIS Pro 3.10. For each flooding simulation, the inundation thresholds reported in Table 19 are considered. The application of a downscaling approach to the regional capital of Trieste is essential to identify and interpret the critical conditions that lead to localised seawater intrusion during high-water ("acqua alta") events. Compared with the other case studies analysed, Trieste represents the site least affected by direct marine intrusion through the urban waterfront. This behaviour is primarily related to the city's geographical setting with respect to the main extreme meteorological forcings acting in the northern Adriatic (Lionello et al., 2012), and secondarily to its sheltered position within the Gulf of Trieste, protected by the Istrian Peninsula. In addition, a key role is played by the elevation of the structures along the urban waterfront and by the pronounced topographic gradient associated with the Carso relief. The downscaling analysis therefore focuses on identifying residual criticalities, particularly in relation to the 12 November 2019 event, which reached sea-level values of approximately 145-150 cm (IGM42). Within the analysed sectors, waterfront elevations range between about 70 cm and 220 cm, allowing a detailed assessment of local vulnerability under different extreme water-level scenarios.

5.9.1 *Downscaling of marine waterfront and promenade*

This section presents the results of the downscaling analysis applied to two specific sectors: (i) the marine waterfront "Le Rive" and (ii) the promenade of the Ponterosso district. The assessment covers part of the Le Rive waterfront and almost the entire extent of the two promenades in Ponterosso (Via Rossini and Via Bellini). Accordingly, the critical sectors were subdivided into three macro-areas (see Figure 53). Table 26 summarises the analysed

promenade sectors, reporting their individual lengths, the total length of the investigated stretch, and the percentage contribution of each section to the overall length.

Waterfront promenade sector	Length (m)	Percent (%) of total length
Via Bellini	273	22
Via Rossini	273	22
Le Rive	713	56
Total promenade	1259	100

Table 26. Trieste marine waterfront and promenade sectors analysed for elevation analysis aimed at the flooding assessment.

The three sectors analysed are described below, namely the Ponterosso promenades along Via Rossini and Via Bellini, and the Le Rive waterfront. The first sector considered corresponds to the Via Rossini promenade in the Ponterosso area. The second sector includes the Via Bellini promenade, while the third concerns the Le Rive waterfront, with a specific focus on the area facing Piazza Unità.

Figure 53. Downscaling area analysis: (a)The subdivision of the waterfront and the promenade into 3 sectors; the extent part of the inhabited area of Trieste municipality is also reported, treating the streets as unobstructed surfaces for water flow while omitting buildings and uninhabited areas. (b) Elevation of the Trieste waterfront and Ponterosso promenade considered in the study, represented by 10 classes subdivided every 0.10 m of elevation.

5.9.1.1 Ponterosso promenade: Via Rossini

The Via Rossini promenade in the Ponterosso sector has a total length of approximately 273 m, corresponding to 22% of the critical sectors analysed for Trieste. The analysis of the promenade edges was based on a total of 10321 surveyed points, with elevations ranging between 70 and 200 cm. The primary pathway for water ingress into the urban fabric of Trieste occurs through this sector, mainly along the western portion of the promenade, in proximity to the Le Rive marine waterfront (Figure 54a). This is confirmed by the plot in Figure 54b, which shows that about 30% of the elevations are submerged for an event with R_P=10 years (Table 19).

Finanziato dall'Unione europea NextGenerationEU
Ministero dell'Università e della Ricerca
Italiadomani
UNIVERSITÀ DEGLI STUDI DI TRIESTE

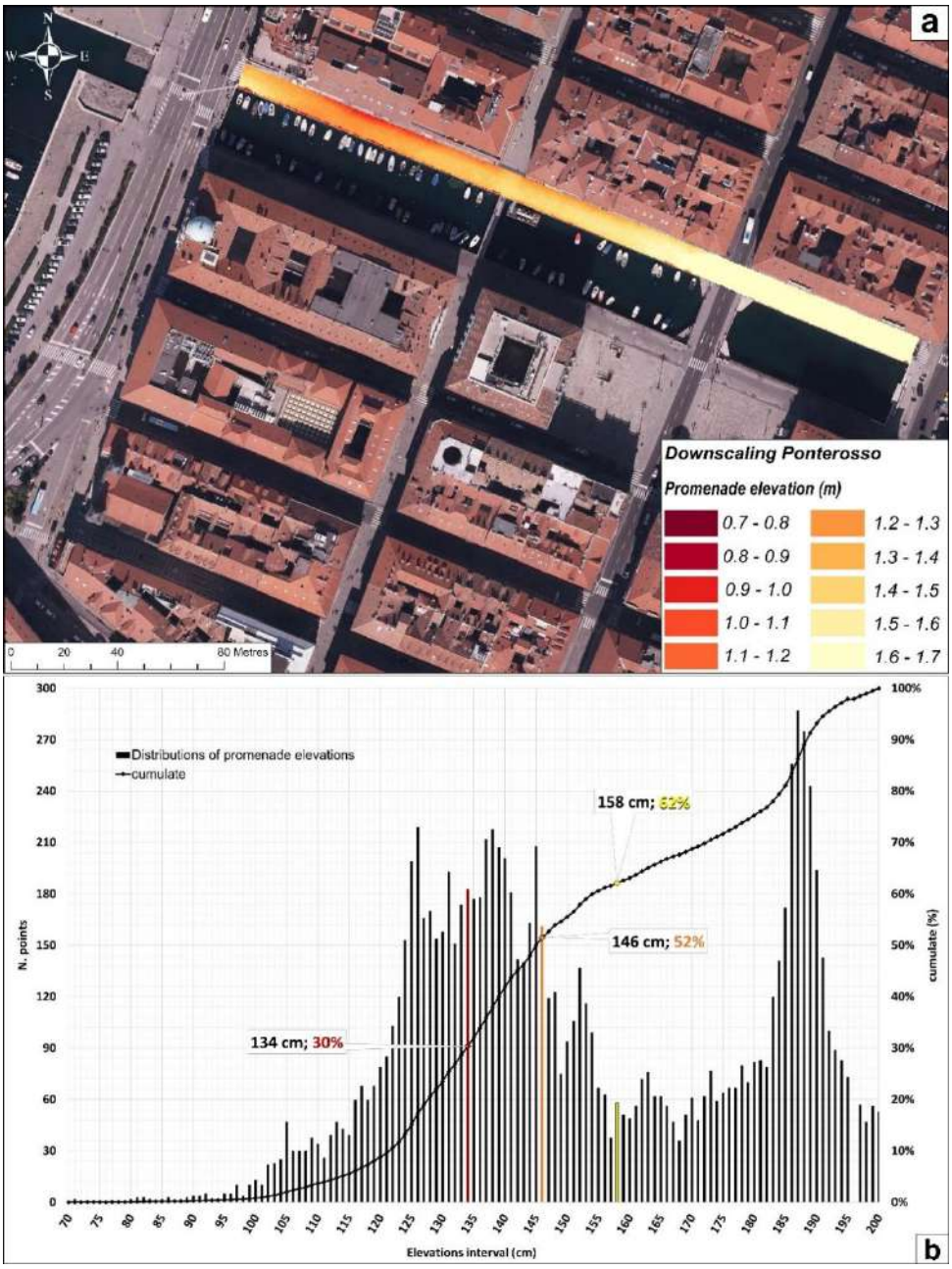

Figure 54. Critical sector of Ponterosso promenade: via Rossini (a) represents the elevations extracted from the 6-m buffer of the Via Rossini promenade. The elevation values of the promenade range from 70 to 200 cm. (b) represents the statistical distribution of the elevations extracted from the promenade of Via Rossini. Shown in red is the 134-cm elevation (R_P=10 years, Table 19) column, which represents 33% of the cumulative statistics. Shown in orange, the promenade is then half flooded with an event with a low probability of occurrence (R_P=30 years), which represents 44% of the cumulative statistics. Shown in yellow, the promenade is then a little bit more flooded with an event with a rare probability of occurrence (R_P = 100 years), especially in the east side of the promenade.

When considering an event with R_P=30 years (146 cm, corresponding to the extreme water level of the 12 November 2019 event), the percentage of submerged elevations increases to 52%, particularly affecting the western part of the sector. Overall, the promenade does not become completely submerged even under a rare R_P=100-year event (158 cm).

Finanziato dall'Unione europea NextGenerationEU
Ministero dell'Università e della Ricerca
Italiadomani PIANO NAZIONALE DI RIPRESA E RESILIENZA
UNIVERSITÀ DEGLI STUDI DI TRIESTE

5.9.1.2 Ponterosso promenade: Via Bellini

The Via Bellini promenade in the Ponterosso sector has the same characteristics of Via Bellini promenade. Via Bellini represents a secondary pathway for water ingress into the urban context of Trieste, again mainly along the western promenade (Figure 55a). However, it is a secondary and relatively less active ingress sector, as will be shown in the reconstruction of the 12 November 2019 event.

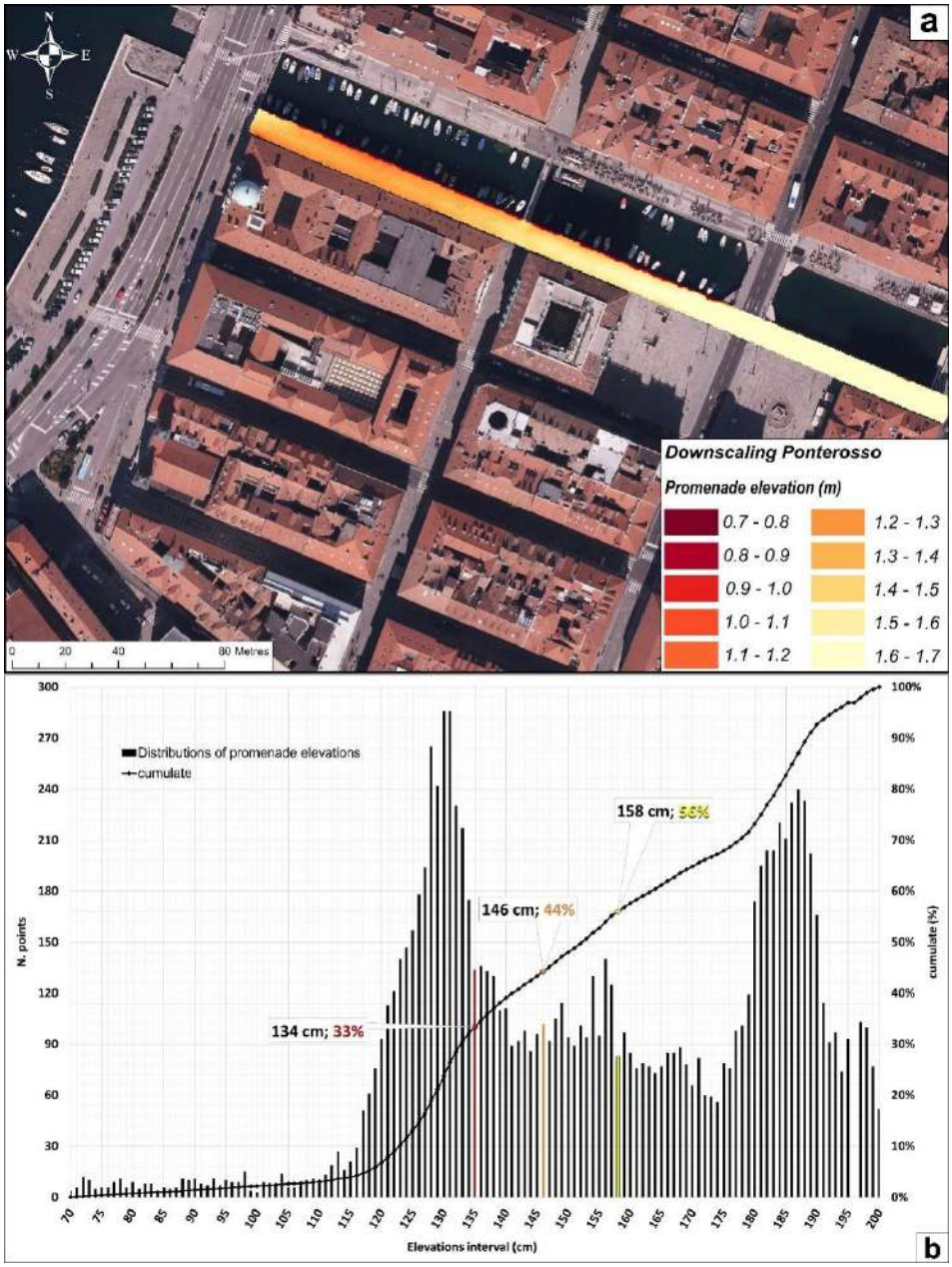

Figure 55. Critical sector of Ponterosso promenade: via Bellini (a) represents the elevations extracted from the 6-m buffer of the Via Rossini promenade. The elevation values of the promenade range from 70 to 200 cm. (b) represents the statistical distribution of the elevations extracted from the promenade of Via Rossini. Shown in red is the 134-cm elevation (R_P=10 years, Table 19) column, which represents 30% of the cumulative statistics. Shown in orange, the promenade is then half flooded with an event with a low probability of occurrence (R_P=30 years), which represents 52% of the cumulative statistics. Shown in yellow, the promenade is then a little bit more flooded with an event with a rare probability of occurrence (R_P=100 years), especially in the east side of the promenade.

Finanziato dall'Unione europea NextGenerationEU
Ministero dell'Università e della Ricerca
Italiadomani PIANO NAZIONALE DI RIPRESA E RESILIENZA
UNIVERSITÀ DEGLI STUDI DI TRIESTE

This behaviour is confirmed by the plot in Figure 55b, which shows that about 33% of the elevations are submerged for an event with R_P=10 years (Table 19). When considering an event with R_P=30 years, the percentage of submerged elevations increases to 44%, which is higher than in the Via Rossini case. Overall, the promenade does not become fully submerged even under a rare R_P = 100-year event, for which about 56% of the elevations experience inundation.

5.9.1.3 Marine waterfront: Le Rive

This represents the most extensive analysed sector, with a total length of 713 m. The analysis of the elevations along the Trieste marine waterfront was carried out using a slightly different approach compared to the other cases described above. In order to evaluate as accurately as possible the elevations of the *Rive* and, consequently, the potential ingress and inland propagation of seawater, a 26-m buffer was adopted, encompassing the entire Trieste waterfront sector. A total of 81725 points were analysed, with elevations ranging from 70 to 220 cm. Based on the extracted elevation statistics, this sector can be considered a potential pathway for water ingress when extreme events exceed thresholds higher than 146 cm (R_P =30 years). As shown in Figure 56a, most of the elevations between 70 and 146 cm are concentrated close to the waterfront, particularly in the central portion facing Piazza Unità d'Italia. This result is confirmed by the plot in Figure 56b which indicates that about 44% of the waterfront is submerged for an R_P=30 years event when considering the 26-m buffer. In contrast, for a rare R_P=100 years event, corresponding to a water level of 158 cm, approximately 67% of the waterfront is submerged (Figure 56b) generating a potential ingress pathway that could lead to the inland expansion of seawater towards the city centre, particularly Piazza Unità and the Borgo Teresiano area.

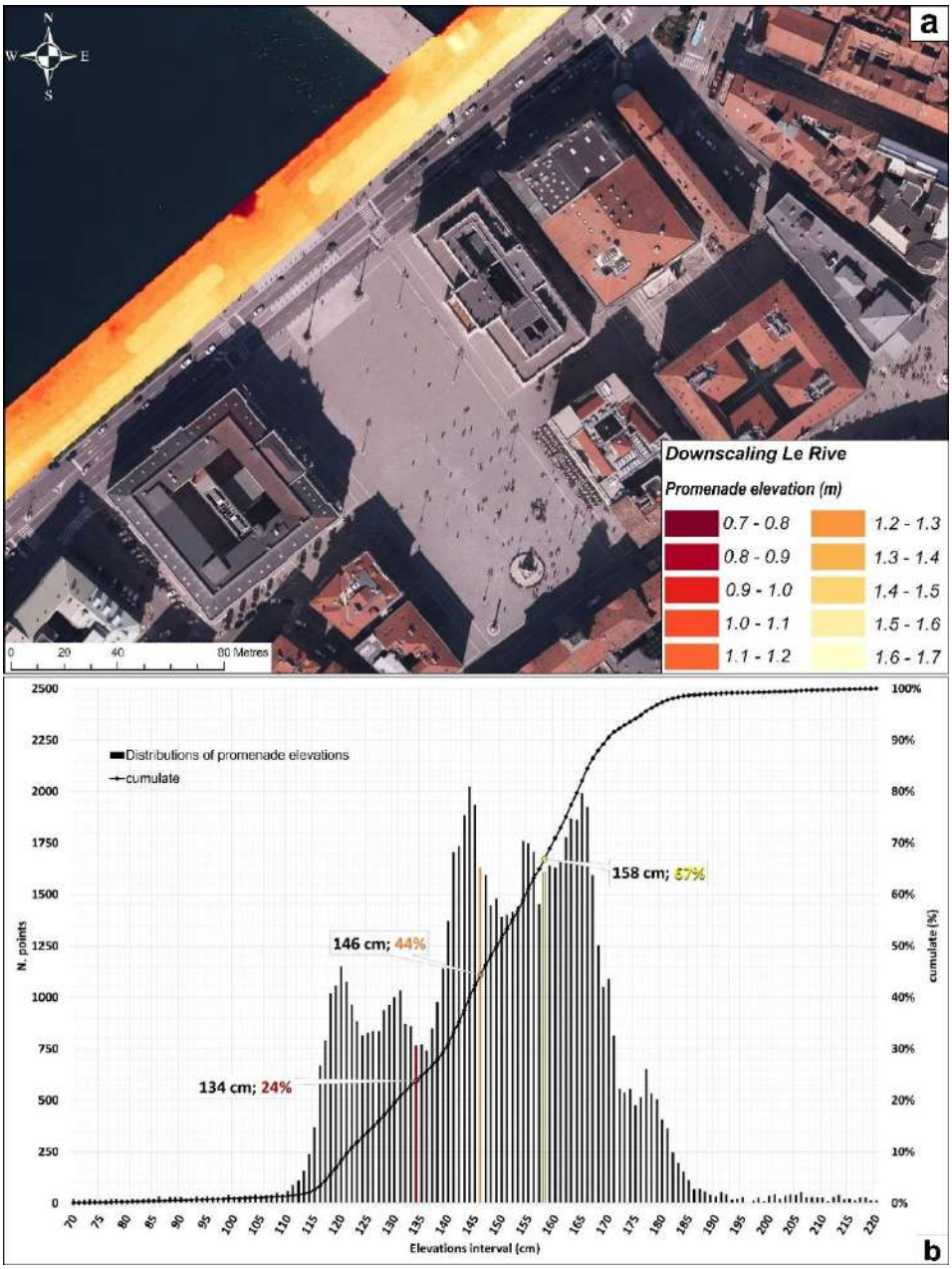

Figure 56. Critical sector of marine waterfront: Le Rive (a) represents the elevations extracted from the 26-m buffer of the waterfront. The elevation values of the waterfront range from 70 to 220 cm. (b) represents the statistical distribution of the elevations extracted from the marine waterfront Le Rive. Shown in red is the 134-cm elevation (R_P=10 years, Table 19) column, which represents 24% of the cumulative statistics. Shown in orange, the promenade is then half flooded with an event with a low probability of occurrence (R_P = 30 years), which represents 44% of the cumulative statistics. Shown in yellow, the promenade is then a little bit more flooded with an event with a rare probability of occurrence (R_P=100 years), especially in the east side of the promenade.

5.9.2 *Bathtub vs. Dynamic modelling*

Using the event of November 12, 2019, as a reference case, a preliminary comparison between the hydrodynamic simulation and the static bathtub approach has also been out for the city of Trieste (highest water levels 149 cm, hourly based recordings from the Molo Sartorio tide gauge), as shown in Figure 57. The bathtub model was first used as a first-order screening method to identify locations that would be flooded based just on elevation thresholds, just like in the earlier case studies. The static approach indicates that once the threshold elevation of roughly 145–149 cm is exceeded, seawater may propagate inland due to the relatively modest topographic gradient of the waterfront sector between Le Rive and Piazza Unità d'Italia. However, unlike Grado and differently from Muggia, the comparison reveals that the hydrodynamic model produces a more constrained and physically coherent flooding pattern. While the static approach assumes direct hydraulic continuity between the waterfront and Piazza Unità, the dynamic simulation demonstrates that the primary inflow pathway is instead located along the Ponterosso promenade, with water propagating southwestward. Essentially, the dynamic model limits direct overflow in front of Piazza Unità, and the maximum extent of flooding remains confined to the areas adjacent to the seafront.

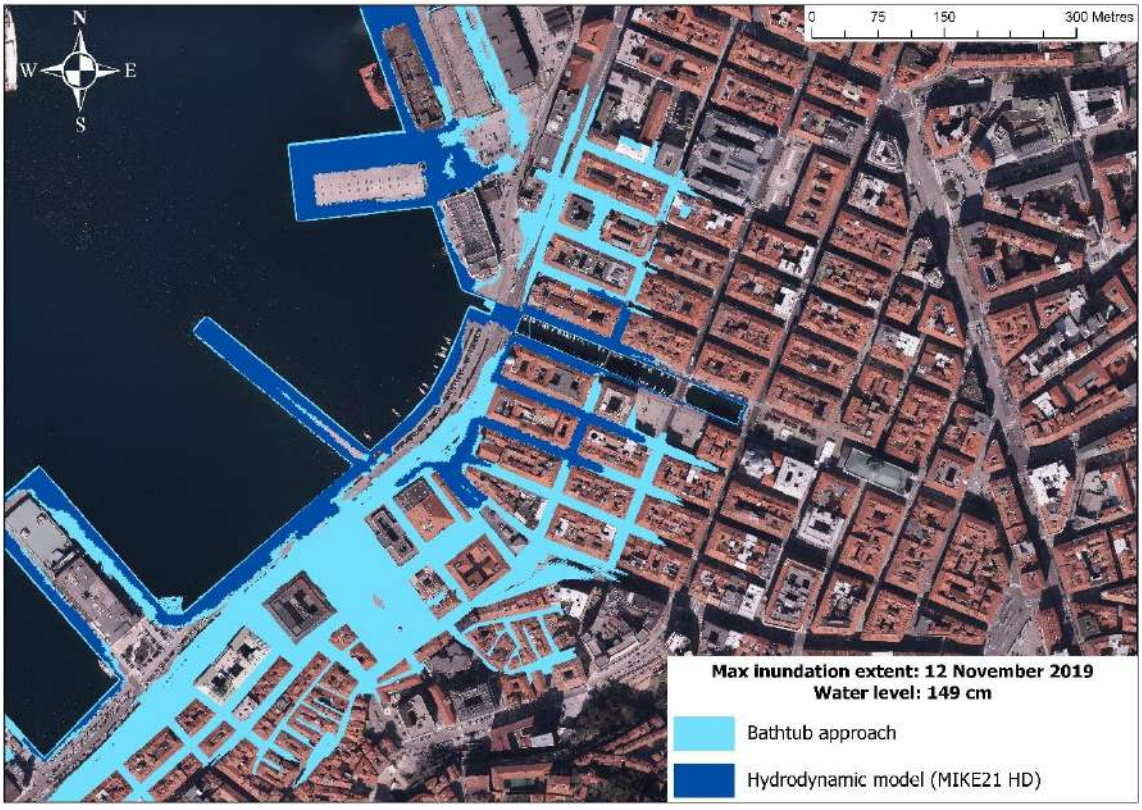

Figure 57. Maximum inundation extent for the 12 November 2019 event in Trieste (peak water level: 149 cm, IGM42), comparing the static bathtub approach (light blue) and the dynamic hydrodynamic model MIKE21 HD (dark blue). The dynamic simulation accounts for hydraulic constraints and flow processes, resulting in a more physically consistent flood pattern compared to the static assumption of uniform water spreading.

The static approach, which disregards hydraulic resistance, the temporal evolution of the peak and the interaction of certain phenomena during the storm surge, may suggest a simplified “basin” expansion that does not fully reflect the physical processes governing the event. In this case study, hydrodynamic simulation proves essential not only for refining the

spatial extent of the flooding, but also for correctly interpreting the mechanisms responsible for the propagation of water inland.

An initial evaluation of Trieste's flood patterns was given by the preliminary comparison of the static and dynamic techniques, but it also brought to light a crucial interpretive problem. Effective hydraulic connectivity during extreme events is not always implied by the DTM-based analysis's suggestion of apparent altimetric continuity between the coastline and Piazza Unità. To determine if topographic continuity alone might account for the inland propagation seen during the incident on November 12, 2019, a specific downscaling analysis of the waterfront elevations was initially conducted. However, in order to determine the real flow routes and quantify the effective propagation mechanisms governing the flooding dynamics, a full 2D hydrodynamic calibration of the 2019 event was subsequently carried out due to the limits of purely geometric analysis. This step represents a necessary transition from morphological interpretation to process-based modelling.

5.9.3 *12 Novembre 2019 event calibration*

However, the analysis of the waterfront elevations raised an additional question regarding the inland expansion of seawater towards Piazza Unità during the 12 November 2019 event. As noted above, the event reached water levels of approximately 149 cm, with oscillations between 142 and 150 cm based on 10-minute records from the Molo Sartorio tide gauge. For this reason, a detailed analysis was carried out in the area facing Piazza Unità d'Italia in order to assess the local elevations that, starting from the marine waterfront, may have enabled the propagation of seawater towards the square, as also reported by local newspapers in the days following the event.(https://www.ilnordest.it/economia/acqua-alta-a-trieste-sommerse-le-rive-e-piazza-unita-la-regione-chiede-lo-stato-di-emergenza-e-non-e-finita-qk77gxpv). The elevations of the Rive were therefore analysed using a 26-m buffer, together with the road elevations using a buffer of approximately 22 m. The aim was to verify whether a topographic continuity could exist between the marine waterfront and Piazza Unità, which are separated by a distance of about 50 m. To assess the contiguity of elevations using the 0.5 × 0.5 m DTM resolution Figure 58a shows a detailed view of the area highlighted by the black dashed rectangle, together with a transect of approximately 140 m oriented NE-SW between the boundary of the Rive buffer and the road buffer. As can be observed from the extracted transect (Figure 58b), the elevations in the area immediately landward of the waterfront and facing Piazza Unità range approximately between 140 and 150 cm. Therefore, considering the 2019 event, it is likely that a topographic continuity existed, allowing the seawater to propagate from the Rive waterfront towards Piazza Unità. This provides a plausible explanation for the flooding observed in this area during that event.(https://www.ilnordest.it/economia/acqua-alta-a-trieste-sommerse-le-rive-e-piazza-unita-la-regione-chiede-lo-stato-di-emergenza-e-non-e-finita-qk77gxpv).

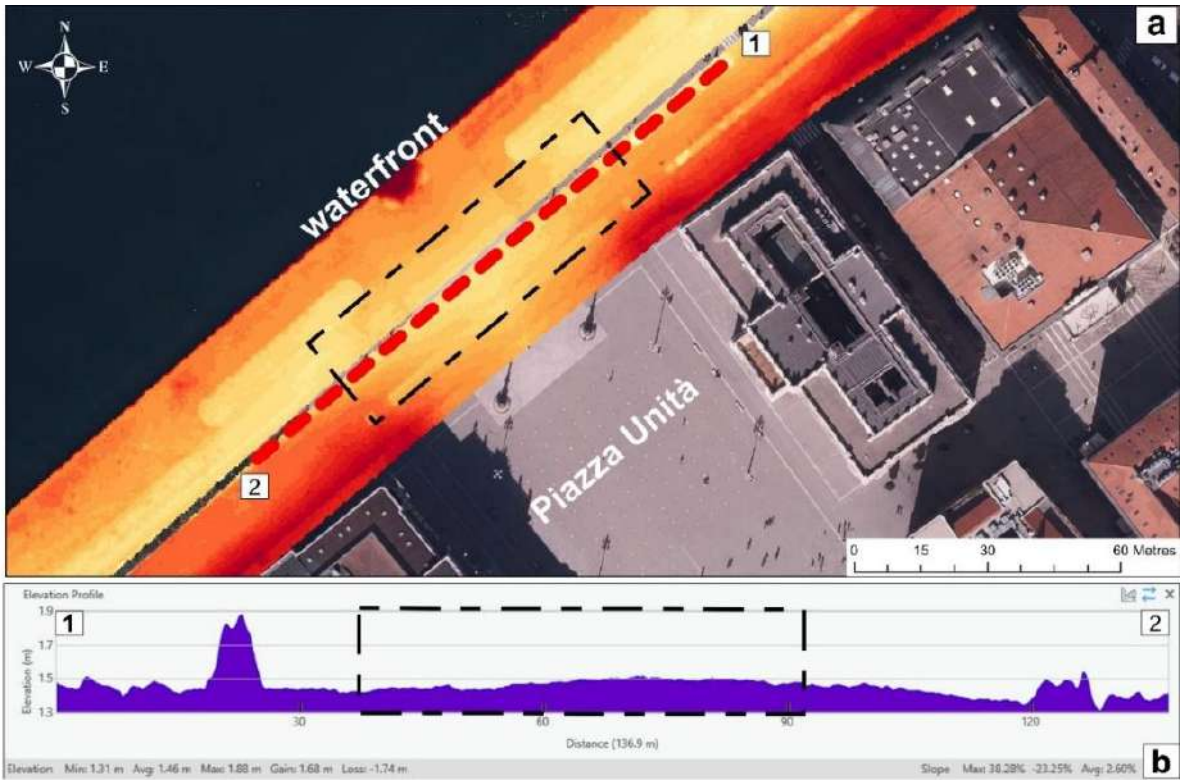

Figure 58. (a) Downscaled intersection between the 26-m buffer of the waterfront (expressed in elevation) and Le Rive Street with a 22-m buffer. The red dashed area represents the 140-m transect. (b) Detailed view of the elevations along the extracted transect from the DTM. The area of contiguity between the waterfront buffer and the street facing Piazza Unità shows elevations ranging between 140 and 150 cm.

Once the downscaling analysis of the contiguity between the waterfront and Piazza Unità was completed, the final step consisted in the calibration of the 12 November 2019 event using MIKE21 with a 2D Hydrodynamic model. The objective was twofold: (i) to verify the spatial extent affected by an acqua alta event comparable to that of 2019 (with total water levels between 140 and 150 cm), and (ii) to reproduce the inflow from the waterfront and the subsequent propagation of the water mass toward Piazza Unità. As shown in Figure 59a the first and primary inflow pathway (around 19:00) is associated with the Ponterosso promenade, specifically along the western sector of Via Rossini, where overtopping begins at water levels of approximately 135 cm (R_P=10 years Table 19) simultaneously mirrored by inflow from the corresponding western sector of Via Bellini. Continuing with the event evolution, around 19:30 an intermediate expansion of flooding occurs (Figure 59b), leading to the involvement of urban grids located northeast and southwest of the Ponterosso promenade, with greater contiguity toward the southwestern sector, in the direction of Borgo Teresiano and Piazza Unità d'Italia.

Finanziato dall'Unione europea NextGenerationEU
Ministero dell'Università e della Ricerca
Italiadomani PIANO NAZIONALE DI RIPRESA E RESILIENZA
UNIVERSITÀ DEGLI STUDI DI TRIESTE

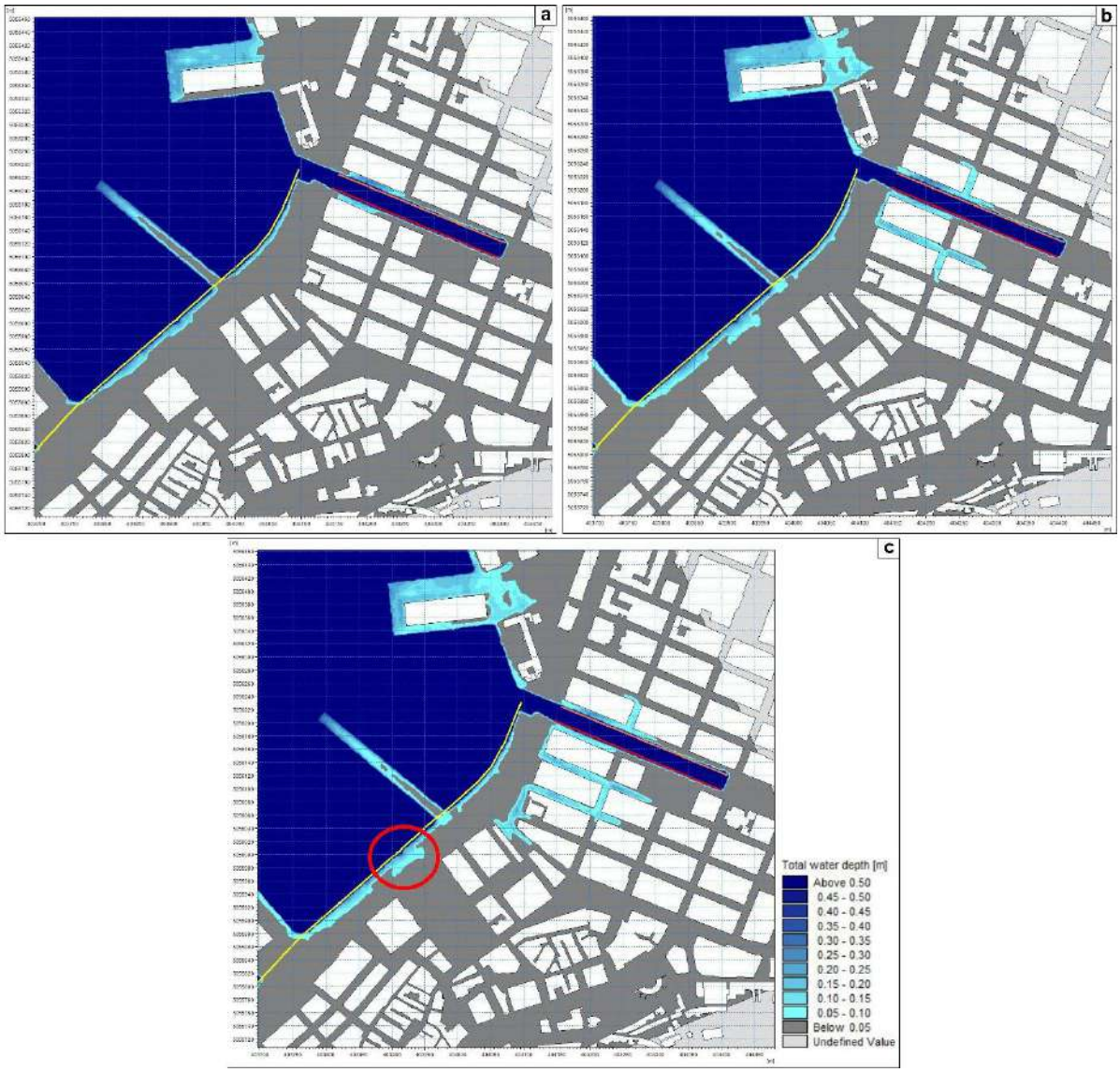

Figure 59. (a) Onset of marine flooding along the Ponterosso promenade (Via Rossini and Via Bellini), primarily along the western section of the promenade. The initial overtopping occurred at an approximate water level of 135 cm**.** (b) Flood extent at 140 cm for streets perpendicular to Via Bellini and 145 cm for those perpendicular to Via Rossini. The affected areas are confined to zones adjacent to the Ponterosso promenade, with documented inundation also impacting the Le Rive waterfront. (c) Maximum flood extent at peak water levels of 145-150 cm, between the Ponterosso promenade and Piazza Unità. Water encroachment is observed within the waterfront area shown in Figure 51a (red circle). Maximum water depths remain within 40-45 cm. Results derived from 2D hydrodynamic simulation**.**

Following a brief phase of partial drainage and stagnation in the Ponterosso area (approximately 20:00-20:30), the maximum expansion of the water mass occurs around 21:10, as shown in Figure 59c. As can be observed, the maximum flood extent, with water depths not exceeding 20 cm, does not reach Piazza Unità. Therefore, contrary to what might be assumed, the waterfront area in front of Piazza Unità was not overtopped by the 150 cm water level (red circle, Figure 59c). Although the transect shown in Figure 58b allows the elevation range orthogonal to the potential expansion of the water mass beyond the marine waterfront to be assessed, these elevations were not exceeded during the 12 November 2019 high-water event, one of the most intense events of the last 50 years. Consequently,

Finanziato dall'Unione europea NextGenerationEU
Ministero dell'Università e della Ricerca
Italiadomani
UNIVERSITÀ DEGLI STUDI DI TRIESTE

the flooding observed in Piazza Unità is likely attributable to a combination of factors: the expansion of the water mass through the Ponterosso promenade toward the southwest, together with the intense precipitation recorded during those days and the hydraulic drainage conditions of the urban sewer system, which are constrained by the local topographic gradient. The superposition of these processes likely produced flooding characterized by a bathtub type effect.

5.9.4 *SLR projections (SSP5-8.5) applied on nuisance extreme events*

Even for events like the one that occurred on November 12, 2019, when the overall water level hit 150 cm IGM42, the city of Trieste is currently in a reasonably safe state. The Ponterosso promenade is primarily home to the few crucial places that permit seawater intrusion, as the dynamic modelling results demonstrate. Although the current state of the waterfront between Le Rive and the Ponterosso area may be regarded as generally stable, future scenarios must take into consideration the additional impact of sea-level rise (SLR) in addition to the overall water levels achieved during extreme high-water occurrences. In order to determine probable key locations and the size of the zones concerned, three scenarios were simulated using a static "bathtub" technique. As was previously mentioned, Trieste is less impacted by extremely high extreme water levels than Grado and Lignano. This is due to the city's elevated waterfront structures, prominent topographic gradient, and different exposure to meteorological forcings. When taking into account simply the hydrometric level and ignoring wave forcing, Trieste has seldom ever encountered extreme events lasting longer than 30 years, excepting uncommon occurrences with a return period of 100 years. Thus, a pessimistic sea-level rise scenario for 2100 is added to events with very high (R_P=2 years), high (R_P=10 years), and medium (R_P=30 years) recurrence. The impact of apparently insignificant events, such the R_P=2 years level of around 115 cm, can be evaluated using this method when combined with the anticipated pessimistic sea-level increase by 2100. Therefore, the projections for Trieste reported in Table 18, are expressed both relative to the reference baseline period (1995-2014) and relative to the year 2022. In the latter case, the observed mean sea-level rise rate at Trieste over the period 1991-2022 (+2.8 mm/yr) was adopted and multiplied by the 18 years elapsed since the baseline, as reported in (Table 27).

Year	**SLR Scenario Reference 2006 Baseline (1995–2014)**	**Total Sea Level Trieste (cm) (2006-2022)**	**Current R_P (years)**	**ESL (cm)**	**2100 ESL (cm)**
2100	SSP5-8.5 (median)	+62	2	115	177
			10	134	196
			30	146	208

Table 27. Local sea-level values for the Trieste under SSP5-8.5, projected for 2100 (cm). Total water level elevations projected for 2100, obtained by summing a storm surge event with a 2, 10 and 30 year and the projected SLR under SSP5-8.5 scenarios.

ArcGIS Pro 3.10 was used to create a set of hazard maps for Trieste, which were similar to those created for the short-term flooding hazard maps for the city of Grado. Only open flow

Finanziato dall'Unione europea NextGenerationEU
Ministero dell'Università e della Ricerca
Italiadomani PIANO NAZIONALE DI RIPRESA E RESILIENZA
UNIVERSITÀ DEGLI STUDI DI TRIESTE

surfaces were regarded as potentially flooded areas, and built-up structures were not included in the analysis, according to the same analytical requirement. Figure 60 demonstrates that an extreme water level of 177 cm is obtained by starting from an event with a return period of R_P=2 years, combining the pessimistic sea-level rise scenario for 2100 (+62 cm), and taking projections from 2022 to 2100 (rather than from 2006, which represents the temporal barycentre of the 1995-2014 reference baseline).

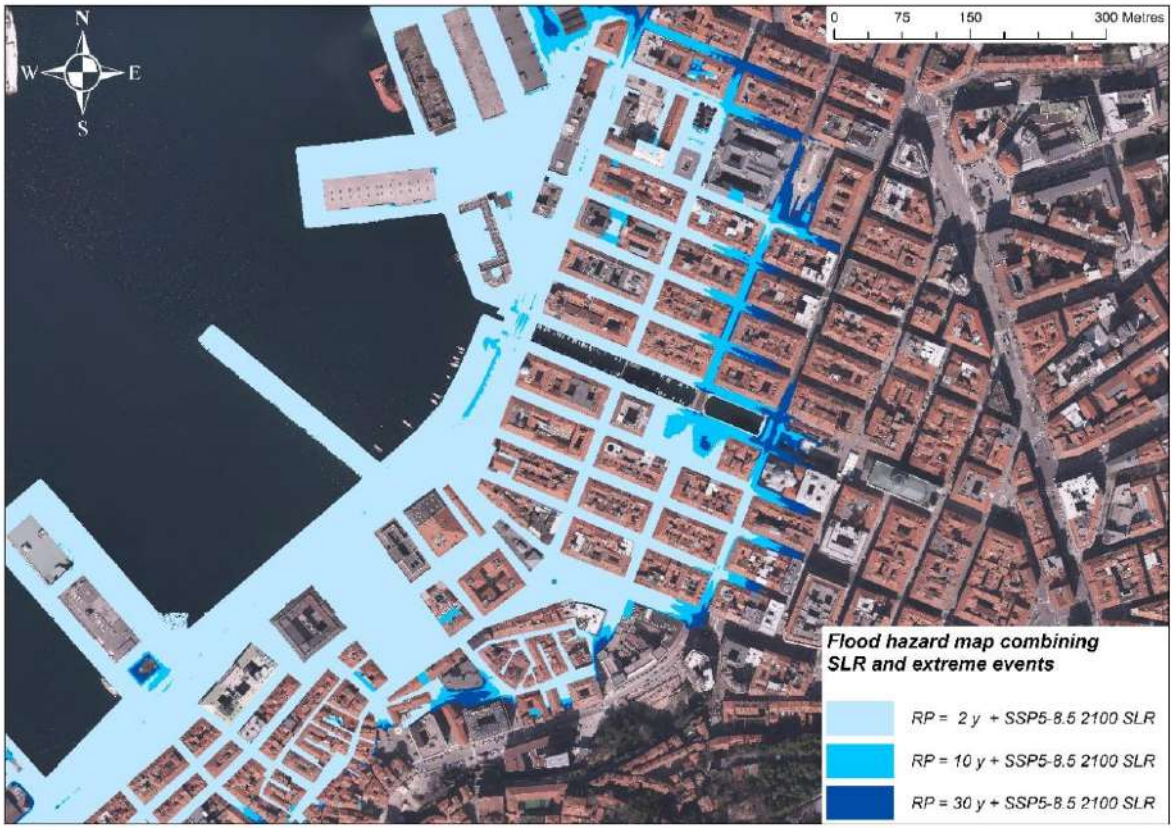

Figure 60. Coastal flood hazard map for the city of Trieste, considering the overlap of extreme events with R_P 2, 10 and 30 years combined with the pessimistic SSP5-8.5 scenario of SLR by 2100 (ArcGis Pro 3.10, 2025).

Assuming the accepted scenario is plausible, this estimated level for 2100 precisely matches the sea level attained on November 26, 1969, which is still Trieste's worst high-water event since the tidal gauge was installed. An event with a high chance of occurrence (R_P=10 years) was then combined with the same sea-level rise prediction, yielding a total water level of 196 cm. (Table *27*). In this case, the hazard map Figure 60 highlights a spatial expansion of flooded areas towards the NE sectors relative to Piazza Unità d'Italia and the Borgo Teresiano. In the end, a medium-probability event (R_P=30 years) was taken into account, resulting in a total estimated water level of 208 cm by 2100 (Table *27*). With regard to Piazza Unità d'Italia, this level causes a gradual but still restricted expansion of inundation, especially along the eastern and northeastern parts. However, the inland penetration of floodwaters remains relatively limited due to the geomorphological and urban characteristics of the territory on which Trieste is constructed, particularly towards the ancient city centre and the Borgo Teresiano neighbourhood.

6 Adaptation Plans and Conclusions

It is now widely known that Northern Adriatic coastal communities situated in low-lying, sandy coastal environments are far more vulnerable to the consequences of sea level rise than other regions (Galluccio et al., 2024). However, severe sea levels and rising mean sea levels are increasingly affecting not only low and sandy shores but also coastal sections with high and heavily populated shorelines, like the town of Muggia. In order to deal with the increasing frequency of extreme events, it has become necessary to implement adaptation and mitigation strategies for other, smaller but equally vulnerable coastal realities, much like the safety measures implemented for the city of Venice with the activation of the Mo.S.E. barrier system in 2020 (van de Wal et al., 2024). Additionally, as current coastal defence infrastructures age and gradually deteriorate, the effects of coastal floods are predicted to worsen (Mel et al., 2021). In order to guarantee a sufficient degree of safety, urban coastal defences, such as waterfronts, promenades, and similar structures, must be evaluated from a structural standpoint and have their crest elevations closely monitored, modified, and, if needed, raised (Shayegh et al., 2016). Plans for elevating embankments and coastal walks should therefore be adjusted in accordance with the anticipated rise in sea level (Sriver et al., 2018), especially in the event of severe weather. The forecasts of future sea-level rise themselves, as well as the level of uncertainty surrounding extreme-value statistics, will determine the kind of measures that should be put in place (Cin et al., 2020; Horton et al., 2020; Hinkel et al., 2021). Extreme coastal flooding events ought to be treated as a risk management and planning issue rather than just a hydrodynamic and/or statistical issue. From the identification of crucial concerns to site-specific design and impact assessment, Rizzo et al. (2025) emphasize how varying degrees of model complexity might be essential in various stages of coastal adaptation planning. As a result, while advanced and complicated dynamic models are required to capture elements like flow velocity, flooding periods, etc., simpler methods like bathtub models can offer an initial evaluation of the most vulnerable areas in cities. The development of coastal places is thus made possible by this kind of practical approach, which is supported by scientific correctness. Thus, it is now possible to develop adaptation and urban-planning hypotheses for the most vulnerable areas of lagoon promenades, like those of Grado and Lignano, as well as for urban waterfronts, like those of Muggia and Trieste, thanks to the statistically updated extreme water-level thresholds, which are site-specific and based on historical data from recent decades. In fact, for many decades to come, the creation of medium- to long-term adaptation plans would enable the identification of definitive answers to site-specific flooding issues. The hopeful SSP1-2.6 pathway, which is impacted by the possible rise in the frequency and severity of extreme events, and short- to medium-term scenarios are now the focus of the most trustworthy future projections. The potential urban adaption solutions for the various coastal environments examined in this thesis study will be covered in the upcoming chapter. As a result, the following factors will be looked at in addition to the statistical analyses created and used in accordance with the particular environmental context: (i) exposure to extreme water levels; (ii) the orientation of the sectors most susceptible to marine intrusion, considering both current episodic events and long-term assessments based on projected sea-level rise; and (iii) the scope of intervention within the urban fabric, assessed in terms of available urban space, the spatial extent of the most vulnerable areas, and the viability of

Finanziato dall'Unione europea NextGenerationEU
Ministero dell'Università e della Ricerca
Italiadomani PIANO NAZIONALE DI RIPRESA E RESILIENZA
UNIVERSITÀ DEGLI STUDI DI TRIESTE

building and/or modifying existing defence structures, taking into consideration the potential reduction of urban impacts.

6.1 Grado adaptation plans

Grado is the first location that underwent a thorough statistical analysis to determine how the frequency of extreme events has gradually increased over the past few decades (Figure 12), This analysis took into account both the most recent extreme-value statistics and the maximum sea levels observed over the previous thirty years. Localized criticalities were then found along particular sections of the lagoon promenade through an evaluation carried out at the size of the urban detail (Figure 27 and Figure 28). Starting from the data of the scenarios and the R_P of the events, the embankment sealing hypothesis starts from the evidence that one must proceed by considering, in a modular way, interventions that, in order of priority, start from the most critical sections. The entire urban stretch facing the lagoon has docks whose elevation cannot guarantee sealing for events with very frequent return times. Consequently, based on the study conducted, a safety threshold level of 180 cm can be chosen. This figure roughly corresponds to a meteomarine event, which statistically occurs with a R_P of approximately 250 years. Thus, considering a pessimistic sea level rise to 2050 calibrated on the city of Grado, equal to an increase of approx. 28 cm, on a probabilistic level, a lowering of the threshold level to 152 cm would occur. The value in question corresponds to an event with a R_P of ca. 30 years, defined as having a medium probability of occurrence. At present, this type of intervention secures the territory and, in the future forecast, will allow sufficient time to prepare –should it be deemed necessary– appropriate modifications or additions. The value of 180 cm, therefore, allows us to have a certain margin of coverage that is much more reliable than a safety value that, correlated with a less reliable projection, would have a greater degree of uncertainty. Once the threshold level of security and the most vulnerable sectors to be safeguarded have been ascertained, based on downscaling simulations and elevation analysis, the next step concerns which adaptation strategies to put in place. The provision of defensive measures depends on various factors, such as political, regional and local decision-making wills. An example of this approach is the SECAP project, undertaken to incorporate adaptation measures and climate mitigation strategies at the municipal level for the city of Trieste (Manzan et al., 2022). Nevertheless, additional factors will be closely related to the layout of the urban fabric (Barnard et al., 2021) and therefore directly controlled by anthropogenic elements, such as urbanisation, accommodation space, adaptability, land-use change, as well as the configuration and size of the road network (Toledo et al., 2024). The first two stretches in need of timely intervention concern the perimeters that extend over two sectors, from Riva Brioni to the Mandracchio Canal inclusive, for a total of 1919 m. Within this section, the two perimeters requiring timely intervention are Riva Brioni (260 m) and the Mandracchio Canal (1392 m). Riva Brioni is characterised by a promenade that, throughout its entire extension, has heights ranging from 70 to 115 cm. The road surface width, measured from the outer edge of the promenade to the pavement on the opposite side, is approximately 14 m (Figure 27). Of this, the space relating to the urban road is approx. 5 m. The area where changes will be made for raising the shoreline or changing the lagoon promenade is about 7 m wide: 3 m for the lagoon promenade and 4 m for parking spaces, which could be adjusted if needed. These characteristics make Riva Brioni one of the few city areas that are most exposed to flooding, where it is possible to implement a significant change in the urban fabric. One possibility concerns the application of bulkhead planter systems or of a bank (see Toledo et al., 2024) extended along the entire affected area (see Figure 61). A

Finanziato dall'Unione europea NextGenerationEU
Ministero dell'Università e della Ricerca
Italiadomani PIANO NAZIONALE DI RIPRESA E RESILIENZA
UNIVERSITÀ DEGLI STUDI DI TRIESTE

further hypothesis is the application of a seawall-walk barrier system that transforms the Riva Brioni promenade into a fully-fledged barrier that maintains the existing pedestrian section connected to the waterfront.

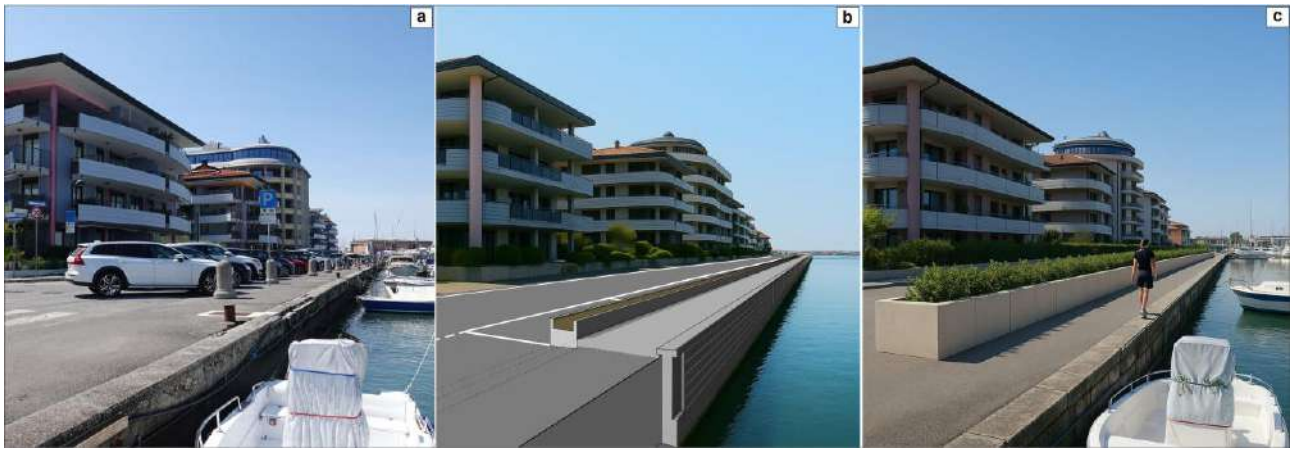

Figure 61. The Riva Brioni promenade. (a) Photo of a promenade section, taken at coordinates 45°68′28.63" N, 13°38′06.56" E (photo credits: Spadotto S.). (b) Design of a bulkhead planter system, built along the entire promenade. Toward the lagoon, the promenade is maintained. Toward the street, parking spaces are created parallel to the bulkhead planter, and the roadway is maintained. (c) Rendering of what Riva Brioni might look like. For the sake of clarity, possible regulated openings needed between the planters for pedestrian transit and dock access are not depicted here.

The situation is different for the Mandracchio Canal. The docks surrounding the canal are characterised by a higher elevation than those at Riva Brioni. However, these fail to provide adequate defence, resulting in a general ingression of the water mass into the built-up area, affecting the historic centre to a certain extent, even with water levels that are not particularly critical, slightly higher than 110 cm. The layout of the streets and buildings surrounding the canal, for nearly their entire length, does not permit significant modifications to the urban fabric. The space available from the docks, where there are boat moorings, to the walls of the buildings on the opposite side is approximately 6 m. It follows that the usable space for a possible intervention is completely absent. For this reason, a possible proposal concerns the design of mobile defence systems at the Mandrachio lagoon entrance (Figure 62a,b), similar conceptually to those already widely used in Northern Europe, especially in the Netherlands with the Maeslant Barrier in Rotterdam (Bol, 2005), designed for protection against very extreme flood events (Jorissen et al., 2016). In Cesenatico, Emilia Romagna, Italy, there exist mobile defence systems known as Porte Vinciane (Da Vinci's gates), a Project by Binini Partners (https://www.bininipartners.it/progetti/porta-vinciana-a-cesenatico/) (Figure 62c). Another possible solution could be a mobile system like the Mo.S.E (Munaretto et al, 2012) designed in Chioggia, called Baby Mo.SE (Il Baby MOSE, 2015) (Figure 62e). Constructing these weirs directly in the upper opening part of the Mandracchio, approximately 20 m wide, can guarantee a safe condition in the city surroundings. Additionally, from an economic perspective, the intervention would be less costly than designing an extended dock elevation for the entire Mandracchio Canal.

Finanziato dall'Unione europea NextGenerationEU
Ministero dell'Università e della Ricerca
Italiadomani
UNIVERSITÀ DEGLI STUDI DI TRIESTE

Figure 62. The Mandracchio Canal docks. (a) View of the Mandracchio C. lagoon entrance (Photo credits: Fontolan G.). (b) Plan view of the Canal opening. (c) Example of Porte Vinciane (Da Vinci's gates) mobile system for flood defence in Cesenatico, a Project by Binini Partners (www.bininipartners.it). (d) Functional design of Baby Mo.SE floodgates in Chioggia (after (www.bininipartners.it) modified). (e) Example of mobile floodgate in operation in Chioggia (after (Il Baby MOSE, 2015) modified).

6.2 Muggia adaptation plans

After Grado, the second coastal town that has been increasingly affected by extreme weather events of marine origin in recent decades is Muggia. Compared to Grado, which is exposed to the Sirocco and Libeccio winds, Muggia is located within a protected area of the Gulf of Trieste (Figure 7). The Istrian peninsula allows for almost total damping of wave forcing. However, meteorological forcing related to extreme hydrometric levels still has a significant impact in this context. Although Muggia is located within a coastal area with high, urbanised coastlines, most of the historic town centre has elevations within the range of 90-120 cm (Figure 46). The elevation of the land and therefore of the urban fabric is gradually leading to a critical situation with regard to the ingress of water, depending on the extreme event. Therefore, as in the case of Grado, the possibility of adapting the urban marine waterfront was also evaluated for Muggia, based on downscaling analysis (Figure 33). Compared to the case applied and discussed for Grado, water ingress in Muggia occurs through the waterfront and promenade of the small Mandracchio Canal. As explained above, the main route of ingress is precisely the waterfront in this sector. The urban areas around the waterfront, which is about 98 meters long, are quite constrained, as illustrated in
Figure 34b. It should be noted that the total buffer employed for the extraction and statistical analysis of the waterfront elevations includes the walkway and road in addition to the embankment itself (Figure 63b). It follows that it would not be a very appropriate solution to raise the embankment along the Mandracchio C. Along the banks of the Mandracchio Canal, specifically on the C. Colombo promenade (Figure 63c), it is evident that space constraints hinder modifications, such as the implementation of a modular embankment rise (Shayegh et al., 2016). Figure 63 illustrates that the promenade section is not a primary access route;

however, it serves as a secondary route connected to the primary waterfront of the Mandracchio Canal. The conditions vary for the promenade of the Sala da Mar restaurant compared to the Circolo della Vela. The space in the first case is significantly larger than that in the two preceding cases. The 6-m-buffer encompasses a smaller area than the entire analysed quay. This section is not a primary connection route to the historic centre, as illustrated in Figure 34. Nonetheless, like the C. Colombo promenade, it may be regarded as a secondary marine access route.

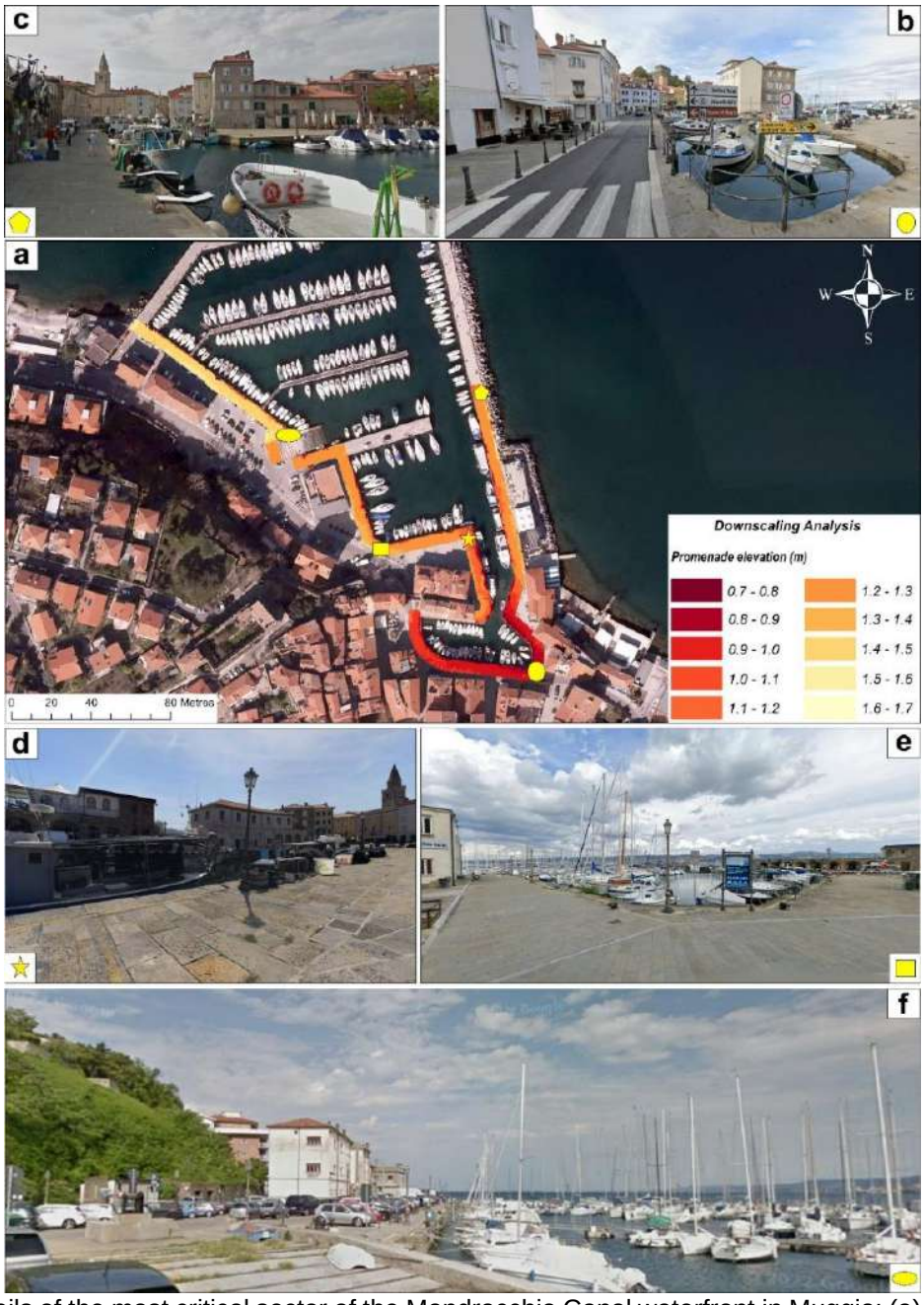

Figure 63. Details of the most critical sector of the Mandracchio Canal waterfront in Muggia: (a) waterfront and promenade elevation along Mandracchio Canal; (b) Google earth photo of the Mandracchio Canal waterfront, main marine water ingression; (c) Google earth photo of C. Colombo promenade; (d) Google earth photo of Sala da Mar restaurant promenade; (e) Google earth photo of the Circolo della Vela promenade; (f) Google earth photo of the Nazario Sauro park promenade.

The modification in this case excludes the embankment elevation due to the absence of a direct connection. Consequently, despite the existing urban space, an intervention in this area would be largely ineffective. In the case of the Circolo della Vela promenade (Figure 63e), the space covers the entire 6-m buffer zone for long stretches (Figure 37). This section of the waterfront similarly does not facilitate a direct connection to the sea ingress in the historic centre. The aforementioned description pertains to events with a recurrence interval ranging from 2 to 10 years, characterised by level thresholds of 115 cm and 134 cm, respectively (Table 19). The incidence of flooding and associated critical issues escalates with the increasing severity of the event. In the scenario with a return period of 30 years (Figure 42), water ingress is observed not only all around the Mandracchio Canal waterfront (Figure 63b) but also due to secondary ingress from the Sala da Mar restaurant promenade. When the water surpasses the maximum elevation of the promenade in this region, it progressively extends towards the historic centre. From an urban planning perspective, it is essential to evaluate the potential risks associated with the most extreme event analysed in this study, specifically the R_P=100 years, which corresponds to a total water level of 158 cm. Figure 41 illustrates that the expansion of the water mass occurs not only through the primary waterfront of the Mandracchio Canal but also via the secondary promenades to the west, namely the Circolo della Vela promenade and the Nazario Sauro car park. Water masses are thus interconnected, influencing the entire road network along the Muggia seafront. Thus, by examining very extreme (R_P=30 years) and rare (R_P=100 years) events, we can derive a comprehensive understanding of urban characteristics in relation to extreme levels. This analysis pertains not only to short-term impacts associated with episodic events influenced by current sea conditions but also to long-term implications related to ongoing climate change. The analysis of return period reduction presented in section 5.3.2 is informative. The urban section adjacent to the waterfront features promenade areas whose elevation fails to ensure resilience against events with high frequency return periods, particularly in proximity to the historic city centre. Consequently, based on the current analysis, it is possible to choose a safety threshold level of 165 cm. A threshold of 165 cm is associated with a meteorological event that statistically has a return period of roughly 250 years (Figure 16). Thus, accounting for a pessimistic sea level rise by 2050 for the city of Muggia, estimated at approximately 21 cm (Table 18), the threshold level would probabilistically decrease to 144 cm. This latter value represents an event with a return period of approximately 30 years, characterised as a scenario with a medium probability of occurrence. This intervention currently secures the waterfront area, particularly the historic centre characterised by low elevations (Figure 46). Future projections indicate that there will be adequate time to implement necessary modifications or additions, if required. The value of 165 cm provides a reliable margin of coverage, surpassing the uncertainty associated with a safety value related to a more uncertain scenario. However, raising the entire waterfront would probably not be the most appropriate choice, both in terms of available urban space and economic cost. In recent years, due to increasingly frequent flooding, it has been decided to install a system of mobile flood barriers that can be erected when high water alerts are issued (https://www.informatrieste.eu/ts/blog/incubo-acqua-alta-scongiurato-test-positivo-paratie-sul-mandracchio-a-muggia/). However, these systems are effective when extreme levels are contained (Figure 64). Raising the entire waterfront may not be the most suitable option, considering the constraints of urban space and associated economic costs. In recent years, the rise in flooding frequency has led to the decision to implement a system of mobile flood barriers that can be deployed during high water alerts (https://www.informatrieste.eu/ts/blog/incubo-acqua-alta-scongiurato-test-positivo-paratie-

Finanziato dall'Unione europea NextGenerationEU
Ministero dell'Università e della Ricerca
Italiadomani PIANO NAZIONALE DI RIPRESA E RESILIENZA
UNIVERSITÀ DEGLI STUDI DI TRIESTE

sul-mandracchio-a-muggia/). However, these systems are effective when storm surge levels are low (Figure 64) and cannot be considered a permanent solution.

Figure 64. Example of a movable gate barrier applied to the Mandracchio Canal waterfront (Figure 34) (from https://www.rainews.it/tgr/fvg/articoli/2025/01/allerta-meteo-acqua-alta-nel-mandracchio-a-muggia-posizionate-le-barriere-mobili-9f41a40f-4d3b-49c4-8962-29ac1471c016.html).

Thus, a potential solution may entail the implementation of a movable gate or flap gate, designed similarly to the MoSE in Venice (Munaretto et al, 2012). Consequently, in light of the aforementioned waterfront issues, the most viable hypothesis pertains to the implementation of a movable floodgate barrier within the Mandracchio Canal. The Mandracchio Canal has a width of approximately 67 m, measured between the Circolo della Vela promenade and the C. Colombo pier promenade (Figure 65). Considering the potential ingress of a 100-year event along the Nazario Sauro park promenade, it is advisable to explore the design possibilities at the mouth of the outermost piers of the small port of Muggia, which features an opening of approximately 55 m (Figure 65). Constructing a singular mobile barrier in this location would offer protection against rare events, particularly considering the ongoing climate change. A recent study by Takagi et al. (2023) in Japan presents a comparable example, proposing the construction of such barriers to mitigate the impacts of storm surges and tsunamis. Also in this context, the suggestion is conceptually similar to that already widely used in Northern Europe, especially in the Netherlands with the Maeslant Barrier in Rotterdam (Bol, 2005), designed for protection against very extreme flood events (Jorissen et al., 2016).

Figure 65. The Mandracchio Canal waterfront. (a) View of the Mandracchio C. marine opening (photo from Google Earth, 2025) (b) details of the different area of urban intervent to apply a movable barrier.

6.3 Lignano adaptation plans

In the case of Lignano, the assessment of extreme scenarios was conducted using the levels estimated for Grado using Gumbel distribution as a reference, given the similar lagoon configuration and the lack of a sufficiently long local historical series. The derived thresholds indicate that the criticality is mainly associated with events with a medium-low or even rare probability of occurrence, such as the event of 12 November 2019 (150 cm water level). On the other hand, as regards more frequent return times, the current conditions are good. In this sense, Lignano can be defined as a conservative territory with respect to current extreme events. Areas most at risk are located along the perimeter bordering the city and the lagoon, in a protected western area that is quite distant from the mouth of Lignano and sheltered from any local Bora winds, which blow in an E-NE direction. Consequently, the ingress of water occurs through specific critical points such as the passage inside the car park of the C. Canottieri promenade, which has already been upgraded and raised to 159 cm. However, from a long-term perspective, the evolution of the risk is mainly attributable to

the reduction in return times induced by the rise in average sea level, suggesting the need for progressive monitoring of protection levels rather than immediate intervention. The evaluation of extreme scenarios for Lignano utilised the levels estimated for Grado as a reference, employing the Gumbel distribution of extreme events due to the comparable lagoon configuration and the absence of an adequately extensive local historical series. The established thresholds suggest that criticality is primarily linked to events with medium-low or rare probabilities of occurrence, exemplified by the event on 12 November 2019 (150 cm level). The territory of Lignano is currently safe from marine flooding caused by high-frequency storm surges. Thus, it can be characterised as a conservative territory in relation to contemporary extreme events. The highest risk areas are situated along the perimeter adjacent to the city and the lagoon, within a safeguarded western region that is relatively far from the Lignano mouth and shielded from local Bora winds, which predominantly blow from the E-NE direction. As a result, water ingress occurs at specific critical points, including the entrance to the car park of the C. Canottieri promenade, which has been upgraded and elevated to 159 cm. From a long-term perspective, the evolution of risk is primarily due to the decreased return times resulting from rising mean sea levels. This indicates a necessity for ongoing monitoring of protection levels rather than immediate intervention.

6.4 Trieste adaptation plans

The evaluation of the statistical dependence between astronomical tide and non-tidal residual (NTR) in conjunction with the direct analysis of extreme sea levels using EVT approaches (GEV and GPD-POT) for the city of Trieste reveals a regime where extreme levels are comparatively moderate and heavily influenced by the urban morphology. In this case, rather than a significant rise in absolute maximum sea levels, future flood risk seems to be primarily linked to an increase in the frequency of exceeding local critical thresholds and the possible amplification owing to combined tide-NTR events. Furthermore, a large percentage of the flooded areas cannot be solely attributable to maritime forcing, as demonstrated by the hydrodynamic calibration of the event on November 12, 2019. Rather, heavy precipitation and the ensuing hydraulic overload of the urban drainage system are mostly linked to flooding patterns, creating a noticeable "bathtub" effect in low-lying regions near the Rive shoreline. Under current circumstances, this process is probably going to be more important than direct marine overtopping. However, the impact of mean sea level rise needs to be taken into account as the changing baseline that severe events arise from. When pessimistic sea-level rise forecasts for 2100 are paired with episodic occurrences with high, medium, and moderate probabilities of occurrence, the resulting impacts become much more severe, as shown by the static modeling findings given in Figure 60. The amount of flooded areas expands significantly under these future conditions, but it is still limited by the city of Trieste's steep topographic gradient. These results imply that focused evaluations of waterfront defenses and urban embankments in the most vulnerable areas should be prioritized from the standpoint of long-term adaptation. In particular, it might be essential to assess a localized raising of the main roadway between the waterfront and Piazza Unità d'Italia, in addition to the possible reconfiguration and elevation of specific sections of the Ponterosso promenade. However, in order to confirm the hydraulic efficiency of the urban drainage system and its ability to handle complex marine-pluvial flooding scenarios, such structural changes should be accompanied in the short to medium term by a comprehensive evaluation of the system.

7 Final remarks

The assessment of coastal flooding hazard in urban environments requires an integrated methodological framework capable of capturing both the statistical behaviour of extreme sea levels and the spatial–temporal dynamics of inundation processes. In this study, a combined approach based on extreme-value statistics and high-resolution hydrodynamic modelling was adopted to support a robust and physically consistent evaluation of flooding risk. To update the statistical characterisation of extreme water levels, measure the return times associated with them, and evaluate current trends in frequency and amplitude, univariate extreme-value analyses (GEV and GPD-POT) were initially used. These techniques offer a crucial starting point for comprehending the evolution of severe sea levels over time and for determining crucial thresholds related to urban floods. In parallel, the dependency between astronomical tide, storm surge, and low-frequency sea-level variability was explicitly taken into account using a multivariate statistical framework that followed the methodology suggested by Ferrarin et al., (2022). In order to accurately depict compound events, which frequently regulate the occurrence of exceptional total water levels in the northern Adriatic, this step proved essential. The probability and intensity of extreme conditions are defined by statistical calculations, but they do not explain how floods spreads across intricate urban networks. Because of this, site-specific downscaling assessments and two-dimensional hydrodynamic modelling were used when necessary. While dynamic models (MIKE21 HD and, for Lignano, HEC-RAS outputs provided by the Regional Civil Protection) were used to resolve the temporal evolution of water ingress, flow pathways, and inundation depths at the urban scale, static "bathtub" approaches were utilized to quickly identify potential inundation areas and critical elevations. Thus, a major strength of this study is the integration of statistical and dynamic modeling, which enables the translation of extreme water levels into realistic flood scenarios pertinent to spatial planning and adaptation techniques.

Grado

Among the case studies that were examined, Grado turns out to be the most vulnerable location. The frequency of threshold exceedances has clearly increased over the past ten years, with relatively minor extreme events already causing extensive flooding, according to the data update on extreme sea levels. The western lagoon side, where low-elevation promenades and embankments serve as preferred channels for water intrusion into the historic centre, is where the most essential regions are concentrated, according to downscaling calculations. Higher return periods cause floodwaters to spread widely inland, although even occurrences with modest return periods (R_P=2 years) have major metropolitan repercussions. Projections of sea level rise show a significant decrease in effective return periods, suggesting that situations that are currently thought to be uncommon could become frequent in the coming decades. Furthermore, its location within the Grado and Marano Lagoon, as well as its greater exposure to sirocco sea winds, makes it even more vulnerable to extremes.

Muggia

Seawater intrusion via the Mandracchio Canal waterfront, which serves as the main entry point into the old centre of Muggia, is the main factor controlling floods. The downscaling analysis identifies a series of crucial micro-sectors with extremely low elevations, where overtopping is caused by even regular occurrences (R_P = 2-10 years). Floodwaters quickly

Finanziato dall'Unione europea NextGenerationEU
Ministero dell'Università e della Ricerca
Italiadomani PIANO NAZIONALE DI RIPRESA E RESILIENZA
UNIVERSITÀ DEGLI STUDI DI TRIESTE

spread inward along little streets once the Mandracchio waterfront is overtopped, according to dynamic modelling, creating water depths that have the potential to seriously alter the medieval urban fabric. Even under optimistic climatic scenarios, long-term predictions demonstrate that even little rises in mean sea level significantly intensify the effects of flooding, resulting in a significant reduction in return periods and exposing significant areas of the town.

Lignano
Given its higher urban elevations, Lignano responds to excessive sea levels more conservatively than Grado and Muggia. However, the downscaling research pinpoints some crucial areas along the lagoon-side promenade that serve as main means of entry during intense events, especially close to the Circolo dei Canottieri and the private marina. Overtopping at these low-elevation regions caused flooding, as confirmed by the reconstruction of the incident on November 12, 2019. In order to improve protection against occurrences with medium return durations, post-event mitigating measures have raised the primary breach's elevation locally. The performance of shoreline defences under high-magnitude extremes should be the primary focus of long-term planning, since forecasts under future sea-level rise scenarios suggest that threshold water levels reached during uncommon events (R_P = 50-100 years) may become substantially more and more frequent.

Trieste
Due to its protected location within the Gulf of Trieste, the existence of elevated waterfront structures, and the steep topography gradient landward of the shore, Trieste is the least vulnerable setting among the sites examined. Direct marine flooding is typically restricted to specific areas, mostly along the Ponterosso promenade, according to statistical and downscaling evaluations. Despite high water levels, dynamic modelling of the event on November 12, 2019, shows that inland flooding was caused by a combination of limited overtopping, heavy precipitation, and restricted urban drainage conditions rather than directly propagating from the marine waterfront toward Piazza Unità. However, static forecasts that combine pessimistic sea-level rise scenarios for 2100 with frequent extreme events show that even Trieste might encounter critical conditions under very low-magnitude events, highlighting the system's long-term vulnerability to mean sea-level increases.

Overall, the results demonstrate that coastal flooding hazard in the northern Adriatic is strongly site-dependent and controlled by the interaction between extreme sea-level statistics, local topography, and urban configuration. The integrated use of statistical extreme-value analysis, multivariate dependence modelling and dynamic flood simulations provides a comprehensive framework to interpret both present-day and future flooding scenarios. This approach supports the identification of critical ingress pathways, the evaluation of defence performance, and the prioritization of adaptation measures tailored to the specific characteristics of each coastal town.

8 References

Agonafir, C., Lakhankar, T., Khanbilvardi, R., Krakauer, N., Radell, D., & Devineni, N. (2023). A review of recent advances in urban flood research. *Water Security, 19*, 100141. https://doi.org/10.1016/j.wasec.2023.100141

Agriconsulting, 2008. S.A.R.A. Sistema aree regionali ambientali Costituzione Sistema regionale delle aree naturali – Piano di Gestione del SIC/ZPS IT3320037 Laguna di Marano e Grado; https://www.regione.fvg.it/rafvg/cms/RAFVG/ambiente-territorio/tutela-ambiente-gestione-risorse-naturali/FOGLIA203/FOGLIA120/

Almeida, L. P., Masselink, G., McCall, R., & Russell, P. (2017). Storm overwash of a gravel barrier: Field measurements and XBeach-G modelling. *Coastal Engineering, 120*, 22–35. https://doi.org/10.1016/j.coastaleng.2016.11.009

Alsina, J. M., van der Zanden, J., Cáceres, I., & Ribberink, J. S. (2018). The influence of wave groups and wave–swash interactions on sediment transport and bed evolution in the swash zone. *Coastal Engineering, 140*, 23–42. https://doi.org/10.1016/j.coastaleng.2018.06.005

Anderson, T. W., & Darling, D. A. (1952). Asymptotic theory of certain goodness-of-fit criteria based on stochastic processes. *Annals of Mathematical Statistics, 23*, 193–212.

Andreadis, K. M., Wing, O. E., Colven, E., Gleason, C. J., Bates, P. D., & Brown, C. M. (2022). Urbanizing the floodplain: global changes of imperviousness in flood-prone areas. *Environmental Research Letters*, *17*(10), 104024.

Anghel, C. G. (2024). Revisiting the use of the Gumbel distribution: A comprehensive statistical analysis regarding modeling extremes and rare events. *Mathematics, 12*(16), 2466. https://doi.org/10.3390/math12162466

Antonellini, M., Mollema, P., Giambastiani, B., Bishop, K., Caruso, L., Minchio, A., ... & Gabbianelli, G. (2008). Salt water intrusion in the coastal aquifer of the southern Po Plain, Italy. *Hydrogeology journal*, *16*(8), 1541-1556. https://doi.org/10.1007/s10040-008-0319-9.

Antonioli F, Anzidei M, Amorosi A, Lo Presti V, Mastronuzzi G, Deiana G, De Falco G, Fontana A, Fontolan G, Lisco S, Marsico A, Moretti M, Orrù PE, Sannino GM, Serpelloni E, Vecchio A (2017) Sea-level rise and potential drowning of the Italian coastal plains: Flooding risk scenarios for 2100. Quatern Sci Rev 158:29–43. https://doi.org/10.1016/j.quascirev.2016.12.021

Anzidei, M., Lambeck, K., Antonioli, F., Furlani, S., Mastronuzzi, G., Serpelloni, E., & Vannucci, G. (2014). Coastal structure, sea-level changes and vertical motion of the land in the Mediterranean. *Geological Society, London, Special Publications, 388*, 453–479. https://doi.org/10.1144/SP388.20

Anzidei, M., Tolomei, C., Trippanera, D., Alberti, T., Bosman, A., Brunori, C. A., Serpelloni, E., Vecchio, A., Falciano, A., & Deli, G. (2025). Multi-Temporal Relative Sea Level Rise Scenarios up to 2150 for the Venice Lagoon (Italy). Remote Sensing, 17(5), 820. https://doi.org/10.3390/rs17050820

Areggi, G., Pezzo, G., Merryman Boncori, J. P., Anderlini, L., Rossi, G., Serpelloni, E., Zuliani, D., & Bonini, L. (2023). Present-Day Surface Deformation in North-East Italy Using InSAR and GNSS Data. *Remote Sensing*, *15*(6), 1704. https://doi.org/10.3390/rs15061704

Arguez, A., & Vose, R. S. (2011). The Definition of the Standard WMO Climate Normal: The Key to Deriving Alternative Climate Normals. *Bulletin of the American Meteorological Society*, *92*(6), 699–704. http://www.jstor.org/stable/26218540

Arns, A., Wahl, T., Wolff, C., Vafeidis, A. T., Haigh, I. D., Woodworth, P., Niehüser, S., & Jensen, J. (2020). *Non-linear interaction modulates global extreme sea levels, coastal flood exposure, and impacts*. Nature Communications, 11, 1918. https://doi.org/10.1038/s41467-020-15752-5

Autorità Di Bacino Distrettuale Delle Alpi Orientali. Relazione e Norme di Attuazione. Allegati. Piano di stralcio per l'assetto idrogeologico dei bacini di interesse regionale (PAIR) (bacini idrografici dei tributari della laguna di Marano - Grado, ivi compresa la laguna medesima, del torrente Slizza e del levante). Relazione tecnica. Settembre 2016. https://distrettoalpiorientali.it/wp-content/uploads/2023/02/PAIR_Allegato_01_relazione_FVG.pdf (accessed on 14 Dicember 2025).

Autorità Di Bacino Distrettuale Delle Alpi Orientali. Aggiornamento e Revisione Del Piano Di Gestione Del Rischio Di Alluvioni (PGRA). Allegato I. Elementi Tecnici Di Riferimento Nell'impostazione Del Piano. Distretto Delle Alpi Orientali. Aggiornamento 2021. Available online: https://sigma.distrettoalpiorientali.it/sigma/documentDownload/downloadDocumentById?documentId=360 (accessed on 14 Dicember 2025).

Bakkensen, L. A. (2017). *Mediterranean hurricanes and associated damage estimates*. *Journal of Extreme Events, 4*(2), 1750008. https://doi.org/10.1142/S2345737617500087.

Balaian, S. K., Sanders, B. F., & Abdolhosseini Qomi, M. J. (2024). How urban form impacts flooding. *Nature Communications, 15*, 6911. https://doi.org/10.1038/s41467-024-50347-4

Baldan, D., Coraci, E., Crosato, F., Ferla, M., Bonometto, A., & Morucci, S. (2022). Importance of non-stationary analysis for assessing extreme sea levels under sea level rise. *Natural Hazards and Earth System Sciences*, *22*(11), 3663-3677.https://doi.org/10.5194/nhess-22-3663-2022.

Baldin, G., & Crosato, F. (2017). L'innalzamento del livello medio del mare a Venezia: eustatismo e subsidenza. *Quaderni Ricerca Marina*, *10*(2017), 1-20.

Baldoni A, Melito L, Marini F, Galassi G, Giacomin P, Filomena G, Barbizzi N, Lorenzoni C and Brocchini M (2024) Modeling coastal inundation for adaptation to climate change at local scale: the case of Marche Region (central Italy). Front. Clim. 6:1334625. doi: 10.3389/fclim.2024.1334625

Balkema, A. A. and de Haan, L.: Residual life time at great age, Ann. Probab., 2, 792–804, https://doi.org/10.1214/aop/1176996548, 1974.

Barbariol, F., Bidlot, J. R., Cavaleri, L., Sclavo, M., Thomson, J., & Benetazzo, A. (2019). Maximum wave heights from global model reanalysis. *Progress in oceanography*, *175*, 139-160.https://doi.org/10.1016/j.pocean.2019.03.009.

Barnard, P. L., Dugan, J. E., Page, H. M., Wood, N. J., Hart, J. A. F., Cayan, D. R., Erikson, L.H.; Hubbard, D.M.; Myers, M.R.; Melack, J.M. Iacobellis, S. F. (2021). Multiple climate change-driven tipping points for coastal systems. *Scientific Reports*, *11*(1), 15560. doi: 10.1038/s41598-021-94942-7

Battistin D., Canestrelli P., (2006). La serie storica delle maree a Venezia. Istituzione Centro Previsioni e Segnalazioni Maree Venezia, p.207.

Battjes, J. A., & Janssen, J. P. F. M. (1978). Energy loss and set-up due to breaking of random waves. In *Coastal Engineering*.

Beirlant, J., Goegebeur, Y., Segers, J. J. J., and Teugels, J.: Statistics of Extremes: Theory and Applications, John Wiley & Sons, Chichester, UK, ISBN 0471976474, 2004.

Belušić, D., M. Pasarić, and M. Orlić (2004), Quasi-periodic Bora gusts related to the structure of the troposphere, Q. J. R. Meteorol. Soc., 130, 1103–1121, doi:10.1256/qj.03.53.

Benito, I., Aerts, J. C. J. H., Eilander, D., et al. (2024). Stochastic coastal flood risk modelling for the east coast of Africa. *npj Natural Hazards, 1*, 10. https://doi.org/10.1038/s44304-024-00010-1

Bezzi, A., Pillon, S., Martinucci, D., & Fontolan, G. (2018). Inventory and conservation assessment for the management of coastal dunes, Veneto coasts, Italy. *Journal of Coastal Conservation*, *22*(3), 503-518. https://doi.org/10.1007/s11852-017-0580-y.

Bezzi, A., Casagrande, G., Fracaros, S., Martinucci, D., Pillon, S., Sponza, S., Bratus, A., Fattor, F., Fontolan, G. (2021). Geomorphological changes of a migrating sandbank: Multidecadal analysis as a tool for managing conflicts in coastal use. *Water*, *13*(23), 3416. https://doi.org/10.3390/w13233416.

Binini Partners. Porta Vinciana a Cesenatico. Sbarramento Mobile per La Difesa Dalle Esondazioni Meteomarine. Available online: https://www.bininipartners.it/progetti/porta vinciana-a-cesenatico/ (accessed on 22 Dicember 2025).

Bisci, C., Cantalamessa, G., De Marco, R., Spagnoli, F., & Tramontana, M. (2021). Caratteri oceanografici dell'Adriatico centro-settentrionale e della costa Marchigiana. *Stud. Costieri*, *30*, 7-12.

Bisht, D. S., Chatterjee, C., Kalakoti, S., Upadhyay, P., Sahoo, M., & Panda, A. (2016). Modeling urban floods and drainage using SWMM and MIKE URBAN: a case study. *Natural hazards*, *84*(2), 749-776. https://doi.org/10.1007/s11069-016-2455-1.

Bol, R. Operation of the "Maeslant Barrier": (Storm Surge Barrier in the Rotterdam New Waterway). In *Flooding and Environmental Challenges for Venice and its Lagoon: State of Knowledge*; Fletcher, C., Spencer, T., Eds.; Cambridge University Press: Cambridge, UK, 2005; pp. 311–315.

Bonaldo, D., Antonioli, F., Archetti, R., Bezzi, A., Correggiari, A., Davolio, S., De Falco, G., Fantini, M., Fontolan, G., Furlani, S., Gaeta, M. g., Leoni, G., Lo Presti, V., Mastronuzzi, G., Pillon, S., Ricchi, A., Stocchi, P., Samaras, A. G., Scicchitano, G., & Carniel, S. (2019). Integrating multidisciplinary instruments for assessing coastal vulnerability to erosion and sea level rise: Lessons and challenges from the Adriatic Sea, Italy. *Journal of Coastal Conservation*, *23*(1), 19-37. https://doi.org/10.1007/s11852018-0633-x.

Brown, J. D., Spencer, T., & Moeller, I. (2007). Modeling storm surge flooding of an urban area with particular reference to modeling uncertainties: A case study of Canvey Island, United Kingdom. *Water Resources Research*, *43*(6). https://doi.org/10.1029/2005WR004597

Bult, S. V., Le Bars, D., Haigh, I. D., &Gerkema, T. (2024). The effect of the 18.6-year lunar nodal cycle on steric sea levelchanges. Geophysical Research Letters,51, e2023GL106563. https://doi.org/10.1029/2023GL106563

Bujak, D., Ilic, S., Miličević, H., & Carević, D. (2023). Wave runup prediction and alongshore variability on a pocket gravel beach under fetch-limited wave conditions. *Journal of marine science and engineering*, *11*(3), 614. https://doi.org/10.3390/jmse11030614

Busetti M., 2011. Nuove evidenze geologiche nel Golfo di Trieste e lungo la sua costa: considerazioni in relazione alle proposte di insediamento di impianti strategici. Tigor: rivista di scienze della comunicazione - A. III (2011) n.2 (luglio-dicembre).

Busetti, A., Leone, C., Corradetti, A., Fracaros, S., Spadotto, S., Rai, P., Zini, L., & Calligaris, C. (2024). Coastal Storm-Induced Sinkholes: Insights from Unmanned Aerial Vehicle Monitoring. Remote Sensing, 16(19), 3681. https://doi.org/10.3390/rs16193681.

Canestrelli P., Mandich M., Pirazzoli P.A., Tomasin A. Venti, depression e sesse: perturbazioni delle maree a Venezia (1950-2000). Centro Previsioni e Segnalazioni Maree, 2001.https://www.comune.venezia.it/sites/default/files/publicCPSM2/pubblicazioni/Venti_depressioni_e_sesse.pdf

Carbognin L., Teatini P., Tosi L., Strozzi T., Tomasin A., (2011) *Present Relative Sea Level Rise in the Northern Adriatic Coastal Area.* In: Coastal and marine spatial planning. Marine Research at CNR, DTA/06 . CNR - Dipartimento Scienze del Sistema Terra e Tecnologie , Roma, pp. 1147-1162. http://eprints.bice.rm.cnr.it/id/eprint/10023

Carton, J. A., Giese, B. S., & Grodsky, S. A. (2005). Sea level rise and the warming of the oceans in the Simple Ocean Data Assimilation (SODA) ocean reanalysis. *Journal of Geophysical Research: Oceans*, *110*(C9). https://doi.org/10.1029/2004JC002817

Caruso, M. F., & Marani, M. (2022). Extreme-coastal-water-level estimation and projection: a comparison of statistical methods. *Natural Hazards and Earth System Sciences*, *22*(3), 1109-1128. https://doi.org/10.5194/nhess-22-1109-2022.

Castillo E, Sarabia JM. Extreme Value Analysis of Wave Heights. J Res Natl Inst Stand Technol. 1994 Jul-Aug;99(4):445-454. doi: 10.6028/jres.099.042.

Castillo, E., Hadi, A.S., Balakrishnan, N. and Sarabia, J.M. (2005) Extreme Value and Related Models with Applications in Engineering and Science. Wiley, New York. ISBN 978-0-471-67172-5.

Cerovečki, I., Orlić, M., & Hendershott, M. C. (1997). Adriatic seiche decay and energy loss to the Mediterranean. *Deep Sea Research Part I: Oceanographic Research Papers*, *44*(12), 2007-2029. http://dx.doi.org/10.1016/S0967-0637(97)00056-3.

Chakravarti, Laha, and Roy, (1967). Handbook of Methods of Applied Statistics, Volume I, John Wiley and Sons, pp. 392-394.

Chen, K. F., & Leandro, J. (2019). A conceptual time-varying flood resilience index. *Water, 11*, 830. https://doi.org/10.3390/w11040830

Chiggiato, J., Schroeder, K., Mourre, B., Miramontes, E., Lionello, P., Marcos, M., et al., (2023). "Chapter 1: Introduction, " in Oceanography of the Mediterranean Sea, eds K. Schoreader and J. Chiggiato (Amsterdam: Elsevier), 1-11. doi: 10.1016/B978-0-12-8236925.00002-9

Choulakian, V. and Stephens, M.A. (2001) Goodness-of-Fit for the Generalized Pareto Distribution. Technometrics, 43, 478-484. https://doi.org/10.1198/00401700152672573

Dal Cin, F., Fleischmann, M., Romice, O., & Costa, J. P. (2020). Climate Adaptation Plans in the Context of Coastal Settlements: The Case of Portugal. *Sustainability*, *12*(20), 8559. https://doi.org/10.3390/su12208559

Città Di Venezia. Grafici e Statistiche. Available online: https://www.comune.venezia.it/it/content/grafici-e-statistiche (accessed on 23 Dicember 2025).

Città Di Venezia. Riferimenti Altimetrici. Available online: https://www.comune.venezia.it/it/content/riferimenti-altimetrici (accessed on 23 Dicember 2025).

Codiga, D.L., (2011). Unified Tidal Analysis and Prediction Using the UTide Matlab Functions. Technical Report 2011-01. Graduate School of Oceanography, University of Rhode Island, Narragansett, RI. 59pp. 2011Codiga-UTide-Report.pdf

Coles, S. *An Introduction to Statistical Modeling of Extreme Values*; Springer-Verlag: London, UK, 2001; p. 209.

Coles S, Tawn J. Bayesian modelling of extreme surges on the UK east coast. Philos Trans A Math Phys Eng Sci. 2005 Jun 15;363(1831):1387-406. doi: 10.1098/rsta.2005.1574. PMID: 16191656.

Cooley, S. R., Schoeman, D. S., Bopp, L., Boyd, P., Donner, S., Ito, S.-I., Kiessling, W., Martinetto, P., Ojea, E., Racault, M.-F., Rost, B., Skern-Mauritzen, M., & Yemane Ghebrehiwet, D. (2023). Oceans and Coastal Ecosystems and Their Services. In *Climate Change 2022: Impacts, Adaptation and Vulnerability: Contribution of Working Group II to the Sixth Assessment Report of the Intergovernmental Panel on Climate Change* Cambridge University Press. https://doi.org/10.1017/9781009325844.005, https://doi.org/10.1017/9781009325844

Comune Di Grado. La Laguna Di Grado. Available online. https://comune.grado.go.it/it/vivere-il-comune-22477/luoghi 22478/la-laguna-di-grado-69770 (accessed on 2 Dicember 2025).

Comune di Muggia. Variante urbanistica generale al P.R.G.C. VAS – Rapporto Ambientale. Elaborato adeguato alla proposta tecnica di controdeduzione alle osservazioni e alle Riserve regionali prevenute al Piano adottato. Giugno 2015. https://www.comune.muggia.ts.it/media/files/md/032003/Rapporto_Ambientale.pdf

Comune di Trieste. Documenti urbanistica. RG-Relazione Geologica. Regione Autonoma Friuli-Venezia Giulia. Comune di Trieste. Area Città e Territorio. Servizio Pianificazione Urbana. Piano Regolatore Generale Comunale. Variante Generale. http://documenti.comune.trieste.it/prg/nuovo-prg/approvazione/All.1_STUDIO_GEOLOGICO/GR_Relazione/GR_NORME_GEOLOGICO-TECNICHE.pdf

Consorzio di Bonifica Bassa Friulana, 2008. Progetto Preliminare. Trasformazione da scorrimento a pioggia del bacino Vittoria nei comuni di Grado e Fiumicello, 1 Lotto. - Relazione Agronomica: 27 pp. https://www.comunegrado.it/attachments/ article/1163/Allegato%2004%20-%20442p_01.c_Relazione_agronomica.pdf

Conte, D., & Lionello, P. (2013). Characteristics of large positive and negative surges in the Mediterranean Sea and their attenuation in future climate scenarios. *Global and Planetary Change*, *111*, 159-173.https://doi.org/10.1016/j.gloplacha.2013.09.006.

Cosolo M., Sponza S., Fattori U. 2015. La laguna di Marano e Grado: un mosaico di biodiversità – un patrimonio da preservare. Regione Autonoma Friuli Venezia Giulia, Udine, 52 pp.

Cramer, W.; Guiot, J.; Fader, M.; Garrabou, J.; Gattuso, J.-P.; Iglesias, A.; Lange, M.A.; Lionello, P.; Llasat, M.C.; Paz, S.; Peñuelas, J., Snoussi, M., Toreti, A., Tisimplis, M. N. & . Xoplaki, E. (2018). Climate change and interconnected risks to sustainable development in the Mediterranean. *Nature climate change*, *8*(11), 972-980. https://doi.org/10.1038/s41558-018-0299-2.

Crisciani, F., Ferraro, S., Raicich, F., 1994. Interannual variability of the sea level at Trieste. Il Nuovo Cimento 17 (4), 377–384. https://doi.org/10.1007/BF02506725

Cushman-Roisin, B., V. Malacic, And M. Gacic (2001), Tides, seiches, and low-frequency oscillations, in The Physical Oceanography of the Adriatic Sea: Past, Present and Future, pp. 217-240, Souinger, New York. ISBN: 978-90-481-5921-5. DOI: 10.1007/978-94-015-9819-4

Da Lio, C., & Tosi, L. (2018). Land subsidence in the Friuli Venezia Giulia coastal plain, Italy: 1992–2010 results from SAR-based interferometry. *Science of the Total Environment*, *633*, 752-764. https://doi.org/10.1016/j.scitotenv.2018.03.244.

Davison, A. C., & Smith, R. L. (1990). Models for exceedances over high thresholds. *Journal of the Royal Statistical Society: Series B (Methodological), 52*(3), 393–442. https://doi.org/10.1111/j.2517-6161.1990.tb01796.x

De Grassi, V. (1952). Le rovine subacquee di San Gottardo a Grado. *Aquila Nostra, 23*, 27–36.

de Haan, L. and Ferreira, A. (2006) Extreme Value Theory: An Introduction. Springer Series in Operations Research and Financial Engineering. Springer, Berlin. https://doi.org/10.1007/0-387-34471-3

De Leo, F., Solari, S., & Besio, G. (2020). Extreme wave analysis based on atmospheric pattern classification: an application along the Italian coast. *Natural Hazards and Earth System Sciences*, *20*(5), 1233-1246. https://doi.org/10.5194/nhess-20-1233-2020.

Demo. Demografia in Cifre. Bilancio Demografico Mensile e Popolazione Residente per Sesso, Anno 2024. Available online: https://demo.istat.it/app/?l=it&a=2024&i=D7B (accessed on 26 Dicember 2025).

De Moel, H., Asselman, N. E. M., & Aerts, J. C. J. H. (2012). Uncertainty and sensitivity analysis of coastal flood damage estimates in the west of the Netherlands. *Natural Hazards and Earth system sciences*, *12*(4), 1045-1058. https://doi.org/10.5194/nhess-12-1045-2012.

De Zolt, S., Lionello, P., Nuhu, A., & Tomasin, A. (2006). The disastrous storm of 4 November 1966 on Italy. *Natural Hazards and Earth System Sciences, 6*(5), 861–879. https://doi.org/10.5194/nhess-6-861-2006

Denamiel, C., Pranić, P., Ivanković, D., Tojčić, I., & Vilibić, I. (2021). Performance of the Adriatic Sea and Coast (AdriSC) climate component–a COAWST V3. 3-based coupled atmosphere-ocean modelling suite: atmospheric part. *Geoscientific Model Development Discussions*, *2021*, 1-46. https://doi.org/10.5194/gmd-14-3995-2021.

DHI. (2023a). *MIKE 21 Spectral Wave Module: Scientific documentation*. Hørsholm, Denmark: DHI A/S. https://manuals.mikepoweredbydhi.help/latest/Coast_and_Sea/M21SW_Scientific_Doc.pdf

DHI. (2023b). *MIKE 21 Flow Model FM: Scientific documentation*. Hørsholm, Denmark: DHI A/S. https://manuals.mikepoweredbydhi.help/latest/Coast_and_Sea/MIKE_21_Flow_FM_Scientific_Doc.pdf

Didier, D., Baudry, J., Bernatchez, P., Dumont, D., Sadegh, M., Bismuth, E., Bandet, M., Dugas, S. & Sévigny, C. (2019). Multihazard simulation for coastal flood mapping: Bathtub versus numerical modelling in an open estuary, Eastern Canada. Journal of Flood Risk Management, 12(S1), e12505. https://doi.org/10.1111/jfr3.12505

Dodet, G., Melet, A., Ardhuin, F., Bertin, X., Idier, D., & Almar, R. (2019). The contribution of wind-generated waves to coastal sea-level changes. *Surveys in Geophysics*, *40*(6), 1563-1601. https://doi.org/10.1007/s10712-019-09557-5.

Dorigo L., 1965. La Laguna di Grado e le Sue Foci. Ricerche e Rilievi Idrografici. Magistrato Alle Acque-Ufficio Idrografico 1–231.

European Union. EUR-Lex. Access to Europena Union Law. Directive 2007/60/EC of the European Parliament and of the Council of 23 October 2007 on the assessment and management of flood risks (Text with EEA relevance) https://eur-lex.europa.eu/legal-content/IT/TXT/PDF/?uri=CELEX:32007L0060

EurOtop. (2007). *Manual on wave overtopping of sea defences and related structures: Assessment manual*. https://www.overtopping-manual.com/assets/downloads/EAK-K073_EurOtop_2007.pdf

EurOtop, 2018. Manual on wave overtopping of sea defences and related structures. An overtopping manual largely based on European research, but for worldwide application. Van der Meer, J.W., Allsop, N.W.H., Bruce, T., De Rouck, J., Kortenhaus, A., Pullen, T., Schüttrumpf, H., Troch, P. and Zanuttigh, B., www.overtopping-manual.com.

Ferla M., et al., Litorali e Lagune del Nord Est 162, 2012. Presentazione Convegno “Aree costiere del Nord Adriatico e gestione delle alluvioni: attuazione della Direttiva 2007/60/CE sulla gestione dal rischio alluvione”, Mestre 5 ottobre 2012. Available online (B7 in elenco): https://www.venezia.isprambiente.it/ricerche#B.

Ferrarin, C., Tomasin, A., Bajo, M., Petrizzo, A., & Umgiesser, G. (2015). Tidal changes in a heavily modified coastal wetland. *Continental Shelf Research*, *101*, 22-33. https://doi.org/10.1016/j.csr.2015.04.002.

Ferrarin, C.; Valentini, A.; Vodopivec, M.; Klaric, D.; Massaro, G.; Bajo, M.; De Pascalis, F.; Fadini, A.; Ghezzo, M.; Menegon, S.; Bressan, L.; Ungendoli, S.; Fettich, A.; Jerman, J.; Ličer, M.; Fustar, L.; Papa, A. & Carraro, E. (2020). Integrated sea storm management strategy: the 29 October 2018 event in the Adriatic Sea. *Natural Hazards and Earth System Sciences*, *20*(1), 73-93. https://doi.org/10.5194/nhess-20-73-2020.

Ferrarin, C.; Bajo, M.; Benetazzo, A.; Cavaleri, L.; Chiggiato, J.; Davison, S.; Davolio, S.; Lionello, P.; Orlić, M.; Umgiesser, G. (2021). Local and large-scale controls of the exceptional Venice floods of November 2019. *Progress in oceanography*, *197*, 102628. https://doi.org/10.1016/j.pocean.2021.102628.

Ferrarin, C., Lionello, P., Orlić, M., Raicich, F., & Salvadori, G. (2022). Venice as a paradigm of coastal flooding under multiple compound drivers. *Scientific reports*, *12*(1), 5754. https://doi.org/10.1038/s41598-022-09652-5

Ferraro S. e Crisciani F. (2001): “La mareografia a Trieste: aspetti scientifici e storici”, CNR - Ist. Talassografico di Trieste, 104 pp.

Fiedler, J. W., Young, A. P., Ludka, B. C., O’Reilly, W. C., Henderson, C., Merrifield, M. A., & Guza, R. T. (2020). Predicting site-specific storm wave run-up. *Natural Hazards*, *104*(1), 493-517. https://doi.org/10.1007/s11069-020-04178-3

Fisher, R. A., & Tippett, L. H. C. (1928). Limiting forms of the frequency distribution of the largest or smallest member of a sample. *Proceedings of the Cambridge Philosophical Society, 24*, 180–190.

Foglini, F., Bosman A., Corregiari A., Remia A., Madricardo F., Prampolini M., Fontolan G., Biscotti E., Ferrero S., Pizzeghello N. & Trincardi F. (2020). CARTA BATIMORFOLOGICA DELL’ADRIATICO SETTENTRIONALE. https://doi.org/10.5281/zenodo.3754625

Fontolan, G., Pillon, S., Bezzi, A., Villalta, R., Lipizer, M., Triches, A., & D'Aietti, A. (2012). Human impact and the historical transformation of saltmarshes in the Marano and Grado Lagoon, northern Adriatic Sea. *Estuarine, coastal and shelf science*, *113*, 41-56. https://doi.org/10.1016/j.ecss.2012.02.007

Fontolan, G., Bratus, A., Bieker, F., Colombetta, L., Gallitelli, D., Lipizer, M., Sgambati, F., Bezzi, A., Casagrande, G., Fracaros, S., Martinucci, D., Pillon, S., Popesso, C., Sponza S., & et al., (2023). Piano Coste – Accordo attuativo di collaborazione per lo studio e monitoraggio morfo-sedimentologico dello stato dei litorali della regione Friuli Venezia Giulia finalizzato alla gestione integrata della zona costiera in applicazione alla convenzione quadro tra la Regione Autonoma Friuli Venezia Giulia e l’Università degli Studi di Trieste (DGR 264/2014). Regione Autonoma Friuli Venezia Giulia, Direzione Centrale Ambiente ed Energia.

Fontolan, G., Bezzi, A., Casagrande, G., Fracaros, S., Popesso, C., Spadotto, S., Favaro, M., Papa, A., 2023a. Real-time monitoring system and an early warning system implemented. Report D 5.4.3_Part B_ Stream project.

Fox-Kemper, B., H.T. Hewitt, C. Xiao, G. Aðalgeirsdóttir, S.S. Drijfhout, T.L. Edwards, N.R. Golledge, M. Hemer, R.E. Kopp, G. Krinner, A. Mix, D. Notz, S. Nowicki, I.S. Nurhati, L. Ruiz, J.-B. Sallée, A.B.A. Slangen, and Y. Yu, 2021: Ocean, Cryosphere and Sea Level Change. In Climate Change 2021: The Physical Science Basis. Contribution of Working Group I to the Sixth Assessment Report of the Intergovernmental Panel on Climate Change [Masson-Delmotte, V., P. Zhai, A. Pirani, S.L. Connors, C. Péan, S. Berger, N. Caud, Y. Chen, L. Goldfarb, M.I. Gomis, M. Huang, K. Leitzell, E. Lonnoy, J.B.R. Matthews, T.K. Maycock, T. Waterfield, O. Yelekçi, R. Yu, and B. Zhou (eds.)]. Cambridge University Press, Cambridge, United Kingdom and New York, NY, USA, pp. 1211–1362, doi:10.1017/9781009157896.011.

Fournier, S., Willis, J., Killett, E., Qu, Z., & Zlotnicki, V. (2022). *JPL MEaSUREs gridded sea surface height anomalies (Version 2205)*. PO.DAAC. https://doi.org/10.5067/SLREF-CDRV3

Gaddi, D. Approdi Nella Laguna Di Grado. *Antichità Altoadriatiche XLVI. Strutture Portuali e Rotte Marittime Nell’alto Adriatico Di Età Romana*; Zaccaria, C., Ed.; EUT Edizione Università Trieste: Trieste, Roma, 2001.

Galassi, G., & Spada, G. (2014). Sea-level rise in the Mediterranean Sea by 2050: Roles of terrestrial ice melt, steric effects and glacial isostatic adjustment. *Global and Planetary Change*, *123*, 55-66. https://doi.org/10.1016/j.gloplacha.2014.10.007

Gallina, V.; Torresan, S.; Zabeo, A.; Rizzi, J.; Carniel, S.; Sclavo, M.; Pizzol, L.; Marcomini, A.; Critto, A. Assessment of climate change impacts in the North Adriatic coastal area. Part II: Consequences for coastal erosion impacts at the regional scale. *Water*, *11*(6), 1300. https://doi.org/10.3390/w11061300.

Galluccio, G.; Hinkel, J.; Fiorini Beckhauser, E.; Bisaro, A.; Biancardi Aleu, R.; Campostrini, P.; Casas, M.F.; Espin, O.; Vafeidis, A.T. Sea Level Rise in Europe: Adaptation Measures and Decision Making Principles. *State of the Planet Discussions*, *2024*, 1-36. https://doi.org/10.5194/sp-3-slre1-6-2024.

Gao, M., Wang, Z., & Yang, H. (2022). Review of urban flood resilience: insights from scientometric and systematic analysis. *International Journal of Environmental Research and Public Health*, *19*(14), 8837. https://doi.org/10.3390/ijerph19148837.

García, M.J., Pérez Gómez, B., Raicich, F., Rickards, L., Bradshaw, E., Plag, H.-P., Zhang, X., Bye, B.L. and Isaksen E. (2007). *European Sea Level Monitoring: Implementation of ESEAS Quality Control*. In: Dynamic Planet: Monitoring and Understanding a Dynamic Planet with Geodetic and Oceanographic Tools; IAG Symposium, Cairns, Australia, 22- 26 August 2005; Tregoning P., Rizos C. (eds.). International Association of Geodesy Symposia, Volume 130, Springer, Berlin, 67-70.

Giorgi, F. (2006). Climate change hot-spots. *Geophysical research letters*, *33*(8). https://doi.org/10.1029/2006GL025734.

Giorgi, F., & Lionello, P. (2008). Climate change projections for the Mediterranean region. *Global and planetary change*, *63*(2-3), 90-104. https://doi.org/10.1016/j.gloplacha.2007.09.005.

Gnedenko, B. (1943). Sur la distribution limite du terme maximum d'une série aléatoire. *Annals of Mathematics, 44*(3), 423–453.

Goda, Y. (1988). On the methodology of selecting design wave height. *Coastal Engineering*, 899–913.

Godin, G. (1972). *The analysis of tides*. Liverpool University Press. p. 272.

Godin, G., & Trotti, L. (1975). *Trieste – Water levels 1952–1971: A study of the tide, mean level, and seiche activity*. Department of the Environment, Fisheries and Marine Service.

Green, J., Haigh, I. D., Quinn, N., Neal, J., Wahl, T., Wood, M., Eilander, D., de Ruiter, M., Ward, P., & Camus, P. (2025). A comprehensive review of compound flooding literature with a focus on coastal and estuarine regions. *Natural Hazards and Earth System Sciences*, *25*(2), 747-816. https://doi.org/10.5194/nhess-25-747-2025.

Gregory, J.M., Griffies, S.M., Hughes, C.W. Lowe, J.A., Church, J. A., Fukimori, I., Gomez, N., E. Kopp, R., Landerer, F., Le Cozannet, G., Ponte, R. M., Stammer, D., Tamisiea, M. E., & van de Wal. R. S. W. (2019). Concepts and terminology for sea level: Mean, variability and change, both local and global. *Surveys in Geophysics*, *40*(6), 1251-1289. https://doi.org/10.1007/s10712-019-09525-z

Grisogono, B., & BelusŠIĆ, D. (2009). A review of recent advances in understanding the mesoand microscale properties of the severe Bora wind. *Tellus A: Dynamic Meteorology and Oceanography*, *61*(1), 1-16.

Guidance for Flood Risk Analysis and Mapping. Flood Insurance Rate Map (FIRM). Database Techinacal Reference. Preparing Flood Insurance Rate Map Databases. November 2023.https://www.fema.gov/sites/default/files/documents/fema_rm-firm-database-technical-reference-nov-2023.pdf

Gumbel, E. *Statistics of Extremes*; Columbia University Press: New York, NY, USA, 1958; p. 375.

Habel, S., Fletcher, C. H., Anderson, T. R., & Thompson, P. R. (2020). Sea-level rise induced multi-mechanism flooding and contribution to urban infrastructure failure. *Scientific reports*, *10*(1), 3796. https://doi.org/10.1038/s41598-020-60762-4.

Haigh, I. D., Winning, A., Toumi, R., et al. (2010). An influence of solar spectral variations on radiative forcing of climate. *Nature, 467*, 696–699. https://doi.org/10.1038/nature09426

Haigh, I. D., Eliot, M., & Pattiaratchi, C. (2011). Global influences of the 18.61-year nodal cycle and 8.85-year cycle of lunar perigee on high tidal levels. *Journal of Geophysical Research: Oceans, 116*, C06025. 10.1029/2010jc006645

Hamdi, Y., Garnier, E., Giloy, N., Duluc, C. M., & Rebour, V. (2018). Analysis of the risk associated with coastal flooding hazards: a new historical extreme storm surges dataset for Dunkirk, France. *Natural Hazards and Earth System Sciences*, *18*(12), 3383-3402. https://doi.org/10.5194/nhess-18-3383-2018.

Hammond, M. J., Chen, A. S., Djordjević, S., Butler, D., & Mark, O. (2015). Urban flood impact assessment: A state-of-the-art review. *Urban Water Journal*, *12*(1), 14-29. https://doi.org/10.1080/1573062X.2013.857421.

Harley, M.D.; Turner, I.L.; Kinsela, M.A.; Middleton, J.H.; Mumford, P.J.; Splinter, K.D.; Phillips, M.S.; Simmons, J.A.; Hanslow, D.J.; Short, A.D. (2017). Extreme coastal erosion enhanced by anomalous extratropical storm wave direction. *Scientific reports*, *7*(1), 6033. https://doi.org/10.1038/s41598-017-05792-1.

Hasselmann, S., Hasselmann, K., Allender, J.H., Barnett, T.P., 1985. Computations and parameterizations of the nonlinear energy transfer in a gravity-wave spectrum. Part II: Parameterizations of the nonlinear energy transfer for application in wave models. J Phys Oceanogr 15, 1378–1391. https://doi.org/doi:10.1175/1520-0485(1985)015<1378:CAPOTN>2.0.CO;2

Herrera-Garcia, G., Ezquerro, P., Tomás, R., Béjar-Pizarro, M., López-Vinielles, J., Rossi, M., Mateos, R. M., Carreón-Freyre, D., Lambert, J., Teatini, P., Cabral-Cano, E., Erkens, G., Galloway, D., Hung, W. C., Kakar, N., Sneed, M., Tosi, L., Wang, H., Ye, S.: (2021). Mapping the global threat of land subsidence. *Science*, *371*(6524), 34-36. doi:10.1126/science.abb8549.

Hinkel, J.; Feyen, L.; Hemer, M.; Le Cozannet, G.; Lincke, D.; Marcos, M.; Mentaschi, L.; Merkens, J.L.; de Moel, H.; Muis, S.; Nicholls, R.J.; Vafeidism A. T.; van de Wal, R.S.W.; Vousdoukas, M.I.; Wahl, T.; Ward, P.J.; Wolff, C. (2021). Uncertainty and bias in global to regional scale assessments of current and future coastal flood risk. *Earth's Future*, *9*(7), e2020EF001882. https://doi.org/10.1029/2020EF001882.

Hlodversdottir, A. O., Bjornsson, B., Andradottir, H. O., Eliasson, J., & Crochet, P. (2015). Assessment of flood hazard in a combined sewer system in Reykjavik city centre. *Water Science and Technology*, *71*(10), 1471-1477. https://doi.org/10.2166/wst.2015.119.

Horsburgh, K. J., & Wilson, C. (2007). Tide-surge interaction and its role in the distribution of surge residuals in the North Sea. *Journal of Geophysical Research: Oceans*, *112*(C8). https://doi.org/10.1029/2006JC004033.

Horton, B.P.; Khan, N.S.; Cahill, N.; Lee, J.S.H.; Shaw, T.A.; Garner, A.J.; Kemp, A.C.; Engelhart, S.E.; Rahmstorf, S (2020). Estimating global mean sea-level rise and its uncertainties by 2100 and 2300 from an expert survey. *NPJ climate and atmospheric science*, *3*(1), 18. https://doi.org/10.1038/s41612-020-0121-5.

Il Baby MOSE per La Difesa Di Chioggia Dalle Acque Alte. Settembre 2015. Available online: http://www.forumtelecontrollo.it/allegati/11.20_progea_angelini.pdf (accessed on 22 Dicember 2025).

Iliadis, C., Galiatsatou, P., Glenis, V., Prinos, P., & Kilsby, C. (2023). Urban Flood Modelling under Extreme Rainfall Conditions for Building-Level Flood Exposure Analysis. *Hydrology*, *10*(8), 172. https://doi.org/10.3390/hydrology10080172

International Oceanographic Commission (IOC). (1993). *Manual of Quality Control Procedures for Validation of Oceanographic Data* (IOC Manuals and Guides 26. UNESCO. https://unesdoc.unesco.org/ark:/48223/pf0000138825

International Oceanographic Commission (IOC). (2020). *Quality control of in situ sea level observations: A review and progress towards automated quality control* (IOC Manuals and Guides No. 83, Vol. 1). UNESCO. https://unesdoc.unesco.org/ark:/48223/pf0000373566

ISPRA. Istituto Superiore per la Protezione e la RIcerca dell'Ambiente. La Direttiva Alluvioni 2007/60/CE e il D.Lgs attuativo 49/2010. https://www.isprambiente.gov.it/pre_meteo/file/DLGS_49_2010_agg2014.pdf

ISTAT. I Flussi Turistici-Anno 2023. Testo integrale e nota metodologica. Available online: https://www.istat.it/wp-content/uploads/2024/11/Statistica-Today_Turismo-2023_rev.pdf (accessed on 23 Dicember 2025).

ISTAT. Annuario statistico Italiano (ASI) 2024. Annuario in capitoli. Capitoli. 1. Territorio. https://www.istat.it/storage/ASI/2024/capitoli/C01.pdf

Janeković, I., & Kuzmić, M. (2005). Numerical simulation of the Adriatic Sea principal tidal constituents. *Annales Geophysicae, 23*, 3207-3218. https://doi.org/10.5194/angeo-23-3207-2005

Janssen, P. A. E. M. (1989). Wave-induced stress and the drag of air flow over sea waves. *Journal of Physical Oceanography, 19*, 745–754. https://doi.org/10.1175/1520-0485(1989)019<0745:WISATD>2.0.CO;2

Janssen, P. A. E. M. (1991). Quasi-linear theory of wind-wave generation applied to wave forecasting. *Journal of Physical Oceanography, 21*, 1631–1642. https://doi.org/10.1175/1520-0485(1991)021<1631:QLTOWW>2.0.CO;2

Jevrejeva, S., Williams, J., Vousdoukas, M. I., & Jackson, L. P. (2023). Future sea level rise dominates changes in worst case extreme sea levels along the global coastline by 2100. *Environmental Research Letters*, *18*(2), 024037. 10.1088/1748-9326/acb504

Johnson, H.K., Kofoed-Hansen, H., 2000. Influence of Bottom Friction on Sea Surface Roughness and Its Impact on Shallow Water Wind Wave Modeling. Horsholm, Denmark. https://doi.org/doi.org/10.1175/1520-0485(2000)030<1743:IOBFOS>2.0.CO;2

Jorissen, R., Kraaij, E., & Tromp, E. (2016). Dutch flood protection policy and measures based on risk assessment. In *E3S Web of Conferences* (Vol. 7, p. 20016). EDP Sciences. https://doi.org/10.1051/e3sconf/20160720016.

Katalinić, M., & Parunov, J. (2020). Uncertainties of estimating extreme significant wave height for engineering applications depending on the approach and fitting technique—Adriatic Sea case study. *Journal of Marine Science and Engineering, 8*(4), 259. https://doi.org/10.3390/jmse8040259

Kendall, M. G. (1938). A new measure of rank correlation. *Biometrika, 30*(1–2), 81–93. https://doi.org/10.2307/2332226

Kendall, M. G. (1975). *Rank correlation methods* (4th ed.). Charles Griffin. Ku, H.; Kim, T.; Song, Y.-I. Coastal Vulnerability Assessment of Sea-Level Rise Associated with Typhoon-Induced Surges in South Korea. *Ocean Coast. Manag.* 2021, *213*, 105884. https://doi.org/10.1016/j.ocecoaman.2021.105884.

Lagarias, A., & Stratigea, A. (2023). Coastalization patterns in the Mediterranean: a spatiotemporal analysis of coastal urban sprawl in tourism destination areas. *GeoJournal*, *88*(3), 2529-2552. https://doi.org/10.1007/s10708-022-10756-8.

Lambeck, K., Antonioli, F., Anzidei, M., Ferranti, L., Leoni, G., Scicchitano, G., & Silenzi, S. (2011). Sea level change along the Italian coast during the Holocene and projections for the future. *Quaternary International*, *232*(1-2), 250-257. https://doi.org/10.1016/j.quaint.2010.04.026

Lang, M., Ouarda, T. B. M. J., & Bobée, B. (1999). Towards Operational Guidelines for Over-Threshold Modeling. *Journal of Hydrology, 225,* 103-117.https://doi.org/10.1016/s0022-1694(99)00167-5

Leder, N., & Orlic, M. (2004, April). Fundamental Adriatic seiche recorded by current meters. In *Annales Geophysicae* (Vol. 22, No. 5, pp. 1449-1464). Copernicus GmbH. https://doi.org/10.5194/angeo-22-1449-2004.

Leon, J. X., Heuvelink, G. B. M., & Phinn, S. R. (2014). Incorporating DEM uncertainty in coastal inundation mapping. *PLOS ONE, 9*(9), e108727. https://doi.org/10.1371/journal.pone.0108727

L.H.N.C. Physical Oceanography By Albert Defant Pergamon Press, London, 1961. Vol. 1, pp. xvi + 729; Vol. 2, pp. viii + 598. Price £10. 10s. od. <i>Journal of Marine Biological Association of the United Kingdom<i>. 1962;42(2):468-468. Doi:10.1017/S0025315400070089

Lionello P, Tomasin A (2005) Sensitivity of free and forced oscillations of the Adriatic Sea to sea level rise. Clim Res 29:23-39 https://doi.org/10.3354/cr029023

Lionello, P., Cavaleri, L., Nissen, K. M., Pino, C., Raicich, F., & Ulbrich, U. (2012). Severe marine storms in the northern Adriatic: Characteristics and trends. *Physics and Chemistry of the Earth, 40–41*, 93–105. https://doi.org/10.1016/j.pce.2010.10.002

Lionello, P., Conte, D., Marzo, L., & Scarascia, L. (2017). The contrasting effect of increasing mean sea level and decreasing storminess on the maximum water level during storms along the coast

of the Mediterranean Sea in the mid 21st century. *Global and Planetary Change*, *151*, 80-91. https://doi.org/10.1016/j.gloplacha.2016.06.012

Lionello, P., Conte, D., & Reale, M. (2019). The effect of cyclones crossing the Mediterranean region on sea level anomalies on the Mediterranean Sea coast. *Natural Hazards and Earth System Sciences*, *19*(7), 1541-1564. https://doi.org/10.5194/nhess-19-1541-2019.

Lionello, P., & Scarascia, L. (2020). The relation of climate extremes with global warming in the Mediterranean region and its north versus south contrast. *Regional Environmental Change*, *20*(1), 31. https://doi.org/10.1007/s10113-020-01610-z.

Lionello, P.; Barriopedro, D.; Ferrarin, C.; Nicholls, R.J.; Orlić, M.; Raicich, F.; Reale, M. Umgiesser, G.; Vousdoukas, M.; Zanchettin, D. (2020). Extremes floods of Venice: characteristics, dynamics, past and future evolution. *Natural Hazards and Earth System Sciences Discussions*, *2020*, 1-34. https://doi.org/10.5194/nhess-21-2705-2021.

Lionello, P., Nicholls, R. J., Umgiesser, G., & Zanchettin, D. (2021). Venice flooding and sea level: past evolution, present issues, and future projections (introduction to the special issue). *Natural Hazards and Earth System Sciences*, *21*(8), 2633-2641. https://doi.org/10.5194/nhess-21-2633-2021.

Lionello, P. Climate Change 2022—Impatti, Adattamento e Vulnerabilità Il Secondo Volume (WG2) Del Sesto Rapporto Di Valutazione Dell'IPCC, La Più Aggiornata e Completa Rassegna Scientifica Sui Cambiamenti Climatici. Available online: https://files.cmcc.it/ar6/wg2/scienziati_italiani_IPCC_ar6_wg2.pdf(accessed on 14 Dicember 2025).

Lionello, P., Giorgi, F., Rohling, E., and Seager, R. (2023). "Mediterranean climate: past, present and future,", in Oceanography of the Mediterranean Seam, eds K. Schroeder and J. Chiggiato (Amsterdam Elsevier), 41-91. Doi: 10.1016/B978-0-12-823692-5.000111-X

Lionello, P., Nicholls, R. J., Umgiesser, G. & Zanchettin, D. Venice flooding and sea level: Past evolution, present issues, and future projections (introduction to the special issue). *Nat. Hazards Earth Syst. Sci.* 21, 2633–2641. https://doi.org/10.5194/nhess-21-2633-2021 (2021).

Locatelli, L., Guerrero, M., Russo, B., Martínez-Gomariz, E., Sunyer, D., & Martínez, M. (2020). Socio-economic assessment of green infrastructure for climate change adaptation in the context of urban drainage planning. *Sustainability, 12*, 3792. https://doi.org/10.3390/su12093792

Longuet-Higgins, M.S., Stewart, R.W., 1963. A note on wave set-up. Journal of Marine Research 21, 4.

Longuet-Higgins, M.S.; Stewart, R.W. Radiation stresses in water waves; a physical discussion, with applications. Deep Sea Res. Oceanogr. 1964, 11, 529–562.

Louisor J, Brivois O, Mouillon P, Maspataud A, Belz P and Laloue J-M (2022) Coastal Flood Modeling to Explore Adaptive Coastal Management Scenarios and LandUse Changes Under Sea Level Rise. Front. Mar. Sci. 9:710086. doi: 10.3389/fmars.2022.710086

Lyddon, C. E., Brown, J. M., Leonardi, N., & Plater, A. J. (2020). Sensitivity of Flood Hazard and Damage to Modelling Approaches. Journal of Marine Science and Engineering, 8(9), 724. https://doi.org/10.3390/jmse8090724

Magrini, G.P., De Marchi, L., Gnesotto, T. (Eds.), 1908. Ricerche Lagunari. vol. 9. Reale Istituto Veneto di Scienze Lettere ed Arti, Venice.

Majumder, R., Reich, B. J., & Shaby, B. A. (2024). Modeling extremal streamflow using deep learning approximations and a flexible spatial process. *The Annals of Applied Statistics*, *18*(2), 1519-1542. 10.1214/23-AOAS1847.

Mann, H. B. (1945). Nonparametric tests against trend. *Econometrica, 13*, 245–259.

Manzan, M.; Bacaro, G.; Nardini, A.; Casagrande, G.; Pezzi, A.; Petruzzellis, F.; Tordoni, E.; Fontolan, G. (2022). Climate change risk and vulnerabilities analysis in Trieste SECAP. *Sustainability*, *14*(10), 5973. https://doi.org/10.3390/su14105973.

Mannarini, G., Salinas, M. L., Verri, G., Da Costa, V. S., Barzaghi, R., & Carrion, D. (2025). Coastal flood hazard for Lecce, Italy, from breaches in the dunes. *Journal of Water and Climate Change*, *16*(9), 2709-2725. https://doi.org/10.2166/wcc.2025.764

Marcos, M., Tsimplis, M. N., & Shaw, A. G. P. (2009). Sea level extremes in southern Europe. *Journal of Geophysical Research: Oceans, 114*, C01007. https://doi.org/10.1029/2008JC004912

Mariano, C., Marino, M., Pisacane, G., & Sannino, G. (2021). Sea level rise and coastal impacts: Innovation and improvement of the local urban plan for a climate-proof adaptation strategy. *Sustainability*, *13*(3), 1565. https://doi.org/10.3390/su13031565.

Marocco, R. Le Spiagge Di Grado: Situazione Attuale, Tendenze Evolutive Ed Ipotesi d'intervento per Il Risanamento Degli Arenili. *GORTANIA—Atti Del Mus. Friul. Di Stor. Naturale.* 2000, *22*, 5–37.

Mark J. Dixon & Jonathan A. Tawn, 1999. "The Effect of Non-Stationarity on Extreme Sea-Level Estimation," Journal of the Royal Statistical Society Series C, Royal Statistical Society, vol. 48(2), pages 135-151.

Masina, M., & Ciavola, P. (2011). Analisi dei livelli marini estremi e delle acque alte lungo il litorale ravennate. *Studi Costieri, 18*, 87–101.

McEvoy, S., Haasnoot, M., & Biesbroek, R. (2021). How are European countries planning for sea level rise?. *Ocean & Coastal Management*, *203*, 105512. https://doi.org/10.1016/j.ocecoaman.2020.105512.

MedECC (2020) Climate and Environmental Change in the Mediterranean Basin. *Current Situation and Risks for the Future. First Mediterranean Assessment Report (MAR1)*; Cramer, W., Marini, K., Guiot, J., Eds.; Union for the Mediterranean, Plan Bleu, UNEP/MAP: Marseille, France, 2020; p. 632. https://doi.org/10.5281/zenodo.7224821 .

Medvedev, I. P., Vilibić, I., & Rabinovich, A. B. (2020). Tidal resonance in the Adriatic Sea: Observational evidence. *Journal of Geophysical Research: Oceans, 125*, e2020JC016168. https://doi.org/10.1029/2020JC016168

Međugorac, I., Orlić, M., Janeković, I., Pasarić, Z., & Pasarić, M. (2018). Adriatic storm surges and related cross-basin sea-level slope. *Journal of marine systems*, *181*, 79-90. https://doi.org/10.1016/j.jmarsys.2018.02.005.

Meier, M. F., & Wahr, J. M. (2002). Sea level is rising: Do we know why? *Proceedings of the National Academy of Sciences of the United States of America, 99*(10), 6524–6526. https://doi.org/10.1073/pnas.112214499

Mel, R., Viero, D. P., Carniello, L., Defina, A., & D'Alpaos, L. (2014). Simplified methods for real-time prediction of storm surge uncertainty: The city of Venice case study. *Advances in water resources*, *71*, 177-185. https://doi.org/10.1016/j.advwatres.2014.06.014.

Mel, R. A., Viero, D. P., Carniello, L., Defina, A., & D'Alpaos, L. (2021). The first operations of Mo. SE system to prevent the flooding of Venice: Insights on the hydrodynamics of a regulated lagoon. *Estuarine, Coastal and Shelf Science*, *261*, 107547. https://doi.org/10.1016/j.ecss.2021.107547.

Melet, A., Meyssignac, B., Almar, R., & Le Cozannet, G. (2018). Under-estimated wave contribution to coastal sea-level rise. *Nature Climate Change*, *8*(3), 234-239.. https://doi.org/10.1038/s41558-018-0088-y.

Melica, G.; De, F.; Rios, L.; Palermo, C.; Ferrario, M.; Baldi, F.; Ulpiani, M.; Hortelano, O.; Barbosa, A. *Covenant of Mayors: 2022 Assessment—Climate Change Mitigation and Adaptation at Local Level*; Publications Office of the European Union: Luxembourg, 2022. https://doi.org/10.2760/930988, JRC130957.

Méndez, F. J., Menéndez, M., Luceño, A., & Losada, I. J. (2007). Analyzing monthly extreme sea levels with a time-dependent GEV model. *Journal of Atmospheric and Oceanic Technology*, *24*(5), 894-911. 10.1175/JTECH2009.1

Merkens, J. L., Reimann, L., Hinkel, J., & Vafeidis, A. T. (2016). Gridded population projections for the coastal zone under the Shared Socioeconomic Pathways. *Global and Planetary Change*, *145*, 57-66. https://doi.org/10.1016/j.gloplacha.2016.08.009.

Merz, B., Basso, S., Fischer, S., Lun,D., Blöschl, G., Merz, R., et al. (2022).Understanding heavy tails of flood peakdistributions. Water Resources Research,58, e2021WR030506. https://doi.org/10.1029/2021WR030506

Miche, M. Le Povoir Réfléchissant des Ouvrages Maritimes Exposés à L'action de la Houle. Ann. Ponts Chaussées 1951, 121, 285–319.

Mignot, E., Li, X., & Dewals, B. (2019). Experimental modelling of urban flooding: A review. *Journal of Hydrology, 568*, 334–342. 10.1016/j.jhydrol.2018.11.001

Ministero dell'Ambiente e della Sicurezza Energetica. Geoportale Nazionale. Direttiva Alluvioni, https://gn.mase.gov.it/portale/direttive-alluvioni

Monserrat, S., Vilibić, I., & Rabinovich, A. B. (2006). Meteotsunamis: atmospherically induced destructive ocean waves in the tsunami frequency band. *Natural hazards and earth system sciences*, *6*(6), 1035-1051. https://doi.org/10.5194/nhess-6-1035-2006.

Morris RL, Bishop MJ, Boon P, Browne NK, Carley JT, Fest BJ, Fraser MW, Ghisalberti M, Kendrick GA, Konlechner TM, Lovelock CE, Lowe RJ, Rogers AA, Simpson V, Strain EMA, Van Rooijen AA, Waters E, Swearer SE. (2021) The Australian Guide to Nature-Based Methods for Reducing Risk from Coastal Hazards. Earth Systems and Climate Change Hub Report No. 26. NESP Earth Systems and Climate Change Hub, Australia.

Muis, S., Verlaan, M., Winsemius, H. C., Aerts, J. C., & Ward, P. J. (2016). A global reanalysis of storm surges and extreme sea levels. *Nature communications*, *7*(1), 11969. https://doi.org/10.1038/ncomms11969

Munaretto, S., Vellinga, P., & Tobi, H. (2012). Flood protection in Venice under conditions of sea-level rise: An analysis of institutional and technical measures. *Coastal Management*, *40*(4), 355-380. https://doi.org/10.1080/08920753.2012.692311.

Nelsen, R. B. *An Introduction to Copulas 272* (Springer, New York, 2006).

Neumann, B., Vafeidis, A. T., Zimmermann, J., & Nicholls, R. J. (2015). Future coastal population growth and exposure to sea-level rise and coastal flooding-a global assessment. *PloS one*, *10*(3), e0118571. https://doi.org/10.1371/journal.pone.0118571.

Nicholls, R.J.; Wong, P.P.; Burkett, V.R.; Codignotto, J.O.; Hay, J.E.; McLean, R.F.; Ragoonaden, S.; Woodroffe, C.D. Coastal Systems and Low-Lying Areas. In *Climate Change 2007: Impacts, Adaptation and Vulnerability. Contribution of Working Group II to the Fourth Assessment Report of the Intergovernmental Panel on Climate Change*; Parry, M.L., Canziani, O.F., et al., Eds.; Cambridge University Press, Cambridge: Cambridge, UK, 2007; pp. 315–356.

Nicholls, R.J.; Adger, W.N.; Hutton, C.W.; Hanson, S.E. (Eds.). *Deltas in the Anthropocene*; Palgrave Macmillan: Cham, Switzerland, 2020; p. 282.

Nicoloso P., 1992, *La città inventata. Idee, progetti e architetture per Lignano Sabbiadoro*. 1903-1939, Edizioni Biblioteca dell'Immagine, Pordenone.

Nimac, I., Cindrić Kalin, K., Renko, T., Vujnović, T., & Horvath, K. (2022). The analysis of summer 2020 urban flood in Zagreb (Croatia) from hydro-meteorological point of view. *Natural hazards*, *112*(1), 873-897. https://doi.org/10.1007/s11069-022-05210-4

Noon, V., Rivière, C., Strosser, P., Manea, E., Gissi, E., & Barbanti, A. (2021). Study on Integrating an Ecosystem-based Approach into Maritime Spatial Planning. *European Commission Report*, 88. https://www.milieu.be/wp-content/uploads/2021/08/Study-on-EBA-in-MSP-NAdriatic-case-study-final-report-25.08.2021.pdf. (accessed on 23 Dicember 2025).

NOAA, 2012. Mapping Coastal Inundation Primer. United States of America. Available Online: https://coast.noaa.gov/data/digitalcoast/pdf/coastal-inundation-guidebook.pdf (accessed on 27 Dicember 2025).

Orlić, M. (2001). Anatomy of sea level variability-an example from the Adriatic. *The Ocean Engineering Handbook*, 1-1. https://api.semanticscholar.org/CorpusID:133631263

Orlić, M., Pasarić, M., Pasarić, Z. (2019). Mediterranean Sea-Level Variability in the Second Half of the Twentieth Century: A Bayesian Approach to Closing the Budget. In: Vilibić, I., Horvath, K., Palau, J. (eds) Meteorology and Climatology of the Mediterranean and Black Seas. Pageoph Topical Volumes. Birkhäuser, Cham. https://doi.org/10.1007/978-3-030-11958-4_15

Papaioannou, G., Efstratiadis, A., Vasiliades, L., Loukas, A., Papalexiou, S. M., Koukouvinos, A., Tsoukalas, I., & Kossieris, P. (2018). An operational method for Floods Directive implementation in ungauged urban areas. *Hydrology, 5*(2), 24. https://doi.org/10.3390/hydrology5020024

Pasarić, M., & Orlić, M. (1992). Response of the Adriatic Sea level to planetary-scale atmospheric forcing. In P. L. Woodworth (Ed.), *Sea level changes: Determination and effects* (Geophysical Monograph Series No. 69, pp. 29–39). American Geophysical Union.

Pasarić, M., & Orlić, M. (1998). Response of the Adriatic sea-level slope to the air-pressure gradient and wind forcing at subsynoptic frequencies. *Rapports et Procès-Verbaux des Réunions CIESM, 35*, 184–185.

Pasarić, M., & Orlić, M. (2001). Long-term meteorological preconditioning of the North Adriatic coastal floods. *Continental Shelf Research*, *21*(3), 263-278. https://doi.org/10.1016/S0278-4343(00)00078-9

Pasarić, Z., Belušić, D., & Chiggiato, J. (2009). Orographic effects on meteorological fields over the Adriatic from different models. *Journal of Marine Systems, 78*, S90–S100. https://doi.org/10.1016/j.jmarsys.2009.01.019

Pasquali, D., & Marucci, A. (2021). The Effects of Urban and Economic Development on Coastal Zone Management. Sustainability, 13 (11), 6071. https://doi.org/10.3390/su13116071

Patterson, M.G. and Hardy, D.J. (2008). "Chapter 9: Economic Drivers of Change and their Oceanic–Coastal Ecological Impacts". In Ecological Economics of the Oceans and Coasts. Cheltenham, UK: Edward Elgar Publishing. Retrivied Feb 2, 2026, from https://doi.org/10.4337/9781782542483

Paxian, A., Hertig, E., Seubert, S., Vogt, G., Jacobeit, J., & Paeth, H. (2015). Present-day and future Mediterranean precipitation extremes assessed by different statistical approaches. *Climate dynamics*, *44*(3), 845-860. https://doi.org/10.1007/s00382-014-2428-6.

Perini, L., Calabrese, L., & Salerno, G. (2016). Il rischio da mareggiata in Emilia-Romagna L'evento del 5–6 febbraio 2015. *Il Geologo dell'Emilia-Romagna, 53*, 8–17. http://www.geologiemiliaromagna.it/wp-content/uploads/Art_Costa.pdf.

Perini, L., Calabrese, L., Salerno, G., Ciavola, P., & Armaroli, C. (2016). Evaluation of coastal vulnerability to flooding: comparison of two different methodologies adopted by the Emilia-Romagna region (Italy). *Natural Hazards and Earth System Sciences*, *16*(1), 181-194. https://doi.org/10.5194/nhess-16-181-2016.

Perini, L., Calabrese, L., Luciani, P., Olivieri, M., Galassi, G., & Spada, G. (2017). Sea-level rise along the Emilia-Romagna coast (Northern Italy) in 2100: Scenarios and impacts. *Natural Hazards and Earth System Sciences, 17*, 2271–2287. https://doi.org/10.5194/nhess-17-2271-2017

Pervan, M., & Šepić, J. (2023). Analysis of the eastern Adriatic Sea level extremes. *ST-OPEN, 4*, e2023.2111.5. https://doi.org/10.48188/so.4.10

Petti, M., Pascolo, S., Bosa, S., Bezzi, A., & Fontolan, G. (2019). Tidal flats morphodynamics: A new conceptual model to predict their evolution over a medium-long period. *Water*, *11*(6), 1176. https://doi.org/10.3390/W11061176

Petti, M., Pascolo, S., Bosa, S., & Busetto, N. (2023). The tidal prism as a dynamic response of a nonlinear harmonic system. *Physics of Fluids*, *35*(1). https://doi.org/10.1063/5.0133390

Pettitt. A.N. and Stephens. M.A. (1977) The Kolmogrov-Smirnov Goodness-of-Fit Statistic with Discrete and Grouped Data. Technometrics, 19, 205-210. http://dx.doi.org/10.1080/00401706.1977.10489529

Pezzetta, E., Lutman, A., Martinuzzi, I., Viola, C., Bernardis, G., & Fuccaro, V. (2011). Iron concentrations in selected groundwater samples from the lower Friulian Plain, northeast Italy: importance of salinity. *Environmental Earth Sciences*, *62*(2), 377-391. https://doi.org/10.1007/s12665-010-0533-3

PGRA, 2016. Piano di Gestione del Rischio di Alluvioni (PGRA), Distretto Idrografico delle Alpi Orientali, 2016. Relazione di Piano + Allegati. https://distrettoalpiorientali.it/wp-content/uploads/2023/02/PGRA_Relazione-di-Piano_Allegati_I_II_III_V_compressed.pdf

PGRA, 2021. Piano di Gestione del Rischio di Alluvioni, 2021; Aggiornamento e revisione del Piano di Gestione del Rischio di Alluvioni; Relazione Generale + Allegato I: Elementi tecnici di riferimento nell'impostazione del Piano; Distretto delle Alpi Orientali. Autorità di Bacino distrettuale delle Alpi Orientali. https://sigma.distrettoalpiorientali.it/sigma/documentDownload/downloadDocumentById?documentId=360

Pickands III, J.: Statistical inference using extreme order statistics, Ann. Stat., 3, 119–131, https://doi.org/10.1214/aos/1176343003,1975.

Pirazzoli P. A., (2006), *Projet Discobole - Contribution à la tâche 5 : calcul de hauteur des niveaux d'eau extrêmes sur le littoral français*, Meudon, CNRS – Laboratoire de Géographie Pysique, p. 93.

Pirazzoli, P. A., Tomasin, A., & Ullmann, A. (2007). Extreme sea levels in two northern Mediterranean areas. *Méditerranée. Revue géographique des pays méditerranéens/Journal of Mediterranean geography*, (108), 59-68. https://doi.org/10.4000/mediterranee.170

Pirazzoli, P. A., & Tomasin, A. (2009). Extreme sea levels on Adriatic coasts: A comparison of estimation methods. *Atti dell'Istituto Veneto di Scienze, Lettere ed Arti, CLXVII*, 53–82.

Poate, T. G., McCall, R. T., & Masselink, G. (2016). A new parameterisation for runup on gravel beaches. *Coastal Engineering*, *117*, 176-190. https://doi.org/10.1016/j.coastaleng.2016.08.003

Polli, S. (1961). *La propagazione delle maree nell'Adriatico*. Istituto Talassografico Sperimentale.

Portmann, R., González-Alemán, J. J., Sprenger, M., & Wernli, H. (2020). How an uncertain short-wave perturbation on the North Atlantic wave guide affects the forecast of an intense Mediterranean cyclone (Medicane Zorbas). *Weather and Climate Dynamics*, *1*(2), 597-615. https://doi.org/10.5194/wcd-1-597-2020.

Pörtner, Hans-Otto & Roberts, Debra & Tignor, Melinda & Poloczanska, Elvira & Mintenbeck, Katja & Alegría, Andrés & Craig, Marlies & Langsdorf, Stefanie & Löschke, Sina & Möller, Vincent & Okem, Andrew & Rama, Bard & Belling, Daniel & Dieck, Wolfgang & Götze, Sandra & Kersher, Tijama & Mangele, Philisiwe & Maus, Bastian & Mühle, Anka & Weyer, Nora. (2022). Climate Change 2022: Impacts, Adaptation and Vulnerability Working Group II Contribution to the Sixth Assessment Report of the Intergovernmental Panel on Climate Change. 10.1017/9781009325844.

Poulter, B., Goodall, J. L., & Halpin, P. N. (2008). Applications of network analysis for adaptive management of artificial drainage systems in landscapes vulnerable to sea level rise. *Journal of Hydrology*, *357*(3-4), 207-217. https://doi.org/10.1016/j.jhydrol.2008.05.022.

Processo verbale delle sedute della Commissione Geodetica Italiana, tenute in Milano nei giorni 5 e 6 Settembre 1895 e 26, 27 e 28 Giugno 1900. Firenze, Tipografia di G. Barbèra (1900), p. 81.

Pugh, S.T. & Vassie, J.M. (1978). EXTREME SEA LEVELS FROM TIDE AND SURGE PROBABILITY. *Coastal Engineering Proceedings*, *1*(16), 52. https://doi.org/10.9753/icce.v16.52

Pugh, D.T. and Vassie, J.M. (1980). Applications of the joint probability method for extreme sea level computations. Proceedings of the Institution of Civil Engineers, Part 2, 69(4), 959-975. https://doi.org/10.1680/iicep.1980.2179

Pugh, D.T. (1987). Tides, Surges and Mean Sea-Level. John Wiley & Sons, Chichester. Reprinted 1996. https://eprints.soton.ac.uk/19157/1/sea-level.pdf

Pugh, D., Woodworth, P. L., & Woodworth, P. (2014). *Sea-level science: understanding tides, surges, tsunamis and mean sea-level changes*. Cambridge university press.

Rabinovich, A. B., Vilibić, I., & Tinti, S. (2009). Meteorological tsunamis: atmospherically induced destructive ocean waves in the tsunami frequency band. *Physics and Chemistry of the Earth, Parts A/B/C*, *34*(17-18), 891-893.

Raicich, F., Crisciani, F., & Ferraro, S. (1994). Interannual variability of the sea level at Trieste. *Il Nuovo Cimento C, 17*(4), 377–384. https://doi.org/10.1007/BF02506725

Raicich, F., Orlić, M., Vilibić, I., & Malačič, V. (1999). A case study of the Adriatic seiches (December 1997). *Il Nuovo Cimento C, 22*, 715–726.

Raicich, F., Crisciani, F., Ceschia, M., & Pierobon, V. (2006). La serie temporale del livello marino a Trieste e un'analisi della sua evoluzione dal 1890 al 2003. *La variabilità del clima locale relazionata ai fenomeni di cambiamento climatico globale, edited by: Cortemiglia, GC, Pàtron, Bologna, Italy*, 199-220.

Raicich, F. (2007). A study of early Trieste sea level data (1875–1914). *Journal of Coastal Research, 23*(4), 1067–1073. https://doi.org/10.2112/04-0325

Raicich, F. (2010). On the contributions of atmospheric pressure and wind to daily sea level in the northern Adriatic Sea. *Continental Shelf Research, 30*, 1575–1581. https://doi.org/10.1016/j.csr.2010.05.017

Raicich, F., V. Malačič, M. Celio, D. Giaiotti, C. Cantoni, R. R. Colucci, B. Čermelj, and A. Pucillo (2013), Extreme air-sea interactions in the Gulf of Trieste (North Adriatic) during the strong Bora event in winter 2012, *J. Geophys. Res. Oceans*, 118, 5238–5250, doi:10.1002/jgrc.20398.

Rafiq, F., Ahmed, S., Ahmad, S., & Khan, A. A. (2016). Urban floods in India. *International Journal of Scientific & Engineering Research*, *7*(1), 721-734.

Ragno, E., Antonini, A., & Pasquali, D. (2023). Investigating extreme sea level components and their interactions in the Adriatic and Tyrrhenian Seas. *Weather and Climate Extremes, 41*, 100590. https://doi.org/10.1016/j.wace.2023.100590

Ranasinghe, R. (2016). Assessing climate change impacts on open sandy coasts: A review. *Earth-science reviews*, *160*, 320-332. https://doi.org/10.1016/j.earscirev.2016.07.011.

Rasmussen, P., Sonnenborg, T. O., Goncear, G., & Hinsby, K. (2013). Assessing impacts of climate change, sea level rise, and drainage canals on saltwater intrusion to coastal aquifer. *Hydrology and Earth System Sciences*, *17*(1), 421-443. https://doi.org/10.5194/hess-17-421-2013.

RAS. Autorità Di Bacino Regionale Della Sardegna. Piano Di Gestione Del Rischio Di Alluvioni. Relazione Metodologica Sulle Inondazioni Costiere. Luglio 2018.https://pianogestionerischioalluvioni.regione.sardegna.it/documenti/1_617_20190124124513.pdf (accessed on 14 Dicember 2025).

RAFVG. Autorità Di Sistema Portuale Del Mare Adriatico Orientale. Piano Regolatore Portuale Del Porto Di Monfalcone, Variante Localizzata. Studio Meteomarino. Progettisti: Modimar, SJS Engineering, Archest. 2019. Available online: https://www.regione.fvg.it/rafvg/export/sites/default/RAFVG/ambiente-territorio/pianificazione-gestione-territorio/FOGLIA9/allegati/Allegato_33_alla_Delibera_2066-2019.pdf (accessed on 27 Dicember 2025).

RAFVG. Comune di Trieste. Dipartimento Territorio, Economica, Ambiente e Mobilità. Servizio di Pianificazione Territoriale e Valorizzazione Porto Vecchio. Variante al P.R.G.C Accordo di programma Porto Vecchio. Relazione Geologica-parere di compatibilità (L.R. 27/88) - Norme geologico-tecniche. RG. Dicembre 2019. https://urbanistica.comune.trieste.it/wp-content/uploads/2020/07/RG_RELAZIONE_GEOLOGICA.pdf (accessed on 27 Dicember 2025).

RAFVG. Comune di Trieste. Dipartimento Territorio, Economica, Ambiente e Mobilità. Servizio di Pianificazione Territoriale e Valorizzazione Porto Vecchio. Piano Particolareggiato del Centro Storico. Marzo 2020. https://urbanistica.online.trieste.it/wp-content/uploads/2020/12/51_SCR-VAS.pdf (accessed on 27 Dicember 2025).

RAFVG. Comune di Trieste. Area Città e Territorio Servizio Pianificazione Urbana. Piano Regolatore Generale Comunale. Relazione sul fabbisogno abitativo e calcolo sulla capacità insediativa residenziale teorica. PO5. Dicembre 2015.https://documenti.comune.trieste.it/prg/nuovo-prg/approvazione/PO5_RELAZIONE_CIRTM/PO5_RELAZIONE_CIRTM_DIC2015.pdf (accessed on 27 Dicember 2025).

RAFVG. Comune di Muggia. Servizio LL.PP. Sviluppo Energetico Ecologia Ambientale -SSP. Collegamento tra la costa e il centro di Muggia. Progetto di fattibilità tecnico-economica. Rapporto preliminare ambientale. Variante n.41 al Piano regolatore generale comunale. Variante n.1 al Piano attuativo del Centro storico di Muggia. Settembre 2023. https://www.comune.muggia.ts.it/media/files/032003/attachment/TCI2210_AM_R01_r1_Rapporto_preliminare_ambientale-REV01.pdf (accessed on 27 Dicember 2025).

RAFVG. Statistica. Regione in Cifre 2024. https://www.regione.fvg.it/rafvg/export/sites/default/RAFVG/GEN/statistica/FOGLIA3/FOGLIA105/allegati/Tavole_e_grafici_2024.zip (accessed on 27 Dicember 2025).

Reimann, L., Vafeidis, A. T., Brown, S., Hinkel, J., & Tol, R. S. (2018). Mediterranean UNESCO World Heritage at risk from coastal flooding and erosion due to sea-level rise. *Nature communications*, *9*(1), 4161. https://doi.org/10.1038/s41467-018-06645-9.

Reiss, R. D., & Thomas, M. (2007). *Statistical analysis of extreme values: with applications to insurance, finance, hydrology and other fields*. Basel: Birkhäuser Basel. 10.1007/978-3-7643-7399-3

Regione Storia FVG. Dedizione di Trieste all'Austria, di Paolo Cammarosano. https://www.regionestoriafvg.eu/tematiche/tema/404/Dedizione-di-Trieste-allAustria

Rizzi, J., Torresan, S., Zabeo, A., Critto, A., Tosoni, A., Tomasin, A., & Marcomini, A. (2017). Assessing storm surge risk under future sea-level rise scenarios: A case study in the North Adriatic coast. *Journal of Coastal Conservation*, *21*(4), 453-471. https://doi.org/10.1007/s11852-017-0517-5.

Rizzo, A., Mattei, G., Steenssens, L. D., Anzidei, M., Aucelli, P. P., Alberti, T., Antonioli, F., Bezzi, A., Bonaldo, D., Fontolan, F., Furlani, S., Serena Liso, I., Parise, M., Sansò, P., Scicchitano, G., Trippanera, D., Vecchio, A. & Mastronuzzi, G. (2025). Methodological advances in sea level rise vulnerability assessment: implications for sustainable coastal management in a climate change scenario. *Ocean & Coastal Management*, *268*, 107751. https://doi.org/10.1016/j.ocecoaman.2025.107751

Robinson, A.R., Tomasin, A. and Artegiani, A. (1973) Flooding of Venice: phenomenology and prediction of the Adriatic storm surge. *Quarterly Journal of the Royal Meteorological Society*, 99, 688–692. https://doi.org/10.1002/qj.49709942210.

Rufat, S., Tate, E., Burton, C. G., & Maroof, A. S. (2015). Social vulnerability to floods: Review of case studies and implications for measurement. *International journal of disaster risk reduction*, *14*, 470-486. https://doi.org/10.1016/j.ijdrr.2015.09.013.

Sánchez, L., Völksen, C., Sokolov, A., Arenz, H., & Seitz, F. (2018). Present-day surface deformation of the Alpine region inferred from geodetic techniques. *Earth System Science Data*, *10*(3), 1503-1526. https://doi.org/10.5194/essd-10-1503-2018.

Sanders, B. F., Wing, O. E. J., & Bates, P.D. (2024). Flooding is not like filling abath. Earth's Future, 12, e2024EF005164. https://doi.org/10.1029/2024EF005164

Santiago-Collazo, F. L., Bilskie, M. V., & Hagen, S. C. (2019). A comprehensive review of compound inundation models in low-gradient coastal watersheds. *Environmental Modelling & Software*, *119*, 166-181. https://doi.org/10.1016/j.envsoft.2019.06.002.

Scarrott, C., & MacDonald, A. (2012). A review of extreme value threshold estimation and uncertainty quantification. *REVSTAT – Statistical Journal, 10*, 33–60. https://doi.org/10.57805/revstat.v10i1.110.

Scheidleger A, Grath J, Lindinger H, 2004. Saltwater intrusion due togroundwater over-exploitation EEA inventory throughout Europe.Page 125 in Proc. 18th Saltwater Intrusion Meet., Cartagena, Spain.

Scicchitano, G., Scardino, G., Monaco, C., Piscitelli, A., Milella, M., De Giosa, F., & Mastronuzzi, G. (2021). Comparing impact effects of common storms and Medicanes along the coast of south-eastern Sicily. *Marine Geology*, *439*, 106556. https://doi.org/10.1016/j.margeo.2021.106556.

Sen, P. K. (1968). Estimates of the regression coefficient based on Kendall's tau. *Journal of the American Statistical Association, 63*, 1379–1389.

Šepić, J., Pasarić, M., Međugorac, I., Vilibić, I., Karlović, M., & Mlinar, M. (2022). Climatology and process-oriented analysis of the Adriatic sea level extremes. *Progress in oceanography*, *209*, 102908. http://dx.doi.org/10.1016/j.pocean.2022.102908

Serinaldi, Francesco & Kilsby, Chris. (2015). Stationarity Is Undead: Uncertainty Dominates the Distribution of Extremes. Advances in Water Resources. 19. 10.1016/j.advwatres.2014.12.013.

Shah, M. A. R., Van Dau, Q., & Wang, X. (2025). Social-ecological vulnerability and risk to coastal flooding and erosion in major coastal cities. *International Journal of Disaster Risk Reduction*, *118*, 105286. https://doi.org/10.1016/j.ijdrr.2025.105286.

Shayegh, S., Moreno-Cruz, J., & Caldeira, K. (2016). Adapting to rates versus amounts of climate change: a case of adaptation to sea-level rise. *Environmental Research Letters*, *11*(10), 104007. https://doi.org/10.1088/1748-9326/11/10/104007.

Shi, S., Yang, B., & Jiang, W. (2022). Numerical simulations of compound flooding caused by storm surge and heavy rain with the presence of urban drainage system, coastal dam and tide gates: A case study of Xiangshan, China. *Coastal Engineering*, *172*, 104064. https://doi.org/10.1016/j.coastaleng.2021.104064.

Sklar, A. (1959). Fonctions de répartition à n dimensions et leurs marges. *Publications de l'Institut de Statistique de l'Université de Paris, 8*, 229–231.

Smith, R. L. (1985). Maximum likelihood estimation in a class of nonregular cases. *Biometrika, 72*(1), 67–90.

Spadotto, S., Fracaros, S., Bezzi, A., & Fontolan, G. (2025). Episodic vs. sea level rise coastal flooding scenarios at the urban scale: Extreme event analysis and adaptation strategies. *Water, 17*(13), 1991. https://doi.org/10.3390/w17131991

Srinivasan, M., & Tsontos, V. (2023). Satellite altimetry for ocean and coastal applications: A review. *Remote Sensing*, *15*(16), 3939. https://doi.org/10.3390/rs15163939.

Sriver, R. L., Lempert, R. J., Wikman-Svahn, P., & Keller, K. (2018). Characterizing uncertain sea-level rise projections to support investment decisions. *PLoS One*, *13*(2), e0190641. https://doi.org/10.1371/journal.pone.0190641.

Stephens, M. A. (1974). EDF statistics for goodness of fit and some comparisons. *Journal of the American Statistical Association, 69*, 730–737. https://doi.org/10.2307/2286009

Stephens, M. A. (1976). Asymptotic results for goodness-of-fit statistics with unknown parameters. *Annals of Statistics, 4*(2), 357–369. https://doi.org/10.1214/aos/1176343411

Stephens, M. A. (1979). Tests of fit for the logistic distribution based on the empirical distribution function. *Biometrika, 66*, 591–595. https://doi.org/10.1093/biomet/66.3.591

Stockdon, H. F., Holman, R. A., Howd, P. A., & Sallenger, A. H. (2006). Empirical parameterization of setup, swash, and runup. *Coastal Engineering, 53*, 573–588. https://doi.org/10.1016/j.coastaleng.2005.12.005

Stravisi, F., Ferraro, S., & Luca, I. (1985). Golfo di Trieste: Previsioni di marea per il 1986. *Nova Thalassia, 7*(Suppl.).

Stravisi F., PurgaN. (1997): La stazione mareografica di Trieste - Porto Lido, N. 60 (97/7), 9 pag.

Supić, N., & Orlić, M. (1999). Seasonal and interannual variability of the northern Adriatic surface fluxes. *Journal of Marine Systems*, *20*(1-4), 205-229. https://doi.org/10.1016/S0924-7963(98)00083-9.

Taherkhani, M., Vitousek, S., Barnard, P. L., Frazer, N., Anderson, T. R., & Fletcher, C. H. (2020). Sea-level rise exponentially increases coastal flood frequency. *Scientific reports*, *10*(1), 6466. https://doi.org/10.1038/s41598-020-62188-4.

Takagi, H., Tomiyasu, R., Araki, T., Oyake, T., Asakawa, N., Ishihara, I., et al. (2023). Feasibility of a self-powered movable seawall using microtidal energy in Japan. *Renewable Energy, 219*, 119563. https://doi.org/10.1016/j.renene.2023.119563

Tarolli, P., Luo, J., Straffelini, E., Liou, Y.-A., Nguyen, K. A., et al. (2023). Saltwater intrusion and climate change impact on coastal agriculture. *PLOS Water, 2*(4), e0000121. https://doi.org/10.1371/journal.pwat.0000121

Tawn J.A., Vassie J.M., (1989), Extreme sea levels: the joint probabilities method revisited and revised, *Proc. Institution Civil Engineers*, Part 2, 87: p. 429-442. (Paper 9476, Water Engineering Group). http://doi.org/10.1680/iicep.1989.2975.

Tomasin, A. and Pirazzoli, P.A. (1999) The Seiches in the Adriatic Sea. Atti Istituto Veneto di Scienze Lettere ed Arti CLVII, Venezia, 299-316.

Tong, S., Bambrick, H., Beggs, P. J., Chen, L., Hu, Y., Ma, W., ... & Tan, J. (2022). Current and future threats to human health in the Anthropocene. *Environment international*, *158*, 106892. https://doi.org/10.1016/j.envint.2021.106892.

Toledo, I.; Pagán, J.I.; López, I.; Aragonés, L.; Olcina, J. Nature-Based Solutions on the Coast in Face of Climate Change: The Case of Benidorm (Spain). *Urban Clim.* 2024, *53*, 101816. https://doi.org/10.1016/j.uclim.2024.101816.

Tortorici, E. Archeologia Subacquea e Trasformazioni Geomorfologiche Del Territorio: Il Caso Della Laguna Di Grado. In Atti Convegno Nazionale di Archeologia Subacquea, Anzio, Italy, 30 May - 1 June 1997, pp. 315–325.

Tosi, L., Teatini, P., Strozzi, T., Carbognin, L., Brancolini, G., & Rizzetto, F. (2010). Ground surface dynamics in the northern Adriatic coastland over the last two decades. *Rendiconti Lincei*, *21*(Suppl 1), 115-129. https://doi.org/10.1007/s12210-010-0084-2

Tosi, L., Da Lio, C., Strozzi, T., & Teatini, P. (2016). Combining L- and X-Band SAR Interferometry to Assess Ground Displacements in Heterogeneous Coastal Environments: The Po River Delta and Venice Lagoon, Italy. *Remote Sensing*, *8*(4), 308. https://doi.org/10.3390/rs8040308.

Tosi, L., Da Lio, C., Bergamasco, A., Cosma, M., Cavallina, C., Fasson, A., ... & Donnici, S. (2021). Sensitivity, hazard, and vulnerability of farmlands to saltwater intrusion in low-lying coastal areas of Venice, Italy. *Water*, *14*(1), 64. https://doi.org/10.3390/w14010064

Touring Club Italiano, Gorizia e provincia: Il Collio, la valle dell'isonzo, Grado e la laguna, il Carso, 2009, 9.92.

Trigo, I.F. and Davies, T.D. (2002) Meteorological conditions associated with sea surges in Venice: a 40-year climatology. *International Journal of Climatology*, 22(7), 787–803. https://doi.org/10.1002/joc 719.

Trobec, A.; Busetti, M. Models of the bathymetry, of the base and of the thickness of Holocene marine sediment in the Gulf of Trieste (Northern Adriatic Sea). OGS SNAP System. 2017. Available online: https://snap.ogs.it/cache/doi/6ad9b1e6-c977-cec9-8 a2d-db10c7f90adc/58074ea270863f0a32214fab4f43d42c.jsp (accessed on 22 Dicember 2025).

Tsimplis, M. N., Proctor, R., & Flather, R. A. (1995). A two-dimensional tidal model for the Mediterranean Sea. *Journal of Geophysical Research: Oceans*, *100*(C8), 16223-16239. https://doi.org/10.1029/95JC01671

Tuel, A., & Eltahir, E. A. (2020). Why is the Mediterranean a climate change hot spot?. *Journal of Climate*, *33*(14), 5829-5843. https://doi.org/10.1175/JCLI-D-19-0910.1.

Umgiesser, G., Bajo, M., Ferrarin, C., Cucco, A., Lionello, P., Zanchettin, D., Papa, A., Tosoni, A., Ferla, M., Coraci, E., Morucci, S., Crosato, F., Bonometto, A., Valentini, A., Orlić, M., Haigh, I. D., Nielsen, J. W., Bertin, X., Fortunato, A. B., Pérez Gómez, B., Alvarez Fanjul, E., Paradis, D., Jourdan, D., Pasquet, A., Mourre, B., Tintoré, J., & Nicholls, R. J. (2021). The prediction of floods in Venice: Methods, models and uncertainty. *Natural Hazards and Earth System Sciences, 21*, 2679–2704. https://doi.org/10.5194/nhess-21-2679-2021

Umgiesser, G., Ferrarin, C., Bajo, M., Bellafiore, D., Cucco, A., De Pascalis, F., Ghezzo, M., McKiver, W., & Arpaia, L. (2022). Hydrodynamic modelling in marginal and coastal seas: The Adriatic Sea as a permanent laboratory. *Ocean Modelling, 179*, 102123. https://doi.org/10.1016/j.ocemod.2022.102123

UNFCCC (United Nations Framework Convention on Climate Change). Defining and Understanding Transformational Adaptation at Different Spatial Scales and Sectors, and Assessing Progress in Planning and Implementing Transformational Adaptation Approaches at the Global Level; 2024. Technical Paper by the Secretariat, FCCC/TP/2024/8. Available online: https://unfccc.int/sites/default/files/resource/tp2024_08.pdf (accessed on 23 Dicember 2025).

Valussi G., 1986, *Lignano Sabbiadoro. Contributo per una geografia del turismo*, Quaderni dell'Istituto di Geografia della Facoltà di Economia e Commercio dell' Università di Trieste, Trieste.

Valle-Levinson, A., Marani, M., Carniello, L., D'Alpaos, A., & Lanzoni, S. (2021). Astronomic link to anomalously high mean sea level in the northern Adriatic Sea. *Estuarine, Coastal and Shelf Science*, *257*, 107418. https://doi.org/10.1016/j.ecss.2021.107418

Van de Sande, B., Lansen, J., & Hoyng, C. (2012). Sensitivity of Coastal Flood Risk Assessments to Digital Elevation Models. Water, 4(3), 568-579. https://doi.org/10.3390/w4030568

van de Wal, R. S., Melet, A., Bellafiore, D., Vousdoukas, M., Camus, P., Ferrarin, C., ... & Staneva, J. (2023). Sea level rise in Europe: Impacts and consequences. *State of the Planet Discussions*, *2023*, 1-65. https://doi.org/10.5194/sp-3-slre1-5-2024.

Vanem, E. (2015). Uncertainties in extreme value modelling of wave data in a climate change perspective. *Journal of Ocean Engineering and Marine Energy*, *1*(4), 339-359. https://doi.org/10.1007/s40722-015-0025-3

Vecchio, A., Anzidei, M., & Serpelloni, E. (2024). Sea Level Rise Projections Up to 2150 in the Northern Mediterranean Coasts. Environmental Research Letters, 19(1), Article 014050. https://doi.org/10.1088/1748-9326/ad127e

Vilibić, I. (2000). *A climatological study of the uninodal free oscillation in the Adriatic Sea*. Acta Adriatica, 41(2), 89-102.

Vilibić, I., & Šepić, J. (2009). Destructive meteotsunamis along the eastern Adriatic coast: Overview. *Physics and Chemistry of the Earth, 34*, 904–917. https://doi.org/10.1016/j.pce.2009.08.004

Vilibić, I., Šepić, J., Pasarić, M., & Orlić, M. (2017). The Adriatic Sea: A long-standing laboratory for sea level studies. *Pure and Applied Geophysics, 174*, 3765–3811. https://doi.org/10.1007/s00024-017-1625-8

Vilibić, I., & Šepić, J. (2017). Global mapping of nonseismic sea level oscillations at tsunami timescales. *Scientific Reports*, *7*(1), 40818. https://doi.org/10.1038/srep40818

Vitousek, S., Barnard, P. L., Limber, P., Erikson, L., & Cole, B. (2017). A model integrating longshore and cross-shore processes for predicting long-term shoreline response to climate change. *Journal of Geophysical Research: Earth Surface*, *122*(4), 782-806. https://doi.org/10.1002/2016JF004065.

Vogt, T., Treu, S., Mengel, M., Frieler, K., & Otto, C. (2024). Modeling surge dynamics improves coastal flood estimates in a global set of tropical cyclones. *Communications Earth & Environment*, *5*(1), 529. https://doi.org/10.1038/s43247-024-01707-x

Von Mises, R. (1936). La distribution de la plus grande de n valeurs. *Revue Mathématique de l'Union Interbalkanique, 1*, 141–160.

Vousdoukas, M. I., Voukouvalas, E., Mentaschi, L., Dottori, F., Giardino, A., Bouziotas, D., Bianchi, A., Salamon, P. & Feyen, L. (2016). Developments in large-scale coastalflood hazard mapping. Natural Hazards and Earth System Sciences, 16(8), 1841–1853. https://doi.org/10.5194/nhess-16-1841-2016

Vousdoukas, M. I., Mentaschi, L., Voukouvalas, E., Verlaan, M., Jevrejeva, S., Jackson, L. P., & Feyen, L. (2018). Global probabilistic projections of extreme sea levels show intensification of coastal flood hazard. *Nature communications*, *9*(1), 2360. https://doi.org/10.1038/s41467-018-04692-w

Vousdoukas, M.I.; Clarke, J.; Ranasinghe, R.; Reimann, L.; Khalaf, N.; Duong, T.M.; Ouweneel, B.; Sabour, S.; Iles, C.E.; Trisos, C.H.; Feyen, L.; Mentaschi, L. & Simpson, N. P. (2022). African heritage sites threatened as sea-level rise accelerates. *Nature Climate Change*, *12*(3), 256-262. https://doi.org/10.1038/s41558-022-01280-1.

Wahl, T., Haigh, I. D., Nicholls, R. J., Arns, A., Dangendorf, S., Hinkel, J., & Slangen, A. B. (2017). Understanding extreme sea levels for broad-scale coastal impact and adaptation analysis. *Nature communications*, *8*(1), 16075. https://doi.org/10.1038/ncomms16075

Williams, J., Horsburgh, K. J., Williams, J. A., & Proctor, R. N. (2016). Tide and skew surge independence: New insights for flood risk. *Geophysical Research Letters*, *43*(12), 6410-6417. https://doi.org/10.1002/2016GL069522.

Wolff C, Vafeidis AT, Lincke D, Marasmi C and Hinkel J (2016). Effects of Scale and Input Data on Assessing the Future Impacts of Coastal Flooding: An Application of DIVA for the Emilia-Romagna Coast. Front. Mar. Sci. 3:41. doi: 10.3389/fmars.2016.00041

Wong, P.P.; Losada, I.J.; Gattuso, J.-P.; Hinkel, J.; Khattabi, A.; Mclennes, K.L.; Saito, Y.; Sallenger, A. Coastal Systems and Low-Lying Areas. In *Climate Change 2014: Impacts, Adaptation, and Vulnerability. Part A: Global and Sectoral Aspects. Contribution of Working Group II to the Fifth Assessment Report of the Intergovernmental Panel on Climate Change*; Field, C.B., Barros, V.R., et al., Eds.; Cambridge University Press: Cambridge, UK; New York, NY, USA, 2014; pp. 361–409.

Woodworth, P. L. (2012). A Note on the Nodal Tide in Sea Level Records. *Journal of Coastal* Research, 28(2), 316–323. https://doi.org/10.2112/JCOASTRES-D-11A-00023.1

Wu, X., Wang, Z., Guo, S., Liao, W., Zeng, Z., & Chen, X. (2017). Scenario-based projections of future urban inundation within a coupled hydrodynamic model framework: a case study in Dongguan City, China. *Journal of Hydrology*, *547*, 428-442. https://doi.org/10.1016/j.jhydrol.2017.02.020.

Xie, W., Tang, B., & Meng, Q. (2021). The impact of sea-level rise on urban properties in Tampa due to climate change. *Water*, *14*(1), 13. https://doi.org/10.3390/w14010013.

Zampato, L., Bajo, M., Canestrelli, P., & Umgiesser, G. (2016). Storm surge modelling in Venice: two years of operational results. *Journal of Operational Oceanography*, *9*(sup1), s46-s57. https://doi.org/10.1080/1755876x.2015.1118804.

Zanchettin, D., Bruni, S., Raicich, F., Lionello, P., Adloff, F., Androsov, A., Antonioli, F., Artale, V., Carminati, E., Ferrarin, C., Fofonova, V., Nicholls, R. J., Rubinetti, S., Rubino, A., Sannino, G., Spada, G., Thiéblemont, R., Tsimplis, M., Umgiesser, G., Vignudelli, S., Wöppelmann, G., and Zerbini, S (2021). Sea-level rise in Venice: historic and future trends. *Natural Hazards and Earth System Sciences*, *21*(8), 2643-2678. https://doi.org/10.5194/nhess-21-2643-2021.

Zerbini, S., Raicich, F., Prati, C. M., Bruni, S., Del Conte, S., Errico, M., & Santi, E. (2017). Sea-level change in the Northern Mediterranean Sea from long-period tide gauge time series. *Earth-Science Reviews*, *167*, 72-87. https://doi.org/10.1016/j.earscirev.2017.02.009.

Zerbini, S., Bruni, S., & Raicich, F. (2021). Tide gauge data archaeology provides natural subsidence rates along the coasts of the Po Plain and of the Veneto–Friuli Plain, Italy. *Geophysical Journal International*, *225*(1), 253-260. https://doi.org/10.1093/gji/ggaa602.

Zheng, Y., & Sun, H. (2020). An integrated approach for the simulation modelling and risk assessment of coastal flooding. *Water, 12*(8), 2076. https://doi.org/10.3390/w12082076

Web references:

COP29, Baku 2024 https://cop29.az/en/home
http://www.emodnet-bathymetry.eu
https://www.informatrieste.eu/ts/blog/incubo-acqua-alta-scongiurato-test-positivo-paratie-sul-mandracchio-a-muggia/
https://www.rainews.it/tgr/fvg/articoli/2025/01/allerta-meteo-acqua-alta-nel-mandracchio-a-muggia-posizionate-le-barriere-mobili-9f41a40f-4d3b-49c4-8962-29ac1471c016.html
https://www.telefriuli.it/cronaca/piogge-e-alta-marea-lacqua-tracima-a-lignano-grado-e-trieste/
https://archiviodistatotrieste.it/documento-del-mese/novembre-2023-mareggiate-a-trieste/
https://www.atlantedeiluoghirivierafriulana.it/
https://archiviodistatotrieste.it/documento-del-mese/novembre-2023-mareggiate-a-trieste/
https://www.lignanoonline.eu/it/storia.php
https://www.domusweb.it/it/dall-archivio/2023/07/11/a-lignano-il-progetto-di-marcello-dolivo.html
https://comune.grado.go.it/it/vivere-il-comune-22477/luoghi-22478/la-laguna-di-grado-69770
https://demo.istat.it/app/?a=2024&i=D7B
https://www.archeocartafvg.it/portfolio-articoli/grado-go-il-castrum/).
https://trieste-di-ieri-e-di-oggi.it/2016/11/15/storia-di-trieste-in-sintesi/
https://www.archeocartafvg.it/portfolio-articoli/muggia-ts-il-centro-storico/
https://www.comune.muggia.ts.it/media/files/032003/attachment/TCI2210_AM_R01_r1_Rapporto_preliminare_ambientale-REV01.pdf
https://tv12.medianordest.it/34515/muggia-acqua-alta-a-muggia-montate-le-paratie-allarme-rientrato-in-mattinata/
https://www.informatrieste.eu/ts/blog/incubo-acqua-alta-scongiurato-test-positivo-paratie-sul-mandracchio-a-muggia/
https://www.rainews.it/tgr/fvg/articoli/2025/01/allerta-meteo-acqua-alta-nel-mandracchio-a-muggia-posizionate-le-barriere-mobili-9f41a40f-4d3b-49c4-8962-29ac1471c016.html
https://www.ilnordest.it/economia/acqua-alta-a-trieste-sommerse-le-rive-e-piazza-unita-la-regione-chiede-lo-stato-di-emergenza-e-non-e-finita-qk77gxpv
https://tomroelandts.com/articles/how-to-create-a-configurable-filter-using-a-kaiser-window

Finanziato dall'Unione europea NextGenerationEU | Ministero dell'Università e della Ricerca | Italiadomani PIANO NAZIONALE DI RIPRESA E RESILIENZA | UNIVERSITÀ DEGLI STUDI DI TRIESTE

9 Acknowledgements

Giunto alla fine del percorso da dottorando, vorrei prima di tutto ringraziare i miei genitori. Nel bene e nel male, senza di loro non sarei arrivato fin qui. Grazie per avermi supportato e soprattutto sopportato in questi anni. Un ringraziamento particolare va dato a mia Nonna Bruna. Mi ha sempre voluto bene e mi ha sempre supportato in tutto e per tutto.
Un grazie va rivolto anche ad alcuni amici con cui ho condiviso diversi momenti della mia avventura. Sicuramente non i migliori in termini di conforto, ma senza dubbio dei cazzari con cui ridere e risollevarsi l'umore. Andriy, Leo, Luc, Roi, il Trick, Freps, e infine Zu e il Presidente di Moruzzo. Un grazie speciale rivolto soprattutto a Nabil, probabilmente il capostipite della rete trofica di tutti i cazzari. In sintesi, tutti personaggi laureati all'Università della Strada con ottimi voti.
Il secondo giro di ringraziamenti è rivolto ovviamente ai membri del Coastal Group, per il supporto tecnico, morale e perché sempre pronti a risollevarti l'umore nonostante le tante avversità degli ultimi tempi. In generale è stata un percorso ricco di insidie non solo sotto l'aspetto lavorativo, ma anche umano. Nonostante questo, desidero ringraziare uno ad uno le persone che mi hanno accompagnato. Un Grazie ad Anne, che nonostante l'entropia è sempre pronta a darti il supporto di cui hai bisogno; a Davide perché è sempre pronto a darti man forte e di stemperare la tensione; a Stefi un grazie per il supporto, i consigli dispensati in certi attimi e le cazzate dette durante le pause caffè ma soprattutto un grazie speciale per avermi fatto capire che il mio tifo è rivolto alla squadra giusta di Milano (si scherza… o forse no); Grazie a Simo per gli aiuti dispensati e per la condivisione di alcuni attimi durante questo percorso. Un grazie anche a Chiara, una mina vagante e buonissima ragazza. Infine, desidero ringraziare le due persone che più di tutte mi hanno aiutato in questo percorso: Giulia e soprattutto Saverio. Nonostante tutto siamo sempre andati d'accordo e ci vogliamo bene. Grazie per le bevute e per i momenti di cazzeggio passati assieme. Probabilmente due "trmoni" così di 'sti tempi non si trovano nemmeno a Beri Vecchia. Per ultimo, ma non per ordine di importanza, desidero ringraziare il Prof. Giorgio Fontolan. Grazie per avermi dato la possibilità di applicare lo studio di tre anni allo stato del mare, tema che fin da subito mi ha completamente affascinato. Non tanto per la bellezza del mare (anche se a me più di tanto non piace), quanto per il suo carattere complesso e avvolto nel mistero. Un grazie per avermi sempre teso la mano e dispensato ogni aiuto di cui avevo bisogno, soprattutto alla fine del percorso delle Laurea Magistrale. Senza dubbio il Barbabianca del gruppo.

Un Grazie Speciale va rivolto a Marisa, dottoranda come me. Siamo subito entrati in sintonia parlando spagnolo. Senza dubbio una gran persona con cui si è creata una bella amicizia. Una persona a cui voglio bene. Un grazie va rivolto anche a Valentina. Anche se è stata poco in università siamo entrati subito in sintonia.

Un Grazie a caratteri cubitali va infine rivolto all'unica persona che non ha mai smesso di supportarmi, nonostante i litigi, le assenze e la lontananza in alcuni periodi, i periodi bui, ma soprattutto per essermi sempre stata a fianco, nonostante le difficoltà degli ultimi anni. Non ha mai smesso di proteggermi e di prendersi cura di me. Nonostante tutte le avversità. MI ha sempre guidato e supportato verso un futuro migliore. Forse le parole che meglio descrivono il nostro legame, oramai duraturo da anni, possono prendono spunto dal tema principale del mio dottorato. Ecco che quindi, senza troppi giri di parole, posso descrivere cosa tu rappresenti per me in questo modo:

Vale, sei e sarai sempre il mio Storm Surge.

Finanziato dall'Unione europea NextGenerationEU
Ministero dell'Università e della Ricerca
Italiadomani PIANO NAZIONALE DI RIPRESA E RESILIENZA
UNIVERSITÀ DEGLI STUDI DI TRIESTE

Quasi dimenticavo. Grazie a Marley perché mi vuoi bene e io te ne voglio a te. Anche se sei un tontolone e puzzi. E Grazie a te Sisley, per essere stata una gattina dolce e per certi aspetti molto più umana di alcune persone. Vale e Io ti ricorderemo sempre e comunque vada. Ti voglio bene.
Per ultimo, ma non per ordine di importanza, voglio ringraziare Duma ma soprattutto il mio Zorro: amico, fratello e compagno di vita. "*Tsuki ga kirei desu ne?"*

This study was carried out within the PNRR research activities of the consortium iNEST (Interconnected North-Est Innovation Ecosystem) funded by the European Union Next-GenerationEU (Piano Nazionale di Ripresa e Resilienza (PNRR) – Missione 4 Componente 2, Investimento 1.5 – D.D. 1058 23/06/2022, ECS_00000043). This manuscript reflects only the Authors' views and opinions, neither the European Union nor the European Commission can be considered responsible for them.

La borsa di dottorato è cofinanziata con risorse dell'Unione europea, NextGeneration EU - Piano Nazionale di Ripresa e Resilienza, Missione 4 – Componente 2 – Investimento 1.5 CUP J43C22000320006

10 Appendix I – Papers and scientific contributions related to PhD project

International ISI papers

- Sabato G., Scardino G., Kushabaha A., Casagrande G., Chirivì M., Fontolan G., Fracaros S., Luparelli A., **Spadotto S.**, Scicchitano G. (2024) Remote measurement of tide and surge using a deep learning system with surveillance camera images. MDPI Water, 2024, 16 (10), 1365. https://doi.org/10.3390/w16101365.
- Busetti A., Leone C., Corradetti A., Fracaros S., **Spadotto S.**, Rai P., Zini L., Calligaris C. Coastal storm-induced sinkholes: insights from UAV monitoring (2024). Remote Sensing 2024, 16 (19), 3681. https://dx.doi.org/10.3390/rs16193681
- **Spadotto S.**, Fracaros S., Bezzi A., Fontolan G. (2025) Episodic vs. sea level rise coastal flooding scenarios at the urban scale: extreme event analysis and adaptation strategies. MDPI Water, 17 (13), 1991, https://doi.org/10.3390/w17131991.

Articles in Italian (not ISI)

- Fontolan G., **Spadotto S.**, Fontanot L., Bezzi A., Bratus A. (2023) Scenari di inondazione costiera: la realtà di Grado. In Segnali dal clima in FVG - cambiamenti impatti azioni (a cura di Flapp F., Stel F.), ARPA FVG – Agenzia Regionale per la Protezione dell'Ambiente del Friuli Venezia Giulia: 38-42 p. https://www.arpa.fvg.it/temi/temi/meteo-e-clima/sezioni-principali/cambiamenti-climatici/segnali-dalclima- in-fvg/

Abstracts in Conference Book, Proceedings

- Sabato G., Scardino G., Kushabaha A., Casagrande G., Chirivì M., Fontolan G., Fracaros S., Luparelli A., **Spadotto S.**, Scicchitano G. (2024) A deep learning method to automatically measure tide and surge in coastal areas. EGU European Geosciences Union General Assembly 2024, Wien, Austria, 14-19 April 2024, EGU24-8103, 2024. https://meetingorganizer.copernicus.org/EGU24/EGU24-8103.html
- Sabato G., Scardino G., Kushabaha A., Casagrande G., Chirivì M., Fontolan G., Fracaros S., Luparelli A., **Spadotto S.**, Scicchitano G. (2024) Developing an automated tide and surge measurement system in coastal regions using deep learning techniques. X AIGeo Italian Young Geomorphologists' Day & III IAG International Young Geomorphologists' Meeting - "Climate change and the role of early-career geomorphologists". Venice, 1-2 March 2024. Abstract Book, pag. 38.
- **Spadotto S.**, Fracaros S., Bezzi A., Casagrande G., Popesso C., Fontolan G. (2024) Coastal flooding risk scenario for the city of Grado, northern Adriatic Sea. Join Congress SGI-SIMP *Geology for a sustainable management of our Planet,* Bari, 2-5 september 2024 (oral presentation: S. Spadotto). Abstract book, pag. 477: https://www.socgeol.it/files/download/pubblicazioni/Abstract%20Book/Abstract%20Congresso%20SGI-SIMP%202024-4.pdf
- Bezzi A., Sponza S., Casagrande G., **Spadotto S.**, Fracaros S., Martinucci D., Pillon S., Fontolan G. (2024) Shoreline dynamics and breeding coastal birds in the Marano and Grado barrier islands. Littoral 2024 European Coastal Challenge Summit, Constanta (Romania) 24-27 settembre 2024, Abstract (poster presentation: A. Bezzi). Book of Abstracts, pag. 59: https://littoral24.univ-ovidius.ro/wp-content/uploads/2024/09/Littoral24_-Book-of-

Abstracts.pdf.

- Bezzi A., Casagrande G., Fracaros S., **Spadotto S.**, Pillon S., Martinucci D., Popesso C., Fontolan G. (2024) Coastal vulnerability assessment of Veneto beaches and barrier islands, northern Adriatic, Italy. Littoral 2024 European Coastal Challenge Summit, Constanta (Romania) 24-27 settembre 2024, Abstract (oral presentation: A. Bezzi). Book of Abstracts, pag. 14: https://littoral24.univ-ovidius.ro/wp-content/uploads/2024/09/Littoral24_-Book-of-Abstracts.pdf.
- Bezzi A., Casagrande G., Fracaros S., Pillon S., Martinucci D., Popesso C., **Spadotto S.**, Sponza S., Fontolan G. (2024) Barrier islands facing sea level rise in Northern Adriatic Sea. Coastal Dynamics 2025, Aveiro (Portugal) 7-11 April 2025, Abstract (oral presentation: Bezzi). Conference Special Issue, Extended abstract, in press.

Speaker to Seminars, Congresses, Workshop

- Cycle of seminars 'THE HYDRAULIC AND COASTAL RISK IN THE VENETIAN SEA FLOOR'. It is hereby certified that Prof. Giorgio Fontolan | University of Trieste Dr. Chiara Popesso | Coastal Group - UNITS Dr. Davide Martinucci | Coastal Group - UNITS |Dr. Annelore Bezzi | Coastal Group - UNITS | **Dr. Sebastian Spadotto** | Coastal Group - UNITS carried out training activities **in the role of speakers** at seminars COASTAL RISK FROM STORM SURGES which was held online on 19 May 2023, from 09:00 to 12:30. Interreg ITA-CRO STREAM Project, organized by Comune di Venezia, Centro Previsione e Segnalazione Maree.
- Congress of the Società Geologica Italiana, 3-5 September 2024, Bari. Title of oral presentation “Coastal flooding risk scenario for the city of Grado, northern Adriatic Sea” by **Spadotto S. (speaker)**, Fracaros S., Bezzi A., Casagrande G., Popesso C. & Fontolan G.
- **Spadotto S., invited speaker** at the workshop “Cambiamenti climatici e rischi costieri - Un approccio multi-rischio in ambiente urbano” held at LignanoSabbiadoro (Hotel Columbus) on 20-21 October 2025. Title Tema 1: rischi costieri e cambiamenti climatici – Mareggiate e inondazioni costiere.

Technical Reports

- Fontolan, G., Bezzi, A., Casagrande, G., Fracaros, S., Popesso, C., **Spadotto, S.**, Favaro, M., Papa, A., 2023a. Real-time monitoring system and an early warning system implemented. Report D 5.4.3_Part B_ Stream project.

In preparation, in press

- **Spadotto S.**, Bezzi, A., Fracaros S., Casagrande G., Pillon S., Popesso C., Fontolan G. I litorali e la laguna del Friuli Venezia Giulia, in Marchigiani E., Centis L., Giannotti E., Maragno D. (a cura di), *Tutto cambia: una diversa mobilità tra acque e terre: Verso progetti di territorio per l’Alto Adriatico e la regione Friuli Venezia Giulia*, vol.2, cap.2. Conegliano: Anteferma, 2025. In prep.
- Bezzi A., Casagrande G., Fracaros S., Martinucci D., Pillon S., Popesso C., **Spadotto S.**, Sponza S., Fontolan G. La gestione dei sedimenti lagunari: conflitti tra usi degli spazi marittimi e dinamiche naturali. in Marchigiani E., Centis L., Giannotti E., Maragno D. (a cura di), *Tutto cambia: una diversa mobilità tra acque e terre: Verso progetti di territorio per l’Alto Adriatico e la regione Friuli Venezia Giulia*, vol.2, cap.4. Conegliano: Anteferma, 2025. In prep.

- **Spadotto S.**, Bezzi, A., Fracaros S., Casagrande G., Pillon S., Popesso C., Fontolan G. Grado: una realtà dinamica tra mare e laguna, in Marchigiani E., Centis L., Giannotti E., Maragno D. (a cura di), *Tutto cambia: una diversa mobilità tra acque e terre: Verso progetti di territorio per l'Alto Adriatico e la regione Friuli Venezia Giulia*, vol.2, cap.4. Conegliano: Anteferma, 2025. In prep.

water

MDPI

Article

Remote Measurement of Tide and Surge Using a Deep Learning System with Surveillance Camera Images

Gaetano Sabato [1], Giovanni Scardino [1], Alok Kushabaha [1,2,*], Giulia Casagrande [3], Marco Chirivì [4], Giorgio Fontolan [3], Saverio Fracaros [3], Antonio Luparelli [4], Sebastian Spadotto [3] and Giovanni Scicchitano [1]

1 Department of Earth and Geoenvironmental Sciences, University of Bari, Via Orabona 4, 70125 Bari, Italy
2 Istituto Universitario di Studi Superiori (IUSS)—School for Advanced Studies, Piazza della Vittoria 15, 27100 Pavia, Italy
3 Department of Mathematics, Informatics and Geosciences, University of Trieste, Via Weiss 2, 34128 Trieste, Italy
4 CETMA (Centro di Ricerca Europeo di Tecnologie Design e Materiali), S.S.7 Km.706 + 030 c/o Cittadella della Ricerca, 72100 Brindisi, Italy
* Correspondence: alok.kushabaha@iusspavia.it

Abstract: The latest progress in deep learning approaches has garnered significant attention across a variety of research fields. These techniques have revolutionized the way marine parameters are measured, enabling automated and remote data collection. This work centers on employing a deep learning model for the automated evaluation of tide and surge, aiming to deliver accurate results through the analysis of surveillance camera images. A mode of deep learning based on the Inception v3 structure was applied to predict tide and storm surges from surveillance cameras located in two different coastal areas of Italy. This approach is particularly advantageous in situations where traditional tide sensors are inaccessible or distant from the measurement point, especially during extreme events that require accurate surge measurements. The conducted experiments illustrate that the algorithm efficiently measures tide and surge remotely, achieving an accuracy surpassing 90% and maintaining a loss value below 1, evaluated through Categorical Cross-Entropy Loss functions. The findings highlight its potential to bridge the gap in data collection in challenging coastal environments, providing valuable insights for coastal management and hazard assessments. This research contributes to the emerging field of remote sensing and machine learning applications in environmental monitoring, paving the way for enhanced understanding and decision-making in coastal regions.

Keywords: deep learning; tide; storm surge; coastal monitoring; convolutional neural network

Citation: Sabato, G.; Scardino, G.; Kushabaha, A.; Casagrande, G.; Chirivì, M.; Fontolan, G.; Fracaros, S.; Luparelli, A.; Spadotto, S.; Scicchitano, G. Remote Measurement of Tide and Surge Using a Deep Learning System with Surveillance Camera Images. *Water* **2024**, *16*, 1365. https://doi.org/10.3390/w16101365

Academic Editor: Jianjun Ni

Received: 10 April 2024
Revised: 30 April 2024
Accepted: 10 May 2024
Published: 11 May 2024

1. Introduction

The rise in global mean sea level, attributed to human-induced climate change [1], is resulting in a global escalation in the frequency of coastal flooding, with a multitude of negative impacts for coastal communities, public safety, and economies [2].

The components of flooding include astronomical and meteorological water levels. The astronomical water level is determined by the tidal cycle, which is primarily caused by the gravitational attraction between the Moon and the Earth. Tides follow a regular pattern and can cause a periodic rise and fall in the water level along coastlines. On the other hand, meteorological water levels are influenced by weather events such as storms, heavy rainfall, or strong winds. These factors can lead to a temporary increase in water level in coastal areas, known as "storm surge". Storm surge can significantly contribute to coastal flooding during extreme weather events. Both of these components can result in an elevation of the water level and contribute to flooding in coastal areas. It is important to consider both factors when evaluating and managing the risk of flooding [3].

Tidal patterns have significant impacts on various aspects of human life and the ecosystem [4]. The positive outcomes of tides include preserving the marine ecosystem, facilitating fishing and harvesting [5], controlling pollution, generating power, and influencing weather circulation [6]. Tides play a vital role in many coastal ecosystems: they influence the habitats, aid in reproductive activities, and support the food chain [7]. In fishing, tides are used to catch fish and harvest seafood, optimizing economic returns [8]. Additionally, they contribute to the generation of renewable energy through tidal energy, harnessing hydraulic forces [9]. Tidal currents impact the circulation of weather, leading to the creation of more favorable climate conditions and contributing to the balance of global temperatures. [10]. They also play a vital role in the movement of sediment along the beach. Phases of high and low tide influence the deposition of sand, gravel, and other particles on the beach [11]. Understanding tides offers opportunities for their optimal utilization in modern society [12].

Significant emphasis must be placed on coastal protection measures in response to storms and the ensuing storm surge.

A storm surge is an anomalous increase in water levels caused by a storm that exceeds the expected astronomical tide. It represents the fluctuation in water level directly influenced by the storm's presence [13].

The primary driver behind storm surges comes from the powerful winds associated with cyclones [14]. The wind patterns surrounding the cloud-free area of a cyclone's 'eye' are determined by a cyclonic circulation through diabatically produced potential vorticity (PV) anomalies in the lower–mid troposphere [15,16]. In offshore areas, this circulation remains largely undisturbed, resulting in minimal signs of storm surge [17]. When the hurricane approaches nearshore areas, the cyclonic circulation is influenced by seabed friction [18], determining the water flow inland [19]. Regarding coastal protection and emergency management, it is important to emphasize that the storm surge can penetrate far inland from the coastline [20,21].

To capture the characteristics of forcing during extreme events and the resulting impacts on the coastal environment, a combination of direct methods (e.g., wave buoys, tide gauges, LiDAR surveys) and indirect methods (e.g., webcam or satellite images) have long been utilized. In recent times, the popularity of indirect methods has increased significantly due to their ability to analyze large volumes of data using artificial intelligence techniques.

Machine learning and deep learning [22], two branches of artificial intelligence [23], are proving to be versatile tools in the examination of coastal environments [24]. This, in turn, can facilitate the informed and sustainable planning and management of coastal regions [25]. Such efforts contribute to safeguarding marine ecosystems and enhancing the tourism appeal of beaches [26]. Machine and deep learning enable the analysis of beach areas through the processing of satellite imagery [27] or footage from surveillance cameras [28]. For instance, machine learning algorithms can be employed to recognize and categorize various aspects of coastal landscapes, such as beach morphology, that are influenced by tides and currents [29]. Additionally, deep learning facilitates the creation of specialized algorithms tailored to the detection of specific coastal features, enhancing the precision and efficiency of monitoring and analysis systems [30]. This, in turn, positively influences beach management by enabling a more precise evaluation of a beach's condition and a more timely response to potential emergencies [31].

In this study, we present the results of experiments conducted using an algorithm for automated tide and surge measurement from images captured by a surveillance camera system. Once an image is acquired and submitted to the system, the algorithm is capable of providing the corresponding tidal height and, consequently, the surge [28]. These results are highly useful in areas where the tide sensor is remotely located, necessitating time corrections [32], and in situations of extreme events, such as Mediterranean Hurricanes, where surge measurement becomes valuable.

The tool presented in this paper represents an upgrade of the Convolutional Neural Network (CNN) for Tide Assessment developed in LEUCOTEA [28]. The forecasts pro-

duced by neural networks were compared to the observational data derived from tide gauge records. The previous code was written in MATLAB and used the GoogLeNet model [33]. This latest update is translated into Python [34] and is based on the Inception V3 model developed by Google [35].

The employment of a comprehensive observational system spanning multiple platforms provides the opportunity for real-time feedback on the occurrence of oceanic and atmospheric events. Moreover, this approach would enable the execution of analyses that are typically reliant on in situ sensors [36], thereby circumventing logistical challenges and facilitating the seamless creation of information databases [37].

The paper was organized as follows:

- Section 2 contains the methodology section, where the study areas, datasets, and deep learning models are reported;
- Section 3 presents the results and discussion, including predictions and hyperparameters;
- Section 4 contains the conclusions.

2. Methodology

In this section, we present a detailed overview of the methodologies and techniques employed in this study. We outline the specific approaches adopted for the remote measurement of tides and surges, as well as details of the deep learning system utilized for analysis. Additionally, we discuss the preprocessing steps applied to the surveillance camera images and the training procedures undertaken to optimize the performance of the model. The following subsections provide a comprehensive overview of the methodologies used in this research endeavor.

2.1. Data Acquisition and Territorial Framework

In the preliminary step, the process begins by choosing a coastal region for investigation and assembling a pertinent set of images to effectively portray the entire spectrum of potential tidal values. A substantial quantity of images is essential for conducting a thorough analysis. In our case, we chose two locations in Italy, and the model was trained and tested using images from surveillance cameras.

2.1.1. Site 1: Santa Lucia

The first site is Santa Lucia, located on the Maddalena peninsula in the municipality of Siracusa (SR), southeastern Sicily (Figure 1a). It features numerous distinct characteristics, various residential settlements, several commercial activities, as well as areas of natural and archaeological interest. In 2004, the Plemmirio Marine Protected Area was established to safeguard the surrounding marine environment and its abundant marine fauna. The management of the Marine Area provided the images from the surveillance camera.

The coastal region of south-eastern Sicily extends over approximately 300 km and is experiencing significant erosion, with the shoreline retreating at a rate of about 5 m/year [38]. This region has faced severe storms over the past few decades, experiencing waves that have reached approximately 6 m in height and storm surges surpassing 1 m [39]. The examined coastal region displays a mix of small rocky headlands and low-lying beach systems, often adjacent to coastal lagoons. The impacts of numerous tsunamis have been recorded by studying accumulations of boulders [40,41], high-energy deposits [42], and the stratigraphy of the lagoon areas [43,44]. Furthermore, the region has also been impacted by severe storms, resulting in the displacement of boulders and cobbles along the coastline [40]. Similar to other Mediterranean coastal areas, these storm occurrences have undergone impacts similar to those witnessed in past extreme marine events, such as tsunamis.

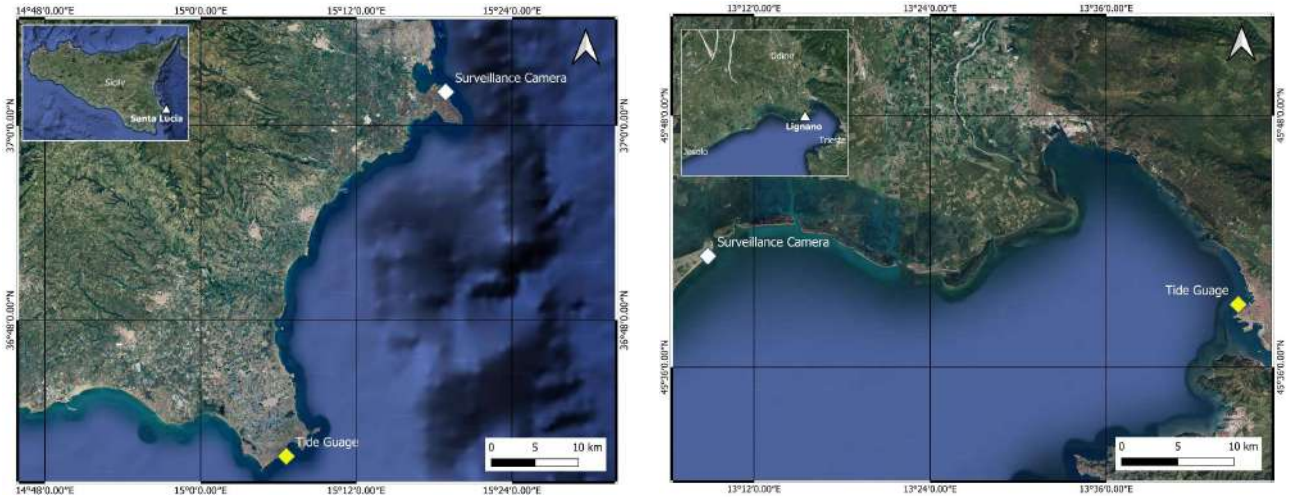

Figure 1. Study areas with surveillance camera locations: (**a**) site 1—Santa Lucia; (**b**) site—2 Lignano.

We also conducted an analysis using data recorded by the Catania wave buoy from the National Wave Network (Rete Ondametrica Nazionale (RON)). The most powerful storm in southeastern Sicily since 1990 was identified, characterized by a substantial wave height (Hs) of around 6.2 m and a peak period (Tp) of 11.3 s. Several medicanes, or Mediterranean hurricanes, have affected the coasts of south-eastern Sicily, and in recent decades, these events have had a greater impact compared to typical seasonal storms. Between 2014 and 2023, ten cyclones passed in the Ionian Sea, with four of them—Qendresa in 2014, Zorbas in 2018, Apollo in 2021, and Helios in 2023 [45]—strongly impacting the coast of south-eastern Sicily. While the Ionian Sea is not typically prone to the formation of tropical cyclones, medicanes result from a process known as Tropical Transition (TT), where an extratropical system transforms into a tropical system or induces a hybrid cyclone [46,47]. However, some studies suggest that climate change may alter medicanes in the future, potentially reducing their frequency but intensifying their impact [48]. Nevertheless, in the Ionian basin, except for 2019, a medicane has crossed the region each year since 2014.

2.1.2. Site 2: Lignano Sabbiadoro

The second site is Lignano Sabbiadoro, a municipality located in the Friuli Venezia Giulia region (Figure 1b). Here, the images, acquired from a webcam placed on the roof of a restaurant overlooking the sea, were provided by the Panomax portal (https://lignano.panomax.com/ (accessed on 4 May 2023)) for tourism in the Friuli Venezia Giulia Region. Despite only having around 7000 inhabitants, it is one of the most important seaside resorts in the Northern Adriatic Sea, with around 3.5 million visitors (ISTAT, 2019). Lignano is located on the peninsula made up of the eastern lobe of the Tagliamento river delta and separates the Adriatic Sea from the Marano and Grado lagoon. The coast, conventionally divided from the Tagliamento river mouth (to the south) to the Lignano inlet (to the north) into the three sectors of Riviera, Pineta and Sabbiadoro, is made up of a single sandy beach approximately 8 km long. The beach has a curvilinear shape: from south to north, the direction rotates progressively clockwise from around 10° N to 45° N at the locality of Sabbiadoro, where the webcam is located, and then rotates in the opposite direction near the tidal inlet. The width of the beach varies from 23 m to 181 m. The seabed facing Sabbiadoro beaches is characterized by the presence of the ebb tidal delta of the Lignano inlet, whose morphological high is evident up to 1600 m from the shoreline, beyond which the depth progressively increases from 2 to 10 m in 1500 m, resulting in an average slope of 3.2‰ [49].

The sediment budget of the shoreface in Sabbiadoro has been positive over the last 20 years [49], although the beach has shown an erosive trend partly compensated by

nourishments and partly by the attempt to protect the beach using seasonal barriers made up of plastic bags filled with sand taken in situ.

The tides in the Northern Adriatic Sea are semi-diurnal, with average mean spring tide and mean neap tide ranges of 78 cm, 105 cm [50], and 22 cm [51], respectively.

The local wind climate is affected by two main winds, "Bora" and "Sirocco". Although the Bora wind (from ENE) is predominant in terms of frequency and strength [52,53], the Sirocco wind (coming from the SSE) is statistically significant, although it holds a subordinate position in terms of strength.

The wave regime tends to exhibit a bimodal pattern due to the prevailing wind conditions. As per data collected from the wave buoy OGS DWRG1 (positioned offshore at coordinates 13.24 E, 45.56 N; 16 m depth), the average significant wave height (Hs) remains below 0.5 m. Instances of Hs exceeding 0.5 m make up 25% of the entire dataset, with prevailing waves originating from the SE (10.7%) and ENE (10.5%). The Sirocco wind contributes to the highest recorded waves, reaching an Hs of 4.4 m [53]. The simultaneous influence of spring tides, seiches, winds, and low atmospheric pressure has the potential to cause a significant elevation in sea level, resulting in a locally recognized surge referred to as "acqua alta".

The storm surges in the Northern Adriatic Sea are mainly related to the Sirocco and secondly to the Bora due to their different fetches. Considering the beach of Lignano, the fetch of the Bora is around 50 km while the Sirocco acts along the entire Adriatic basin for around 800 km, being able to produce greater and more persistent storm surges at the end of the basin [54].

Extreme storm events in the northern Adriatic have been the subject of multiple studies, most of which are associated with the city of Venice due to its important artistic and cultural heritage. The major extreme events were recorded between late October and December (1966, 1979, 2018, and 2019), while the 1986 event occurred in February [55]. Cavaleri et al. [56] studied the event of 29 October 2018, identifying extreme storm surge values above 150 cm, limited by the out-of-phase astronomical tide, and assuming that much more catastrophic consequences would occur in the case of concomitant in-phase factors. Moreover, the authors observed a significant increase in the nearshore sea level associated with the wave set-up and surface wind stress, caused by the progressive decrease in depth shoreward. Ferrarin et al. [57] analyzed the meteorological characteristics of the November 2019 event, comparing it with previous extreme events in 1966, 1979, and 2018. Unlike previous events, characterized by high storm surges associated with a low astronomical tidal range, the 2019 event showed how the in-phase concomitance of even non-extreme factors can lead to an exceptional rise in sea level. Mel et al. [58] analyzed the event at the end of November 2022, associated with a persistent low pressure over central Italy which generated both Sirocco winds along the Adriatic and Bora winds over the northern Adriatic, causing storm surges of 173 cm (refer to the Punta della Salute gauge datum, ZMPS) and wave heights of up to 4.5 m at the CNR platform, located 12 m offshore from the Venice lagoon.

The barrier islands of the adjacent Marano and Grado lagoon were also affected by such extreme events, and were frequently overwashed and breached with the formation of multiple washover fans [59].

2.2. Creation of the Dataset

The dataset creation constitutes the initial step and is essential for training the Convolutional Neural Network (CNN). This task is typically performed manually by the research team. In our case, we tested the system using two different datasets of images during significant meteorological events. In each frame, a value was assigned based on the real data recorded during the event from the tide gauge sensors. Starting from the historical data that were acquired, the overall range of tidal values in the considered area is divided into intervals, with each representing a membership class. The amplitude value must be as representative as possible of the event type to consider the excursion values of the

site. For site 1, a minimum value of −81.4 cm and a maximum value of 89.9 cm were considered, while for site 2, a minimum value of −20 cm and a maximum value of 145 cm were considered. The image datasets were split into groups based on the membership class of the corresponding tidal value. To address class imbalances (Figure 2), a function was implemented to calculate the respective weights for each class. These weights were then converted into a dictionary where the keys represent the unique classes in the training data and the values correspond to the class weights. This approach helps prevent the model from being overly influenced by more represented classes at the expense of less represented ones. The characteristics of each dataset are listed in Table 1.

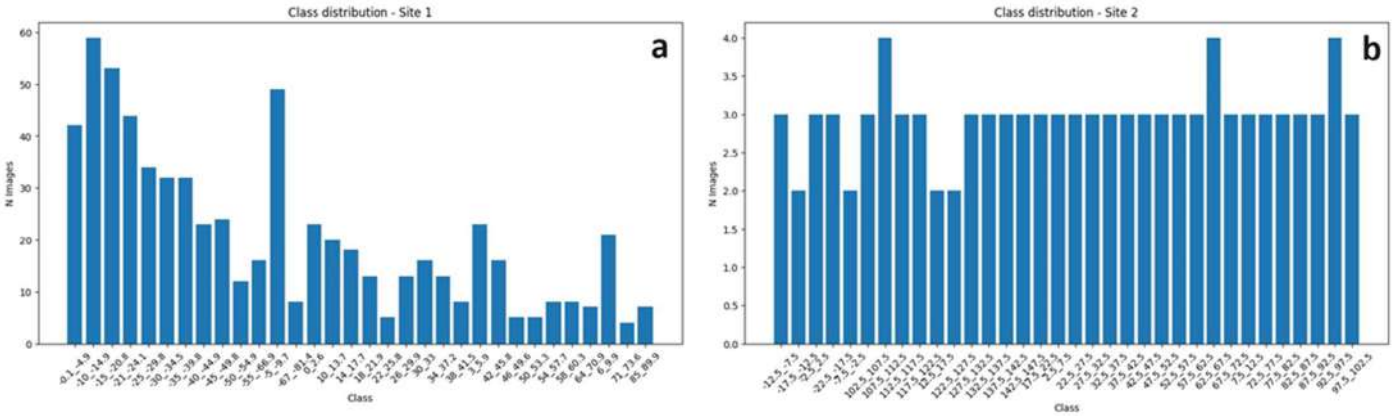

Figure 2. Dataset class distribution: (**a**) Santa Lucia; (**b**) Lignano Sabbiadoro.

Since there were no sensors at the specific sites, the nearest ones were used, and all corrections for tidal lag were applied: in the case of Santa Lucia, Capo Passero's (SR) tide gauge was used, while Trieste's tide gauge was used for Lignano. For Santa Lucia, the images of the impact of the cyclone Helios (8–11 February 2023) were analyzed (Figure 3a). In the case of Lignano, a severe storm surge that occurred between 21 November and 23 November 2022 was analyzed (Figure 3b).

Figure 3. Images extracted from the surveillance cameras in the following areas: (**a**) Santa Lucia; (**b**) Lignano Sabbiadoro.

Table 1. Dataset and site information.

Name Dataset	Basement	N° Imgs	Train	Test	N° Classes	Site	Coordinates UTM Wgs84
Santa Lucia	Rock	3.266	2.605	661	32	Santa Lucia (SR), Italy	37°02′03.19″ N 15°18′54.41″ E
Lignano	Sand	430	248	101	34	Lignano Sabbiadoro (UD), Italy	45°41′18.36″ N 13°08′51.08″ E

2.3. Installation and Requirements

It is necessary to set up the entire script by creating an environment with the necessary and suitable requirements for its proper functioning. The open-source TensorFlow 2 library was used for model training [60]. For convenience and to ensure a better performance, we proceeded to install the system on the Google Collaboratory platform, which temporarily provides high-performance workstations [61].

In our case, the features provided by the Google Colab workstation were as follows:

- CPU: Intel Xeon 2.00 GHz (×2)
- GPU: NVIDIA Tesla T4 16 GB
- Driver Version: 525.85.12
- CUDA Version: 12.0
- RAM: 12.7 GB

2.4. Training Model Process and Testing

We opted for the Inception v3 model as our foundation, a convolutional neural network specifically designed for image analysis and object detection [35]. Originally developed as a module for GoogLeNet, it is the third iteration of Google's Inception Convolutional Neural Network. Similar to how ImageNet serves as a classified visual object database [62], Inception assists in object classification within the realm of computer vision. The Inception v3 architecture has found widespread use across various applications [63], and is frequently employed in a "pre-trained" state from ImageNet. One notable application lies within the life sciences field, where it contributes to leukemia research [64–66].

The next step involves training our dataset to enable the system to recognize high tides based on previously organized classes. The images were automatically resized to a dimension of 224 × 224 pixels, and augmentation techniques, including rescale, horizontal and vertical flip, width and height shift, and zoom, were applied. The duration of the computational processes relies on several factors, chiefly the computational capacity. Given that the training of models encompasses CNN and image processing procedures, substantial resource utilization is expected, particularly involving the CPU, GPU, and RAM. We delegated the training to the GPU instead of the CPU, which has specialized functional units such as the 'tensor core' and parallel computing, thereby speeding up processing times [67]. The configuration of hyperparameters represents the second factor affecting both the time required and the accuracy achieved by the trained model [68]. Hyperparameters in a deep learning model are not learned directly through the training process; instead, they are selected manually by the user or through automated hyperparameter search techniques. These parameters play a pivotal role in controlling the model's behavior during training and influencing its generalization capabilities. Examples of hyperparameters include the learning rate, the number of epochs, and the batch size.

Optimal hyperparameter selection is essential to ensure a deep learning model achieves strong generalization capabilities without succumbing to issues like overfitting or underfitting [69]. The hyperparameters used were chosen after repeated fine-tuning and they are as follows: batch Size = 8, Starting LR = 0.003, Epochs = 35.

Image analysis follows a step-by-step procedure incorporating three layers: convolutional layers, pooling layers, and fully connected layers. Two-dimensional convolutional layers are employed to process two-dimensional signals, like images. These layers apply

a convolution kernel to the image, executing convolutions at each position between the kernel and the corresponding image segment. The kernel then shifts by a set number of pixels, referred to as the stride. It is important to consider the stride value, as a small stride can lead to redundant information. To control the output size, zero padding is introduced, which adds a border of zeros (of size l) around the image. The convolutional operations are complemented by an activation function known as the Rectified Linear Unit (ReLU), which is typically applied as an activation layer. This is a common activation function in deep learning neural networks that introduces non-linearity, facilitating the learning of complex models. The advantages of ReLU include its simplicity and computational efficiency, its ability to mitigate the vanishing gradient problem in deep neural networks, and the promotion of sparsity in the representation of outputs, which can be beneficial in certain contexts [70].

Moreover, to normalize each activation across different channels, a cross-channel normalization operation was employed. It improves model performance by ensuring a consistent scale of features, expediting convergence during training, enhancing stability, and acting as an implicit regularization. This process contributes to more efficient and robust model learning [71]. The CNN architecture also incorporates pooling layers, which serve to reduce the dimensionality of the input by subsampling, either through mean-pooling or max-pooling applied to patches of the image. Much like convolutional layers and pooling layers, these work on different parts of the image and incorporate a stride parameter. In the context of this specific deep learning network, 2D max-pooling layers were employed, extracting the maximum values from within the patches [72]. To handle inputs with the same height and width, depth concatenation layers were employed, which concatenate the inputs along the third dimension, representing the channels. The CNN concludes with a fully connected layer, establishing connections between each element of the preceding layer and every element within the softmax layer. The softmax layer, which estimates relative probabilities, is instrumental in determining the ultimate and most probable value. The structural framework of the deep neural network is crafted around Inception modules [33].

The Inception V3 model was trained using a deep learning technique called "transfer learning" [73]. This involves using a pre-trained deep learning model on a large dataset and updating the last layers of the model on a specific dataset of interest [74]. This approach allows the knowledge gained during the pre-training of the model to improve the model's ability to generalize to new data [75]. These modules enable the network to select from various convolutional filter sizes within each block, enhancing its flexibility and adaptability.

The original architecture of Inception v3 was modified to tailor it to this application; the last layer was removed, and a Global Average 2D pooling layer was implemented to allow the CNN to better adapt to the specific case study. This is a special layer employed in Convolutional Neural Networks to compress the input tensor space. Unlike traditional pooling layers with fixed-size windows, Global Average Pooling calculates the average of all values in the feature map, generating a single mean value for each channel. This process reduces the spatial dimensions of the feature map while preserving crucial information about the features. The use of this layer is often considered to reduce the number of parameters in the model, prevent overfitting, and improve generalization. Additionally, it makes the network less sensitive to variations in the position and size of objects in images. Our modified architecture has 313 layers, of which 184 are trainable.

During the training process, the CNN was trained using 70% of the available images for training purposes and the remaining 30% for validation, which is considered by the literature as the optimal partition of the dataset for training these types of CNNs [35,76].

Figure 4 shows the training curves for the model in both case studies.

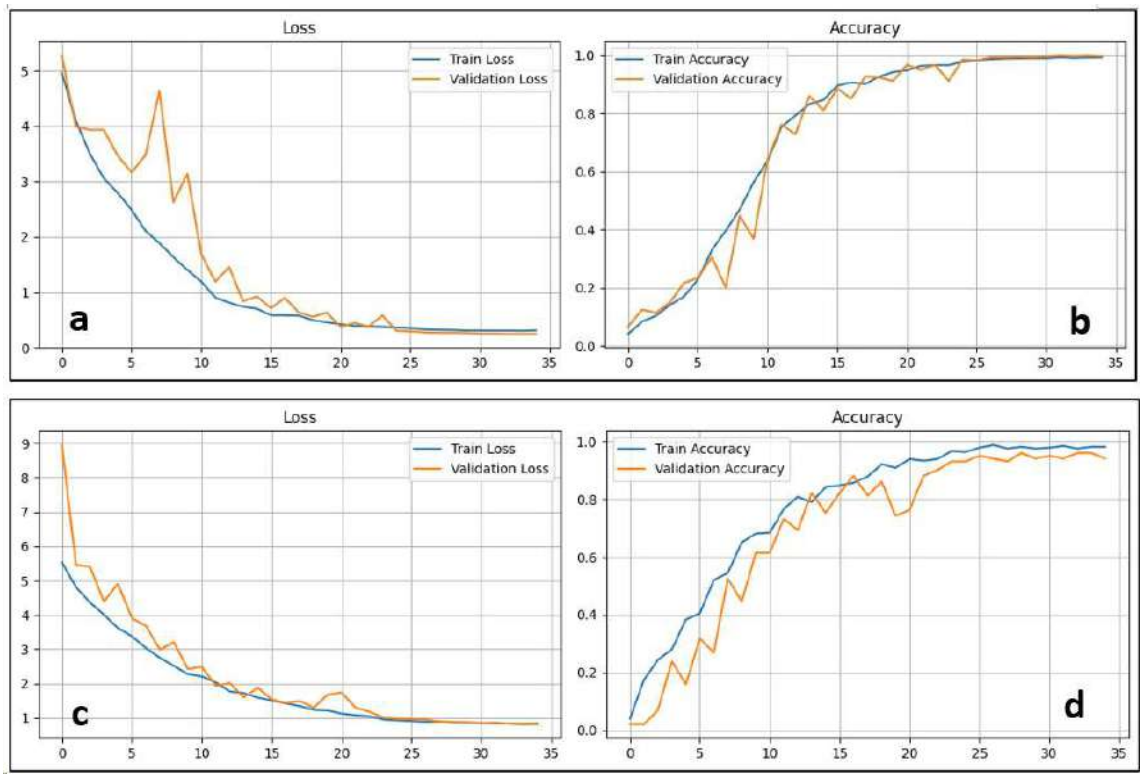

Figure 4. Training curves produced by machine learning model: (**a**) loss values for Santa Lucia; (**b**) accuracy values for Santa Lucia; (**c**) loss values for Lignano Sabbiadoro; (**d**) accuracy values for Lignano Sabbiadoro.

3. Results and Discussion

The CNN outputs deliver the probabilities corresponding to tide classes linked to a specific video frame captured by the webcams. In Figure 5a,b, the probabilities of tide classes related to a given image are illustrated. To depict tide phases across a continuous temporal spectrum, various snapshots were automatically extracted from the video recordings, with tide classes assigned to each image. The CNN achieved an accuracy exceeding 90%, and the Categorical Cross-Entropy Loss function yielded a value below 1 at the conclusion of the iterations. Detailed results can be found in Table 2. The evaluation of the CNN output metrics involved the examination of the confusion matrix (depicted in Figure 6a,b), which illustrates the relationship between predicted classes (CNN output) and true classes (spatial reference from field surveys). The confusion matrix stands as a commonly employed metric in the domain of classification problem-solving. Its versatility extends to both binary and multiclass classification scenarios. This matrix furnishes a tabulated representation of counts stemming from predicted and actual values [77].

Table 2. Results from training.

Location	Accuracy	Loss
Santa Lucia	99.55%	0.25
Lignano	94.06%	0.88

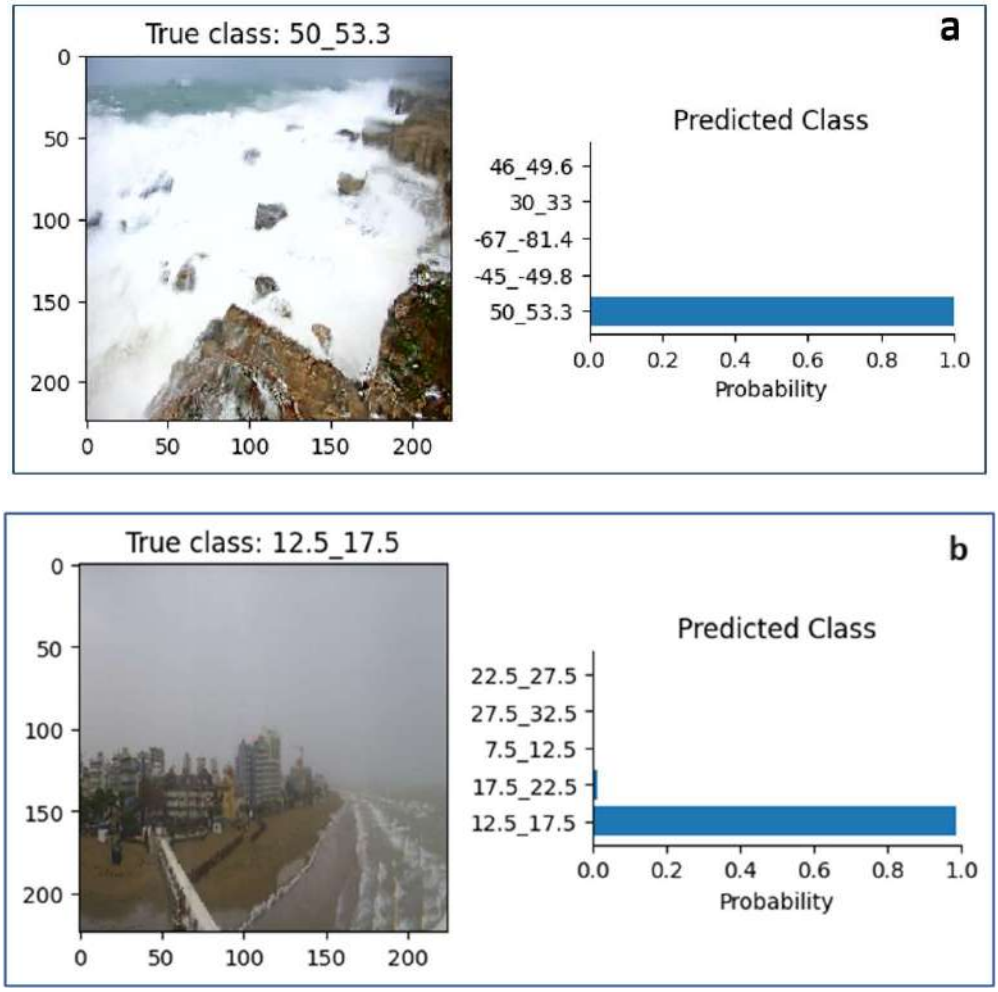

Figure 5. Comparison between the true class and the predicted class for (**a**) Santa Lucia and (**b**) Lignano Sabbiadoro.

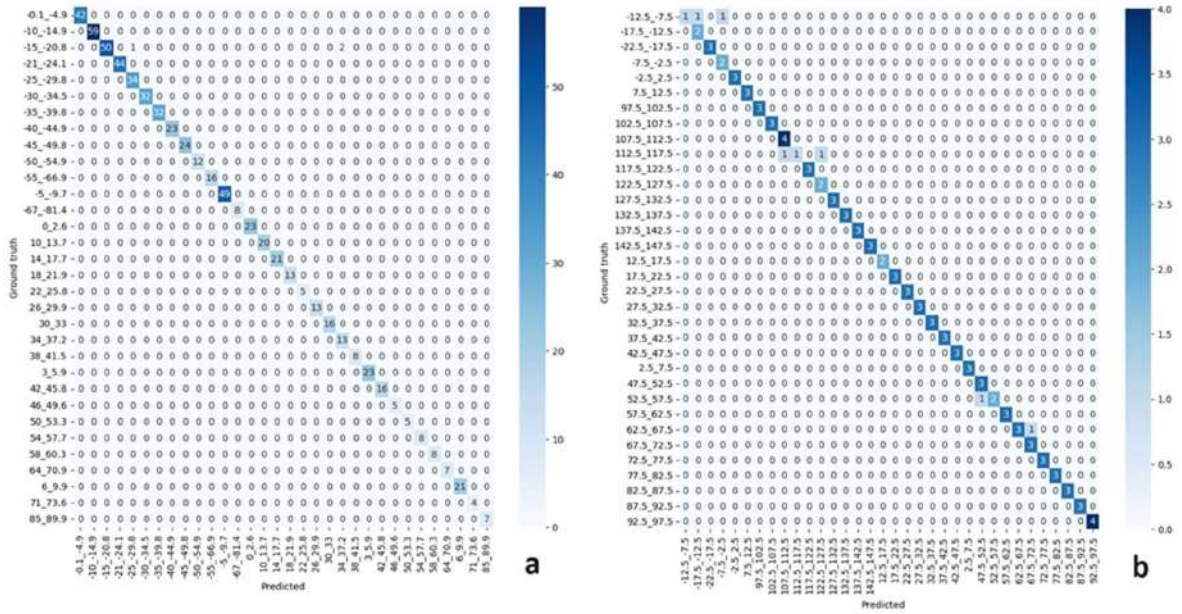

Figure 6. Confusion matrix derived from test datasets for (**a**) Santa Lucia and (**b**) Lignano Sabbiadoro.

As tide classes are mutually exclusive and encompass all potential tide phases, the most probable predicted class was chosen as a dependable representation of tide values. It is worth noting that during storms and medicanes, exceptional values may arise, wherein predicted classes may be linked to higher values than those typically associated with common tide phases.

In addition to considering the accuracy and loss metrics mentioned above, F1 scores in the various classes are presented below for a deeper understanding of the performance of the CNN model. The F1 score combines accuracy and recall through its harmonic mean and offers insight into the model's effectiveness in handling class imbalances [78].

In both cases, the obtained weighted average is significantly higher, over 90%, indicating a good overall performance for all classes.

In particular, for the Santa Lucia site, the F1 scores show a weighted average of 0.9955. Most of the classes in this series achieve perfect scores (1.0). There is a slight decrease in the F1 score for class 2 (0.9709) and class 20 (0.9286). Although these scores are slightly lower than the results obtained by the other classes, they are still considered good and indicate the substantial ability of the model to correctly classify images belonging to the respective classes.

For the Lignano site, the weighted average is 0.9339. Specifically, classes 0 and 9 show lower F1 scores (0.5), suggesting difficulty in accurately predicting these particular tidal classes. This could be attributed to their limited representation in the training data. In contrast, many other classes, such as 2, 4, 5, and 6, achieve perfect scores (1.0), highlighting the excellent performance of the model within these tidal classes. Other classes, such as 1, 3, 24, 25, and 27, show moderate F1 scores ranging from (0.8 to 0.8571), indicating areas where improvements can be made.

Overall, the F1 scores for both sites demonstrate the effectiveness of the model in accurately classifying tidal heights into different categories, revealing areas of strength and scope for additional improvement.

The widespread use of deep learning models integrated with monitoring sensors, and they are becoming a low-cost tool for engineering and oceanographic studies [4,79–81]. On the other hand, using surveillance cameras allows for an increase in the density of data in coastal areas without monitoring stations. Remote sensing data combined with machine learning models have usually been applied to obtain physical features of the coastal areas, like water depth [82,83], storm surge [10,11,84], and hydrological parameters [85]. To date, few studies have focused on the assessment of meteo-marine parameters through deep learning and video monitoring [86–88]. Here, classification techniques using the Inception V3 model allowed us to obtain new observations of tide phases characterizing sandy and rocky coasts.

In summary, the outcomes of the study are influenced by factors such as image quality and landscape complexity. Convolutional neural networks (CNNs) have shown impressive effectiveness in classifying data across diverse applications, but it is important to note that using CNNs requires substantial computational resources. However, the advantages include the high precision in image classification, demonstrated by the elevated F1 scores at specific sites. The efficiency of CNNs is notable due to their parallel processing, making them suitable for large datasets. Additionally, CNNs automate image identification and classification, reducing the need for human intervention, and their customization feature allows for adaptation to specific application requirements through fine-tuning with representative image data.

However, from the evidence, it can be concluded that training the model is sufficient to implement and correlate it to the new environment. Training is necessary only once, after which it will be possible to perform classification of all the images that are inserted to recognize the tide height.

Using a temporal denomination for the images, it is possible to recreate the time-sheet of the extreme event to provide a better understanding of its temporal progression (Figure 7) and also for potential comparison with real data. Regarding Lignano, the images do not

cover the entire 24 h period as the camera does not record during the night. One of the benefits of using systems like this is that they can reduce the workload of the operator, who has to manually analyze and view the images, and obtain almost instantaneous results. This approach could be relevant for the study of extreme events and for measuring hydrodynamic parameters in order to model the high frequency in the coastal dynamic. Similar approaches to the high-frequency dynamic are also applied to predict coastal changes, like shoreline movements [89], sea surface temperature changes [90], and tropical cyclone forecasting [91,92].

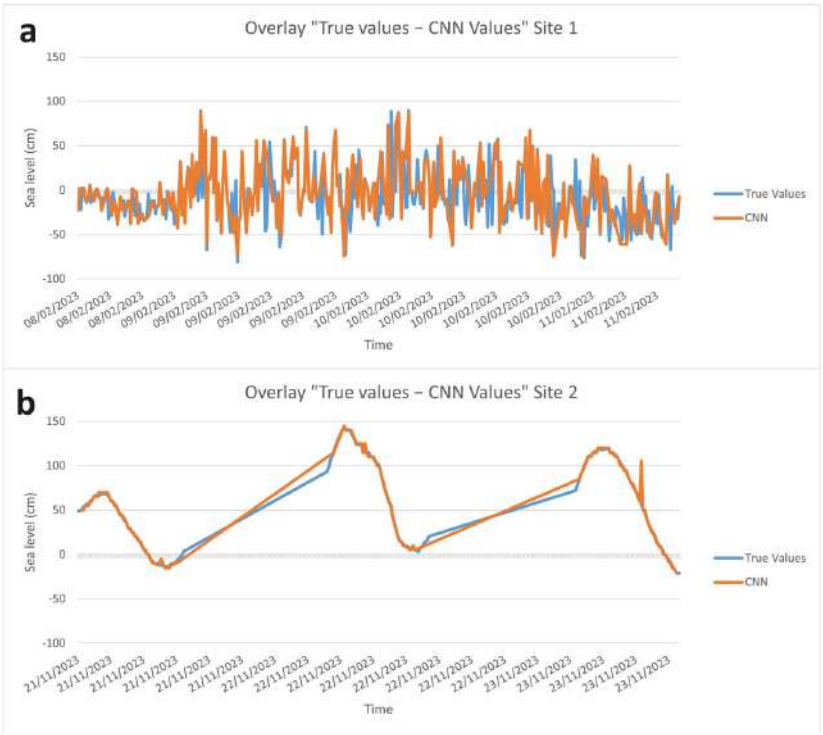

Figure 7. Comparison between extracted tide values using CNN and observed values through tide gauge from different locations (**a**) Santa Lucia and (**b**) Lignano Sabbiadoro.

The field of application is diverse and could be of interest for those institutions that deal with the research and monitoring of beaches. Classification techniques could be integrated with segmentation techniques for beach monitoring [93–95] in order to obtain a reliable assessment of sedimentary balance.

4. Conclusions

In this study, we introduced a deep learning-based system for the automatic measurement and classification of tides in surveillance camera images. Deep learning techniques offer a cost-effective solution for coastal monitoring by increasing the availability of data that are sparsely distributed along coastlines. Furthermore, video footage serves as a valuable resource for gaining insights into high-energy occurrences, exemplified by the impact of Helios in southeastern Sicily in February 2023. Leveraging convolutional neural networks (CNN) in these scenarios enables the evaluation of hydrodynamic characteristics such as storm surge, which are challenging to assess in the field during actual events.

Accumulating a significant volume of data is essential for the development of prediction models that forecast the intensity of future extreme marine events. The application of deep learning in coastal monitoring facilitates the expansion of available datasets, thus proving valuable in this context.

The findings suggest that, even with a limited test dataset, the algorithm is capable of accurately recognizing the value of the tide or the relative surge during extreme events. The

trained models achieved accuracy values exceeding 90% and a loss below 1. The generated confusion matrices also exhibited excellent results, with predicted values rarely deviating from the reference diagonal. Furthermore, by comparing the time-series of actual values with those predicted by the CNN for the two intense weather events, it is evident that the curves follow very similar patterns.

The precision of the outcomes relies on multiple factors, encompassing image quality and the intricacy of objects within the images. Overall, convolutional neural networks have proven highly effective in tasks involving classification and measurement across diverse applications. The incorporation of deep learning technology could yield even more advantages. Introducing such a system would offer the chance to receive instantaneous feedback on the consequences of atmospheric events in real-time. In addition, it would empower remote analysis, eliminating the necessity of in-person visits. This not only addresses logistical challenges but also facilitates the establishment of comprehensive databases of information. Utilizing systems like this could also alleviate the workload of operators who would otherwise need to manually analyze and review images, enabling almost instantaneous results.

Author Contributions: G.S. (Gaetano Sabato): conceptualization, methodology, software, validation, data curation, writing—original draft, visualization. G.S. (Giovanni Scardino): conceptualization, methodology, validation and review. A.K.: software, data curation and review. G.C.: data curation, writing. M.C.: methodology, software, writing and review. G.F.: writing and review, conceptualization and founding. S.F.: data curation, writing. A.L.: methodology, software, validation and review. S.S.: data curation. G.S. (Giovanni Scicchitano): conceptualization, review, supervision, validation and founding. All authors have read and agreed to the published version of the manuscript.

Funding: This research has been funded by the PRIN 2022 PNRR project titled "ARCHIMEDE-MultidisciplinARy approaCH to better define vulnerabIlity and hazard of MEDicanEs along the Ionian coasts of Sicily" (CUP H53D23011380001, Principal Investigator Prof. G. Scicchitano). Part of this study was funded by the consortium iNEST (Interconnected North-Est Innovation Ecosystem) funded by the European Union Next-GenerationEU (Piano Nazionale di Ripresa e Resilienza (PNRR)-Missione 4 Componente 2, Investimento 473 1.5-D.D. 1058 23/06/2022, ECS_00000043).

Data Availability Statement: Name of the code/library: tide_measurement-using-Mechine-Learning-Model-inception-V3; Contact e-mail and phone number: alok.kushabaha@iusspavia.it/0805442604; Hardware requirements: CPU: Intel Xeon 2.00 GHz (x2), GPU: NVIDIA Tesla T4 16GB, Driver Version: 525.85.12, CUDA Version: 12.0, RAM: 12.7 GB; Program language: Python (3.10 version); Software required: Google Colaboratory, Jupiter Notebook; Program size: 803 MB; The source codes are available for downloading at the link: https://github.com/alokkush2024/tide_measurement-using-Mechine-Learning-Model-inception-V3-/tree/tide_measurement_code (accessed on 9 January 2024).

Acknowledgments: This research is part of the activities conducted under the RIPARTI project, specifically the LEUCOTEA initiative (CUP: B83C22004070002), led by Giovanni Scicchitano from the Department of Earth and Environmental Sciences at the University of Bari "Aldo Moro". This research was supported by the Civil Protection of the Autonomous Region of Friuli Venezia Giulia as part of a collaboration with the Department of Mathematics, Informatics, and Geosciences at the University of Trieste.

Conflicts of Interest: The authors declare no conflicts of interest.

References

1. Lee, H.; Calvin, K.; Dasgupta, D.; Krinner, G.; Mukherji, A.; Thorne, P.W.; Trisos, C.; Romero, J.; Aldunce, P.; Barrett, K.; et al. *IPCC, 2023: Climate Change 2023: Synthesis Report. Contribution of Working Groups I, II and III to the Sixth Assessment Report of the Intergovernmental Panel on Climate Change*; Core Writing Team, Lee, H., Romero, J., Eds.; First Intergovernmental Panel on Climate Change (IPCC); IPCC: Geneva, Switzerland, 2023. [CrossRef]
2. Intergovernmental Panel On Climate Change (IPCC). *Climate Change 2022–Impacts, Adaptation and Vulnerability: Working Group II Contribution to the Sixth Assessment Report of the Intergovernmental Panel on Climate Change*, 1st ed.; Cambridge University Press: Cambridge, UK, 2023. [CrossRef]
3. Chaumillon, E.; Bertin, X.; Fortunato, A.B.; Bajo, M.; Schneider, J.; Dezileau, L.; Walsh, J.P.; Michelot, A.; Chauveau, E.; Créach, A.; et al. Storm-induced marine flooding: Lessons from a multidisciplinary approach. *Earth-Sci. Rev.* **2017**, *165*, 151–184. [CrossRef]

4. Jones, O.; Barker, N. Tides, coasts and people: Culture, ecology and sustainability. In *Littoral 2010–Adapting to Global Change at the Coast: Leadership, Innovation, and Investment*; EDP Sciences: Cambridge, UK, 2011. [CrossRef]
5. Bezerra, D.M.M.; Nascimento, D.M.; Ferreira, E.N.; Rocha, P.D.; Mourão, J.S. Influence of tides and winds on fishing techniques and strategies in the Mamanguape River Estuary, Paraíba State, NE Brazil. *An. Acad. Bras. Ciências* **2012**, *84*, 775–788. [CrossRef]
6. Purnaini, R.; Purwono, S. Tidal Influence on water quality of Kapuas Kecil River downstream. *E3S Web Conf.* **2018**, *31*, 04006. [CrossRef]
7. GSGislason & Associates Ltd. British Columbia Seafood Sector and Tidal Water Recreational Fishing: A Strengths, Weaknesses, Opportunities, and Threats Assessment. Technical Report: British Columbia Canada, 2004. Available online: https://www.for.gov.bc.ca/hfd/library/documents/bib105375_sum.pdf (accessed on 20 January 2024).
8. U.S. Department of Energy, Office of Efficiency & Renewable Energy. Powering the blue economy: Exploring opportunities for marine renewable energy in maritime markets. In *Chapter 4-Offshore Marine Aquaculture*; 2019. Available online: https://www.energy.gov/sites/prod/files/2019/03/f61/73355.pdf (accessed on 15 February 2024).
9. Hafner, M.; Luciani, G. (Eds.) *The Palgrave Handbook of International Energy Economics*; Springer International Publishing: Cham, Switzerland, 2022. [CrossRef]
10. Müller, M.; Haak, H.; Jungclaus, J.H.; Sündermann, J.; Thomas, M. The effect of ocean tides on a climate model simulation. *Ocean Model.* **2010**, *35*, 304–313. [CrossRef]
11. Webb, P. Introduction to Oceanography. 2023. Available online: http://rwu.pressbooks.pub/webboceanography (accessed on 7 April 2024).
12. Hicks, S.D. Understanding Tides. Technical Report, U.S. Department of Commerce National Oceanic and Atmospheric Administration National Ocean Service, 2006; 66p. Available online: https://tidesandcurrents.noaa.gov/publications/Understanding_Tides_by_Steacy_finalFINAL11_30.pdf (accessed on 15 February 2024).
13. Von Storch, H.; Woth, K. Storm surges: Perspectives and options. *Sustain. Sci.* **2008**, *3*, 33–43. [CrossRef]
14. Bullock, J.A.; Haddow, G.D.; Coppola, D.P. 3-Hazards. In *Homeland Security*, 2nd ed.; Bullock, J.A., Haddow, G.D., Coppola, D.P., Eds.; Butterworth-Heinemann: Oxford, UK, 2018; pp. 45–66. [CrossRef]
15. Oddo, P.; Bonaduce, A.; Pinardi, N.; Guarnieri, A. Sensitivity of the Mediterranean Sea level to atmospheric pressure and free surface elevation numerical formulation in NEMO. *Geosci. Model Dev.* **2014**, *7*, 3001–3015. [CrossRef]
16. Rooney, A. *Hurricane!* Nature's Fury E-Book Series; Britannica Digital Learning: Chicago, IL, USA, 2012; 32p.
17. Idier, D.; Bertin, X.; Thompson, P.; Pickering, M.D. Interactions between mean sea level, tide, surge, waves and flooding: Mechanisms and contributions to sea level variations at the coast. *Surv. Geophys.* **2019**, *40*, 1603–1630. [CrossRef]
18. Miles, T.; Seroka, G.; Glenn, S. Coastal ocean circulation during hurricane Sandy. *J. Geophys. Res. Ocean.* **2017**, *122*, 7095–7114. [CrossRef]
19. Mulligan, R.P.; Walsh, J.P.; Wadman, H.M. Storm surge and surface waves in a shallow lagoonal estuary during the crossing of a hurricane. *J. Waterw. Port Coast. Ocean Eng.* **2015**, *141*, A5014001. [CrossRef]
20. Ren, H.; Dudhia, J.; Li, H. The size characteristics and physical explanation for the radius of maximum wind of hurricanes. *Atmos. Res.* **2022**, *277*, 106313. [CrossRef]
21. Nott, J. *Extreme Events: A Physical Reconstruction and Risk Assessment*; Cambridge University Press: Cambridge, UK, 2006.
22. Shinde, P.P.; Shah, S. A Review of Machine Learning and Deep Learning Applications. In Proceedings of the 2018 Fourth International Conference on Computing Communication Control and Automation (ICCUBEA), Pune, India, 16–18 August 2018; pp. 1–6. [CrossRef]
23. Ongsulee, P. Artificial intelligence, machine learning and deep learning. In Proceedings of the 15th International Conference on ICT and Knowledge Engineering (ICT&KE), Bangkok, Thailand, 22–24 November 2017. [CrossRef]
24. Pourzangbar, A.; Jalali, M.; Brocchini, M. Machine learning application in modelling marine and coastal phenomena: A critical review. *Front. Environ. Eng.* **2023**, *2*, 1235557. [CrossRef]
25. Moksness, E.; Dahl, E.; Støttrup, J. *Integrated Coastal Zone Management*; John Wiley & Sons: Hoboken, NJ, USA, 2009. [CrossRef]
26. Northrop, E.; Schuhmann, P.; Burke, L.; Fyall, A.; Alvarez, S.; Spenceley, A.; Becken, S.; Kato, K.; Roy, J.; Some, S.; et al. Opportunities for Transforming Coastal and Marine Tourism—Towards Sustainability, Regeneration and Resilience. Technical Report Commissioned by High Level Panel for a Sustainable Ocean Economy (Oceanpanel.org), 2022; 135p. Available online: https://oceanpanel.org/wp-content/uploads/2022/06/22_REP_HLP-Tourism_v6.pdf (accessed on 6 January 2024).
27. Choung, Y.-J.; Jung, D. Comparison of machine and deep learning methods for mapping sea farms using high-resolution satellite image. *J. Coast. Res.* **2021**, *114*, 420–423. [CrossRef]
28. Scardino, G.; Scicchitano, G.; Chirivì, M.; Costa, P.J.M.; Luparelli, A.; Mastronuzzi, G. Convolutional neural network and optical flow for the assessment of wave and tide parameters from video analysis (LEUCOTEA): An innovative tool for coastal monitoring. *Remote Sens.* **2022**, *14*, 2994. [CrossRef]
29. Tsiakos, C.-A.D.; Chalkias, C. Use of machine learning and remote sensing techniques for shoreline monitoring: A review of recent literature. *Appl. Sci.* **2023**, *13*, 3268. [CrossRef]
30. Dang, K.B.; Dang, V.B.; Ngo, V.L.; Vu, K.C.; Nguyen, H.; Nguyen, D.A.; Nguyen, T.D.L.; Pham, T.P.N.; Giang, T.L.; Nguyen, H.D.; et al. Application of deep learning models to detect coastlines and shorelines. *J. Environ. Manag.* **2022**, *320*, 115732. [CrossRef]
31. Merz, B.; Kuhlicke, C.; Kunz, M.; Pittore, M.; Babeyko, A.; Bresch, D.N.; Domeisen, D.I.V.; Feser, F.; Koszalka, I.; Kreibich, H.; et al. Impact forecasting to support emergency management of natural hazards. *Rev. Geophys.* **2020**, *58*, e2020RG000704. [CrossRef]

32. Meli, M.; Olivieri, M.; Romagnoli, C. Sea-level change along the Emilia-Romagna coast from tide gauge and satellite altimetry. *Remote Sens.* **2020**, *13*, 97. [CrossRef]
33. Szegedy, C.; Liu, W.; Jia, Y.; Sermanet, P.; Reed, S.; Anguelov, D.; Erhan, D.; Vanhoucke, V.; Rabinovich, A. Going deeper with convolutions. *arXiv* **2014**, arXiv:1409.4842.
34. Ozgur, C.; Colliau, T.; Rogers, G.; Hughes, Z. MatLab vs. Python vs. R. *J. Data Sci.* **2021**, *15*, 355–372. [CrossRef]
35. Szegedy, C.; Vanhoucke, V.; Ioffe, S.; Shlens, J.; Wojna, Z. Rethinking the inception architecture for computer vision. *arXiv* **1512**, arXiv:1512.00567.
36. Pytharouli, S.; Chaikalis, S.; Stiros, S.C. Uncertainty and bias in electronic tide-gauge records: Evidence from collocated sensors. *Measurement* **2018**, *125*, 496–508. [CrossRef]
37. Ganti, V.; Gehrke, J.; Ramakrishnan, R. Mining very large databases. *Computer* **1999**, *32*, 38–45. [CrossRef]
38. Anzidei, M.; Scicchitano, G.; Scardino, G.; Bignami, C.; Tolomei, C.; Vecchio, A.; Serpelloni, E.; De Santis, V.; Monaco, C.; Milella, M.; et al. Relative sea-level rise scenario for 2100 along the coast of South Eastern Sicily (Italy) by InSAR data, satellite images and high-resolution topography. *Remote Sens.* **2021**, *13*, 1108. [CrossRef]
39. Anzidei, M.; Scicchitano, G.; Tarascio, S.; De Guidi, G.; Monaco, C.; Barreca, G.; Mazza, G.; Serpelloni, E.; Vecchio, A. Coastal retreat and marine flooding scenario for 2100: A case study along the coast of Maddalena peninsula (Southeastern Sicily). *Geogr. Fis. Din. Quat.* **2018**, *41*, 5–16.
40. Scicchitano, G.; Pignatelli, C.; Spampinato, C.R.; Piscitelli, A.; Milella, M.; Monaco, C.; Mastronuzzi, G. Terrestrial laser scanner techniques in the assessment of tsunami impact on the Maddalena peninsula (South-Eastern Sicily, Italy). *Earth Planets Space* **2012**, *64*, 8. [CrossRef]
41. Nandasena, N.A.K.; Scicchitano, G.; Scardino, G.; Milella, M.; Piscitelli, A.; Mastronuzzi, G. Boulder displacements along rocky coasts: A new deterministic and theoretical approach to improve incipient motion formulas. *Geomorphology* **2022**, *407*, 108217. [CrossRef]
42. Scardino, G.; Rizzo, A.; De Santis, V.; Kyriakoudi, D.; Rovere, A.; Vacchi, M.; Torrisi, S.; Scicchitano, G. Insights on the origin of multiple tsunami events affected the archaeological site of Ognina (South-Eastern Sicily, Italy). *Quat. Int.* **2022**, *638–639*, 122–139. [CrossRef]
43. De Martini, P.M.; Barbano, M.S.; Smedile, A.; Gerardi, F.; Pantosti, D.; Del Carlo, P.; Pirrotta, C. A unique 4000 year long geological record of multiple tsunami inundations in the Augusta bay (Eastern Sicily, Italy). *Mar. Geol.* **2010**, *276*, 42–57. [CrossRef]
44. De Martini, P.M.; Barbano, M.S.; Pantosti, D.; Smedile, A.; Pirrotta, C.; Del Carlo, P.; Pinzi, S. Geological evidence for paleotsunamis along eastern Sicily (Italy): An Overview. *Nat. Hazards Earth Syst. Sci.* **2012**, *12*, 2569–2580. [CrossRef]
45. D'Adderio, L.P.; Panegrossi, G.; Dafis, S.; Rysman, J.-F.; Casella, D.; Sanò, P.; Fuccello, A.; Miglietta, M.M. Helios and Juliette: Two falsely acclaimed medicanes. *Preprint* **2023**. [CrossRef]
46. Bentley, A.M.; Keyser, D.; Bosart, L.F. A dynamically based climatology of subtropical cyclones that undergo tropical transition in the North Atlantic basin. *Mon. Weather. Rev.* **2016**, *144*, 2049–2068. [CrossRef]
47. Flaounas, E.; Davolio, S.; Raveh-Rubin, S.; Pantillon, F.; Miglietta, M.M.; Gaertner, M.A.; Hatzaki, M.; Homar, V.; Khodayar, S.; Korres, G.; et al. Mediterranean cyclones: Current knowledge and open questions on dynamics, prediction, climatology and impacts. *Weather Clim. Dyn.* **2022**, *3*, 173–208. [CrossRef]
48. Romera, R.; Gaertner, M.A.; Sánchez, E.; Domínguez, M.; González-Alemán, J.J.; Miglietta, M.M. Climate change projections of medicanes with a large multi-model ensemble of regional climate models. *Glob. Planet. Chang.* **2017**, *151*, 134–143. [CrossRef]
49. Fontolan, G.; Bratus, A.; Bieker, F.; Colombetta, L.; Gallitelli, D.; Lipizer, M.; Sgambati, F.; Bezzi, A.; Casagrande, G.; Fracaros, S.; et al. Piano Coste—Accordo attuativo di collaborazione per lo studio e monitoraggio morfo-sedimentologico dello stato dei litorali della regione Friuli Venezia Giulia finalizzato alla gestione integrata della zona costiera in applicazione alla convenzione quadro tra la Regione Autonoma Friuli Venezia Giulia e l'Università degli Studi di Trieste (DGR 264/2014). 2023. Unpublished Technical Report.
50. Petti, M.; Pascolo, S.; Bosa, S.; Busetto, N. The tidal prism as a dynamic response of a nonlinear harmonic system. *Phys. Fluids* **2023**, *35*, 017124. [CrossRef]
51. Dorigo. La Laguna di Grado e le sue foci. Ricerche e rilievi idrografici. *Uff. Idrogr. Del Magistr. Alle Acque* **1965**, *155*, 231.
52. Bezzi, A.; Pillon, S.; Martinucci, D.; Fontolan, G. Inventory and conservation assessment for the management of coastal dunes, Veneto coasts, Italy. *J. Coast. Conserv.* **2018**, *22*, 503–518. [CrossRef]
53. Regione Autonoma Friuli Venezia Giulia. Piano Regolatore Portuale Del Porto Di Monfalcone Variante Localizzata. Studio Meteomarino. Progettisti: Modimar, SJS Engineering, Archest. Technical Report, 2019. Available online: https://www.regione.fvg.it/rafvg/export/sites/default/RAFVG/ambiente-territorio/pianificazione-gestioneterritorio/FOGLIA9/allegati/Allegato_33_alla_Delibera_2066-2019.pdf (accessed on 26 November 2023).
54. Lionello, P.; Cavaleri, L.; Nissen, K.M.; Pino, C.; Raicich, F.; Ulbrich, U. Severe marine storms in the northern Adriatic: Characteristics and trends. *Phys. Chem. Earth Parts A/B/C* **2012**, *40–41*, 93–105. [CrossRef]
55. Umgiesser, G.; Bajo, M.; Ferrarin, C.; Cucco, A.; Lionello, P.; Zanchettin, D.; Papa, A.; Tosoni, A.; Ferla, M.; Coraci, E.; et al. The prediction of floods in Venice: Methods, models and uncertainty (review article). *Nat. Hazards Earth Syst. Sci.* **2021**, *21*, 2679–2704. [CrossRef]

56. Cavaleri, L.; Bajo, M.; Barbariol, F.; Bastianini, M.; Benetazzo, A.; Bertotti, L.; Chiggiato, J.; Davolio, S.; Ferrarin, C.; Magnusson, L.; et al. The October 29, 2018 storm in Northern Italy—An exceptional event and its modeling. *Prog. Oceanogr.* **2019**, *178*, 102178. [CrossRef]
57. Ferrarin, C.; Bajo, M.; Benetazzo, A.; Cavaleri, L.; Chiggiato, J.; Davison, S.; Davolio, S.; Lionello, P.; Orlić, M.; Umgiesser, G. Local and large-scale controls of the exceptional Venice floods of November 2019. *Prog. Oceanogr.* **2021**, *197*, 102628. [CrossRef]
58. Mel, R.A.; Coraci, E.; Morucci, S.; Crosato, F.; Cornello, M.; Casaioli, M.; Mariani, S.; Carniello, L.; Papa, A.; Bonometto, A.; et al. Insights on the extreme storm surge event of the 22 November 2022 in the Venice Lagoon. *J. Mar. Sci. Eng.* **2023**, *11*, 1750. [CrossRef]
59. Casagrande, G.; Bezzi, A.; Fracaros, S.; Martinucci, D.; Pillon, S.; Salvador, P.; Sponza, S.; Fontolan, G. Quantifying transgressive coastal changes using UAVs: Dune migration, overwash recovery, and barrier flooding assessment and interferences with human and natural assets. *J. Mar. Sci. Eng.* **2023**, *11*, 1044. [CrossRef]
60. Abadi, M.; Agarwal, A.; Barham, P.; Brevdo, E.; Chen, Z.; Citro, C.; Corrado, G.S.; Davis, A.; Dean, J.; Devin, M.; et al. TensorFlow: Large-Scale Machine Learning on Heterogeneous Distributed Systems. 2015. Available online: http://download.tensorflow.org/paper/whitepaper2015.pdf (accessed on 5 March 2024).
61. Carneiro, T.; Medeiros Da NóBrega, R.V.; Nepomuceno, T.; Bian, G.-B.; De Albuquerque, V.H.C.; Filho, P.P.R. Performance analysis of google colaboratory as a tool for accelerating deep learning applications. *IEEE Access* **2018**, *6*, 61677–61685. [CrossRef]
62. Yu, Z.; Dong, Y.; Cheng, J.; Sun, M.; Su, F. Research on face recognition classification based on improved GoogleNet. *Secur. Commun. Netw.* **2022**, *2022*, 7192306. [CrossRef]
63. Warkar, K.V.; Pandey, A.B. A survey on multiclass image classification based on Inception-v3 transfer learning model. *Int. J. Res. Appl. Sci. Eng. Technol.* **2021**, *9*, 169–172. [CrossRef]
64. Anilkumar, K.K.; Manoj, V.J.; Sagi, T.M. Automated detection of leukemia by pretrained deep neural networks and transfer learning: A comparison. *Med. Eng. Phys.* **2021**, *98*, 8–19. [CrossRef]
65. Mulya, R.F.; Utami, E.; Ariatmanto, D. Classification of acute lymphoblastic leukemia based on white blood cell images using inceptionv3 model. *J. RESTI (Rekayasa Sist. Dan Teknol. Inf.)* **2023**, *7*, 947–952. [CrossRef]
66. Ramaneswaran, S.; Srinivasan, K.; Vincent, P.M.D.R.; Chang, C.-Y. Hybrid Inception v3 XGBoost model for acute lymphoblastic leukemia classification. *Comput. Math. Methods Med.* **2021**, *2021*, 2577375. [CrossRef]
67. Raihan, M.A.; Goli, N.; Aamodt, T. Modeling deep learning accelerator enabled GPUs. IEEE International Symposium on Performance Analysis of Systems and Software (ISPASS). *arXiv* **2019**, arXiv:1811.08309.
68. Yang, L.; Shami, A. On hyperparameter optimization of machine learning algorithms: Theory and practice. *Neurocomputing* **2020**, *415*, 295–316. [CrossRef]
69. Zhang, H.; Zhang, L.; Jiang, Y. Overfitting and underfitting analysis for deep learning based end-to-end communication systems. In Proceedings of the 11th International Conference on Wireless Communications and Signal Processing (WCSP), Xi'an, China, 23–25 October 2019; pp. 1–6. [CrossRef]
70. Agarap, A.F. Deep learning using rectified linear units (ReLU). *arXiv* **2019**, arXiv:1803.08375.
71. Shanker, M.; Hu, M.Y.; Hung, M.S. Effect of data standardization on neural network training. *Omega* **1996**, *24*, 385–397. [CrossRef]
72. Gholamalinezhad, H.; Khosravi, H. Pooling methods in deep neural networks, a review. *arXiv* **2020**, arXiv:2009.07485.
73. Han, D.; Liu, Q.; Fan, W. A new image classification method using CNN transfer learning and web data augmentation. *Expert Syst. Appl.* **2018**, *95*, 43–56. [CrossRef]
74. Zhuang, F.; Qi, Z.; Duan, K.; Xi, D.; Zhu, Y.; Zhu, H.; Xiong, H.; He, Q. A comprehensive survey on transfer learning. *arXiv* **2020**, arXiv:1911.02685.
75. Shin, H.-C.; Roth, H.R.; Gao, M.; Lu, L.; Xu, Z.; Nogues, I.; Yao, J.; Mollura, D.; Summers, R.M. Deep convolutional neural networks for computer-aided detection: CNN architectures, dataset characteristics and transfer learning. *IEEE Trans. Med. Imaging* **2016**, *35*, 1285–1298. [CrossRef]
76. Götz, T.I.; Göb, S.; Sawant, S.; Erick, X.F.; Wittenberg, T.; Schmidkonz, C.; Tomé, A.M.; Lang, E.W.; Ramming, A. Number of necessary training examples for neural networks with different number of trainable parameters. *J. Pathol. Inform.* **2022**, *13*, 100114. [CrossRef]
77. Kulkarni, A.; Chong, D.; Batarseh, F.A. 5-Foundations of data imbalance and solutions for a data democracy. In *Data Democracy. At the Nexus of Artificial Intelligence, Software Development, and Knowledge Engineering*; Batarseh, F.A., Yang, R., Eds.; Academic Press: Cambridge, MA, USA, 2020; pp. 83–106. [CrossRef]
78. Huang, H.; Xu, H.; Wang, X.; Silamu, W. Maximum F1-score discriminative training criterion for automatic mispronunciation detection. *IEEE/ACM Trans. Audio Speech Lang. Process.* **2015**, *23*, 787–797. [CrossRef]
79. Yin, L.; Wang, L.; Li, T.; Lu, S.; Tian, J.; Yin, Z.; Li, X.; Zheng, W. U-Net-LSTM: Time Series-Enhanced Lake Boundary Prediction Model. *Land* **2023**, *12*, 1859. [CrossRef]
80. Sabato, G.; Scardino, G.; Kushabaha, A.; Chirivi, M.; Luparelli, A.; Scicchitano, G. Automatic Seagrass Banquettes Detection from Surveillance Camera Images with Detectron2. *Geogr. Fis. E Din. Quat.* **2023**, *45*, 229–235. [CrossRef]
81. Ibaceta, R.; Almar, R.; Catalán, P.A.; Blenkinsopp, C.E.; Almeida, L.P.; Cienfuegos, R. Assessing the Performance of a Low-Cost Method for Video-Monitoring the Water Surface and Bed Level in the Swash Zone of Natural Beaches. *Remote Sens.* **2018**, *10*, 49. [CrossRef]

82. Al Najar, M.; Thoumyre, G.; Bergsma, E.; Almar, R.; Benshila, R.; Wilson, D. Satellite Derived Bathymetry Using Deep Learning. *Mach. Learn.* **2023**, *112*, 1107–1130. [CrossRef]
83. Zhou, G.; Su, S.; Xu, J.; Tian, Z.; Cao, Q. Bathymetry Retrieval From Spaceborne Multispectral Subsurface Reflectance. *IEEE J. Sel. Top. Appl. Earth Obs. Remote Sens.* **2023**, *16*, 2547–2558. [CrossRef]
84. Chen, W.; Liu, W.; Liang, H.; Jiang, M.; Dai, Z. Response of Storm Surge and M2 Tide to Typhoon Speeds along Coastal Zhejiang Province. *Ocean Eng.* **2023**, *270*, 113646. [CrossRef]
85. Zhang, K.; Li, Y.; Yu, Z.; Yang, T.; Xu, J.; Chao, L.; Ni, J.; Wang, L.; Gao, Y.; Hu, Y.; et al. Xin'anjiang Nested Experimental Watershed (XAJ-NEW) for Understanding Multiscale Water Cycle: Scientific Objectives and Experimental Design. *Engineering* **2022**, *18*, 207–217. [CrossRef]
86. Andriolo, U.; Mendes, D.; Taborda, R. Breaking Wave Height Estimation from Timex Images: Two Methods for Coastal Video Monitoring Systems. *Remote Sens.* **2020**, *12*, 204. [CrossRef]
87. Callens, A.; Morichon, D.; Liria, P.; Epelde, I.; Liquet, B. Automatic Creation of Storm Impact Database Based on Video Monitoring and Convolutional Neural Networks. *Remote Sens.* **2021**, *13*, 1933. [CrossRef]
88. Davidson, M.A.; Aarninkhof, S.G.J.; Van Koningsveld, M.; Holman, R.A. Developing Coastal Video Monitoring Systems in Support of Coastal Zone Management. *J. Coast. Res.* **2006**, *39*, 49–56.
89. Calkoen, F.; Luijendijk, A.; Rivero, C.R.; Kras, E.; Baart, F. Traditional vs. Machine-Learning Methods for Forecasting Sandy Shoreline Evolution Using Historic Satellite-Derived Shorelines. *Remote Sens.* **2021**, *13*, 934. [CrossRef]
90. Xiao, C.; Chen, N.; Hu, C.; Wang, K.; Xu, Z.; Cai, Y.; Xu, L.; Chen, Z.; Gong, J. A Spatiotemporal Deep Learning Model for Sea Surface Temperature Field Prediction Using Time-Series Satellite Data. *Environ. Model. Softw.* **2019**, *120*, 104502. [CrossRef]
91. Giffard-Roisin, S.; Yang, M.; Charpiat, G.; Kumler Bonfanti, C.; Kégl, B.; Monteleoni, C. Tropical Cyclone Track Forecasting Using Fused Deep Learning from Aligned Reanalysis Data. *Front. Big Data* **2020**, *3*, 1. [CrossRef]
92. Jiang, G.-Q.; Xu, J.; Wei, J. A Deep Learning Algorithm of Neural Network for the Parameterization of Typhoon-Ocean Feedback in Typhoon Forecast Models. *Geophys. Res. Lett.* **2018**, *45*, 3706–3716. [CrossRef]
93. Diakogiannis, F.I.; Waldner, F.; Caccetta, P.; Wu, C. ResUNet-a: A Deep Learning Framework for Semantic Segmentation of Remotely Sensed Data. *ISPRS J. Photogramm. Remote Sens.* **2020**, *162*, 94–114. [CrossRef]
94. Sabato, G.; Scardino, G.; Kushabaha, A.; Chirivi, M.; Luparelli, A.; Scicchitano, G. Deep Learning-Based Segmentation Techniques for Coastal Monitoring and Seagrass Banquette Detection. In Proceedings of the 2023 IEEE International Workshop on Metrology for the Sea; Learning to Measure Sea Health Parameters (MetroSea), La Valletta, Malta, 4–6 October 2023; pp. 524–527.
95. Yang, T.; Jiangde, S.; Hong, Z.; Zhang, Y.; Han, Y.; Zhou, R.; Wang, J.; Yang, S.; Tong, X.; Kuc, T. Sea-Land Segmentation Using Deep Learning Techniques for Landsat-8 OLI Imagery. *Mar. Geod.* **2020**, *43*, 105–133. [CrossRef]

remote sensing

MDPI

Article

Coastal Storm-Induced Sinkholes: Insights from Unmanned Aerial Vehicle Monitoring

Alice Busetti, Christian Leone, Amerigo Corradetti, Saverio Fracaros, Sebastian Spadotto, Pietro Rai, Luca Zini and Chiara Calligaris *

Department of Mathematics, Informatics and Geosciences, University of Trieste, 34127 Trieste, Italy; abusetti@units.it (A.B.); christian.leone@units.it (C.L.); amerigo.corradetti@units.it (A.C.); saverio.fracaros@phd.units.it (S.F.); sebastian.spadotto@phd.units.it (S.S.); pietro.rai@phd.units.it (P.R.); zini@units.it (L.Z.)

* Correspondence: calligar@units.it

Abstract: In recent decades, the scientific community has increasingly focused on extreme events linked to climate change, which are leading to more intense and frequent natural disasters. The Mediterranean can be considered a hotspot where the effects of these changes are expected to be more intense compared to other regions of the planet. Italy is not exempt; in fact, with its extensive shoreline, it is particularly vulnerable, especially to high sea levels and coastal erosions. In this framework, from late October to early November 2023, six storm surges occurred in the Gulf of Trieste (NE Italy). These events, characterized by winds from 190°N to 220°N and the significant wave height, which reached up to 1.81 m nearshore—an uncommon meteorological condition in the northern Adriatic Sea—caused the occurrence of eight coastal sinkholes and substantial damages to man-made structures. Thanks to Unmanned Aerial Vehicles (UAVs) and their derived products (high-resolution orthomosaics, Digital Elevation Models—DEMs, and point clouds), it was possible to study these features over time, enabling long-term coastal dynamics monitoring, which can be crucial for timely and effective response and restoration efforts.

Keywords: coastal sinkholes; climate changes; UAV monitoring; high-resolution orthomosaics; DEMs; point clouds; wave modelling; geological hazard; Italy

Citation: Busetti, A.; Leone, C.; Corradetti, A.; Fracaros, S.; Spadotto, S.; Rai, P.; Zini, L.; Calligaris, C. Coastal Storm-Induced Sinkholes: Insights from Unmanned Aerial Vehicle Monitoring. *Remote Sens.* **2024**, *16*, 3681. https://doi.org/10.3390/rs16193681

Academic Editor: Paraskevas Tsangaratos

Received: 29 August 2024
Revised: 26 September 2024
Accepted: 28 September 2024
Published: 2 October 2024

1. Introduction

The First Report on the Climate and Environmental Change Assessment (MedECC) [1] highlights that the Mediterranean is warming 20% faster than the global average [2–4], affecting both terrestrial and marine environments. This makes it a hotspot [5] where the effects of climate change are expected to be more intense compared to other regions of the planet [6,7]. Within this context, scientists unanimously agree that coastal areas are among the most impacted: even a small increase in sea level can have devastating effects on coastal habitats [4,8,9], leading to the loss of sandy shores and causing damage to settlements, infrastructure, and ecosystems [10–13].

In recent years, the Mediterranean basin has experienced an increase in both the intensity and frequency of coastal flooding events [14–16]. Therefore, direct impacts generated by storms hold significant social and scientific interest within this area [17–23]. This interest is not solely due to sea level rise [24]; it is also correlated with the growing population, considering that about 75% of the Mediterranean inhabitants are concentrated along coastal areas [25], and this percentage is expected to increase further in the future [10,26]. However, the critical issues are not only limited to low-lying coasts. Rising sea levels and wave activity could also exacerbate erosive phenomena even on typically high, rocky coasts [27]. In this regard, a possible effect of storm surges is a worldwide little-known phenomenon called coastal sinkholes [28,29]. Sinkholes are closed, depressed landforms that can form suddenly due to a collapse or which can have a lower development as in the

suffosion processes or in the dissolution ones [28]. These features (intended as subsidence sinkholes—*sensu* [28]) can significantly affect the geomorphological evolution of coastlines by controlling the formation and preferential orientation of bays and inlets as observed in the Apulia region (SE Italy) and Malta Island [30–40]. Despite their importance, these phenomena have caught little interest in the scientific community while they generally become trending topics in local news (Table 1 and Figure 1).

Table 1. Recent coastal sinkholes occurred around the world and appeared on the news.

Location	Date	Dimension	Causes	References
Scotland	4 February 2021	Diameter: 3 m	storm	[41]
Scotland	30 October 2023	Diameter: 5 m	storm	[42]
England	7 October 2019	Axis: 2.4 × 6 m Depth: 2.4 m	very heavy rainfall combined with the highest tide of the year	[43]
England	10 January 2022	Diameter: 12 m	coastal erosion	[44]
Australia	10 June 2021		ongoing coastal erosion	[45]
Oregon (USA)	22 January 2023	Diameter: 6 m Depth: 4.5 m	coastal erosion	[46]
Oregon (USA)	8 May 2023	Diameter: 3 m	coastal erosion	[47]
Italy (Otranto)			progressive erosion by sea wave action	[28]
Italy (Sicily)	11 December 2021		coastal erosion	[48]
Italy (Sicily)	28 November 2023		floods	[49]
Italy (Naples)	November 2023		persistent rainfall and high tide	[50]

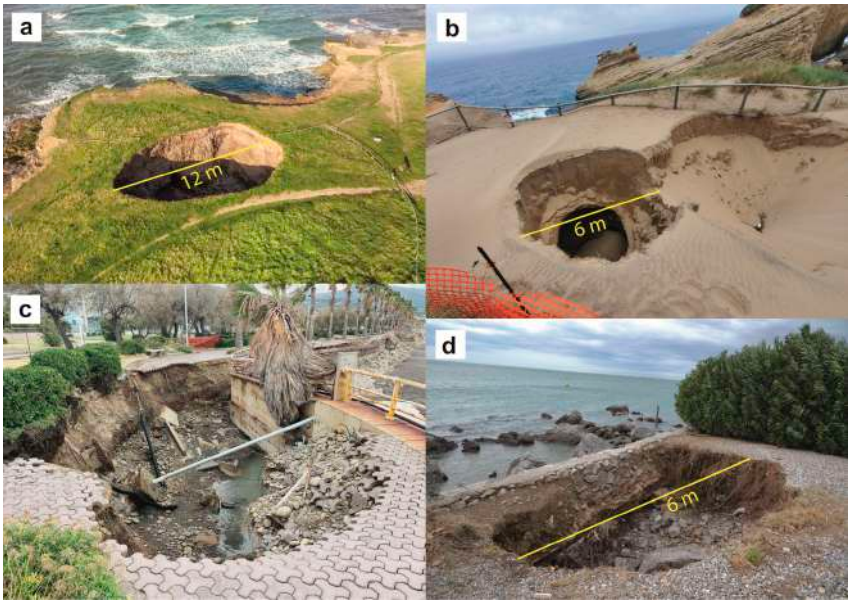

Figure 1. Recent coastal sinkhole worldwide: (**a**) Aerial view of Souter sinkhole and surrounding coastal landscape in Sunderland, England (photo credits: National Trust Images/Annapurna Mellor, Souter Lighthouse and The Leas, Tyne and Wear); (**b**) Sinkhole formed on January 2023 in Cape Kiwanda State Park, Oregon (photo credits: Oregon Parks and Recreation Department Media Hub); (**c**) Sinkhole due to a storm surge event on November 2023 in Sant'Agata di Militello (Sicily, Italy) (photo credits: "In Alto Mare-Sant'Agata di Militello" [49]; (**d**) Sinkhole formed at the Sistiana Bay (Friuli Venezia Giulia, Italy) after a storm surge on October 2023 (photo credits: Busetti A).

The occurrence and evolution of sinkholes, typically associated with inland environments due to the presence of carbonates and evaporites ([28,51–56], and all the references within), can be monitored through the use of tools such as Unmanned Aerial Vehicles (UAVs). UAVs facilitate frequent, rapid, accurate, and low-cost surveying [57,58]. UAVs

and particularly the digital photogrammetry technique relying on the well-known Structure from Motion-Multi View Stereo (SfM-MVS) photogrammetry workflow [59] have been used to produce terrain models for predictive purposes (e.g., [60–62]) and to conduct post-event assessments (e.g., [63]). These technologies were also employed to monitor the impact of extreme events on anthropized areas (e.g., [64]) and, particularly, have recently been used for surveys (e.g., [65–69]) and the assessment of erosive effects and post-event morphological impacts (Rapid Environmental Assessment—REA) on low coasts [70,71]. Despite this broad application of UAVs in various contexts, to the authors' knowledge, UAVs have never been used to investigate storm-induced coastal sinkholes and their evolution, as proposed in the present paper. This study focused on the Northern Adriatic Sea (the NE of the Mediterranean Sea) and specifically on the Gulf of Trieste (Figure 2), which experienced significant meteorological and marine phenomena along high and urbanized coasts, such as the event that occurred in November 1969 [72]. More recently, in late October and early November 2023, a similar event occurred in the same areas, severely affecting the localities of Sistiana Mare and Barcola. This event resulted in substantial damage to infrastructure, buildings, and beach facilities, as well as the formation of several coastal sinkholes. To assess the evolution of the latter, high-resolution (HR) orthomosaics, Digital Elevation Models (DEMs), and point clouds were created from UAV imagery and compared. Several UAV surveys were carried out between September 2023 and February 2024. Furthermore, for the sake of data reproducibility and future comparisons, as well as to better document the phenomena, three additional 3D models of the storm-induced sinkholes were produced.

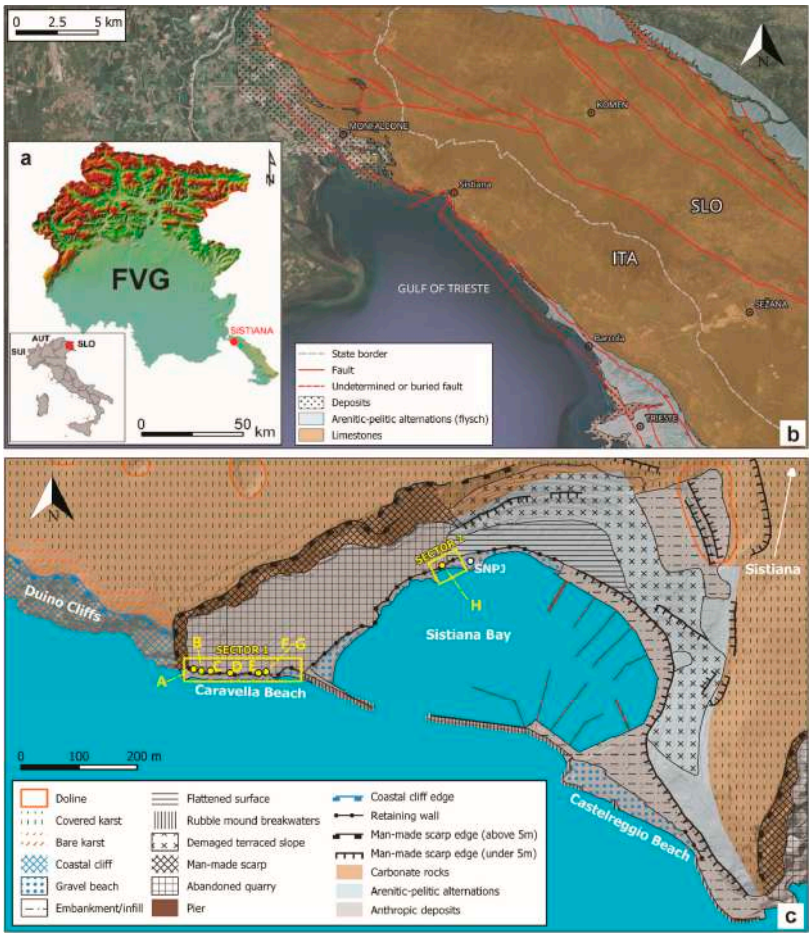

Figure 2. Study area location: (**a**) Friuli Venezia Giulia (FVG) region; (**b**) simplified lithological map of part of the Classical Karst Region; (**c**) geomorphological map of the study area. Yellow rectangles identify SECTOR 1 and SECTOR 2, and the letters are related to the occurred sinkholes.

Finally, to simulate the intensity of waves in the study area, wave motion modeling related to the storm events of autumn 2023 was conducted. This approach enabled the study of the correlation between the characteristics of the storm events in terms of wave parameters and their direct effects on the Sistiana Mare coastline.

2. Study Area

Sistiana Mare is located in the western sector of the Gulf of Trieste (Friuli Venezia Giulia Region, NE Italy), which is in the northernmost part of the Adriatic Sea (Figure 2a). The area is part of the Classical Karst Region, a carbonate plateau (approximately 750 km^2) shared between Italy and Slovenia (Figure 2b). The region is renowned worldwide for its abundance and variety of epigean and hypogean karst landforms [73]. From a geological point of view, this carbonate plateau belongs to the northwestern sector of the External Dinarides (e.g., [74]), a fold-and-thrust belt formed during the NE-SW-oriented Jurassic-Eocene convergence between the European and Adria-related units [75–77]. The plateau is characterized by an SW-verging asymmetrical anticline affecting Mesozoic to lower Eocene shallow-water carbonates. As a result of the convergence, during Eocene times, these shallow-water carbonates were subjected to drowning—marked by the deposition of a siliciclastic unit—caused by the accelerating flexural subsidence related to the development of the Dinaric fold-and-thrust belt and foreland basin system (e.g., [74,78–80]). Geomorphologically, the area is defined as a mature karst, as evidenced by the abundance of karst features such as more than 4000 caves and over 32,800 dolines, which give the topographical surface an irregular and rough appearance [81].

The study area is characterized by distinctive morphologies linked not only to the main structural characteristic of the Classical Karst Region but also to the anthropogenic modifications that occurred over time. On the westernmost side of the area, the shoreline is a limestone-plunging cliff towering 70 m high [82] known as the Duino Cliffs [72], characterized by steeply dipping to overturned stratification [82] belonging to the frontal flank of the karst anticline (Figure 2b,c). Moving southeastward, the area is characterized by a disused quarry that was converted into an urbanized area, which includes beach facilities such as Caravella Beach, a small sewage treatment plant, and a tourist area partially occupied by a parking place. Between the two rubble mound breakwaters lies Sistiana Bay, a fully anthropized area featuring gravel beaches, sailing clubs, a small harbor, asphalted parking areas, and spaces for recreational activities. At the extreme southeastern side of the bay, beyond the breakwater, Castelreggio Beach is sited. The stretches of coastline considered for the present study are the gravel beach of Caravella (SECTOR 1) and the western sector of the Sistiana Bay up to the Pietas Julia sailing club (SNPJ) (SECTOR 2) (Figure 2). In the entire area described above, immediately upstream of the beaches and separating them from the man-made plain areas, a stone retaining wall, 1 to 3 m high, is present.

Physiographically, the Gulf of Trieste is a shallow basin with a mean depth of 16.2 m and a maximum depth of 32.6 m [83]. The shoreface has steeper slopes in the southeast and gentler slopes in the northern sector, where the 20 m isobath extends up to 8 km away from the coastline (Figure 3). Additionally, the Gulf is characterized by bathymetric highs, such as the Mula Muggia sandbank (Figure 3) [84–86] and the seabed rocky outcrops of Trezza Grande and Trezza Piccola [86,87], located in the northern part of the Gulf. Bathymetric lows, such as the depression of Cape Madona just north of Piran [82], are also present. This bathymetric variability can influence wave height depending on the wind direction. Sistiana Mare is exposed only to the southwest winds at angles between 200 and 220 degrees, where the fetch exceeds 100 km. In all the other directions, the fetch is limited below 30 km (Figure 3).

Based on data recorded by three buoys (DWRG1, DWRG3, and Paloma), several considerations were made on the wave and wind characteristics in this area.

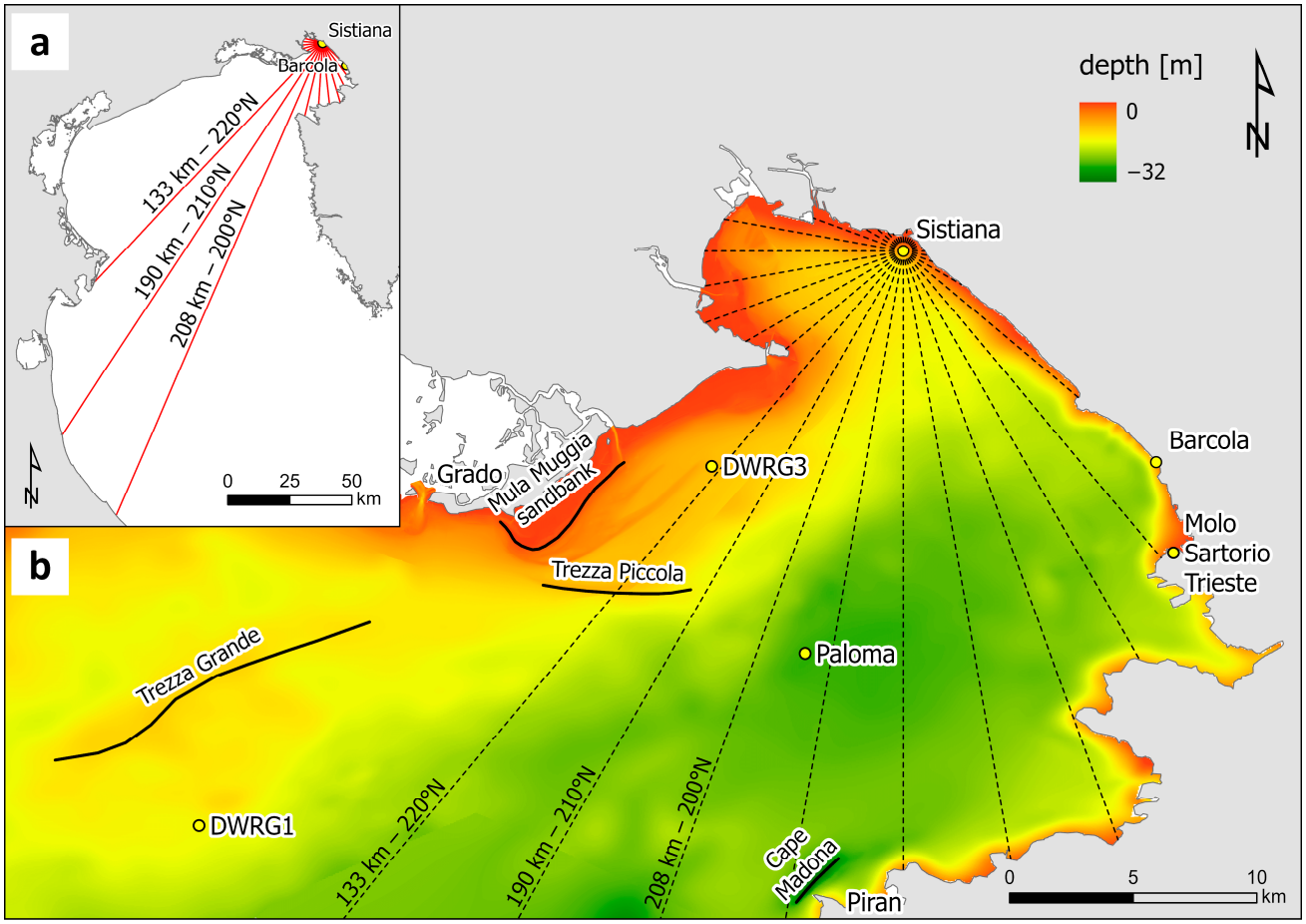

Figure 3. (**a**) Fetch referred to the study area and (**b**) bathymetric model of the Gulf of Trieste and monitoring system locations: DWRG1 (13.24°E, 45.56°N, 15.2 m depth) and DWRG3 (13.52°E, 45.69°N, 9.7 m depth) wave buoys, Paloma station (13.57°E, 45.62°N, 10 m height), and Molo Sartorio (Trieste) tide gauge (13.76°E, 45.65°N). DWRG1 and DWRG3 (installed and managed by Istituto Nazionale di Oceanografia e di Geofisica Sperimentale (OGS), record semi-hourly data; Paloma (Italian acronyms of Advanced Platform Oceanographic Laboratory Adriatic Sea), installed 8 nautical miles off the coast of Trieste between Piran (Slovenia) and Grado, measure both wind speed and direction with a sampling rate of 15 min. The bathymetric model was obtained from one of the European Marine Observation and Data Network (EMODnet) of 2022 [88] integrated with the bathymetry provided by [89] and higher resolution bathymetry of the northern coastal area.

The Gulf usually experiences anticlockwise semi-diurnal tides with a mean range of 76 cm [90]. Spring tides average about 105 cm, while neap tides average about 22 cm [91]. Based on data collected at the DWRG1 buoy (Figure 3), NE and SE winds generate a bimodal wave regime (Figure 4a), with a mean significant wave height (Hs) of less than 0.5 m. Events with Hs greater than 0.5 m account for 25.2% of the overall record, with prevailing waves from the SSE (10.7%) and ENE (10.5%). The highest wave heights, reaching up to 4.4 m, are associated with SE-wind due to its longer fetch with respect to the buoy [92]. The wave buoy DWRG3 (Figure 3), closer to the study area, recorded only 11.5% of events with Hs greater than 0.5 m, originating from two main directions. However, data from both buoys indicate that waves recorded at DWRG3 (Figure 4b) are rotated clockwise with respect to those at DWRG1 (Figure 4a).

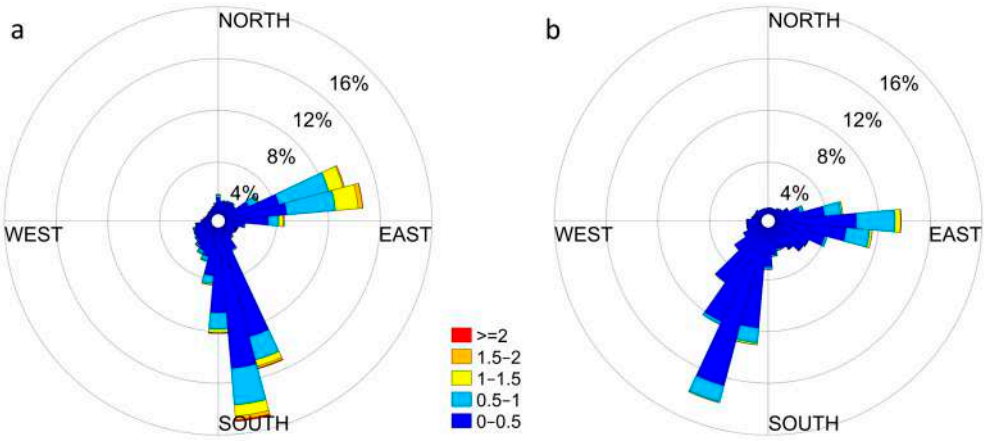

Figure 4. Wave roses of (**a**) DWRG1 relating to the time interval 2004–2023, and (**b**) DWRG3 relating to the time interval 2007–2023.

3. The Extreme Storm Events

From the local news [93], it emerges that severe storms, accompanied by significant damages, occurred in the past in the study area (Figure 5). Historical chronicles report events such as that of June 14, 1911, another in 1969, and a more recent one in 1984. All of them had a violent impact on the Trieste waterfront. Similarly to these past events, between October and November 2023, a new period of bad weather characterized by multiple storm events impacted the Barcola waterfront and Sistiana Mare (a coastline of approximately 4.5 km). The estimated damages, including those associated with the occurrence of several coastal sinkholes, amounted to millions of euros (Figure 5) [94]. Based on wind recordings from the Paloma weather station and wave recordings from the DWRG1 buoy, six different storm events were identified (Table 2). Unluckily, the DWRG3 buoy ceased functioning shortly before the series of storm events and was therefore not considered.

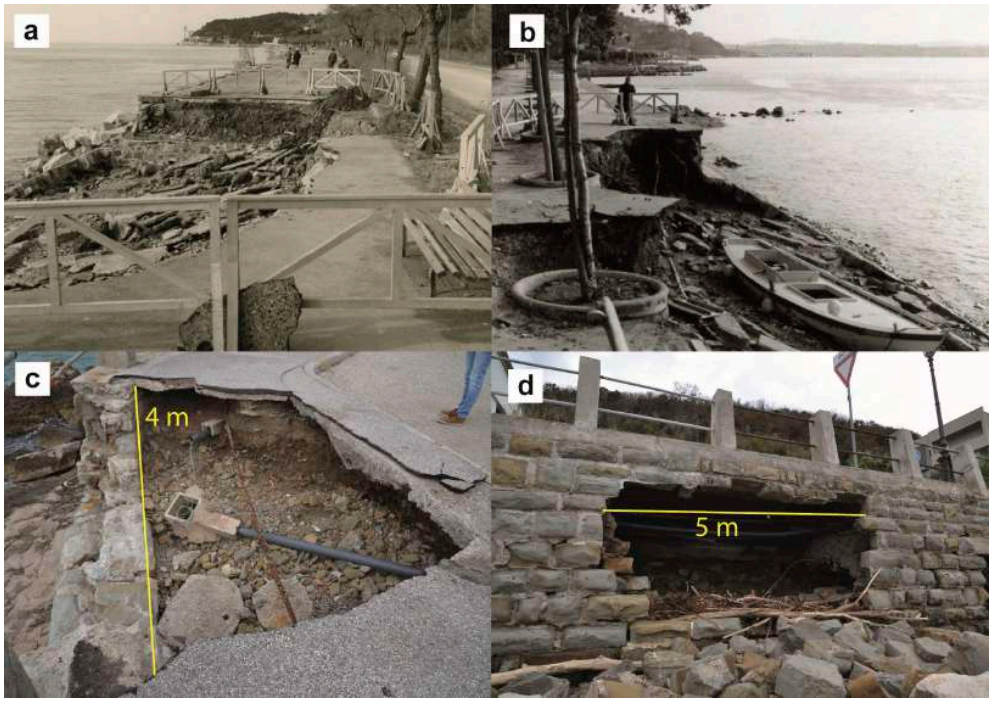

Figure 5. Historical (**a**,**b**) and recent (**c**,**d**) images of the damages that occurred along Barcola waterfront (a and b, photo credits: ASTS, Commissariato del Governo nella Regione Friuli Venezia Giulia, Fototeca (b. 1, ex b. 8, in riordinamento) [72]; c and d, photo credits: Busetti A).

Table 2. Storm events: meteo-marine characteristics.

Storm Event	Storm Date	Hs (Direction) at DWRG1 [m]	Wind Speed (Direction) at Paloma [m/s]
EVENT 1	27 October 2023 06:00	2.26 (170°N)	15.0 (220°N)
EVENT 2	30 October 2023 20:30	2.28 (166°N)	12.2 (179°N)
EVENT 3	31 October 2023 13:00	2.07 (205°N)	13.9 (265°N)
EVENT 4	2 November 2023 17:30	3.24 (175°N)	12.2 (187°N)
EVENT 5	3 November 2023 14:00	2.72 (197°N)	18.3 (221°N)
EVENT 6	5 November 2023 03:00	3.77 (172°N)	14.7 (235°N)

4. Materials and Methods

To calculate the intensity of surge events on the Sistiana Mare coastline and to correlate the evolution of the observed sinkholes with the storm events, wave modeling was performed using MIKE 21. In addition, the evolution of sinkholes along the Sistiana Mare coastline was assessed by creating and comparing High Resolution (HR) 3D models, orthomosaics, and DEMs. These data products were created by applying an SfM-MVS photogrammetry processing workflow to six sets of UAV images acquired between 29 September 2023 and 13 February 2024. Furthermore, to better define the geometry and characteristics of four storm-induced landforms among the largest observed, three additional small-scale and higher-resolution 3D models were produced. A lower-resolution version of these models has been made available in the Sketchfab 3D model public repository (see Section 5.3. HR 3D Models) for documentation and accessibility purposes.

4.1. Wave Modelling

Modelling is a widely used tool to study coastal dynamics [95–99], serving as a knowledge base for both morphodynamic interpretations and engineering purposes of designing coastal works. The lack of wave buoys near the study area necessitated wave modeling to accurately represent the wave motion impacting the Gulf of Trieste. The spectral wave module of the model MIKE 21 by ©DHI was used to simulate the spatial distribution of the wave parameters (significant wave height, mean wave direction, peak wave period, and wave power) during the extreme storm events of autumn 2023.

Spatial discretization was carried out using the finite volume approach applied to unstructured meshes. The mesh was divided into 3 zones with different resolutions: an offshore zone generated starting from a vertex spacing of 675 m on the edge, a central zone built from a spacing of 225 m, and an area near the coast where the spacing between the vertices was 75 m. The resulting mesh has a total of 40,992 nodes and 81,128 elements. Four boundaries were defined: the northern Adriatic boundary towards the southwest, a closed boundary representing the shoreline, and two lateral boundaries connecting the closed and the Adriatic boundaries.

To simulate wave motion during the storm surges, wave parameters obtained from the wave buoy DWRG1 (significant wave height, mean wave direction, peak period, wave spreading), weather data from the Paloma station (wind speed and direction, air temperature, precipitation), and water level obtained from the Trieste tide gauge at Molo Sartorio were used. Wind, air temperature, and water level were set as varying in time and constant in the domain, while wave parameters were set constant along the Adriatic boundary.

The mesh was interpolated starting from the bathymetry of the Gulf of Trieste, obtained from the bathymetric model of the European Marine Observation and Data Network (EMODnet) of 2022 [89] on a grid of 1/16 × 1/16 arc minute of longitude and latitude (ca. 115 × 115 m) integrated with the bathymetric model provided by [90] and higher resolution bathymetric models of the northern coastal area on a grid of 2 × 2 m.

4.2. Orthomosaics and DEMs Creation and Point Cloud Comparison

4.2.1. UAV Survey

The UAV used for the acquisition was a DJI Mavic 3T (DJI Enterprise series). The Mavic 3T is equipped with a 48 MP and 1/2″ CMOS camera sensor with an f/2.8 wide angle lens (24 mm equivalent), stabilized by a 3-axis gimbal. The drone was equipped with a DJI RTK (Real Time Kinematic) module (Mavic 3 Enterprise series), which provided NRTK-corrected (Net Real Time Kinematic) GNSS positioning data, enabling accurate georeferencing of each image. This module has a horizontal nominal accuracy of 1 cm (+1 ppm) and a vertical nominal accuracy of 1.5 cm (+1 ppm).

UAV surveys were carried out on 29 September, 27 October, 7 November, 29 November, 4 December 2023, and on 13 February 2024. All acquisitions were conducted with pre-planned and self-consistent surveys defined using the DJI Pilot 2 application (version 1.1.5). The flights were designed to maintain a constant flight route altitude of 90 m a.s.l. (considering the EGM96 geoid as the sea level), with the camera pointed orthogonally to the ground. Acquisitions were planned, maintaining a side and a frontal overlap ratio between images of 85% and a flight speed of 7 m/s. A total of 471 images were acquired for each survey.

4.2.2. GNSS Survey

To improve the georeferencing accuracy of models and to facilitate comparison between them, 11 Ground Control Points (GCPs) were chosen. Their locations were acquired using a Leica GS07 GNSS antenna in an NRTK configuration, utilizing real-time corrections provided by the GNSS net Hexagon (HxGN) SmartNet. The Leica GS07 GNSS antenna, supported by an RTK net, can reach a horizontal accuracy of 10 mm (+0.5 ppm) and a vertical accuracy of 20 mm (+0.5 ppm). The recording of GCPs was set to be carried out when the accuracy of planar and quote coordinates was less than 3 cm.

4.2.3. SfM-MVS Photogrammetry

The UAV image processing was conducted using Agisoft Metashape 2.0.1. This software is renowned for its reliability and widespread adoption in the field of 3D reconstructions from digital imagery [100]. The processing workflow of each set of images was performed independently in Metashape, where the alignment process was configured to high accuracy and no point limit settings. This initial stage entails the employment of SfM algorithms [101] to retrieve the spatial coordinates of points within the scene by correlating and subsequently analyzing the 2D pixel coordinates across various images [102,103]. The resulting matched tie points form a sparse point cloud that represents the reconstructed scene. The georeferencing was provided by both the RTK position of the images and by the GCPs. Subsequently, iterative steps of gradual selection filtering of points and camera optimization were conducted to enhance the quality of the model (e.g., [104]). Specifically, the point cloud was filtered using gradual selection tools of Metashape based on reconstruction uncertainty, projection accuracy, and reprojection error. After each filtering step, cameras were optimized, resulting in an overall significant decrease in the estimated error associated with the SfM reconstruction of the GCP positions. The subsequent phase involved the calculation of the image depth maps and the creation of multitemporal DEMs and orthomosaics of the study site. DEMs and orthomosaics obtained after the application of the described workflow to the different sets of images show a resolution of about 6.3 cm (≈250 points/m^2) and 2.9 cm, respectively.

Within a sub-area focused on the studied landforms, the multitemporal point clouds were densified using the point cloud building step of Metashape, which relies on Multi-View Stereo (MVS) algorithms [105], thereby completing the comprehensive SfM-MVS photogrammetry workflow [59,106]. Before cloud-to-cloud comparison, the sub-models were re-aligned by registering using only the GCPs positions, thus minimizing georeferencing error between different acquisitions. Finally, the cloud-to-cloud comparison between dense point clouds was carried out using CloudCompare (version 2.14.4), an open-source software for point cloud processing and analysis (available at [107]).

4.3. HR 3D Models Creation

4.3.1. UAV Survey

To acquire HR 3D models of the studied storm-induced landforms, a different UAV device was used: a DJI Mini 3 Pro equipped with a 3-axis gimbal-stabilized 48 MP and 1/1.3″ CMOS camera sensor with an f/1.7 lens (24 mm equivalent). The low weight and compact size of this UAV made it ideal for flights at lower altitudes and closer proximity to the target scene.

The flights were conducted on 29 November 2023, when the studied landforms (sinkholes C, F, G in SECTOR 1 and H in SECTOR 2) were at their maximum extent, except for the sinkhole H, for which the restoration works had already begun (Figure 2). The flights were carried out manually, ensuring that all images depicted the chosen subjects from various angles. Georeferencing of the images was provided by the standalone GNSS system equipped on the UAV (without RTK correction), ensuring an accuracy of a few meters (e.g., [108,109]). Correct scaling of these models was granted by adding four markers at known distances, employing the methodology established by Corradetti [110]. The relative distances between the markers were measured using a laser distance meter (model Bosch GLM 50–27 CG Professional), which has a nominal measuring accuracy of ± 1.5 mm, corresponding to the scale accuracy of the HR 3D models.

4.3.2. SfM-MVS Photogrammetry

The processing of these subsets of UAV images was performed using the Metashape software (version 2.0.1), replicating most of the workflow already described in Section 4.2.3. The main difference was the absence of accurate positioning of the images during the registration of models, which was provided by the known relative distances between the markers. In addition, these HR 3D models were also meshed and textured, achieving a final ground resolution between 2.33 and 3.34 mm/pix (value provided by Agisoft Metashapefinal reports).

5. Results

5.1. Wave Modelling

Between late October and early November 2023, the coastal area of the Gulf of Trieste was hit by 6 storm events with significant intensity and wave height (exceeding 2 m, according to DWRG1 recordings). These storms caused extensive damage along the entire coast, particularly in the area of Sistiana Mare, where eight sinkholes formed, severely damaging the existing man-made structures. Since no wave-monitoring systems are present near Sistiana Mare, wave motion in the Gulf of Trieste from 27 October to November 9 was simulated through the spectral wave module of MIKE 21 2024 Update 1 modeling software, and the time series of the significant wave height was extracted at the study area (13.63°E, 45.76°N, 10 m depth).

Of the six peaks representing the storm events, only the four originating from SW winds produced waves impacting the coastline with Hs greater than 1 m (Table 3). These storms occurred on 27 October (EVENT 1) and 31 (EVENT 3) and on 3 November (EVENT 5) and 5 (EVENT 6) (Figure 6). In the two events with waves and wind from the south, which occurred on 30 October (EVENT 2) and 2 November (EVENT 4), the Hs was dampened by about 70% compared to the DWRG1 buoy data due to the misalignment of wind and offshore waves relative to the longest fetches. EVENTs 1 and 3 experienced similar nearshore wave attenuation of about 40%, despite differing wave and wind characteristics. The first was characterized by offshore wave motion from SSE (170°N) and SW winds (220°N) up to 15.0 m/s, while the latter experienced waves coming from SSW (205°N) and wind blowing from WSW (265°N) up to 13.9 m/s. The most severe storm at Sistiana Mare was the fifth (3 November). During this storm, SSW wave motion (197°N) and SW winds (221°N) blowing up to 18.3 m/s were able to generate the highest nearshore waves, reaching up to 1.8 m of Hs, resulting in the least damped event with only a 33% nearshore attenuation. Finally, the last event (5 November), characterized by waves from SSE (172°N)

and wind up to 14.7 m/s from SW (235°N), was significantly dampened (71%), producing waves with Hs up to 1.08 m near the coast, although the waves recorded at DWRG1 were the highest, reaching up to 3.77 m.

Table 3. Storm events: marine characteristics simulated through MIKE21 Spectral Waves by ©DHI at Sistiana Mare. Hs is the significant wave height.

Storm Event	Storm Date	Hs at Sistiana Mare [m]	Hs Sistiana Mare/HS DWRG1 (%)	Time over 1 m Threshold [Hours:Minutes]
EVENT 1	27 October 2023 06:00	1.30	58%	3:50
EVENT 2	30 October 2023 20:30	0.67	29%	-
EVENT 3	31 October 2023 13:00	1.24	60%	2:00
EVENT 4	2 November 2023 17:30	0.97	30%	-
EVENT 5	3 November 2023 14:00	1.81	67%	8:35
EVENT 6	5 m November 2023 03:00	1.08	29%	1:05

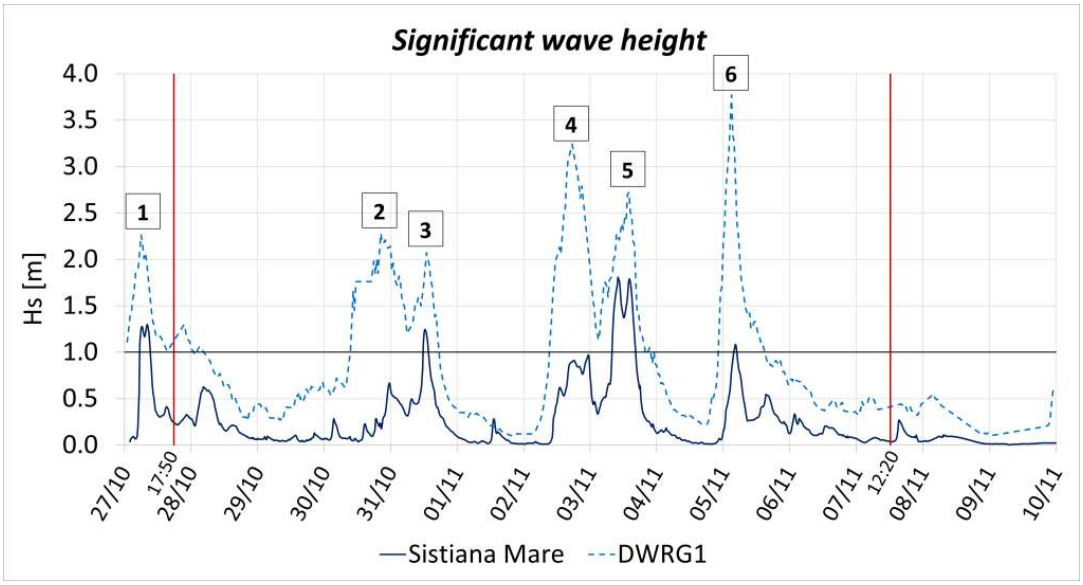

Figure 6. Graph representing the significant wave height recorded at the DWRG1 buoy (open sea, light blue dashed line) and simulated through MIKE21 Spectral Waves by ©DHI at the study area (Sistiana Mare, dark blue line). The different storm surge events are here indicated with their corresponding numbers (from 1 to 6 and refers to those of Tables 2 and 3). UAV surveys of 27 October, following the first event, and 9 November, following the whole multi-event, are evidenced (vertical red lines).

At Sistiana Mare, the significant wave height exceeded the threshold of 1 m for a total of 15 h and 30 min: 3:50 h during EVENT 1, prior to the second UAV survey (29 October), and 11 h and 40 min between surveys 2 and 3 (9 November), divided among EVENT 3 (2 h), EVENT 5 (8 h and 35 min), and EVENT 6 (1 h and 5 min).

5.2. Observations on Orthomosaics and DEMs

Using UAV surveys and the associated products obtained (orthomosaics, DEMs, and 3D models), it was possible to monitor the formation and evolution of the eight sinkholes that occurred along the coast of Sistiana Mare, which were identified (Figures 7–9) and measured (Table 4). For clarity, the formed sinkholes were named in alphabetical order from west to east.

Table 4. Geometric characteristics of the identified sinkholes at their maximum extension were measured on 4 December, except for sinkhole H, whose maximum dimensions were measured on 7 November. The depth of sinkhole E (*) (as for the initial phase of sinkhole C) is underestimated due to the absence of light inside it, which did not allow an efficient application of SfM methods.

Sinkhole	Major Axis (*a*) [m]	Minor Axis (*b*) [m]	Flattening Factor $(1-\frac{b}{a})$	Maximum Depth [m]	Perimeter [m]	Area [m^2]
A	1.68	1.21	0.28	0.30	4.77	1.37
B	5.69	2.01	0.65	1.18	13.21	9.18
C	5.72	3.64	0.36	1.87	15.81	17.04
D	6.86	2.39	0.65	1.06	16.31	11.67
E	1.40	1.15	0.18	0.26 *	4.31	1.03
F	3.24	2.12	0.35	0.84	8.75	5.39
G	3.89	3.68	0.05	0.80	13.28	9.88
H	5.84	2.87	0.51	1.68	14.79	13.05

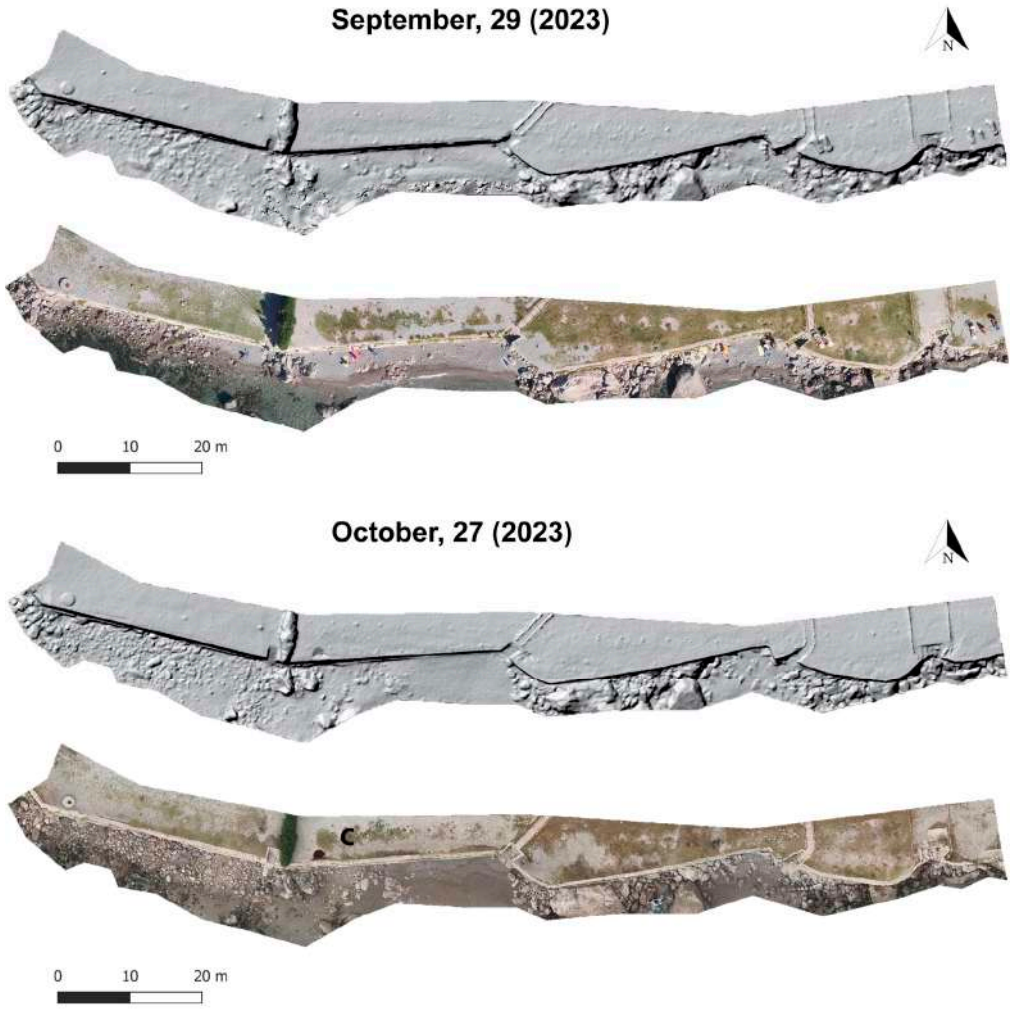

Figure 7. Caravella Beach shaded relief and orthomosaics (SECTOR 1) comparison between two different surveys: pre-storm event of 29 September (2023) and on 27 October (2023), just after the EVENT 1. The storm surge event that occurred during the night between 26 and 27 October (2023) produced the opening of only one sinkhole, the one identified with letter C, but also caused the removal of the finest material along the beach and in particular in its western part.

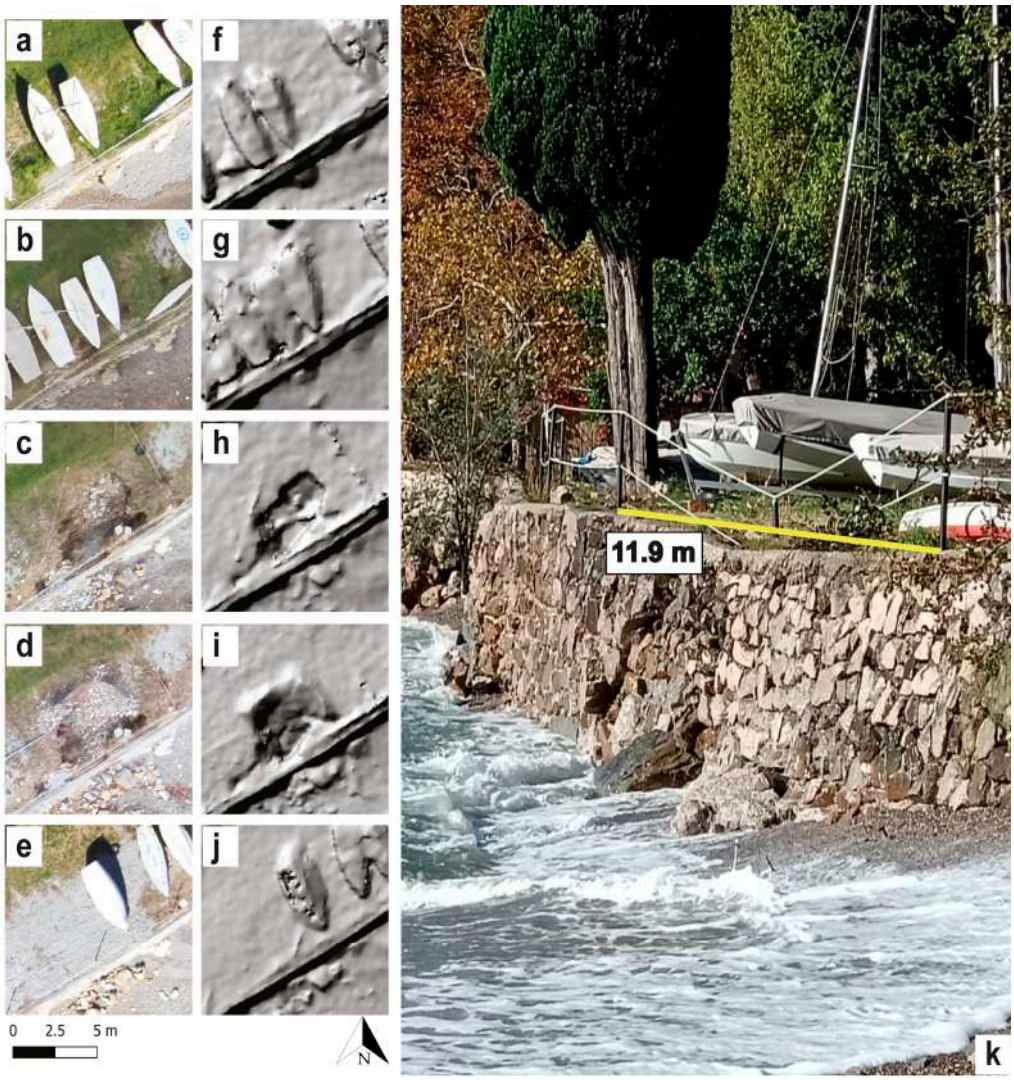

Figure 8. Orthomosaics (**a**–**e**) and shaded relief (**f**–**j**) representing sinkhole H. The scene depicted represents sinkhole H on 29 September 2023 (**a**,**f**), on 27 October 2023 (**b**,**g**), on 7 November 2023 (**c**,**h**), on 4 December 2023 (**d**,**i**) and on 27 February 2024 (**e**,**j**). (**k**) A detail of the collapsed retaining wall on 28 October.

The UAV survey realized on 27 October, and the derived orthomosaics and shaded relief allowed the evaluation of the effects of storm EVENT 1, which caused the opening of the first sinkhole (identified as sinkhole C) (Figure 7). The estimated void had an area of 1.61 m^2 (more than ten times smaller than its maximum extent reached on 4 December, equal to 17.04 m^2) and a flattening factor (defined as the difference in magnitude between the semimajor and the semiminor axis divided by the semimajor axis) of 0.26 (Table 4) (lower than that measured at its final stage, equal to 0.36). Data comparison between the two UAV acquisitions (29 September and 27 October) captured the formation stage of this sinkhole, revealing a circular surface shape. According to the DEM (Figure 7), the depth of sinkhole C was evaluated to be 0.5 m, though this is an underestimate due to the total absence of light inside it, which impaired the effectiveness of the Structure from Motion method and, consequently, the accurate depth reconstruction.

Sinkhole H was the only one that occurred in SECTOR 2 (Figure 2c). Orthomosaics and shaded relief representing this sector after EVENT 1 showed the formation of a depression beneath the boats (Figure 8b,g). Unfortunately, the presence of boats parked in the embanked area obscured the depressed feature, making it difficult to clearly evaluate the slopes of its side walls. A photograph taken the day after EVENT 1 (Figure 8k) shows

the collapse of the retaining wall and the creation of the sinkhole (the iron pole inside the sinking feature is not aligned with the other two placed outside).

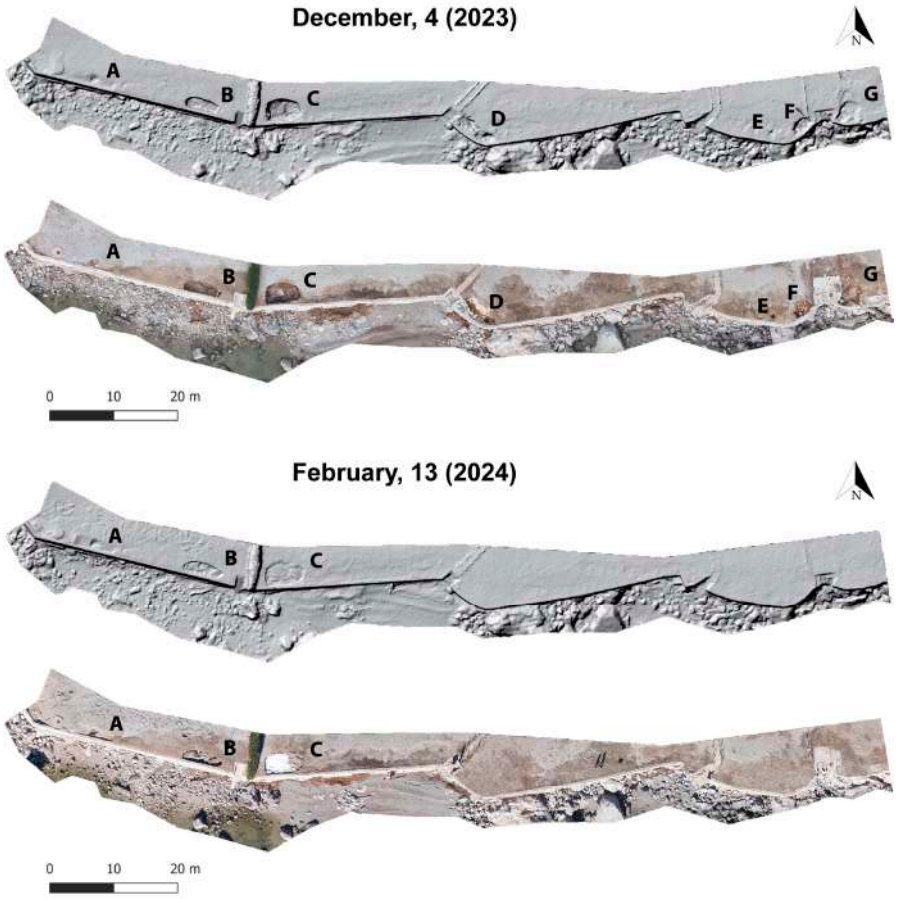

Figure 9. Caravella Beach shaded relief and orthomosaics (SECTOR 1) comparison between two different surveys: 4 December (2023) and 13 February (2024). The storm surge events between 31 October and 5 November (2023) caused the occurrence of most of the sinkholes in this sector (A, B, D, E, F, and G) and enlarged sinkhole C. The last acquisitions on 13 February show the ongoing restauration phase, with the leveling of the embankment behind the retaining wall and the consequent disappearance of sinkholes D, E, F, and G and the beach replenishment (mainly in front of sinkhole C).

The subsequent series of five storm surge events caused the paroxysm of all the other sinkholes in both sectors (Figure 8c,h, and Figure 9).

Unfortunately, due to adverse weather conditions, further UAV surveys were not possible until 7 November. Since the orthomosaics and shaded relief associated with acquisitions performed on 7 November and 4 December showed only negligible differences in the features, the acquisitions of 4 December were considered to represent the final evolutionary stage of sinkholes before the start of restoration activities (Figure 8e–j). Overall, the DEMs reveal that different sinkholes exhibit distinct geometries and varying degrees of erosion. For instance, Sinkhole A (Figure 9) displays an early stage of development with gently sloping sides.

By 13 February, restoration works were underway across the entire study area. Sinkholes D, E, F, and G (Figure 9) had already been filled, and the embankment had been levelled. Additionally, the replenishment of gravel beaches had begun, particularly on the stretch in front of sinkhole C.

Thanks to the use of UAVs, orthomosaics, DEMs, and point clouds, the most important morphometric parameters for each phenomenon were obtained and later validated by on-site manual measurements. The geometrical characteristics at the phase of maximum

detected expansion are summarized in Table 4. They have variable dimensions and show that, while the smaller ones maintain a circular shape (low flattening factor), the larger ones tend towards an elliptical shape (with a higher flattening factor), aligning parallel to the retaining wall.

5.3. HR 3D Models

To better understand the dynamic of sinkhole occurrence, three HR 3D models were reconstructed and analyzed (Figures 10 and 11). The 3D model of sinkhole B, reconstructed after all the storm events on 29 November (Figure 10a), revealed that the stone retaining wall upstream of the beach, including its curb foundations, appeared to be intact (label 1 in Figure 10a). However, beneath it, a horizontally elongated excavation was observed (label 2 in Figure 10a). The analyzed sinkhole was characterized by an area of 9.18 m^2, a maximum depth of 1.18 m, and a flattening factor of 0.65.

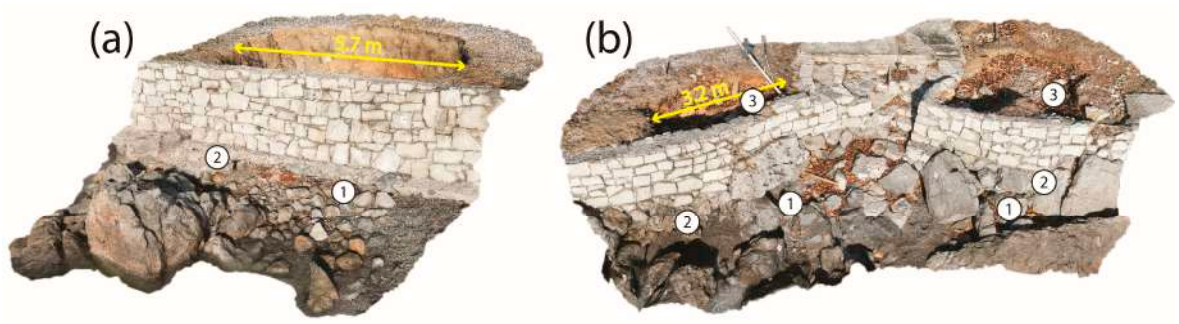

Figure 10. (**a**) HR 3D model of sinkhole B on 29 November 2023 (https://skfb.ly/p7U7E, accessed on 21 August 2024); (**b**) HR 3D model of sinkholes F and G on 29 November 2023 (https://skfb.ly/p7Uws, accessed on 21 August, 2024). (1) foundations of the retaining wall; (2) horizontally elongated hole; (3) collapsed material. View towards North. The ground resolutions of the models (provided by Agisoft Metashape reports) are respectively 2.86 (**a**) and 2.33 mm/pix (**b**).

Figure 11. Three-dimension model of the sinkhole H on 29 November 2023 (https://skfb.ly/p7Uzu, accessed on 21 August 2024). It was already partially filled with landfill material. The retaining wall is almost completely broken. View towards the north-west. The ground resolution of the model (provided by the Agisoft Metashape report) is equal to 3.34 mm/pix.

Considering the 3D model of sinkholes F and G (Figure 10b), their area is equal to 5.39 and 9.88 m^2, with maximum depths of 0.84 and 0.80 m and flattening factors of 0.35 and 0.05, respectively. The model analysis reveals similar characteristics to those previously described for sinkhole B. In both cases, the sinkholes are confined by the intact retaining wall, and a linear hole is present beneath them. In this sector, the wall is built directly on large boulders, with its foundations merged into them.

Sinkhole H presents a depressed landform that had already partially filled with landfill material (Figure 11), as restoration works for sinkhole H had already begun on 29 November (Figure 8e,j). In this case, the retaining wall is almost completely broken, its foundations remain covered, and no under-excavation voids are present.

This landform is one of the largest in the entire study area and is characterized by an area of 13.05 m^2, a maximum depth of 1.68 m, and a flattening factor of 0.51.

5.4. Point Clouds Comparison

The cloud-to-cloud comparison between dense point clouds contributed to shed further light on the evolution of SECTOR 1, but offered limited information for SECTOR 2, where some boats covered sinkhole H during the acquisition days.

By analyzing the difference between the point clouds of 29 September and 27 October 2023 (Figure 12a), the effects of storm EVENT 1 become evident. In addition to the formation of sinkhole C, which was previously identified through the analysis of orthomosaics and shaded relief, the applied method highlights the concentration of surge erosion in the areas in front of the retaining wall, where sinkholes B, C, and D subsequently appeared (identified with number 1 on Figure 12a,b). On the embankment, in the areas identified with number 3, small depressions elongated in the direction of the retaining wall are already present, acting as precursor signs of further collapses. Despite the predominance of erosional processes on the beach during the first storm event, a zone of gravel sediment accumulation just in front of the wall is present in the middle of SECTOR 1 (identifiable with number 2 in Figure 12a).

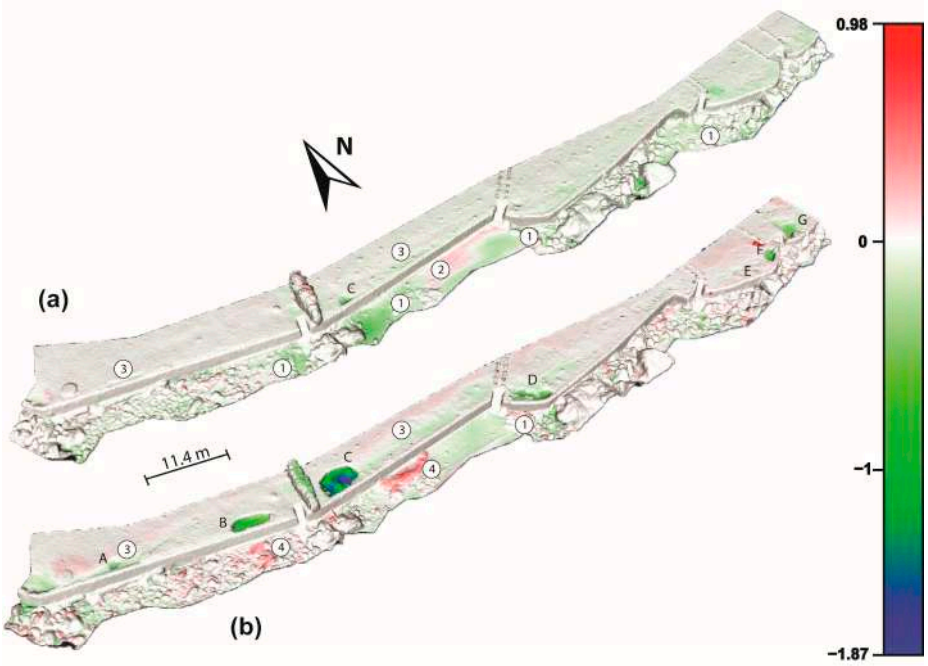

Figure 12. Cloud-to-cloud comparison between dense point clouds of (**a**) 29 September (2023) and 27 October (2023) and (**b**) between 27 October (2023) and 4 December (2023). Highlighted in green are the areas where the wave erosion was concentrated (1); in red are the areas of accumulation of gravel sediments (2) after EVENT 1, and the wooden material accumulation (4) occurred after the last four storm events hit Caravella Beach. Number (3) identifies the linear depressions located immediately beyond the retaining wall and parallel to it.

In the area in front of sinkhole D, erosion is present in both point cloud comparisons, denoting a higher continuity of the process during all surge events impacting the beach. Furthermore, the accumulation of wooden material in front of the retaining wall is also evident (Figures 9 and 12b, number 4). Finally, in both the models' comparisons, a slight deformation immediately beyond the wall and parallel to it is visible (Figure 12 number 3), highlighting the pervasiveness of storm surge erosion along the entire western part of the area considered.

6. Discussion

The formation of coastal sinkholes in Sistiana Mare during the storm events of late 2023 underscores the vulnerability of coastal areas in the northern Adriatic to extreme meteorological conditions. The results obtained through UAV monitoring and wave modeling provide critical insights into both the processes driving sinkhole formation and the potential mitigation strategies.

6.1. Wave Modelling

The model of the series of storm events highlights that the nearshore significant wave height is not always proportional to open sea data recorded by the DWRG1 wave buoy. Indeed, the modeling revealed that nearshore the Hs at Sistiana Mare is strongly influenced by both the offshore wave motion and wind characteristics in terms of intensity and direction (Figure 6). Specifically, events generated by winds and involving waves with directions not aligned with the longest fetches (from 220°N to 190°N) (Figure 3) were significantly dampened compared to their intensity at the DWRG1 buoy. This was the case for the second (31 October), fourth (2 November), and sixth (5 November) events (Figure 6). On the other hand, when both offshore waves and wind are directed within the major fetches, as occurred during EVENT 5, the nearshore waves can be quite high, capable of delivering substantial energy to the shoreline and the existing infrastructure. However, such events are uncommon in the northern Adriatic, as shown by the recordings from the DWRG1 wave buoy (Figure 4), making them exceptional occurrences for the Gulf of Trieste.

6.2. Coastal Sinkhole Formation

The study revealed the progressive development of coastal sinkholes in Sistiana Mare during six main storm events that hit the area. The analysis of orthomosics and shaded reliefs reveals that the storm event on 27 October (EVENT 1) created the conditions for the subsequent openings of the remaining sinkholes in SECTOR 1 by removing fine material from Caravella Beach, leaving only larger particles such as pebbles and boulders (Figure 7). In the areas where the most aggressive erosion occurred, small evidence of surface accommodations was already visible during the survey on 27 October. Subsequently, sinkholes developed in some of these locations (Figure 9).

The coastal erosion caused by the subsequent storm surges removed finer material, eventually leading to under-excavation of the stone retaining walls and the formation of sinkholes. This process was particularly evident in the formation and enlargement of sinkhole C, which evolved from a small circular depression into one of the largest features.

The DEM analysis of sinkhole A after all events, evidencing gentleness of the sinkhole sides suggests a plastic behavior, leading to a gradual accommodation of the ground surface as it deformed smoothly over the underlying void. This feature could still represent an initial evolutionary stage, indicating that the collapse forming sinkholes occurs only when a critical threshold of underlying material loss is reached. The elliptical shape linked to the final evolutionary stage is due to the linear shape of the wall, which acts as a constraint.

In SECTOR 2, sinkhole H showed subsiding evidence after EVENT 1 (Figure 8). Despite the presence of boats to hinder the true characteristics of the sinkhole, a certain gentleness in the slopes could indicate that this landform corresponded to an initial stage of the future sinkhole. Similarly, the analysis of the HR 3D model of sinkhole B (Figure 10a), characterized by an intact retaining wall and a horizontally elongated excavation under-

neath, indicates that the genesis of the sinkhole was linked to diffuse wave erosion, which initially removed the finer material and subsequently caused the under-excavation of the man-made structure. The verticality of the sinkhole's walls suggests an initial sagging followed by a collapse mechanism. The absence of the collapsed material is due to its subsequent removal by waves and marine tides. The presence of large boulders in front of the beach, though detached from the retaining wall, partially protected the man-made structure by dampening significantly Hs.

The characteristics of sinkholes F and G (Figure 10b), along with the verticality of their walls, suggest a similar genesis to that of sinkhole B. The only appreciable difference is that sinkholes F and G contain a considerable amount of collapsed material. The presence of this material can be explained by a lower vulnerability of the site to wave impacts, higher protection from erosive action due to the greater presence of boulders, and/or a later occurrence of the collapse, which allowed the waves to remove only a small portion of the material.

A slightly different scenario is observed when analyzing the HR 3D model of sinkhole H (Figure 11), where the retaining wall was almost completely broken and no under-excavation voids are present. After the removal of the finer components of the beach, the waves eroded the base of the wall, leading to its collapse. The absence of the concrete curb at the bottom of the retaining wall further facilitated its collapse.

The analysis of the difference between dense point clouds of 27 October (Figure 12a) and 4 December 2023 (after the entire series of subsequent storm events) (Figure 12b) in SECTOR 1 confirms the predisposing effect of the first event on the sinkholes' formation. Indeed, in the area where sinkholes B and C formed, the model shows a decrease in beach erosion, the occurrence of sinkhole B, and the expansion of sinkhole C. The wave energy was no longer used to remove the fine material from the beach but to under-excavate the retaining wall, causing the appearance of horizontal voids and, consequently, collapses.

6.3. Protective Role of Boulders

This study also evidenced the protective role of boulders in mitigating the impact of storm surges. Indeed, data analysis of SECTOR 1 (Figure 9) revealed that sinkholes were more concentrated in areas lacking large carbonate boulders in front of the stone retaining wall. These boulders acted as a natural barrier, preserving the man-made retaining wall by preventing the under-excavation of the structure and the consequent collapse of the loose material. Thus, the appearance of sinkholes was influenced not only by the characteristics of the events (with wave direction ranging from SSE to SSW) but also by geomorphological factors, such as the presence of stone-retaining walls partially protected by boulders embedded in the beaches.

7. Conclusions

The phenomenon of coastal sinkholes, though little studied, has proven to be particularly relevant in the coastal sector of the northern Adriatic Sea. This area, notably including the Venice lagoon, has been extensively studied concerning issues related to sea level rise. However, limited information exists regarding the impacts of storm events in surrounding areas, such as the Trieste waterfront analyzed in this study. The storm events of autumn 2023 provided an opportunity to shed light on the vulnerability of these coasts, enabling researchers to monitor the occurrence and evolution of specific features using Unmanned Aerial Vehicles (UAVs).

Damages to the coastline and the man-made structures in these locations are generally rare: only events characterized by winds from 190°N to 220°N, uncommon meteorological conditions in the northern Adriatic Sea, have the longest fetch to generate high and energetic wave motion with the right impact angle relative to the coastline orientation. The multi-event that occurred in autumn 2023 represents a rare example of a SW-storm, during which the significant wave height exceeded the 1-m threshold nearshore for 15 h and 30 min, reaching up to 1.81 m.

The six UAV flights conducted between 29 September 2023 (with the availability of a crucial baseline acquisition before the storm events) and 14 February 2024 enabled the creation of orthomosaics, shaded reliefs, 3D models, and point cloud comparisons. These tools were instrumental in clarifying the genesis of the eight coastal sinkholes that formed in Sistiana Mare. The area, characterized by gravel beaches with a limited backshore (<10 m) and landward retaining stone walls, experienced six storm events that resulted in:

- Preliminary removal of finer material from the beaches;
- Under-excavation of the retaining stone walls, causing sagging of the landward embankment behind the retaining wall;
- Subsequent collapse of the materials, including the destruction of the retaining wall in the most representative case of sinkhole H.

The study highlighted several advantages of using UAV remote sensing technology for coastal monitoring, including:

- Fast and precise damage assessment, as UAVs allow for rapid HR morphometric analysis and assessment of damage, which can be crucial for timely and effective response and restoration efforts;
- Monitoring over time, as repeated UAV surveys allow for the tracking of tem-poral changes, facilitating long-term observation of coastal dynamics as well as the assessment of catastrophic events.

One significant outcome of this study was the assessment of the protective role exerted by boulders placed at sea in front of the retaining walls. These boulders can serve as a fundamental defense for the coasts; their presence mitigated the severity of coastal sinkhole formation and protected the integrity of the retaining walls.

This study was made possible in part due to the availability of a baseline, underscoring the critical importance of conducting regular monitoring studies along coastal areas that may be susceptible to such events. With climate change, these events are likely to become more frequent and severe, making it even more crucial to understand their evolution. Periodic monitoring allows for a detailed and in-depth understanding of these phenomena and provides essential data to enhance coastal protection strategies. By establishing a continuous and systematic observation framework, we can implement more effective measures to mitigate the impacts of future events, thereby safeguarding coastal environments and communities that depend on them.

Author Contributions: Conceptualization, C.C., A.B. and C.L.; methodology, C.L., S.F., P.R. and S.S.; software, C.L., S.F. and S.S.; validation, A.C.; data curation: A.C. and C.L.; investigation, C.L., A.B. and P.R.; data curation, C.L.; writing—original draft preparation, C.C., C.L., A.B., P.R., S.F., S.S. and A.C.; writing—review and editing, C.C., C.L., A.B., P.R., S.F., S.S., A.C. and L.Z.; funding acquisition, L.Z. and C.C. All authors have read and agreed to the published version of the manuscript.

Funding: This research was funded by Servizio Geologico Friuli Venezia Giulia Region in the framework of the following projects: (1) Grant number CUP J95F21002770002 "Realizzazione dei Fogli geomorfologici alla scala 1:50.000 n. 110 Trieste e n. 131 Caresana della Carta Geologica ufficiale d'Italia e per lo studio geomorfologico applicato del territorio regionale e relativa cartografia", scientific coordinator Prof. Luca Zini; (2) grant number ALP-B/10/AG—447 "Aggiornamento continuo del censimento e della pericolosità dei sinkhole del territorio regionale", scientific coordinator Prof. Chiara Calligaris. Part of this study was funded by the consortium iNEST (Interconnected North-Est Innovation Ecosystem) funded by the European Union Next-GenerationEU (Piano Nazionale di Ripresa e Resilienza (PNRR)-Missione 4 Componente 2, Investimento 473 1.5-D.D. 1058 23/06/2022, ECS_00000043).

Data Availability Statement: All the data/models used in this study can be made available upon request to interested parties.

Acknowledgments: The authors would like to thank the scientific coordinators of the abovementioned projects, functionaries of the Geological Survey of the Friuli Venezia Giulia Region, in the persons of Chiara Piano.

Conflicts of Interest: The authors declare no conflicts of interest. The funders had no role in the design of the study, in the collection, analysis, or interpretation of data, in the writing of the manuscript, or in the decision to publish the results.

References

1. MedECC. Climate and Environmental Change in the Mediterranean Basin–Current Situation and Risks for the Future. In *First Mediterranean Assessment Report 2020*; Cramer, W., Guiot, J., Marini, K., Eds.; Union for the Mediterranean, Plan Bleu, UNEP/MAP: Marseille, France, 2020; p. 632. ISBN 978-2-9577416-0-1.
2. Cramer, W.; Guiot, J.; Fader, M.; Garrabou, J.; Gattuso, J.P.; Iglesias, A.; Lange, M.A.; Lionello, P.; Llasat, M.C.; Paz, S.; et al. Climate change and interconnected risks to sustainable development in the Mediterranean. *Nat. Clim. Change* **2018**, *8*, 972–980. [CrossRef]
3. Lionello, P.; Scarascia, L. The relation of climate extremes with global warming in the Mediterranean region and its north versus south contrast. *Reg. Environ. Change* **2020**, *20*, 31. [CrossRef]
4. IPCC. Climate Change 2022: Impacts, Adaptation, and Vulnerability. In *Contribution of Working Group II to the Sixth Assessment Report of the Intergovernmental Panel on Climate Change*; Pörtner, H.-O., Roberts, D.C., Tignor, M., Poloczanska, E.S., Mintenbeck, K., Alegría, A., Craig, M., Langsdorf, S., Löschke, S., Möller, V., et al., Eds.; Cambridge University Press: Cambridge, UK; New York, NY, USA, 2022; p. 3056. [CrossRef]
5. Tuel, A.; Eltahir, E.A.B. Why is the mediterranean a climate change hotspot? *J. Clim.* **2020**, *33*, 5829–5843. [CrossRef]
6. Giorgi, F. Climate changes hot-spots. *Geophys. Res. Lett.* **2006**, *33*, L08707. [CrossRef]
7. Giorgi, F.; Lionello, P. Climate change projections for the Mediterranean region. *Glob. Planet Change* **2008**, *63*, 90–104. [CrossRef]
8. Xie, W.; Tang, B.; Meng, Q. The Impact of Sea-Level Rise on Urban Properties in Tampa Due to Climate Change. *Water* **2022**, *14*, 13. [CrossRef]
9. IPCC. *Climate Change 2021: The Physical Science Basis. Contribution of Working Group I to the Sixth Assessment Report of the Intergovernmental Panel on Climate Change*; Masson-Delmotte, V., Zhai, A.P., Pirani, S.L., Connors, C., Péan, S., Berger, N., Caud, Y., Chen, L., Goldfarb, M.I., Gomis, M., et al., Eds.; Cambridge University Press: Cambridge, UK; New York, NY, USA, 2021; p. 2391. [CrossRef]
10. Neumann, B.; Vafeidis, A.T.; Zimmermann, J.; Nicholls, R. Future coastal population growth and exposure to sea-level rise and coastal flooding—A global assessment. *PLoS ONE* **2015**, *10*, e0118571. [CrossRef]
11. Ranasinghe, R. Assessing climate change impacts on open sandy coasts: A review. *Earth Sci. Rev.* **2016**, *160*, 320–332. [CrossRef]
12. Nicholls, R.J.; Adger, N.; Hutton, C.W.; Hanson, S.E. *Deltas in the Anthropocene*; Palgrave Macmillan: Cham, Switzerland, 2020; p. 282. [CrossRef]
13. Vousdoukas, M.I.; Mentaschi, L.; Voukouvalas, E.; Verlaan, M.; Jevrejeva, S.; Jackson, L.P.; Feyen, L. Global probabilistic projections of extreme sea levels show intensification of coastal flood hazard. *Nat. Commun.* **2018**, *9*, 2360. [CrossRef] [PubMed]
14. Bakkensen, L.A. Mediterranean hurricanes and associated damage estimates. *J. Extreme Events* **2017**, *4*, 1750008. [CrossRef]
15. Portmann, R.; González-Alemán, J.J.; Sprenger, M.; Wernli, H. How an uncertain short-wave perturbation on the North Atlantic wave guide affects the forecast of an intense Mediterranean cyclone (Medicane Zorbas). *Weather Clim. Dynam.* **2020**, *1*, 597–615. [CrossRef]
16. Scicchitano, G.; Scardino, G.; Monaco, C.; Piscitelli, A.; Milella, M.; De Giosa, F.; Mastronuzzi, G. Comparing impact effects of common storms and Medicanes along the coast of southeastern Sicily. *Mar. Geol.* **2021**, *439*, 106556. [CrossRef]
17. Sanuy, M.; Duo, E.; Jäger, W.S.; Ciavola, P.; Jiménez, J.A. Linking source with consequences of coastal storm impacts for climate change and risk reduction scenarios for Mediterranean sandy beaches. *NHESS* **2018**, *18*, 1825–1847. [CrossRef]
18. Lira-Loarca, A.; Cobos, M.; Losada, M.Á.; Baquerizo, A. Storm characterization and simulation for damage evolution models of maritime structures. *Coast Eng.* **2020**, *156*, 103620. [CrossRef]
19. Amores, A.; Marcos, M.; Carrió, D.S.; Gómez-Pujol, L. Coastal impacts of Storm Gloria (January 2020) over the northwestern Mediterranean. *NHESS* **2020**, *20*, 1955–1968. [CrossRef]
20. Cavaleri, L.; Bajo, M.; Barbariol, F.; Bastianini, M.; Benetazzo, A.; Bertotti, L.; Chiggiato, J.; Davolio, S.; Ferrarin, C.; Magnusson, L.; et al. The October 29, 2018 storm in Northern Italy–an exceptional event and its modelling. *Prog. Oceanogr.* **2019**, *178*, 102178. [CrossRef]
21. Jiménez, J.; Sanuy, M.; Ballesteros, C.; Valdemoro, H. The Tordera Delta, a hotspot to storm impacts in the coast northwards of Barcelona (NW Mediterranean). *Coast Eng.* **2018**, *134*, 148–158. [CrossRef]
22. Amarouche, K.; Akpınar, A.; Cakmak, R.E.; Houma, F.; Bachari, N.E.I. Assessment of storm events along the Algiers coast and their potential impacts. *Ocean Eng.* **2020**, *210*, 107432. [CrossRef]
23. Anfuso, G.; Postacchini, M.; Di Luccio, D.; Benassai, G. Coastal sensitivity/vulnerability characterization and adaptation strategies: A review. *J. Mar. Sci. Eng.* **2021**, *9*, 72. [CrossRef]
24. Melet, A.; Meyssignac, B.; Almar, R.; Le Cozannet, G. Under-estimated wave contribution to coastal sea-level rise. *Nat. Clim. Change* **2018**, *8*, 234–239. [CrossRef]
25. McEvoy, S.; Hassnoot, M.; Biesbroek, R. How are European countries planning for sea level rise? *Ocean Coast Manag.* **2021**, *203*, 105512. [CrossRef]

26. Harley, M.D.; Turner, I.L.; Kinsela, M.A.; Middleton, J.H.; Mumford, P.J.; Splinter, K.D.; Phillips, M.S.; Simmons, J.A.; Hanslow, D.J.; Short, A.D. Extreme coastal erosion enhanced by anomalous extratropical storm wave direction. *Sci. Rep.* **2017**, *7*, 6033. [CrossRef]
27. Biolchi, S.; Denamiel, C.; Devoto, S.; Korbar, T.; Macovaz, V.; Scicchitano, G.; Vilibić, I.; Furlani, S. Impact of the October 2018 Storm Vaia on Coastal Boulders in the Northern Adriatic Sea. *Water* **2019**, *11*, 2229. [CrossRef]
28. Parise, M. Sinkholes. In *Encyclopedia of Caves*, 3rd ed.; William, B., White, D.C., Culver, T.P., Eds.; Academic Press: Cambridge, MA, USA, 2019; pp. 934–942. [CrossRef]
29. Liso, I.S. Sinkhole occurrence and evolution, and seawater intrusion in a low-coastal setting of Apulia. *Ital. J. Eng. Geol. Environ.* **2024**, 197–204. [CrossRef]
30. Forth, R.A.; Butcher, D.; Senior, R. Hazard mapping of karst along the coast of the Algarve, Portugal. *Eng. Geol.* **1999**, *52*, 67–74. [CrossRef]
31. Bruno, E.; Calcaterra, D.; Parise, M. Development and morphometry of sinkholes in coastal plains of Apulia, southern Italy. Preliminary sinkhole susceptibility assessment. *Eng. Geol.* **2008**, *99*, 198–209.
32. Delle Rose, M.; Parise, M. Karst subsidence in south-central Apulia Italy. *Int. J. Speleol.* **2002**, *31*, 181–199. [CrossRef]
33. Delle Rose, M.; Parise, M. Slope instability along the Adriatic coast of Salento, southern Italy. In Proceedings of the IX International Symposium on Landslides, Rio de Janeiro, Brasil, 28 June 2004–2 July 2004; Volume 1, pp. 399–404.
34. Delle Rose, M.; Parise, M. Speleogenesi e geomorfologia del sistema carsico delle Grotte della Poesia nell'ambito dell'evoluzione quaternaria della costa Adriatica Salentina. *Atti E Mem. Comm. Grotte "E. Boegan"* **2005**, *40*, 153–173.
35. Delle Rose, M.; Federico, A.; Parise, M. Sinkhole genesis and evolution in Apulia, and their interrelations with the anthropogenic environment. *NHESS* **2004**, *4*, 747–755. [CrossRef]
36. Parise, M. I sinkholes in Puglia. In *I Fenomeni Naturali di Sinkhole Nelle Aree di Pianura Italiana*; Nisio, S., Ed.; Memorie descrittive della Carta Geologica d'Italia: Rome, Italy, 2008; Volume 85, pp. 309–334.
37. Del Prete, S.; Iovine, G.; Parise, M.; Santo, A. Origin and distribution of different types of sinkholes in the plain areas of Southern Italy. *Geodin. Acta* **2010**, *23*, 113–127. [CrossRef]
38. Margiotta, S.; Negri, S.; Parise, M.; Valloni, R. Mapping the susceptibility to sinkholes in coastal areas, based on stratigraphy, geomorphology and geophysics. *Nat. Hazards* **2012**, *62*, 657–676. [CrossRef]
39. Coratza, P.; Galve, J.P.; Soldati, M.; Tonelli, C. Recognition and assessment of sinkholes as geosites: Lessons from the Island of Gozo (Malta). *Quaest. Geogr.* **2012**, *31*, 25–35. [CrossRef]
40. Soldati, M.; Tonelli, C.; Galve, J.P. Geomorphological evolution of palaeosinkhole features in the Maltese archipelago (Mediterranean Sea). *GFDQ* **2013**, *36*, 189–198. [CrossRef]
41. The Scottish Sun. Available online: https://www.thescottishsun.co.uk/news/6634343/sinkhole-fife-coastal-path-west-wemyss-harbour/ (accessed on 23 April 2024).
42. Edinburghlive. Available online: https://www.edinburghlive.co.uk/news/edinburgh-news/east-lothian-locals-warned-huge-28012627 (accessed on 23 April 2024).
43. Chroniclelive. Available online: https://www.chroniclelive.co.uk/news/north-east-news/what-caused-giant-sinkhole-blyth-17049690 (accessed on 23 April 2024).
44. Independent. Available online: https://www.independent.co.uk/tv/climate/huge-sinkhole-appears-at-coastal-beauty-spot-revealing-hidden-underground-beach-b2195003.html (accessed on 23 April 2024).
45. Newsweek. Available online: https://www.newsweek.com/coastal-sinkhole-suck-people-ocean-appears-overnight-1599411 (accessed on 23 April 2024).
46. The news tribune. Available online: https://www.thenewstribune.com/news/nation-world/national/article271602352.html (accessed on 23 April 2024).
47. OPB. Available online: https://www.opb.org/article/2023/05/20/2-sinkholes-have-appeared-on-oregons-north-coast-heres-more-on-why-they-happen/ (accessed on 23 April 2024).
48. MeteoWeb. Available online: https://www.meteoweb.eu/2021/12/maltempo-mareggiata-a-marsala-cede-tratto-del-lungomare/1746896/ (accessed on 23 April 2024).
49. In Alto Mare–Sant'Agata di Militello. Available online: https://www.facebook.com/inaltomare.santagata/ (accessed on 23 April 2024).
50. IlFattoVesuviano. Available online: https://www.ilfattovesuviano.it/2023/11/forti-mareggiate-crolla-la-litoranea-di-torre/#google_vignette (accessed on 23 April 2024).
51. Cooper, A.H. The classification, recording, databasing and use of information about building damage caused by subsidence and landslides. *QJEGH* **2008**, *41*, 409–424. [CrossRef]
52. Gutierrez, F. Sinkhole hazards. In *Oxford Research Encyclopedia of Natural Hazard Science 2016*; Oxford University Press: Oxford, UK, 2016. [CrossRef]
53. Calligaris, C.; Devoto, S.; Zini, L. Evaporite sinkholes of the Friuli Venezia Giulia region (NE Italy). *J. Maps* **2017**, *13*, 406–414. [CrossRef]
54. Busetti, A.; Calligaris, C.; Forte, E.; Areggi, G.; Mocnik, A.; Zini, L. Non-invasive methodological approach to detect and characterize high-risk sinkholes in urban cover evaporite karst: Integrated reflection seismics, PS-InSAR, leveling, 3D-GPR and ancillary data. A NE Italian case study. *Remote Sens.* **2020**, *12*, 3814. [CrossRef]

55. Parise, M. Sinkholes, subsidence and related mass movements. In *Treatise on Geomorphology 5*; Shroder, J.J.F., Ed.; Academic Press: Cambridge, MA, USA; Elsevier: Amsterdam, The Netherlands, 2022; pp. 200–220. [CrossRef]
56. Sevil, J.; Gutiérrez, F. Morphometry and evolution of sinkholes on the western shore of the Dead Sea. Implications for susceptibility assessment. *Geomorphology* **2023**, *434*, 108732. [CrossRef]
57. Gonçalves, J.A.; Henriques, R. UAV photogrammetry for topographic monitoring of coastal areas. *ISPRS J. Photogramm.* **2015**, *104*, 101–111. [CrossRef]
58. Turner, I.L.; Harley, M.D.; Drummond, C.D. UAVs for coastal surveying. *Coast Eng.* **2016**, *114*, 19–24. [CrossRef]
59. Carrivick, J.L.; Smith, M.W.; Quincey, D.J. *Structure from Motion in the Geosciences*; Collection of New Analytical Methods in Earth Environ Sci; John Wiley & Sons: Chichester, UK, 2016. [CrossRef]
60. Seong, K.; Leeb, T.; Singhc, V.P. UAV Photogrammetry-based Sea Level Establishment for a Storm Surge Early Warning System in Wolpo-beach, South Korea. *KSCE J. Civ. Eng.* **2024**, *28*, 2505–2514. [CrossRef]
61. Albuquerque, M.; Alves, D.C.L.; Espinoza, J.M.A.; Oliveira, U.R.; Simões, R.S. Determining shoreline response to meteo-oceanographic events using remote sensing and unmanned aerial vehicle (UAV): Case study in southern Brazil. *J. Coast Res.* **2018**, *85*, 766–770. [CrossRef]
62. Brunetta, R.; Duo, E.; Ciavola, P. Evaluating Short-Term Tidal Flat Evolution Through UAV Surveys: A Case Study in the Po Delta (Italy). *Remote Sens.* **2021**, *13*, 2322. [CrossRef]
63. Duo, E.; Trembanis, A.C.; Dohner, S.; Grottoli, E.; Ciavola, P. Local-scale post-event assessments with GPS and UAV-based quick-response surveys: A pilot case from the Emilia–Romagna (Italy) coast. *NHESS* **2018**, *18*, 2969–2989. [CrossRef]
64. Adams, S.M.; Friedlandb, C.J.; Levitanc, M.L. Unmanned Aerial Vehicle Data Acquisition for Damage Assessment in Hurricane Events. In Proceedings of the 8th International Workshop on Remote Sensing for Disaster Management, Tokyo, Japan, 30 September–1 October 2010.
65. Biolchi, S.; Furlani, S.; Devoto, S.; Scicchitano, G.; Korbar, T.; Vilibić, I.; Šepić, J. The origin and dynamics of coastal boulders in a semi-enclosed shallow basin: A northern Adriatic case study. *Mar. Geol.* **2019**, *411*, 62–77. [CrossRef]
66. Pinton, D.; Canestrelli, A.; Moon, R.; Wilkinson, B. Estimating Ground Elevation in Coastal Dunes from High-Resolution UAV-LIDAR Point Clouds and Photogrammetry. *Remote Sens.* **2023**, *15*, 226. [CrossRef]
67. Casella, E.; Drechsel, J.; Winter, C.; Benninghoff, M.; Rovere, A. Accuracy of sand beach topography surveying by drones and photogrammetry. *Geo-Mar. Lett.* **2020**, *40*, 255–268. [CrossRef]
68. Laporte-Fauret, Q.; Marieu, V.; Castelle, B.; Michalet, R.; Bujan, S.; Rosebery, D. Low-Cost UAV for High-Resolution and Large-Scale Coastal Dune Change Monitoring Using Photogrammetry. *J. Mar. Sci. Eng.* **2019**, *7*, 63. [CrossRef]
69. Mancini, F.; Dubbini, M.; Gattelli, M.; Stecchi, F.; Fabbri, S.; Gabbianelli, G. Using unmanned aerial vehicles (UAV) for high-resolution reconstruction of topography: The structure from motion approach on coastal environments. *Remote Sens.* **2013**, *5*, 6880–6898. [CrossRef]
70. Casagrande, G.; Bezzi, A.; Fracaros, S.; Martinucci, D.; Pillon, S.; Salvador, P.; Sponza, S.; Fontolan, G. Quantifying Transgressive Coastal Changes Using UAVs: Dune Migration, Overwash Recovery, and Barrier Flooding Assessment and Interferences with Human and Natural Assets. *J. Mar. Sci. Eng.* **2023**, *11*, 1044. [CrossRef]
71. Fontolan, G.; Bezzi, A.; Casagrande, G.; Fracaros, S.; Popesso, C.; Spadotto, S.; Favaro, M.; Papa, A. Real-Time Monitoring System and an Early Warning System Implemented. Report D 5.4.3_Part B_ Stream project 2023. Available online: https://programming14-20.italy-croatia.eu/web/stream/docs-and-tools-details?id=2136615&nAcc=5&file=12 (accessed on 23 April 2024).
72. Archivio di Stato di Trieste. Available online: https://archiviodistatotrieste.it/documento-del-mese/novembre-2023-mareggiate-a-trieste/ (accessed on 23 April 2024).
73. Zini, L.; Calligaris, C.; Cucchi, F. Along the hidden Timavo. *GFT&M* **2022**, *14*, 1–69. [CrossRef]
74. Jurkovšek, B.; Biolchi, S.; Furlani, S.; Kolar-Jurkovšek, T.; Zini, L.; Jež, J.; Tunis, G.; Bavec, M.; Cucchi, F. Geology of the Classical Karst Region (SW Slovenia–NE Italy). *J. Maps* **2016**, *12*, 352–362. [CrossRef]
75. Schmid, S.M.; Bernoulli, D.; Fügenschuh, B.; Matenco, L.; Schefer, S.; Schuster, R.; Tischler, M.; Ustaszewski, K. The Alpine-Carpathian-Dinaridic orogenic system: Correlation and evolution of tectonic units. *Swiss J. Geosci.* **2008**, *101*, 139–183. [CrossRef]
76. van Unen, M.; Matenco, L.; Nader, F.H.; Darnault, R.; Mandic, O.; Demir, V. Kinematics of foreland-vergent crustal accretion: Inferences from the Dinarides evolution. *Tectonics* **2019**, *38*, 49–76. [CrossRef]
77. van Hinsbergen, D.J.; Torsvik, T.H.; Schmid, S.M.; Maţenco, L.C.; Maffione, M.; Vissers, R.L.; Gürer, D.; Spakman, W. Orogenic architecture of the Mediterranean region and kinematic reconstruction of its tectonic evolution since the Triassic. *Gondwana Res.* **2020**, *81*, 79–229. [CrossRef]
78. Korbar, T. Orogenic evolution of the External Dinarides in the NE Adriatic region: A model constrained by tectonostratigraphy of Upper Cretaceous to Paleogene carbonates. *Earth-Sci. Rev.* **2009**, *96*, 296–312. [CrossRef]
79. Balling, P.; Tomljenović, B.; Schmid, S.M.; Ustaszewski, K. Contrasting along-strike deformation styles in the central external Dinarides assessed by balanced cross-sections: Implications for the tectonic evolution of its Paleogene flexural foreland basin system. *Global Planet Change* **2021**, *205*, 103587. [CrossRef]
80. Consorti, L.; Corradetti, A.; Hadi, M.; Franceschi, M.; Sabbatino, M.; Bensi, S.; Bertone, N.; Bonini, L. Biostratigraphic investigations assisted by virtual outcrop modeling: A case study from an Eocene shallow-water carbonate succession (Val Rosandra gorge, Trieste, NE Italy). *Ital. J. Geosci.* **2024**, *143*, 60–74. [CrossRef]

81. Zini, L.; Calligaris, C.; Forte, E.; Turpaud, P. Flood hazard assessment in a polje: The case of Mucille (Classical Karst Region, NE Italy). *Environ. Earth Sci.* **2023**, *82*, 293. [CrossRef]
82. Furlani, S.; Ninfo, A.; Zavagno, E.; Paganini, P.; Zini, L.; Biolchi, S.; Antonioli, F.; Coren, F.; Cucchi, F. Submerged notches in Istria and The Gulf of Trieste: Results from the Geoswim Project. *Quat. Int.* **2014**, *332*, 37–47. [CrossRef]
83. Trobec, A.; Busetti, M.; Zgur, F.; Baradello, L.; Babich, A.; Cova, A.; Gordini, E.; Romeo, R.; Tomini, I.; Poglajen, S.; et al. Thickness of marine Holocene sediment in the Gulf of Trieste (northern Adriatic Sea). *Earth Syst. Sci. Data* **2018**, *10*, 1077–1092. [CrossRef]
84. Bezzi, A.; Casagrande, G.; Fracaros, S.; Martinucci, D.; Pillon, S.; Sponza, S.; Bratus, A.; Fattor, F.; Fontolan, G. Geomorphological changes of a migrating sandbank: Multidecadal analysis as a tool for managing conflicts in coastal use. *Water* **2021**, *13*, 3416. [CrossRef]
85. Brambati, A. Modificazioni costiere nell'arco lagunare dell'Adriatico Settentrionale. *Antich. Altoadriatiche* **1985**, *27*, 13–47.
86. Marocco, R. Lineamenti geomorfologici della costa e dei fondali del Golfo di Trieste e considerazioni sulla loro evoluzione tardo-quaternaria. *Int. J. Speleol.* **1989**, *18*, 87–110. [CrossRef]
87. Gordini, E.; Caressa, S.; Marocco, R. Nuova carta morfo-sedimentologica del Golfo di Trieste (Da Punta Tagliamento alla foce dell'Isonzo). *Gortania. Atti. Mus. Friul. Stor. Nat.* **2003**, *25*, 5–29.
88. European Marine Observation and Data Network (EMODnet). Available online: http://www.emodnet-bathymetry.eu (accessed on 10 June 2024).
89. Trobec, A.; Busetti, M. Models of the bathymetry, of the base and of the thickness of Holocene marine sediment in the Gulf of Trieste (Northern Adriatic Sea). *OGS SNAP System*. 2017. Available online: https://snap.ogs.it/cache/doi/6ad9b1e6-c977-cec9-8a2d-db10c7f90adc/58074ea270863f0a32214fab4f43d42c.jsp (accessed on 10 June 2024).
90. Petti, M.; Pascolo, S.; Bosa, S.; Bezzi, A.; Fontolan, G. Tidal Flats Morphodynamics: A new Conceptual Model to Predict Their Evolution over a Medium-Long Period. *Water* **2019**, *11*, 1176. [CrossRef]
91. Dorigo, L. La Laguna di Grado e le Sue Foci. Ricerche e Rilievi Idrografici. *Magistr. Alle Acque-Ufficio Idrografico* **1965**, *155*, 1–231.
92. RAFVG. Piano Regolatore Portuale del Porto di Monfalcone, Variante Localizzata. Studio Meteomarino. 2019. Available online: https://www.regione.fvg.it/rafvg/export/sites/default/RAFVG/ambiente-territorio/pianificazione-gestione-territorio/FOGLIA9/allegati/Allegato_33_alla_Delibera_2066-2019.pdf (accessed on 23 April 2024).
93. Triestenews. Available online: https://www.triesteallnews.it/2023/11/uno-spettacolo-di-desolazione-la-mareggiata-che-travolse-trieste-nel-1911/ (accessed on 23 April 2024).
94. Il Piccolo. Available online: https://ilpiccolo.gelocal.it/trieste/cronaca/2023/11/13/news/mareggiata_trieste_danni_quattro_milioni-13856672/ (accessed on 25 September 2024).
95. Amoudry, L.O.; Souza, A.J. Deterministic coastal morphological and sediment transport modeling: A review and discussion. *Rev. Geophys.* **2011**, *49*. [CrossRef]
96. Baldoni, A.; Melito, L.; Marini, F.; Galassi, G.; Giacomin, P.; Filomena, G.; Barbizzi, N.; Lorenzoni, C.; Brocchini, M. Modeling coastal inundation for adaptation to climate change at local scale: The case of Marche Region (central Italy). *Front. Clim.* **2024**, *6*, 1334625. [CrossRef]
97. Chaumillon, E.; Bertin, X.; Fortunato, A.B.; Bajo, M.; Schneider, J.L.; Dezileau, L.; Walsh, J.P.; Michelot, A.; Chauveau, E.; Créach, A.; et al. Storm-induced marine flooding: Lessons from a multidisciplinary approach. *Earth-Sci. Rev.* **2017**, *165*, 151–184. [CrossRef]
98. Chen, Z.; Luo, F.; Zhou, G.; Zhu, F.; Wu, H.; Li, R.; Zhang, C. Hydrodynamic modeling study of nature-based hybrid coastal defense strategy applied in salt marsh restoration. *Estuar. Coast Shelf Sci.* **2024**, *298*, 108666. [CrossRef]
99. Yaiche Temam, I.; Bouhmadouche, M.; Hemdane, Y.; Kessali, N.; Amiri, H. Analysis of the hydrosedimentary circulation in the mouth of dominated wave environment using grain size analysis, wave/current modeling and image processing case of the principal Rivers in Zemmouri bay. *MESE* **2024**, *10*, 4279–4294. [CrossRef]
100. Verhoeven, G. Taking computer vision Aloft-archaeological three-dimensional reconstructions from aerial photographs with photoscan. *Archaeol. Prospect* **2011**, *18*, 67–73. [CrossRef]
101. Ullman, S. The interpretation of structure from motion. *Proc. R Soc. Lond. B* **1979**, *203*, 405–426. [CrossRef] [PubMed]
102. Grün, A.; Remondino, F.; Zhang, L. Photogrammetric reconstruction of the Great Buddha of Bamiyan, Afghanistan. *Photogramm. Rec.* **2004**, *19*, 177–199. [CrossRef]
103. Szeliski, R. Image processing. In *Computer Vision: Algorithms and Applications*; Springer: Cham, Switzerland, 2022; pp. 85–151. [CrossRef]
104. Vaccher, V.; Hastewell, L.; Devoto, S.; Corradetti, A.; Mantovani, M.; Korbar, T.; Furlani, S. The application of UAV-derived SfM-MVS photogrammetry for the investigation of storm wave boulder deposits on a small rocky island in the semi-enclosed Northern Adriatic Sea. *Geomat. Nat. Haz. Risk* **2024**, *15*, 2295817. [CrossRef]
105. Seitz, S.M.; Curless, B.; Diebel, J.; Scharstein, D.; Szeliski, R. A comparison and evaluation of multi-view stereo reconstruction algorithms. In Proceedings of the 2006 IEEE Computer Society Conference on Computer Vision and Pattern Recognition—Volume 1 (CVPR'06), New York, NY, USA, 5 June 2006; pp. 519–528. [CrossRef]
106. Corradetti, A.; Seers, T.; Mercuri, M.; Calligaris, C.; Busetti, A.; Zini, L. Benchmarking Different SfM-MVS Photogrammetric and iOS LiDAR Acquisition Methods for the Digital Preservation of a Short-Lived Excavation: A Case Study from an Area of Sinkhole Related Subsidence. *Remote Sens.* **2022**, *14*, 5187. [CrossRef]

107. CloudCompare: 3D Point Cloud and Mesh Processing Software Open Source Project. Available online: https://www.danielgm.net/cc/ (accessed on 10 June 2024).
108. Kim, H.; Kim, H.; Hyun, C.-U.; Park, H.-D.; Cha, J. Image Mapping Accuracy Evaluation Using UAV with Standalone, Differential (RTK), and PPP GNSS Positioning Techniques in an Abandoned Mine Site. *Sensors* **2023**, *23*, 5858. [CrossRef]
109. Tavani, S.; Pignalosa, A.; Corradetti, A.; Mercuri, M.; Smeraglia, L.; Riccardi, U.; Seers, T.; Pavlis, T.; Billi, A. Photogrammetric 3D Model via Smartphone GNSS Sensor: Workflow, Error Estimate, and Best Practices. *Remote Sens.* **2020**, *12*, 3616. [CrossRef]
110. Corradetti, A.; Seers, T.D.; Billi, A.; Tavani, S. Virtual Outcrops in a Pocket: The Smartphone as a Fully Equipped Photogrammetric Data Acquisition Tool. *GSA Today* **2021**, *31*, 4–9. [CrossRef]

water

MDPI

Article

Episodic vs. Sea Level Rise Coastal Flooding Scenarios at the Urban Scale: Extreme Event Analysis and Adaptation Strategies

Sebastian Spadotto [1,*], Saverio Fracaros [1], Annelore Bezzi [1] and Giorgio Fontolan [1,2,*]

[1] Department of Mathematics Informatics and Geosciences, University of Trieste, Via E. Weiss 1, 34128 Trieste, Italy; saverio.fracaros@phd.units.it (S.F.); bezzi@units.it (A.B.)
[2] National Interuniversity Consortium for Marine Sciences, CoNISMa, Piazzale Flaminio 9, 00196 Rome, Italy
* Correspondence: sebastian.spadotto@phd.units.it (S.S.); fontolan@units.it (G.F.)

Abstract

Sea level rise (SLR) and increased urbanisation of coastal areas have exacerbated coastal flood threats, making them even more severe in important cultural sites. In this context, the role of hard coastal defences such as promenades and embankments needs to be carefully assessed. Here, a thorough investigation is conducted in Grado, one of the most significant coastal and historical towns in the Friuli Venezia Giulia region of Italy. Grado is located on a barrier island of the homonymous lagoon, the northernmost of the Adriatic Sea, and is prone to flooding from both the sea and the back lagoon. The mean and maximum sea levels from the historical dataset of Venice (1950–2023) were analysed using the Gumbel-type distribution, allowing for the identification of annual extremes based on their respective return periods (RPs). Grado and Trieste sea level datasets (1991–2023) were used to calibrate the statistics of the extremes and to calculate the local component (subsidence) of relative SLR. The research examined the occurrence of annual exceedance of the minimum threshold water level of 110 cm, indicating Grado's initial notable marine ingression. The study includes a detailed analysis of flood impacts on the urban fabric, categorised into sectors based on the promenade elevation on the lagoon side, the most vulnerable to flooding. Inundated areas were obtained using a high-resolution digital terrain model through a GIS-based technique, assessing both the magnitude and exposure of the urban environment to flood risk due to storm surges, also considering relative SLR projections for 2050 and 2100. Currently, approximately 42% of Grado's inhabited area is inundated with a sea level threshold value of 151 cm, which occurs during surge episodes with a 30-year RP. By 2100, with an optimistic forecast (SSP1-2.6) of local SLR of around +53 cm, the same threshold will be met with a surge of ca. 100 cm, which occurs once a year. Thus, extreme levels linked with more catastrophic events with current secular RPs will be achieved with a multi-year frequency, inundating more than 60% of the urbanized area. Grado, like Venice, exemplifies trends that may impact other coastal regions and historically significant towns of national importance. As a result, the generated simulations, as well as detailed analyses of urban sectors where coastal flooding may occur, are critical for medium- to long-term urban planning aimed at adopting proper adaptation measures.

Keywords: sea level rise; storm surge; coastal flooding; extreme water levels; urban planning; local adaptation strategy; risk management; northern Adriatic Sea

Academic Editor: Maria Mimikou

Received: 29 May 2025
Revised: 30 June 2025
Accepted: 1 July 2025
Published: 2 July 2025

Citation: Spadotto, S.; Fracaros, S.; Bezzi, A.; Fontolan, G. Episodic vs. Sea Level Rise Coastal Flooding Scenarios at the Urban Scale: Extreme Event Analysis and Adaptation Strategies. *Water* **2025**, *17*, 1991. https://doi.org/10.3390/w17131991

1. Introduction

Sea level rise (SLR) is already affecting the Mediterranean and Adriatic coasts. Defined as a hot spot of climate change [1], especially in terms of extreme events [2], this area is

gradually warming 20% faster than global trends [3–6], as the effects are expected to be more intense than in other areas of the planet [7,8]. Globally, the imminent effects of SLR will lead to heightened risks of erosion, salinisation, and particularly coastal flooding [9,10]. The primary consequences include the loss of low-lying and sandy shoreline areas, shoreline retreat, saline intrusion [11], and the degradation of ecosystems [12–15]. In recent decades, coastal flooding events in the Mediterranean have intensified and become more frequent, linked to significant storms and severe surge phenomena [16–18]. Flooding is especially pertinent to the Adriatic Sea, where storm surge components are more pronounced than in other regions of the Mediterranean basin [19,20].

The northern Adriatic is noteworthy regarding meteorological and marine forcing [21]. The highest sea levels, resulting from storm surge events, may exceed the elevation of one meter in certain instances [22]. Extreme levels are attained during the autumn season, specifically in November, when the surge effect is pronounced due to the interplay of various factors, including the combined influence of strong Sirocco winds from the southeast [21] and the inverse effect of atmospheric pressure. South-easterly winds propel the water mass for durations of hours or days along the Adriatic Sea, leading to flooding events [23]. The impact of the generated storm surge is significantly greater in the shallow waters of the northern Adriatic [21,22,24,25].

The increase in sea level, coupled with the storm surge, can result in an enhanced response, particularly when combined with subsidence, notably for alluvial plain and deltaic-lagoon coastlines. For these reasons, whole northern Adriatic coastlines, encompassing the Venice and Grado-Marano lagoons along with the Po Delta territory, are among the Mediterranean regions most vulnerable to relative sea level rise (RSLR) and marine flooding [26–28], particularly during extreme events [29].

Furthermore, Rizzi et al. [30], Melet et al. [31], and Bonaldo et al. [32] have observed that sensitivity to SLR in Mediterranean regions, especially the northern Adriatic Sea (or the Nile Delta), is intensified by the high population density and significance concentrated along coastal strips [33,34]. Moreover, the coastal territories of the study area include several historical cities and important tourist destinations.

Densely populated coastal regions, which hold significant economic and tourism value, face the risk of disappearance due to a combination of factors [35,36]. Alongside the global and regional effects of SLR, rapid urban development has notably increased flood risks in coastal areas [37,38]. This has led to socio-economic damage [39–44], attributed to a growing population at risk of flooding [45] and recurring critical issues within urban environments [12]. This encompasses issues such as transport disruptions [46], vehicle accidents, and building collapses [47], along with impacts on land use [15] and human activities [48], thereby endangering significant cultural sites in certain coastal regions [49,50].

For this reason, careful studies should be carried out to analyse and define the impact and effects of marine flooding, especially in urbanised coastal areas [51].

The need to develop adaptation and mitigation plans [52–54] in response to the effects of climate change, sometimes by making substantial modifications to the territory at risk of extreme events [6,55], has increased public awareness and concern about political responsibilities in translating these issues into urban planning programmes [56]. Since 2008, starting with the Covenants of Mayor, European local governments have signed SECAPs, Sustainable Energy and Climate Action Plans, committing to increasing energy efficiency and the use of renewable energy sources, as well as incorporating adaptation measures and climate mitigation strategies [57]. Following the SECAP's guidelines, it was possible, for instance, to draw up coastal flood hazard maps for the urban area of Trieste [58], to assess the incidence of flooding at a local scale. Multiple studies [56,59–64] indicate that ad-hoc simulations are essential for designing flood management plans and for regular urban maintenance programs. This ap-

proach aids regional and municipal governments in formulating effective planning strategies and mitigation actions, thereby significantly reducing management costs in the short term [65].

In this work, we present a comprehensive study of flooding scenarios for the town of Grado, situated in the northern Adriatic Sea, which is recognised as one of the most significant coastal and heritage towns in Friuli Venezia Giulia. The town is built on a barrier island and experiences flooding, both from the sea and from the lagoon located behind it. In recent years, the local Civil Protection of the Friuli Venezia Giulia region has been quite active regarding flooding issues, particularly due to the challenges posed by water ingress from the lagoon side and the resulting inconveniences within the urban fabric. The objective of this work arises from the necessity to explore the criticality of flooding at an urban detail scale, where we can achieve sufficiently accurate altimetric precision to conduct various types of flooding simulations, including surge occurrence and RSLR projections. The analyses hold significant relevance for coastal areas like Grado, which has faced considerable challenges, particularly over the past decade.

2. Study Area

2.1. The Town of Grado

The municipality of Grado lies in the easternmost part of the Grado and Marano lagoon, bordering the northern part of the Adriatic Sea, in the Friuli Venezia Giulia region, Italy (Figure 1). The municipality has a total area of 115.5 km^2, 45 km^2 of dry land and 70.5 km^2 of lagoon [66]. The dry land represents the easternmost part of the barrier island systems bordering the Grado Lagoon and is almost entirely devoted to tourism and agriculture [67]. Despite having just over 7550 inhabitants [68], a number that triples during the summer season, it represents one of the most important tourist hubs in the region with 1.4 million visitors per year [69]. The settlement is connected to the mainland by a long artificial dam and includes a scenic lagoon-type core, around which more recent districts have developed. After the post-war period, the major urban development of the town took place, alongside the expansion of coastal accommodations and bathing facilities, including the "Costa Azzurra" popular beach, the seawall protecting the historic centre and the Main Beach [70].

Figure 1. Overview of the municipality area of Grado, located in the northern Adriatic Sea: (**a**) northern Adriatic Sea; (**b**) the eastern part of the northern Adriatic Sea and Grado and Marano Lagoon. The position of the DWRG1 wave buoy is also reported. The white rectangle identifies the study site; (**c**) orthophotography representing in detail the town of Grado.

Grado, after Aquileia, is an important archaeological site. Over the decades, significant cultural heritage has been discovered, ranging from the Roman to the early Christian and early medieval periods. Numerous relics have been discovered along the shoreline, particularly in front of the Grado seawall, including old church dykes and Roman structures [71–73]. The most significant remains are found in what is known as the *castrum*, the historic centre (Figure 1) that corresponds to the original urban core. Early Christian architectural relics include the St. Eufemia Cathedral, the baptistery and church of Santa Maria delle Grazie, and the ruins of the Basilica delle Corte.

2.2. Oceanographic and Meteoclimatic Forcing

The northern Adriatic wind climate is marked by the dominance of Bora winds, primarily originating from the E-NE direction, in both frequency and intensity [74,75]. The Sirocco winds originating from the southeast are also significant. The warm and humid Sirocco winds exhibit lower intensity compared to the Bora winds, yet they are distinguished by a significantly extended fetch of approximately 800 km. Under particularly persistent conditions, the Sirocco can produce waves of considerable heights along the North Adriatic coast [76].

Data from the wave buoy OGS-DWRG1 (coordinates 13.24° E, 45.56° N, −15.2 m depth) indicate that the mean significant wave height (Hs) is below 0.5 m. Events with significant wave heights exceeding 0.5 m constitute 25% of the total dataset, with predominant wave directions from the southeast (10.7%) and east-northeast (10.5%). The Scirocco exhibits the highest recorded wave heights, with Hs measured at 4.4 m [75]. The annual wave energy flux for the northern Adriatic region is 1.95 kW/m. Longshore drift is oriented westward from the mouth of the Isonzo River [77]. The astronomical tide in the Gulf of Trieste is semi-diurnal, with a mean value of 76 cm [78], 105 cm for spring tide, and 22 cm for neap tide [79]. The combination of spring tide, seiche, and low-pressure forcing, as well as strong SE winds that push the water mass below the coast, causes a significant rise in sea level [21,80], also known as surge or locally "acqua alta". The waves are bimodal due to the Bora and Scirocco winds [74].

3. Materials and Methods

The elaboration developed in this work includes a series of statistical analyses on tide gauge data and flooding map construction according to the following steps.

- Analysing the time series of sea level data recorded in three important tide gauges in the northern Adriatic Sea, to define the return period (RP) of extreme sea levels.
- Defining the threshold for the urban flooding of the city of Grado and estimating the occurrence and possible exceedance above the threshold.
- Using the LiDAR-derived digital terrain model (DTM), dividing the Grado territory into sectors with varying levels of vulnerability to obtain a series of downscaling maps of episodic flood-inducing extreme events with different RPs. The analysis also includes a detailed inspection of the promenade elevation along the lagoon border.
- Estimating relative sea level rise (RSLR) for the town of Grado, by comparing the IPCC AR6 Report [35], tide gauge data from Trieste and Grado, and the literature, for inferring the vertical land motion (VLM) component.
- Combining the RSLR predictions for 2050 and 2100 with the episodic events statistics and RPs, in order to assess the reduction of the same RPs of given flooding thresholds.

3.1. Statistics of the Extreme Water Levels

The total water level (TWL) data were derived from the records of the Meteo-Mareographic Network of the Lagoon of Venice (RMLV), pertaining to the Zero Mare

Punta della Salute 1897 (ZMPS datum). The historical series spanning 1950 to 2023 was examined to evaluate the likelihood of severe level occurrences. Given the large number of years available, we simplify our approach by adopting the Gumbel distribution, a specific case of the Generalized Extreme Value (GEV), using the Block Maxima (BM) methodology [81] in order to identify maximum values for uniform time intervals. The use of over 70 years of data provides a sufficient number of annual maxima to support a statistically sound application of the GEV-BM approach. As shown by Caruso and Marani [82], GEV-BM applied to the long time series of Venice exhibits low estimation uncertainty for return periods up to approximately 100 years, particularly when long calibration windows are available. Additionally, from the perspective of risk management, the moderate overestimation of return levels by GEV-BM in the short-to-intermediate return period range obtained by [82] can be interpreted as conservative, providing an additional safety margin in applications such as coastal infrastructure design, as in the case of Grado.

Annual maximum values exceeding 110 cm, referenced to ZMPS, were retrieved from the time series. The data spanning from 1950 to 2020 (prior to the closure system of the Venice Lagoon, called Mo.S.E.) are sourced from the 'Centro Previsione e Segnalazioni Maree' of the Municipality of Venice [83], whereas the data from 2021 to 2023 are provided by the same organisation but recorded offshore Venice by the 'Piattaforma Oceanografica Acqua Alta ISMAR-CNR' during the Mo.S.E operation. The subsequent procedure entailed a calibration process of the studied historical series about the SLR trend. A SLR rate of roughly 2.5 mm per year was utilised. The reference rate utilised was derived using the 1996–2023 reference period to examine the latest trends, based on the local history series documented by the Trieste tide gauge (Table 1), in relation to the national IGM datum (ref. Genova 1942).

Table 1. List of tide gauges in the northern Adriatic considered in this study.

Site	Station Name	Latitude (°)	Longitude (°)
Venice	RMLV	45° 25′ 50.49″	12° 20′ 11.97″
Trieste	Molo Sartorio	45° 38′ 50.00″	13° 45′ 33.90″
Grado	RMLV	45° 40′ 59.26″	13° 23′ 00.38″

The analysis of extremes utilised 2006 as the reference year, with a baseline from 1995 to 2014, according to the latest IPCC report [35], which reflects the most recent trends. A detrending operation was performed on the overall historical series values from 1950 to 2023, adjusting them based on 2006 as the barycentre of the baseline. Consequently, SLR rates should be subtracted from the years following the baseline and added to the years preceding the baseline, in relation to the trend observed from 1950 to 2023. The extreme values sample underwent statistical inference analysis to ascertain the parameters of the Gumbel distribution [84]. The data sample was arranged in descending order, and for each m-th value, the sample frequency of non-exceedance is computed using the plotting position formula based on Gringorten's formulation [85]. The least squares method was subsequently applied.

Once the non-exceedance probability function was defined, considering that this is linked to the return time of the value, it was possible to evaluate the extreme sea level value corresponding to an assigned RP. Finally, the obtained thresholds were adjusted according to the IGM datum, subtracting 23.56 cm from the level value referred to the ZMPS datum [86].

3.2. Annual Exceedance of Flooding Threshold

The analysis initially assessed the mean SLR trend for Grado concerning the duration of exceedances of the previously updated extreme thresholds. The sea level trend recorded by the tide gauge station in Grado (Table 1), reference ZMPS, is accessible in the ISPRA database [87]. The data, accessible since 1991, were collected at 5-min intervals until 2019 and at 10-min intervals from 2020 to 2023. The data were subsequently converted to the

IGM datum by subtracting 23.56 cm from the ZMPS reference level value. The mean sea level trend was compared to the maximum levels trend recorded in Grado, in order to check whether there was also a significant increase in extreme events, as reported by [82]. After comparing the trends, the issue arising from the duration of the events was evaluated to consider only events with a significant impact. The analysis was conducted by comparing the maximum recorded values against their duration, taking into account the total number of records for each year. The threshold value is here defined as the cumulative duration at the extreme 99.96 percentile, which represents approximately 0.04% of the total time, or 3 h.

3.3. Base for Downscaling Analysis

Flood hazard maps were developed concerning the urban and territorial context of the city of Grado. A "bathtub approach" [88] was employed using high-resolution DTMs with ESRI ArcGIS Pro 3.1.0 software. The objective involves assessing the elevations of the town's perimeter promenade (Figure 2a) to identify critical issues concerning both current water levels and projected future levels. To analyse the elevation of the lagoonal promenade and embankment, the procedure adopted is as follows. The Grado Digital Terrain Model (DTM), derived from a LiDAR survey conducted in 2018 (courtesy of Regione Friuli Venezia Giulia), was initially utilised. The derived DTM product exhibits a spatial resolution of 0.5×0.5 m. A 6-m-thick buffer was generated from the DTM elevations, derived from the outermost section of the promenade, specifically the part nearest to the water, moving inward. Given the different elevation statistics, the promenade has been segmented into four sectors (Figure 2b). This approach enabled a detailed analysis of the promenade and embankment elevations, assessing both point-specific and area-wide criticalities.

Figure 2. Downscaling area analysis: (**a**) elevation of the lagoon promenade considered in the study, represented by 10 classes subdivided every 0.10 m of elevation. (**b**) The subdivision of the promenade and lagoon embankment into 4 macro sectors; the extent of the inhabited area of Grado municipality is also reported, treating the streets as unobstructed surfaces for water flow while omitting buildings and uninhabited areas.

The calculation of the elevation value for the extracted cells became necessary to obtain averaged elevation information surrounding the cells, based on the fixed-width buffer. A GIS analysis tool (Cell Statistics, part of the Spatial Analyst extension in ArcGIS Pro 3.1.0) was used to perform this operation, enabling the calculation of an average value over a 6m radius for the entire length of the embankment section examined. To finalise the survey, the elevation values at the centre of the previously considered cells were extracted and subsequently subjected to statistical analysis. The analysed elevation points were filtered to exclude negative elevations exceeding a specified threshold. To assess bank heights in relation to extreme events, a range of heights from 70 cm to a maximum of 155 cm was evaluated, contingent upon the specific bank stretch examined. The heights obtained were represented through a graph illustrating the cumulative statistics as a function of the considered height ranges, indicating the percentage of embankment in safety relative to the threshold value of an extreme event associated with the return time.

3.4. Short-Term (Surge) Analysis

To represent the effects of storm surge events through water level thresholds, updated for recent decades, scenarios with varying probabilities of occurrence were analysed. The processing aims to create a mapping of flood hazards resulting from extreme events, serving as the foundation for assessing and managing flood risks, in accordance with the Flood Directive 2007/60/CE, which was later implemented in Italy through Legislative Decree 49/2010. The Flood Directive allows for reference solely to extreme events, contingent upon an evaluation of the protection level. Some Italian methodological reports on coastal flooding, such as those from the Sardinia region, have indicated that the absence of a precise regulatory definition of the "adequate level of protection" [89] suggests refraining from utilising this prerogative. In contrast, based on territorial urban planning and civil protection measures, particularly in Emilia Romagna [90–92], a region with a comparable coastal physiography to Friuli Venezia Giulia, an assessment was conducted to evaluate the impact of marine events with short RPs. Consequently, the development of flood hazard maps for RPs of 2, 10, 30, and 100 years was undertaken. The maps were developed by assessing the inhabited regions according to the boundaries of the municipality of Grado, treating the streets as unobstructed surfaces for water flow while omitting buildings and uninhabited areas. The analysis primarily concentrated on the historical centre, the area exhibiting the highest vulnerability, and extended in an eastward direction. The analysed municipal area of Grado extends for approximately 0.96 km^2 (Figure 2b).

3.5. Long-Term (RSLR) Analysis

To develop a projection of RSLR over the medium to long term, the mean sea level of Grado was analysed for the period from 1991 to 2023. To compare the data from Grado and assess their significance, the dataset from Trieste was utilised. The temporal trend of sea level is assessed by CNR-ISMAR in Trieste and is accessible in the database of the Permanent Service for Mean Sea Level [93]. The analysed data encompasses the recorded sea level and the subsidence component, a critical factor for long-term level projections. To undertake a long-term analysis, subsidence data from Da Lio and Tosi [94] and Areggi et al. [95] were used as a reference. The computed value for Grado, acquired using SAR and GNSS interferometry between 2003 and 2010 [94] and 2015 and 2019 [95], was then compared to the residual produced by correlating Grado and Trieste's sea level changes. The mean value was used to generate long-term RSLR projections for 2050 and 2100. Using the values recorded by satellite and reported by the NASA Sea Level Projection Tool [96] for Trieste, the RSLR and tectonic contribution data were adjusted based on a correction factor, averaged across the territory of Grado. After calculating the increases for 2050 and 2100

based on ongoing climate changes, the reductions in RPs for certain significant episodic events were evaluated.

This analysis assessed both the magnitude of flooding and the exposure of the urban environment to flood risk. The scenarios mentioned focus on a single short-term event related to the threshold update, followed by that event along with sea level predictions for 2050 and 2100, as detailed in the latest IPCC AR6 Report [35].

4. Results and Discussion

4.1. Extreme Water Levels

The results of the sample fit analysis to Gumbel's distribution law on extreme water levels are shown in Figure 3. The RPs indicated in Table 2 (reference baseline: 1995–2014; central year: 2006) are paired with the corresponding updated extreme thresholds. According to the Flood Risk Management Plan of the Eastern Alps Hydrographic District for Zone 2 (PGRA) [97], the values obtained are related to the mere water component, or to the sum of the meteorological component, astronomical tide, and mean sea level component.

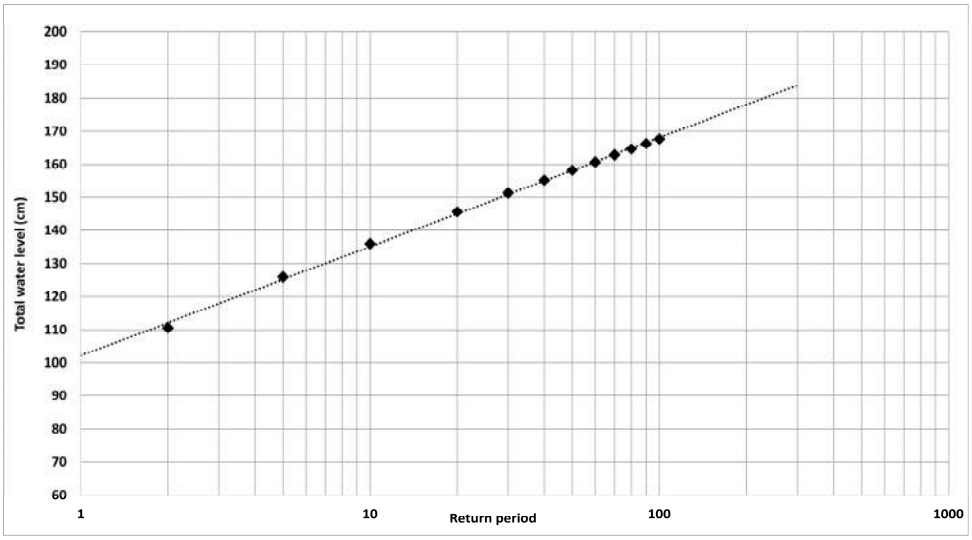

Figure 3. Extreme water level statistical analysis (Gumbel distribution) observed at the RMLV meteo-mareographic station in Venice (reference period 1950–2023).

Table 2. Updated extreme level values as a function of return period (reference year 2006, Gumbel distribution).

Return Period (Years)	Extreme Water Levels (cm)	Confidence Interval (95%)
2	111	107–115
10	136	125–146
30	151	136–165
100	168	147–186

The values listed in Table 2 serve as an update to the PGRA, which is based on the time baseline of 1985–2005 and includes data from the severe tidal level statistics compiled by Pirazzoli and Tomasin [98]. The extreme water levels reported within the PGRA, relating to events with a RP of 30 and 100 years, are lower by approximately 8/10 cm.

4.2. Analysis of Mean vs. Max Levels and Threshold Exceedance

The evolution of mean sea level is commonly utilised for long-term projections; however, in the short and medium term, the temporal changes in maximum levels may offer more pertinent information regarding the risk of storm surge. Our aim is to compare the

evolution of mean sea level with that of maximum levels, as illustrated in Figure 4. The selected time interval spans just over 30 years, providing a sufficiently extensive historical series to assess the annual inter-variability of the meteorological component [99].

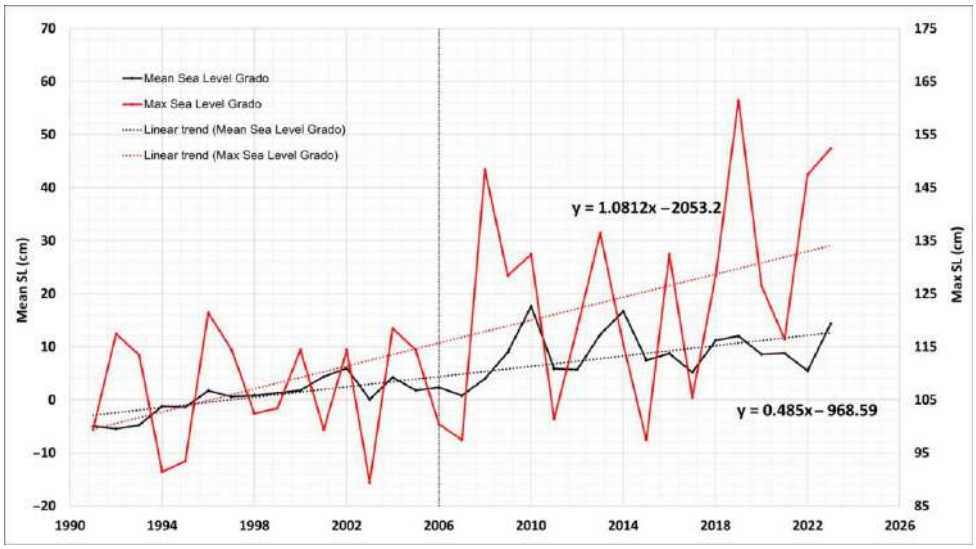

Figure 4. Comparison of the mean sea level (black line) and the maximum sea level (red line) observed in Grado from 1991 to 2023 (IGM42 reference). The left axis indicates the scale for mean sea level, whereas the right axis signifies the maximum levels.

The maximum levels observed are rising at a rate of 10.8 mm/y, which is more than double the mean values of 4.9 mm/y. This suggests, within the limits of thirty-year statistics, that the risk is escalating more substantially than indicated by current projections.

The risk associated with storm surge events is not solely determined by the peak levels attained but also by the duration of the events. Consequently, it was determined to evaluate the level exceeded over a specified duration within a year, specifically a minimum of 3 h. The graph in Figure 5 illustrates the temporal trend of maximum levels recorded in Grado that persisted for a minimum of 3 h. The 2006 as the barycentric year for the thirty-year reference trend, consistently corresponds to the latest IPCC AR6 report [35], thus allowing for projections that are approximately aligned with the most recent trend.

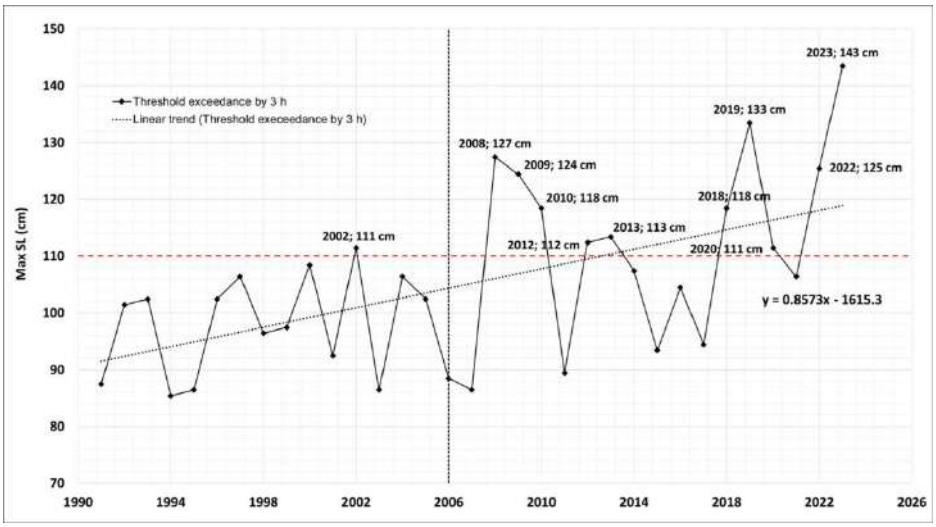

Figure 5. The 30-year trend of maximum sea levels recorded in Grado that persisted for a minimum of 3 h (threshold exceedance by 3 h). The threshold level of 110 cm (ref. IGM42 datum) is here reported as a reference value for flooding phenomena in the 'Old Town' (see Figure S1 in the Supplementary Materials).

By observing the graph in Figure 5, an analysis can be conducted on the average trend of sea level maxima exceeding a minimum of 3 h annually. The angular coefficient is 8.6 mm/y. The average value indicated by the trend line demonstrates a duration of 3 h for events commencing in 1991, with an initial extrapolated value of 93 cm, increasing to approximately 118 cm by 2023. Over a period of slightly more than 30 years, maximum levels have risen by 25 cm. The graph indicates a minimum threshold value of 110 cm, serving as a precautionary reference. This value corresponds to an event with an approximate RP of 2 years and a high probability of occurrence. In the town of Grado, an ingress level of 110 cm indicates substantial submersion in the historic centre, particularly along the docks of the Mandracchio Canal. In 10 of the past 18 years, the city of Grado has experienced flooding events with water levels exceeding 110 cm for a duration of almost 3 h.

4.3. Downscaling Analysis of Short-Term Flooding

This section presents and discusses various marine flooding hazard maps derived from the results of the developed flood scenarios. The elaborations depict the episodic event scenario along with the corresponding RP. Each event is defined by a critical threshold that indicates the total elevation of the water mass throughout the event. The simulations employed a static methodology alongside qualitative data analysis, omitting variables such as ingress speed and flooding duration from consideration. The wave component was excluded from the analysis, as the water mass traverses the Grado inlet (see Figure 1c) and propagates into the lagoon, resulting in a progressive damping of the wave set-up parameter.

Table 3 depicts a summary diagram of the many scenarios evaluated, represented by the RP associated with the threshold value, as well as the overall extension of the inhabited region impacted by marine ingression, expressed in square kilometres and as a percentage of the entire municipality.

Table 3. Extreme water levels with return periods (levels expressed in cm), which correspond to the relative flooded areas, expressed in terms of size (km^2) and percentage value with respect to the built-up area of the Municipality of Grado of 0.96 km^2.

Return Period	Extreme Water Levels (cm)	Inhabitated Area (km^2)	Flooded Area (%)
2	111	0.016	1.67
10	136	0.20	20.8
30	151	0.40	41.7
100	168	0.61	63.5

Below are the hazard maps drawn up on the basis of the episodic events considered. The hazard maps are realised by means of the water depth representation, i.e., the hypothetical maximum water elevation above the ground reached during flooding. The water depth is extrapolated as a function of the heights of the starting DTM and the flooded area.

4.3.1. The 2-Year Return Period Episodic Event

In the case of a meteomarine event with a RP of 2 years, the water level has a total elevation of approximately 111 cm. The flood hazard map is shown in Supplementary Materials (Figure S1). The downscaling analysis (scale 1:5000) enables detailed verification of the problems caused by flooding. On the map, it is possible to establish that the criticalities occur mostly around the Mandracchio Canal and the Brioni promenade. Both stretches correspond to the lowest urban areas that allow the water mass to advance inwards. The criticalities found mostly concern the propagation of the water mass into the interior of the old town by means of the urban network. The nearby historic centre, located south of the Mandracchio Canal, does not exhibit any particular criticality.

4.3.2. The 10-Year Return Period Episodic Event

In the case of a meteomarine event with a RP of 10 years, the water level has a total elevation of 136 cm. The flood hazard map is shown in Figure 6.

Figure 6. Flood hazard map representing an event with a 10-year RP (136 cm). The blue colours represent the water depths as a function of the city's DTM elevations: (**a**) The inundation map of the 'Old Town' sector shows that this area is almost entirely affected by the extent of the flooding. Flooding also affects parts of the historic centre. (**b**) It depicts the slight expansion of flooding to the east as well, with some ingressions of the water mass toward the built-up area by the Moreri Canal. (**c**) Flooding in the western part of the historic centre during 27 October 2023 (photo credits: Cester E.). (**d**) Expansion of the water mass along the western docks of the Mandracchio Canal during 27 October 2023 (photo credits: Cester E.). (**e**) expansion flooding along A. Manzoni Street during 29 October 2018 (photo credits: Folla M.).

The 1:5000 downscaling analysis made it possible to observe more clearly the extended criticality along the lagoon promenade of Riva Brioni, the town's primary western encroachment area. We could also observe a generalised extension of the water mass around the Mandracchio Canal through its perimetral docks. Compared to the previous simulation, the water mass extends both to the east and west of Mandracchio, almost completely affecting the old town and partially affecting the historic core to the south. There is also an eastern expansion of the water mass through two areal criticalities of the lagoon promenade along the Moreri Canal.

4.3.3. The 30-Year Return Period Episodic Event

Compared to the previous scenario, in the simulation of a storm surge event with a return time of 30 years and a total elevation of 151 cm, the urban flooding also extends along the eastern part of the town (Figure 7).

Figure 7. Flood hazard map representing an event with a 30-year RP (151 cm). The blue colours represent the water depths as a function of the city's DTMs elevations: (**a**) The inundation map of the 'Old Town' sector shows that this area is completely flooded. The extent of the flooding also affects much of the historic centre. (**b**) The widespread flooding in the city's 'Grado East' area. Water flows inland through the Moreri Canal's embankment at several places. (**c**) Flooding near the southwest dock of the Mandracchio Canal during 27 October 2023 (photo credits: Cester E.). (**d**) Flooding in front of the St. Eufemia Cathedral during 12 November 2019 (photo credits: Patruno V.). (**e**) Extensive flooding along the end of the Moreri Canal embankment, Monfalcone Street during 27 October 2023 (photo credits: Rai Tgr Fvg website).

The flooding affects the entire old town, particularly the historic core surrounding the St. Eufemia Cathedral and the Baptistery. It extends approximately 2000 metres along the lagoon promenade of the Moreri Canal, impacting many areas in the eastern part of the city. The additional 15 centimetres, compared to the 10-year RP scenario, clearly illustrate how a meteomarine event of this magnitude can lead to an expansion of the water mass covering a significant portion of the urban fabric.

4.3.4. The 100-Year Return Period Episodic Event

This statistically rare event is characterized by a water mass elevation of 168 cm, thus representing a real calamity for the town of Grado. The event is responsible for a large inundation effect, which extends throughout the old town. Some of these areas are affected by a very high water depth. Compared to the 30-year return time event, the water mass penetrates the lagoon promenade of Moreri Canal for its entirety, generating flooding that affects almost the entire eastern urban fabric, spreading the water mass into areas close to the Main Beach. The flood hazard map is shown in Supplementary Materials (Figure S2).

4.3.5. Lagoon Promenade Downscaling Analysis

We performed the promenade elevation analysis along the complete boundary that divides the town from the lagoon. The assessment encompasses the full perimeter embankment stretching from Riva Brioni to the easternmost part of the Moreri Canal, divided into four macro-sectors. This approach enabled a more thorough examination of the embankments, assessing both specific and broader critical issues. Table 4 presents the analysed promenade/embankment sectors along with their respective lengths, the total length of the embankments, and the percentage of each section in relation to the total length.

Table 4. Lagoon promenade/embankment sectors analysed for elevation analysis aimed at the flooding assessment.

Promenade/Embankment Sector	Length (m)	Percent (%) of Total Length
Riva Brioni-Mandracchio C.	573	9
Mandracchio C.	1392	22
Schiusa Island	1681	27
Mandracchio C.–Moreri C.	2685	42
Total embankment	6334	100

The two lagoon promenade and docks sectors most vulnerable to marine ingression are described below. The first stretch considered concerns the Riva Brioni—Mandracchio sector. The second section concerns the Mandracchio Canal. The other two sectors, Moreri Canal and Schiusa Island, are shown and described in the Supplementary Materials (Figure S3 and Figure S4, respectively).

Riva Brioni—Mandracchio C.

The section considered has a total length of 260 m. Figure 8 displays the analysis of the promenade's heights along the entire Riva Brioni. The survey covered a total of 6188 measured points within an elevation range of 70 to 125 cm. Hence, approximately 85% of the height of the promenade section considered is below 111 cm (Figure 8b). This means that, already with a meteomarine event with a high probability of occurrence, having a RP of 2 years, the perimeter promenade is not in a safe condition. On the other hand, considering an episodic event with a RP of about 5 years and approximately 125 cm of water level, the entirety of the promenade is not in a safe condition, causing the expansion of the water mass in the western area of the urban centre.

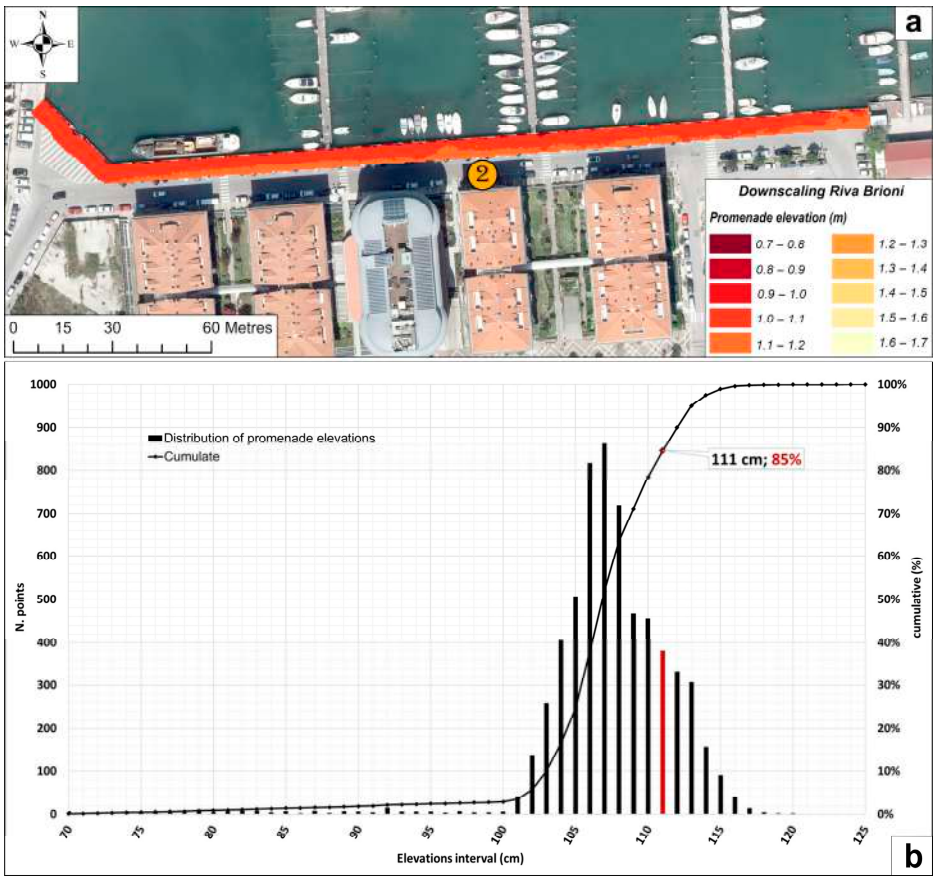

Figure 8. Critical sector promenade of Riva Brioni (see Figure 6a, number 2 for the position): (**a**) represents the elevations extracted from the 6-m buffer of the promenade. The elevation values of the promenade range from 70 to 125 cm. (**b**) represents the statistical distribution of the elevations extracted from the promenade of Riva Brioni. Shown in red is the 111-cm elevation column, which represents about 85% of the cumulative statistics. The promenade is then flooded with an event with a very high probability of occurrence (RP = 2 years).

Mandracchio C.

The Mandracchio Canal has a total length of 1392 m, corresponding to 22% of the total lagoon promenade. The analyses of the canal's banks covered a total of 31,782 measured points within an elevation range of 70 to 155 cm. Historically, the main flooding within the built-up area of Grado occurs through the docks of the Mandracchio Canal, the preferential route of water ingression within the ancient centre. In fact, as described in Section 4.2, the 110 cm threshold has been exceeded for 3 h in a year almost 9 times in the last 15 years (2008–2023). This statistic is corroborated by the graph in Figure 9b, which shows that 50% of the Mandracchio docks are not in a safe condition for an event with a RP-2 year. It follows that even with a very low elevation threshold, the historic centre is experiencing significant flooding. On the other hand, considering a RP of 10 years, with a medium-high frequency of occurrence and a level of 136 cm, the entire docks of the Canal do not guarantee any safety, entailing extensive flooding both to the west and east of the Mandracchio itself, also affecting the portion of the historic core post south of the Canal (Figure 6a,c).

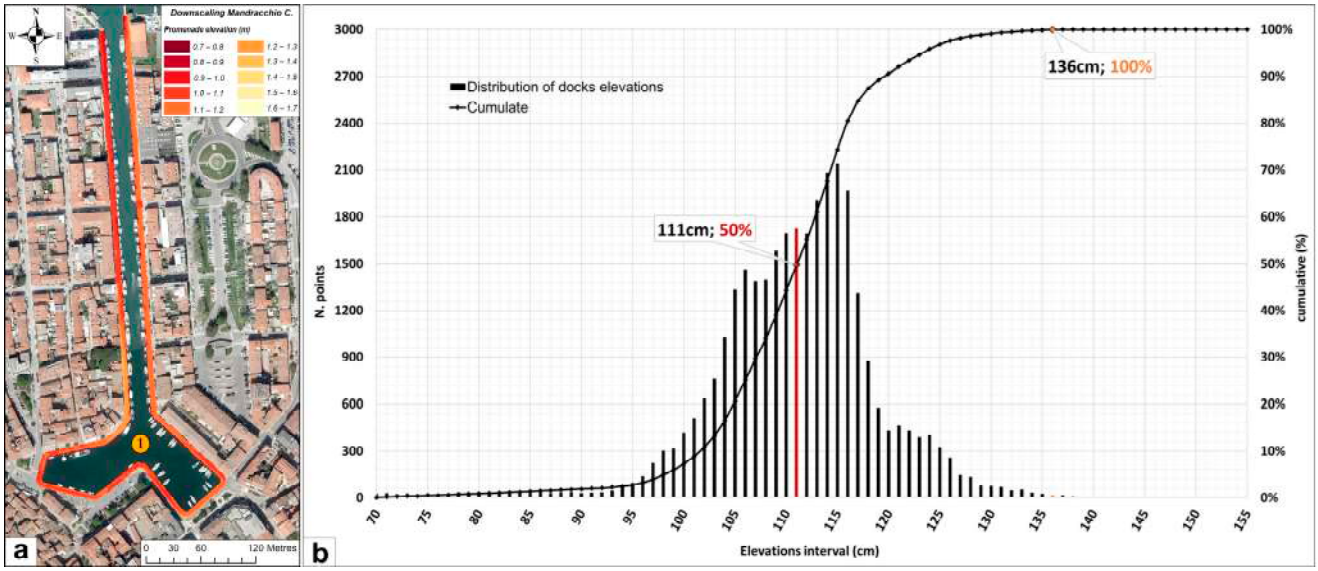

Figure 9. Critical sector of Mandracchio Canal docks (see Figure 6a, number 1 for the position): (**a**) represents the elevations extracted from a 6-m buffer of the docks. The elevation values of the canal docks range from 70 to 155 cm. (**b**) represents the statistical distribution of the elevations extracted from the Mandracchio Canal docks. Shown in red is the 111 cm elevation column, which represents about 50% of the cumulative statistics. Shown in orange is the elevation of 136 cm, the level of an event with a medium to high probability of occurrence (RP = 10 years), resulting in complete submergence of the canal docks.

4.4. Downscaling Analysis of Long-Term Flooding

Considering the last 30 years, from 1991 to 2023, the SLR trend of Grado falls back to values of 4.8 mm/y (Figure 10). Reducing the reference time interval tends to increase the trend. The level fluctuations can reach up to 10 cm from one year to the next, as demonstrated in the year 2010.

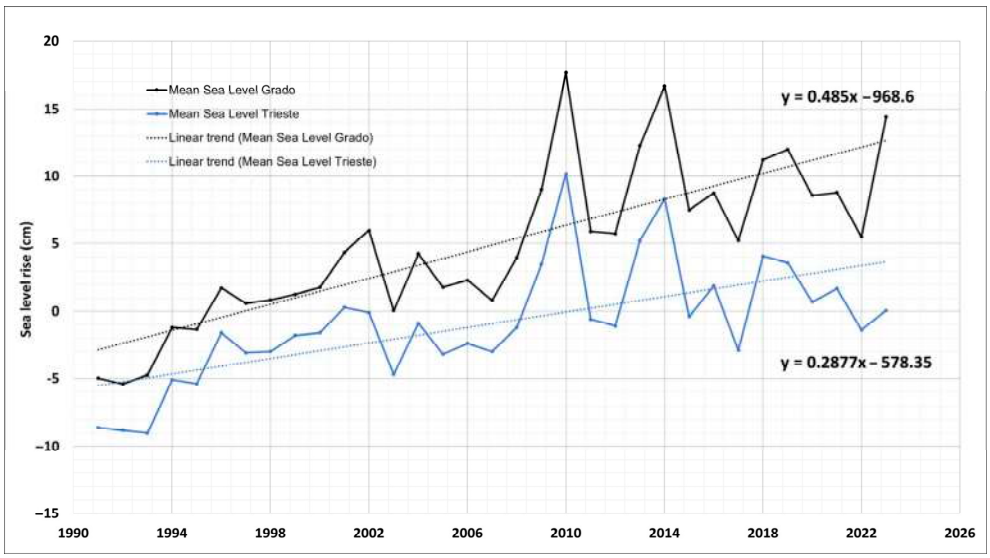

Figure 10. The 30-year trend of sea level change in Grado (black line) and Trieste (blue line) with IGM42 reference. Elevation in ordinate has been kept to scale for each series. Trends can be calculated on the basis of linear regression.

The sea level trends in Grado and Trieste exhibit notable similarities. The difference in rates, specifically 4.8 and 2.8 mm/year, can be attributed to the subsidence component (vertical land motion, VLM). Trieste is the only location where subsidence is minimal

relative to the rest of the northern Adriatic [100,101]. The VLM inferred from sea level trend comparison and the literature data [94,95] falls within the interval 1–2 mm/year. Accordingly, we chose to apply a mean subsidence rate of 1.5 ± 0.5 mm/year for Grado, which is pertinent for formulating RSLR projections for 2050 and 2100. Using the nearest sea level data from Trieste, sourced from the NASA Sea Level Projection Tool [96], an increase of 1.5 mm/year should be calculated by multiplying this rate by the number of years since the barycentre of 2006. Specifically, this results in 44 years if the projection is extended to 2050 and 94 years if extended to 2100. The values for VLM to incorporate into the SLR scenarios are 6.6 ± 2.2 cm for 2050 and 14.1 ± 4.7 cm for 2100, respectively.

Table 5 summarises the sea levels projected to 2050 and 2100 according to the calculations made above.

Table 5. Projection of sea level in 2050 and 2100 according to IPCC AR-6, as reported in the NASA Sea Level Projection Tool [96]. Sea level projections refer to the city of Trieste. Vertical land motion (VLM) for Grado is assumed at a rate of 1.5 ± 0.5 mm/year (see text for explanation). The total sea level for Grado is calculated by adding the two components.

Year	SLR Scenario Reference 2006 Baseline (1995–2014)	Trieste Sea Level (cm)	Total VLM (cm) for Grado (Average Rate)	Total Sea Level for Grado (cm)
2050	SSP1-2.6 (median)	17	6.6	23.6
	SSP5-8.5 (median)	21	6.6	27.6
2100	SSP1-2.6 (median)	39	14.1	53.1
	SSP5-8.5 (median)	67	14.1	81.1

At this stage, by looking at the most important rare events and taking into account city planning and the expected RPs of 10, 30, and 100 years, we can figure out how much the RPs change by examining the expected sea level rise for 2050 and 2100 under the best- or worst-case scenario.

In the context of an extreme episodic event that has a low probability of occurrence and is linked to a RP of 100 years, along with projected sea level rises for both 2050 and 2100 under a pessimistic SSP5-8.5 scenario, we can anticipate a potential situation as follows:

$$\text{critical threshold to 2050} = \text{current RP 100 y} - \text{RSLR 2050} = 168\ \text{cm} - 28\ \text{cm} = 140\ \text{cm}.$$

Considering a pessimistic scenario, the value of 168 cm at 2050 becomes, after subtracting the 28 cm SLR, approximately 140 cm. The latter value corresponds to a threshold reached by an episodic event with a RP of about 14/15 years. On a probabilistic level, exceeding the 168 cm threshold in 2050 could occur almost seven times more frequently. For this reason, the frequency of extreme events is bound to increase significantly in the near future. We can apply the same reasoning to a 100-year episodic event with an optimistic projection to 2100. In this case, 53 cm will have to be subtracted. At 2100, the value of 168 cm will become approximately 115 cm. The latter corresponds to an episodic event with a return time of about two to three years. On a probabilistic level, exceeding the 168 cm threshold in 2100 may occur 33 times more frequently. The values found, typical for the eastern part of the northern Adriatic, are quite similar to those reported by Lionello et al. [102], which looks at how RPs change based on sea level rise rates expected for 2050 and 2100 in the western part of the northern Adriatic. The application of SLR's worst-case scenario for 2100 is now rendered pointless.

4.5. Adaptation Plans

Grado, like other coastal resorts in the northern Adriatic that rise in contexts characterised by low and sandy coasts, is subject to the effects of sea level rise in a much more evident way than other territories [103]. Similarly to the safety measures adopted for the

city of Venice through the activation of the Mo.S.E barrier in 2020 [104], the need to adopt adaptation and mitigation strategies to address the rising frequency of extreme events has also emerged for the town of Grado. In addition, the impacts of coastal flooding are expected to increase due to ageing defence infrastructures [105]. For this reason, urban embankments need to be structurally verified, and their heights carefully checked and adapted (and thus raised, [106]) to a safe level.

Consequently, plans to raise embankments and promenades need to be adjusted based on how much the sea levels are expected to rise [107] during extreme weather events. The types of actions to take depend on how uncertain we are about the extreme value statistics and future sea level rise predictions [108–110]. Therefore, the updated extreme level thresholds, based on the case histories of the past decades, made it possible to formulate hypotheses for adaptation and urban planning in the most vulnerable promenade sectors. Indeed, strategising for the medium- to long-term future would enable a decisive solution to site-specific flooding for many decades to come. However, the most reliable future projections focus on short-to-medium-term scenarios and the pessimistic SSP5-8.5 projections, which also depend on the potential increase in extreme events.

Starting from the data of the scenarios and the RP of the events, the embankment sealing hypothesis starts from the evidence that one must proceed by considering, in a modular way, interventions that, in order of priority, start from the most critical sections. The entire urban stretch facing the lagoon has docks whose elevation cannot guarantee sealing for events with very frequent return times. Consequently, based on the study conducted, a safety threshold level of 180 cm can be chosen. This figure roughly corresponds to a meteomarine event, which statistically occurs with a RP of approximately 250 years. Thus, considering a pessimistic sea level rise to 2050 calibrated on the city of Grado, equal to an increase of approx. 28 cm, on a probabilistic level, a lowering of the threshold level to 152 cm would occur. The value in question corresponds to an event with a RP of ca. 30 years, defined as having a medium probability of occurrence. At present, this type of intervention secures the territory and, in the future forecast, will allow sufficient time to prepare—should it be deemed necessary—appropriate modifications or additions. The value of 180 cm, therefore, allows us to have a certain margin of coverage that is much more reliable than a safety value that, correlated with a less reliable projection, would have a greater degree of uncertainty.

Once the threshold level of security and the most vulnerable sectors to be safeguarded have been ascertained, based on downscaling simulations and elevation analysis, the next step concerns which adaptation strategies to put in place. The provision of defensive measures depends on various factors, such as political, regional and local decision-making wills. An example of this approach is the SECAP project, undertaken to incorporate adaptation measures and climate mitigation strategies at the municipal level for the city of Trieste [58]. Nevertheless, additional factors will be closely related to the layout of the urban fabric [111] and therefore directly controlled by anthropogenic elements, such as urbanisation, accommodation space, adaptability, land-use change, as well as the configuration and size of the road network [112].

The first two stretches in need of timely intervention concern the perimeters that extend over two sectors, from Riva Brioni to the Mandracchio Canal inclusive, for a total of 1919 m. Within this section, the two perimeters requiring timely intervention are Riva Brioni (260 m) and the Mandracchio Canal (1392 m). Riva Brioni is characterised by a promenade that, throughout its entire extension, has heights ranging from 70 to 115 cm. The road surface width, measured from the outer edge of the promenade to the pavement on the opposite side, is approximately 14 m (Figure 8). Of this, the space relating to the urban road is approx. 5 m. The area where changes will be made for raising the shoreline or

changing the lagoon promenade is about 7 m wide: 3 m for the lagoon promenade and 4 m for parking spaces, which could be adjusted if needed. These characteristics make Riva Brioni one of the few city areas that are most exposed to flooding, where it is possible to implement a significant change in the urban fabric. One possibility concerns the application of bulkhead planter systems or of a bank (see Toledo et al., [113]) extended along the entire affected area (see Figure 11). A further hypothesis is the application of a seawall-walk barrier system that transforms the Riva Brioni promenade into a fully-fledged barrier that maintains the existing pedestrian section connected to the waterfront.

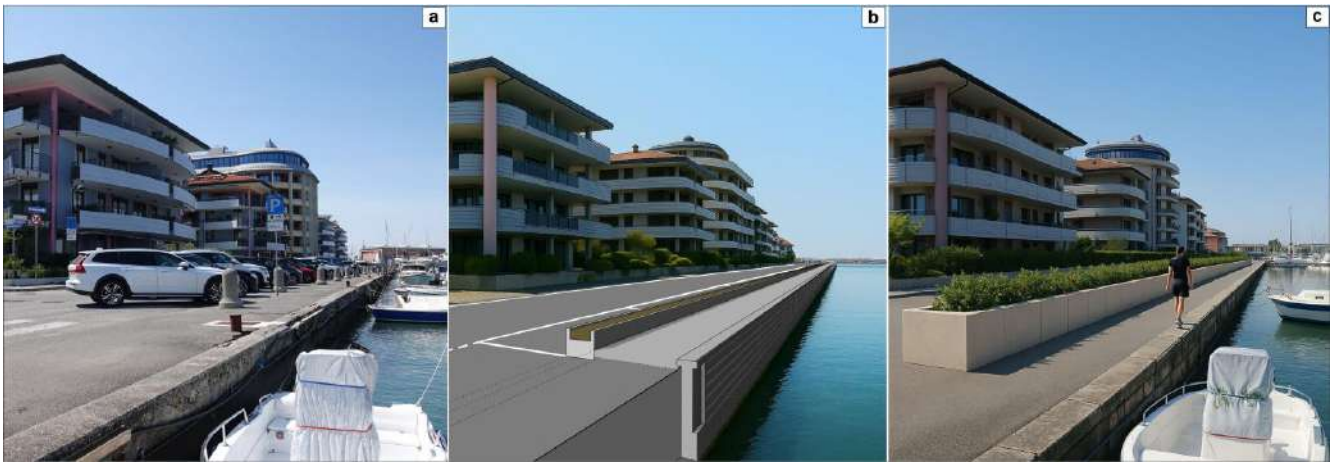

Figure 11. The Riva Brioni promenade. (**a**) Photo of a promenade section, taken at coordinates 45°68′28.63″ N, 13°38′06.56″ E (photo credits: Spadotto S.). (**b**) Design of a bulkhead planter system, built along the entire promenade. Toward the lagoon, the promenade is maintained. Toward the street, parking spaces are created parallel to the bulkhead planter, and the roadway is maintained. (**c**) Rendering of what Riva Brioni might look like. For the sake of clarity, possible regulated openings needed between the planters for pedestrian transit and dock access are not depicted here.

The situation is different for the Mandracchio Canal. The docks surrounding the canal are characterised by a higher elevation than those at Riva Brioni. However, these fail to provide adequate defence, resulting in a general ingression of the water mass into the built-up area, affecting the historic centre to a certain extent, even with water levels that are not particularly critical, slightly higher than 110 cm. The layout of the streets and buildings surrounding the canal, for nearly their entire length, does not permit significant modifications to the urban fabric. The space available from the docks, where there are boat moorings, to the walls of the buildings on the opposite side is approximately 6 m. It follows that the usable space for a possible intervention is completely absent. For this reason, a possible proposal concerns the design of mobile defence systems at the Mandracchio lagoon entrance (Figure 12), similar conceptually to those already widely used in Northern Europe, especially in the Netherlands with the Maeslant Barrier in Rotterdam [114], designed for protection against very extreme flood events [115]. In Cesenatico, Emilia Romagna, Italy, there exist mobile defence systems known as Porte Vinciane (Da Vinci's gates), a Project by Binini Partners [116] (Figure 12c).

Figure 12. The Mandracchio Canal docks. (**a**) View of the Mandracchio C. lagoon entrance (Photo credits: Fontolan G.). (**b**) Plan view of the Canal opening. (**c**) Example of Porte Vinciane (Da Vinci's gates) mobile system for flood defence in Cesenatico, a Project by Binini Partners (after [116]). (**d**) Functional design of Baby Mo.SE floodgates in Chioggia (after [117], modified). (**e**) Example of mobile floodgate in operation in Chioggia (after [117]).

Another possible solution could be a mobile system like the Mo.S.E [118] designed in Chioggia, called Baby Mo.SE [117] (Figure 12d,e). Constructing these weirs directly in the upper opening part of the Mandracchio, approximately 20 m wide, can guarantee a safe condition in the city surroundings. Additionally, from an economic perspective, the intervention would be less costly than designing an extended dock elevation for the entire Mandracchio Canal.

5. Conclusions

In evaluating sea level estimates, the issue of flooding in coastal regions and towns vulnerable to marine intrusions emerges as a critical priority for spatial planning. In this paper, we presented an exhaustive investigation of the reality of Grado, an Adriatic coastal town that has experienced significant marine flooding, especially during the last decade. The objective of the study is to assess, identify, and delineate urban regions susceptible to flooding, based on current episodic occurrences and projections of future sea level rise that may exacerbate extreme events.

A statistical update of extreme water levels, analysing trends in maximum levels and the hourly duration of their exceedance, and evaluating medium and long-term sea rise projections, revealed the need for the town to verify the elevations of the perimeter embankments and promenades that separate the lagoon from the urban centre. As a result of the current defensive status, which does not provide adequate assurances during even minor surge events, some preliminary intervention hypotheses have been developed to improve the condition of the lagoon promenade, particularly in the most problematic locations. These options can be considered in future adaptation plans, thus contributing to urban planning procedures.

A downscaling analysis found that the most important challenges are concentrated near the town's western lagoon edge. Even with very high recurrence times (i.e., a 2-year RP), equivalent to water levels of 111 cm, significant challenges were identified in two adjacent urban sectors that are crucial for the propagation of seawater into the historic centre.

Increasing the RP of the events, criticalities also spread toward the eastern lagoon edge. Accordingly, urban criticalities extend outward along the eastern perimeter, and the area of the regions impacted by the water mass expands significantly. An episode with a 10-year RP affects 21% of the whole municipality but entirely impacts the western historic centre, causing significant issues for both the people and the road network.

Sea level rise would cause floods to occur more frequently and with greater severity in the future, which will eventually result in shorter RPs. Between 2008 and 2023, ten flooding events occurred, exceeding the 110 cm water threshold for almost 3 h. Therefore, the trend to date is 1.5 events per year, with a greater size during the previous two years taken into consideration. Even with an optimistic sea rise forecasting for 2050 (short-medium projection period), it is possible to heavily reduce even very extreme events that have RP longer than 200 years.

These simulations demonstrate how crucial it is to downscale coastal urban locations in order to promptly define critical situations involving the existence of ingression points, presently insufficient perimeter embankments and promenades, and/or depressions in the urban fabric that allow water to easily enter and cause damage and inconvenience to the population.

With respect to the predisposition of climate change adaptation strategies by prompt evaluation of the phenomenon's incidence at the municipal level, the analyses suggested in this paper are crucial. Extreme events and return times aid in forecasting the future development of the phenomena, encouraging the first meaningful conversations regarding adaptation measures required to create comprehensive urban planning procedures for the town of Grado. Relying on defensive systems that are planned and constructed using a modular approach, considering the rates of sea rise and the potential for an increase in severe events, and that can be adjusted based on the configuration of the urban fabric, will be the issue and the challenge for the near future.

Supplementary Materials: The following supporting information can be downloaded at: https://www.mdpi.com/article/10.3390/w17131991/s1, Figure S1: Flood hazard RP 2 y (111 cm); Figure S2: Flood hazard RP 100 y (168 cm); Figure S3: Statistics of elevation and flooding occurrence of Schiusa Island promenade; Figure S4: Statistics of elevation and flooding occurrence of Moreri Canal promenade.

Author Contributions: Conceptualization, S.S., S.F. and G.F.; methodology, validation, formal analysis, S.S., S.F., A.B. and G.F.; data elaborations, S.S. and G.F.; writing—original draft preparation, S.S. and G.F.; writing—review and editing, S.S., S.F., A.B. and G.F.; supervision, G.F.; project administration, A.B. and G.F.; funding acquisition, G.F. All authors have read and agreed to the published version of the manuscript.

Funding: This study was funded by (i) the consortium iNEST (Interconnected North-Est Innovation Ecosystem) funded by the European Union Next-GenerationEU (Piano Nazionale di Ripresa e Resilienza (PNRR)-Missione 4 Componente 2, Investimento 473 1.5-D.D. 1058 23/06/2022, ECS_00000043); (ii) the Civil Protection of the Autonomous Region Friuli Venezia Giulia, through the Collaboration Agreement with the Department of Mathematics, Informatics and Geosciences (DMG) of the University of Trieste, Project D86-AARFVGE23FONTO_01 "Forecast and Prevention of Coastal Criticalities"; CUP J93C22002670002.

Data Availability Statement: Data are available to the corresponding author upon request.

Acknowledgments: Chiara Popesso, Giulia Casagrande, Davide Martinucci, Stefano Sponza and Simone Pillon are fully acknowledged for their technical assistance.

Conflicts of Interest: The authors declare no conflicts of interest.

Abbreviations

The following abbreviations are used in this manuscript:

SLR	Sea Level Rise
RSLR	Relative Sea Level Rise
VLM	Vertical Land Motion
RP	Return Period
DTM	Digital Terrain Model

References

1. Tuel, A.; Eltahir, E.A.B. Why Is the Mediterranean a Climate Change Hot Spot? *J. Clim.* **2020**, *33*, 5829–5843. [CrossRef]
2. Paxian, A.; Hertig, E.; Seubert, S.; Vogt, G.; Jacobeit, J.; Paeth, H. Present-Day and Future Mediterranean Precipitation Extremes Assessed by Different Statistical Approaches. *Clim. Dyn.* **2015**, *44*, 845–860. [CrossRef]
3. Cramer, W.; Guiot, J.; Fader, M.; Garrabou, J.; Gattuso, J.-P.; Iglesias, A.; Lange, M.A.; Lionello, P.; Llasat, M.C.; Paz, S.; et al. Climate Change and Interconnected Risks to Sustainable Development in the Mediterranean. *Nat. Clim. Change* **2018**, *8*, 972–980. [CrossRef]
4. Lionello, P.; Scarascia, L. The Relation of Climate Extremes with Global Warming in the Mediterranean Region and Its North versus South Contrast. *Reg. Environ. Change* **2020**, *20*, 31. [CrossRef]
5. MedECC. Climate and Environmental Change in the Mediterranean Basin. In *Current Situation and Risks for the Future. First Mediterranean Assessment Report (MAR1)*; Cramer, W., Marini, K., Guiot, J., Eds.; Union for the Mediterranean, Plan Bleu, UNEP/MAP: Marseille, France, 2020; p. 632. [CrossRef]
6. IPCC. *IPCC, 2022: Climate Change 2022: Impacts, Adaptation, and Vulnerability. Working Group II Contribution of to the Sixth Assessment Report of the Intergovernmental Panel on Climate Change*; Pörtner, H.-O., Roberts, D.C., Tignor, M.M.B., Poloczanska, E., Mintenbeck, K., Alegría, A., Craig, M., Langsdorf, S., Löschke, S., Möller, V., et al., Eds.; Cambridge University Press: Cambridge, UK; New York NY, USA, 2022; p. 3056.
7. Giorgi, F. Climate Change Hot-Spots. *Geophys. Res. Lett.* **2006**, *33*, L08707. [CrossRef]
8. Giorgi, F.; Lionello, P. Climate Change Projections for the Mediterranean Region. *Glob. Planet. Change* **2008**, *63*, 90–104. [CrossRef]
9. Vitousek, S.; Barnard, P.L.; Limber, P.; Erikson, L.; Cole, B. A Model Integrating Longshore and Cross-Shore Processes for Predicting Long-Term Shoreline Response to Climate Change. *J. Geophys. Res. Earth Surf.* **2017**, *122*, 782–806. [CrossRef]
10. Taherkhani, M.; Vitousek, S.; Barnard, P.L.; Frazer, N.; Anderson, T.R.; Fletcher, C.H. Sea-Level Rise Exponentially Increases Coastal Flood Frequency. *Sci. Rep.* **2020**, *10*, 6466. [CrossRef]
11. Ku, H.; Kim, T.; Song, Y.-I. Coastal Vulnerability Assessment of Sea-Level Rise Associated with Typhoon-Induced Surges in South Korea. *Ocean Coast. Manag.* **2021**, *213*, 105884. [CrossRef]
12. Neumann, B.; Vafeidis, A.T.; Zimmermann, J.; Nicholls, R.J. Future Coastal Population Growth and Exposure to Sea-Level Rise and Coastal Flooding—A Global Assessment. *PLoS ONE* **2015**, *10*, e0131375. [CrossRef]
13. Ranasinghe, R. Assessing Climate Change Impacts on Open Sandy Coasts: A Review. *Earth Sci. Rev.* **2016**, *160*, 320–332. [CrossRef]
14. Vousdoukas, M.I.; Mentaschi, L.; Voukouvalas, E.; Verlaan, M.; Jevrejeva, S.; Jackson, L.P.; Feyen, L. Global Probabilistic Projections of Extreme Sea Levels Show Intensification of Coastal Flood Hazard. *Nat. Commun.* **2018**, *9*, 2360. [CrossRef] [PubMed]
15. Nicholls, R.J.; Adger, W.N.; Hutton, C.W.; Hanson, S.E. (Eds.) *Deltas in the Anthropocene*; Palgrave Macmillan: Cham, Switzerland, 2020; p. 282.
16. Bakkensen, L.A. Mediterranean Hurricanes and Associated Damage Estimates. *J. Extrem. Events* **2017**, *4*, 1750008. [CrossRef]
17. Portmann, R.; González-Alemán, J.J.; Sprenger, M.; Wernli, H. How an Uncertain Short-Wave Perturbation on the North Atlantic Wave Guide Affects the Forecast of an Intense Mediterranean Cyclone (Medicane Zorbas). *Weather Clim. Dynam.* **2020**, *1*, 597–615. [CrossRef]
18. Scicchitano, G.; Scardino, G.; Monaco, C.; Piscitelli, A.; Milella, M.; De Giosa, F.; Mastronuzzi, G. Comparing Impact Effects of Common Storms and Medicanes along the Coast of South-Eastern Sicily. *Mar. Geol.* **2021**, *439*, 106556. [CrossRef]
19. Marcos, M.; Tsimplis, M.N.; Shaw, A.G.P. Sea Level Extremes in Southern Europe. *J. Geophys. Res. Ocean.* **2009**, *114*, C01007. [CrossRef]
20. Conte, D.; Lionello, P. Characteristics of Large Positive and Negative Surges in the Mediterranean Sea and Their Attenuation in Future Climate Scenarios. *Glob. Planet. Change* **2013**, *111*, 159–173. [CrossRef]
21. Lionello, P.; Cavaleri, L.; Nissen, K.M.; Pino, C.; Raicich, F.; Ulbrich, U. Severe Marine Storms in the Northern Adriatic: Characteristics and Trends. *Phys. Chem. Earth* **2012**, *40–41*, 93–105. [CrossRef]

22. Međugorac, I.; Orlić, M.; Janeković, I.; Pasarić, Z.; Pasarić, M. Adriatic Storm Surges and Related Cross-Basin Sea-Level Slope. *J. Mar. Syst.* **2018**, *181*, 79–90. [CrossRef]
23. Pervan, M.; Šepić, J. Analysis of the Eastern Adriatic Sea Level Extremes. *ST-OPEN* **2023**, *4*, e2023.2111.5. [CrossRef]
24. Mel, R.; Pietro Viero, D.; Carniello, L.; Defina, A.; D'Alpaos, L. Simplified Methods for Real-Time Prediction of Storm Surge Uncertainty: The City of Venice Case Study. *Adv. Water Resour.* **2014**, *71*, 177–185. [CrossRef]
25. Ferrarin, C.; Valentini, A.; Vodopivec, M.; Klaric, D.; Massaro, G.; Bajo, M.; De Pascalis, F.; Fadini, A.; Ghezzo, M.; Menegon, S.; et al. Integrated Sea Storm Management Strategy: The 29 October 2018 Event in the Adriatic Sea. *Nat. Hazards Earth Syst. Sci.* **2020**, *20*, 73–93. [CrossRef]
26. Perini, L.; Calabrese, L.; Luciani, P.; Olivieri, M.; Galassi, G.; Spada, G. Sea-Level Rise along the Emilia-Romagna Coast (Northern Italy) in 2100: Scenarios and Impacts. *Nat. Hazards Earth Syst. Sci.* **2017**, *17*, 2271–2287. [CrossRef]
27. Gallina, V.; Torresan, S.; Zabeo, A.; Rizzi, J.; Carniel, S.; Sclavo, M.; Pizzol, L.; Marcomini, A.; Critto, A. Assessment of Climate Change Impacts in the North Adriatic Coastal Area. Part II: Consequences for Coastal Erosion Impacts at the Regional Scale. *Water* **2019**, *11*, 1300. [CrossRef]
28. Noon, V.; Rivière, C.; Strosser, P.; Manea, E.; Gissi, E.; Barbanti, A. Study on Integrating an Eco-System-Based Approach into Maritime Spatial Planning—Valuation Case Study: Assessing and Valuing Ecosystem Services in the Northern Adriatic. Final Report. 2021. Available online: https://www.milieu.be/wp-content/uploads/2021/08/Study-on-EBA-in-MSP-NAdriatic-case-study-final-report-25.08.2021.pdf (accessed on 23 May 2025).
29. Ferrarin, C.; Bajo, M.; Benetazzo, A.; Cavaleri, L.; Chiggiato, J.; Davison, S.; Davolio, S.; Lionello, P.; Orlić, M.; Umgiesser, G. Local and Large-Scale Controls of the Exceptional Venice Floods of November 2019. *Prog. Oceanogr.* **2021**, *197*, 102628. [CrossRef]
30. Rizzi, J.; Torresan, S.; Zabeo, A.; Critto, A.; Tosoni, A.; Tomasin, A.; Marcomini, A. Assessing Storm Surge Risk under Future Sea-Level Rise Scenarios: A Case Study in the North Adriatic Coast. *J. Coast. Conserv.* **2017**, *21*, 453–471. [CrossRef]
31. Melet, A.; Meyssignac, B.; Almar, R.; Le Cozannet, G. Under-Estimated Wave Contribution to Coastal Sea-Level Rise. *Nat. Clim. Chang.* **2018**, *8*, 234–239. [CrossRef]
32. Bonaldo, D.; Antonioli, F.; Archetti, R.; Bezzi, A.; Correggiari, A.; Davolio, S.; De Falco, G.; Fantini, M.; Fontolan, G.; Furlani, S.; et al. Integrating Multidisciplinary Instruments for Assessing Coastal Vulnerability to Erosion and Sea Level Rise: Lessons and Challenges from the Adriatic Sea. *J. Coast. Conserv.* **2019**, *23*, 19–37. [CrossRef]
33. McEvoy, S.; Haasnoot, M.; Biesbroek, R. How Are European Countries Planning for Sea Level Rise? *Ocean. Coast. Manag.* **2021**, *203*, 105512. [CrossRef]
34. Lagarias, A.; Stratigea, A. Coastalization Patterns in the Mediterranean: A Spatiotemporal Analysis of Coastal Urban Sprawl in Tourism Destination Areas. *GeoJournal* **2023**, *88*, 2529–2552. [CrossRef]
35. Masson-Delmotte, V.; Zhai, P.; Pirani, A.; Connors, S.L.; Péan, C.; Chen, Y.; Goldfarb, L.; Gomis, M.I.; Robin Matthews, J.B.; Berger, S.; et al. (Eds.) *IPCC, 2021: Climate Change 2021: The Physical Science Basis. Working Group I Contribution of to the Sixth Assessment Report of the Intergovernmental Panel on Climate Change*; Cambridge University Press: Cambridge, UK; New York, NY, USA, 2021.
36. Lionello, P. Climate Change 2022—Impatti, Adattamento e Vulnerabilità Il Secondo Volume (WG2) Del Sesto Rapporto Di Valutazione Dell'IPCC, La Più Aggiornata e Completa Rassegna Scientifica Sui Cambiamenti Climatici. Available online: https://files.cmcc.it/ar6/wg2/scienziati_italiani_IPCC_ar6_wg2.pdf (accessed on 14 May 2025).
37. Merkens, J.L.; Reimann, L.; Hinkel, J.; Vafeidis, A.T. Gridded Population Projections for the Coastal Zone under the Shared Socioeconomic Pathways. *Glob. Planet. Change* **2016**, *145*, 57–66. [CrossRef]
38. Andreadis, K.M.; Wing, O.E.J.; Colven, E.; Gleason, C.J.; Bates, P.D.; Brown, C.M. Urbanizing the Floodplain: Global Changes of Imperviousness in Flood-Prone Areas. *Environ. Res. Lett.* **2022**, *17*, 104024. [CrossRef]
39. Nicholls, R.J.; Wong, P.P.; Burkett, V.R.; Codignotto, J.O.; Hay, J.E.; McLean, R.F.; Ragoonaden, S.; Woodroffe, C.D. Coastal Systems and Low-Lying Areas. In *Climate Change 2007: Impacts, Adaptation and Vulnerability. Contribution of Working Group II to the Fourth Assessment Report of the Intergovernmental Panel on Climate Change*; Parry, M., Canziani, O., Palutikof, J., van der Linden, P., Hanson, C., Eds.; Cambridge University Press: Cambridge, UK, 2007; pp. 315–356.
40. Wong, P.P.; Losada, I.J.; Gattuso, J.-P.; Hinkel, J.; Khattabi, A.; Mclennes, K.L.; Saito, Y.; Sallenger, A. Coastal Systems and Low-Lying Areas. In *Climate Change 2014: Impacts, Adaptation, and Vulnerability. Part A: Global and Sectoral Aspects. Contribution of Working Group II to the Fifth Assessment Report of the Intergovernmental Panel on Climate Change*; Field, C.B., Barros, V.R., Dokken, D.J., Mach, K.J., Mastrandrea, M.D., Eds.; Cambridge University Press: Cambridge, UK; New York, NY, USA, 2014; pp. 361–409.
41. Hlodversdottir, A.O.; Bjornsson, B.; Andradottir, H.O.; Eliasson, J.; Crochet, P. Assessment of Flood Hazard in a Combined Sewer System in Reykjavik City Centre. *Water Sci. Technol.* **2015**, *71*, 1471–1477. [CrossRef] [PubMed]
42. Harley, M.D.; Turner, I.L.; Kinsela, M.A.; Middleton, J.H.; Mumford, P.J.; Splinter, K.D.; Phillips, M.S.; Simmons, J.A.; Hanslow, D.J.; Short, A.D. Extreme Coastal Erosion Enhanced by Anomalous Extratropical Storm Wave Direction. *Sci. Rep.* **2017**, *7*, 6033. [CrossRef]
43. Wu, X.; Wang, Z.; Guo, S.; Liao, W.; Zeng, Z.; Chen, X. Scenario-Based Projections of Future Urban Inundation within a Coupled Hydrodynamic Model Framework: A Case Study in Dongguan City, China. *J. Hydrol.* **2017**, *547*, 428–442. [CrossRef]

44. Locatelli, L.; Guerrero, M.; Russo, B.; Martínez-Gomariz, E.; Sunyer, D.; Martínez, M. Socio-Economic Assessment of Green Infrastructure for Climate Change Adaptation in the Context of Urban Drainage Planning. *Sustainability* **2020**, *12*, 3792. [CrossRef]
45. Rufat, S.; Tate, E.; Burton, C.G.; Maroof, A.S. Social Vulnerability to Floods: Review of Case Studies and Implications for Measurement. *Int. J. Disaster Risk Reduct.* **2015**, *14*, 470–486. [CrossRef]
46. Hammond, M.J.; Chen, A.S.; Djordjević, S.; Butler, D.; Mark, O. Urban Flood Impact Assessment: A State-of-the-Art Review. *Urban Water J.* **2015**, *12*, 14–29. [CrossRef]
47. Agonafir, C.; Lakhankar, T.; Khanbilvardi, R.; Krakauer, N.; Radell, D.; Devineni, N. A Review of Recent Advances in Urban Flood Research. *Water Secur.* **2023**, *19*, 100141. [CrossRef]
48. Cooley, S.; Schoeman, D.; Bopp, L.; Boyd, P.; Donner, S.; Ghebrehiwet, D.Y.; Ito, S.-I.; Kiessling, W.; Martinetto, P.; Ojea, E.; et al. Oceans and Coastal Ecosystems and Their Services. In *Climate Change 2022—Impacts, Adaptation and Vulnerability*; Pörtner, H.-O., Roberts, D.C., Tignor, M., Poloczanska, E.S., Mintenbeck, K., Alegría, A., Craig, M., Langsdorf, S., Löschke, S., Möller, V., et al., Eds.; Cambridge University Press: Cambridge, UK; New York, NY, USA, 2022; pp. 379–550.
49. Reimann, L.; Vafeidis, A.T.; Brown, S.; Hinkel, J.; Tol, R.S.J. Mediterranean UNESCO World Heritage at Risk from Coastal Flooding and Erosion Due to Sea-Level Rise. *Nat. Commun.* **2018**, *9*, 4161. [CrossRef]
50. Vousdoukas, M.I.; Clarke, J.; Ranasinghe, R.; Reimann, L.; Khalaf, N.; Duong, T.M.; Ouweneel, B.; Sabour, S.; Iles, C.E.; Trisos, C.H.; et al. African Heritage Sites Threatened as Sea-Level Rise Accelerates. *Nat. Clim. Change* **2022**, *12*, 256–262. [CrossRef]
51. Tong, S.; Bambrick, H.; Beggs, P.J.; Chen, L.; Hu, Y.; Ma, W.; Steffen, W.; Tan, J. Current and Future Threats to Human Health in the Anthropocene. *Environ. Int.* **2022**, *158*, 106892. [CrossRef] [PubMed]
52. Rafiq, F.; Ahmed, S.; Ahmad, S.; Khan, A.A. Urban Floods in India. *Int. J. Sci. Eng. Res.* **2016**, *7*, 721–734.
53. Shah, M.A.R.; Rahman, A.; Chowdhury, S.H. Challenges for Achieving Sustainable Flood Risk Management. *J. Flood Risk. Manag.* **2018**, *11*, S352–S358. [CrossRef]
54. Chen, K.F.; Leandro, J. A Conceptual Time-Varying Flood Resilience Index for Urban Areas: Munich City. *Water* **2019**, *11*, 830. [CrossRef]
55. UNFCCC (United Nations Framework Convention on Climate Change). Defining and Understanding Transformational Adaptation at Different Spatial Scales and Sectors, and Assessing Progress in Planning and Implementing Transformational Adaptation Approaches at the Global Level; 2024. Technical Paper by the Secretariat, FCCC/TP/2024/8. Available online: https://unfccc.int/sites/default/files/resource/tp2024_08.pdf (accessed on 23 May 2025).
56. Mariano, C.; Marino, M.; Pisacane, G.; Sannino, G. Sea Level Rise and Coastal Impacts: Innovation and Improvement of the Local Urban Plan for a Climate-Proof Adaptation Strategy. *Sustainability* **2021**, *13*, 1565. [CrossRef]
57. Melica, G.; De, F.; Rios, L.; Palermo, C.; Ferrario, M.; Baldi, F.; Ulpiani, M.; Hortelano, O.; Barbosa, A. *Covenant of Mayors: 2022 Assessment—Climate Change Mitigation and Adaptation at Local Level*; JRC130957; Publications Office of the European Union: Luxembourg, 2022. [CrossRef]
58. Manzan, M.; Bacaro, G.; Nardini, A.; Casagrande, G.; Pezzi, A.; Petruzzellis, F.; Tordoni, E.; Fontolan, G. Climate Change Risk and Vulnerabilities Analysis in Trieste SECAP. *Sustainability* **2022**, *14*, 5973. [CrossRef]
59. Bisht, D.S.; Chatterjee, C.; Kalakoti, S.; Upadhyay, P.; Sahoo, M.; Panda, A. Modeling Urban Floods and Drainage Using SWMM and MIKE URBAN: A Case Study. *Nat. Hazards* **2016**, *84*, 749–776. [CrossRef]
60. Mignot, E.; Li, X.; Dewals, B. Experimental Modelling of Urban Flooding: A Review. *J. Hydrol.* **2019**, *568*, 334–342. [CrossRef]
61. Habel, S.; Fletcher, C.H.; Anderson, T.R.; Thompson, P.R. Sea-Level Rise Induced Multi-Mechanism Flooding and Contribution to Urban Infrastructure Failure. *Sci. Rep.* **2020**, *10*, 3796. [CrossRef]
62. Gao, M.; Wang, Z.; Yang, H. Review of Urban Flood Resilience: Insights from Scientometric and Systematic Analysis. *Int J Env. Res Public Health* **2022**, *19*, 8837. [CrossRef] [PubMed]
63. Shi, S.; Yang, B.; Jiang, W. Numerical Simulations of Compound Flooding Caused by Storm Surge and Heavy Rain with the Presence of Urban Drainage System, Coastal Dam and Tide Gates: A Case Study of Xiangshan, China. *Coast. Eng.* **2022**, *172*, 104064. [CrossRef]
64. Balaian, S.K.; Sanders, B.F.; Abdolhosseini Qomi, M.J. How Urban Form Impacts Flooding. *Nat. Commun.* **2024**, *15*, 6911. [CrossRef]
65. Xie, W.; Tang, B.; Meng, Q. The Impact of Sea-Level Rise on Urban Properties in Tampa Due to Climate Change. *Water* **2022**, *14*, 13. [CrossRef]
66. Comune Di Grado. La Laguna Di Grado. Available online: https://comune.grado.go.it/it/vivere-il-comune-22477/luoghi-22478/la-laguna-di-grado-69770 (accessed on 2 April 2025).
67. Bezzi, A.; Casagrande, G.; Fracaros, S.; Martinucci, D.; Pillon, S.; Sponza, S.; Bratus, A.; Fattor, F.; Fontolan, G. Geomorphological Changes of a Migrating Sandbank: Multidecadal Analysis as a Tool for Managing Conflicts in Coastal Use. *Water* **2021**, *13*, 3416. [CrossRef]
68. Demo. Demografia in Cifre. Bilancio Demografico Mensile e Popolazione Residente per Sesso, Anno 2024. Available online: https://demo.istat.it/app/?a=2024&i=D7B (accessed on 26 May 2025).

69. ISTAT. I Flussi Turistici—Anno 2023. Available online: https://www.istat.it/comunicato-stampa/i-flussi-turistici-anno-2023/ (accessed on 23 May 2025).
70. Marocco, R. Le Spiagge Di Grado: Situazione Attuale, Tendenze Evolutive Ed Ipotesi d'intervento per Il Risanamento Degli Arenili. *GORTANIA—Atti Del Mus. Friul. Di Stor. Naturale.* **2000**, *22*, 5–37.
71. De Grassi, V. Le Rovine Subacquee Di San Gottardo a Grado. *Aquil. Nostra* **1952**, *23*, 27–36.
72. Gaddi, D. *Approdi Nella Laguna Di Grado. Antichità Altoadriatiche XLVI. Strutture Portuali e Rotte Marittime Nell'alto Adriatico Di Età Romana*; Zaccaria, C., Ed.; EUT Edizione Università Trieste: Trieste, Roma, 2001.
73. Tortorici, E. Archeologia Subacquea e Trasformazioni Geomorfologiche Del Territorio: Il Caso Della Laguna Di Grado. In Proceedings of the Atti Convegno Nazionale di Archeologia Subacquea, Anzio, Italy, 30 May–1 June 1997; pp. 315–325.
74. Bezzi, A.; Pillon, S.; Martinucci, D.; Fontolan, G. Inventory and Conservation Assessment for the Management of Coastal Dunes, Veneto Coasts, Italy. *J. Coast. Conserv.* **2018**, *22*, 503–518. [CrossRef]
75. Regione Autonoma Friuli Venezia Giulia-Autorità Di Sistema Portuale Del Mare Adriatico Orientale. Piano Regolatore Portuale Del Porto Di Monfalcone, Variante Localizzata. Studio Meteomarino. Progettisti: Modimar, SJS Engineering, Archest. 2019. Available online: https://www.regione.fvg.it/rafvg/export/sites/default/RAFVG/ambiente-territorio/pianificazione-gestioneterritorio/FOGLIA9/allegati/Allegato_33_alla_Delibera_2066-2019.pdf (accessed on 27 March 2025).
76. Ferla, M.; Crosato, F.; Ragazzo, M. Litorali e Lagune Del Nord Est. Presentazione Convegno "Aree Costiere Del Nord Adriatico e Gestione Delle Alluvioni: Attuazione Della Direttiva 2007/60/CE Sulla Gestione Dal Rischio Alluvione", Mestre 5 Ottobre 2012. Available online: https://www.venezia.isprambiente.it/ispra/upload/en_home/ricerche/litorali_e_lagune_del_nord-est.pdf (accessed on 27 March 2024).
77. Casagrande, G.; Bezzi, A.; Fracaros, S.; Martinucci, D.; Pillon, S.; Salvador, P.; Sponza, S.; Fontolan, G. Quantifying Transgressive Coastal Changes Using UAVs: Dune Migration, Overwash Recovery, and Barrier Flooding Assessment and Interferences with Human and Natural Assets. *J. Mar. Sci. Eng.* **2023**, *11*, 1044. [CrossRef]
78. Petti, M.; Pascolo, S.; Bosa, S.; Bezzi, A.; Fontolan, G. Tidal Flats Morphodynamics: A New Conceptual Model to Predict Their Evolution over a Medium-Long Period. *Water* **2019**, *11*, 1176. [CrossRef]
79. Dorigo, L. *La Laguna di Grado e le Sue Foci. Ricerche e Rilievi Idrografici*; Pubbl. 165; Magistrato Alle Acque—Ufficio Idrografico: Venezia, Italy, 1965; p. 231.
80. Perini, L.; Emilia-Romagna, R.; Calabrese, L.; Luciani, P. Il Rischio Da Mareggiata in Emilia-Romagna: L'evento Del 5-6 Febbraio 2015. *Il Geol.* **2016**, *53*, 8–17.
81. Coles, S. *An Introduction to Statistical Modeling of Extreme Values*; Springer: London, UK, 2001; p. 209.
82. Caruso, M.F.; Marani, M. Extreme-Coastal-Water-Level Estimation And Projection: A Comparison Of Statistical Methods. *Nat. Hazard Earth Syst. Sci.* **2022**, *22*, 1109–1128. [CrossRef]
83. Città Di Venezia. Grafici e Statistiche. Available online: https://www.comune.venezia.it/it/content/grafici-e-statistiche (accessed on 23 May 2025).
84. Gumbel, E. *Statistics of Extremes*; Columbia University Press: New York, NY, USA, 1958; p. 375.
85. Goda, Y.; Asce, M. On the Methodology of Selecting Design Wave Height. In Proceedings of the 21st Coastal Engineering Conference, ASCE, New York, NY, USA, 20–25 June 1988; pp. 899–913.
86. Città Di Venezia. Riferimenti Altimetrici. Available online: https://www.comune.venezia.it/it/content/riferimenti-altimetrici (accessed on 23 May 2025).
87. ISPRA. Dati. La Rete Meteo-Mareografica Della Laguna Di Venezia (RMLV). Le Stazioni Meteo-Mareografiche. Available online: https://www.venezia.isprambiente.it/rete-meteo-mareografica (accessed on 23 May 2025).
88. National Oceanic and Atmospheric Administration (NOAA). *Mapping Coastal Inundation Primer*; National Oceanic and Atmospheric Administration: Washington, DC, USA, 2012. Available online: https://coast.noaa.gov/data/digitalcoast/pdf/coastal-inundation-guidebook.pdf (accessed on 27 May 2025).
89. Regione Autonoma Della Sardegna; Autorità Di Bacino Regionale Della Sardegna. Piano Di Gestione Del Rischio Di Alluvioni. Relazione Metodologica Sulle Inondazioni Costiere. Available online: https://pianogestionerischioalluvioni.regione.sardegna.it/documenti/1_617_20190124124513.pdf (accessed on 14 May 2025).
90. Perini, L.; Calabrese, L.; Deserti, M.; Valentini, A.; Ciavola, P.; Armaroli, C. *Le Mareggiate e Gli Impatti Sulla Costa in Emilia-Romagna 1946–2010*; I Quaderni ARPA; Regione Emilia Romagna Ambiente: Emilia-Romagna, Italy, 2011; p. 144. Available online: https://www.researchgate.net/publication/290441941 (accessed on 26 May 2025).
91. Perini, L.; Calabrese, L.; Salerno, G.; Luciani, P. Mapping of flood risk in Emilia-Romagna coastal areas. In Proceedings of the Abstracts 86° Congresso Nazionale della Società Geologica Italiana, Arcavacata di Rende (CS), Cosenza, Italy, 18–20 September 2012. [CrossRef]
92. Perini, L.; Calabrese, L.; Salerno, G.; Ciavola, P.; Armaroli, C. Evaluation of Coastal Vulnerability to Flooding: Comparison of Two Different Methodologies Adopted by the Emilia-Romagna Region (Italy). *Nat. Hazards Earth Syst. Sci.* **2016**, *16*, 181–194. [CrossRef]

93. Permanent Service for Mean Sea Level (PSMSL). Trieste. *Tide Gauge Data.* Available online: https://www.psmsl.org/data/obtaining/stations/154.php (accessed on 23 May 2025).
94. Da Lio, C.; Tosi, L. Land Subsidence in the Friuli Venezia Giulia Coastal Plain, Italy: 1992–2010 Results From SAR-Based Interferometry. *Sci. Total Environ.* **2018**, *633*, 752–764. [CrossRef]
95. Areggi, G.; Pezzo, G.; Merryman Boncori, J.P.; Anderlini, L.; Rossi, G.; Serpelloni, E.; Zuliani, D.; Bonini, L. Present-Day Surface Deformation in North-East Italy Using InSAR and GNSS Data. *Remote Sens.* **2023**, *15*, 1704. [CrossRef]
96. IPCC AR6 Sea Level Projection Tool. Nasa Earth Data, Sea Level Change. Available online: https://sealevel.nasa.gov/ipcc-ar6-sea-level-projection-tool (accessed on 23 May 2025).
97. Autorità Di Bacino Distrettuale Delle Alpi Orientali. Aggiornamento e Revisione Del Piano Di Gestione Del Rischio Di Alluvioni. *Allegato I. Elementi Tecnici Di Riferimento Nell'impostazione Del Piano. Distretto Delle Alpi Orientali.* Available online: https://sigma.distrettoalpiorientali.it/sigma/documentDownload/downloadDocumentById?documentId=360 (accessed on 14 May 2025).
98. Tomasin, A.; Pirazzoli, P.A. Extreme Sea Levels on Adriatic Coasts: A Comparison on Estimation Methods. In *Atti dell'Istituto Veneto di Scienze, Lettere ed Arti*; Tomo CLXVII (2008-2009)—Classe Scienze Matematiche, Fisiche e Naturali; Istituto Veneto di Scienze, Lettere ed Arti: Venice, Italy, 2008; pp. 53–82.
99. Arguez, A.; Vose, R.S. The Definition of the Standard WMO Climate Normal: The Key to Deriving Alternative Climate Normals. *Bull. Am. Meteorol. Soc.* **2011**, *92*, 699–704. [CrossRef]
100. Sánchez, L.; Völksen, C.; Sokolov, A.; Arenz, H.; Seitz, F. Present-Day Surface Deformation of the Alpine Region Inferred from Geodetic Techniques. *Earth Syst. Sci. Data* **2018**, *10*, 1503–1526. [CrossRef]
101. Zerbini, S.; Bruni, S.; Raicich, F. Tide Gauge Data Archaeology Provides Natural Subsidence Rates along the Coasts of the Po Plain and of the Veneto-Friuli Plain, Italy. *Geophys. J. Int.* **2021**, *225*, 253–260. [CrossRef]
102. Lionello, P.; Barriopedro, D.; Ferrarin, C.; Nicholls, R.J.; Orlić, M.; Raicich, F.; Reale, M.; Umgiesser, G.; Vousdoukas, M.; Zanchettin, D. Extreme Floods of Venice: Characteristics, Dynamics, Past and Future Evolution (Review Article). *Nat. Hazards Earth Syst. Sci.* **2021**, *21*, 2705–2731. [CrossRef]
103. Marsico, A.; Lisco, S.; Lo Presti, V.; Antonioli, F.; Amorosi, A.; Anzidei, M.; Deiana, G.; De Falco, G.; Fontana, A.; Fontolan, G.; et al. Flooding Scenario for Four Italian Coastal Plains Using Three Relative Sea Level Rise Models. *J. Maps* **2017**, *13*, 961–967. [CrossRef]
104. Galluccio, G.; Hinkel, J.; Fiorini Beckhauser, E.; Bisaro, A.; Biancardi Aleu, R.; Campostrini, P.; Casas, M.F.; Espin, O.; Vafeidis, A.T. Sea Level Rise in Europe: Adaptation Measures and Decision-Making Principles. *State Planet* **2024**, *2024*, 1–36. [CrossRef]
105. van de Wal, R.; Melet, A.; Bellafiore, D.; Camus, P.; Ferrarin, C.; Oude Essink, G.; Haigh, I.D.; Lionello, P.; Luijendijk, A.; Toimil, A.; et al. Sea Level Rise in Europe: Impacts and Consequences. *State Planet* **2023**, *2023*, 1–65. [CrossRef]
106. Mel, R.A.; Viero, D.P.; Carniello, L.; Defina, A.; D'Alpaos, L. The First Operations of Mo.S.E. System to Prevent the Flooding of Venice: Insights on the Hydrodynamics of a Regulated Lagoon. *Estuar. Coast. Shelf Sci.* **2021**, *261*, 107547. [CrossRef]
107. Shayegh, S.; Moreno-Cruz, J.; Caldeira, K. Adapting to Rates versus Amounts of Climate Change: A Case of Adaptation to Sea-Level Rise. *Environ. Res. Lett.* **2016**, *11*, 104007. [CrossRef]
108. Sriver, R.L.; Lempert, R.J.; Wikman-Svahn, P.; Keller, K. Characterizing Uncertain Sea-Level Rise Projections to Support Investment Decisions. *PLoS ONE* **2018**, *13*, e0190641. [CrossRef]
109. Horton, B.P.; Khan, N.S.; Cahill, N.; Lee, J.S.H.; Shaw, T.A.; Garner, A.J.; Kemp, A.C.; Engelhart, S.E.; Rahmstorf, S. Estimating Global Mean Sea-Level Rise and Its Uncertainties by 2100 and 2300 from an Expert Survey. *NPJ Clim. Atmos. Sci.* **2020**, *3*, 18. [CrossRef]
110. Hinkel, J.; Feyen, L.; Hemer, M.; Le Cozannet, G.; Lincke, D.; Marcos, M.; Mentaschi, L.; Merkens, J.L.; de Moel, H.; Muis, S.; et al. Uncertainty and Bias in Global to Regional Scale Assessments of Current and Future Coastal Flood Risk. *Earths Future* **2021**, *9*, e2020EF001882. [CrossRef]
111. Cin, F.D.; Fleischmann, M.; Romice, O.; Costa, J.P. Climate Adaptation Plans in the Context of Coastal Settlements: The Case of Portugal. *Sustainability* **2020**, *12*, 8559. [CrossRef]
112. Barnard, P.L.; Dugan, J.E.; Page, H.M.; Wood, N.J.; Hart, J.A.F.; Cayan, D.R.; Erikson, L.H.; Hubbard, D.M.; Myers, M.R.; Melack, J.M.; et al. Multiple Climate Change-Driven Tipping Points for Coastal Systems. *Sci. Rep.* **2021**, *11*, 15560. [CrossRef]
113. Toledo, I.; Pagán, J.I.; López, I.; Aragonés, L.; Olcina, J. Nature-Based Solutions on the Coast in Face of Climate Change: The Case of Benidorm (Spain). *Urban Clim.* **2024**, *53*, 101816. [CrossRef]
114. Bol, R. Operation of the "Maeslant Barrier": (Storm Surge Barrier in the Rotterdam New Waterway). In *Flooding and Environmental Challenges for Venice and its Lagoon: State of Knowledge*; Fletcher, C., Spencer, T., Eds.; Cambridge University Press: Cambridge, UK, 2005; pp. 311–315.
115. Jorissen, R.; Kraaij, E.; Tromp, E. Dutch Flood Protection Policy and Measures Based on Risk Assessment. *E3S Web Conf.* **2016**, *7*, 20016. [CrossRef]
116. Binini Partners. Porta Vinciana a Cesenatico. Sbarramento Mobile per La Difesa Dalle Esondazioni Meteomarine. Available online: https://www.bininipartners.it/progetti/porta-vinciana-a-cesenatico/ (accessed on 22 May 2025).

117. Il Baby MOSE per La Difesa Di Chioggia Dalle Acque Alte. Available online: http://www.forumtelecontrollo.it/allegati/11.20_progea_angelini.pdf (accessed on 22 May 2025).
118. Munaretto, S.; Vellinga, P.; Tobi, H. Flood Protection in Venice under Conditions of Sea-Level Rise: An Analysis of Institutional and Technical Measures. *Coast. Manag.* **2012**, *40*, 355–380. [CrossRef]

IL MARE E I GHIACCI

SEGNALI DAL CLIMA IN FVG (2023):

LIVELLO MEDIO DEL MARE: IN CRESCITA ANCHE A TRIESTE 26

SCENARI FUTURI DI INNALZAMENTO DEL LIVELLO DEL MARE 29

TEMPERATURA MEDIA DEL MARE, FRA LE PIÙ ALTE DEGLI ULTIMI VENTI ANNI 32

ONDATE DI CALORE MARINE: LA SITUAZIONE GENERALE E IL CASO DEL 2022 33

L'ACIDIFICAZIONE MARINA: UN FENOMENO GLOBALE CHE INTERESSA ANCHE I NOSTRI MARI 35

SCENARI DI INONDAZIONE COSTIERA: LA REALTÀ DI GRADO 38

LA MARINIZZAZIONE DELLA LAGUNA DI MARANO E GRADO 43

LA CRIOSFERA DELLE ALPI GIULIE, EVOLUZIONE PASSATA E RECENTE 47

LA VALANGA DI GHIACCIO IN MARMOLADA 52

Foto: Agostino Manzato

IL MARE E I GHIACCI

estratto da:

SEGNALI DAL CLIMA IN FVG

CAMBIAMENTI – IMPATTI – AZIONI

maggio 2023

notizie dal

Gruppo di lavoro tecnico-scientifico

Clima FVG

“Segnali dal Clima in FVG” è realizzato da:

ARPA FVG - Agenzia Regionale per la Protezione dell’Ambiente del Friuli Venezia Giulia

nell’ambito dell’attività di coordinamento e segreteria del “Gruppo di lavoro tecnico scientifico Clima FVG” istituito dalla Regione Autonoma Friuli Venezia Giulia con Decreto DC Difesa dell’ambiente, energia e sviluppo sostenibile, n. 2137 del 04/05/2022

Coordinamento editoriale:
Federica Flapp, Fulvio Stel

Elaborazione grafica:
Ester Curci, Federica Flapp, Michela Mauro

Ove non diversamente specificato, le immagini sono state fornite dagli autori dei diversi contributi, che se ne assumono la responsabilità, o sono tratte da:

https://pixabay.com/it/
https://www.google.com/maps
https://it.freepik.com/

La foto di copertina è di Agostino Manzato.

ARPA FVG
Via Cairoli, 14 - 33057 Palmanova (UD)
Tel +39 0432 922 611 - Fax +39 0432 922 626
www.arpa.fvg.it
https://twitter.com/arpafvg

Segnali dal Clima

Segnali dal Clima in FVG è una pubblicazione divulgativa che racconta i cambiamenti climatici partendo da un'ottica locale e regionale e affronta questo grande tema da tre prospettive: CAMBIAMENTI, IMPATTI, AZIONI.

Nasce dall'impegno del Gruppo di lavoro tecnico-scientifico Clima FVG e dalla convinzione che le sfide che i cambiamenti climatici pongono alla nostra società si possano affrontare efficacemente solo se allo sviluppo scientifico e tecnologico si accompagnano una crescita della conoscenza e una consapevolezza sempre più diffusa sul tema da parte di tutta la popolazione.

Segnali dal Clima affronta diversi aspetti dei cambiamenti climatici partendo dal racconto di eventi e situazioni che hanno riguardato il Friuli Venezia Giulia nel 2022, ma anche evidenziando come la dimensione locale sia collegata a quella globale attraverso riferimenti a eventi e situazioni verificatisi al di fuori della nostra regione e su scala più ampia.

Al racconto degli eventi e dei fenomeni si accompagnano le spiegazioni delle cause che li hanno prodotti. Un filo rosso – CAMBIAMENTI, IMPATTI, AZIONI - unisce i diversi articoli, i nostri "segnali dal clima", collegando i cambiamenti in atto con i loro effetti sull'ambiente e sulle attività umane, ma anche con le azioni che possiamo mettere in campo sia per limitare il riscaldamento globale e i cambiamenti del clima (mitigazione) che per ridurre gli impatti che ne conseguono (adattamento).

Il 2022 è stato l'anno più caldo mai registrato in Friuli Venezia Giulia: alle alte temperature si è associata una grave e prolungata siccità, che ha determinato pesanti conseguenze per il nostro territorio. Alle criticità più acute che hanno occupato le pagine dei giornali per diversi mesi si affianca però un flusso più graduale e meno evi-dente di effetti che si manifestano negli anni. Il racconto parte quindi dagli argomenti più propriamente "climatici" – a iniziare dalle temperature dell'aria e dalle precipitazioni e dai loro effetti sul mare e sui ghiacci – e indaga poi alcuni ambiti in cui gli effetti dei cambiamenti climatici si manifestano in Friuli Venezia Giulia: dalle modifiche graduali, ma profonde, degli ecosistemi, agli incendi che hanno devastato i nostri boschi nell'estate 2022, all'agricoltura, mettendo in luce alcune possibili risposte e soluzioni e come queste emergano dalle conoscenze prodotte dagli enti scientifici e di ricerca e dalle attività delle agenzie e strutture regionali.

Segnali dal Clima in FVG non è quindi un report sullo "stato del clima" in Friuli Venezia Giulia: non ha l'obiettivo di fornire un quadro completo ed esaustivo della tematica, non ne esplora tutti gli aspetti e i settori ambientali e socioeconomici coinvolti, non passa in rassegna tutte le conoscenze disponibili. È però, appunto, un segnale: un segnale di cosa sta accadendo, di quanto sia importante prenderne coscienza ed agire, di come la società, la pubblica amministrazione e il mondo scientifico si stiano già attivando.

Il gruppo di lavoro tecnico-scientifico Clima FVG

L'ABC DEL CLIMA

Per rendere gli argomenti accessibili a tutti, negli articoli sono inseriti alcuni box a sfondo arancione pensati per avvicinare al pubblico alcuni termini e concetti tecnico-scientifici a cui è necessario fare riferimento quando si spiegano argomenti e fenomeni collegati ai cambiamenti climatici.

DAL LOCALE AL GLOBALE

Con uno sfondo grigio sono evidenziati gli articoli che riportano notizie e informazioni relative a realtà extra-regionali e che ci consentono di ampliare la nostra visione, collegando ciò che avviene in Friuli Venezia Giulia con conoscenze generali e con fenomeni a scala più ampia.

Gruppo di lavoro Clima FVG

Il "Gruppo di lavoro tecnico-scientifico Clima FVG" istituito dalla Regione autonoma Friuli Venezia Giulia nel 2022 riunisce le eccellenze tecniche e scientifiche presenti in FVG, in grado di fornire all'Amministrazione regionale e a tutti gli enti e soggetti del FVG le conoscenze più aggiornate per affrontare i cambiamenti climatici sul nostro territorio.

Ad ARPA FVG è stato affidato il coordinamento del team, che è composto da esperti di ICTP, OGS, CNR, delle Università di Udine e di Trieste e della stessa Regione: gli stessi che avevano elaborato e pubblicato, nel 2018, il primo Studio conoscitivo dei cambiamenti climatici e di alcuni loro impatti in Friuli Venezia Giulia.

Il Gruppo di lavoro Clima FVG innanzitutto facilita la condivisione e la collaborazione tra i soggetti esperti che in regione producono conoscenze tecnico-scientifiche sui cambiamenti climatici e sui loro effetti.

Fornisce quindi un orientamento e un supporto consultivo alla pianificazione regionale delle azioni per il clima e in particolare per l'adattamento ai cambiamenti climatici.

L'attività del gruppo di lavoro Clima FVG favorisce anche il trasferimento delle conoscenze scientifiche ai tecnici che le applicano sul territorio.

E infine, tutti i componenti del gruppo di lavoro credono che sia indispensabile divulgare queste conoscenze alla cittadinanza, promuovendo quella che si chiama *"climate literacy"* ovvero l'alfabetizzazione climatica, che mette ciascuno di noi in condizione di comprendere la propria influenza sul clima e l'influenza del clima su ciascuna persona e sulla società.

La redazione di "Segnali dal Clima in FVG" è un primo passo per dare concretezza a questo fondamentale obiettivo

.

Chi siamo?

ARPA FVG – Agenzia Regionale per la Protezione dell'Ambiente	Fulvio Stel (coordinatore) e Federica Flapp
CNR - Istituto di Scienze Marine di Trieste	Fabio Raicich
CNR - Istituto di Scienze Polari	Renato Colucci
ICTP - International Centre for Theoretical Physics di Trieste	Filippo Giorgi
OGS - Istituto nazionale di oceanografia e di geofisica sperimentale di Trieste:	Cosimo Solidoro
Regione autonoma Friuli Venezia Giulia	Silvia Stefanelli ed Enzo Dall'Osto
Università degli Studi di Trieste	Giovanni Bacaro
Università degli Studi di Udine	Alessandro Peressotti

Immagine di muammark su Freepik

SCENARI DI INONDAZIONE COSTIERA: LA REALTÀ DI GRADO

Le zone costiere sono vulnerabili agli eventi di acqua alta causati da una combinazione di alta marea e condizioni meteoclimatiche. Grazie al modello altimetrico delle coste del FVG, preciso e aggiornato, è possibile simulare mappe di allagamento potenziali, sia nelle condizioni attuali che considerando scenari futuri di innalzamento del mare, come fatto ad esempio per Grado.

Le zone costiere sono per loro natura vulnerabili all'ingressione marina determinata dalle condizioni meteoclimatiche (vento, bassa pressione, precipitazioni intense) che possono provocare mareggiate e, unite all'alta marea, le acque alte.

VULNERABILITÀ E PROTEZIONI DELL'AREA COSTIERA

In Friuli Venezia Giulia questa vulnerabilità è enfatizzata dal fatto che molte aree costiere hanno quote molto basse rispetto al livello del mare, se non addirittura al di sotto di esso. Queste ultime aree, in prevalenza agricole, sono il risultato dei lunghi e complessi lavori di bonifica idraulica realizzati nel passato e sono oggi mantenute solo grazie a un sistema di argini che le protegge verso mare, oltre a canali e idrovore che pompano l'acqua in mare al di là degli argini stessi.

IL RISCHIO DI ALLAGAMENTO

La conoscenza dell'altimetria del nostro territorio costiero è molto precisa e aggiornata grazie al rilievo condotto nel 2018 dalla Protezione Civile del Friuli Venezia Giulia con un sofisticato strumento di scansione laser (LIDAR). Il prodotto è un modello digitale, tridimensionale, aggiornato e di estremo dettaglio dei territori costieri.

Grazie alla disponibilità di questo modello altimetrico è possibile simulare mappe di allagamento potenziali per le realtà costiere più importanti della nostra regione, immaginando sia singoli eventi di mareggiata sia un futuro scenario di innalzamento di livello del mare, in conseguenza del riscaldamento globale.

LIDAR (acronimo dall'inglese Light Detection and Ranging): è una tecnologa basata sull'uso di un sensore che emette raggi laser. Montato su un aereo o su un drone consente di rilevare milioni di punti della superfice terrestre in breve tempo, determinandone l'altimetria con grande precisione.

Altimetria delle zone costiere

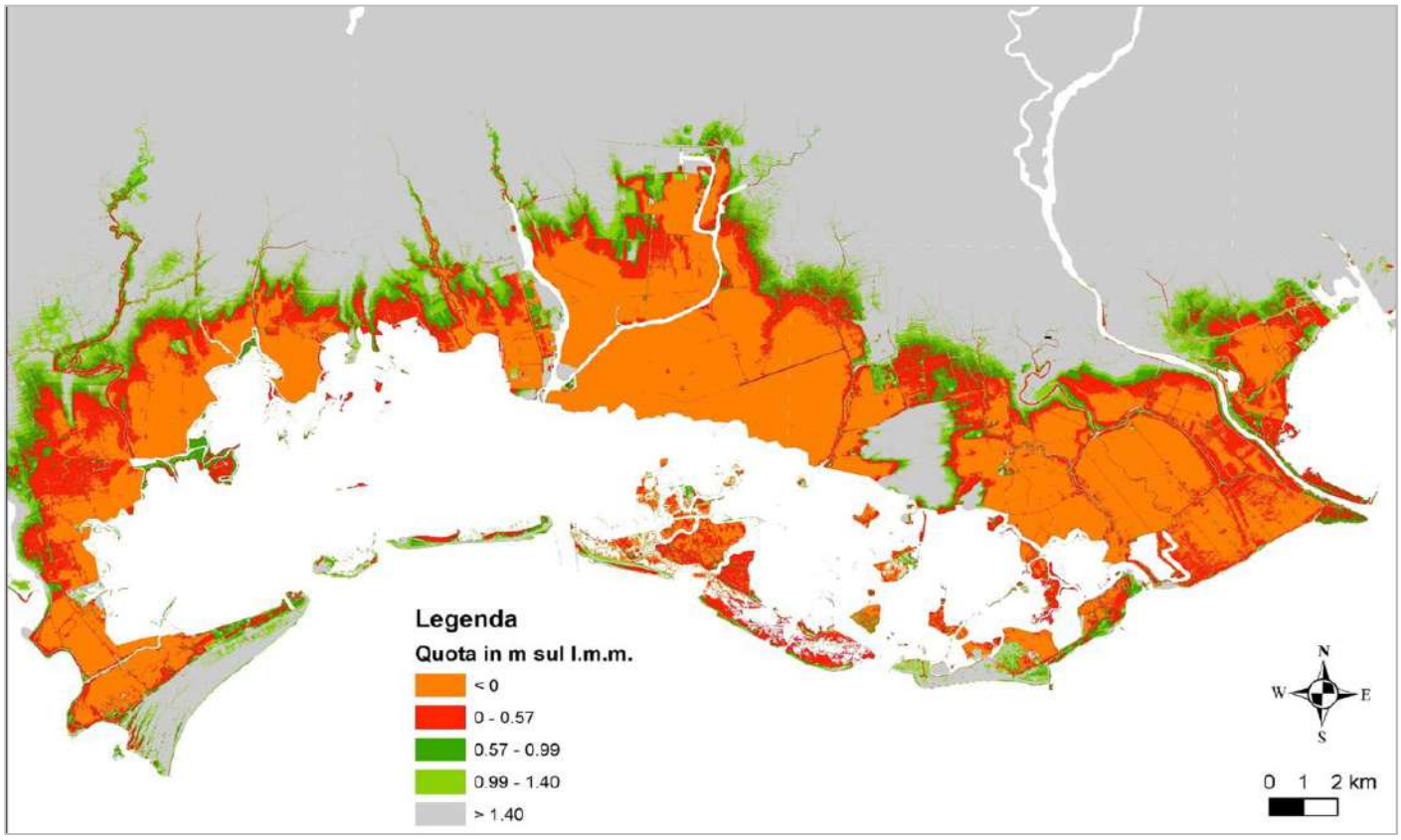

Mappa delle quote sul livello del mare delle aree costiere del Friuli Venezia Giulia tra Monfalcone e la foce del Tagliamento (elaborazione Università di Trieste)

Protezioni costiere

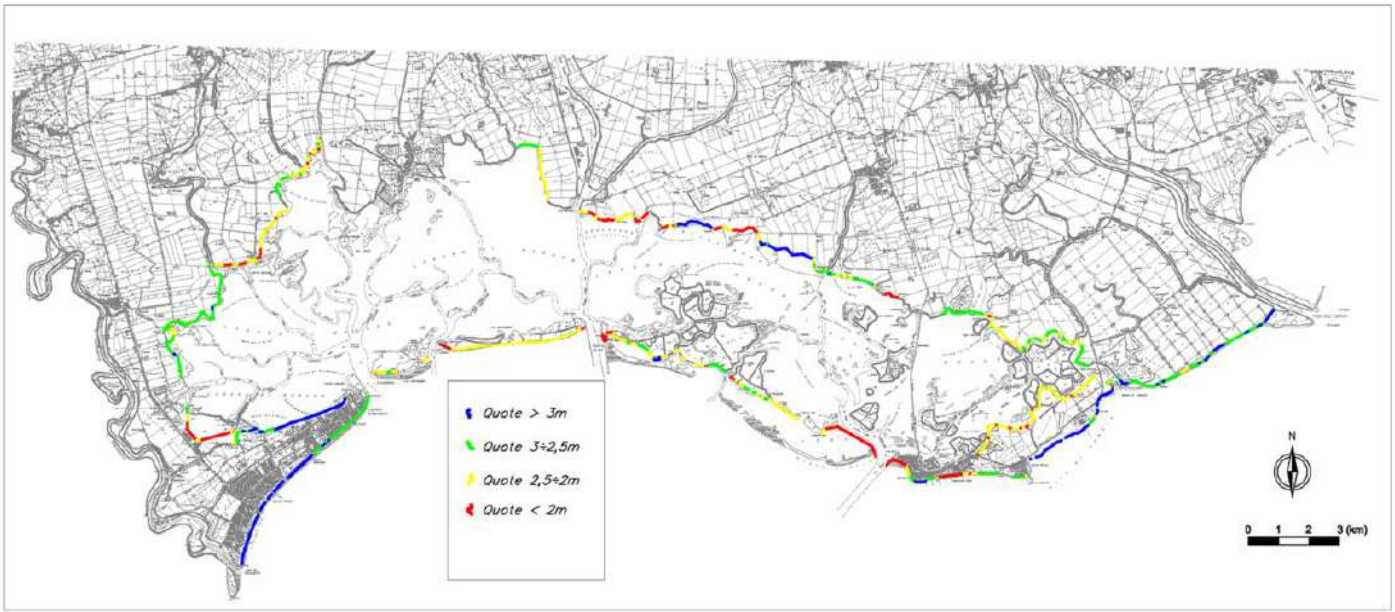

Mappa degli argini di difesa delle coste e dei margini lagunari del Friuli Venezia Giulia tra le foci dell'Isonzo e del Tagliamento. La mappa è ricavata dall'Indagine sullo stato degli argini della bassa pianura realizzate del 2005 dall'Università di Trieste- Dipartimento di Scienze Geologiche Ambientali e Marine

LE MAREGGIATE A GRADO

Se immaginiamo un sovralzo marino da mareggiata che provoca un aumento episodico del livello del mare pari a 128 cm - come statisticamente si prevede possa accadere ogni 30 anni - otteniamo una mappa di possibile allagamento per la cittadina di Grado che mostra come gran parte delle vie del centro risultino allagate.

Mappa di allagabilità attuale di Grado

Mappa di allagabilità di Grado a oggi, nell'ipotesi di un aumento episodico del livello del mare pari a 128 cm.
La mappa è stata elaborata dal Coastal Group dell'Università di Trieste sulla base del rilievo LIDAR della protezione Civile FVG del 2018. La base della figura è la foto aerea del 2018 (da Regione Autonoma Friuli Venezia Giulia - https://eaglefvg.regione.fvg.it)

L'INNALZAMENTO DEL LIVELLO DEL MARE

Considerando una proiezione futura di innalzamento del livello del mare all'anno 2100, pur utilizzando quella più "ottimistica" immaginata dall'IPCC (Intergovernmental Panel on Climate Change) cioè quella indicata con lo scenario RCP2.6, il livello medio delle acque sarà stabilmente ben più elevato di oggi.

Di conseguenza, nel 2100, lo stesso evento di mareggiata ipotizzato precedentemente si sommerà a un livello medio del mare più alto di 40 cm rispetto a quello attuale: gli effetti dell'inondazione risulterebbero molto più rilevanti, in quanto sommergerebbero gran parte della cittadina di Grado.

Mappa di allagabilità futura di Grado

Mappa di allagabilità di Grado al 2100, nell'ipotesi di un aumento episodico del livello del mare pari a 128 cm che si sommi a un aumento del livello medio del mare di 40 cm (scenario RCP2.6).
La mappa è stata elaborata dal Coastal Group dell'Università di Trieste sulla base del rilievo LIDAR della protezione Civile FVG del 2018. La base della figura è la foto aerea del 2018 (da Regione Autonoma Friuli Venezia Giulia - https://eaglefvg.regione.fvg.it)

IL FUTURO

Queste simulazioni sono di fondamentale importanza per la definizione delle possibili future situazioni di criticità. Analisi più approfondite saranno eseguite grazie alla collaborazione avviata tra l'Università degli studi di Trieste e la Protezione Civile regionale del Friuli Venezia Giulia e riguarderanno sia lo stato degli argini sia una migliore definizione delle mappe di allagabilità, soprattutto nelle aree più vulnerabili. Ad esempio saranno individuati e analizzati nel dettaglio i punti critici, ossia i "varchi" attraverso i quali l'acqua proveniente dal mare o dalla laguna può trovare facile accesso, causando danni e disagi alla popolazione.

LE DIVERSE SOGLIE DEL LIVELLO DEL MARE

Il livello del mare in una determinata località varia continuamente a differenti scale di tempo.

Un elevato rialzo del livello del mare che si verifica a scala di ore può essere considerato un evento episodico ed essere il risultato di varie componenti. In primo luogo l'alta mare astronomica che interessa le coste del Friuli Venezia Giulia con periodicità semidiurna (ogni 12 ore).

Una differenza di pressione atmosferica lungo il bacino dell'Adriatico può provocare un sovralzo meteorologico ("surge") del livello del mare noto anche come "sessa" che, sommato all'alta marea astronomica, causa la cosiddetta "acqua alta".

Se a questo si accompagna l'azione del vento sul bacino si ha la formazione di onde che, quando giungono vicino alla costa, diventano più ripide e si rompono (frangenza) andando a formare uno "strato di acqua" in più, chiamato sovralzo d'onda (setup).

Sulla spiaggia infine l'onda può provocare un flusso d'acqua che ne risale la superficie inclinata (risalita dell'onda o runup).

Tutte queste componenti se sommate tra loro rappresentano dei "livelli" di cui bisogna tener conto nella pianificazione territoriale, nei piani di emergenza e nella progettazione delle opere di difesa costiera.

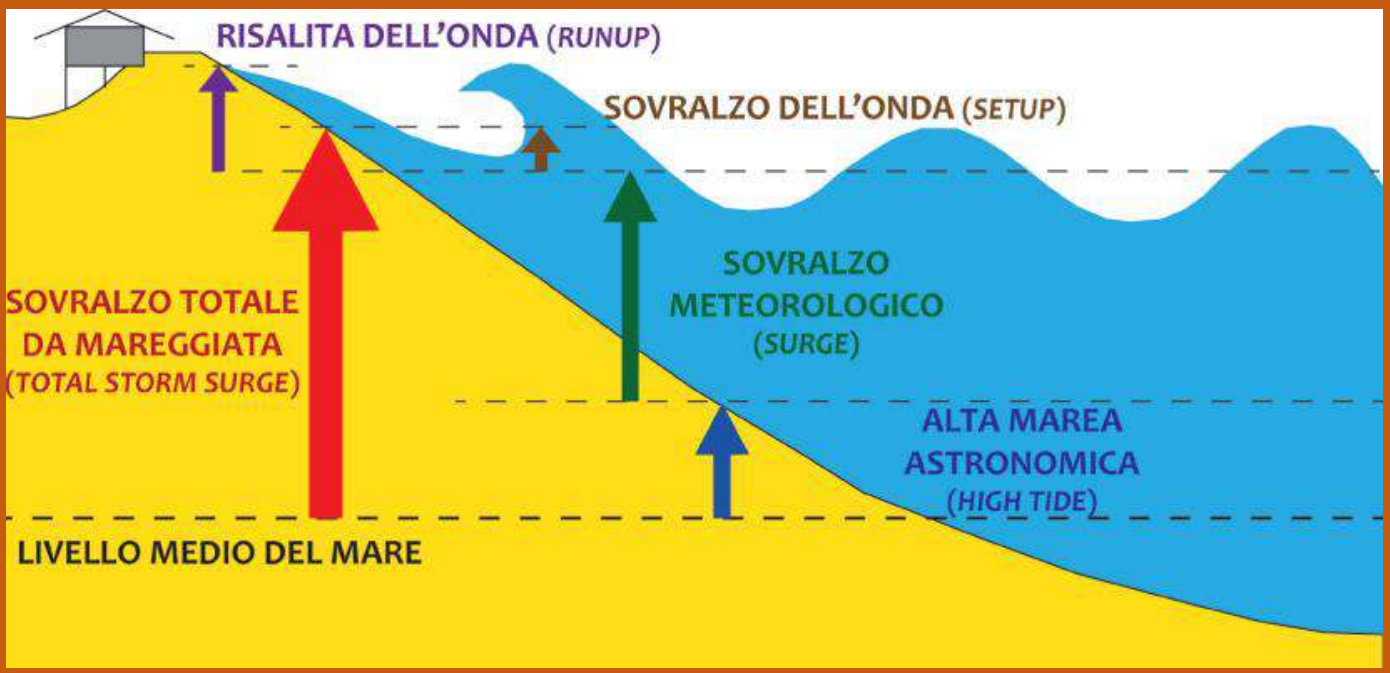

Figura tratta da *Mareggiate e impatti sulla costa - aggiornamento dei dati al 2020, degli indicatori e analisi delle tendenze. A cura del Servizio Geologico, Sismico e dei Suoli della Regione Emilia-Romagna, in collaborazione con Arpae-Servizio Idro-Meteo-Clima e Università di Ferrara, nell'ambito del progetto EU Micore (2008-2011) - Gennaio 2021*

Giorgio Fontolan, Sebastian Spadotto, Luisa Fontanot, Annelore Bezzi – Università di Trieste
Antonio Bratus – Regione Autonoma Friuli Venezia Giulia

https://doi.org/10.3301/ABSGI.2024.01

Venice, 1-2 March 2024

ABSTRACT BOOK

a cura della Società Geologica Italiana

X AIGeo Italian Young Geomorphologists' Day &
III IAG International Young Geomorphologists' Meeting

"Climate change and the role of early-career geomorphologists"

Università Ca'Foscari Venezia
Dipartimento di Scienze Ambientali, Informatica e Statistica

Developing an Automated Tide and Surge Measurement System in Coastal Regions Using Deep Learning Techniques

Sabato G.[1*], Scardino G.[1], Kushabaha A.[1,4], Casagrande G.[2], Chirivì M.[3], Fontolan G.[2], Fracaros S.[2], Luparelli A.[3], Spadotto S.[2] & Scicchitano G.[1]

[1]Department of Earth and Geoenvironmental Sciences, University of Bari, Italy.
[2]Department of Mathematics, Informatics and Geosciences, University of Trieste, Italy.
[3]CETMA (Centro di Ricerca Europeo di Tecnologie Design e Materiali), Brindisi, Italy.
[4]IUSS – School for Advanced Studies, Pavia, Italy.

Corresponding author e-mail: gaetano.sabato@uniba.it

Keywords: deep learning, tide, storm surge, coastal monitoring.

The most recent advances in machine learning and deep learning methodologies are generating great interest in a variety of research fields, including environmental studies. By facilitating automated and remote collection of data, these new tools have changed approaches to measuring maritime features. This research focuses on the development of a deep learning model to automatically measure tide and surge, with the goal of achieving precise results through the analysis of security camera data. The deep learning model was used to predict tide and storm surge from surveillance cameras strategically placed in two different coastal locations namely Santa Lucia in southeastern Sicily and Lignano Sabbiadoro in Friuli Venezia Giulia, Italy, adopting the Inception v3 architecture. The deep learning model uses categorization methods to assign a water level value to a given frame. This approach is especially useful in situations where typical tidal sensors are inaccessible or too far away from measurement stations, such as during extreme events requiring precise surge observations. The dataset employed to train and validate the deep learning model encompasses the full range of tide values observed in the study areas. The accuracy of the system was evaluated by comparing the predictions generated by the deep learning model with the corresponding tide gauge values. The experiments conducted clearly show that the model is quite effective in measuring tide and surge remotely, achieving an accuracy of over 90% and keeping the loss value below 1 for the deep learning model. These results highlight the model's ability to address the absence of data collection in difficult coastal environments, providing valuable information for coastal management and hazard assessment. This research significantly contributes to the expanding realm of remote sensing and machine learning applications in environmental monitoring, enhancing understanding and decision-making in coastal regions.

https://doi.org/10.3301/ABSGI.2024.02

Bari, 2-5 September 2024

ABSTRACT BOOK

a cura della Società Geologica Italiana

BARI 2024

Geology for a sustainable management of our Planet

Using deep learning system-based for tide and surge measurement

Sabato G.*[1], Scardino G.[1], Kushabaha A.[1-4], Casagrande G.[2], Chirivì M.[3], Fontolan G.[2], Fracaros S.[2], Luparelli A.[3], Spadotto S.[2] & Scicchitano G.[1]

[1] Dipartimento di Scienze della Terra e Geoambientali, Università di Bari "Aldo Moro". [2] Dipartimento di Matematica, Informatica e Geoscienze, Università di Trieste. [3] CETMA Centro di Ricerca Europeo di Tecnologie Design e Materiali, Brindisi. [4] Istituto Universitario di Studi Superiori, IUSS, Pavia.

Corresponding author email: gaetano.sabato@uniba.it

Keywords: deep learning, storm surge, coastal monitoring.

In recent years, the development of artificial intelligence and machine and deep learning techniques have attracted the attention of various research fields. Among them, the field of land and environmental study has seen some development in applications of this type by placing some interest in remote data acquisition, measurement of marine parameters and their automated analysis (Scardino et al., 2022; Sabato et al., 2023). This work focuses on the implementation of a deep learnig model based on Inception V3 capable of automatically measuring, after appropriate training, the height of tides and storm surge at a given site using fixed camera images. This solution is useful at sites where tide gauges are far from the measurement point and especially for calculating storm surge at the site of interest. The study was carried out on two different Italian locations, the first in southeastern Sicily, in the center of the Mediterranean and called Santa Lucia, and the second in the north of the country called Lignano Sabbiadoro. For convenience and better performance, the development environment was created on Google Colab. To train the deep learning model, a dataset of images was created for each site, and each frame was axed with the corresponding value measured by an in situ instrument. The dataset partitioning was done according to the literature, which as the best partitioning has 70% of the images used for Convolutional Neural Network (CNN) training and the remaining 30% for validation (Götz et al., 2022). Once the model was trained, prediction was performed on images of the site. The algorithm performed well with accuracy above 90% and Categorical Cross Entropy Loss less than 1. Confusion matrices also show good results and the calculated F1 score is above 0.9 (Huang et al., 2015). Finally, from the comparison of the actual values and those processed by CNN, it was possible to see that the values are very similar to each other and the corresponding time-sheets could be processed. In conclusion, the incorporation of systems such as the one presented in this paper could bring many advantages, such as having almost instantaneous feedback on the consequences from intense weather events and eliminating the need for in-person inspection by the operator. These findings underscore its potential to fill the data collection gap in challenging coastal environments, offering valuable insights for coastal management and hazard assessment. This study makes an important contribution to the rapidly growing field of remote sensing and machine learning applications in environmental monitoring, facilitating greater comprehension and decision-making in coastal areas.

Götz TI et al. (2022) - Number of necessary training examples for Neural Networks with different number of trainable parameters. J. Pathol. Inform., 13, https://doi.org/10.1016/j.jpi.2022.100114.

Huang H. et al. (2015) - Maximum F1-Score Discriminative Training Criterion for Automatic Mispronunciation Detection. IEEE/ACM Transactions on Audio, Speech, and Language Processing, 23(4), 787-797, https://doi.org/10.1109/TASLP.2015.2409733.

Sabato G. et al. (2023) - Deep learning-based segmentation techniques for coastal monitoring and seagrass banquette detection. 2023 IEEE International Workshop on Metrology for the Sea; Learning to Measure Sea Health Parameters (MetroSea), La Valletta, Malta, 524-527, https://doi.org/10.1109/MetroSea58055.2023.10317577.

Scardino G. et al. (2022) - Convolutional Neural Network and Optical Flow for the Assessment of Wave and Tide Parameters from Video Analysis (LEUCOTEA): An Innovative Tool for Coastal Monitoring. Remote Sens., 14, 2994, https://doi.org/10.3390/rs14132994.

https://doi.org/10.3301/ABSGI.2024.02

Bari, 2-5 September 2024

ABSTRACT BOOK

a cura della Società Geologica Italiana

BARI 2024

Geology for a sustainable management of our Planet

Coastal flooding risk scenario for the city of Grado, northern Adriatic Sea

Spadotto S.*[1], Fracaros S.[1], Bezzi A.[1], Casagrande G.[1], Popesso C.[1] & Fontolan G.[1-2]

[1] Dipartimento di Matematica, Informatica e Geoscienze, Università di Trieste.
[2] Consorzio Nazionale Interuniversitario per le Scienze del Mare CoNISMa, Roma.

Corresponding author email: sebastian.spadotto@phd.units.it

Keywords: coastal flooding, storm surge, sea level rise.

Sea level rise, along with fast urbanization, has significantly raised flood hazards in coastal areas due to both increased population and the frequent urgent situations encountered in the urban context (Neumann, 2015). Rigid defensive systems along shorelines, backshore, and perimeter embankments at the lagoon border must therefore undergo structural verification and accurate elevation control, adapted to the expected sea level rise over which extreme events emerge.

In this regard, a thorough investigation was conducted on the city of Grado, located in the North Adriatic Sea and representing one of the most important coastline and heritage sites in Friuli Venezia Giulia. The city is located on a barrier island and is prone to flooding from both the sea and from the back lagoon.

The examination of the historical dataset of mean sea level and maximum levels recorded between 1991 and 2022 allowed us to first obtain local elevation estimates while also including subsidence. The study then looked at the duration of annual exceedance of the minimal threshold level of 110 cm, which marks Grado's first significant marine ingression. Annual extremes were then processed using the Gumbel-type distribution law (Gumbel, 1958; Coles, 2001), which modulated the level thresholds with their respective return times for the location. Finally, the reconnaissance includes a downscaling examination of the impacts on the urban fabric, which is divided into regions of different vulnerability. Inundated areas were compared from high-resolution DEMs using a GIS-based technique and a modeling approach utilizing MIKE software, analyzing both the magnitude and exposure of the urban setting to flood risk estimated for 2050 and 2100. As of today, approximately 56% of Grado's inhabited area is inundated with a sea level threshold value of 151 cm, which occurs during surge episodes with a 30-year return period. By 2100, with an optimistic forecast (SSP1-2.6) of local sea level rise of around +50 cm, the same threshold will be met with events with a 30 times shorter return time. As a result, by 2100, 56% of the land area will be submerged at least once a year due to 101 cm surges. Extreme levels linked with more catastrophic events with secular recurrence times will be achieved on a multi-year basis, flooding more than 70% of the urbanized area. This makes it more important than ever to develop proper adaptation measures from the outset. The simulations developed are thus essential for medium to long-term urban planning, with the goal of securing the city, which, like Venice, is indicative of the processes that may affect other coastal realities and historical cities of great national worth.

Coles S. (2001) - An Introduction to Statistical Modeling of Extreme Values, Springer Series in Statistics, Springer, London, 209 pp., https://doi.org/10.1007/978-1-4471-3675-0.

Gumbel E. (1958) - Statistics of Extremes, Columbia University Press, New York, 378 pp., https://doi.org/10.7312/gumb92958.

Neumann B. et al. (2015) - Future coastal population growth and exposure to sea-level rise and coastal flooding-a global assessment. PLoS One, 10(3), e0118571, https://doi.org/10.1371/journal.pone.0118571.

Littoral 24

European Coastal Challenge Summit

17th EUCC International Conference

Book of Abstracts

September 2024

Constanța, Romania

littoral24.univ-ovidius.ro

Poster session I

SHORELINE DYNAMICS AND BREEDING COASTAL BIRDS IN THE MARANO AND GRADO BARRIER ISLANDS

Annelore Bezzi*, Stefano Sponza, Giulia Casagrande, Sebastian Spadotto, Saverio Fracaros, Davide Martinucci, Simone Pillon, Giorgio Fontolan

Università degli Studi di Trieste, Dipartimento di Matematica, Informatica e Geoscienze

**Corresponding author: bezzi@units.it; sponza@units.it*

Covering almost 12% of the world's coasts, barrier islands are ideal habitat for many species of coastal birds. The functionality and benefits related to these coastal environments have recently been threatened by the reduction in sedimentary input, sea level rise, and human activities. Part of the Natura 2000 network, the system of sand banks and barrier islands of the Marano and Grado Lagoon (NE Italy) maintains a high degree of naturalness. Here, the Oystercatcher (Haematopus ostralegus), the Little tern (*Sternula albifrons*), and the Kentish plover (*Charadrius alexandrinus*) are the most distinctive bird nesting species of conservation concern. We examine the monitoring of target species during the nesting phase over a ten-year period (2013 to 2023) and look into the possible effect and/or constraint exerted by the morphodynamic setting of the nesting habitat. The analysis focuses on key geomorphological indicators, such as coastline advance or retreat, as well as variations in the island extent. The results indicate that the barrier system is self-sustaining despite a general rollover process. An external longshore sediment input is responsible for supplying a compensating longshore process that counteracts short-term, localised morphological changes such as spit progradation and washover development. In this morphodynamic context, the nesting population of Oystercatchers has grown over the years, while greater difficulties have been registered for the Little tern and the Kentish plover, whose breeding success has been more limited and is probably more constrained by the high dynamism and ephemeral characteristics of the barrier islands habitat. This underlines how, despite sharing the same nesting habitat, the response to different pressures could vary from species to species. Furthermore, our results allowed to provide a first set of management indications for species protection, based on the principles of adaptive management and maintenance of morphodynamic processes.

Keywords: *barrier islands, coastal birds, morphodynamics, monitoring,*

Acknowledgements: The monitoring activity is founded by the Biodiversity Office, Regione Friuli Venezia Giulia. We especially thank Dr. Umberto Fattor.

Littoral 24

European Coastal Challenge Summit

17th EUCC International Conference

Book of Abstracts

September 2024

Constanța, Romania

littoral24.univ-ovidius.ro

Session I. Climate change adaptation strategies

COASTAL VULNERABILITY ASSESSMENT OF VENETO BEACHES AND BARRIER ISLANDS, NORTHERN ADRIATIC, ITALY

Annelore Bezzi [1*], Casagrande G. [1], Fracaros S. [1] ,Spadotto S[1]., Pillon S[1]., Martinucci D. [1], Popesso C. [1], Fontolan G. [1]

[1] *Università degli Studi di Trieste, Dipartimento di Matematica, Informatica e Geoscienze*

[*]*Corresponding author: bezzi@units.it*

The assessment of coastal vulnerability to sea storms is critical in coastal management since sea level rise and human pressure affect both the morphological and sedimentary constraints, thus increasing coastal risks. In this work we present an assessment of sea storm vulnerability for the 170 km of coastline of the Veneto area (Northern Adriatic, Italy), using an adaptation of the Coastal Vulnerability Index. The methodology relies on a comprehensive coastal geodatabase and includes the estimate of the Intrinsic Vulnerability (Vi): several variables were analysed and weighted to define the physical and evolutionary conditions of the coast, under the assumption that there is no defence against sea storms. Subsequently, the classification and evaluation of coastal defences (hard and soft) allows the shift from intrinsic to Real vulnerability (Vr). Owing to a methodological adjustment made for the various coastal types (barrier islands or beaches), the results show varying grades of Vi depending on distinct morpho-evolutive conditions. Low values of Vi are typical of coastal tracts acting as sedimentary traps in proximity to jettied or unjettied tidal inlets. At the same time, along the Po delta, some barrier islands have dissipative characteristics and positive sedimentary budget due to the sandy load from river branches. In many cases, beaches with moderate Vi benefit from the widespread distribution of hard coastal defences and the presence of coastal dunes, which mitigate vulnerability. Finally, littoral sections with high Vi are mostly afflicted by a persistent sedimentary deficit, resulting in absent or narrow beaches with steep shoreface. Overall, the massive use of hard defence works ensures safety, although impeding any resilience of the morpho-sedimentary system.

Keywords: *coastal vulnerability index, sea storm, beach, barrier island, Northern Adriatic sea*.

Acknowledgements: Research funded by the consortium iNEST (Interconnected North-Est Innovation Ecosystem) funded by the European Union Next-GenerationEU (Piano Nazionale di Ripresa e Resilienza (PNRR)-Missione 4 Componente 2, Investimento 473 1.5-D.D. 1058 23/06/2022, ECS_00000043), and Interreg Italy - Croatia Stream. This research was supported by the Civil Protection of the Autonomous Region of Friuli Venezia Giulia as part of a collaboration with the Department of Mathematics, Informatics, and Geosciences at the University of Trieste.